Energy, Environment, and Sustainability
Series Editor: Avinash Kumar Agarwal

Akhilendra Pratap Singh
Dhananjay Kumar
Avinash Kumar Agarwal *Editors*

Alternative Fuels and Advanced Combustion Techniques as Sustainable Solutions for Internal Combustion Engines

Springer

Energy, Environment, and Sustainability

Series Editor

Avinash Kumar Agarwal, Department of Mechanical Engineering, Indian Institute of Technology Kanpur, Kanpur, Uttar Pradesh, India

AIMS AND SCOPE

This books series publishes cutting edge monographs and professional books focused on all aspects of energy and environmental sustainability, especially as it relates to energy concerns. The Series is published in partnership with the International Society for Energy, Environment, and Sustainability. The books in these series are edited or authored by top researchers and professional across the globe. The series aims at publishing state-of-the-art research and development in areas including, but not limited to:

- Renewable Energy
- Alternative Fuels
- Engines and Locomotives
- Combustion and Propulsion
- Fossil Fuels
- Carbon Capture
- Control and Automation for Energy
- Environmental Pollution
- Waste Management
- Transportation Sustainability

Review Process

The proposal for each volume is reviewed by the main editor and/or the advisory board. The chapters in each volume are individually reviewed single blind by expert reviewers (at least four reviews per chapter) and the main editor.

Ethics Statement for this series can be found in the Springer standard guidelines here https://www.springer.com/us/authors-editors/journal-author/journal-author-helpdesk/before-you-start/before-you-start/1330#c14214

More information about this series at http://www.springer.com/series/15901

Akhilendra Pratap Singh · Dhananjay Kumar ·
Avinash Kumar Agarwal
Editors

Alternative Fuels and Advanced Combustion Techniques as Sustainable Solutions for Internal Combustion Engines

Springer

Editors
Akhilendra Pratap Singh
Department of Mechanical Engineering
Indian Institute of Technology Kanpur
Kanpur, Uttar Pradesh, India

Dhananjay Kumar
Department of Mechanical Engineering
Indian Institute of Technology Kanpur
Kanpur, Uttar Pradesh, India

Avinash Kumar Agarwal
Department of Mechanical Engineering
Indian Institute of Technology Kanpur
Kanpur, Uttar Pradesh, India

ISSN 2522-8366 ISSN 2522-8374 (electronic)
Energy, Environment, and Sustainability
ISBN 978-981-16-1512-2 ISBN 978-981-16-1513-9 (eBook)
https://doi.org/10.1007/978-981-16-1513-9

This Springer imprint is published by the registered company Springer Nature Singapore Pte Ltd.
The registered company address is: 152 Beach Road, #21-01/04 Gateway East, Singapore 189721, Singapore

Preface

Energy demand has been rising remarkably due to increasing population and urbanization. Global economy and society are significantly dependent on the energy availability because it touches every facet of human life and activities. Transportation and power generation are the two major examples. Without the transportation by millions of personalized and mass transport vehicles and availability of 24×7 power, human civilization would not have reached contemporary living standards.

The International Society for Energy, Environment and Sustainability (ISEES) was found at Indian Institute of Technology Kanpur (IIT Kanpur), India, in January 2014 with an aim to spread knowledge/awareness and catalyze research activities in the fields of energy, environment, sustainability and combustion. The society's goal is to contribute to the development of clean, affordable and secure energy resources and a sustainable environment for the society and to spread knowledge in the above-mentioned areas and create awareness of the environmental challenges, which the world is facing today. The unique way adopted by the society was to break the conventional silos of specializations (engineering, science, environment, agriculture, biotechnology, materials, fuels, etc.) to tackle the problems related to energy, environment and sustainability in a holistic manner. This is quite evident by the participation of experts from all fields to resolve these issues. ISEES is involved in various activities such as conducting workshops, seminars and conferences in the domains of its interests. The society also recognizes the outstanding works done by the young scientists and engineers for their contributions in these fields by conferring them awards under various categories.

The Fourth International Conference on 'Sustainable Energy and Environmental Challenges' (IV-SEEC) was organized under the auspices of ISEES from November 27 to 29, 2019, at NEERI, Nagpur. This conference provided a platform for discussions between eminent scientists and engineers from various countries including India, USA, China, Italy, Mexico, South Korea, Japan, Sweden, Greece, Czech Republic, Germany, Netherland and Canada. In this conference, eminent speakers from all over the world presented their views related to different aspects of energy, combustion, emissions and alternative energy resource for sustainable development and cleaner environment. The conference presented one high-voltage plenary talk

by Mrs. Rashmi Urdhwareshe, Director, Automotive Research Association of India (ARAI), Pune.

The conference included 28 technical sessions on topics related to energy and environmental sustainability including 1 plenary talk, 25 keynote talks and 54 invited talks from prominent scientists, in addition to 70+ contributed talks and 80+ poster presentations by students and researchers. The technical sessions in the conference included fuels, engine technology and emissions, coal and biomass combustion/gasification, atomization and sprays, combustion and modeling, alternative energy resources, water and wastewater treatment, automobile and other environmental applications, environmental challenges and sustainability, nuclear energy and other environmental challenges, clean fuels and other environmental challenges, water pollution and control, biomass and biotechnology, waste to wealth, microbiology, biotechnological and other environmental applications, waste and wastewater management, cleaner technology and environment, sustainable materials and processes, energy, environment and sustainability, technologies and approaches for clean, sensors and materials for environmental, biological processes and environmental sustainability. One of the highlights of the conference was the Rapid-Fire Poster Sessions in (i) engine/fuels/emissions, (ii) environment and (iii) biotechnology, where 50+ students participated with great enthusiasm and won many prizes in a fiercely competitive environment. Three hundred plus participants and speakers attended this three-day conference, where 12 ISEES books published by Springer, Singapore, under a special dedicated series 'Energy, environment and sustainability' were released. This was the third time in a row that such a significant and high-quality outcome has been achieved by any society in India. The conference concluded with a panel discussion on 'Balancing Energy Security, Environmental Impacts and Economic Considerations: Indian Perspective,' where the panelists were Dr. Anjan Ray, CSIR-IIP Dehradun; Dr. R. R. Sonde, Thermax Ltd.; Prof. Avinash Kumar Agarwal, IIT Kanpur; Dr. R. Srikanth, National Institute of Advanced Studies, Bengaluru; and Dr. Rakesh Kumar, NEERI, Nagpur. The panel discussion was moderated by Prof. Ashok Pandey, Chairman, ISEES. This conference laid out the roadmap for technology developments, opportunities and challenges in energy, environment and sustainability domains. All these topics are relevant for the country and the world in the present context. We acknowledge the support received from various funding agencies and organizations for the successful conduct of the Fourth ISEES Conference (IV-SEEC), where these books germinated. We would therefore like to acknowledge SERB, Government of India (special thanks to Dr. Sandeep Verma, Secretary); NEERI, Nagpur (special thanks to Dr. Rakesh Kumar, Director), CSIR, and our publishing partner Springer (special thanks to Swati Mehershi).

The editors would like to express their sincere gratitude to authors from all over the world for submitting their high-quality work in a timely manner and revising it appropriately at a short notice. We would like express our special thanks to Dr. Pravesh Chandra Shukla, Dr. Nirendra Nath Mustafi, Prof. V. Ganeshan, Dr. Joonsik Hwang, Dr. Sayan Biswas, Dr. Vikram Kumar, Dr. Dhinesh Balasubramanian, Dr. Prashant Malik, Ashutosh Jena, Ankur Kalwar, Utkarsha Sonawane, Harsimran Singh, Sulav Kafle, Manojit Pal, Sam Joe, Gaurav Chaudhary, Arun Lal, Akash Rai, Ayush Tripathi

and Tushar Kakkar, who reviewed various chapters of this monograph and provided their valuable suggestions to improve the manuscripts.

This book covers different aspects related to utilization of alternative fuels in internal combustion (IC) engines with a focus on biodiesel, dimethyl ether, alcohols, biogas, etc. The main objective of this book is to present the engine combustion, performance and emission characteristics of IC engines fueled by different alternative fuels. One section of this book also covers the adaptation of advanced combustion and engine technologies for utilization of alternative fuels as well as conventional fuels in an energy-efficient manner to reduce the harmful pollutants emitted from IC engines. Technologies described in different chapters of this book are focused on current trends of the automotive sector. Overall, this book will be useful for both engine researchers and energy experts. We hope that the book would be of great interest to the professionals and post-graduate students involved in fuels, IC engines, engine instrumentation and environmental research.

Kanpur, India

Akhilendra Pratap Singh
Dhananjay Kumar
Avinash Kumar Agarwal

Contents

Editors and Contributors

About the Editors

Dr. Akhilendra Pratap Singh is currently working at the Indian Institute of Technology (IIT) Kanpur, India. He received his Master's and Ph.D. in Mechanical Engineering from IIT Kanpur, India in 2010 and 2016, respectively. He worked at the Engine Research Center, University of Wisconsin at Madison, USA as a postdoctoral fellow (2017–2018). His areas of research include advanced low temperature combustion, optical diagnostics with special reference to engine endoscopy and PIV, combustion diagnostics, engine emissions measurement, particulate characterization and their control, and alternative fuels. Dr. Singh has edited 10 books and authored 27 book chapters, 45+ research articles in international journals and conferences. He has been awarded with ISEES Best Ph.D. Thesis Award (2017), SERB Indo-US Postdoctoral Fellowship (2017) and IEI Young Engineer Award (2017). He is a member of numerous professional societies, including SAE, ASME, and ISEES.

Dhananjay Kumar is a research scholar at the Engine Research Laboratory, Indian Institute of Technology (IIT) Kanpur, India. He received his B.Tech. in Mechanical Engineering from National Institute of Technology (NIT) Mizoram, India in 2017. His research area includes laser ignition technology, alternative fuels, combustion simulations, particulate characterization, etc. He has published several international journal papers and authored book chapters in the area of laser ignition, combustion simulations and alternative fuel like methanol, DME, etc.

Prof. Avinash Kumar Agarwal joined the Indian Institute of Technology (IIT) Kanpur, India in 2001 after working as a post-doctoral fellow at the Engine Research Center, University of Wisconsin at Madison, USA. His interests are IC engines, combustion, alternate and conventional fuels, lubricating oil tribology, optical diagnostics, laser ignition, HCCI, emissions and particulate control, and large bore engines. Prof. Agarwal has published 290+ peer reviewed international journal and conference papers, 42 edited books, 78 books chapters and has 10,000+ Scopus and 15,300+ Google scholar citations. He is a Fellow of SAE (2012), Fellow of ASME (2013), Fellow of ISEES (2015), Fellow of INAE (2015), Fellow of NASI (2018), Fellow of Royal Society of Chemistry (2018), and a Fellow of American Association of Advancement in Science (2020). He is recipient of several prestigious awards such as Clarivate Analytics India Citation Award-2017 in Engineering and Technology, NASI-Reliance Industries Platinum Jubilee Award-2012; INAE Silver Jubilee Young Engineer Award-2012; Dr. C. V. Raman Young Teachers Award-2011; SAE Ralph R. Teetor Educational Award-2008; INSA Young Scientist Award-2007; UICT Young Scientist Award-2007; INAE Young Engineer Award-2005. Prof. Agarwal received Prestigious Shanti Swarup Bhatnagar Award-2016 in Engineering Sciences. For his outstanding contributions, Prof. Agarwal is conferred upon Sir J. C. Bose National Fellowship (2019) by SERB.

Contributors

Avinash Kumar Agarwal Engine Research Laboratory, Department of Mechanical Engineering, Indian Institute of Technology Kanpur, Kanpur, India

Mamta Awasthi Centre for Energy and Environmental Engineering, NIT Hamirpur, Hamirpur, India

Dhinesh Balasubramanian Department of Mechanical Engineering, Mepco Schlenk Engineering College, Sivakasi, Tamil Nadu, India;
Mechanical Engineering Division, Faculty of Engineering, Khon Kaen University, Khon Kaen, Thailand;
Center for Alternative Energy Research and Development, Khon Kaen University, Khon Kaen, Thailand

Lepakshi Barbora Centre for Energy, Indian Institute of Technology Guwahati, Guwahati, Assam, India

Debarshi Baruah Centre for Energy, Indian Institute of Technology Guwahati, Guwahati, Assam, India

Sayan Biswas University of Minnesota Twin Cities, Minneapolis, MN, USA

Deep Bora Centre for Energy, Indian Institute of Technology Guwahati, Guwahati, Assam, India

Arup Jyoti Borah Department of Biotechnology, National Institute of Technology Arunachal Pradesh, Yupia, Papum Pare, Arunachal Pradesh, India

Hiren Dave U. V. Patel College of Engineering, Ganpat University, Kherva, Gujarat, India

Akash Deep School of Mechanical Engineering, Lovely Professional University, Jalandhar, Punjab, India

S. K. Gugulothu Department of Mechanical Engineering, National Institute of Technology Andhra Pradesh, Tadepalligudem, Andhra Pradesh, India

P. V. Inbanaathan Department of Mechanical Engineering, Mepco Schlenk Engineering College, Sivakasi, Tamil Nadu, India

Ashutosh Jena Engine Research Laboratory, Department of Mechanical Engineering, Indian Institute of Technology Kanpur, Kanpur, India

Pankaj Kalita Centre for Energy, Indian Institute of Technology Guwahati, Guwahati, Assam, India

Ankur Kalwar Engine Research Laboratory, Department of Mechanical Engineering, Indian Institute of Technology Kanpur, Kanpur, India

Ramalingam Krishnamoorthy Department of Mechanical Engineering, CK College of Engineering and Technology, Cuddalore, Tamil Nadu, India

Dhananjay Kumar Department of Mechanical Engineering, Indian Institute of Technology Kanpur, Kanpur, India

Pankaj Kumar Department of Mechanical Engineering, College of Engineering and Technology, SRM Institute of Science and Technology, Chennai, TN, India

Vikram Kumar Engine Research Laboratory, Department of Mechanical Engineering, Indian Institute of Technology Kanpur, Kanpur, India

Pinakeswar Mahanta Department of Mechanical Engineering, Centre for Energy, Indian Institute of Technology Guwahati, Guwahati, Assam, India;
Department of Mechanical Engineering, National Institute of Technology Arunachal Pradesh, Yupia, Papum Pare, Arunachal Pradesh, India

Sunil Kumar Mahla Department of Mechanical Engineering, IKG Punjab Technical University, Kapurthala, India

Prashant Malik Centre for Energy and Environmental Engineering, NIT Hamirpur, Hamirpur, India

Vijayanand Suryakant Moholkar Department of Chemical Engineering, Centre for Energy, Indian Institute of Technology Guwahati, Guwahati, Assam, India

Nalini Kanta Mukherjee Centre of Excellence, TAFE Motors and Tractors Ltd., Alwar, India

Marcin Noga Institute of Automobiles and Internal Combustion Engines, Cracow University of Technology, Kraków, Poland

Manojit Pal Engine Research Laboratory, Department of Mechanical Engineering, Indian Institute of Technology Kanpur, Kanpur, India

Brijesh Patel Gdhyana Sanshodhana Nagari Foundations, Vadodara, Gujarat, India

Tran Dang Quoc School of Transportation Engineering, Hanoi University of Science and Technology, Hanoi, Vietnam

Amudhan Rajarajan Department of Mechanical Engineering, CK College of Engineering and Technology, Cuddalore, Tamil Nadu, India

Vigneswaran Rajendran Department of Mechanical Engineering, Sri Sairam Institute of Technology, Chennai, India

D. Siva Krishna Reddy Department of Mechanical Engineering, College of Engineering and Technology, SRM Institute of Science and Technology, Chennai, TN, India

Akhilendra Pratap Singh Department of Mechanical Engineering, Indian Institute of Technology Kanpur, Kanpur, India

Harsimran Singh Engine Research Laboratory, Department of Mechanical Engineering, Indian Institute of Technology Kanpur, Kanpur, India

Utkarsha Sonawane Engine Research Laboratory, Department of Mechanical Engineering, Indian Institute of Technology Kanpur, Kanpur, India

Bharatkumar Sutaria S. V. National Institute of Technology, Surat, Gujarat, India

S. Vedharaj Department of Mechanical Engineering, National Institute of Technology, Tiruchirappalli, Tamil Nadu, India

General

Introduction to Alternative Fuels and Advanced Combustion Techniques as Sustainable Solutions for Internal Combustion Engines

Akhilendra Pratap Singh, Dhananjay Kumar, and Avinash Kumar Agarwal

In the last few decades, internal combustion (IC) engines have been declared as the prime source of pollutants, which is highly undesirable for environment as well as human health. Sustainability of IC engines has become another issue due to rapidly decreasing fossil fuel reserves, which is the main source of energy for IC engines. Researchers are continuously trying to resolve these issues by exploring alternative energy resources and advanced combustion and engine technologies for IC engines. Among different alternative energy resources, renewable fuels have been universally adopted for IC engines, which has significant potential to resolve the above mentioned issues. On the other side, researchers have also developed several advanced combustion and engine technologies, which can simultaneously improve the engine performance along with reduced exhaust emissions. This book covers these two technology road maps for resolving the issues associated with IC engines.

The second section of this book is completely based on alternative fuels, in which various alternative fuels such as dimethyl-ether (DME), biodiesel, biogas and producer gas have been discussed. The first few chapters of this book discuss the potential of DME for IC engines. DME can be used as a next-generation fuel in the existing compression ignition (CI) engines because of the ultra-low emission (Soot and oxides of nitrogen (NOx)) discharged. This chapter also includes variety of methods for DME production, and its physical and chemical characteristics. The main objective of this chapter is to provide information related to modifications required for DME adaptation in IC engines. This chapter suggests that several components including fuel tank, fuel supply lines, valves, filters, fuel feed pump, fuel high pressure pump and fuel injectors need to be changed for adapting DME as fuel in CI engines. The next chapter of this section deals with handling of liquid DME and development of DME fuel injection system for fueling CI engines. This chapter

A. P. Singh · D. Kumar · A. K. Agarwal (✉)
Department of Mechanical Engineering, Indian Institute of Technology Kanpur, Kanpur, India
e-mail: akag@iitk.ac.in

A. P. Singh et al. (eds.), *Alternative Fuels and Advanced Combustion Techniques as Sustainable Solutions for Internal Combustion Engines*, Energy, Environment, and Sustainability, https://doi.org/10.1007/978-981-16-1513-9_1

also cover the safety aspects of DME utilization as DME liquid detection system. Compatibility of DME with sealing and gasket materials has also been discussed in this chapter. This chapter also discusses various other aspects of DME including techniques for lubricant addition, mixing and circulation in pressurized conditions, etc. The next chapter of this section describes about the energy resource as unutilized pine needles, especially in hilly regions, which has significant potential to meet out the energy demand. Pine needles are used in biomass gasifiers as a feedstock for producer gas production and successively used for combustion in IC engines for electricity generation. This chapter suggests that producer gas formed from pine needles can be easily used in diesel engines as hybrid fuel or stand-alone fuel. Techno-economic analysis of this solution is the novel aspect of this chapter. The next chapter of this section discusses another gaseous alternative fuel such as biogas for IC engine applications. Biogas produced from anaerobic digestion of organic resources may be considered as a significant bioenergy with the potential to address energy crisis concerns. This chapter also describes the cleaning of biogas to remove the impurities like carbon dioxide (CO_2) and hydrogen sulphide (H_2S), which is necessary to enhance the applicability of biogas as a clean alternative fuel. This chapter summarizes different physico-chemical (viz. cryogenic, adsorption, membrane separations and absorption) and biological (in situ and ex situ) techniques for biogas upgradation. These operations are critical for upgrading the fuel properties similar to standards for vehicular applications, for injection in the natural gas grid, to be used as substrate for the production of chemicals or for fuel cell applications. The next chapter of this book talks about the biomass gasification, which is a carbon–neutral mode of energy conversion and a promising option to meet the growing needs of energy. This chapter attempts to address various aspects related to the utilization of producer gas in IC engines, including both CI and spark ignition (SI) engines. This chapter also describes the issues such as tar formation and engine derating, which adversely affects the potential of producer gas as an IC engine fuel. The measures required to address these issues are briefly discussed in this chapter. Several case studies related to producer gas-fueled IC engines are the important aspect of this chapter. The next chapter of this section describes about the biodiesel as an alternative fuel for IC engines. This chapter briefly described the biodiesel production aspects. In this chapter, a case study of biodiesel utilization in IC engine has been discussed. This chapter provides interesting results about the performance and emission characteristics of a CI engine fueled with blends of biodiesel and mineral diesel. This section also includes another chapter on biodiesel, which is produced from waste cooking oil (WCO). In this chapter, emission, performance and combustion characteristics of a single-cylinder CI engine fueled with biofuel/diesel blends have been discussed. This chapter exhibited that lower blends of biodiesel with mineral diesel can be effectively used to reduce smoke, carbon monoxide (CO) and hydrocarbon (HC) emissions. Biodiesel-fueled engine resulted in relatively inferior engine performance; however, performance of lower blends of biodiesel was almost similar to baseline results. The last chapter of this section discusses the emulsified fuels for IC engines. This chapter discusses the utilization of 1,4-dioxane emulsified fuel in direct-injection diesel engine to reduce the engine-out emissions and salvage the

fossil fuel from depletion. The test fuel was made with 79.8% diesel, 10% water, 10% 1,4-dioxane, and 0.2% surfactant. This chapter was based on the results of the experiments, which were performed at different start of injection (SoI) timings. This chapter exhibited the great potential of emulsified fuels in IC engines.

The third section of this book discusses the advanced combustion and engine technologies for IC engines. The first chapter of this book discusses lean-burn spark-ignition engines, which are beneficial in comparison with conventional SI engine as lower in-cylinder temperature, reduced heat losses, better thermodynamic and combustion efficiency and lower HC, CO and NO_x emissions. This chapter also describes several practical difficulties involved with lean-burn SI engines, which include combustion instability, engine misfire and lower flame speed. Several solutions such as advanced ignition systems have been also discussed in this chapter, which includes laser ignition (LI), turbulent jet ignition (TJI), radio-frequency corona ignition (RFCI) and microwave-assisted spark-ignition (MASI) system. Important aspects of all these advanced ignition systems as principle of operation, fundamental understanding, engine characteristics, advantages, limitation and challenges are described in this chapter. The second chapter of this section is based on TJI technique. In TJI, a pre-chamber combustion generated turbulent jet consisting of hot combustion products and active radicals ignite a lean mixture. This chapter covers the fundamentals as well as the scalability aspect of the TJI strategy. A lot of results using detailed analysis is the key feature of this chapter, which provide useful insights about the TJI fundamentals and serve as a guideline for future pre-chamber design and optimization. The next chapter of this section is based on advanced engine technology for SI engines as gasoline direct-injection (GDI). GDI engines are beneficial in terms of fuel economy and higher power output compared to identical port-fuel injected SI engines. This chapter discusses the two modes of operation of GDI engine, namely stratified mode and homogeneous mode. The main objective of this chapter is to highlight the advantages of stratified mode and challenges involved. This chapter describes the causes for combustion variability, which results in partial burn and misfire cycles. Important information related to ignition parameters, spray characteristics of different nozzles, injection strategies, cylinder charge control and utilization of alternate fuels is the key feature of this chapter, which have been summarized in the chapter. The next chapter of this section is based on another engine technology named as gasoline compression ignition (GCI). This is an advanced and promising low-temperature combustion (LTC) technology, which takes advantage of higher volatility and auto-ignition temperature of gasoline-like fuels and higher compression ratio inherent to diesel engines. It has potential to reduce PM and NO_x emissions simultaneously without compromising with CI engine like efficiency. However, practical implementation of GCI technology in heavy-duty applications is a challenging due to higher combustion loss and combustion instability at lower engine loads, combustion noise at higher engine loads, difficulty in maintaining a balance between maximum pressure rise rate, higher CO and HC emissions, etc. This chapter provides solution for these issues and discusses the way-forward of GCI technology for IC engines. The next chapter of this section covers the design aspects of intake pipe and

piston bowl of engine, which significantly affect the engine performance and emission characteristics. In this chapter, 1-D engine performance simulations were used to optimize the length and diameter of the intake pipe because air flow rate is significantly affected by these parameters. These findings were validated on steady-state engine dynamometer, which exhibited that the optimized intake pipe had different characteristics compared to that predicted from simulations. This chapter includes a detailed analysis of probable reasons for this deviation and reported that defective components and associated testing procedures were the main reasons for this anomaly. This study also included a comparison of engine performance and emission characteristics obtained from optimized intake pipes w.r.t. original intake pipes. The results exhibited that superior engine performance and emission characteristics of optimized intake pipe compared to original intake pipe. For detailed combustion investigations, 3-D combustion CFD simulations were performed using two piston bowl designs as original and modified designs. They differ in geometric parameters of the bowl with the identical compression ratio, which promoted better fuel–air mixing, which was also exhibited in performance and emission characteristics. The last chapter of this section discusses the suitability of pilot injections for IC engines. This chapter describes about the smoke-brake specific fuel consumption (BSFC) trade-off, which exists between smoke/soot emissions and BSFC under pilot injection mode. This chapter suggests the solution for this problem as use of a fuel injector with increased number of nozzle holes. The detailed results of numerical simulations having two different injector configurations are discussed in this chapter. Overall, this chapter suggests that replacement of a three-hole injector with a six-hole injector results in lower BSFC and smoke emissions.

Specific topics covered in the monograph include:

- Introduction to Alternative Fuels and Advanced Combustion Techniques as Sustainable Solutions for Internal Combustion Engines
- Prospects of Fuel Injection System for Dimethyl Ether Applications in Compression Ignition Engines
- Material Compatibility, Technical Challenges and Modifications Required for DME Adaptation in Compression Ignition Engines
- Techno-Economic and Environmental Evaluation of Producer Gas-Based IC Engine in a Hybrid Energy System
- A Comparative Assessment of Biogas Upgradation Techniques and its Utilization as an Alternative Fuel in Internal Combustion Engines
- A Comprehensive Study on Utilization of Producer Gas as IC Engine Fuel
- Experimental Investigation of Unmodified Diesel Engine on Performance, Combustion and Emission with Various Proportions of Jatropha Biofuel in Diesel
- Characterization of Single-Cylinder DI Diesel Engine Fueled with Waste Cooking Oil Biofuel/Diesel Blends
- Effect of 1,4-Dioxane Emulsified Fuel on Diesel Engine Performance and Emission Operating with Varying Injection Timing
- Advanced Ignition System to Extend the Lean Limit Operation of Spark-ignited (SI) Engines

- Dimensionless Quantities in Pre-chamber Turbulent Jet Ignition of Premixed Methane/Air
- Lean-Burn Combustion in Direct-Injection Spark-Ignition Engines
- Potential of Gasoline Compression Ignition Combustion for Heavy-Duty Applications in Internal Combustion Engines
- Application of CFD in the Design of Reciprocating Engine for Light Commercial Vehicle Applications
- An Approach to Improve Smoke-Fuel Consumption Trade-Off under Pilot Injection Mode in a Diesel Engine-Experimental and Numerical Study

The topics are organized in three different sections: (i) General, (ii) Alternative Fuels for IC Engines, (iii) Advanced Combustion and Engine Technologies.

Alternative Fuels for IC Engines

Prospects of Fuel Injection System for Dimethyl Ether Applications in Compression Ignition Engines

Manojit Pal, Vikram Kumar, Ankur Kalwar, Nalini Kanta Mukherjee, and Avinash Kumar Agarwal

1 Introduction

Dimethyl ether (DME), being a synthetic fuel, enables energy security. DME is a clean fuel, and its use in energy sector (industries and transport) can reduce environmental pollution and paves way for sustainable development of transport sector. Other alternatives, such as electric vehicles (EV), are also being implemented, but they have limitations of low peak power output compared to internal combustion (IC) engines. IC engines are the backbone of transportation sector globally. Owing to higher torque output and thermal efficiency of diesel engines compared to gasoline engines, they are extensively used in heavy-duty applications such as generators, agricultural applications and road transport vehicles. However, higher emissions of nitrogen oxides (NO_x) and particulate matter (PM) from diesel-fueled compression ignition (CI) engines are hazardous to human health and the environment. These emissions can be reduced by using oxygenated fuels such as DME to displace diesel. DME is the simplest ether, and absence of carbon-to-carbon bond in its chemical structure allows soot-free combustion in CI engines. Hence, DME as an alternative fuel is an excellent replacement for diesel.

DME is a gaseous fuel at normal temperature and pressure (NTP). It becomes liquid, when pressurized to 6 bar at 25 °C temperature, which makes its handling convenient. It can be handled similar to liquid petroleum gas (LPG). Existing infrastructure of LPG can be used for handling DME with some specific modifications due to its inherent corrosive nature. DME is not compatible with rubber, and therefore,

M. Pal · V. Kumar · A. Kalwar · A. K. Agarwal (✉)
Engine Research Laboratory, Department of Mechanical Engineering,
Indian Institute of Technology Kanpur, Kanpur 208016, India
e-mail: akag@iitk.ac.in

N. K. Mukherjee
Centre of Excellence, TAFE Motors and Tractors Ltd., Alwar, India

A. P. Singh et al. (eds.), *Alternative Fuels and Advanced Combustion Techniques as Sustainable Solutions for Internal Combustion Engines*, Energy, Environment, and Sustainability, https://doi.org/10.1007/978-981-16-1513-9_2

we need alternate sealant material. Due to its high cetane number (~55–60), DME is suitable for CI engines, unlike LPG, which is used as alternate fuel in the SI engines mainly. Liquid DME can be inducted directly into the combustion chamber of a CI engine, which can be ignited by high-temperature compressed air toward the end of compression stroke. Many researchers have studied DME by premixing it in gaseous form with the intake air and triggering the ignition by diesel pilot injection [1]. Later, liquid DME was blended with other liquid fuels such as diesel, and then, these blends were injected in conventional diesel engines, which improved the combustion characteristics [2]. However, presence of conventional diesel deteriorates the emission characteristics of DME. Subsequently now, direct injection of 100% DME in CI engines has been implemented for several modern applications [3, 4]. Prerequisite to inject DME as fuel in a CI engine is to liquefy it at a pressure above its vapor pressure. Liquid state of DME should be maintained in fuel supply line, in order to avoid the vapor lock. Liquefied DME is injected into the combustion chamber after proper fuel conditioning, such as maintaining appropriate pressure corresponding to local fuel temperature. Fuel supply line should be well-sealed in order to prevent any leakage of high-pressure DME. Leakage through static parts can be avoided by choosing appropriate DME compatible sealing materials. However, leakage through the clearances of various moving parts such as plunger barrel pump and fuel injector needs to be arrested. In addition, leakage of gaseous DME into the cylinder through fuel injector is also required to be arrested. Injector holds up to ~200 mm^3 fuel [5] in off-condition. After the engine shutdown, the liquefied DME present in the injector vaporizes due to loss of pressure. This gaseous DME leaks into the engine cylinder through needle-seat interface of the injector. Such a leakage may raise safety issues, if upper flammability limit is reached. Hence, there is a need to purge the fuel lines after the engine shutdown. During engine run, diesel injectors are exposed to high temperatures of the combustion chamber, which increases the fuel temperature. This leads to flashing of DME into vapor phase due to its high vapor pressure, leading to instability in the injection pattern. Therefore, there is a requirement of certain modifications in the fuel injection system, which needs to be done for adaption of DME in conventional CI engines. Automotive industry is looking for solutions for adaption of DME with minimal changes in the current engine designs. Moreover, additional DME adaption cost should be kept to a minimum without any loss in power output and engine performance. Lower energy density of DME compared to diesel requires high volume flow rate to achieve similar power output. Extensive research in these areas has led to development of fuel injection system capable of handling liquid DME for CI engine applications. Various approaches for the modifications of conventional fuel injection systems for DME adaption have been discussed in the subsequent sections.

2 DME Handling

In a fuel injection system, fuel flows through components operating at different pressures, such as low-pressure line, in-line pump and fuel injectors, including expansion notches. The fuel pressure should be sufficient throughout the fuel line to avoid formation of two-phase mixtures, which will damage the fuel injection system components. Very few experimental studies are available in the literature to develop a dense map of pressure versus temperature for DME in liquid state. AVL Powertrain Technologies, Inc. [6] calculated the thermodynamic properties of DME using molecular thermodynamics, which had an accuracy of ~95% compared to the experimental data. At 25 °C, the saturation pressure of DME was around 6 bar, which was the minimum pressure of DME required in the fuel line to retain liquid state at that temperature. Critical temperature of DME is 127 °C. The temperature of DME should not exceed this value, irrespective of the pressure throughout the fuel line, in order to avoid flashing and vapor lock situations. For common rail fuel injection system, the maximum temperature should be maintained below 50 °C, in order to avoid vapor/ bubble formation. The return line should be maintained at 8 to 10 bar by a back-pressure regulator [7]. To verify this pressure, a pressure gauge can be installed upstream of the back-pressure regulator. Fuel return needs to be cooled by recirculating it through a heat exchanger. After cooling, the fuel can be fed to the fuel line at the inlet of the feed pump using a T-joint, to equalize the pressure with that of the tank pressure. Thermo-physical properties of DME with working temperature range are given in Table 1 [6].

Higher vapor pressure of DME at normal temperature makes it more susceptible to leak. DME is heavier than air, which creates further safety issues. Material compatibility is a key aspect in design of leakage arrestors for DME injection system. Popular materials, such as Viton and Buna-N rubber used for sealing fuel lines, are incompatible with DME. Thus, more corrosive resistance material, e.g., Kalrez (trade name) is used for sealing. Other materials such as Teflon, butyl rubber,

Table 1 Variations in saturation pressure and density of DME with respect to temperature [6]

Temperature (°C)	Saturation pressure (bar)	Liquid density (kg/m^3)	Vapor density (kg/m^3)
5.0	3.367	682.90	7.292
10.0	3.934	675.72	8.456
15.0	4.570	668.40	9.757
20.0	5.287	660.92	11.23
25.0	6.107	653.28	12.91
30.0	7.055	645.46	14.87
35.0	8.108	637.44	17.06
40.0	9.273	629.22	19.49
45.0	10.56	620.75	22.21
50.0	11.96	612.04	25.23

neoprene, hydrogenated acrylonitrile-butadiene rubber (H-NBR) are also compatible with DME. However, Kalrez is found to be the most suitable by several studies [8, 9]. Hansen and Mikkelsen [8] used Teflon for sealing, where metal-to-metal sealing was not possible. They also used graphite and Kalrez O-rings, where dynamic load assemblies were present. Sato et al. [9] replaced the pump seals and rubber O-rings with H-NBR. They also reported that sensors used for safety monitoring such as level sensors have lower lifetime, when used with DME.

2.1 Transfer of Liquefied DME from Fuel Tank

Vapor pressure is a function of temperature. In a closed vessel filled with DME, the vapor pressure determines the percentage of liquid and vapor phase fuels at a particular temperature. The pressure in the closed vessel may increase with possible rise in temperature. Hence, containers are partially filled with DME gas. DME compressed gas containers have provision to extract both liquid and gas phases [10]. Small cylinders have a long dip tube, which runs from the inlet valve to the bottom of the vessel so that DME liquid can be extracted from the vessel. A simple valve at the top is used to withdraw DME gas from the vessel, as shown in Fig. 1a. However, ton tanks used in cars and trucks are laid on their sides. Short length goose-neck type bent dip tubes are used in such cases, as shown in Fig. 1b. These tubes are bent in upward and downward directions for extraction of gaseous and liquid DME, respectively. The extraction pressure of DME liquid is equal to its vapor pressure at local temperature.

Hence, tank outlet pressure of DME is at max equal to its vapor pressure, and any pressure drop can cause DME to flash into vapor. Therefore, the tank can be placed at a certain height to increase the outlet pressure through gravitational pull [9]. The

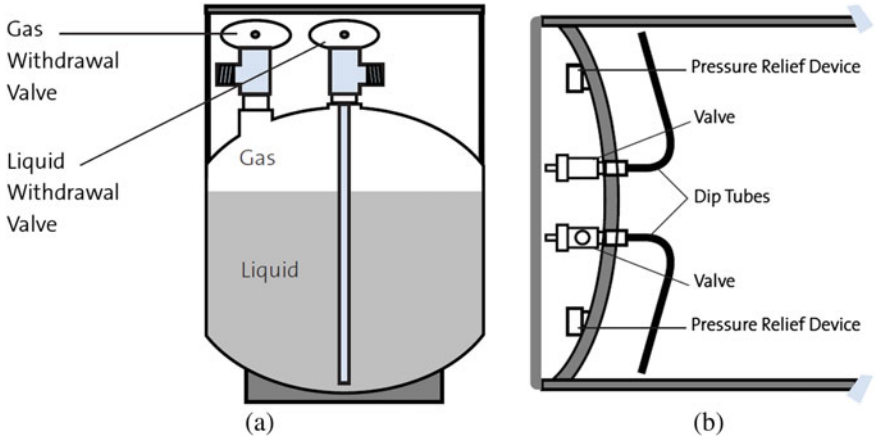

Fig. 1 **a** Cylinder tank with long straight dip tube; **b** ton tank with short goose-neck type dip tubes [10]

feed pump must be connected as close as possible to the outlet of the DME tank. The feed pump can be installed inside the tank, dipped in liquid phase DME [5, 11–17]. Besides this, padding can be used to pressurize the DME. Padding is a process of raising the pressure of a container by inducting pressurized gas into it. Inert gases such as nitrogen or helium can be used to pressurize DME up to 10 bar [18–21]. Stainless steel tubes should be used for the complete fuel line, running from the outlet of the fuel tank till the injectors, including the return line due to its excellent corrosive resistance property when used with DME [9]. Moreover, other components such as regulators, valves and fittings should be made of stainless steel.

2.2 Additive Mixing in DME and Its Arrangement

Besides higher vapor pressure, another challenging thermo-physical property of DME is its low lubricity and viscosity. AVL Powertrain Technologies Inc. developed a mathematical model to predict the transport properties of liquefied DME, which were verified by the experimental data [6]. It was found that at 25 °C, the kinematic viscosity would be 0.151 cP. This finding was consistent with the experimental data, which was 0.150 cP. This value was almost 1/10th of the kinematic viscosity of mineral diesel. In a conventional diesel engine fuel pump, the fuel itself serves as a lubricating agent for its moving parts. The use of liquid DME in these fuel pumps causes corrosion of metallic parts, as reported by many researchers [3, 4, 9]. Hence, lubricity additives are required to improve the lubricity of DME. DME forms heterogeneous mixture with lubricity additives used for diesel. It has been found that additives mixed with DME settle down, when left unattended after mixing. This may lead to seizure of fuel injection pump due to insufficient lubricity. Various lubricity additives and their dosage amounts have been reported in the literature such as Lubrizol LZ539N (1000 ppm) [13]; Lubrizol LZ539ST (800 ppm) [22]; Hitech-580, an Ethyl Japan Corp. product (500 ppm) [19]. However, additives in DME affect engine-out emissions. Hence, the quantity of these additives should be optimized so as not to compromise the ultra-low emission characteristics of DME. Another issue with DME as an alternative fuel for automobiles is that it is odorless. Hence, the leakage cannot be sensed easily. Therefore, for safety purposes, ethyl mercaptan, which is used for LPG, can be used in DME as well with dosage as low as 20 ppm [13] to give it a characteristic smell. At NTP, these additives (lubricity and odor) remain in liquid state unlike DME. Therefore, dosing of additive must be done when both substances, i.e., DME and additives are in liquid phase. Continuous circulation of fuel has to be carried out in the fuel supply tank such that the additives do not settle down after a prolonged duration from the time of dosing. Since the dosing rate is very low, a precision dosing pump should be used to facilitate the process using an on-board control system. This integration will be useful in optimizing the additive quantity in order to meet both the objectives of lower corrosion of metallic parts along with minimum compromise with emissions. A schematic of the dosing system is shown in Fig. 2.

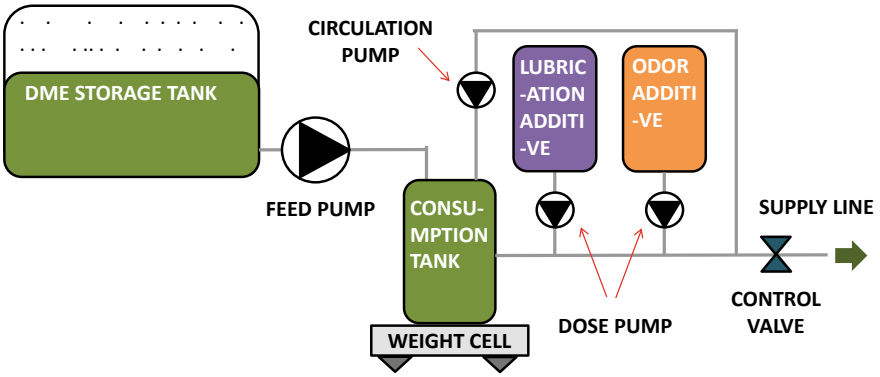

Fig. 2 Arrangement for mixing additives in liquefied DME [13]

The mixing arrangement consists of a DME storage tank and a consumption tank. Through the feed pump, fixed amount of DME is transferred to consumption tank. A mixing fuel line is attached to the consumption tank, which consists of two dose pumps, one each for lubricant additive and odor additive. A circulation pump, placed downstream of dosing pump, helps in continuous circulation of the fuel, to avoid heterogeneous mixing. DME for the engine is supplied from the consumption tank through the control valve. An electronic weight balance is used to measure the fuel consumption from the consumption tank. This weight balance gives input to the control system, which controls the flow of DME from the storage tank. An alternate way to enhance the fuel lubricity is by blending DME with diesel. Chapman et al. [7] conducted experiments with DME-diesel blends in a 7.3 L Navistar diesel engine. The blending was done by first adding diesel in an airtight transparent chamber according to predetermined mixing ratio. Then, DME was added without any physical mixing. Since DME has relatively lower specific gravity, the two liquids gradually diffuse into each other up to 60% of DME addition. The fuel tank can be a modified LPG cylinder, which should be tested to withstand an internal pressure up to 10–12 bar.

3 Fuel Injection System Component Modifications

Fuel injection system is said to be the heart of an engine, which pumps fuel into the combustion chamber via the fuel injectors. Various components of the fuel injection system are feed pump, low-pressure line, high-pressure pump, high-pressure line, injector and return line. The design of fuel injection system is specific to a particular fuel and is tuned to the engine requirements. Physical and chemical properties of DME such as high vapor pressure, low viscosity, low lubricity, low calorific value (about half of diesel) and liquid density are quite different from that of mineral diesel. Therefore, most parts of the fueling system of an existing diesel engine need to be

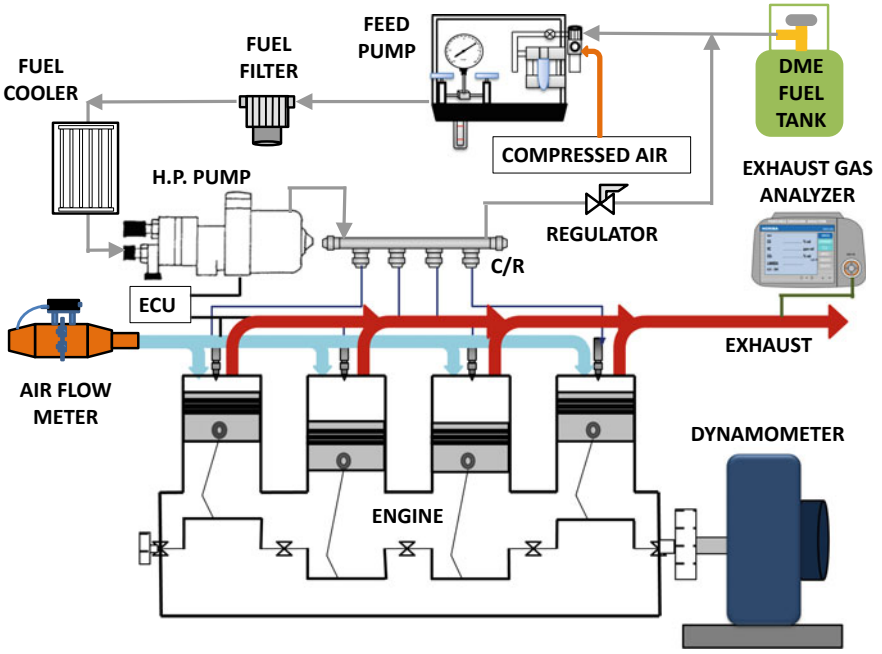

Fig. 3 Schematic of common rail fuel injection system for DME-fueled CI engine [22]

re-designed for DME implementation. A schematic of typical DME-fueled engine with its fueling system is shown in Fig. 3.

Modifications in the fuel injection system include but not limited to fuel filter, low-pressure stage, high-pressure stage, return line and purging, accumulator, fuel cooler and electronic control unit (ECU).

3.1 Low-pressure Line and Feed Pump

A low-pressure line and feed pump are used to supply fuel to the high-pressure pump. This line is maintained at relatively lower pressure compared to other parts of the fuel injection system; hence, it is defined as a low-pressure line or low-pressure stage. In conventional engines, feed pumps are mainly used for two reasons: (a) high-pressure pump pressurizes the fuel almost 250 times; hence, fuel line at the inlet of this pump needs sufficient volume flow rate of the fuel. Further, cooling of the high-pressure pump is done by continuous circulation of fuel in its galleries. Adequate fuel flow rate is maintained by the feed pump. (b) Fuel filters are designed such that the fuel needs to be forced through the filter elements to keep it free from debris and sludge. DME needs to be maintained above a certain pressure in order to retain its liquid phase during its transmission through the lines and filters. Hence, an additional function of

the feed pump for a DME-fueled engine is to raise the pressure of the fuel above its vapor pressure, corresponding to the maximum temperature that might be attained by the fuel. In low-pressure line, the temperature of the fuel might increase due to the following reasons: increased ambient temperature, frictional heating through the lines and due to the pressure rise of the fuel by the feed pump itself. Hence, feed pump pressure may vary from 10 to 30 bar [11, 13–15, 18, 23]. Such high pressure enables higher amount of heat absorption. A regulator can be installed in parallel to the supply pump in order to maintain adequate pressure at the inlet of the high-pressure pump [20]. The feed pump must be powered before the engine starts, in order to retain the liquid state of fuel due to its high vapor pressure characteristics [9]. An excess fuel flow stop valve can be used downstream of the feed pump, or a regulator can be installed in parallel to the supply pump in order to restrict the fuel flow pressure above a predetermined maximum pressure [17, 20]. The use of pressure regulator will avoid high pressure buildup in the line and maintain adequate pressure at the inlet of the high-pressure pump. Fuel lines must not come close to the hot surface of the engine in order to avoid vaporization of DME. Positive displacement pumps such as vane-type pumps, diaphragm pumps and gear pumps are found to be suitable for DME due to low viscosity and lubricity of DME [13, 18]. Polyphenylene sulfate can be used as suitable material for gear type feed pump, which is compatible with DME, while the sealing material and gaskets need to be replaced with Teflon [13].

3.2 Fuel Filter

Fuel filters are said to be the lifeguard of a fuel injection system, which clean the fuel by arresting the foreign particles chocking the fuel pump and fuel line. Hence, fuel filters increase the service life of the engine. In the DME injection system, low-pressure line is maintained at ~5–6 times higher pressure than that of existing diesel engines. Thus, the fuel filter needs to sustain this elevated pressure of fuel. DME at the outlet of the fuel tank is in a pressurized state, and hence, the fuel filter need not to be placed downstream of the feed pump, like in a conventional diesel injection systems. Thus, the fuel filter can be installed upstream of the feed pump. This will allow a compensation in the pressure rating of the fuel filter. Since the vapor pressure characteristics of DME are similar to that of LPG, the same fuel filter can be used for DME [7].

3.3 High-pressure Pump and DME Detection System

Fuel pump requires lubrication for its moving components such as at the plunger and barrel interface. Diesel being liquid at NTP greatly offers enough lubricity due to its higher viscosity. However, DME has low lubricity properties, and it may get vaporized in the fuel line, while pumped from DME tank to high-pressure pump, if

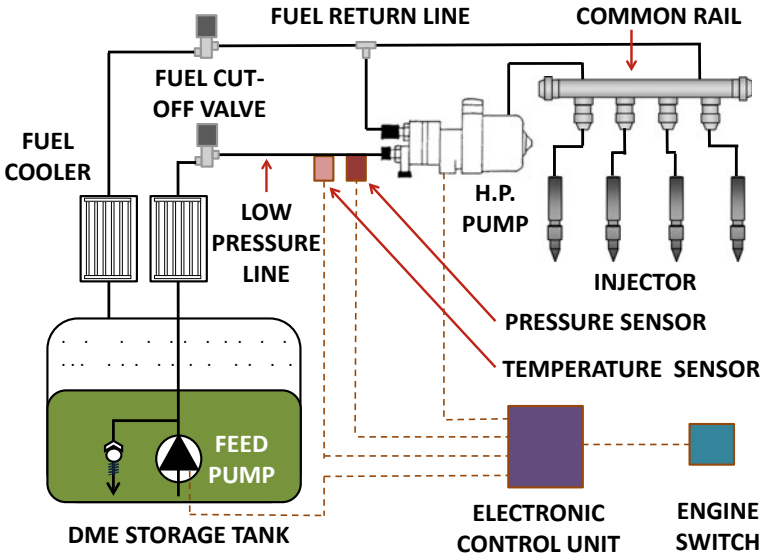

Fig. 4 Schematic of a fuel injection system with liquid DME detection system [16]

line pressure is not maintained above its vapor pressure. Lack of lubrication would severely damage the high-pressure pump components. Fuel pump generally accounts for substantial amount of the vehicle cost. To mitigate this issue, a DME liquid detection system can be used upstream of the high-pressure pump, as shown in Fig. 4 [16]. The high-pressure pump is not activated until the low-pressure line is filled with liquid DME for its satisfactory operation. An electronic control device can be used to operate all the fuel injection components in synchronous with the liquid detection system. DME liquid detection system comprises a pressure and a temperature sensor, which send pressure and temperature signals to the ECU of the engine. A map of the vapor pressure of DME corresponding to different temperatures is fed into the ECU. Thus, the ECU ensures that the pressure of the low-pressure pressure line is above the saturation pressure, before the high-pressure pump is switched on and injectors are activated. This integration will also ensure safe operation of high-pressure pump throughout its service life. If the pressure of low-pressure line drops below the vapor pressure of DME at local temperature, the ECU would shut off the high-pressure pump and would prevent the pump from getting seized due to lubrication failure.

A simple alternative design can be incorporated by eliminating the DME detection system and replacing the complex programming of the ECU with a simple electronic timer. An engine body temperature sensor needs to be coupled with the control unit for this purpose. The timer will store the data of time duration required by the feed pump to raise the line pressure above the vapor pressure, corresponding to the temperature of the engine surroundings. High-pressure pump activation will be delayed from the feed pump activation by the specific time duration for a given temperature. This preset time should be enough to ensure that the fuel at the high-pressure pump is only

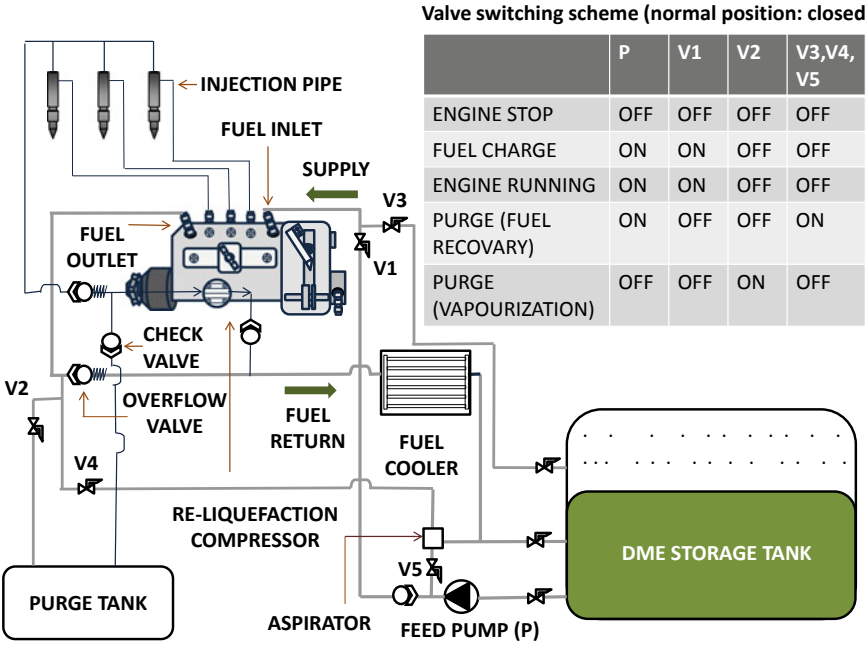

Valve switching scheme (normal position: closed)

	P	V1	V2	V3,V4, V5
ENGINE STOP	OFF	OFF	OFF	OFF
FUEL CHARGE	ON	ON	OFF	OFF
ENGINE RUNNING	ON	ON	OFF	OFF
PURGE (FUEL RECOVARY)	ON	OFF	OFF	ON
PURGE (VAPOURIZATION)	OFF	OFF	ON	OFF

Fig. 5 Layout of in-line fuel injection system for DME [9]

in the liquid phase. In mechanical DME injection system, a minimum pressure of the fuel injection pump can be maintained by attaching two valves, one at the inlet (V1) and the other at the return line of the pump [9, 11, 23]. The intercept valve (V1) and the overflow valve are used to maintain the pressure in the low-pressure line above the vapor pressure of DME, as shown in Fig. 5.

To compensate for lower lubricity of DME, all moving components of the fuel pump, which come in contact with the fuel, can be sulphurized [22]. Sulfurizing can help improve the lubrication without letting the sulfur burn in the combustion chamber. DME can easily leak through the clearance between the plunger and the barrel of the in-line pump. Hence, there is a high probability that DME will dissolve in the lubricating oil and make its way to the oil sump. This may lead to explosion in the crankcase. Hence, the lubricating oil circuit of the in-line pump should be separated from the engine lubrication system [22]. To match the power output of a diesel engine, equivalent energy input from DME needs to be the same. Density of liquefied DME is ~80% that of diesel, and the energy density is ~70% that of diesel [22]. Hence, DME needs to be injected in almost double the quantity compared to diesel, when operating the same engine [18]. This can be done easily by varying the fuel injection pressure and injection duration using common rail injection system. However, the mechanical injection system is not that flexible. Hence, to control the injection parameters, the in-line pump cam profile needs to be modified such that the surface pressure to activate nozzle opening is low. A higher capacity of the in-line

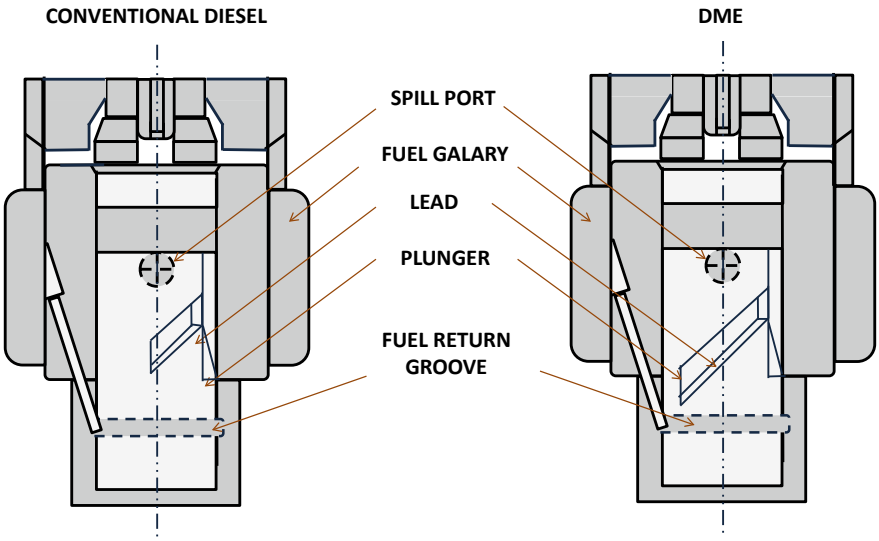

Fig. 6 Illustration showing plunger's helical position in conventional in-line fuel pump and rotated plunger in case of DME with longer effective stroke [9]

pump of the same series can be utilized to match the increased flow rate requirement. In addition, the effective plunger stroke can be altered to increase the fuel quantity per stroke [9]. The schematic is illustrated in Fig. 6.

Existing high-pressure pumps are incompatible with DME and require substantial modifications. However, DME can be adopted with conventional diesel injection pumps with additional retrofitment, as shown in Fig. 7 [7]. The fuel pump will feed diesel to a shuttle valve, and thereby, DME will get pressure pulses according to the timing of the fuel pump camshaft. The shuttle valve is a normal spring-loaded valve, in which DME is separated from diesel by a spring-operated piston. As the diesel gets pressurized by the fuel pump according to the camshaft timing, it pushes the spring-loaded piston, which eventually develops pressure in the high-pressure line filled with DME for working of the injector. Upstream of the shuttle valve, a non-return valve needs to be attached such that high pressure does not propagate into the low-pressure line and remains confined to the high-pressure line only.

3.4 Accumulator

Accumulator or buffer is used in the fuel injection system to minimize the pressure fluctuation or pulsation caused due to substantial reduction in fuel quantity from a high-pressure line during the fuel injection. With DME, the pressure fluctuation further increases because of its low bulk modulus. In common rail injection system, the accumulator can be attached to the rail with initial pressurization up to 200 bar

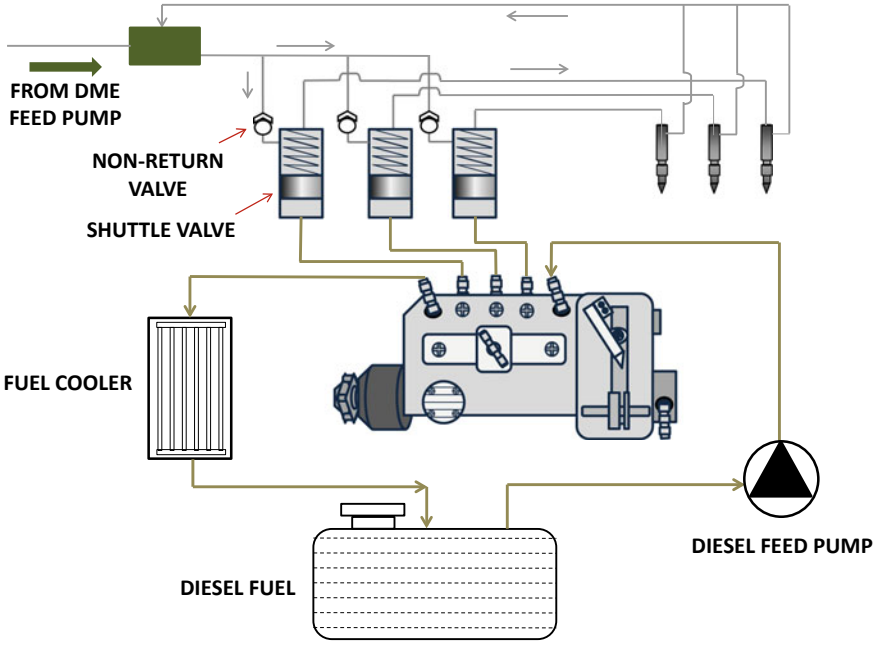

Fig. 7 Fuel injection system with shuttle valve [5]

[24]. While for an in-line fuel pump injection system, the accumulator can be placed at the inlet of the injection pump [20].

3.5 Injector

Fuel injectors are continuously exposed to high temperature of the combustion chamber. DME may get vaporized easily, when exposed to such high temperature because of its high vapor pressure. Hence, a highly thermal resistant material should be used between the fuel passage and the injector surface. Injectors are explicitly designed as per the engine requirements. Fuel injection quantity requirement of DME is nearly double that of diesel for the same power output. To compensate the flow rate, the cross section area of the injector nozzle orifice (A_o) needs to be twice that of the existing orifice, as shown in Fig. 8 [18, 22]. However, pressure in sac region decreases with increasing nozzle orifice area. Hence, in order to compensate for the pressure, the nozzle seat area (A_s) needs to be altered because the pressure in the sac region (P_s) also depends upon the seat area (A_s) [9, 25]. Using continuity and Bernoulli's equations, the relationship between $P_{s,}$ and A_s can be determined for a given orifice area (A_o) and nozzle room pressure (P_n) (Eq. 1)

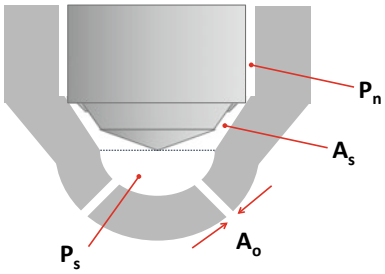

Fig. 8 Indication of pressure in the sac region (P_s), nozzle room (P_n) and the area of nozzle seat (A_s) and the orifice (A_n) [9]

$$P_s/P_n = \frac{(A_s/A_o)^2}{(A_s/A_o)^2 + 1} \tag{1}$$

The variations in the ratio of sac pressure and nozzle room pressure (P_s/P_n) with the ratio of seat area and orifice area (A_s/A_o) has been formulated using Eq. 1. It has been found that there is a significant reduction in sac region pressure (P_s), when the ratio of nozzle seat and orifice area (A_s/A_o) reduces below 2 [9]. Hence, the nozzle seat area needs to be more than twice the orifice area in order to maintain sufficient pressure in the sac region. DME having low bulk modulus requires more energy to build up pressure compared to diesel. Thus, a conventional fuel pump that is designed for diesel would generate insufficient pressure with DME for lifting the injector needle of the mechanical injector. Hence, nozzle opening pressure should be reduced along with increasing the diameter of the nozzle. However, low opening pressure may lead to secondary injections or dribbles. Reduction in nozzle pressure as well as increase in nozzle orifice diameter affects fuel atomization adversely, which results in inferior engine performance and higher exhaust emissions. However, atomization characteristics of DME are superior to diesel due to its higher vapor pressure, and hence, DME can be injected at a relatively lower pressure than that of diesel. Nozzle opening pressure can be reduced to 90 bar, in order to accommodate 1.8 times fuel flow rate of DME in the existing diesel nozzle at a nozzle opening pressure of 200 bar [11, 19, 21]. This pressure reduction can be achieved by replacing pressure adjustment shim in the existing injectors using a lower thickness shim in mechanical fuel injection system.

In the electronic fuel injection systems, high-pressure lines are connected to the injectors through electronic three-way valves (inj_V), as shown in Fig. 9.

When this valve is in 'on-position', the rail is connected to the injector, while the control line is disconnected. And when the engine is shut down, the valve (inj_V) is in 'off-position' so that the high-pressure line gets disconnected, while the injector is connected to the control line [5, 12]. Control line pressure is maintained below nozzle opening pressure (though above vapor pressure), and this connection will ensure maintaining a residual pressure at the injector and also a closure state of injector valve seat (opening pressure of ~180 bar). It has been reported earlier that injectors act as

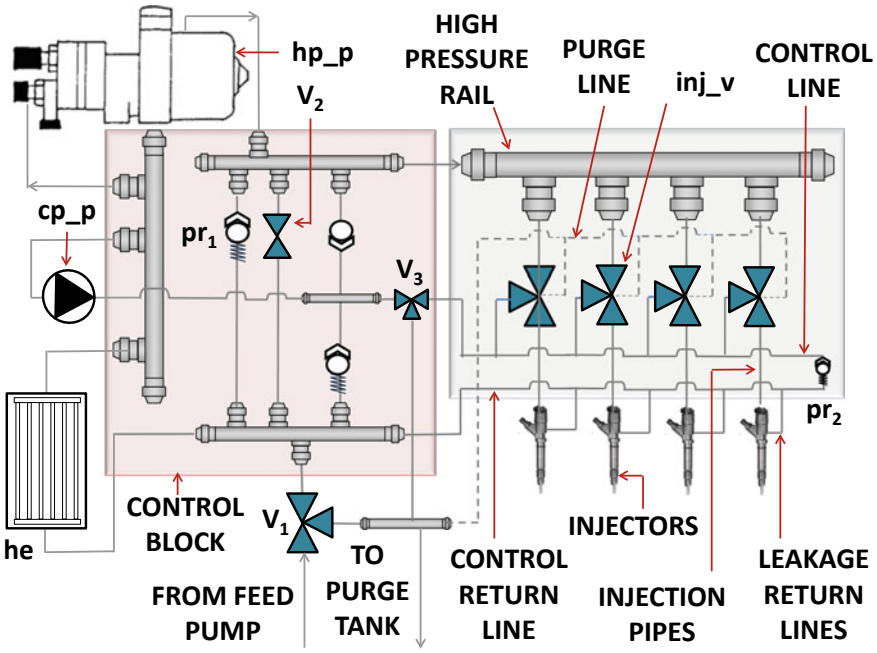

Fig. 9 Typical layout of common rail fuel injection system equipped DME engine [5]

hot spots for DME vaporization due to their high-temperature exposure, which may cause instability in the operation of the nozzle. Appropriate pressure regulation of the control line may mitigate this problem. Residual pressure is built up in the control line by an electrical motor-operated secondary pump (c_p), and pressure regulator valve (pr_2) is used to control the aforesaid pressure. As the control line maintains the liquefied state of DME upstream of the injector, the valve (v3), which operates the control line, is used to separate the fuel injection system from the combustion chamber. Hence, during initial part of cranking, the supply in the control line can be cut off by the valve (v3) until there is a significant pressure rise in the high-pressure line. Further, the valve (v3) can also be used to depressurize the control line instead of depressurizing the whole fuel injection system for a small stoppage of the engine.

3.6 Injector Return Line and Heat Exchanger

In a conventional fuel injection system, return lines are maintained at atmospheric pressure. Excess fuel is returned back to the fuel tank through a heat exchanger. Heat exchanger cools down the heated fuel returning from the engine. However, DME remains in gaseous state at atmospheric conditions, and therefore, the return lines must be pressurized to retain DME in liquid state (Fig. 10). Later, it can be connected

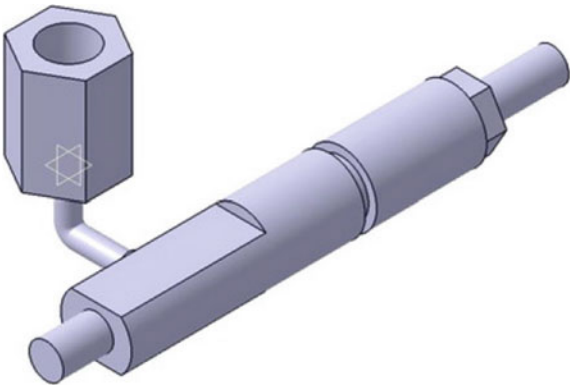

Fig. 10 Modifications for pressurizing the fuel in injector return line [21]

to the inlet of the fuel pump using a T-joint via the heat exchanger, as shown in Fig. 9 [5, 9, 12, 16, 21].

Alternatively, DME in the return line can be expanded to vapor and fed into the gaseous phase of DME tank through a solenoid valve [17]. This solenoid valve is kept open, when the engine is in operating condition in order to clear the return line of the injector. The valve needs to be turned off, when the engine is shut off to restrict the reverse flow of gaseous DME from the fuel tank.

3.7 Purging Facility

Purging a line means to evacuate fuel line from the existing fluid. DME fuel lines are pressurized above the vapor pressure of DME, in order to maintain the liquid phase using a feed pump. After the engine is turned off, the line pressure gradually drops. With time, DME in the high-pressure lines will get depressurized and turned into vapor. These vapors can leak into the combustion chamber through these metal-to-metal seals and can cause self-ignition during the next cranking [9, 11, 21]. Also, substantial leakage is possible into the cam-case via the clearance in the plunger barrel system. Hence, after each shutdown of the engine, along with the high-pressure line, fuel injection pump should also be ventilated. Three methods are used to purge the fuel lines by using a purge tank, a carbon canister or by reverse rotation of the feed pump. These methods are described in detail in the following subsections. The fuel lines can be connected to a purge tank via a purge line to depressurize the DME. The purge tank is maintained below the saturation pressure of DME (near atmospheric) such that the liquefied DME can be easily expanded and stored in the purge tank [5, 11, 12, 22]. Thus, the fuel can be evacuated through the purge line. The purge line is operated through a two-way, three-stage valve, v1 as shown in Fig. 11.

The supply port (S) of the valve (V1) is connected to the fuel tank, and the fuel is supplied to the injection system via the exit port (E). The drain port (D) of the valve (V1) is connected to the purge line. During engine run, the valve is in ‘on’ position,

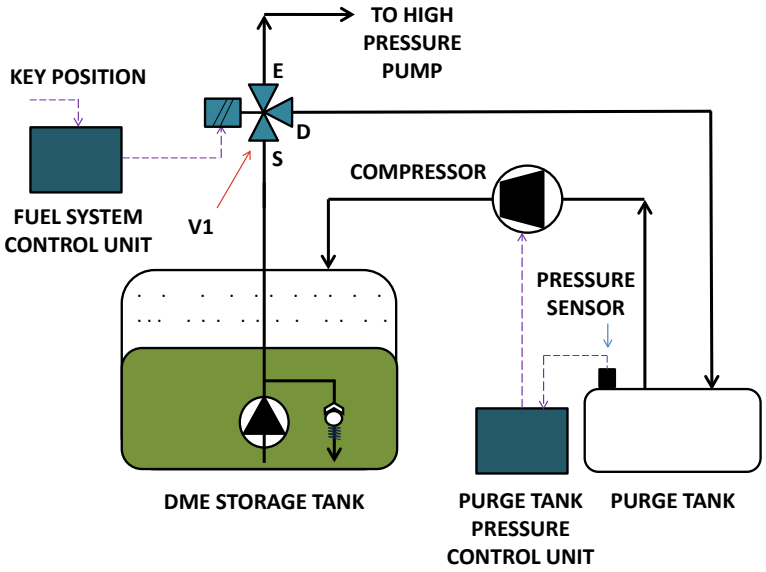

Fig. 11 DME purge tank and its connections [12]

and the exit port (E) is connected to the supply port (S). When the engine is shut down, the valve is turned 'off', and the exit port (E) gets connected to the drain port (D) for purging the lines. Hence, this valve cuts off the fuel supply to the injection system and connects the purge line with the engine fuel line, whenever required. Therefore, this valve also acts as a safety valve of the engine. In a conventional mechanical fuel injection system, spill port is used to drain off the excess fuel in the barrel. The volume of drain-off is adjusted by a rack and pinion mechanism, which is attached to the pump governor. Similarly, pressurized DME in the high-pressure line and in-line pump plunger barrel system can be drained through a slot called purge slot and a purge port, which are grooved in the cylinder and plunger of the in-line pump, respectively, as shown in Fig. 12 [9]. After engine shutoff, the plunger needs to be rotated such that the slot and port are made in-line with each other. Thus, remaining DME in the high-pressure line can be discharged to the low-pressure line.

For safety reasons, the purge system attached to the fuel line can be automated [5, 12, 13]. When DME reaches a certain maximum level in the purge tank, the compressor attached with it is turned on to compress the gaseous DME present in the purge tank and supply it to the DME storage tank. The compressor is turned off when a preset minimum value of the purge tank pressure is reached. Switching off of the compressor is determined based upon the signal from a level indicator, installed in the purge tank. This indication is required to avoid liquid accumulation in the purge tank and to maintain enough pressure drop in the purge line for natural expansion of liquid DME from the fuel line. The compressor can be operated by the compressed air of the vehicle's pneumatic brake system.

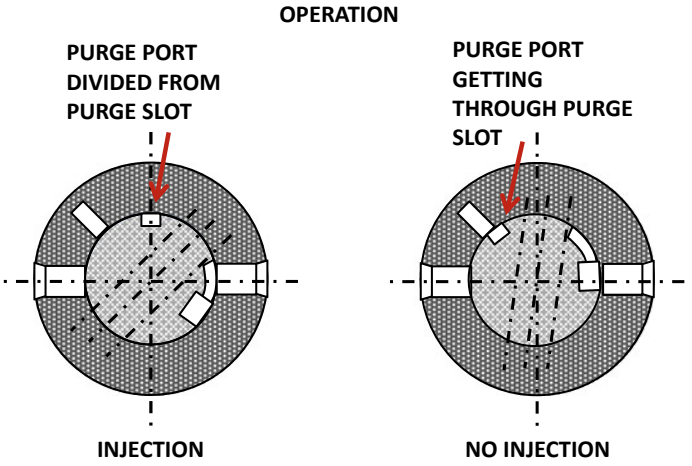

Fig. 12 Strategy for purging the high-pressure DME line [9]

In the mechanical injection system, a re-liquefaction compressor can be coupled with the in-line pump, which is operated by the rotation of the camshaft of the in-line pump, as shown in Fig. 13 [9, 22]. Return line of the injectors, purge tank outlet, and in-line pump camshaft case is directly connected to the inlet of the re-liquefaction compressor. It returns the liquefied DME to the fuel line or feeds to the fuel tank after appropriate cooling. Figure 13 depicts the position of various valves used in this operation. To purge the fuel line at the inlet of the fuel pump, a T-joint is connected through a valve (V3) leading to the fuel tank. Additionally, in the return line of the fuel pump, an aspirator is connected downstream of the overflow valve through a valve (V4).

Another method to purge the fuel line is by using a charcoal canister [5]. This is similar to the canister-purge mechanism used in automobiles to arrest the fuel vapor emissions from the tank. In this method, the fuel line will be allowed to depressurize, and the expanded DME gas will get absorbed in the carbon/charcoal canister. Later, DME can be regenerated from the carbon canister and fed into the intake manifold of the engine along with fresh air. The regeneration process is timely controlled by two valves (V2 and V3), as shown in Fig. 14, to control the intake air flow through the carbon canister.

The methods discussed so far for purging come with additional cost and sacrifices space. An alternative solution to these methods can be to reverse the rotation of the gear type pump (used as feed pump) and pull back the stagnant DME from the fuel injection system to the DME tank [17]. To facilitate this process, solenoid valves need to be installed at various locations with the alteration in the state of each valve accordingly, as shown in Fig. 15. To clear the downstream of each high-pressure device such as high-pressure pump, common rail and injectors, return lines are connected to the liquid part of the DME tank via solenoid valves and feed pump. These solenoid valves are turned on, when the engine is shut off, and the pressurized

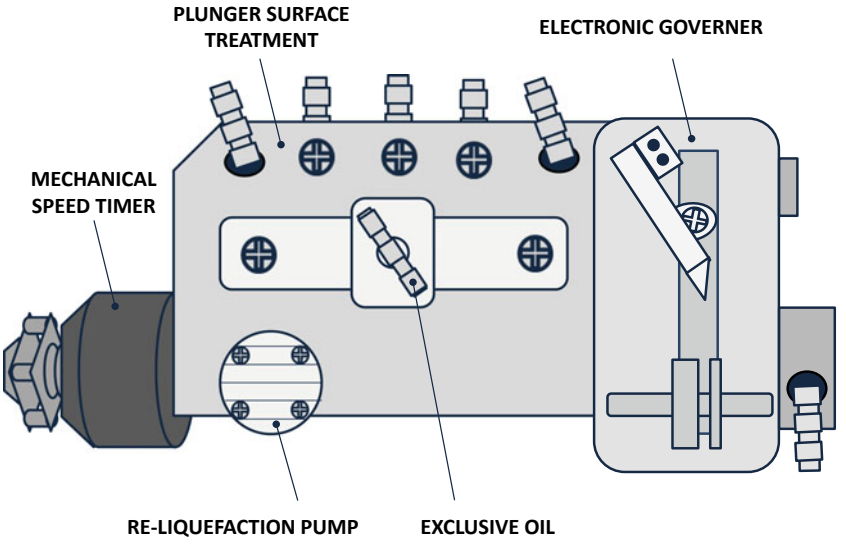

Valve switching scheme (normal position: closed)

	P	V1	V2	V3,V4, V5
ENGINE STOP	OFF	OFF	OFF	OFF
FUEL CHARGE	ON	ON	OFF	OFF
ENGINE RUNNING	ON	ON	OFF	OFF
PURGE (FUEL RECOVARY)	ON	OFF	OFF	ON
PURGE (VAPOURIZATION)	OFF	OFF	ON	OFF

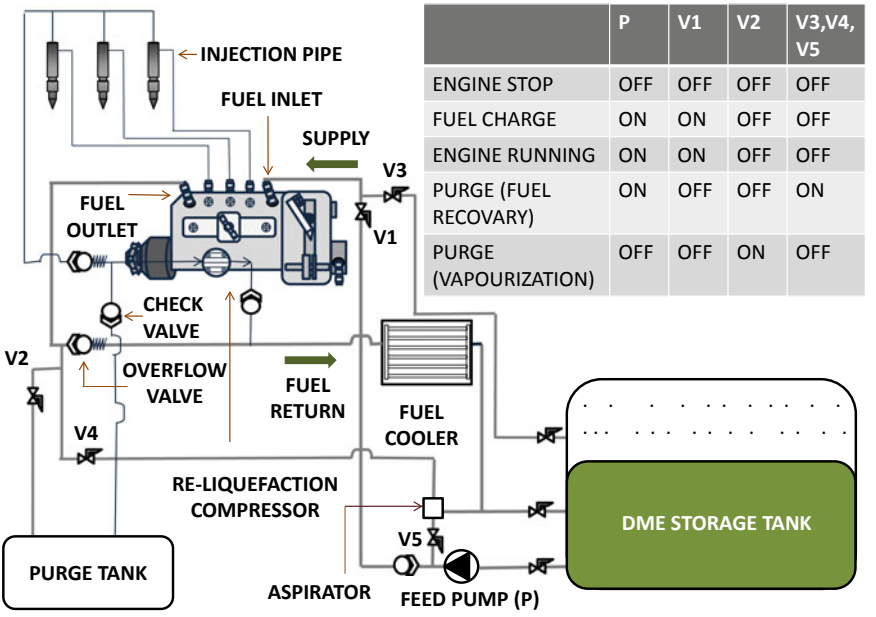

Fig. 13 Modified in-line fuel injection pump for purging [22]

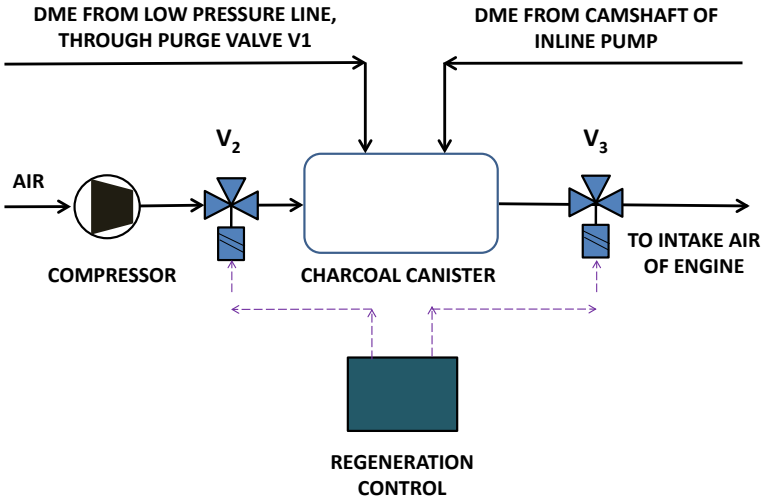

Fig. 14 Purging DME fuel line by using charcoal canister [5]

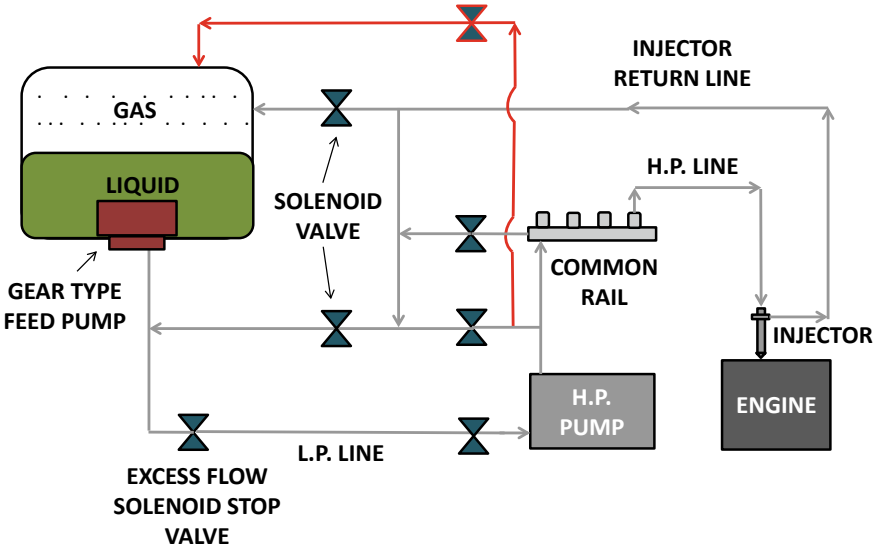

Fig. 15 Schematic of fuel injection system without purging chamber [17]

DME in the high-pressure line is returned to the DME tank by the reverse rotation of the feed pump. At this stage, the valve upstream of the high-pressure pump should be turned off. The reverse flow of the gear type feed pump will clear the low-pressure and high-pressure lines along with the injector return line. The solenoid valve between the gaseous part of the DME tank and the injector return line should be turned off so

that feed pump does not create any suction at the gaseous part of the DME tank. In addition to the operation of feed pump in the reverse direction, existing pressure in the fuel line can be reduced by connecting the high-pressure line to the gaseous part of the fuel tank through a solenoid valve (highlighted with red in Fig. 15). This valve will be turned off, when the engine is in running condition, and it will be turned on to depressurize the fuel line, when the engine is shut off.

This process will ensure that liquefied DME does not remain stagnant in the fuel line, though gaseous DME may be left over in the fuel line as gear pump is used to purge these lines. This gas can leak into the combustion chamber through a conventional nozzle, as explained earlier. An ejector can be used to transfer the gaseous DME from injection system to DME tank, as shown in Fig. 16. The ejector is a device that incorporates a diffuser, which creates a low-pressure zone to suck the gaseous DME from the injection fuel line. Liquid DME from the DME tank is forced through a diffuser by the regular rotation of the feed pump, creating a low-pressure zone at the entry of the diffuser. This low-pressure zone will create a suction effect to suck the remaining gaseous DME from the return line and the high-pressure line. When the prerequisite time for reversal of feed pump to clear the liquefied fuel is passed, the solenoid valves connected upstream and downstream of the ejector are made operational. At this point of time, the feed pump is used to operate the diffuser in the ejector. The diffuser is operated by regular direction rotation of the feed pump, i.e., forcing liquid DME out of the tank, while the valve in the return line connected to feed pump is turned off, in order to restrict the flow back to the return line. The liquid DME from the feed pump is forced to enter the diffuser through a nozzle.

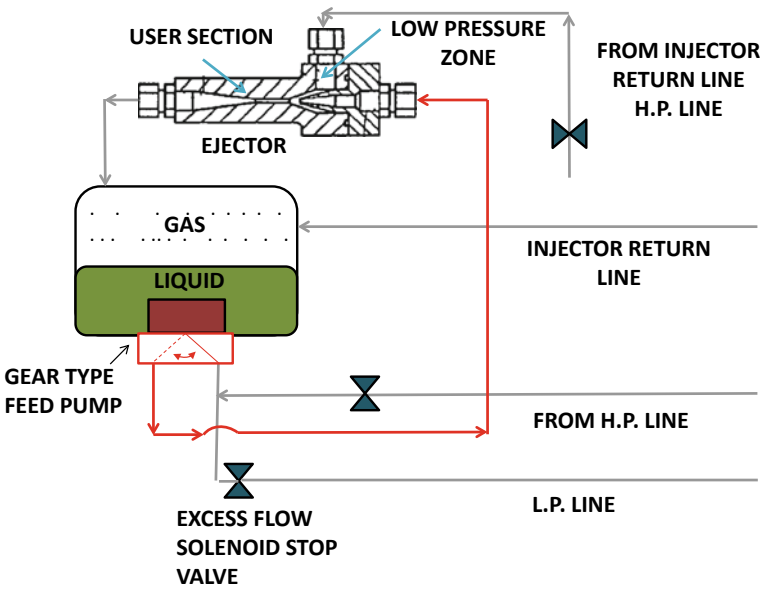

Fig. 16 Schematic of fuel injection system with purging using an ejector [17]

This creates a low-pressure zone at the entry of the diffuser. The valve connecting the return line and high-pressure line is attached to this zone, by turning on the corresponding valve. This process permits mixing of remaining gaseous DME in the fuel line with the circulating DME in the ejector, and it finally returns to the DME tank. However, liquid DME can be directly supplied to the ejector. This is achieved by incorporating a solenoid switch along with a compression chamber attached with the feed pump containing two different outlet ports. One such port will function for the low-pressure supply line, and the second one will be used to supply liquid to the ejector at an appropriate interval of time, as shown in Fig. 16. The port toward the low-pressure line needs to be switched on, when the engine is on till the prerequisite time of the return of liquid DME by reversal rotational direction of the feed pump has not elapsed.

After the engine is turned off and passage of prerequisite time, outlet of the feed pump will be changed to the second port by controlling the solenoid switch. This will activate the passage of the ejector. By regular rotation of the feed pump, the diffuser can be operated to draw the gas phase DME from the injection system, as described in the earlier section.

4 Adaptation of DME Fuel Injection System in a Test Engine

The fuel injection system of DME-fueled engine fundamentally operates in three modes due to the fuel's elevated vapor pressure [13].

(a) Purge mode: In this mode, the high-pressure line and injectors are connected to the purge tank; hence, the fuel lines are maintained below the saturation pressure of DME. DME will get expanded and stored in the purge tank in this mode.
(b) Starting mode: In this mode, high-pressure line is maintained at the pressure of the feed pump (above saturation pressure of DME). As the high-pressure pump is coupled to the engine crankshaft, therefore before cranking the engine, the inlet of the high-pressure pump should be supplied with liquid DME for its proper lubrication and functioning. Hence, feed pump should be turned on well in advance of the engine such that sufficient pressure is developed at the inlet of the high-pressure pump.
(c) Operational mode: At this mode, both low-pressure pump and injection pump work in tandem and maintain sufficient pressure for the proper functioning of the engine while avoiding cavitation.

For experimentation and mapping the DME quantity with respect to load and speed, various equipments such as strain gauge and flow rate measurement device need to be incorporated in the fuel injection system. As the properties of DME are different from that of diesel, conventional fuel flow rate measurement techniques such as gravity flow measurement will not be applicable. For liquefied DME flow

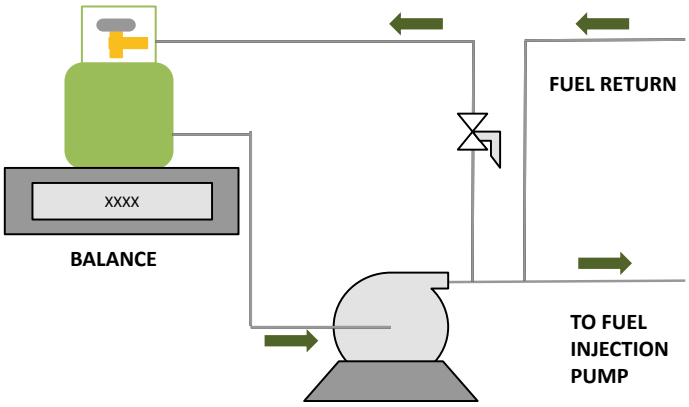

Fig. 17 Fuel consumption measurement technique [11]

measurement, DME compatible flow meter is required. Flow meters can be connected at the outlet of the DME tank, given that the return line of DME is fed back to the low-pressure line, and none should be returned to the DME tank [20]. Since flow meters are quite expensive, the fuel flow rate can be measured alternatively by a precision weighing balance of an initially filled DME consumption tank as shown in Fig. 17 and noting the weight reduction with respect to time [11, 22]. The fuel consumption can be verified by balancing the exhaust gas composition and intake air quantity.

Adopting DME as an injection fuel requires increased flow rate quantity by increasing the injection area, as explained earlier in addition to modification in the cam profile of the in-line pump. The equivalent injection rate profile of DME to diesel can be verified by the principle of the Zeuch technique [9]. The schematic of an experimental setup is depicted in Fig. 18. In this experiment, temperature of DME was maintained constant at 40 °C. The leaked fuel was released into the atmosphere rather than collecting it into the purge tank as the flow meter was used to directly measure the quantity injected by the injector. Piezo-electric type pressure sensors were used to monitor the pressure in the high-pressure line, placed just before entry to the nozzle. This was used to monitor the injection behavior for DME [11]. Pulse for each cycle of injection was measured by attaching a standard type pulse generator to the camshaft of the in-line pump, as shown in Fig. 18. The injection period was segregated by the start and stop for each injection data.

5 DME Fuel Injection System in an On-road Truck

DME fuel injection system was implemented in on-road vehicles by many research groups. Sato et al. [9] implemented the modified fuel injection system (discussed in Sect. 3.3) in a truck engine of 88 KW rated power, having displacement volume of

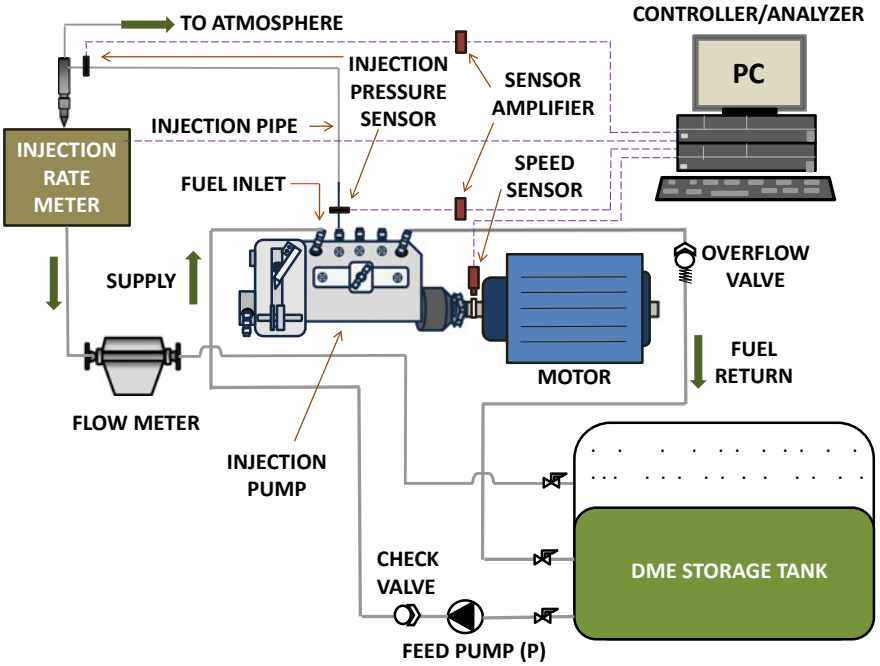

Fig. 18 Illustration of injection rate profile measurement instrument [9]

4570 cc. Other relevant parts of the engine, such as air intake and engine combustion chamber, were unchanged. DME fuel tank was of 120 L capacity. Half-inch NTP fittings were used at the bottom of the DME tank to draw liquid DME from the tank due to gravitational effect, as shown in Fig. 19. DME was supplied to the fuel injection system by an electrically driven feed pump, which was placed between the DME fuel pump and the DME tank. This was done in order to ensure that the inlet of the feed pump was maintained in a liquid state. Tank was pressurized up to 7 bar by an inert gas (Helium), which eliminated the need of a transfer pump. As DME in the fuel tank was pre-pressurized, the fuel filter did not require a feed pump for its operation. The overflow valve attached at the pump return line was used to maintain low-pressure line at ~10 to 15 bars. The in-line fuel injection system showed higher reliability for DME injection in terms of its pressure distribution characteristics.

With all-mechanical in-line DME pump at low-speed conditions, pressure rise was found to be inadequate. But at high engine speeds, injection pressure increased. As reported in this study, an in-line fuel pump has excellent operating characteristics with low lubricity fuel such as DME. The fuel consumption was calculated by the carbon balance of the exhaust gas. Finally, these values were converted to specific fuel consumption of diesel equivalent. The lubricity of DME used in the test was enhanced by adding lubricant LZ539ST (880 ppm), which maintained DME purity level >99%. Modified DME engine could achieve equivalent energy output as that

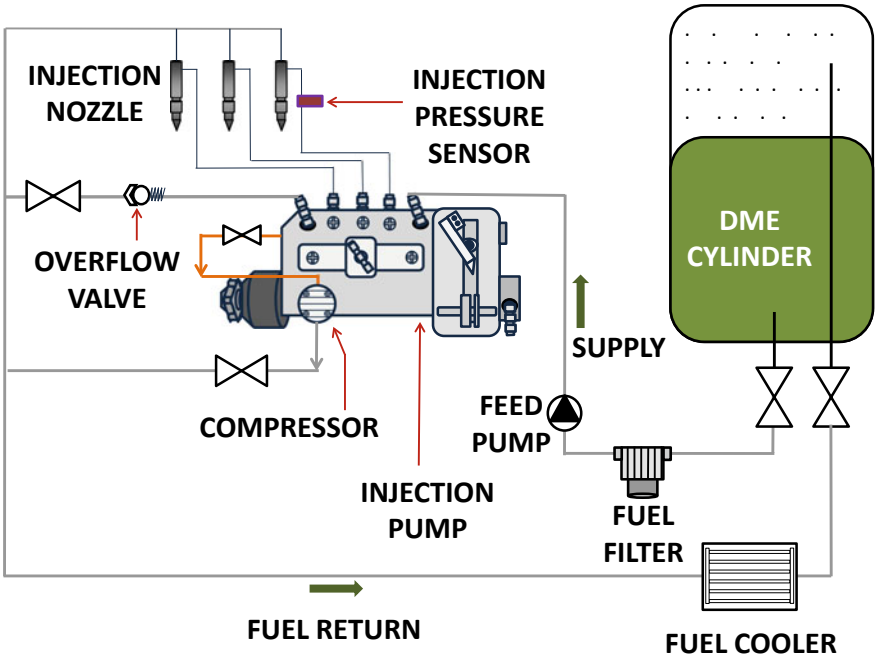

Fig. 19 Vehicular test setup with DME injection system [9]

of the diesel variant with comparable brake specific energy consumption. Emissions data revealed that NOx and CO_2 reduced by ~40% and ~20%, respectively, while CO increased at heavy-load condition for all speed ranges. It was also reported that total hydrocarbons (THC) were extremely low.

6 Conclusions

DME is a fuel of future for CI engines as it is renewable and environment friendly. However, its adoption in CI engines is challenging. It cannot be directly implemented in existing engines due to its physical and chemical properties and issues of compatibility with existing fuel injection system material. Hence, material used for manufacturing several components of the fuel injection system is required to be changed. Substantial design modifications are required to match the performance level of conventional diesel engines. From an in-depth analysis of current state of the art of DME utilization in CI engines, the following points are concluded:

(a) Fuel tank needs to be pressurized at ~10–12 bar at normal temperature for DME's vapor-free operation. Fuel outlet should be at the bottom of the tank, so that only liquid phase is extracted from the tank. The tank must be kept at a

certain height such that any pressure drop during extraction of DME and further supply does not lead to reduction in pressure below its saturation pressure.

(b) Feed pump should be operated independent of the engine itself as fuel line pressure should be raised to adequate level before running the fuel injection pump. Capacity of the fuel pump should be higher so that it can maintain the same equivalent energy input to the engine cylinder in each cycle, as that of diesel. An accumulator should be installed to compensate for the pressure pulsations in the high-pressure line, which is prominent due to lower bulk modulus (high compressibility) of DME.

(c) Fuel wetted regions should be coated to prevent corrosion by DME, and to increase lubrication, an adequate amount of lubrication additive should be added to DME, in order to avoid erosion of the moving parts. Odor additives are also required to provide a characteristic smell to the odorless DME for safety reasons. The mixture should be well-circulated before feeding it to the fuel pump to prevent the separation of additives.

(d) Fuel filter should be capable of handling increased pressure of liquefied fuel. A regulation valve should be provided both upstream and downstream of the fuel pump, in order to ensure fuel pressure above the saturation pressure throughout the fuel pump.

(e) Injector nozzle opening pressure should be reduced, and the injection area should be increased accordingly to facilitate the requirement of higher injection quantity of DME. DME injector return line should be pressurized to avoid significant loss of fuel leakage past the nozzle. Return fuel should be cooled before feeding it to the inlet of the fuel pump.

(f) Provision for the purging of the fuel pump should be provided along with a separate lubrication system. Proper purging connections should be incorporated in the fuel injection system, which need to be actuated either by ECU control or manually. High-pressure line should be depressurized after the engine is shut off, in order to avoid any leakage of gaseous DME into the combustion chamber and the environment.

(g) The materials such as elastomers and plastics used for sealing and gaskets of the engine must be replaced with suitable DME compatible materials.

References

1. Zhao, Y., Wang, Y., Li, D., Lei, X., & Liu, S. (2014). Combustion and emission characteristics of a DME (dimethyl ether)-diesel dual fuel premixed charge compression ignition engine with EGR (exhaust gas recirculation). *Energy, 72,* 608–617.
2. Eirich, J., Chapman, E., Glunt, H., Klinikowski, D., Boehman, A. L., & Hansel, J. G. (2003). *Development of a dimethyl ether (DME)-fueled shuttle bus.* SAE Technical Paper 2003; 2003-01-0756.
3. Oguma, M., Goto, S., & Watanabe, T. (2004). *Engine performance and emission characteristics of DME diesel engine with in-line injection pump developed for DME.* SAE Technical Paper 2004; 2004-01-1863.

4. Park, S. H., & Lee, C. S. (2014). Applicability of dimethyl ether (DME) in a compression ignition engine as an alternative fuel. *Energy Conversion and Management, 86,* 848–863.
5. Ofner, H., & Gill, D. W. (1999). Design guideline for dimethyl ether injection systems. In *Dimethyl ether as an automotive fuel*. AVL LIST GMBH.
6. Teng, H., McCandless, J. C., & Schneyer, J. B. (2004). *Thermodynamic properties of dimethyl ether—An alternative fuel for compression-ignition engines.* SAE transactions (pp. 134–157).
7. Chapman, E. M., Bhide, S., Stefanik, J., Glunt, H., Boehman, A. L., Homan, A., & Klinikowski, D. (2003). *Dimethyl Ether (DME)-Fueled Shuttle Bus Demonstration Project 2003*. Pennsylvania State University (US).
8. Hansen, J. B., & Mikkelsen, S. E. (2001). *DME as a transportation fuel*. Haldor Topsøe A/S 2001.
9. Sato, Y., Nozaki, S., Noda, T. (2004). *The performance of a diesel engine for light duty truck using a jerk type in-line DME injection system.* SAE Transactions 2004 (pp. 1210–1222).
10. Air Products and Chemicals, Inc. (2013). (36219) 900-13-108-US.
11. Sorenson, S. C., & Mikkelsen, S. E. (1995). *Performance and emissions of a 0.273 liter direct injection diesel engine fuelled with neat dimethyl ether*. SAE transactions 1995 (pp. 80–90).
12. Ofner, H., Gill, D. W., Krotschec, C., & Krotscheck, C. (1998). *Dimethyl ether as fuel for CI engines-a new technology and its environmental potential*. SAE transactions 1998 (pp. 425–437).
13. Hansen, K. F., Nielsen, L., Hansen, J. B., Mikkelsen, S. E., Landälv, H., Ristola, T., & Vielwerth, K. (2000). *Demonstration of a DME (dimethyl ether) fuelled city bus.* SAE Technical Paper 2000; 2000-01-2005.
14. Gill, D., Ofner, H., Schwarz, D., Sturman, E., & Wolverton, M. A. (2001). *The performance of a heavy duty diesel engine with a production feasible DME injection system.* SAE Technical Paper 2001; 2001-01-3629.
15. Gill, D., Ofner, H., Sturman, E., Carpenter, J., & Wolverton, M. A. (2001). *Production feasible DME technology for direct injection CI engines.* SAE Technical Paper 2001; 2001-01-2015.
16. Yanagisawa, N. (2004). Isuzu Motors Ltd. Fuel supply system for dimethyl ether engine. U.S. Patent 6,742,479.
17. Moroi, T., Suzuki, S., Ota, & M., Toyota Industries Corp. (2008). *Fuel supply system for DME engine*. U.S. Patent Application 11/827,636.
18. Fleisch, T., McCarthy, C., Basu, A., Udovich, C., Charbonneau, P., Slodowske, W., Mikkelsen, S. E., & McCandless, J. (1995). *A new clean diesel technology: demonstration of ULEV emissions on a Navistar diesel engine fueled with dimethyl ether*. SAE transactions 1995 (pp. 42–53).
19. Konno, M., Kajitani, S., Oguma, M., Iwase, T., & Shima, K. I. (1999). *NO emission characteristics of a CI engine fueled with neat dimethyl ether*. SAE transactions 1999 (pp. 460–467).
20. Longbao, Z., Hewu, W., Deming, J., & Zuohua, H. (1999). *Study of performance and combustion characteristics of a DME-fueled light-duty direct-injection diesel engine*. SAE Technical Paper 1999; 1999-01-3669.
21. Wattanavichien, K. (2009). Implementation of DME in a small direct injection diesel engine. *Journal of Renewable Energy and Smart Grid Technology, 4*(2), 1–12.
22. Tsuchiya, T., & Sato, Y. (2006). *Development of DME engine for heavy-duty truck*. SAE Technical Paper 2006; 2006-01-0052.
23. Christensen, R., Sorenson, S. C., Jensen, M. G., & Hansen, K. F. (1997). *Engine operation on dimethyl ether in a naturally aspirated, DI diesel engine.* SAE transactions 1997 (pp. 1863–1872).
24. Egnell, R. (2001). Comparison of heat release and NO_x formation in a DI diesel engine running on DME and diesel fuel. SAE Paper 2001-01-0651. *SAE Trans J Fuel Lubr 2001, 110*(4), 492–506.
25. Goto, S., Oguma, M., & Suzuki, S. (2005). *Research and development of a medium duty DME truck*. SAE Technical Paper 2005; 2005-01-s2194.

Material Compatibility, Technical Challenges and Modifications Required for DME Adaptation in Compression Ignition Engines

Vikram Kumar and Avinash Kumar Agarwal

1 Introduction

The compression ignition (CI) engines are mostly used in heavy-duty applications such as generators, buses, trucks, construction equipment, agricultural machines and heavy vehicles for defense services. Diesel-fueled CI engines offer several benefits over gasoline-fueled spark-ignition (SI) engine counterparts of similar capacity, which includes higher engine torque, superior thermal efficiency, better fuel economy and extended durability. In CI engines, only air is inducted through the intake port, which is compressed during the compression stroke. Fuel is then injected into the combustion chamber, which contains air at high temperature. Fine droplets of injected fuel spray then evaporate, get mixed with the hot air and then get ignited. Although CI engine offers many benefits, however here are serious concerns of harmful emissions from CI engines such as hydrocarbons (HC), carbon monoxide (CO), oxides of nitrogen (NO_x) and particulate matter (PM). PM and NO_x formation in a diesel engine is higher than gasoline engine counterparts. In addition, in a CI engine, there exists a trade-off between PM and NO_x emissions [1]. Hence, PM and NO_x cannot be reduced simultaneously. These can only be reduced simultaneously by applying advanced low temperature combustion (LTC) techniques such as reactivity controlled compression ignition (RCCI), premixed charge compression ignition (PCCI) and homogeneous charge compression ignition (HCCI), but the deployment of these technologies to practical engines remains cumbersome and complex with limited success. Therefore, there is a need of adopting clean combustion technologies and use of alternative fuels to control the damage to the environment. Fossil fuel reserves are very limited, and energy demand is exponentially increasing, thereby making the

V. Kumar · A. K. Agarwal (✉)
Engine Research Laboratory, Department of Mechanical Engineering,
Indian Institute of Technology Kanpur, Kanpur 208016, India
e-mail: akag@iitk.ac.in

A. P. Singh et al. (eds.), *Alternative Fuels and Advanced Combustion Techniques as Sustainable Solutions for Internal Combustion Engines*, Energy, Environment, and Sustainability, https://doi.org/10.1007/978-981-16-1513-9_3

energy resources scarce. To resolve these issues, eco-friendly renewable alternative fuels such as biodiesel, methanol, ethanol, butanol, hydrogen and dimethyl ether (DME) are being explored for large-scale deployment in the IC engines.

Among these alternative fuel candidates, DME is a very promising alternate fuel candidate offering cleaner combustion, compared to conventional diesel. DME is a gaseous fuel at normal temperature and pressure (NTP) conditions, and it has quite similar handling characteristics as that of liquefied petroleum gas (LPG). DME could be produced from various feedstocks such as biomass, municipal solid waste (MSW), coal, crude oil and natural gas. Many researchers investigated suitability of DME as fuel in diesel engines. DME is an efficient and excellent fuel for diesel engines with smoke-free emissions due to low ignition temperature, fast vaporization, high oxygen content and the absence of carbon-to-carbon bonds [2]. Initially, DME was used as additives in alcohol-fueled combustion engines due to its lower self-ignition temperature but higher cost. High percentage of DME in methanol/ DME blend also showed similar combustion behavior as that of methanol [3]. Low-cost production of DME has enhanced applicability of DME as fuel in IC engines. Several DME-fueled engine studies have demonstrated very low emissions and noise with excellent efficiency [4].

The objective of this chapter is to review DME production aspects, its physical, chemical, and thermal properties, compatibility with engine components, challenges in DME adaptation, engine modifications required, vehicular adaptation and current status of DME-fueled vehicle development. DME's commercial availability is also a challenge for its large-scale application as fuel in CI engines.

2 DME Production, Material Compatibility, and Challenges in Adaptation

DME can be produced from renewable and non-renewable feedstock resources. DME is quite different from mineral diesel in terms of physical properties. DME is not compatible with many components of the fuel injection equipment (FIE) due to its corrosive nature. There are many challenges in application of DME as a substitute for mineral diesel in CI engines. All these aspects are discussed in the following subsections.

2.1 DME Production

The production of DME started in 1996, and its annual production was 100,000–150,000 tons [2, 5]. Today, global production of DME stands at 10 million tons annually. DME is a synthetic fuel, which can be produced by various pathways. DME can be synthesized by conversion of several carbonaceous feedstocks such as

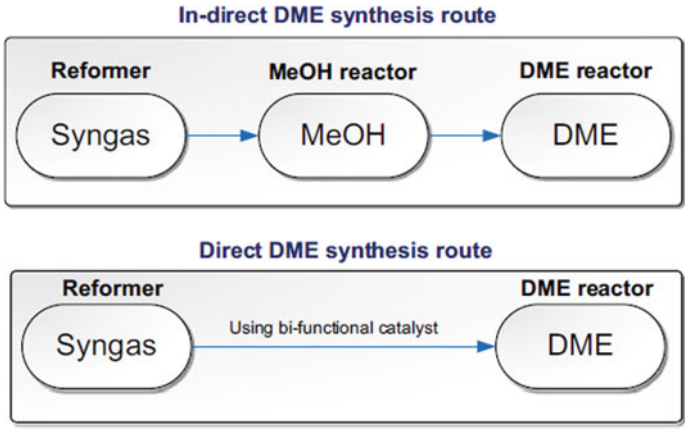

Fig. 1 Indirect and direct DME synthesis route from syngas [8]

biomass, MSW, coal, oil residues and natural gas. Production cost of DME from biomass is generally higher than the one produced from natural gas, and lower fuel prices are necessary from economics of operations point of view [6]. The process of DME production by natural gas is quite similar to that of methanol production; however, the production cost is relatively lower. DME can be produced on a large scale at a low price, and it removes 'special chemical' status of DME. Natural gas reserves are available in several remote areas which are inaccessible by pipelines globally, can be used for DME production. Natural gas present in excess at oil production sites can be used for DME production at lower cost. DME can also be synthesized using syngas (a mixture of CO and H_2 and a small amount of CH_4 and CO_2) [7] by two routes, namely (i) direct DME synthesis and (ii) indirect DME synthesis, as shown in Fig. 1.

The DME production reactions from syngas using different catalyst are as follows [8].

$$CO + 2H_2 \leftrightarrow CH_3OH \tag{1}$$

$$2CH_3OH \leftrightarrow CH_3OCH_3 + H_2O \tag{2}$$

$$2CO + 4H_2 \leftrightarrow CH_3OCH_3 + H_2O \tag{3}$$

Two different methods are used to produce DME at a large scale, as shown in Fig. 2. These methods include a direct route, in which syngas is used in one reactor with bi-functional catalysts, and in an indirect route via methanol catalytic dehydration [8, 9]. DME is also produced from coal and biomass using thermal pretreatment, followed by gasification and direct conversion from natural gas using thermal reformer mechanism [2, 10]. Currently, the maximum amount of DME is produced

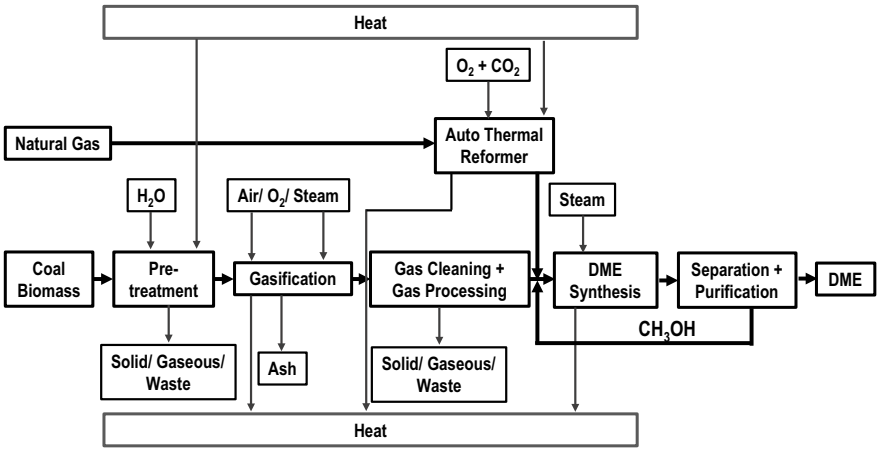

Fig. 2 Synthesis of DME from natural gas and coal/biomass

by dehydrogenation of methanol generated from the syngas. Syngas is a mixture of CO (30–60%), CO_2 (5–15%), CH_4 (0–5%) and H_2 (25–30%), and the constituent percentage of syngas is dependent on the feedstock and gasification processes. It may contain a small amount of CH_4 as an impurity. Simultaneous production of DME and methanol takes place from the syngas in direct conversion method. Initial step of direct DME production is the generation of syngas from the feedstock, which could be natural gas, oil residues, coal or biomass. Syngas is produced from steam reforming of natural gas or by partial oxidation of biomass, coal and oil residues through gasification. In the second step, methanol is synthesized using a copper-based catalyst, and in the third step, methanol is dehydrated to DME using alumina-based or zeolite-based catalysts. Finally, DME is purified, and traces of moisture and methanol are removed. Ignition characteristics of pure DME are excellent; however, presence of traces of moisture and methanol acts as contaminants and degrades the ignition quality of DME. On the other hand, presence of DME traces in methanol acts as an ignition improver. DME produced from biomass gasification is called bio-DME. Bio-DME is a highly renewable and attractive CI engine fuel, but bio-DME production cost is higher than the DME produced from fossil resources.

2.2 DME Properties

DME is an environmentally benign, colorless, odorless, non-toxic hydrocarbon species, which has combustible properties very similar to mineral diesel. DME has no adverse health effect on the human health upon mild exposure; however, large exposure of DME leads to a narcotic effect. DME burns with visible blue flames, which is an important DME characteristic from safety viewpoint. Combustion of

DME can occur in a very wide range of fuel–air ratios, which requires extra precautions and attention in designing DME combustion systems. Combustion, performance and emission characteristics of DME-fueled CI engine are very exciting. However, its physical and chemical properties demand extensive modifications in the FIE of a typical CI engine. DME's physical properties such as physical state, viscosity, modulus of elasticity and vapor pressure are the most important characteristics for its application as fuel in CI engine. Important physical and chemical properties of DME are given in Table 1. DME's vapor pressure at 25 °C is 5.1 bars. DME has relatively lower heating value and lower liquid density compared to mineral diesel, and therefore, nearly double volume flow rate is required compared to diesel for the identical engine power output.

DME has a very low boiling point (−24.83 °C) and high latent heat of vaporization (460 kJ/kg at −24.8 °C). In contrast, the latent heat of vaporization of mineral diesel is 250 kJ/kg at NTP [13]. Lower boiling point temperature of DME promotes faster vaporization of DME spray compared to mineral diesel in engine test conditions. Higher latent heat of vaporization of DME leads to reduction in NO_x emissions because DME absorbs a lot of heat during fuel spray in the combustion chamber, which lowers the in-cylinder temperature. The compression characteristics of a liquid are represented by fuel's bulk modulus. DME has very low bulk modulus compared

Table 1 Important physical and chemical properties [11–13]

Properties	DME	Diesel
Chemical formulae	CH_3OCH_3	C_{12}–C_{20}
Molecular weight	46.07	170
Carbon content (mass %)	52.2	86
Hydrogen content (mass %)	13	14
Oxygen content (mass %)	34.8	0
Stoichiometric air–fuel ratio (kg/kg)	9.1	14.6
Lower heating value (MJ/kg)	28.8	42.5
Latent heat of vaporization (kJ/kg@24.8 °C)	460	250
Bulk modulus (MN/m^2)	637	1486
Liquid density (kg/m^3@25 °C)	657	831
Critical density (kg/m^3)	259	–
Boiling point/ range (°C)	– 24.83	450–43
Viscosity (kg/m.s@25 °C)	0.12–0.15	3
Vapor pressure (bar@25 °C)	5.17	<<0.10
Critical pressure (bar)	53.7	30
Critical temperature (°C)	127	435
Ignition temperature (°C)	235	135
Flammability limits in air (volume %)	3.4–18	0.6–7.5
Cetane number	55–60	48–50

to mineral diesel or any other conventional engine fuel. Hence, the compressibility of DME is much higher than any other fuel hydrocarbon fuel [14]. Therefore, the work required to compress DME in the fuel pump is relatively higher than other hydrocarbon fuels, and significantly, higher pressure oscillation are observed during the compression of DME, when jerk type fuel pumps are used. Higher compressibility causes reduction in DME density at full load operation of the engine due to higher temperature, and hence, fuel cooling is necessary. Since the viscosity of DME is ~20 times lower than diesel, there is possibility of leakage through very small clearances present in the injector nozzles, pump plungers, common rail and solenoid injectors. Leakages of DME could be avoided by using appropriate sealing of DME compatible materials. DME has very poor lubrication properties, which leads to wear of fuel pump and other components of the FIE. Hence, there is a need for extra surface treatment of components, which are in direct contact with DME, and they need to be lubricated as well. Additives to the DME enhance lubrication properties of DME and prevent wear of components in contact with DME. Reactivity of DME in photochemical reactions is rather low, and therefore, it has one of the lowest ozone-forming potentials amongst all hydrocarbons used as fuel [15]. In the case of DME, formaldehyde does not form as a result of photochemical reactions, whereas other oxygenated fuels produce formaldehyde [16]. Since DME is stored in a closed and pressurized tank, there are no evaporative emissions, and it has a very low impact on the ambient air due to evaporative losses. Reactivity of organic compounds emitted in DME-fueled engine exhaust is also very low [17]. Nearly negligible amount of PM is emitted in the DME engine exhaust. Main advantages of DME as fuel in CI engines are as follows:

- **High Oxygen Content and Absence of C–C Bond**: Absence of C–C bond and presence of oxygen in DME molecule is the main reason for smokeless combustion of DME in CI engines.
- **Low Boiling Point**: Due to very low boiling point of DME, it evaporates very quickly in the combustion chamber upon being injected and forms a homogeneous mixture leading to more complete combustion.
- **High Cetane Number**: High cetane number (>55) of DME results in very low auto-ignition temperature. Auto-ignition and fuel vaporization occur at nearly the same time in the combustion chamber, and hence, the combustion duration reduces quite significantly.

2.3 DME Material Compatibility

DME is completely miscible in diesel, and the DME-diesel blend has low vapor pressure. DME is compatible with most metals and metallic alloys. Compatibility of DME with polymers is not much studied, and very few studies have been performed in this domain. DME is not compatible with polymeric components of the engine. These polymeric components could be valve seals, hoses, tanks, fuel pipes or FIE

components. Compatibility of DME with plastics and elastomers is limited. Conventional rubber-based materials deteriorate quickly after coming in contact with DME, and rubber solubility in DME is high. Hence, there is a need for DME compatible materials for different engine and FIE, components.

Polymers such as elastomers and plastics are used in manufacturing of several engine components such as seals and hoses of FIE. DME has a very strong ability to dissolve most polymers (elastomers and plastics) used in the diesel engine's FIE, and therefore, it is necessary to use DME compatible materials. Compatibility of these elastomers and plastics with DME is not the same for all manufacturers, and it is given in Table 2. Nitrile rubber (NBR) is commonly used in hoses and seals, and it is recommended as a compatible material by a few companies; however, Allorings indicated that it is not compatible with DME [18]. The compatibility of elastomers and plastics can be measured by 'solubility test'. In this test, polymers are dipped into DME for prolonged period. If the elastomer/plastic is unaffected, then it is compatible with DME, otherwise it is incompatible with DME. Fluorocarbon-based polymers are compatible with DME and can be applied in place of elastomers/plastics. DME compatible materials include stainless steel, aluminum, copper, zinc, monel, brass, Teflon, kynar, Kel-F, tetzel, butyl rubber, KalRez, H-NBR, styrene-butadiene rubber (SBR), neoprene, polyurethane, silicone and ethylene propylene terpolymer rubber (EPDM) [18–21]. Teflon has high creep characteristics and stiffness, and hence, it is suitable for sealing applications.

Most elastomers are not compatible with DME, and hence, they are not used in DME-fueled conventional diesel engines. A very careful approach for material selection for DME-fueled engine is therefore necessary in order to avoid deterioration of seals, which are in contact with DME for prolonged periods of time. Most common materials used in existing diesel injection systems are Viton and Buna-N rubber, which are not compatible with DME. Hence, material of these components should be replaced with DME compatible materials. Sealing of DME tank should be made of inert materials such as polytetrafluoroethylene (PTFE), which does not react with DME. Polyphenylene sulfate is another compatible material with diesel as well as DME, which should be used in the high pressure pump and low pressure pump of the FIE. Material used for sealing in DME FIE is Teflon, which is compatible with DME. Other corrosion-resistant material used for modifications of DME FIE is KalRez. Butyl rubber and neoprene are the other materials, which are acceptable

Table 2 DME compatibility of commonly used seal materials as recommended by various industries [18]

Company	NBR/ SBR	Fluorocarbon	Fluorosilicone	Silicone	PTFE
Mykin	Satisfactory	Satisfactory	–	–	–
Geotech	Acceptable	Unacceptable	–	–	Acceptable
Hargraves	–	Acceptable	Acceptable	–	–
Allorings	Unacceptable	–	Acceptable	Acceptable	–
Parr	Acceptable	Acceptable	Acceptable	Acceptable	–

sealing materials for DME FIE. Gasket material of the fuel pump should be changed to Teflon, to ensure its compatibility with DME. Stainless steel also has excellent corrosion resistance properties, when in contact with DME. Hence, entire fuel supply line from the fuel tank to the engine, including the return line, should be made of stainless steel tubes. Other components, such as regulators, valves and fittings, should also be made of stainless steel.

3 Challenges and Engine Modifications Required for DME Adaptation in the Engines

Adaptation of DME in CI engines has many challenges due to its distinct physical properties such as high vapor pressure, very low boiling point, high compressibility, low density and low viscosity. Corrosive nature of DME leads to damages to the elastomers/plastics used in the FIE components. Some of these aspects are discussed in the following paragraphs.

Physical State: DME is in gaseous phase at atmospheric conditions. Hence, engine components such as feed pump, high pressure pump, high pressure DME supply and return lines and pressure regulators need to be modified in order to avoid DME leakage. DME detectors and purging systems are also installed on the DME-fueled engines to ensure safety.

Combustion Enthalpy: Combustion enthalpy of DME is relatively lower than mineral diesel, and due to which, relatively larger volume of DME injection for longer duration is required in order to produce same power generated as that of diesel.

Viscosity: Lower viscosity of DME compared to mineral diesel causes leakage of DME from various parts such as fuel tank and FIE. DME FIE needs relatively smaller clearances, further sealed by DME compatible materials. Lower viscosity and inferior lubricity of DME increase the wear of FIE components. Special attention is required to resolve these issues.

Bulk Modulus: The bulk modulus of DME is lower than the diesel, and the difference is higher at lower pressures. Compressibility of DME in a closed system is four to six times higher than diesel, which requires higher compression work to be done by DME fuel pump compared to diesel fuel pump for the same engine power output. DME leaks through the seals of the plunger barrel of the high pressure pump, and it goes into the camshaft housing of the pump and crankcase during DME compression.

Vapor Pressure: During full load operation of DME-fueled engine, it is very difficult to inject the required DME quantity because of higher vapor pressure at higher injector temperature, which causes cavitation and consequent engine issues. There is no perfect sealing at injection nozzle seat due to DME vapor formation.

3.1 Engine Modifications

A direct injection (DI) low compression ratio (CR) CI engine fueled with DME exhibits the highest possible thermal efficiency because of lower compression ratio (12:1), larger ignition delay due to lower CR, lower NO_x emissions, and constant HC, and CO emissions [22]. Engines with lower compression ratios for DME have lighter structures, resulting in reduced costs. An existing diesel engine requires modifications, mainly the FIE for the adaptation of DME as fuel because of the physical state of DME at NTP. Engine components made of polymers need to be replaced with DME compatible materials. Figure 3 shows different components of typical DME-fueled CI engine. DME FIE contains a pressurized DME tank, pressure regulator, valves, pipelines, DME supply pump which supplies DME to high pressure pump at nearly 15 bar line pressure to avoid the cavitation in fuel line, and high pressure fuel pump [23]. An intercooler is installed in the DME return line for reducing the temperature of the returned DME.

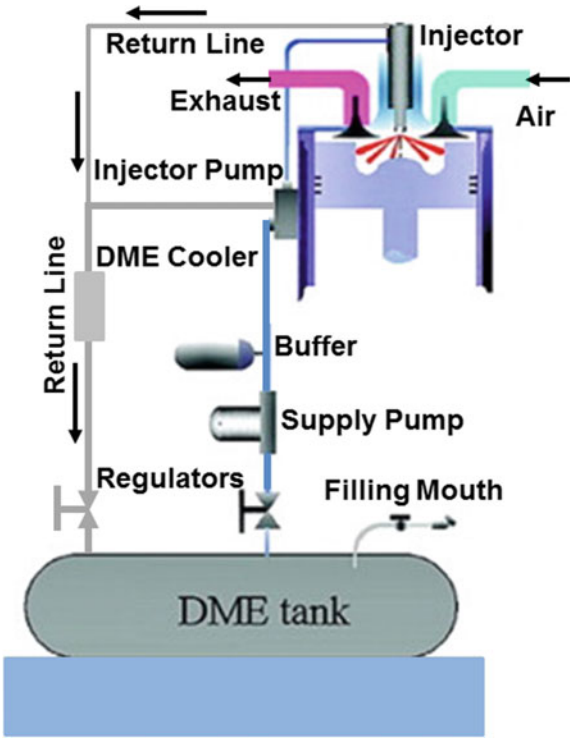

Fig. 3 Schematic of DME-fueled CI engine

3.1.1 Fuel Tank

Storage of DME is a big challenge because at NTP, DME exists in gaseous phase. Hence, DME is stored in a pressurized tank above its saturation pressure as liquid. A very important part of DME storage tank is the feed pump, which is a low pressure pump and compresses the gaseous DME to liquid phase. Pressure required for liquefaction of gaseous DME is more than 5.1 bar at 25 °C. Vapor pressure of DME is a function of its temperature. The size of DME tank should be twice that of the diesel tank due to DME's lower volumetric energy density [24]. DME is stored in a high pressure tank, and the pressure of DME tank is maintained at nearly 10 bar in order to keep DME in liquid state. The temperature versus pressure curve of DME is shown in Fig. 4. DME can also be stored in saturated condition in the pressurized tank. The saturation pressures at -15 °C and 50 °C are 1.616 bar and 11.96 bar, respectively [25].

Vapor pressure of DME lies in between the vapor pressure of propane and butane at any temperature, as shown in Fig. 4, and the mixture of propane and butane is known as liquefied petroleum gas (LPG) [26]. Therefore, a modified LPG cylinder can be used as a DME tank, which should be tested to withstand an internal pressure of 9 bar or above before use as DME tank. DME tank is visually quite similar to a diesel tank, and major difference is being that the filler cap is replaced with hemispherical endcaps (disks) and sight glass, as shown in Fig. 5 [27]. These disks act as a pressure relief valve and blow-off valve. The most noticeable modification to any DME powered engine is the elimination of its diesel tank and inclusion of the DME tank. DME tank must be a corrosion-resistant pressure vessel, and it should not be affected by salt/oxidation. Pressure vessel is placed physically at a location such

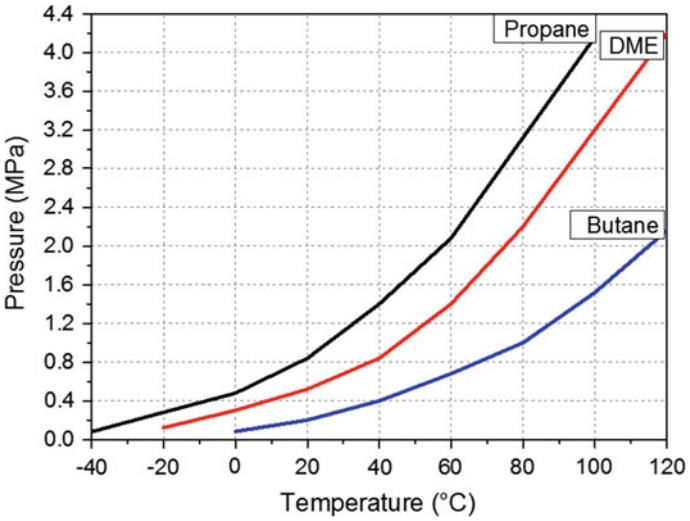

Fig. 4 Vapor pressure variation with temperature of various fuels

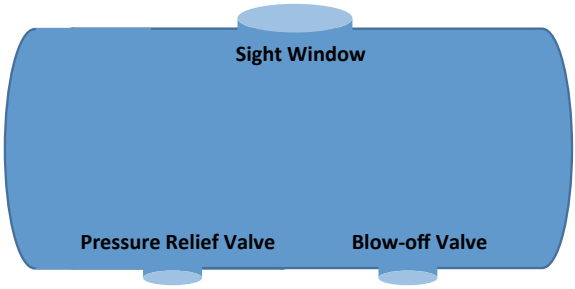

Fig. 5 DME tank

that the exposure to direct sunlight and chemicals is avoided. Function of DME tank should be to support required engine operating range, and test fuel must be in liquid state all the time. The pressure vessel should be able to bear minimum pressures in the range of 5 bar (~75 psi) in order to retain DME in liquid phase, because at NTP conditions, DME exists in gaseous phase [28]. DME has 66% and 53% lower energy compared to mineral diesel on a mass basis and on a volume basis, respectively.

3.1.2 Fuel Injection Equipment

FIE is the heart of any engine since it supplies the fuel to the engine combustion chamber via different components starting from the fuel tank, ending at the fuel injector. DME FIE includes a low pressure fuel pump, high pressure fuel pump, high pressure fuel lines, common rail control valve, common rail, solenoid injectors, electronic injection controller, fuel cooling system and purge system. Features of a DME injection system and flow characteristics of injector nozzles are very distinct from the mineral diesel engine because of differences in chemical and physical properties. DME is in the gaseous phase at NTP like LPG. Hence, DME FIE should be similar to LPG FIE. DME is kept in pressurized condition in the FIE because of its very low boiling point (−24.8 °C). Hence, the DME supply system must be closed and pressurized in order to maintain DME in liquid state throughout the fuel supply line. Vapor pressure of DME causes cavitation in the FIE, which hampers stable fuel injection. Hence, the fuel supply from the fuel tank to the high pressure pump must be at 12–30 bar in order to prevent cavitation. Cavitation is not only due to high vapor pressure of DME at high temperature, but also due to dynamic flow effects of DME during engine operation, which leads to formation of vapor regions in the injector nozzles/ fuel lines [29]. DME gasifies very fast when it is injected even at low fuel injection pressures (FIP) due to its very low boiling point. Hence, low FIP of 200–300 bar for DME can deliver a similar engine performance as that of diesel at 500 bar [30]. Existing diesel fuel injection systems are not acceptable for DME because of DME leak from clearances at atmospheric conditions due to its very low viscosity. Up to 40 to 50% DME could be leaked from the pump plunger in such systems [29]. Hence, sealing components should be replaced with anti-corrosive sealing components such as O-rings coated with Teflon and high tension sealing

components made of PTFE [31]. Very small amount (~100–1000 ppm) of additives could be added to enhance the lubricity of DME in order to avoid wear of FIE components, which are in relative motion [29, 32].

3.1.3 Fuel Pump

Fuel pumps are used to transfer the fuel under higher pressure conditions. Supply of fuel from the fuel tank is initiated by a feed pump, which is also called the primary pump or pre-supply pump. DME-fueled engine requires a modified fuel injection pump. Physical, chemical, and thermal characteristics (Table 1) of DME are considered for designing the fuel pump. Primary pump is used for the supply system of DME to the high pressure pump, and it is designed according to the fuel quantity required for the engine power rating and engine type. The power required for operating the high pressure pump and low pressure feed pump is directly related to the fuel flow rate and pressure difference between inlet and outlet fuel flows. DME's physical characteristics to be considered include lower bulk modulus (high compressibility), higher vapor pressure, lower viscosity and density as compared to mineral diesel. Higher vapor pressure and higher compressibility of DME cause fuel leakage and hence increase the power required for DME supply. Higher reactivity of DME with sealing materials such as rubber and plastic components damages the seals. Because of higher vapor pressure of DME, there is a requirement of a high pressure line to maintain DME in liquid state. Viscosity of DME is nearly one tenth compared to diesel. Lubricity of DME is also very low, which causes internal leakages due to increased frictional wear of the FIE components. These issues should be resolved by adding lubricant additives in DME [33, 34].

DME fuel pump generates high pressure in fuel supply line in order to maintain DME in liquid state. There is a relative motion of the fuel pump components such as movement of swash plate of pump against the sealing surface, and it can cause internal leakage of DME from the high-pressure compartment to the low-pressure compartment in the fuel pump. DME leakage rate is relatively higher due to lower viscosity and lubricity, leading to high wear of seals [35]. Application of DME as fuel in CI engine requires increase in fuel injection capacity/displacement volume. These changes are to be made in such a way that DME leakage can be avoided from the seals of the pump components under motion. Any leakage of DME from the pump and injector is sent back to the DME tank via a high pressure return line, as shown in Fig. 6. The displacement volume of fuel pump can be enhanced by increasing the plunger diameter and stroke length. Nozzle dimensions should be changed to make them suitable for increased duel flow rate. DME compatible materials should be used for sealing and manufacturing components of the fuel pump. Some of these materials are Teflon, H-NBR, butyl rubber, neoprene, KalRez and graphite. Teflon is used wherever metallic sealing is not possible. KalRez and graphite are used as O-ring materials for the engine components assemblies.

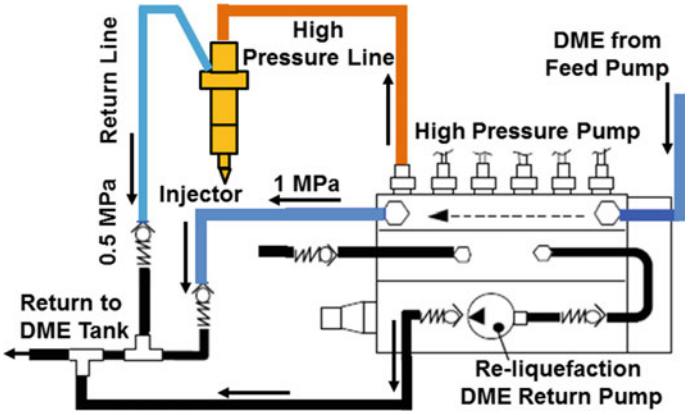

Fig. 6 Schematic of DME high-pressure pump, fuel supply and return lines

3.1.4 Fuel Line

DME supply and return to/from the tank and to/from the injectors is maintained via high-pressure fuel lines. DME fuel lines should be designed in such a way that they can bear the pressure of >5 bar to maintain liquid state of DME. The diameter of fuel supply line should be more than conventional diesel supply line, because higher DME quantity is required for power generation as diesel. Fuel line material should be steel, which would avoid corrosion, since DME is corrosive in nature. Valves, pressure regulators and other measuring instruments attached to the fuel line should be made of DME compatible materials such as steel, brass and copper. Supply of DME from the tank to the high pressure fuel injection pump is quite similar to the LPG-fueled engine. DME supply line of an electronically controlled FIE consists of a DME feed pump, low pressure line, high pressure pump, high pressure line and a fuel return line. An electronically controlled high pressure common rail FIE makes it easier to optimize the fuel injection timing and the injector solenoid energizing duration, which control rate of injection and injected fuel quantity [36–40].

3.1.5 Fuel Injector

The injector is a very crucial part of the FIE. DME is supplied to the combustion chamber by the injector. The injection and fuel spray characteristics are affected by fuel flow rate. DME has relatively lower heating value than diesel and requires ~48% more mass of DME than diesel for the identical heat generation [41]. Hence, by using the same injector for both DME and diesel, DME injection duration increases by 37% compared to diesel for identical test conditions. Therefore, it is important to design separate injectors for DME for increasing the DME flow rate by modifying

the injector nozzle (orifice size and cone angle). It is also necessary to modify the combustion chamber geometry for an appropriate injection strategy.

DME required more fuel injected into the engine cylinder for diesel equivalent power generation due to its lower calorific value. The amount of DME injected into the combustion chamber is dependent on the FIP and injection duration. Fuel injection duration could be reduced by injecting DME at high pressure and in multiple injections. High FIP is not required for DME injection in the combustion chamber, because DME has excellent vaporization and spray atomization characteristics. DME spray characteristics in the combustion chamber are affected by the nozzle hole size, cone angle and FIP. Since the bulk modulus of DME is nearly 2.3 times lower than diesel, investigation of DME injection rate with respect to FIP is very important. The spray behavior of DME at high FIP in different ambient pressure conditions shows that DME spray characteristics are at variance from diesel. Spray penetration length of DME is smaller than diesel, and it decreases with increasing ambient pressure for both fuels, as shown in Fig. 7 [42].

The DME injection characteristics in the combustion chamber are different from diesel due to different physical properties. Figure 8 shows the fuel injection rate, effective velocity of the fuel spray and energy supply rate for a fixed energy input from DME and diesel injectors. The hole size of the injector nozzle should be enlarged to inject higher mass of DME for the same power output as diesel. Nozzle should be coated with the self-lubricating DME compatible materials in order to avoid wear of nozzle holes.

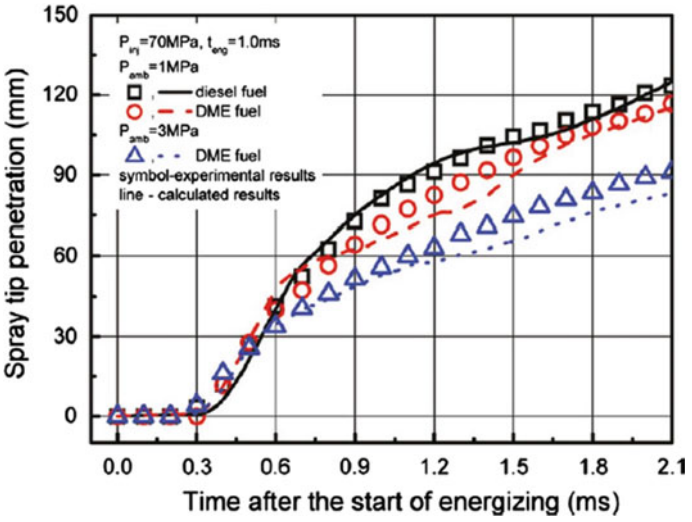

Fig. 7 Comparison of spray tip penetration length of DME and diesel at different ambient pressures [42]

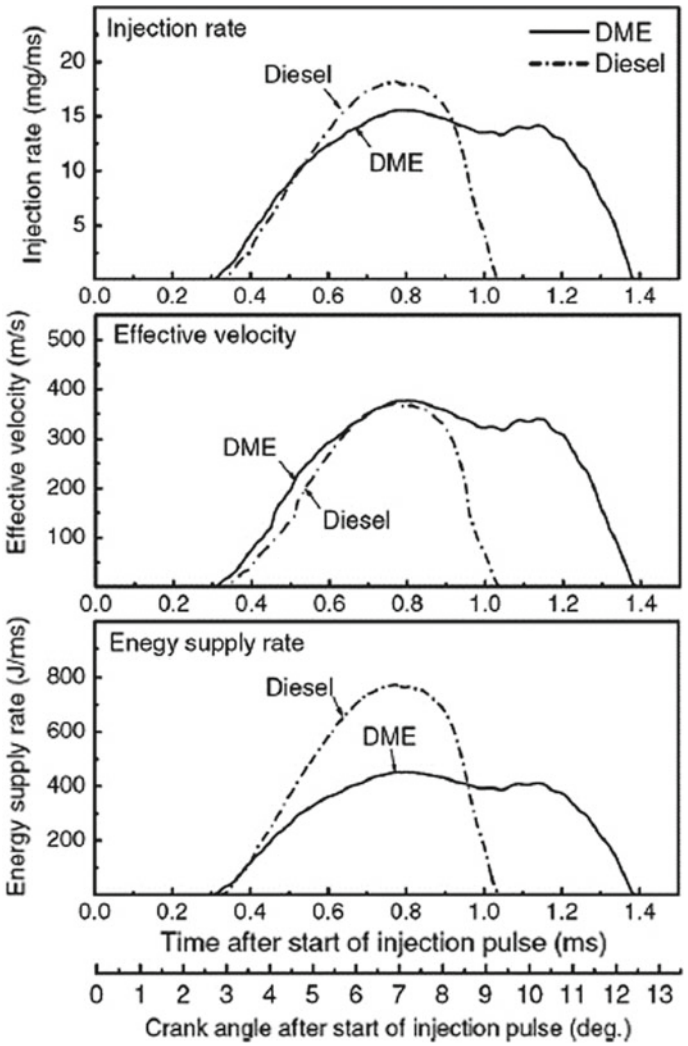

Fig. 8 Comparison of DME and diesel injection rates, energy supply rates and effective velocity for constant energy output [43]

3.1.6 DME-Fueled LTC Engines

Several new low-temperature combustion (LTC) engine concepts, such as HCCI engines and low compression ratio direct-injection (DI) diesel engines, are used for DME application, which increase the thermal efficiency and reduce emissions. HCCI engines fueled with DME have great potential to enhance the thermal efficiency and reduce noise and NO_x and soot emissions; however, here are combustion control issues. DME can also be used in premixed charge compression ignition

(PCCI) engines. PCCI combustion strategy is a combination of HCCI combustion and conventional diffusion combustion (direct injection of diesel and port injection of DME) or PCCI direct injection (DI) of DME (PCCI-DI). In PCCI-DI combustion, pilot injection of DME is used, and pilot quantity can be varied [31, 44]. The smoke, PM and NO_x emissions are reduced simultaneously in PCCI engines.

4 Vehicle Adaptation of DME

The environmental concerns regarding the pollution due to transport sector can be resolved by development of environment-friendly vehicles with zero/ negligible emissions by deploying new technology. DME-fueled vehicle development has emerged as a vital solution for resolving environmental issues due to transport vehicles. DME-fueled vehicles emit negligible harmful emissions. In spite of poor lubrication behavior, lower viscosity and calorific value of DME, development of DME-fueled vehicles is being considered seriously for reduction of NO_x and soot emissions. These emissions are dangerous for the human health. Usage of DME in transport sector and other applications can be a solution for energy scarcity, because DME can be manufactured from renewable and natural resources. Therefore, research organizations and automobile companies world over are undertaking research and development programs for DME-fueled vehicles.

4.1 Europe

The first DME-fueled vehicle was developed in Europe in 1996 by Haldor Topsoe (Denmark). A EURO-IV norms emission compliant DME engine was developed in 1998, and the first DME-fueled bus was developed by Volvo (Sweden) in 1999. This was a first-generation DME-fueled bus with a fuel economy of 1.17 km/l. It exhibited improved performance and reduced emissions (NO_x, HC, CO and PM), which are shown in Table 3 [45]. Volvo started working on development of DME-

Table 3 DME-fueled vehicle and engine test results [45]

Test results	EURO-IV Norms	Vehicle test	Engine test
NO_x (g/kWh)	3.5	3.3	2.99
HC (g/kWh)	0.46	0.25	0.25
CO (g/kWh)	1.5	0.03	0.12
PM (g/kWh)	0.02	–	<0.02
Power @ 2000 rpm, kW	–	186	109
Torque @ 1450 rpm, Nm	–	1050	727

fueled heavy-duty vehicles in 2002. They developed the second-generation DME-fueled vehicle with power output of 224 kW in 2005. They also developed a third-generation DME-fueled truck with engine power of 343 kW and engine torque of 2732.56 Nm. Presently, Volvo and EU are jointly working on bio-DME project, in which bio-DME pilot plant is on the verge of completion and large-scale production of DME would start for its application as a transport fuel.

4.2 Asia

In Asia, Japan is the only country where researchers first started working on the development of DME-fueled vehicles. The National Traffic Safety and Environment Laboratory (NTSEL), along with Nissan diesel motors and Bosch Japan, developed DME-fueled heavy-duty buses during 1998–2001 and used a mechanical fuel injection system. In 2003, DME-fueled heavy- and medium-duty vehicle development was started by the National Institute of Advanced Industrial Science and Technology (AIST), in collaboration with oil companies and motor companies. They converted a four cylinder diesel-fueled engine to DME, and this engine was fitted successfully in a minibus/truck [46]. AIST and Japan Oil, Gas, and Metals National Corporation (JOGMEC) collaboratively developed a DME-fueled medium-duty truck that showed very low emissions in 2005, as shown in Table 4 [47]. This development demonstrated that average DME fuel economy of trucks was 2.61 km/l. Nissan diesel motors and NTSEL developed a DME-fueled six-cylinder in-line truck, which was turbocharged with intercooler along with EGR, and after-treatment devices (NO_x reduction catalyst and oxidation catalyst) [37]. Isuzu Motors also worked on development of DME-fueled light-duty and medium-duty vehicles and engines and reported that mileages of medium-duty and light-duty vehicles were 3.81 km/l and 2.83 km/l, respectively [48].

In China, first-generation DME-fueled engines and vehicles were developed in 2005 under the scheme of National Clean Vehicle Action Program. Shanghai Jiao Tong University (SJTU), Shanghai Motor Company, Shanghai Coking & Chemical Corporation collaboratively manufactured ten buses fueled with DME, in which DME was injected by using a mechanical fuel injection system. They also developed DME filling stations. These vehicles were tested successfully for more than

Table 4 Japanese emission limits and vehicle test emission results of DME-fueled vehicle and diesel-fueled vehicle [47]

Test results	Japanese emission limits (2005)	DME fueled	Diesel fueled
NO_x (g/kWh)	3.38	2.479	2.99
HC (g/kWh)	0.87	0.222	0.89
CO (g/kWh)	2.22	0.117	3.17
PM (g/kWh)	0.18	0.01	0.17

220,000 km in commercial applications. Second- and third-generation vehicles were developed to comply with EURO-V emission standards using a common rail FIE. They used after-treatment devices for further reduction in emissions. SJTU worked on more than 863 projects funded by the Chinese government to develop new technology for vehicles (trucks, buses and taxis) fueled with DME [49] and to meet current emission norms.

The first DME-fueled engine development research project in Korea was started in 2000 by the Korea Institute of Energy Research (KIER). They manufactured a prototype DME-fueled truck in 2003. In 2005, KIER started research project for DME-fueled bus development, and they had successfully operated 33 passenger bus on the road by 2010. A passenger car was developed by Hanyang University (HYU). They used a common rail fuel injection system for DME and successfully drove the car on the road. In 2009, Korea Automotive Technology Institute (KATEC) developed a modern advanced DME vehicle fueled by modifying existing sports utility vehicle (SUV). They also developed a DME-fueled truck using common rail DME FIE and tested its performance and emission characteristics according to New European Driving Cycle (NEDC). This truck complied with Euro-5 emission regulation [50].

In India, Engine Research Laboratory (ERL), IIT Kanpur, has started development of DME-fueled engine and tractor in collaboration with TAFE Motors and Tractor limited (TMTL), and Science and Engineering Research Board (SERB), Government of India. Tractor prototype is expected to be ready for on-field trials by 2022.

4.3 North America

In USA, DME-fueled bus development program was initiated jointly by the Department of Energy (DOE), Pennsylvania State University, Air Products and Chemicals, Inc., Caterpillar, and Navistar International between 1999 and 2001. They chose a turbocharged, 7.1 L displacement engine for shuttle bus. For avoiding the lubricity problems of DME, they used DME/ diesel blend (14% to 30% DME v/v) as a fuel. They reported 80% lower PM emissions using 25% DME blended fuel [51].

4.4 Summary

This chapter provides an inclusive review of DME production, properties, challenges, material compatibility and modifications required in CI engines/ components for DME adaptation as fuel. The review includes all aspects of DME as fuel in CI engine, starting from production to vehicle adaptation. DME can be produced by many renewable (biomass, syngas, solid waste) and non-renewable (coal, natural gas, crude oil, oil residues) feedstock resources. DME is a gas at NTP and can be liquefied at higher pressures, similar to LPG. DME is also non-toxic, environment-friendly and easy to handle fuel candidate. It is a very efficient fuel for CI engine

application due to higher cetane number (55–60) than diesel. Higher evaporation of DME results in excellent mixing with air in the combustion chamber. Absence of C–C bond and presence of oxygen in DME structure along with superior air–fuel mixing lead to more complete and smokeless combustion. However, due to relatively lower calorific value and density of DME, higher volume of DME needs to be injected for an energy generation equivalent to diesel. Fuel injection system of DME engine requires additives to enhance its lubricity. DME compatible materials should be used in the components of fuel injection system and fuel tank. Anti-corrosive sealing materials are required for the DME supply system, and fuel pumps safe and leak-free operation. Fuel injection system components such as fuel tank, fuel lines, fuel pumps and fuel injectors of DME-fueled CI engines should be modified according to DME properties. Use of DME in different vehicles is increasing globally, and new research and development efforts are in place for improving these vehicles. However, broad studies of DME's impact on the environment are required for evaluation of full potential of its large-scale application. Overall, this chapter demonstrated that DME is a strong alternative fuel candidate for CI engines, which delivers higher thermal efficiency and lower emissions. Based on the physical and chemical characteristics of DME, fuel system components which are in direct or indirect contact with DME need to be made of DME compatible materials. More research and development are required before mass production of DME and DME-fueled vehicles for automotive sector.

Acknowledgements Financial support from SRA scheme of Council for Scientific and Industrial Research (CSIR), Government of India, to Dr. Vikram Kumar is gratefully acknowledged, which supported his stay at ERL, IIT Kanpur, for contributing to this chapter.

References

1. Agarwal, A. K., Singh, A. P., & Maurya, R. K. (2017). Evolution, challenges and path forward for low temperature combustion engines. *Progress in Energy and Combustion Science, 61,* 1–56.
2. Verbeek, R. P., Van Doom, A., & Van Walwijk, M. (1996). Global assessment of di-methyl ether as an automotive fuel, 2nd edn., 96.OR.VM.029. 1/RV, TNO Road-Vehicles Research Institute.
3. Murayama, T., Chikahisa, J., Guo, J., & Miyano, M. A. (1992). *Study of compressions ignition methanol engine with converted dimethyl ether as an ignition improver*. SAE Technical Paper 1992, 922212.
4. Sorenson, S. C., & Mikkelsen, S. E. (1995). *Performance and emissions of a 0.273 liter direct injection diesel engine fueled with neat dimethyl ether*. SAE Technical Paper 1995, 950964.
5. Arcoumanis, C. (2000). *The second European Auto-Oil programme (AOLII).* European Commission 2.
6. Greszler, A. (2013). DME from natural gas or biomass: A better fuel alternative. In *Presentation to the SAE International World Congress 2013.*
7. Kajitani, S., & Chen, Z. (2003). *Fundamental research on the next generation fuel (dimethyl ether) engines 2003.*

8. Luu, M. T., Milani, D., Wake, M., & Abbas, A. (2016). Analysis of di-methyl ether production routes: Process performance evaluations at various syngas compositions. *Chemical Engineering Science, 149,* 143–155.
9. https://en.wikipedia.org/wiki/File:DME_Process_diagram.jpg.
10. Mills, A. (1994). Status and future opportunities for conversion of synthesis gas to liquid fuels. *Fuel, 73,* 1243–1279.
11. Sorenson, S. C. (2001). Dimethyl ether in diesel engines: Progress and perspectives. *Journal of Engineering for Gas Turbines and Power, 123*(3), 652–658.
12. Park, S. H., & Lee, C. S. (2013). Combustion performance and emission reduction characteristics of automotive DME engine system. *Progress in Energy and Combustion Science, 39,* 147–168.
13. Sezer, I. (2011). Thermodynamic, performance and emission investigation of a diesel engine running on dimethyl ether and diethyl ether. *International Journal of Thermal Science, 50,* 1594–1603.
14. Sorenson, S. C., Glensvig, M., & Abata, D. L. (1998). *Dimethyl ether in diesel fuel injection system.* SAE Tech Paper 1998, SAE 981159.
15. Bowman, F. M., & Seinfeld, J. H. (1995). Atmospheric chemistry of alternative fuels and reformulated gasoline components. *Progress in Energy and Combustion Science., 21,* 387–417.
16. Japar, S. M., Wallington, T. J., Richert, J. F. O., & Ball, J. C. (1990). The atmospheric chemistry of oxygenated fuel additives: t-butyl alcohol, dimethyl ether, and methyl t-butyl ether. *International Journal of Chemical Kinetics, 22,* 1257–1269.
17. Mikkelsen, S. E., Hansen, J. B., & Sorenson, S. C. (1996). *Dimethyl ether as an alternate fuel for diesel engines: Application of powertrain and fuel technologies to meet emissions standards*, Institution of Mechanical Engineers London (pp. 289–298).
18. Kass, M. D., & Daw, C. (2016). Compatibility of dimethyl ether (DME) and diesel blends with fuel system polymers: A Hansen solubility analysis approach. *SAE International Journal of Fuels and Lubricants, 9*(1), 71–79.
19. Wu, N., Zhang, W., & Huang, Z. (2008). Impact of dimethyl ether on engine seal materials. *Frontiers of Energy and Power Engineering in China, 2*(3), 279–284.
20. www.mathesongas.com/pdfs/products/Materials-Compatibility-Guide.
21. www.graco.com/content/dam/graco/ipd/literature/misc/chemical-compatibility-guide/Graco_ChemCompGuideEN-B.
22. Kajitani, S., Chen, Z., Oguma, M., & Konno, M. (2002). A study of low-compression-ratio di-methyl ether diesel engines. *International Journal of Engine Research, 2,* 1–11.
23. Zhao, Y., Wang, Y., & Liu, S. (2014). *Combustion and emission characteristics in a DME premixed charge compression ignition diesel engine.* SAE Technical Paper 2014, 2014-01-1292.
24. Ying, W., Longbao, Z., & Wei, L. (2010). Effects of DME pilot quantity on the performance of a DME PCCI-DI engine. *Energy Conversion and Management, 51*(4), 648–654.
25. Huang, Z., Qiao, X., Zhang, W., Wu, J., & Zhang, J. (2009). Dimethyl ether as alternative fuel for CI engine and vehicle. *Frontiers of Energy and Power Engineering in China, 3*(1), 99–108.
26. Teng, H., McCandless, J. C., & Schneyer, J. B. (2004). *Thermodynamic properties of dimethyl ether—an alternative fuel for compression-ignition engines.* SAE Technical Paper 2004, 2004-01-0093.
27. Szybist, J. P., McLaughlin, S., & Iyer, S. (2014). Emissions and performance benchmarking of a prototype dimethyl ether fueled heavy-duty truck. *Papers of the American Chemical Society, 248,* 1155.
28. Fleisch, T., McCarthy, C., Basu, A., Udovich, C., Charbonneau, P., Slodowske, W., Mikkelsen, S. E., & McCandless, J. (1995). *A new clean diesel technology: Demonstration of ULEV emissions on a Navistar diesel engine fueled with dimethyl ether*. SAE Technical Paper 1995, 950061.
29. DME-another choice alternative fuel Samuel Mclaughlin Volvo Group Trucks Technology.
30. Kitamura, T., Ito, T., Senda, J., & Fujimoto, H. (2002). Mechanism of smokeless diesel combustion with oxygenated fuels based on the dependence of the equivalence ratio and temperature on soot particle formation. *International Journal of Engine Research, 3,* 223–248.

31. Kim, M. Y., Yoon, S. H., Ryu, B. W., & Lee, C. S. (2008). Combustion and emission characteristics of DME as an alternative fuel for compression ignition engines with a high pressure injection system. *Fuel, 87,* 2779–2786.
32. Edgar, B., Dibble, R. W., & Naegeli, D. W. (1997). *Autoignition of di-methyl ether and dimethoxy methane sprays at high pressures*. SAE Technical Paper 1997, 971677.
33. Tsuchiya, T., & Sato, Y. (2006). *Development of DME engine for heavy-duty truck*. SAE Paper 2006, 2006-01-0052.
34. Yu, J., & Bae, C. (2003). Dimethyl ether (DME) spray characteristics compared to diesel in a common-rail fuel injection system. *Proceedings of the Institution of Mechanical Engineers, Part D: Journal of Automobile Engineering, 217,* 1135–1144.
35. Kapus, P., & Ofner, H. (1995). *Development of fuel injection equipment and combustion system for DI diesels operated on di-methyl ether*. SAE Technical Paper 1995, 950062.
36. Kim, H. J., Park, S. H., Suh, H. K., & Lee, C. S. (2009). Atomization and evaporation characteristics of biodiesel and dimethyl ether compared to diesel fuel in a high-pressure injection system. *Energy and Fuel, 23,* 1734–1742.
37. Tsuchiya, T., & Sato, Y. (2006). *Development of DME engine for heavy-duty truck*. SAE Technical Paper 2006, 2006-01-0052.
38. McCandless, J., Teng, H., & Schneyer, J. (2000). *Development of a variable-displacement, rail-pressure supply pump for dimethyl ether*. SAE tech paper 2000, 2000-01-0687.
39. Sorenson, S. C., & Mikkelsen, S. E. (1995). *Performance and emissions of a 0.273 liter direct injection diesel engine fuelled with neat dimethyl ether*. SAE Technical Paper 1995, 950064.
40. Zhang, G. D., Liu, H., Xia, X. X., & Yang, Q. L. (2004). Study on the injection process of a direct injection diesel engine fuelled with dimethyl ether. *Proceedings of the Institution of Mechanical Engineers, Part D: Journal of Automobile Engineering, 218,* 1341–1347.
41. Kapus, P. E., & Cartellieri, W. P. (1995). *ULEV potential of a DI/TCI diesel passenger car engine operated on dimethyl ether*. SAE Technical Paper 1995, 952754.
42. Christensen, R., Sorenson, S. C., Jensen, M. G., & Hansen, K. F. (1997). *Engine operation on dimethyl ether in a naturally aspirated, DI diesel engine*. SAE Technical Paper 1997, 971665.
43. McCandless, J. C., & Li, S. (1997). *Development of a novel fuel injection system (NFIS) for dimethyl ether e and other clean alternative fuels*. SAE Technical Paper 1997, 970220.
44. Park, S. H., Kim, H. J., & Lee, C. S. (2011). Study on the dimethyl ether spray characteristics according to the diesel blending ratio and the variations in the ambient pressure, energizing duration, and fuel temperature. *Energy and Fuel, 25,* 1772–1780.
45. Hansen, K. F., Nielsen, L., Hansen, J. B., Mikkelsen, S., Landalv, H., Ristola. T., & Vielwerth, K. (2000). *Demonstration of a DME (dimethyl ether) fuelled city bus.* SAE Technical Paper 2000, 2000-01-2005.
46. Goto, S., Oguma, M., & Suzuki, S. (2005). *Research and development of a medium duty DME truck*. SAE Technical Paper 2005, 2005-01-2194.
47. Kinoshita, K., Oguma, M., Goto, S., Sugiyama, K., Mori, M., & Watanabe, T. (2003). *Effects of fuel injection conditions on driving performance of a DME diesel vehicle.* SAE Technical Paper 2003, 2003-01-3193.
48. Hara, T., Shimazaki, N., Yanagisawa, N., Seto, T., Takase, S., Tokumaru, T., & Sato, Y. (2011). *Study of DME diesel engine for low NOx and CO_2emission and development of DME trucks for commercial use*. SAE Technical Paper 2011, 2011-01-1961.
49. Huang, Z., Zhang, W., Fang, J., & Qiao, X. (2010). Shanghai DME bus demonstration: recent progress. In *4th International DME conference 2010, Stockholm.*
50. Jeong, S., & Park, J. (2012). Development and prospect of common rail vehicle fueled with di-methyl ether. *Auto Journal (Written in Korean), 33*(8), 64–69.
51. Eirich, J., Chapman, E., Glunt, H., Klinikowski, D., Boehman, A. L., & Hansel, J. G. (2003). *Development of a dimethyl ether (DME)-fueled shuttle bus.* SAE Technical Paper 2003, 2003-01-0756.

Techno-economic and Environmental Evaluation of Producer Gas-Based IC Engine in a Hybrid Energy System

Prashant Malik and Mamta Awasthi

Abbreviations

MHP	Micro hydro plant
COE	Cost of energy
SPV	Solar photovoltaic
BM	Biomass gasifier system
HRES	Hybrid renewable energy system
DG	Diesel generator
GHG	Greenhouse gases
CR	Compression ratio
TNPC	Total net present cost
LHV	Lower heating value
RF	Renewable fraction
SOC	State of charge
CV	Calorific value
HC	Hydrocarbons
TG	Travelling grate
GCV	Gross calorific value

P. Malik (✉) · M. Awasthi
Centre for Energy and Environmental Engineering, NIT Hamirpur, Hamirpur, India

A. P. Singh et al. (eds.), *Alternative Fuels and Advanced Combustion Techniques as Sustainable Solutions for Internal Combustion Engines*, Energy, Environment, and Sustainability, https://doi.org/10.1007/978-981-16-1513-9_4

1 Introduction

Energy conversion and production is continuing to play a crucial role in attaining the goal of sustainability. Rapid technological progress and prolonged development have placed immense pressure on the natural resources to meet the rising demand for energy, which may create a stern hazard to the imminent fuel security. So, the world is now searching for alternative fuels (solar, wind, biomass, geothermal, etc.) to generate power. Utilization of renewable energy is contributing in increasing demand. Advancement in the current system and conversion technologies to develop a more effective conversion system is needed. Around 14% population have access to electricity on a worldwide scale, and most of the rural area do not have electricity in their houses or having for a small-time frame [1]. Therefore, off-grid renewable energy systems could be a healthier solution because of abundantly nearby availability of renewable resources such as MHP, biomass and solar PV. Single resource-based energy system having a major issue of intermittency could be solved by hybrid of more than one resources. Unutilized form of biomass can be a better choice to improve reliability of system and resolve the other issues like as intermittency in solar or wind energy systems, better electricity quality and efficiency improvement. It has lot of advantages over fossil fuels such as carbon neutral, abundantly available, low cost, renewability, ability to replacement of diesel energy system and higher employment.

There is always a need of techno-economic analysis of an energy system prior to installation. Lot of studies based on techno-economic analysis of hybrid system has been carried out by researchers. As instance, Makhija and Dubey [2] found that the biomass gasifier system with grid connection offered the lowest COE in cement factories in India. Parihar et al. [3] suggested that the biomass gasifier system with battery is more cost-effective in comparison with the alone gasifier system, the hybrid system and solar PV with a battery storage. Garrido et al. [4] investigated feasibility and sensitivity analysis of SPV/BM HRES to satisfy of rural villages demand in Mozambique, Southern Africa. The proposed system is found to be more competitive with COE of 0.33 $/kWh as compared to the SPV/DG hybrid system. Sava et al. [5] carried out the technical and economic analysis of a grid-connected hybrid system for an educational building in Bucharest, Romania. SPV/BG/Battery-based hybrid is found to be the most optimized system with the least COE of 0.343 $/kWh. Grid-connected SPV/BM HRES has been proposed by Barrozo et al. [6] to reduce the GHG emission in Colombia. The analyzed results show that the biomass-based proposed hybrid system reduces total GHG emissions by 38% when compared to the existing system. The system feasibility depends on various key factors such as plant location and fuel type. Therefore, COE will change from location to location, and it means that feasibility analysis is the first step before experimental setup for each location.

In this chapter, techno-economic and environmental analysis has been carried out of a producer gas-based IC engine integrated in a hybrid system with the help of a simulation software (HOMER). An actual educational building load with realistic weather data of Hamirpur, Himachal Pradesh, was used for analysis, and unutilized pine needles are used as a gasifier fuel. Pine needles are a serious problem especially

in hilly regions because these are the main cause of forest fires in summer seasons. Pine needles as a gasifier fuel will not only reduce the forest fire incidents but also help in carbon dioxide reduction.

The chapter is organized as follows: First section describes the IC engine with their alternative gaseous fuels, and modification steps to run on producer gas are discussed in Sect. 2, Sect. 3 provides the overview of biomass conversion technologies, and simulation study with different cases is described in Sects. 4 and 5. The conclusion part is presented in last section.

1.1 IC Engines for Energy Transformation

A turbine or a generator is being used after combustion of any fuel irrespective of its origin for heat generation. This heat is consequently being used for electricity generation. Much work has been done on internal combustion engine since its inception.

The IC engines first came into the picture 150 years ago, when J.J.E. Lenoir developed an engine with 5% efficiency and used a cylinder integrated with a piston to combust the coal–air mixture without compression. Later, Nicolaus A. Otto developed an improved engine with the Lenoir concept with greater efficiency of 11%. Otto constructed the first engine based on four-stroke concept, which serving as a prime operation cycle in today's engines [7]. From this stage and with the efforts of some great developers like as Rudolf Diesel, Robert Bosch, Sir Harry Ricardo and Charles Kettering, the IC engine is now one of the energy-efficient, economical, simple to operate and reliable power system accessible to people.

The internal combustion engine (IC) is a type of heat engine in which the fuel's chemical energy is altered into mechanical energy with the help of combustion of fossil fuel at high pressure. It has two main parts—one is stationary cylinder and second is piston. The piston is used for compressing fuel and air mixture, which is erupted, and high-pressure and high-temperature gases are produced inside the combustion chamber. The produced gas accelerates the piston and mechanical energy transferred to the spinning shaft.

The spark ignition (Otto cycle) and the compression ignition (Diesel cycle) are the two types of engines. In case of spark-ignition engine, carburetor or an injection system is basically used to inject fuel. If carburetor is used, the fuel is throttled by jets and mixed to the air, which passes through the carburetor valve. Later, the mixture of air and fuel moves into cylinder, where spark plug erupts the mixture. Fuel injection systems are mostly used in advanced engine systems because it uses various sensors and electronic devices to control the air–fuel mixture, which basically improves the efficiency. In recent years due to fuel price increment and environmental concerns, the use of fuel injection systems in smaller engines has been increased. For an engine without carburetor, the fuel injection in air stream has been through throttle body. Otherwise, in some systems, a single injector has been placed at the throttle body, which meters the fuel in cylinders. In case of an IC engine, the fuel is directly pumped

into the combustion chamber, and the injection is scheduled before top dead center on the combustion cycle. Combustion happens almost instantly because compression is the reason of temperature increment of air up to 1,000 °F and above. Hence, there is no requirement of spark plug for fuel ignition, and the fuel amount has been controlled by injector pump.

1.2 Alternative Gaseous Fuels for IC Engine

The utilization of alternate fuels in engines has become the subject of significant interest due to growing issues related to environmental safety and crude oil shortages. Producer gas, CNG, LPG, biogas and hydrogen have been identified as alternative fuels. CNG and LPG gaseous fuels are petroleum-based fuels and widely accessible. These are mostly used for transportation applications, while CNG could be used in industrial applications. On other hand, hydrogen, syngas and biogas fuels are produced from renewable resources, which are chiefly used for power generation in remote areas where grid availability is not present.

Hydrogen: It is also comes under an environmental friendly fuels category because of least CO and HC compared to fossil fuels. Coal, crude oil and natural gas are the major sources of hydrogen production. Electrolysis of water is also a renewable method of hydrogen production. Hydrogen's fast flammability speed is the cause of rapid combustion, which is nice in terms of thermodynamics and helps to achieve higher engine efficiency [8–10]. Hydrogen-operated engine has good thermal efficiency because of its high auto-ignition temperature, which supports to run the engine at high CR. Wide flammability, high flame speed, self-ignition temperature and low ignition energy necessity are the most advantageous characteristics. However, low CV by volume, low density and uncolored flame are some adverse properties of hydrogen fuel. Higher cost associated with engine modification, protection, handling and supply is some other glitches, which have to be tackled to increase viability of such systems.

In Changwei and Wang [11], H_2 enrichment was used for performance enhancement of a gasoline engine under small load and low-load circumstances. The study found a huge increment in brake thermal efficiency and torque due to addition of H_2. The emission results found reduction in CO and HC emission, but NO_x shows increment because of hydrogen addition. Karagoz et al. [12] examined the various properties (performance, emission and combustion) of a diesel engine running at various hydrogen levels. The study revealed that CO and smoke emission was reduced with increment of hydrogen percentage. Hernández et al. [13] evaluates the effect on diesel engine performance, emission and combustion properties due to addition of hydrogen, CH_4 and carbon monoxide. The results show higher emission of HC and CO in case of CO and CH_4. The reduction in thermal efficiency with diesel replacement was also get noticed because of increment in unburnt gaseous fuel. But a substantial decrement was attained in particulate matter with a small change in NO_x emissions. Wang et al.'s [14] experimental investigation of H_2 addition has

been carried out on a SI engine. The emission results show reduction in CO, HC and CO_2 with increment of the hydrogen percentage, but NO_x emission shows increasing trend against cylinder cutoff and increment in hydrogen blend ratio.

Biogas: It is a renewable resource of energy, which is produced during an anaerobic condition. Animal waste, agricultural waste, sewage, food waste, plant waste, etc., are major raw materials used in a biogas digestor. CH_4 and CO_2 have the highest share in biogas with small fraction of H_2S and moisture. Biogas is basically used in rural areas to meet out the energy and heat demand [15]. It may be used in IC engines and generators with suitable alteration for electricity production in rural areas. Biogas is an appropriate fuel with high CR because of higher octane number, which is also a cause of increment in thermal efficiency [16]. Biogas has lower emission than fossil fuels because of less % of carbon content [17]. It has low energy density, small flammability, high self-ignition temperature, high octane number and less amount of H_2S. There is a need of close control on air–fuel ratio to achieve the good performance, but H_2S presence in biogas could be a reason of rust on engine parts.

Chandara et al. [18] investigated performance of 5.9 kW diesel engine which has been carried out with different fuels (CNG, bio-CNG and biogas). The highest power loss 46.3% was achieved in biogas, while methane enriched biogas and CNG show almost same engine performance (thermal efficiency, gas consumption and brake power output). Jung et al. [19] carried out a simulation analysis to investigate the performance and NO_x emission of a biogas-fueled turbocharged IC engine, and experimental validation also has been done. The results show that thermal efficiency and NO_x emissions were increased as per the % increment in methane content. The author achieved about 90% reduction in NO_x emissions by minimizing the combustion temperature. Makareviciene et al. [20] stated that unmodified diesel engine with biogas is a cause of higher fuel consumption rate, low thermal efficiency and higher pollutant emissions excluding NO_x. Therefore, there was a need of exhaust gas recirculation system and change start of injection timing to attain the best performance in biogas fuel IC engines. Faria et al. [21] suggested a simulation model with minimum computational price to check the performance of a SI engine with biogas as a fuel. The developed model was also validated experimentally and found only 5% error in simulated and experimental values.

Liquefied petroleum gas (LPG): it is a product of petroleum plants and mainly consisting of propane and butane with some % of other hydrocarbons. LPG is mostly used for heating, cooking, cooling appliances and vehicles applications. The transportation and storage of LPG are very easy compared to other gaseous fuel because it can be liquefied at very low pressure 0.7–0.8 Mpa. LPG is a good alternative fuel in SI engines because of its high calorific value and high octane number, while it is difficult to use with CI engines due to low cetane number [22, 23]. Low cost and low CO_2 emission are basically two major advantages of LPG used as a fuel. Selim et al. [24] stated that LPG as a fuel in SI engines could be a best approach to reduce the carbon dioxide emission and other pollutants. Performance and emission characteristics of a modified diesel engine have been carried out by Ngang and Abbe [25]. The study results found that increment in LPG mass fraction would decrease the pollutants

(NO_X, HC) and enhance the engine performance. Saleh [26] investigated the impact of variation in LPG composition on dual-fuel diesel engine to identify the optimal composition to enhance the performance and reduction in emission of engine. The study found that LPG with 70% propane and 30% butane composition gives the best results in dual-fuel mode. A critical review of experimental studies on performance, emission and combustion properties of LPG based dual-fuel engine has been carried out by Ashok et al. [27]. The studies indicate that part load characteristics may be enhanced by improving the operating and design parameters of engine.

Compressed natural gas (CNG): Crude oil refineries and gas wells are the main sources of CNG production. CNG comprises the highest % (about 98%) of CH_4 and very less % of H_2S, CO_2, ethane, propane, water vapor and N_2. It is an environment friendly fuel due to its low emission of pollutants in IC engines. CNG is a compressed form of natural gas, which is stored in a cylindrical or spherical shape container at 20–25 Mpa pressure. CNG is safer compared to LPG, diesel and petrol fuels because it is lighter than air and spreads at faster rate in case of leakage. At normal atmospheric circumstances, it has higher miscibility and dispersion with gaseous air, which is very helpful in proper combustion. Volumetric efficiency drops about 10% because of air displacement which is a major issue with CNG [28, 29], while cost, non-renewability and fuel placement are other barriers in adoption of CNG as a better fuel. Semin and Bakar [30] critically reviewed the technical studies on CNG as a fuel in IC engines and compared with gasoline and diesel as a fuel. The authors stated that CNG fuel is superior to gasoline and diesel in terms of fuel cost and GHG emissions. Aslam et al. [31] carried out a comparative analysis of gasoline and CNG fueled SI engine based on performance and emissions. The study revealed that CNG has higher efficiency, low fuel consumption and lower CO, HC and carbon dioxide emission compared to gasoline. Jahirul et al. [32] investigated a comparative analysis and stated that CNG fueled engine has better efficiency and low pollutants emission except NO_x. A comparison analysis between H_2 and CNG fuel in a SI engine has been done by Das et al. [33]. The study found higher thermal efficiency (31.19%) in case of hydrogen fuel compared to CNG (27.59%), and break specific fuel consumption was also less in hydrogen case.

Producer gas: Producer gas is a mixture of about 40% combustible gases (CO, H_2 and CH_4), and rest 60% are non-combustible (N_2, CO_2). The gas composition is mainly reliant on the biomass type and gasification conditions. The producer gas production has been done by using the gasification process in which solid biomass is transformed into producer gas, and further, the produced gas can be used in CI engines in dual-fuel mode or SI engine in 100% gas mode. Producer gas production from waste has gained tremendous publicity over the last few years. The use of waste biomass energy by gasification is not only cost effective but also environmentally sustainable [34]. Earlier, producer gas was an effective replacement of oil in IC engines but vanished after Second World War due to the techno-economic hindrances relative to cheap imported fuels. Again, in mid-1970s, the gasification technologies could gain the attention due to the increment in oil prices. Thus, biomass was capable to reduce the dependency on imported oil [35]. Additionally, it has environmental benefits like as GHG emission reduction and easy availability.

The hydrogen fuel-based engine has lot of attractive characteristics, but in high-load situations, premature ignition is a serious problem due to hydrogen's lesser ignition energy, shorter quenching distance and broader flammability range [36–38]. In case of producer gas-based engine, premature ignition is less serious problem since it contains 12–20% hydrogen [39]. Producer gas as a fuel have lot of advantages over other gaseous fuels. As instance, producer gas has better knock resistivity, low pollutants emission, better safety, lower cost of energy generation, renewable in nature, etc., and it has better octane rating in comparison with biogas and natural gas. Experimental analysis of a producer gas-based SI engine on the basis of performance, emission and combustion has been carried out by Hagos et al. [40]. The results show that heat release rate was higher in case of producer gas compared to CNG. However, brake thermal efficiency and fuel consumption rate were better than producer gas. The emission analysis revealed that emission of HC and CO from producer gas-fueled engine were enormously low at higher loads. Shah et al. [41] found 30–96% decrement in CO emission with producer gas compared to petrol and 54–94% lower NO_x emission in comparison with gasoline as a fuel, but there is need of enhancement in power output and exhaust heat recovery in producer gas-operated systems. Babu et al. [42] investigated an experimental analysis of modified SI engine with gasoline and producer gas. The study shows that producer gas-based system saves around 70% on fuel consumption compared to gasoline, and further, 5% reduction in energy consumption is achieved in fuel conversion examination. Producer gas-based IC engines are economically viable and could be a better option for electricity production in rural areas after some modifications in engines [43].

2 IC Engine Modification to Run on Producer Gas

IC engines are mostly used with downdraft gasifier, and lot of substantial research has been done for efficiency improvement and performance enhancement of producer gas-fueled IC engine. As a fuel, producer gas is a lower quality fuel than gasoline and natural gas. Therefore, engine needs to be marginally modified to operate on dual-fuel mode or 100% producer gas. Two different approaches could be applied to enhance the engine performance. One could boost the fuel quality by concentrating on raising the H_2 and CO content in fuel, which can be attained by advancement in gasifier design, combustion process and fuel (biomass) characteristics [44]. In another method, engine design could be modified to improve the use of producer gas.

The following important steps has to be performed to run a IC engine on producer gas:

Step 1: First, the diesel injection nozzles are replaced by spark plugs. The plugs are coupled to an ignition system, which controls the ignition timing and generates electricity to produce the spark.

Step 2: A gas train must be installed, connecting the thermal gasifier and the engine. The gas train will cut off the gas supply in case of an engine stop.
Step 3: Air and fuel must be mixed before entering the engine. This is normally done by a carburetor, which assures a homogeneous mixture and makes it possible to regulate the air–fuel ratio (λ).
Step 4: A gas carburetor is coupled to a constant pressure regulator, ensuring that the pressure of the gas from the gasifier is constant.
Step 5: An oxygen probe, which measures the oxygen content in the exhaust gases, must also be attached to the engine. When operating on producer gas, the oxygen content in the exhaust gases is an indirect indication of λ. The reason for this is that the composition of the producer gas varies, and the result is a shift in the heating value, the stoichiometric and the air consumption.
Step 6: For a precise control of λ, measurements of the gas composition must be made before the intake manifold, with subsequent adjustments of the root blower.
Step 7: For commercial plants, the oxygen probe is precise enough, and adjustments based on the gas composition are not necessary. Also, a governor, controlling the throttle valve through an actuator and a magnet pickup, needs to be installed. The governor control is only necessary during start-up, as the throttle valve will be fully open in case of producer gas.

In a diesel engine, the temperature of the air in the combustion chamber must be high enough, for the diesel to ignite. Generally, the compression ratio in diesel engines is very high—between 14:1 and 25:1. Most diesel engines are built with a compression ratio around 17:1–18:1, which is higher than for a petrol or natural gas engine. The compression ratio should be left unchanged in conversion of diesel engine (DG) to run on producer gas, since a high compression ratio improves the efficiency. Lot of literatures are available in which producer gas engines were operated at various CR. Dasappa et al. [45] investigated a 100 kW producer gas-operated SI engine with 1000 incessant hour running at 8.5 CR. The results revealed that the power output was 45% less, whereas the overall efficiency was found to be 18%.

Raman and Ram [46] have investigated a 100% producer gas-operated 75 kW power generator and found 21% overall power generation efficiency at 85% load. Sridhar et al. [47] transformed a CI engine to run on producer gas at 11.5–17:1 CR. The study reported 21% overall efficiency at CR 17:1 for a 24 kW power rating engine with reduction in power output by 17–19%. Homdoung et al. [48] converted a small CI engine to run on producer gas at CR 14:1 and achieved thermal efficiency around 19%. Table 1 shows some other studies related to diesel engine operated on 100% producer gas. The performance of producer gas-based IC engines depends on some key factors such as producer gas heating value, engine displaced volume, fuel octane number, air/fuel mixture flame speed, auto-ignition postponement time, engine CR ratio and spark timing.

Table 1 Studies on 100% producer gas-based IC engines

Biomass type	RPM	CR	Power (kW)	Spark timing	Exhaust gas temp. (°C)	Overall efficiency (%)	Ref
Wood	1500	11.5:1	12–16	35	360–430	21–24	[49]
Wood	1500	17:1	2.3	10	310–370	n.a	[50]
Coconut shell	1500	18.5:1	13.22	n.a	448.2	11.69	[51]
Wood	1500	17:1	17.5	6	n.a	16.6	[52]
Wood chips	n.a	n.a	15–20	n.a	n.a	25	[53]
Wood	1500 ± 50	11.5:1–17:1	15.3–17.5	n.a	n.a	18–21	[54]
Wood charcoal	1100–1900	9.7:1–17:1	3.2	35–45	n.a	11.5–21	[44]

3 Biomass Conversion Methods

Lot of conversion technologies are available for biomass resources for electrical and thermal energy applications, but broadly it could be studied under two different methods.

1. Rankine cycle (based on combustion)
2. Gasification.

The conversion technology processes selection depends on many factors, such as end-use applications, biomass type, technology cost, biomass quantity, environmental standards and energy conversion efficiency [55, 56].

3.1 Combustion Method

The systems based on combustion are most flexible, and it can be used for all forms of biomass resources including waste. Here, the biomass is combusted in a boiler for steam production, which is fed to the steam turbine, and finally, power is being generated with turbine rotation. The technology and component specification are very similar to the thermal power plant except for the boiler as shown in Fig. 1. Many methods have been established for biomass fired boilers based on the different types of biomass and plant sizes. Travelling grate (TG) is the most adaptable because all types of biomass could be used in this technology. However, fluidized-based combustion (FBC) has higher efficiency compared to TG, but FBC is extremely reactive to physical and chemical properties of the biomass fuel [57]. FBC could be a better choice for grainy biomass like woodchips, shells and rice husks because of

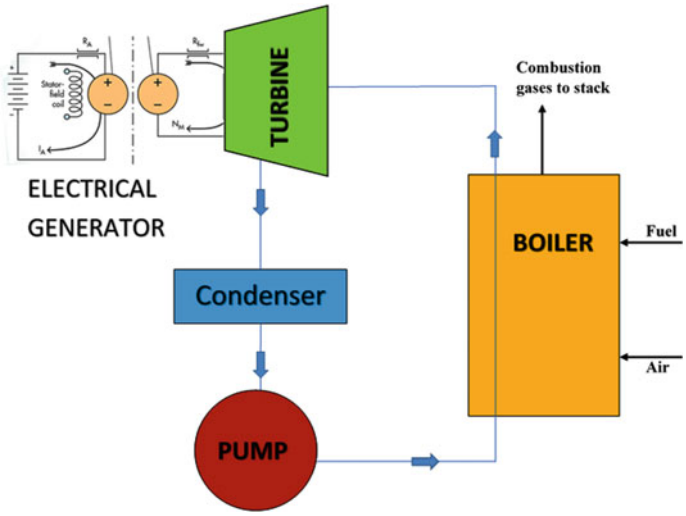

Fig. 1 Schematic diagram of Rankine cycle

their high efficiency performance, while the TG is basically used for other forms of biomass like leaves, stalks and straws, bagasse etc.

In most of the cases, the system size varies between 1 and 10 MW, but in the case of bagasse, the size strongly depends on cane-crushing capacity and bagasse quantity. The minimum size of the plant depends on the techno-economic analysis, whereas the maximum size is governed by fuel quantity availability within the area.

3.2 Gasification Technology

The gasification technology-based decentralized electricity generation system sizes could be few kilowatts to 1 megawatt. In biomass gasification process, a partial biomass combustion under controlled air flow results in a mixture of gases normally identified as producer gas as shown in Fig. 2. In first step of this process, raw biomass or pretreated biomass is fed to gasifier and remove moisture. In second stage, low moisture biomass goes through the gasification process (described in next section) with the help of various types of gasifiers (fixed bed and fluidized bed). The final generated producer gas is fed to a gas-cleaning chamber to remove the unwanted contents from producer gas. In final stage, the producer gas is supplied to IC engine after cooldown of the gas temperature with the help of gas cooler chamber, and finally, electricity is generated for end user. Power plants usually utilize the locally available biomass which not only reduce the fuel management cost but also decrease the transportation cost and GHG emission. The biomass gasifier can be operated in grid-integrated system as well as off-grid systems for power generation to supply

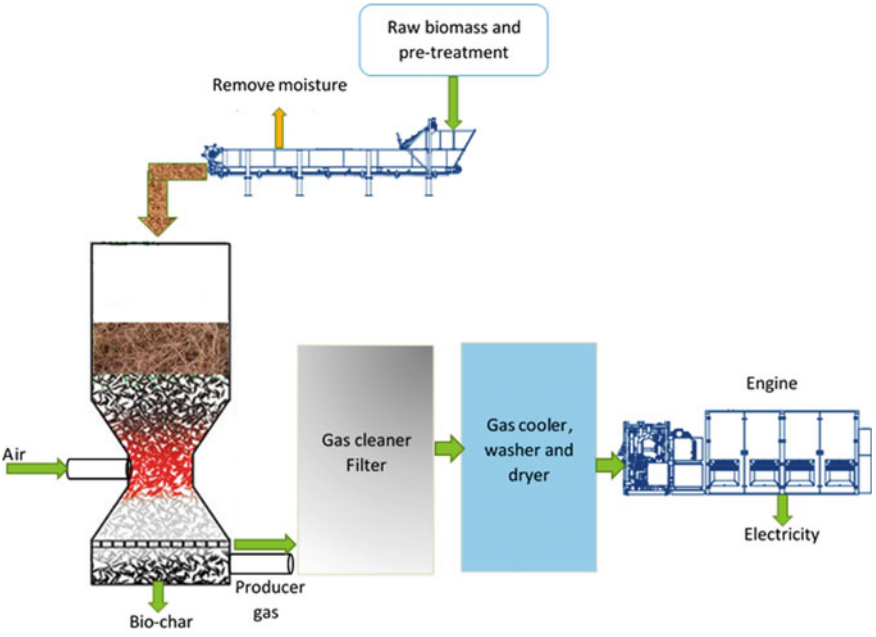

Fig. 2 Schematic of biomass gasifier power generation system

electricity in various industries for different applications and rural electrification [58, 59].

3.3 Producer Gas Production Plants

The producer gas is produced as a result of thermochemical transformation of dry hydrocarbon-containing biomass. The gasification process is accomplished in an air-sealed closed chamber. The complete process has been explained in this section. Figure 3 shows the general execution steps of gasification.

Gasification is a thermochemical method which is quite complicated, and it is not practical to break the gasifier into purely different regions, but still it is necessary for better understanding conceptually. In this process, different stages (shown in Fig. 3) happen at the same time in various parts of gasifier. Different gasifier system is mainly differentiated based on air vent location in gasifier body to inject the air in fuel column. In gasification process, very first step is drying the wet biomass at 100–150 °C temperature to reduce the moisture level, and no biomass decomposition occurs at this stage. In next stage, pyrolysis occurs at temperature range of 150–700 °C, where thermal decomposition of dry biomass takes place in absence of oxygen. Three different forms, solid (charcoal), liquid (Tar) and gas (low heating value gas), are by-product of this stages, and the output percentage of individual

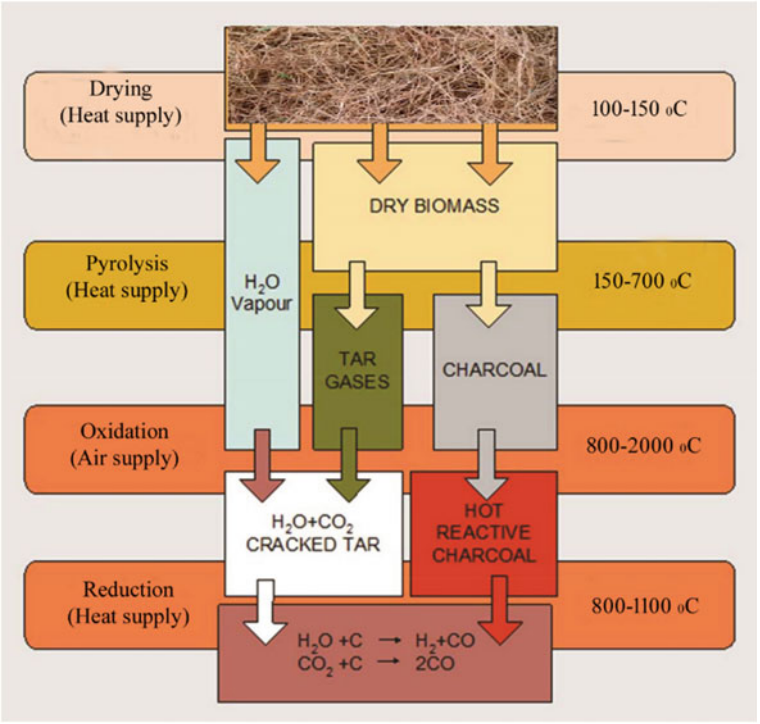

Fig. 3 Gasification process inside a gasifier chamber

product depends on the biomass chemical properties and operating conditions. In third stage, air is supplied from outside, and oxidation occurs at high temperature (800–2000 °C). Solid carbonized fuel reacts with oxygen present in air and produces the CO and steam which are also generated due to hydrogen reaction with supplied oxygen that present in air. Oxidation stage is responsible for complete combustion, which occurs when combustible gases mix with supplied oxygen. Next step is reduction, which is opposite to the oxidation stage. At this stage, four different reactions namely Boudouard, water–gas, water shift and methane production occur; in Boudouard reaction, carbon dioxide react with carbon and form carbon monoxide. In water gas reaction carbon reacts with steam and produces CO and H_2. These two reactions are endothermic reaction (take heat), while other two reactions are exothermic (release heat) in which it removes water vapors (water shift) and produces methane (methane production).

3.4 Types of Biomass Gasification Systems

Various types of technology are used in gasification process to improve the efficiency and increment in producer gas production, as illustrated in Fig. 4. In general, both fixed-bed and fluidized-bed technologies are used for the gasification of biomass, while indirect heating technology is still under development.

3.4.1 Fixed-Bed Gasifier

In this technology, the biomass is fed from top by using a hopper, and it moves from top to down, during which the biomass is converted into gases. The gasifiers are distinguished on the behalf of air and producer gas flow direction in the gasification chamber. These types of gasifiers are capable to handle a moderate moisture and ash content type fuel. The basic properties of biomass fuel, which can be used in these types of gasifier, are given in Table 2. Fixed-bed gasifiers include updraft and downdraft designs. These have distinctive operating characteristics.

Fig. 4 Different biomass gasification technologies

Table 2 Fuel characteristics in fixed-bed gasifier [60]

Description	Range
Fuel dimensions	5–100 mm
Fuel moisture content	<60%
Ash content (weight %)	<6%
Operating temperature	800–1200 °C
Turn down ratio	4:1
GCV of gas	3–5 MJ/kg
Gas composition	Producer gas

Updraft Gasifiers

This is also defined as counterflow gasification. The updraft design is the ancient and user-friendly structure of gasifier, which is mostly used in coal gasification. The updraft gasifier has specifically described all gasification zones such as partial combustion, reduction and pyrolysis. The biomass is fed from the reactor top, and a grate is positioned at the reactor base to protect the reacting pad. Under the grate, air or oxygen and/or steam are added and diffused into the biomass bed and char. The entire char combustion occurs at the bed bottom, producing CO_2 and H_2O. Such high temperature gases (~1000 °C) travel thru the bed above and decreased to H_2 and CO and condensed to 750 °C. The sensible heat from the hot gas is used in pyrolyzing the dry biomass and drying the entering wet biomass. The advantages and disadvantages of this technology has been described in Table 4.

Downdraft Gasifier

This is also identified as co-current flow gasification, and the downdraft gasifier has the similar mechanical design as the updraft gasifier apart from the oxidant and product gases flow, which flow down the reactor (same as biomass path). A main modification is that such a method can combust up to 99.9% of the tars produced. In the reaction zone at the top of the reactor, low moisture biomass (<20%) and air or oxygen are ignited. The flame produces pyrolysis gas/vapor, which burns vigorously having left 5–15% char and hot combustion gas. The produce gases move down and react to char at 800–1200 °C, generate additional CO and H_2 and then cool down to lower 800 °C. Finally, unreacted char and ash slip into the bottom of the grate, which are sent to disposal. This type of gasifier is most appropriate for integration with IC engines to achieve the better efficiency and power output. The advantages and disadvantages are described in Table 4. The schematics of updraft and downdraft is shown in Fig. 5a, b, respectively.

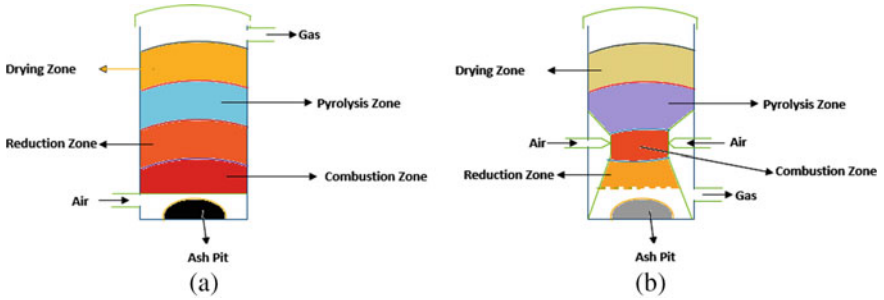

Fig. 5 **a** Schematic of updraft gasifier, **b** Schematic of downdraft gasifier

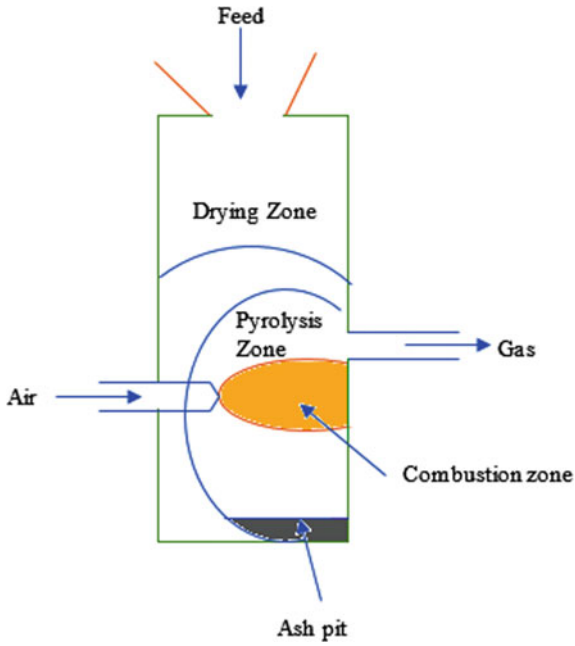

Fig. 6 Schematic of cross-draft gasifier

Cross-Draft Gasifier

The cross-draft gasifier has some drawbacks such as higher temperature of exit gas, least efficient for CO_2 reduction and higher gas velocity. It has isolated ashbin, fire and reduction zone as shown in Fig. 6. The cross-draft gasifier is more suitable for low ash and dry fuels like as wood, coke and charcoal due to its designing characteristics. Cross-draft gasifier has very less starting time (5–10 min), and it also has better load-following ability. The emission reduction ability of such type of gasifiers is very less with reduction in hydrogen and methane content in output gas because of attained higher temperature (around 2000 °C).

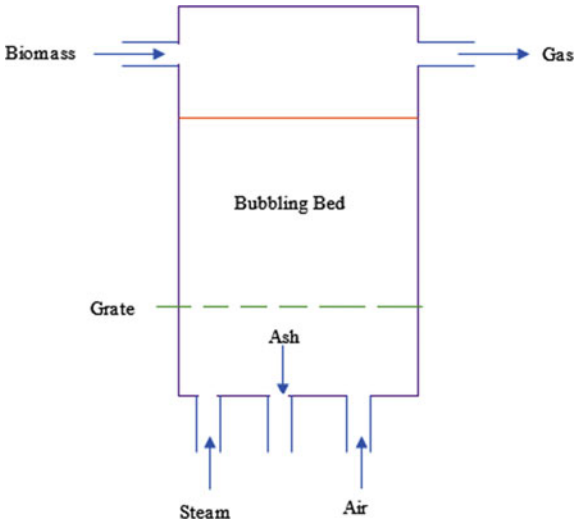

Fig. 7 Schematic of bubbling FBG

3.4.2 Fluidized-Bed Gasifier (FBG)

In such type of gasifier systems, biomass fuel is combusted in suspension mode and the fluidization process has been done with the help of air. This process mainly has two configurations.

Bubbling FBG

In bubbling FBG, air is inoculated from the bottom side of the gasifier as shown in Fig. 7, while the produced gases release from the top and biomass is introduced to the bubbling bed. The bubbling bed could be a bed of inert material (sand) or catalytic material like as CaO. It comprises of fine inactive particles of sand or alumina, which have been chosen for dimensions, density and thermal properties, and gasification has been occurred in suspension zone. The increment in heat and mass transfer among solid and gas is because of fluidization of biomass and bed material, which helps in gasification reactions and controlling of targeted temperature. It has good reaction rate and carbon conversion efficiency, but tar content is higher than downdraft gasifiers. These are suitable for medium-to-large-scale (25 MW) power generation plants.

Circulating FBG

Circulating FBG could be used in few MW to 100 MW biomass gasification process because of long residence time. Therefore, it can handle biomass with high volatile

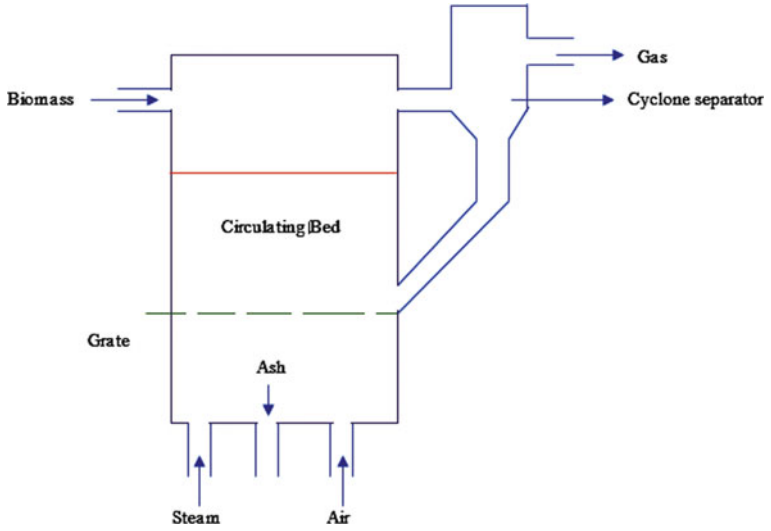

Fig. 8 Schematic of circulating FBG

Table 3 Fuel properties of FBG [60]

Description	Range
Fuel size	0.25–20 mm
Fuel moisture content	<20%
Ash content (weight %)	5–25%
Operating temperature	750–1000 °C
Turn down ratio	3:1
GCV of gas	5–6 MJ/kg
Gas composition	Producer gas

contents. In such type of gasifiers, the gasifying agent is fed from bottom side at higher speed (3.5–5.5 m/s) for proper mixing and move bed material in a circular loop. In this, biomass is fed from side, and entrained particles in the gas which eliminate from the reactor top are segregated in a cyclone and restored to the reactor as shown in Fig. 8. The designing of circulating FBG has some advantages over bubbling FBG such as better gas–solid contact, higher biomass heat rate, better efficiency and less tar production. Such type of gasifiers is reliable for a wide biomass range.

Circulating FBG works at gas rates greater than the lowest fluidization point, which is the cause of particle entrainment in the gas stream. The fuel properties, which can be used in these gasifiers, are described in Table 3.

The fixed-bed downdraft gasifiers are mainly used up to 1 MW plant size, while updraft is used for 1–10 MW. The fluidized-bed gasifiers are basically used in larger-scale gasification process. In electricity production at smaller stages, updraft and downdraft gasifiers are largely used.

Table 4 Advantages and drawbacks of down and upward gasifiers [61–63]

Technology	Advantages	Drawback
Updraft gasifier	Easy and low-cost method Higher moisture % range Established technology	Producer gas cleanup is required because it comprises 10–20% tar by weight Large quantities of tars in the product gas, which are susceptible to plugging the syngas pipe Required a tight control of feedstock particle size to assure a fixed bed of uniform void age It can form a slag in low melting-point ash-contained biomass
Downdraft gasifier	Less formation of tar NO need of a cyclone unit Established, easy in use and low-cost method Plant operation time is less (20–30 min) than updraft	Needed a low moisture biomass (<20%) Heat recovery system is required Around 4–7% unreacted carbon is got into ash pit
Crossdraft gasifier	Least design height Very quick response time to load Flexibility in gas production Can be operated for small-scale systems	High sensitive to slag formation Higher pressure drop Very sensitive to moisture content High exit gas temperature Less CO_2 reduction
Bubbling FBG	Mostly used in high scale applications Capable in production of higher heating value gases Flexibility in biomass feed size High velocity air is not required	Medium tar production Higher particle loading Less gasification efficiency Mixing is not good as circulating FBG
Circulating FBG	High gasification efficiency Less tar production Better mixing than bubbling FBG Less NO_x and SO_2 emission than bubbling FBG	Complex process control Required fuel particle size is less than bubbling FBG High velocity of gasifying agent required

The overall electricity generation cost of various gasification technologies sturdily depends on key parameters such as O&M cost, fuel cost, initial capital cost, interest rate and project life. Capital cost with overall cost of energy (COE) generation for different biomass power technologies is presented in Table 5 [64]. Only electricity generation from gasifiers is found to be more economical as compared to the gasifier CHP based systems. Therefore, gasifier electricity generation system is mostly used for small-scale power generation plants in rural areas, where raw biomass is an easily available at least cost [65].

Table 5 Economical details of different biomass power technologies

Technology	Capital cost ($/kW)	COE ($/kWh)
Fixed- and fluidized-bed gasifiers	2140–5700	0.07–0.024
Gasifier CHP	5570–6545	0.11–0.28
Digesters	2574–6104	0.06–0.15
Co-firing	140–850	0.04–0.13
Bubbling and circulating fluidized boilers	2170–4500	0.07–0.021

4 Simulated Case Study for Comparative Analysis

In this study, a comparative analysis of diesel engine and gasifier-integrated producer gas-based engine in stand-alone mode and hybrid mode has been carried out for electricity production.

4.1 Software Description

In the present study, hybrid optimization of multiple energy resources (HOMER) developed by NREL [66] is used for simulation. It is a micro-system simulation tool that can simulate both dual-fuel mode and 100% producer gas mode-based electricity generation system. HOMER simulates the system for 8760 h in a year and scales the results based upon total net present cost (TNPC). Additionally, sensitivity can also be performed to reveal how the outputs change according to the sensitivity inputs. Figure 9 presents a graphical depiction of HOMER with input and output parameters.

HOMERs Inputs

It needs six different types of data input for simulation and optimization process. First data is meteorological information (solar radiation, wind speed, humidity, temperature, etc.) of the plant location. This information is used for the power calculation of different energy generation units. Second data is load profile on hourly bases for the calculation of generators sizes. Load could be weekly and weekdays. Third data is equipment information, which includes power output at optimal condition, working temperature range, etc., next data is search space, which is defined by the user as per the requirement, and HOMER generates results according to the defined search space. Economical data of components is also needed to calculate the cost of the project, energy generation cost and other costs that occur during plant installation.

HOMER Outputs

After proving input data, it simulates the configuration for 1 year and shows the most optimum solution to user on the basis of least TNPC and COE. It also provides

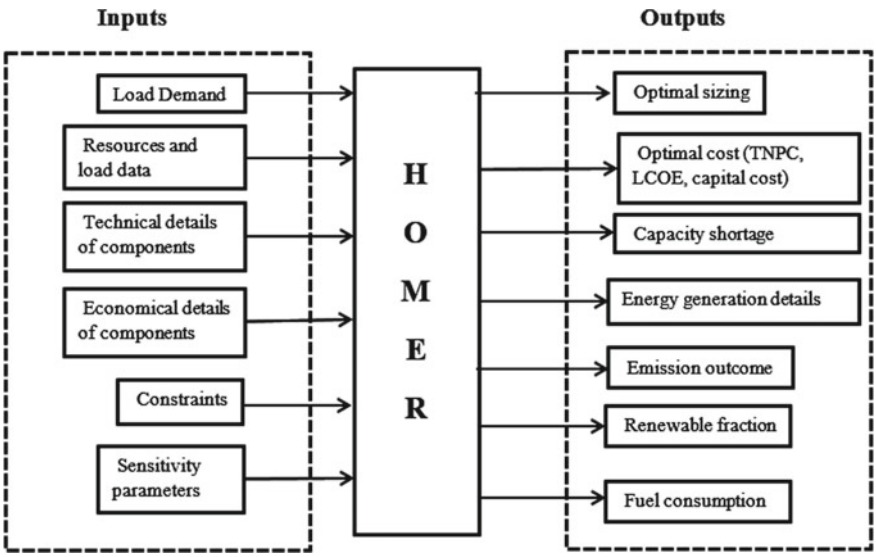

Fig. 9 Schematic representation of HOMER software

various other informations such as different components sizes, electricity generation information of individual component, initial investment, O&M cost, emission outcomes, renewable fraction in case of renewable resources-based energy system designing, capacity shortage and excess energy generation.

4.2 Fuel Properties

In the present study, pine needles are used as a biomass fuel in downdraft biomass gasifier, and the properties of pine needles are given in Table 6. Pine needles are forest wastage mostly produced in hilly regions, and about 76.2 lakh hectare of pine forest in Himalayan subtropical region is the largest in Indo-Pacific region. The shedding period of pine needles is from middle of March to end of July. The pine needles have high flammability due to resin content, and it is a major cause of forest fires in summer seasons because summer is the falling season of pine needles. Additionally, pine needles are also a reason of flora and fauna destruction with reduction in soil fertility [67]. It is not useful as a cattle feedstuff. Therefore, it has to be removed from forest floor to reduce the chances of forest fires, which further helps in reduction of environmental pollution and improvement in ecosystem.

Unutilized pine needles could be a better option for electricity generation by using gasifiers in rural areas. For example, Avani Bio Energy (NGO) setup a 9 kW pine needles based gasifier power plant in Uttarakhand to meet the energy demand of rural households and additionally provide employment to local peoples. Another 120 kW

Table 6 Properties of fuel (pine needles) used in biomass gasifier [68]

Parameters	Values	Parameters	Values
Carbon content	52.60%	*Physical properties*	
Calorific value	20 MJ/kg	Diameter (mm)	0.7–1.3
LHV	18.97 MJ/kg	Bulk density (kg/m^3)	1.808
Moisture content	9.76%	Length (mm)	170–250
Ash	1.31%	Mass (mg)	0.6
H	7%	*Chemical analysis (% by wt.)*	
O	40.40%	Lignin	33.4
		Holocellulose	67.3
		Extractives	15

power plant was setup by Avani Bio Energy, and pine needles are used as a fuel in gasifier. The plant was a grid-connected plant, which sold the energy to the state grid. Dhaundival and Gupta [67] stated that pine needles used in gasifiers would generate about 12.8% average CO_2 emission compared to emission in forest (15.46%), and further, it will also increase the fertility of soil.

In this chapter, Educational institute campus in Hamirpur, Himachal Pradesh, is considered as case study, and its forest covers around 58 hec. pine forest inside the campus. One hectare area of pine trees normally produce 11.9 ton pine needles per year [59]. Therefore, study location produces 690 tons pine needles per year at very cheaper price 14.57 $/ton.

4.3 Electrical Load Profile

To calculate the economic and technical analysis of both the systems, a real-time load data is required. Therefore, in this study, the hourly consumption details of the CEEE building were used for weekdays of a year. Most of the energy requirement for a typical weekday is between 9 a.m. and 6 p.m. The average daily load demand, mean energy demand, peak load demand and building load factor is 3.65 kW, 87.6 kWh/day, 29.2 kW and 0.125, respectively. Figure 10 shows the monthly trend of load requirements.

5 Producer Gas- and Diesel Fuel-Integrated Energy Systems

The electricity generation from producer gas is possible only with an IC engine after some modifications which are discussed in Sect. 2. The engine basically is used as

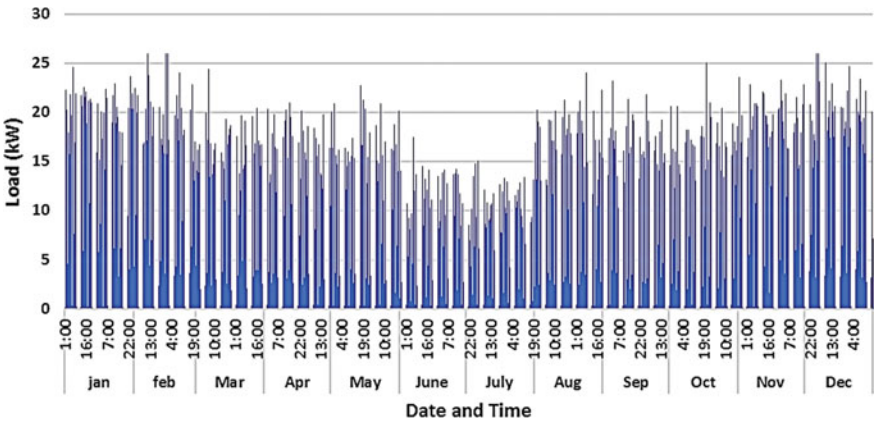

Fig. 10 Month-wise electric load profile of CEEE building

an intermediate system, which converts biochemical energy into mechanical energy. The stand-alone off-grid energy system with DG and BG is shown in Fig. 11. The goal of this study is to design and investigation of an optimized biomass-based energy system. The simulation has been done for four different cases based on resource data after providing the necessary input parameters. This section describes and discusses the technical and economical results of all four cases.

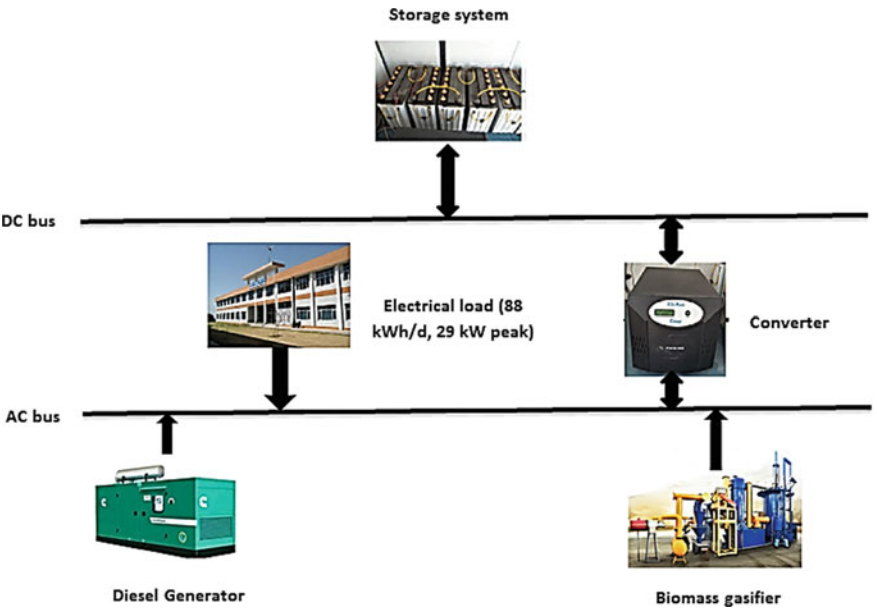

Fig. 11 Representation of a proposed energy system with different components

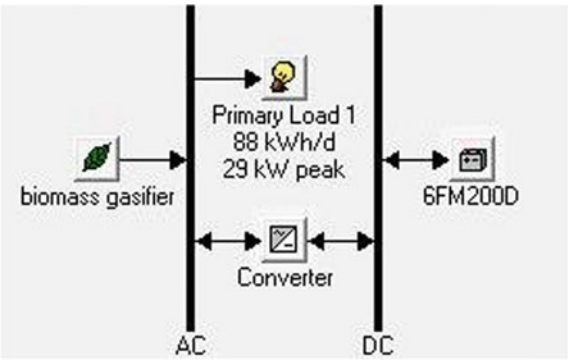

Fig. 12 Biomass-based off-grid energy system

5.1 Stand-Alone Cases

5.1.1 Case 1: BG System Only (Integrated with 100% Producer Gas-Based IC Engine)

In this case, downdraft BG energy system is used with battery to satisfy the total load demand as simulated with a range of parameters in HOMER. The optimal configuration of this case comprises of 16 kW biomass gasifier system, 20 units of 12 V, 200 Ah batteries and 16 kW converter. Figure 12 shows the schematic of case 1. The TNPC of this combination was found to be $78,964 at COE 0.192 $/kWh.

5.1.2 Case 2: DG Only (100% Diesel-Based System)

In this case, DG with battery is used to fulfill the load requirement of study area, and the optimum configuration consists of 15 kW DG, 11 kW converter and 30 units of 12 V, 200 Ah batteries. Figure 13 shows the schematic of case 2. The TNPC was found to be $205,615 at COE 0.501 $/unit.

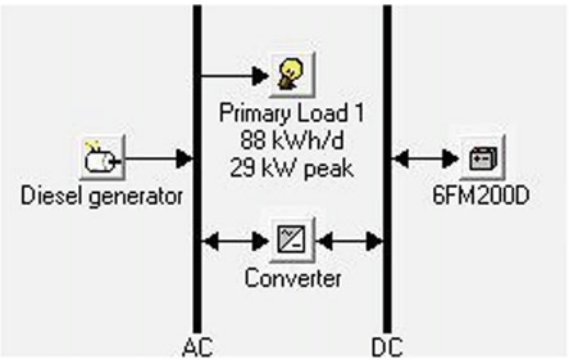

Fig. 13 DG based off-grid energy system

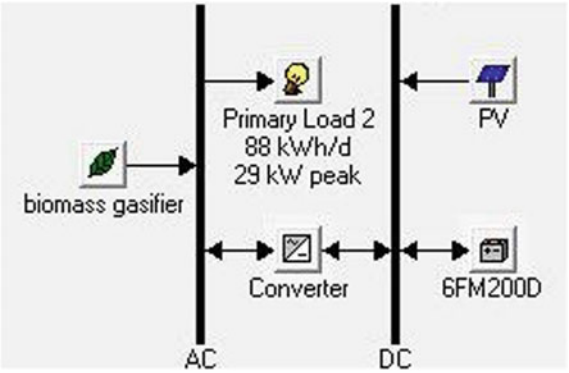

Fig. 14 PV/BM off-grid hybrid energy system

5.2 Hybrid Energy Systems Cases

5.2.1 Case 3: PV/BM Hybrid System

The optimum combination of this case consists of 13 kW PV, 13 kW biomass gasifier, 20 no. of 12 V batteries and 14 kW converter. Figure 14 shows the schematic of case 3. The TNPC of this combination is $76,080 at the LCOE $ 0.185 per unit.

5.2.2 Case 4: PV/DG Hybrid System

The most favorable combination of this case consists of 42 kW PV array, 13 kW DG, 30 no. of 12 V batteries and 24 kW converter. The TNPC and LCOE of this combination have been estimated as $129,081 and 0.314 $/kWh, respectively, for RF 0.86. Figure 15 shows the schematic of PV/DG hybrid energy system.

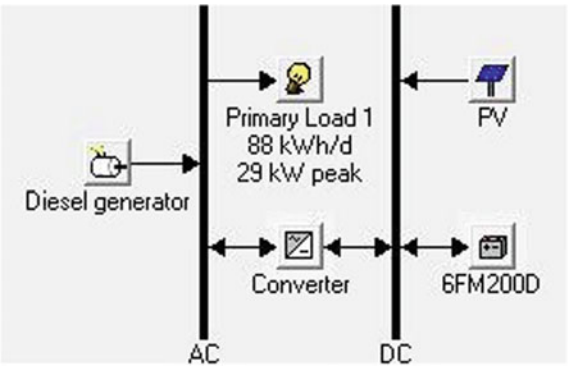

Fig. 15 PV/DG hybrid off-grid energy system

Table 7 Relative simulation results of stand-alone configurations with battery storage

Parameters	Case1 (BG/Batt.)	Case2 (DG/Batt.)
BG (kW)	16	0
DG (kW)	0	15
Battery	20	30
Converter (kW)	16	11
Initial capital cost ($)	28,240	19,297
Operating cost ($/YEAR)	3949	14,506
TNPC ($)	78,964	205,615
COE ($/kWh)	0.192	0.501
Diesel (l/year)	0	10,563
Biomass (ton/year)	17	0
BG (hours)	2546	0
DG (hours)	0	2579
Total generation (kWh/year)	33,836	34,015
Renewable fraction (%)	100	0
Losses in battery (kWh/year)	1275	1392
Annual battery throughput (kWh/year)	5745	6271

5.3 Technical and Economic Analysis

The simulation results of optimal configurations in stand-alone and hybrid cases are given in Tables 7 and 8. It has been observed from the analysis that configuration of case 1 and case 3 offers the lowest COE, TNPC, operating cost and battery storage in stand-alone and hybrid configurations, respectively.

5.4 Stand-Alone Cases Analysis (Case 1 & 2)

Technically, the optimal configuration of diesel-based engine required a larger number of battery units compared to 100% producer-based system, but it would require a small size power generator. Therefore, the battery numbers will affect the initial investment, which is found least in case 1. Capacity shortage value was also found less in biomass case as compared to case 2. Therefore, case 1 is found more suitable with technical point of view. Figures 16 and 17 show the yearly power generation variation of BG and DG in stand-alone mode with energy demand and SOC of battery bank variation. The battery bank mainly used in two cases

(1) Fulfill the load demand, which is not meet out by main generation units (BG or DG).

Table 8 Relative simulation results of hybrid configurations with battery storage

Parameters	Case 3 (PV/BG/Batt.)	Case 4 (PV/DG/Batt.)
PV (kW)	13	42
BG (kW)	13	0
DG (kW)	0	13
Battery	20	30
Converter (kW)	14	24
Initial capital cost ($)	34,154	50,927
Operating cost ($/Year)	3264	6085
TNPC ($)	76,080	129,081
COE ($/kWh)	0.185	0.314
Diesel (l/year)	0	2661
Biomass (ton/year)	12	0
BG (hours)	2268	0
DG (hours)	0	734
Total generation (kWh/year)	38,310	59,487
Renewable fraction (%)	100	86
Losses in battery (kWh/year)	996	1560
Annual battery throughput (kWh/year)	4462	7358

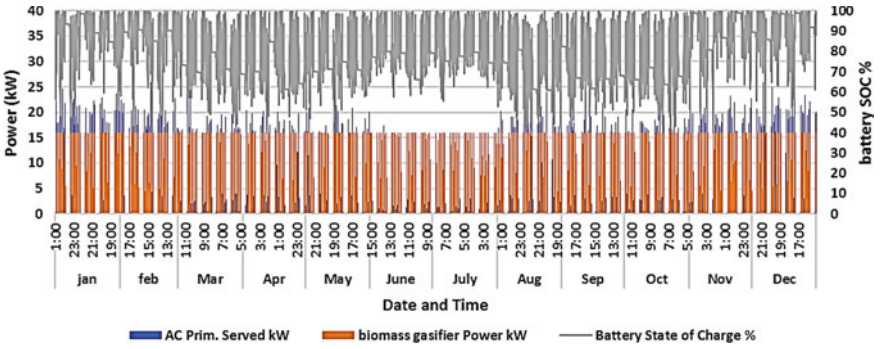

Fig. 16 Yearly power generation profile with primely served load and battery SOC in case 1

(2) If load demand is deficient and it can be fulfilled by battery bank only, then the main unit will not start and the only battery bank will be used.

The battery SOC variation is also found less (50–100%) in case 2, while in case 1, it was 40–100%. It means battery life would be higher in case 2 because most of the time the load demand is fulfilled through DG. The SOC variation has been found lower (45–100% and 50–100% in BG and DG cases, respectively) in summer seasons because of different load profiles during these seasons.

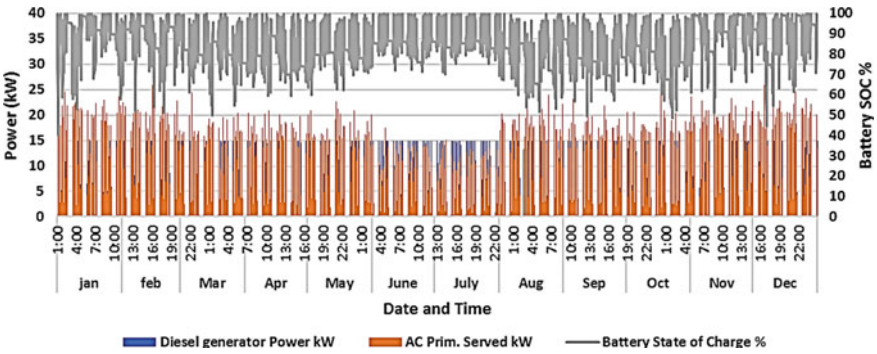

Fig. 17 Yearly power generation profile with primely served load and battery SOC in case 2

From economical point of view, case 1 is found to be the most appropriate because the overall generation cost in BG case is much lower than case 2. The cash flow summary of both the cases has been shown in Figs. 18 and 19. In case 2, initial capital cost is found around 31% lower than BG case, but the O&M cost was 73% higher compared to case 1 because of higher fuel price and larger number of battery units. Finally, the overall total net present cost of case 1 is obtained around 62% lower than case 2 at an estimated COE 0.192 $/kWh. Therefore, case 1 is the best configuration economically as compared to case 2.

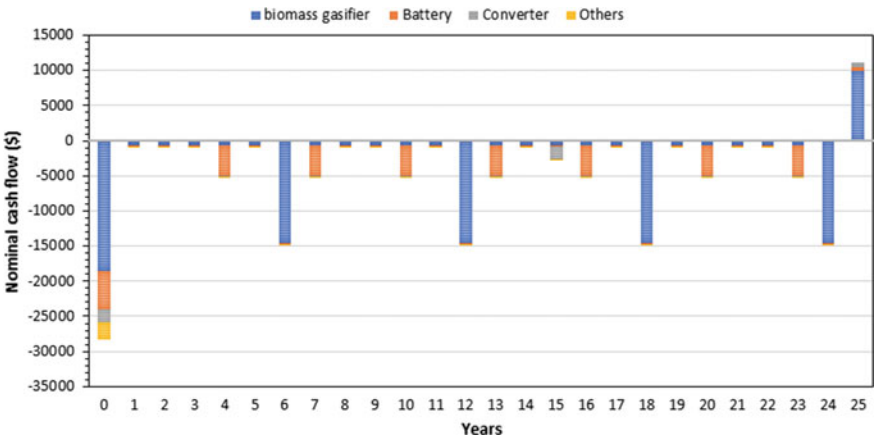

Fig. 18 Cash flow summary for 25 years in case 1

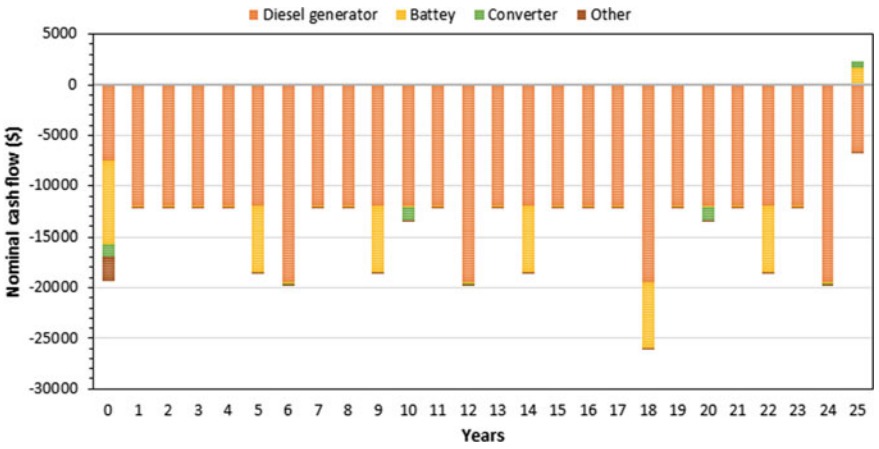

Fig. 19 Cash flow summary for 25 years in case 2

5.5 Hybrid Cases Analysis (Case 3 & 4)

In case of hybrid energy system, solar PV is integrated with BG and DG units because of its wide availability at every location worldwide. In case of DG based hybrid systems, large number of batteries will be required, which additionally increase the initial cost of the system. According to the comparison Table 8, DG based hybrid system requires large capacity solar PV (46 kW) to meet out the load demand. Therefore, large installation area will be required to setup this plant as compared to case 3 (BM/PV). From storage point of view, loss per annum was found to be higher in DG case, while battery loss was minimum in case 3 with less amount of excess energy. In case of hybrid system, the consumption of biomass also reduces from 17 ton/year to 12 ton/year, which further reduces the overall COE of the system. Therefore, technically as well as economically biomass-based stand-alone or hybrid system is more optimal solution for electricity generation. Figures 20 and 21 show the yearly power generation variation of cases 3 and 4, respectively, with energy demand and SOC of battery bank variation. The storage unit mostly is required in cloudy or night hours, when sun radiation is not available. The variation of SOC is found higher in the case of DG hybrid, which affects the battery life.

Case 3 was the winner from economical point of view in hybrid as well as stand-alone cases. The 25 years' cash flow summary in cases 3 and 4 is shown in Figs. 22 and 23, respectively. In case of BG hybrid, there is a need of gasifier and battery unit replacement after its lifetime. Therefore, cash flow diagram shows a replacement cost occurs regularly in biomass gasifier and battery. While initial investment in case 4 is more than 3 because of larger capacity of PV power plant, overall cost is also higher than case 3 due to higher fuel cost (diesel cost). The normalized daily average power generation units from DG and BG are also shown in Fig. 24, where DG generates higher units per day compared to biomass gasifier.

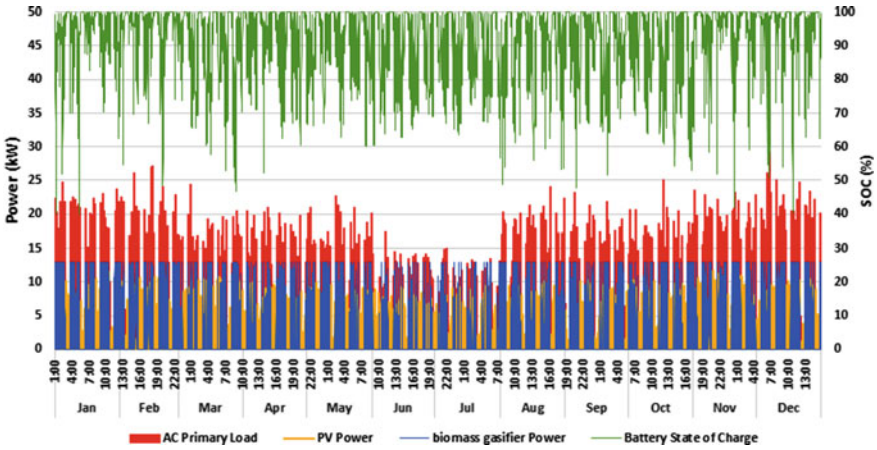

Fig. 20 Yearly power generation profile with primely served load and battery SOC in case 3

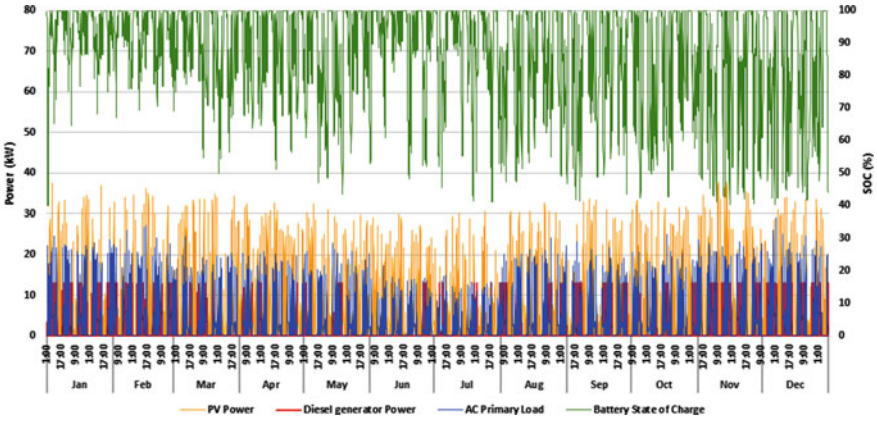

Fig. 21 Yearly power generation profile with primely served load and battery SOC in case 4

5.6 Environment and Social Analysis

In the environmental analysis, the annual CO_2 emissions in both the cases have been calculated. In case 1, pine needles is fed as a fuel in biomass gasifier system, and biomass is a carbon-neutral fuel. Therefore, in this case, the CO_2 emission is found very less as 3.5 Mt/year. In case 2, diesel is used as a fuel in DG, and the CO_2 emission is found around 84% (28.3 Mt/year) which is higher than case 1. In social aspect, biomass-based energy systems would generate more employment for local peoples, which will improve their living standards. Overall with environmental and social analysis, it has been observed that biomass-based cases are more favorable compared to DG based cases.

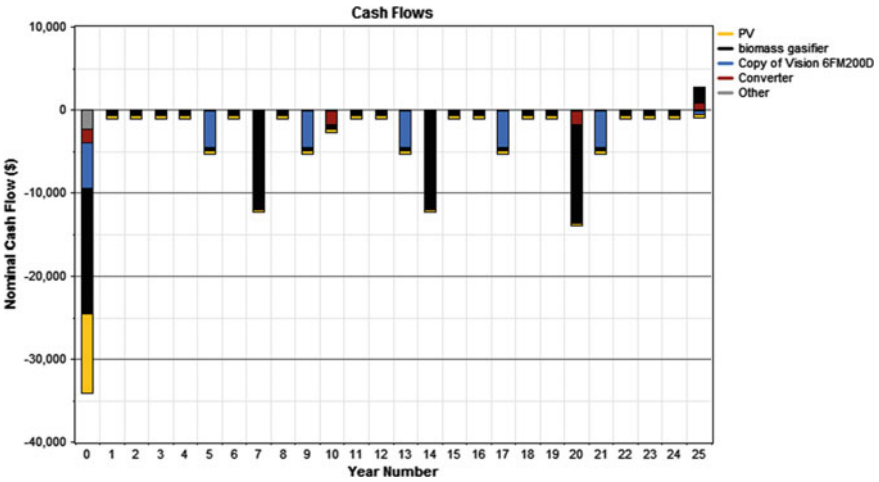

Fig. 22 Cash flow summary for 25 years in case 3

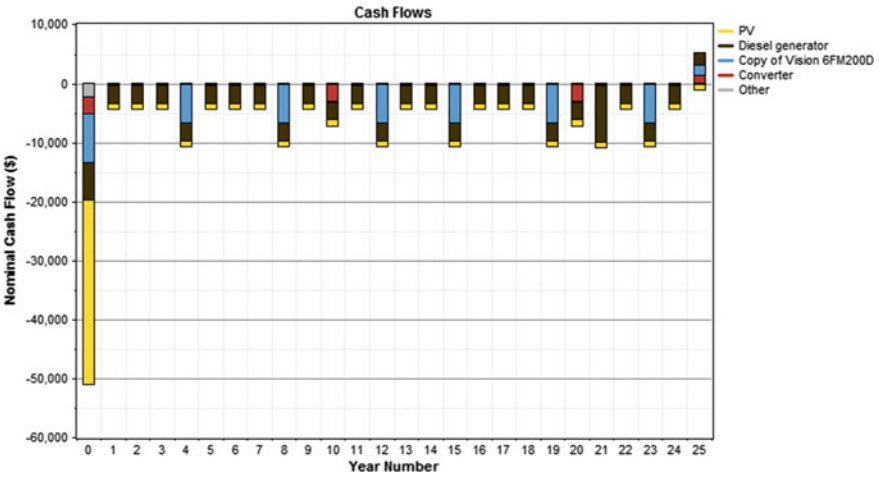

Fig. 23 Cash flow summary for 25 years in case 4

6 Conclusions

In this study, techno-economic and environmental analysis of biomass gasifier and diesel generator-based energy system has been carried out. In biomass gasifier, unutilized locally available pine needles are used as a fuel in biomass gasifier. The overall analysis shows that biomass gasifier is a wise selection as a main energy generation system or backup system in biomass-rich areas benefitting environment as well as economic and social aspects. The biomass gasifier energy system's overall COE and

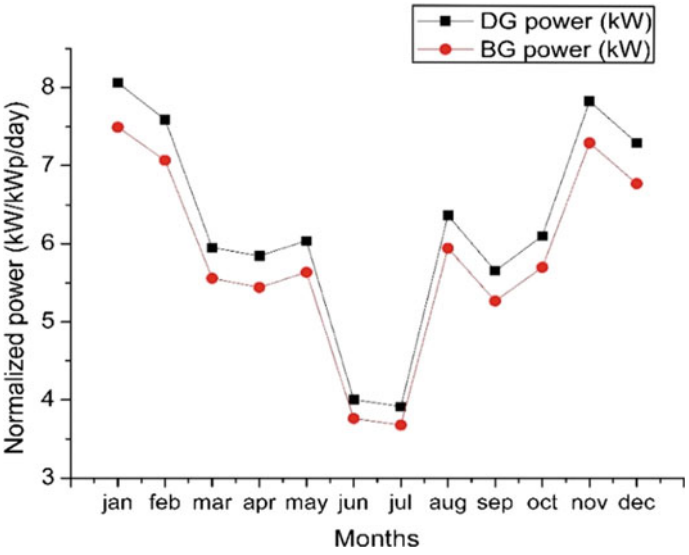

Fig. 24 Normalized daily power generation of BG and DG systems

TNPC in stand-alone mode are found to be 62% lower (0.192 $/kWh, 78,964 $) than diesel-based energy generation system (0.501 $/kWh, 205,615 $), while hybrid system further reduces the COE up to 3–4% (0.185 $/kWh) in BG hybrid case. Case 3 was the most optimal case with least COE and TNPC among all (stand-alone and hybrid) from technical and economical point of view.

The practical use of unutilized biomass for energy generation by using gasifier will not only aid in protecting the environment, but also will help achieve the renewable energy goals of the country. Decentralized biomass energy systems can play a significant role in electrification purpose because of their higher reliability, low generation costs and environmental friendly nature.

References

1. Renewables 2017 Global Status Report, www.REN21.net.
2. Makhija, S. P., & Dubey, S. P. (2019). Feasibility analysis of biomass-based grid-integrated and stand-alone hybrid energy systems for a cement plant in India. *Environment, Development and Sustainability, 21*(2), 861–878.
3. Parihar, A. K., Sethi, V., & Banerjee, R. (2019). Sizing of biomass based distributed hybrid power generation systems in India. *Renewable Energy, 134,* 1400–1422.
4. Garrido, H., Vendeirinho, V., & Brito, M. C. (2016). Feasibility of KUDURA hybrid generation system in Mozambique: Sensitivity study of the small-scale PV-biomass and PV-diesel power generation hybrid system. *Renewable Energy, 92,* 47–57.

5. Sava, G. N., Ionescu, G., Necula, H., Scripcariu, M., Duong, M.Q., Leva, S., & Mussetta, M. (2017). Efficiency analysis of a hybrid power system for a campus in Romania. In *2017 IEEE International Conference on Environment and Electrical Engineering and 2017 IEEE Industrial and Commercial Power Systems Europe (EEEIC/I&CPS Europe)* (pp. 1–5). IEEE.
6. Barrozo Budes, F., Cardenas Escorcia, Y., & Valencia, O. G. (2017). Biomass generator to reduce the gas emission and operation cost in a grid-connected renewable energy systems. *International Journal of ChemTech Research, 10,* 311–316.
7. Cummins, C., Jr. (1976). Early IC and automotive engines. *SAE Transactions, 85*(SAE Paper No. 760604), 1960–1971.
8. Saravanan, N., & Nagarajan, G. (2008). An experimental investigation of hydrogen-enriched air induction in a diesel engine system. *International Journal of Hydrogen Energy, 33*(6), 1769–1775.
9. Priyam, A., Chand, P., & Lata, D. B. (2019). Effect of hydrogen and producer gas addition on the performance and emissions on a dual-fuel diesel engine. In *Advanced Engine Diagnostics* (pp. 29–56). Singapore: Springer.
10. Sharma, P., & Dhar, A. (2019). Particulate emissions from hydrogen diesel fuelled CI engines. In *Engine exhaust particulates* (pp. 199–211). Singapore: Springer.
11. Ji, C., & Wang, S. (2011). Effect of hydrogen addition on lean burn performance of a spark-ignited gasoline engine at 800 rpm and low loads. *Fuel, 90*(3), 1301–1304.
12. Karagöz, Y., Güler, İ, Sandalcı, T., Yüksek, L., & Dalkılıç, A. S. (2016). Effect of hydrogen enrichment on combustion characteristics, emissions and performance of a diesel engine. *International Journal of Hydrogen Energy, 41*(1), 656–665.
13. Hernández, J. J., Lapuerta, M., & Barba, J. (2016). Separate effect of H_2, CH_4 and CO on diesel engine performance and emissions under partial diesel fuel replacement. *Fuel, 165,* 173–184.
14. Wang, S., Ji, C., & Zhang, B. (2010). Effects of hydrogen addition and cylinder cutoff on combustion and emissions performance of a spark-ignited gasoline engine under a low operating condition. *Energy, 35*(12), 4754–4760.
15. Pohare, J. Y. O. T. I., Pandey, K. C., & Mahalle, D. M. (2010). Improve the operation of IC engine with 100% biogas as fuel. *Engineering and Technology in India, 1*(2), 56–60.
16. Yoon, S. H., & Lee, C. S. (2011). Experimental investigation on the combustion and exhaust emission characteristics of biogas–biodiesel dual-fuel combustion in a CI engine. *Fuel Processing Technology, 92*(5), 992–1000.
17. Walsh, J. L., Ross, C. C., Smith, M. S., & Harper, S. R. (1989). Utilization of biogas. *Biomass, 20*(3–4), 277–290.
18. Chandra, R., Vijay, V. K., Subbarao, P. M. V., & Khura, T. K. (2011). Performance evaluation of a constant speed IC engine on CNG, methane enriched biogas and biogas. *Applied Energy, 88*(11), 3969–3977.
19. Jung, C., Park, J., & Song, S. (2015). Performance and NOx emissions of a biogas-fueled turbocharged internal combustion engine. *Energy, 86,* 186–195.
20. Makareviciene, V., Sendzikiene, E., Pukalskas, S., Rimkus, A., & Vegneris, R. (2013). Performance and emission characteristics of biogas used in diesel engine operation. *Energy Conversion and Management, 75,* 224–233.
21. de Faria, M. M. N., Bueno, J. P. V. M., Ayad, S. M. E., & Belchior, C. R. P. (2017). Thermodynamic simulation model for predicting the performance of spark ignition engines using biogas as fuel. *Energy Conversion and Management, 149,* 1096–1108.
22. Tira, H. S., Herreros, J. M., Tsolakis, A., & Wyszynski, M. L. (2012). Characteristics of LPG-diesel dual fuelled engine operated with rapeseed methyl ester and gas-to-liquid diesel fuels. *Energy, 47*(1), 620–629.
23. Oguma, M., Goto, S., Sugiyama, K., Kajiwara, M., Mori, M., Konno, M., & Yano, T. (2003). Spray characteristics of LPG direct injection diesel engine (No. 2003-01-0764). SAE Technical Paper.
24. Selim, M. Y., Al-Omari, S. B., & Al-Aseery, A. A. (2009). Effects of steam injection to dual fuel engine on performance, noise and exhaust emission (No. 2009–01–1831). SAE Technical Paper.

25. Ngang, E. A., & Abbe, C. V. N. (2018). Experimental and numerical analysis of the performance of a diesel engine retrofitted to use LPG as secondary fuel. *Applied Thermal Engineering, 136,* 462–474.
26. Saleh, H. E. (2008). Effect of variation in LPG composition on emissions and performance in a dual fuel diesel engine. *Fuel, 87*(13–14), 3031–3039.
27. Ashok, B., Ashok, S. D., & Kumar, C. R. (2015). LPG diesel dual fuel engine—A critical review. *Alexandria Engineering Journal, 54*(2), 105–126.
28. Prasad, R. K., Kar, T., & Agarwal, A. K. (2019). Prospects and challenges for deploying direct injection technology for compressed natural gas engines. In *Natural gas engines* (pp. 117–141). Singapore: Springer.
29. Geok, H. H., Mohamad, T. I., Abdullah, S., Ali, Y., Shamsudeen, A., & Adril, E. (2009). Experimental investigation of performance and emission of a sequential port injection natural gas engine. *European Journal of Scientific Research, 30*(2), 204–214.
30. Semin, R. A. B. (2008). A technical review of compressed natural gas as an alternative fuel for internal combustion engines. *American Journal of Engineering and Applied Sciences, 1*(4), 302–311.
31. Aslam, M. U., Masjuki, H. H., Kalam, M. A., Abdesselam, H., Mahlia, T. M. I., & Amalina, M. A. (2006). An experimental investigation of CNG as an alternative fuel for a retrofitted gasoline vehicle. *Fuel, 85*(5–6), 717–724.
32. Jahirul, M. I., Masjuki, H. H., Saidur, R., Kalam, M. A., Jayed, M. H., & Wazed, M. A. (2010). Comparative engine performance and emission analysis of CNG and gasoline in a retrofitted car engine. *Applied Thermal Engineering, 30*(14–15), 2219–2226.
33. Das, L. M., Gulati, R., & Gupta, P. K. (2000). A comparative evaluation of the performance characteristics of a spark ignition engine using hydrogen and compressed natural gas as alternative fuels. *International Journal of Hydrogen Energy, 25*(8), 783–793.
34. Mukunda, H. S., Dasappa, S., & Shrinivasa, U. (1993). Open-top wood gasifiers. In *Renewable energy—Sources for fuels and electricity* (pp. 699–728). Island Press.
35. Mohan, D., Pittman, C. U., Jr., & Steele, P. H. (2006). Pyrolysis of wood/biomass for bio-oil: A critical review. *Energy & Fuels, 20*(3), 848–889.
36. Gopal, G., Srinivasa Rao, P., Gopalakrishnan, K. V., & Murthy, B. S. (1982). Use of hydrogen in dual-fuel engines. *International Journal of Hydrogen Energy, 7*(3), 267–272 (1982).
37. Li, J. D., Lu, Y. Q., & Du, T. S. (1986). Improvement on the combustion of a hydrogen fueled engine. *International Journal of Hydrogen Energy, 11*(10), 661–668 (1986).
38. Karim, G. A. (2003). Hydrogen as a spark ignition engine fuel. *International Journal of Hydrogen Energy, 28*, 569–577.
39. Anon. (1986). Wood gas as engine fuel. A Report of the Mechanical Wood Products Branch of FAO Forestry, Food and Agriculture Organization of United Nations, Rome.
40. Hagos, F. Y., Aziz, A. R. A., & Sulaiman, S. A. (2014). Syngas (H_2/CO) in a spark-ignition direct-injection engine. Part 1: Combustion, performance and emissions comparison with CNG. *International Journal of Hydrogen Energy, 39*(31), 17884–17895.
41. Shah, A., Srinivasan, R., To, S. D. F., & Columbus, E. P. (2010). Performance and emissions of a spark-ignited engine driven generator on biomass based syngas. *Bioresource Technology, 101*(12), 4656–4661.
42. Babuak, M. S., Clementb, S., & Rajanc, N. K. S. (2016). Fuel Conversion benefit of producer gas over gasoline—An experimental analysis. *Energy Procedia, 100,* 203–209.
43. Yaliwal, V. S., Banapurmath, N. R., Gireesh, N. M., & Tewari, P. G. (2014). Production and utilization of renewable and sustainable gaseous fuel for power generation applications: A review of literature. *Renewable and Sustainable Energy Reviews, 34,* 608–627.
44. Jaojaruek, K., Jarungthammachote, S., Gratuito, M. K. B., Wongsuwan, H., & Homhual, S. (2011). Experimental study of wood downdraft gasification for an improved producer gas quality through an innovative two-stage air and premixed air/gas supply approach. *Bioresource Technology, 102*(7), 4834–4840.
45. Dasappa, S., Subbukrishna, D. N., Suresh, K. C., Paul, P. J., & Prabhu, G. S. (2011). Operational experience on a grid connected 100 kWe biomass gasification power plant in Karnataka, India. *Energy for Sustainable Development, 15*(3), 231–239.

46. Raman, P., & Ram, N. K. (2013). Performance analysis of an internal combustion engine operated on producer gas, in comparison with the performance of the natural gas and diesel engines. *Energy, 63,* 317–333.
47. Sridhar, G., Sridhar, H. V., Dasappa, S., Paul, P. J., Rajan, N. K. S., & Mukunda, H. S. (2005). Development of producer gas engines. *Proceedings of the Institution of Mechanical Engineers, Part D: Journal of Automobile Engineering, 219*(3), 423–438.
48. Homdoung, N., Tippayawong, N., & Dussadee, N. (2014). Effect of ignition timing advance on performance of a small producer gas engine. *International Journal of Applied Engineering Research, 9*(13), 2341–2348.
49. Tinaut, F. V., Melgar, A., Horrillo, A., & De La Rosa, A. D. (2006). Method for predicting the performance of an internal combustion engine fuelled by producer gas and other low heating value gases. *Fuel Processing Technology, 87*(2), 135–142.
50. Reed, T. B., & Das, A. (1988). *Handbook of biomass downdraft gasifier engine systems.* Biomass Energy Foundation.
51. Garcia-Bacaicoa, P., Bilbao, R., Arauzo, J., & Salvador, M. L. (1994). Scale-up of downdraft moving bed gasifiers (25–300 kg/h)—Design, experimental aspects and results. *Bioresource Technology, 48*(3), 229–235.
52. Kirubakaran, V., Sivaramakrishnan, V., Nalini, R., Sekar, T., Premalatha, M., & Subramanian, P. (2009). A review on gasification of biomass. *Renewable and Sustainable Energy Reviews, 13*(1), 179–186.
53. Dogru, M., Howarth, C. R., Akay, G., Keskinler, B., & Malik, A. A. (2002). Gasification of hazelnut shells in a downdraft gasifier. *Energy, 27*(5), 415–427.
54. Sridhar, G., Paul, P. J., & Mukunda, H. S. (2001). Biomass derived producer gas as a reciprocating engine fuel—An experimental analysis. *Biomass and Bioenergy, 21*(1), 61–72.
55. Kalita, P., & Baruah, D. (2018). Investigation of biomass gasifier product gas composition and its characterization. In *Coal and biomass gasification* (pp. 115–149). Singapore: Springer.
56. Searcy, E., & Flynn, P. (2009). The impact of biomass availability and processing cost on optimum size and processing technology selection. *Applied Biochemistry and Biotechnology, 154*(1–3), 92–107.
57. Malik, A., & Mohapatra, S. K. (2013). Biomass-based gasifiers for internal combustion (IC) engines—A review. *Sadhana, 38*(3), 461–476.
58. Malik, P., Awasthi, M., & Sinha, S. (2020). Study on an existing PV/wind hybrid system using biomass gasifier for energy generation. *Pollution, 6*(2), 335–346.
59. Malik, P., Awasthi, M., & Sinha, S. (2020). Study of grid integrated biomass-based hybrid renewable energy systems for Himalayan terrain. *International Journal of Sustainable Energy Planning and Management, 28,* 71–88.
60. https://www.epa.gov/sites/production/files/2015-07/documents/biomass_combined_heat_and_power_catalog_of_technologies_5._biomass_conversion_technologies.pdf.
61. Chopra, S., & Jain, A. (2007). A review of fixed bed gasification systems for biomass. *Agricultural Engineering International: The CIGR Ejournal. Invited Overview, 9*(5).
62. Balat, M., Balat, M., Kirtay, E., & Balat, H. (2009). Main routes for the thermo-conversion of biomass into fuels and chemicals. Part 2: Gasification systems. *Energy Conversion Management, 50*, 3158–3168.
63. Asadullah, M. (2014). Barriers of commercial power generation using biomass gasification gas: A review. *Renewable & Sustainable Energy Reviews, 29,* 201–215.
64. Gielen, D. (2012). Renewable energy technologies: Cost analysis series. *Sol Photovolt, 1*(1), 52.
65. Somashekhar, H. I., Dasappa, S., & Ravindranath, N. H. (2000). Rural bioenergy centres based on biomass gasifiers for decentralized power generation: Case study of two villages in southern India. *Energy for Sustainable Development, 4*(3), 55–63.

66. Lilienthal, P. (2005). HOMER micropower optimization model (No. NREL/CP-710–37606). National Renewable Energy Lab. (NREL), Golden, CO (United States). https://www.osti.gov/servlets/purl/860993.
67. Dhaundiyal, A., & Gupta, V. K. (2014). The analysis of pine needles as a substrate for gasification. *Hydro Nepal: Journal of Water, Energy and Environment, 15,* 73–81.
68. Kumar, A., & Randa, R. (2014). Experimental analysis of a producer gas generated by a chir pine needle (leaf) in a downdraft biomass gasifier. *International Journal of Engineering Research and Applications, 4*(10).

A Comparative Assessment of Biogas Upgradation Techniques and Its Utilization as an Alternative Fuel in Internal Combustion Engines

Deep Bora, Lepakshi Barbora, Arup Jyoti Borah, and Pinakeswar Mahanta

Abbreviations

AD	Anaerobic digestion
CH_4	Methane
CO_2	Carbon dioxide
N_2	Nitrogen
H_2S	Hydrogen sulfide
NH_3	Ammonia
ppm	Parts per million
HRT	Hydraulic retention time
FVW	Fruit and vegetable wastes
CN	Carbon Nitrogen
pH	Potential of hydrogen
IC	Internal combustion
MEA	Monoethanolamine

D. Bora · L. Barbora (✉) · P. Mahanta (✉)
Centre for Energy, Indian Institute of Technology Guwahati, Guwahati, Assam 781039, India
e-mail: lopab@iitg.ac.in

P. Mahanta
e-mail: pinak@iitg.ac.in

P. Mahanta
Department of Mechanical Engineering, Indian Institute of Technology Guwahati, Guwahati, Assam 781039, India

Department of Mechanical Engineering, National Institute of Technology Arunachal Pradesh, Yupia, Papum Pare, Arunachal Pradesh 791112, India

A. J. Borah
Department of Biotechnology, National Institute of Technology Arunachal Pradesh, Yupia, Papum Pare, Arunachal Pradesh 791112, India

A. P. Singh et al. (eds.), *Alternative Fuels and Advanced Combustion Techniques as Sustainable Solutions for Internal Combustion Engines*, Energy, Environment, and Sustainability, https://doi.org/10.1007/978-981-16-1513-9_5

DEA	Diethanolamine
TEA	Triethanolamine
DGA	Diglycolamine
MDEA	Methyldiethanolamine
PZ	Piperazine
AMP	2-Amino-2-methyl-1-propanol
KOH	Potassium hydroxide
$CaCO_3$	Calcium carbonate
Na_2CO_3	Sodium carbonate
K_2CO_3	Potassium carbonate
NaOH	Sodium hydroxide
$Ca(OH)_2$	Calcium hydroxide
PSA	Pressure swing adsorption
MMMs	Mixed matrix membranes
VFA	Volatile fatty acids
ATBR	Anaerobic trickle-bed reactors
CSTR	Continuous stirred tank reactor
SI	Spark ignition
CI	Compression ignition
CR	Compression ratio
NO_x	Nitrogen oxide
R&D	Research and development

1 Introduction

Fossil fuel exhaustion and increasing concern in environmental pollution at alarming rate have encouraged the researchers to look for environment friendly as well as cost-effective sources of energy [10]. Thus, various forms of renewable energy, for instance wind, tidal wave, solar and biomass, are getting attention globally during the last few decades [22]. Solar photovoltaic systems are limited due to high cost of production while use of wind, tidal and wave energy is site specific. One of the options to convert biomass to energy is the production of biogas through anaerobic digestion. The advantage of biogas technology is ease in production and sustainability. Harnessing energy from biomass is gaining popularity in developing countries due to the high availability of biomass and bio-waste. Landfills and wastewater treatment plants serve as the natural basis for enormous amount of biogas production. Many arable farmlands universally have now implemented in constructing anaerobic digesters to produce small quantities of biogas from organic waste such as kitchen waste, sludge and manure. Widespread availability of the organic materials is required for biogas synthesis, and it is considered as a potentially effective and sustainable energy source [24]. World Bioenergy Association reported that around

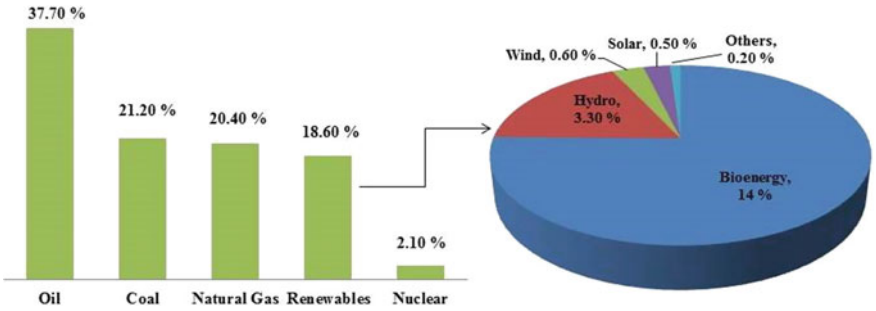

Fig. 1 Global energy consumption in 2014

18.6% of the total global energy consumption was contributed by renewable energy, in which approximately 14% comprise of bioenergy Fig. 1 [42].

Internal combustion (IC) engines provide outstanding drivability and durability, due to its comparatively compact size, high power-to-weight ratio, high compression ratio and safe to operate with less time required to start the engine. A series of fossil fuels comprising gasoline or diesel and alternative fuels such as natural gas, biomethane gas, biodiesel or ethanol have been studied on IC engines [64]. The engine serves as the major automobile mover in today's generation and is expected to continue for years to come. Although there are alterations, the basic operational principles of the IC engines have not shifted significantly [60]. Using of biogas in IC engine has certain advantages, being an eco-friendly carbon-neutral fuel, it has the potential to solve problems related to waste management. It has high compression ratio and comparatively lower proportion of sulfur than diesel engine. This has an impact on the cost, performance and environment with high emission, loud noise and low comfortability. The fuel can be used in both light- and heavy-duty vehicles with no or slight modification. However, high self-ignition temperature (650 °C) of biogas prevents its direct usage in CI engine and involves utilizing a dual-fuel engine constituting of biogas and other fuel in combination. Investigation on the combustion characteristic and their effects on exhaust emission with different fuel combination mode has been reported. Dual-fuel approach demonstrated lesser emission of NO*x* and particulate matter but sharply increased unburnt hydrocarbon emissions in contrast to diesel fueling mode [67]. The presence of CO_2 lowers its calorific value, flame and burning speed, traces of H_2S in raw biogas may corrode the metal parts, these are identified as additional lacunae associated with biogas utilization and need to be addressed. There are several reports on enrichment of CH_4 by removal of CO_2 and H_2S gas by scrubbing [32].

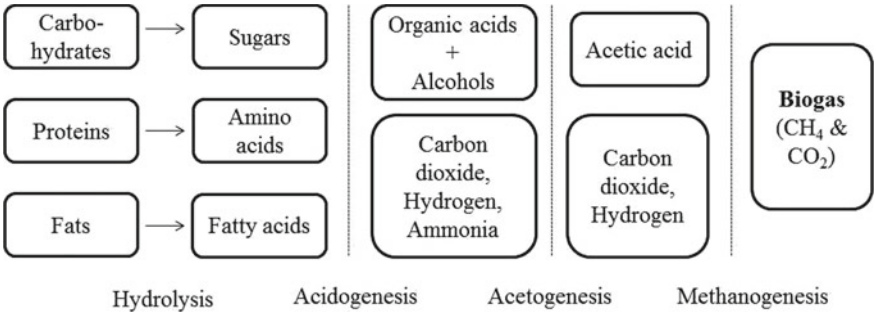

Fig. 2 Breakup of anaerobic digestion process

1.1 Process of Biogas Production: Anaerobic Digestion

Biogas is a mixture of combustible gases obtained from anaerobic digestion (AD) of organic matter by a community of microbial consortia. The digestion process takes place through various reactions and interactions among the methanogens and substrates which are fed into the digester as input [46]. The anaerobic digestion process generally consists of four steps—hydrolysis, acidogenesis, acetogenesis and methanogenesis [26], as shown in Fig. 2.

Biogas typically is a mixture of methane (CH_4) and carbon dioxide (CO_2) ranging from 45 to 60% each and a small amount of other gases like hydrogen (H_2), nitrogen (N_2), hydrogen sulfide (H_2S) and ammonia (NH_3) (ranges in between 100 and 1000 ppm), respectively [47]. The variable composition of biogas is due to the variety of materials that can be used for its production (Fig. 3). Temperature plays a key role in biogas production. Hydraulic retention time (HRT) is normally inversely proportional to the process temperature and varies from place to place. The feed materials are generally animal by-products, which are fed to the digester. In some cases, the feed materials first go through a controlled pre-sanitation process for deactivation of pathogens and for breaking their proliferation cycles. The digested residue after the AD process is transferred automatically to the outlet tanks, which are typically covered with a concrete to prevent methane leakage to the atmosphere. The digested residue has an added advantage of high nutrient value and can be reprocessed directly as fertilizer for the agricultural fields.

1.2 Biogas Production from Co-digestion

The availability of various types of feed materials in the same geographical area facilitates integrated residue management, posing substantial environmental benefits, like recycling of nutrients back to the agricultural land, energy savings, cost benefits and reduction of CO_2 emissions [37]. In recent times, co-digestion has gained much

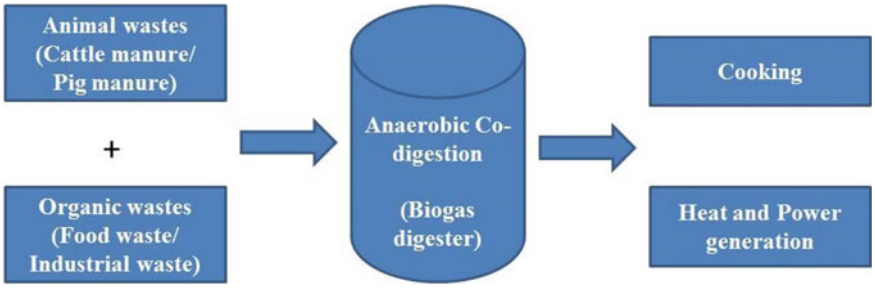

Fig. 3 Schematic representation of anaerobic co-digestion

attention in many countries since it increases the yield of AD. Co-digestion helps in managing different types of organic waste at one place in production of biogas. Due to a balanced mixture composition of waste materials, digestion of more than one substrate in the same digester can establish a positive synergism in the digestion medium, and the added nutrients can support microbial growth for enhancing biogas production [48, 56]. Co-digestion helps in accomplishing a better NPK ratio attributed to mixing of multiple organic wastes, thereby enhancing the digestate as a fertilizer. Co-digestion of cattle manure and fruit and vegetable wastes (FVW) under mesophilic condition (35 °C) in a continuous stirred tank reactor increased the percentage of FVW from 20 to 50%, and the methane yield enhanced from 230 to 450 L/kg VS added [18]. FVW are rapidly degraded by contaminating microorganisms, and this takes place even faster when they exhibit signs of excessive ripening or are subjected to mechanical damage. An effective co-digestion is not simply a blend of multiple feed materials treated at the equal time. Biogas production and stability of the process are fully dependent on waste composition like C:N ratio (25:1 to 30:1), process conditions like pH (6.8–7.2), operation temperature (35–37 °C) and the population of microbial community in the system. If not mixed in a proper ratio, co-digestion may also cause antagonistic interactions, leading to lower methane yields than expected [55].

1.3 Enhanced Biogas Production Using Pre-treatment

For AD, generally animal dung (cattle, pig, horse, mule and donkey) has been the most preferable feedstock. However, because of limited feedstock availability, it has become essential for researchers to explore new substrate suitable for utilization in AD while simultaneously contributing to the growing energy needs. Lignocellulosic biomasses are abundantly available worldwide as well as their high carbohydrate content make these materials an attractive feedstock for biofuel production [77]. Unfortunately, the challenge associated with utilization of lignocellulosic biomasses as feedstock for biogas production is their recalcitrant structure [31]. The recalcitrant

structure of lignocellulosic biomass makes it fairly impervious to bacterial attack. The rigid outer layer of lignin makes it very difficult for microorganisms to access the cellulose and hemicellulose components inside it. Hence, the hydrolysis step is often considered as the rate-limiting step when utilizing these kind of substrates [71]. An initial pre-treatment step prior to AD process is of utmost importance in order to rupture the recalcitrant structure of the lignocellulosic biomass to release the cellulose and hemicellulose to the microbial consortia present in the digester, which in turn increases the rate of biomass degradation along with an increase in the biogas yield [82]. However, in some cases, the chemical agent used for the pre-treatment process can act as a budding inhibitor for the microorganisms involved in the AD. Generally, the pre-treatment should yield a polysaccharidic-rich substrate with minimum amounts of inhibitory by-products and also be cost effective. A number of authors have reported different pre-treatment methods using different types of lignocellulosic biomass for enhancing biogas production [31, 52, 78]. Some of them are mentioned below:

- Physical (liquid hot water)
- Physico-chemical
- Chemical (acidic and alkaline processes)
- Microbial Processes (fungi, bacterial consortium, etc.)
- Ionic liquid process
- Irradiation (Microwave, gamma, X-ray, etc.).

Using alcohols or weak organic acids as a pre-treatment agent for degradation of lignocellulosic biomass seems to be an interesting process. During the process of AD, alcohols or weak organic acids generally form as intermediary products. So the above-mentioned inhibitory problems could be avoided as after the pre-treatment these solvents can be converted into additional methane production. Pre-treatment of forest residues using methanol, ethanol or acetic acid before AD resulted in higher methane yields in a batch experimental process. The techno-economic calculations presented that treatment with methanol was more viable economically due to its lower price and easy recovery after the treatment [36].

1.4 Challenges of the Current Processes and Need for Biogas Upgradation

The methane in biogas is a high-valued energy source, although other constituents are impurities that pose key obstacles to the viable use of biogas [1]. CO_2 through combustion has no energy yield and greatly diminish the heating value per volume of biogas due to its high content. Calorific value of biogas with CO_2 varies from 18.7 to 26 MJ/m^3 and that of without CO_2 varies from 33.5 to 35.3 MJ/m^3 [51]. Apart from CO_2, another major impurity is H_2S. It is always present in biogas, while concentrations differ with the feedstock [76]. It is toxic and highly corrosive in nature,

Table 1 Properties of biogas [33, 68]

Properties	Biogas
Composition	55–70% CH_4, 30–45% CO_2 and traces of other gases
Energy value	6.0–6.5 kW/m^3
Fuel equivalent	0.6–0.65 L oil/m^3 biogas
Explosion limits	6–12% biogas in air
Ignition temperature	650–750 °C
Critical pressure	75–89 bar
Critical temperature	−82.5 °C
Normal density	1.2 kg/m^3
Flame speed	25 cm/s
Odor	Bad eggs (the smell of H_2S)
Lower heating value	17 MJ/kg
Research octane number	110
Heat of vaporization	0.5 MJ/kg

often damaging gas burners, gas storage tanks, compressors, engines and pipelines to transport. Upon combustion, it also forms a risky pollutant sulfur dioxide [39]. That is why to use the biogas effectively, it is very important to remove the CO_2 and H_2S from it. Thus, removal of CO_2 and H_2S from biogas will enhance the fuel efficiency which could serve as a source of immense energy that can be used effectively for different purposes like main power source for transport vehicles and also used for powering of generators for electrical energy [3]. This possibility of use is justified by biogas properties, which makes it convenient for IC engines. The actual calorific value of biogas mainly depends on CH_4 percentage, temperature and absolute pressure and is a vital parameter for the performance of an engine. The fuel consumption of IC engine using biogas is often specified in m^3n/h or m^3n/kWh. After scrubbing, biogas can be compressed and stored in gas cylinder and transported wherever it is required. Also, this scrubbed biogas decreases greenhouse gas emissions [63]. The properties of biogas are given in Table 1.

2 Biogas Upgradation Technologies

Biogas upgrading to biomethane is a novel degree of gas purification. The splitting of minor impurities (moisture, H_2S, etc.) and especially CO_2 is essential and critical operation. The removal of these impurities is necessary for all generally used gas applications like CHP engines, boilers, vehicles or injection in the natural gas grid. The qualitative requirements for removal of key constituents from biogas fitting to its uses are given in Table 2 [65]. Currently, an amount of altered biogas upgradation technologies to fulfill the job of producing biomethane of sufficient quality are

Table 2 Requirement of purification

Applications	H_2S	CO_2	Moisture
Boiler	Recommended	No	No
CHP engine	Yes	No	No condensation
Vehicle fuel	Yes	Recommended	Yes
Natural gas grid	Yes	Yes	Yes

commercially available and have proven to be technically and economically feasible. The major step comprises drying of the raw biogas and the removal of CO_2 and thus enhancement of the heating value of the produced gas. Several essential mechanisms are involved to achieve selective separation of gas components. These may include physical or chemical absorption, adsorption on a solid surface, membrane separation, cryogenic separation and chemical hydrogenation [54]. All biogas upgradation technologies have their own specific advantages and disadvantages and are different for different biogas upgrading sites. The accurate choice of the economically feasible technology is strongly rely on the quality and quantity of the raw biogas to be raised the biomethane quality to be attained and its utilization.

2.1 Physical Absorption Method Using Water and Organic Solvents

Physical absorption employing water as a solvent for dissolving CO_2 and H_2S is considered as the simplest, requiring fewer infrastructure, eco-friendly, cost-effective and widely accepted method for biogas upgradation [69]. For biogas scrubbing, physical absorption method is generally applied as they are effective even at low flow rates that the biogas plants are normally operated at. In this case, the absorbed gas components are physically bound to the scrubbing agent. The absorption in water is employed because CO_2 and H_2S have higher solubility in water than CH_4 and will therefore be dissolved to a higher extend, particularly at lower temperatures and higher pressures. This method can tolerate H_2S concentrations of around 300–2500 ppm, but higher H_2S concentrations are detrimental to the scrubbing system as it lowers the pH of the scrubbing liquid [53]. In this process, the raw biogas is compressed and fed into a packed-bed column from bottom, and pressurized water is sprayed from the top which flows downward. The process is thus a counter-current one. Purified biogas (biomethane) leaves column at the top and dissolves CO_2 as well as H_2S in water, which are collected at the bottom of the tower. In order to maintain the absorption performance, the scrubbing liquid has to be replaced by fresh liquid or regenerated in a separated step (desorption or regeneration step). The regenerated water is then pumped back to the absorber as fresh scrubbing liquid. CO_2 is released into atmosphere as an off-gas in case of water recirculation system or stays in water in case of a single-pass system [58]. Any CH_4 dissolved in water is captured and

recycled in the absorption column in order to alleviate methane losses. Viyaj et al. [73] designed a water scrubbing system in which the CO_2 content was reduced by 99%. The setup used a gas inlet pressure and flow rate of 1.0 MPa and 1.5 m^3/h, respectively, while the corresponding water flow rate was 1.8 m^3/h. The limitation of this technique is that the air constituents, oxygen and nitrogen, are dissolved in the water stream during regeneration and thus elated to the upgraded biomethane. Therefore, biomethane produced with this technology always contains small amount of oxygen and nitrogen. This technology also uses an organic solvent solution (e.g., polyethylene glycol) instead of water as a scrubbing agent. Solubility of CO_2 in these solvents is found higher than in water. As a result, less scrubbing liquid circulation is required for higher CO_2 absorption, and thereby, smaller apparatus is needed for the same raw biogas upgradation. Some of the commercially available organic physical scrubbing agents used for biogas upgrading technologies are Genosorb®, Selexol® and Rektisol® [6].

2.2 Chemical Absorption Method

The mechanism of chemical absorption is quite similar as water scrubbing process where a chemical reaction takes place connecting scrubbing agent components and absorbed gas components within the liquid phase. But the conformation of chemical absorption is much simpler with improved performance because of higher CO_2 solubility at low pressure in highly reactive chemical absorbents [7]. The separation principle of absorption is established on different solubility of various gas constituents in a liquid-scrubbing solution. As the process includes development of reversible chemical bonds among the solute and the solvent, regeneration of the solvent, thus, involves breaking of these bonds and requires significantly a very great energy input [59]. The most employed chemical solvents are generally diglycolamine (DGA), monoethanolamine (MEA), triethanolamine (TEA), diethanolamine (DEA), methyldiethanolamine (MDEA) and sterically hindered amines, such as 2-amino-2-methyl-1-propanol (AMP) and piperazine (PZ) which in comparison with water can dissolve significantly much more CO_2 per unit volume of biogas [38]. Usually, amine scrubbing plants are operated at slightly high pressure which is already available in the raw biogas, and no extra compression of the gas is required. The high selectivity and absorptivity of the amine solution has an advantage during absorption but turns out to be a hindrance during regeneration of the scrubbing solution. MEA is the cheapest amine, and it is the most commonly used as a scrubbing agent due to its high absorption capacities for CO_2. The amine scrubbing agent can also absorb H_2S from the raw biogas, but higher temperature is needed during regeneration of the solution. Hence, it is advisable to remove this component prior to the amine scrubber. Inorganic solvents generally employed for this process are sodium hydroxide (NaOH), potassium hydroxide (KOH) and calcium hydroxide $Ca(OH)_2$. The solubility of CO_2 in NaOH is higher in comparison with amines [2]. Theoretically, to absorb 1 ton of CO_2, 1.39 tons of MEA will be required, and when compared with NaOH, only 0.9

tons is required [8]. Alkali hydroxides are more efficient, cost effective and easily available in the market as compared to amines. But regeneration of these hydroxides is complex and challenging because of the formation of thermally stable products such as Na_2CO_3, K_2CO_3 and $CaCO_3$ salts. Yeh et al. [79] studied a chemical absorption and desorption process for the removal of CO_2. They used MEA as scrubbing agent in a conventional and structured packed column. Significant improvements in CO_2 removal above 90% were obtained with the structured packing. Tippayawong and Thanompongchart [72] investigated a method for biogas scrubbing and CH_4 enrichment where they used aqueous solutions of NaOH, $Ca(OH)_2$ and MEA for the chemical absorption of CO_2 and H_2S in a packed column. Test results revealed that the aqueous solutions used were effective in reacting with CO_2 in biogas (over 90% removal efficiency), making CH_4 an enriched fuel.

2.3 Pressure Swing Adsorption (PSA)

Pressure swing adsorption (PSA) is an established and developed technology for biogas upgradation. The method is based on specific adsorption behavior of at least one gaseous component (adsorbate) on a solid surface (adsorbent) under elevated pressure mainly as a result of physical or Van der Waals or electrostatic forces [28]. Adsorbent materials are able to capture some gaseous component of a mixture by adsorption affinity and molecular size of the adsorbent. The physico-chemical properties of gaseous components present in biogas are given in Table 3. The size of CO_2 molecules is smaller than the size of CH_4 molecules. Consequently, in the instance of biogas, the molecules of CO_2 easily adsorbed on a selective adsorbent material and later enriching CH_4 content of the gas. The efficiency of adsorption process depends mainly on temperature, pore size of adsorbent and partial pressure of adsorbate. Normally, solids with a large surface area per unit volume adsorbents are commercially available. Gas purification can also be performed using some form of activated carbon, alumina, silica or silicates, which are also known as molecular sieves. Usually adsorbents with molecular sieve, a regular pore size of 3.7 Å is used to capture CO_2 (molecular size of 3.4 Å) into the pores, while rejecting CH_4 molecules (molecular size of 3.8 Å). By an appropriate choice of adsorbent, the process is

Table 3 Physico-chemical properties of biogas components [40]

Gaseous component	σ (Å)	α (Å^3)	μ (D)
CH_4	3.80	2.448	0.000
CO_2	3.40	2.507	0.000
H_2S	3.60	3.630	0.970
N_2	3.64	1.710	0.000
H_2O	2.65	1.501	1.850

where σ kinetic diameter (Å: Angstrom), α polarizability (Å^3: Angstrom^3) and μ dipole moment (D: coulomb-meter).

able to eliminate CO_2, H_2S, moisture and other impurities either simultaneously or selectively from biogas [70]. Conventional PSA usually consist of four adsorption columns packed with adsorbents. One cycle has typically four basic steps: pressure build-up, adsorption, depressurization and regeneration. After building pressure, CO_2 is captured from raw biogas in adsorbent and consequently leaves the adsorber as off-gas by a stepwise decrease in pressure. Enriched CH_4 leaves the column as a biomethane stream. Afterward, the pressure is increased again with raw biogas or biomethane, and the adsorber is ready for the next sequence of loading. Biogas feeding and column pressurization are usually carried out at 4–10 bars to increase CO_2 adsorption inside the pores [14]. The CH_4 concentration in the raw biogas can be upgraded up to 96–98%; however, up to 4% CH_4 can be lost in the off-gas stream [65]. Since the adsorption of H_2S is irreversible and harm the adsorbent material, these components have to be removed before reusing the adsorption column.

2.4 Membrane Separation

Separation by membrane is a mature commercialized technology with a market stake of 10%. It has emerged as an attractive process for biogas upgradation [57]. The process established on the principle of selective permeation of different components through a semi-permeable membrane. The carriage of each component is driven by the change in partial pressure over the membrane and highly relies on the permeability of the membrane material in the component. It is additionally resolute by other factors such as changes in temperature, concentration and electric charges of different gases. Membranes for biogas upgradation are made of materials that are mainly permeable for CO_2, H_2S and water while CH_4 passes only to a very low extent [14]. For high methane purity, the difference in permeability of CH_4 and CO_2 must be high. Basically, for gas separation, there are three types of membranes use, inorganic, polymeric and mixed matrix membranes (MMMs). Some of the polymeric and non-polymeric membrane materials for biogas upgrading are given in Table 4. Polymeric

Table 4 Membrane constituents for biogas upgrading [7, 12]

Polymeric materials	Non-polymeric materials
Polysulfane, polyethersulfone	Carbon molecular sieves
Cellulose acetate, cellulose triacetate	Non-porous carbon
Polyphenyleneoxide	Palladium alloys
Polycarbonate	Zeolites and non-zeolitic molecular sieves
Polyaramide	Mixed conducting perovskites
Polyimide, polyetherimide	Ultramicroporous amorphous silica

membranes are the most widely used membranes in biogas sector. The polymeric membranes are preferred for the separation of biogas because of their low cost, high selective permeability, easy production and stability at high pressures. To offer adequate membrane surface area in compact biogas plants, these membranes are used in the form of hollow fibers combined to a number of parallel membrane modules [12]. Solid membrane fabricated from acetate–cellulose polymer has permeability for CO_2 and H_2S up to 20 and 60 times, respectively, higher than CH_4. However, a pressure of 25–40 bar is required for the process [30]. Using high-pressure gas separation, the raw biogas can be filtered up to 94% CH_4 in one-stage performance, and it can be improved up to 96% CH_4 by using two- or three-stage performance [75].

2.5 *Cryogenic Separation*

The cryogenic method of purification is based on the principle of separation of different gases by fractional condensations and distillations at low temperatures. As different gases liquefy at different temperature and pressure domains, it is possible to separate gas components by cooling and compressing the biogas. The process has an advantage that it allows recovery of pure component in the form of a liquid, which can be transported conveniently [27]. The boiling point of CH_4 at 1 atm pressure is −161.5 °C which is quite lower than the boiling point of CO_2 (−78.2 °C), thus facilitating the separation of CO_2 from biogas by liquefying CO_2 at very low temperatures [29].

Removal of water and H_2S from biogas is necessary in order to avoid freezing and other problems; however, the gases like N_2 and O_2 can be condensed during CH_4 separation [20]. The cryogenic separation is carried out by initially drying followed by multistage compression of the raw biogas with intermediate cooling up to 80 bar. The pressurized biogas is stepwise cooled to −55 °C to achieve the liquefaction of CO_2 and finally expanded to 8–10 bar in a flash tank at −110 °C to facilitate biomethane purification via CO_2 solidification [65]. This method can upgrade the raw biogas up to 97% and CH_4 loss lower than 2%. The process requires large number of equipment facilities and thus consumes high investment and a large amount of energy which increases the final cost of biomethane production [23]. The operating cost and practical problems of clogging and freezing due to high concentration of solid CO_2 or presence of rest impurities limit the wider implementation of this technique. Table 5 summarizes the advantages and disadvantages of biogas upgradation techniques for CO_2 removal.

Table 5 Summary of advantages and disadvantages of biogas upgradation processes [65, 81]

Upgradation technologies	Advantages	Disadvantages
Physical absorption	Simple process, can remove both H_2S and CO_2 simultaneously, eco-friendly solvents, low cost to operate and maintain	Requires high pressure, need a larger column compared to chemical absorption
Chemical absorption	High purity CH_4 (>95%), More efficient in low pressure, column volume is smaller than water scrubbing	Chemicals are corrosive in nature and expensive, Higher energy required to regenerate the solvent
Pressure swing adsorption	Simple in design, economy in production with comparatively high purity, good moisture removal capacities	High capital cost, high pressure is required, CH_4 losses when malfunctioning of valves, pre-treatment of H_2S is required
Membrane separation	Fast installation and startup, High purity CH_4 (>96%), Production output is flexible	High cost membrane, Consumes more energy
Cryogenic separation	High purity CH_4 (90–98%), Produce CO_2 in marketable form, such as dry ice, Liquid CH_4 decreases gas volume, thus can be easily transported	Consumes relatively more electricity per unit of gas production, Uses lots of process equipment

3 Emerging Technologies for Biogas Upgradation

Though conventional technologies are promising in upgradation of biogas, the market for biogas upgrading is often characterized by harder competition with the establishment of new upgrading technologies. Biological technologies are one of the recent developments in biogas upgrading technology. Both conventional and emerging biogas upgradation technologies are currently being developed for enhancing performance, for increasing CO_2 reduction efficiency and for rendering them cost effective to get a wider implementation network.

3.1 Biological CO_2 Removal Technologies

Biological biogas upgradation involves the employment of microbes for conversion of CO_2 and H_2 into CH_4. On comparison with the conventional technologies, the major advantage of biological technology is that the CO_2 is converted into other value-added products at atmospheric pressure and moderate temperature contributing significantly to a sustainable bio-based and circular economy [62]. Biological biogas upgrading consists of two types of metabolic pathways. The first metabolic pathway involves the role of hydrogenotrophic methanogens

which converts CO_2 directly to CH_4. The other metabolic pathway chooses an indirect route where homoacetogenic bacteria first convert CO_2 to acetate and then converted to CH_4 by the acetoclastic methanogens [8]. The former pathway is more preferable as hydrogenotrophic methanogens (*Methanobacterium, Methanoculleus* and *Methanomicrobium*) are more abundant than acetoclastic methanogens such as *Methanosarcina* [4]. The biological biogas upgrading process is classified into two types:

(a) In situ biological methane enrichment and
(b) Ex situ biological methane enrichment

3.1.1 In Situ Biological Methane Enrichment

Biological in situ biogas upgradation implicates the injection of H_2 inside the biogas digester in order to couple with the endogenous CO_2 produced in the anaerobic digester to convert into CH_4 by the action of autochthonous hydrogenotrophic methanogens [41]. The process can enrich CH_4 up to nearly 99% if the operational parameters (e.g., pH, temperature, H_2 flow rate, etc.) are fully monitored and controlled [74]. Though in situ biogas upgrading is a cost-effective method, it has also some technical challenge with the increase of pH values above 8.5 due to the elimination of the key buffering agent, i.e., bicarbonate, thus leading to inhibition of methanogenesis [44]. Therefore, 8.5 is measured as the threshold pH for ideal biomethanation process in both conventional and emerging biogas production systems. In order to overcome this technical challenge, co-digestion of manure with acidic waste was anticipated to arrest the pH in an optimal range during the biogas upgrading process [45]. Another challenge is that the oxidation of volatile fatty acids (VFA) and alcohols are thermodynamically viable only if the partial pressure of H_2 is very low [25]. On the other hand, addition of H_2 in the biogas digester increases the concentration of H_2 inside the digester which inhibits the process of VFA oxidation [13]. Due to this concern, the in situ methane enrichment process is limited to laboratory-scale studies only and more process optimization is required to get a wider implementation worldwide.

3.1.2 Ex Situ Biological Methane Enrichment

The concept of ex situ biogas upgradation came into existence to overcome the challenges incurred in in situ biogas upgradation. The ex situ biogas upgradation implicates the accumulation of CO_2 from biogas and H_2 from external sources in a separate anaerobic reactor having the hydrogenotrophic methanogenic archaea, resulting in their subsequent conversion to CH_4. In this process, CO_2 is utilized as carbon source and H_2 as reducing agent for the production of CH_4 [41].

Some advantages of this method compared to the in situ process [9] are:

- Simple biochemical process since no biomass is required for degradation.

Table 6 Assessment of in situ and ex situ biogas advancement processes

Process	Reactor type	Temperature (°C)	pH	CH_4 (%)	References
In situ	CSTR	55	7.7–7.9	75	Luo and Angelidaki [45]
Ex situ	Fixed-bed reactor	50	6.9	> 90	Alitalo et al. [5]
In situ	Batch	35 and 55	7.2	96	Yun et al. [80]
Ex situ	CSTR	37	8.17	88	Bassani et al. [11]
In situ	CSTR	37	8	98.9	Wang et al. [74]
Ex situ	ATBR	37	7.2–7.4	98	Burkhardt et al. [17]

- The conversion occurs in a separate unit which ensures the stability of existing biogas plant.
- External source of waste makes the process more flexible (e.g., CO_2 from syngas and H_2 from hydrolysis of water).
- The process takes less retention time as it can handle high volumes of influent gases.

The efficiency of biogas upgradation strongly depends on the reactor type, partial pressure of H_2 and operating temperature inside the bioreactor, which can result in methane conversion from 79 to 98%. On comparison with mesophilic culture, the enriched thermophilic culture resulted in >60% higher H_2 and CO_2 bioconversion in batch assay [43]. The types of reactors that can address the challenges of gas–liquid mass transfer of H_2 are fixed-bed reactors, anaerobic trickle-bed reactors (ATBR), continuous stirred tank reactor (CSTR) and series up-flow reactors. A methane upgradation of 95.4% was achieved in a thermophilic CSTR functioned with mixed methanogenic culture [45]. In a recent study, it was shown that 96% CH_4 production was achieved by operating the process in a mesophilic ATBR using immobilized hydrogenotrophic culture [62]. An assessment of different in situ and ex situ methane enrichment processes is given in Table 6.

4 Application of Biogas in IC Engines

With increasing pollutant exhaust emissions, regulations and policies are being tightened worldwide to combat the problem of poor ambient air quality. Therefore, fostering use of clean alternative fuels as substitutes for IC engines is the need of the hour [34, 66]. There are various fuels that can be used in IC engines, but they should meet certain physical and chemical properties. Usually fuels used in IC engines are re-designed to satisfy requirements of engine performance effectively. The physico-chemical properties of biogas justify the applicability of biogas as an alternate fuel for IC engines. The actual calorific value of biogas is the key factor for the performance of an engine. For both spark ignition (SI) and compression ignition

(CI) engines, biogas provides a clean fuel. To use biogas effectively in SI engines, a higher compression ratio (CR) engine with magneto ignition and modification of piston and carburetor is required, while in CI engine it can be employed efficiently in dual-fuel mode with diesel as a pilot fuel. For use of biogas as a vehicle fuel, upgradation of biogas is necessary which has been discussed in Sects. 2 and 3. After removal of impurities like CO_2, H_2S and water, it can be compressed in a three- or four-stage compressor up to a pressure of 20 MPa and stored in a gas cascade for enabling quick refueling of cylinders. Compression of biogas is required to put more volume of gas in a small cylinder, so that the engine will run for a longer time [19, 21].

4.1 Biogas in SI Engines

The use of biogas in SI engines is gaining popularity because of higher auto ignition temperature, ability to form homogeneous mixture and higher hydrocarbon ratio. Being a clean fuel with a high auto-ignition temperature and high octane number, biogas can resist knocking in SI engines. Due to higher anti-knock index, SI engines fueled by biogas have relatively higher CR than that of petrol which enhances the thermal efficiency of the engine. In the case of operation using simulated biogas, SI engine CR can even be raised in a range from 11:1 to 13:1 because of the high self-ignition temperature and has been found to be appropriate for operation without knock [21]. The presence of impurities such as CO_2 and N_2 affects in characteristics of combustion, calorific value, flammability limit and flame speed. Also, increase in impurities percentage aggravates cyclic variation and also lowers power output. In order to achieve low emission and the best fuel conversion efficiency for a biogas-fueled SI engine, it is highly recommended to maintain the air–fuel ratio, accurate CR and ignition timing [35, 61]. The modification of an SI engine to operate with biogas is simple and quite easier than CI engine because the engine is designed to operate on an air–fuel mixture with spark ignition. The basic alteration is to provide a biogas–air mixture instead of a carburetor. The engine is controlled by variation of the mixture supplied to the engine through operating the butterfly valve placed between the biogas mixer and engine intake system. Adequate design of the mixing device along with the precise control of butterfly valve can ensure the provision of constant air/fuel ratio irrespective of the actual amount sucked into the engine [49].

4.2 Biogas in CI Engines

Due to high self-ignition temperature, biogas cannot be utilized as a stand-alone fuel in CI engine; however, it could be applied in CI engine in dual-fuel mode. The dual-fuel engine is a modified diesel engine includes an initial supply of a mixture of fresh air and gaseous fuels to a cylinder and injection of a small amount of diesel,

usually termed pilot fuel for ignition of the combustible mixture. The pilot fuels are generally of high cetane value. The amount of diesel required for sufficient ignition is between 10 to 20% of the amount required for operation on diesel fuel alone. Gaseous fuel quickly mixes with air to form a standardized air–fuel mixture that improves the emission characteristics and retain high efficiency, leading to the widespread utilization of biomass energy [15, 16]. The use of biogas fuel in dual CI engine shows less emission of NO_x and particulate matter when compared with diesel mode engine. A dual-fuel CI engine can attain higher efficiency owing to its high CR as compared to a sole biogas-fueled SI engine. Faster and complete combustion takes place in the combustion chamber as the diesel fuel injected provides multi-point ignition sources, which increases the stability of the engine performance [19, 50]. Additionally, recent inclusions of hydrogen and LPG with simultaneous lowering of CO_2 emissions are considered as major developments in the performance of biogas dual-fuel engines [21]. However, the process parameters such as fuel composition, air–fuel ratio, inlet temperature as well as emission characteristics have to be monitored considerably for effective application of biogas in IC engines.

5 Conclusions

The biogas production from different organic wastes through anaerobic digestion and physico-chemical properties is discussed for use as an alternative fuel in IC engines. The changes that have to be made in the existing engines to use biogas as a fuel are being discussed. The biogas purification is necessary as it contains not only CH_4 but also other gases, considered as impurities, such as CO_2 and H_2S. Different existing and emerging biogas upgradation technologies for CO_2 and H_2S removal are discussed, among which water scrubbing is found to be a simple and cost-effective method for purification. Reduction of CO_2 in biogas for both SI and CI engines increases the calorific value of the fuel, thermal efficiency and power output. Use of biogas as a fuel could decrease carbon emissions compared to other fossil fuels. Another advantage of using upgraded biogas in vehicles is that it leads to lower emissions of NO_x and particulate matter. Enriched methane from biogas is a potential source of energy and can be used as an alternative fuel for IC engines. However, scale-up of this highly potential technology and appropriate R&D measures is required to fulfill the demand of alternate energy for IC engines worldwide.

Acknowledgements The authors gratefully acknowledge the financial support of the Ministry of New and Renewable Energy, Government of India, for the above project (256/3/2017-BIOGAS).

References

1. Abatzoglou, N., & Boivin, S. (2008). A review of biogas purification processes. *Biofuels, Bioproducts & Biorefining, 3*(1), 42–71.
2. Abdeen, F. R. H., Mel, M., Jami, M. S., Ihsan, S. I., & Ismail, A. F. (2016). A review of chemical absorption of carbon dioxide for biogas upgrading. *Chinese Journal of Chemical Engineering, 24,* 693–702.
3. Abushammala, M. F. M., Qazi, W. A., Azam, M. H., Mehmood, U. A., Al-Mufragi, G. A., & Alrawahi, N. A. (2016). Generation of electricity from biogas in Oman. In *3rd MEC International Conference on Big Data and Smart City*.
4. Agneessens, L. M., Ottosen, L. D. M., Voigt, N. V., Nielsen, J. L., de Jonge, N., Fischer, C. H., & Kofoed, M. V. W. (2017). In-situ biogas upgrading with pulse H_2 additions: The relevance of methanogen adaption and inorganic carbon level. *Bioresource Technology, 233,* 256–263.
5. Alitalo, A., Niskanen, M., & Aura, E. (2015). Biocatalytic methanation of hydrogen and carbon dioxide in a fixed bed bioreactor. *Bioresource Technology, 196,* 600–605.
6. Allegue, L. B., & Hinge, J. (2012). Report: Biogas and bio-syngas upgrading. Danish Technological Institute. https://www.teknologisk.dk/_/media/52679_Report-Biogasandsyngasupgrading.pdf.
7. Andriani, D., Wresta, A., Atmaja, T. D., & Saepudin, A. (2014). A review on optimization production and upgrading biogas through CO_2 removal using various techniques. *Applied Biochemistry and Biotechnology, 172,* 1909–1928.
8. Angelidaki, I., Treu, L., Tsapekos, P., Luo, G., Campanaro, S., Wenzel, H., & Kougias, P. G. (2018). Biogas upgrading and utilization: Current status and perspectives. *Biotechnology Advances, 2,* 452–466.
9. Aryal, N., Kvist, T., Ammam, F., Pant, D., & Ottosen, L. D. M. (2018). An overview of microbial biogas enrichment. *Bioresource Technology, 264,* 359–369.
10. Bansal, N., Srivastava, V. K., & Kheraluwala, J. (2019). Renewable energy in India: Policies to reduce greenhouse gas emissions. In: *Greenhouse gas emissions, energy, environment, and sustainability* (pp. 161–178).
11. Bassani, I., Kougias, P. G., Treu, L., & Angelidaki, I. (2015). Biogas upgrading via hydrogenotrophic methanogenesis in two-stage continuous stirred tank reactors at mesophilic and thermophilic conditions. *Environmental Science and Technology, 49,* 12585–12593.
12. Basu, S., Khan, A., Cano-, A., Liu, C., & Vankelecom, I. (2010). Membrane-based technologies for biogas separations. *Chemical Society Reviews, 39,* 750–768.
13. Batstone, D. J., Keller, J., Angelidaki, I., Kalyuzhnyi, S. V., Pavlostathis, S. G., Rozzi, A., et al. (2002). The IWA anaerobic digestion model no 1 (ADM1). *Water Science and Technology, 45,* 65–73.
14. Bauer, F., Persson, T., Hulteberg, C., & Tamm, D. (2013). Biogas upgrading – technology overview, comparison and perspectives for the future. *Biofuels, Bioproducts and Biorefining, 7,* 499–511.
15. Bora, B. J., Saha, U. K., Chatterjee, S., & Veer, V. (2014). Effect of compression ratio on performance, combustion and emission characteristics of a dual fuel diesel engine run on raw biogas. *Energy Conversion Management, 30*(87), 1000–1009.
16. Borah, A. J., Singh, S., Goyal, A., & Moholkar, V. S. (2016). An Assessment of Invasive Weeds as Multiple Feedstocks for Biofuels Production. *RSC Advances, 6,* 47151–47163.
17. Burkhardt, M., Koschack, T., & Busch, G. (2015). Biocatalytic methanation of hydrogen and carbon dioxide in an anaerobic three-phase system. *Bioresource Technology, 178,* 330–333.
18. Callaghan, F. J., Wase, D. A. J., Thayanithy, K., & Forster, C. F. (2002). Continuous co-digestion of cattle slurry with fruit and vegetable wastes and chicken manure. *Biomass and Bioenergy, 27*(1), 71–77.
19. Chandra, R., Vijay, V. K., Subbarao, P. M. V., & Khura, T. K. (2011). Performance evaluation of a constant speed IC engine on CNG methane enriched biogas and biogas. *Applied Energy, 88*(11), 3969–3977.

20. Chen, X. Y., Vinh-Thang, H., Ramirez, A. A., Rodrigue, D., & Kaliaguine, S. (2015). Membrane gas separation technologies for biogas upgrading. *RSC Advances, 5,* 24399–24448.
21. Crookes, R. J. (2006). Comparative biofuel performance in internal combustion engines. *International Journal of Biomass and Bioenergy, 30,* 461–468.
22. Demirbas, A. (2010). Use of algae as biofuel sources. *Energy Conversion and Management, 5*(1), 2738–2749.
23. Deublein, D., & Steinhauser, A. (2010). *Biogas from waste and renewable resources: An introduction* (2nd ed.). Weinheim: Wiley.
24. Diaz, I., Perez, S. I., Ferrero, E. M., & Fdz, M. (2011). Effect of oxygen dosing point and mixing on the microaerobic removal of hydrogen sulphide in sludge digesters. *Bioresource Technology, 102*(4), 3768–3775.
25. Dolfing, J., Jiang, B., Henstra, A. M., Stams, A. J., & Plugge, C. M. (2008). Syntrophic growth on formate: A new microbial niche in anoxic environments. *Applied and Environment Microbiology, 74,* 6126–6131.
26. Gerardi, M. (2003). *The microbiology of anaerobic digesters. Waste water microbiology series* (Vol. 7). Wiley, United States of America.
27. Goffeng, B. (2013). *Crynotechnology for biogas.* Dept of Chem Eng: Lund University.
28. Grande, C. A. (2012). Advances in pressure swing adsorption for gas separation. *ISRN Chemical Engineering*. https://doi.org/10.5402/2012/982934.
29. Green, D. W., & Perry, R. H. (2008). *Perry's chemical engineers' hand book* (8th ed.). New York: McGraw-Hill Companies Inc.
30. Hagen, M., Polman, E. (2001). Adding gas from biomass to the gas grid. Final report submitted to Danish Gas. Agency (pp. 26–47).
31. Hendriks, A. T. W. M., & Zeeman, G. (2009). Pretreatments to enhance the digestibility of lignocellulosic biomass. *Bioresource Technology, 100*(1), 10–18.
32. Hernandez, N. M., & Villanueva, E. P. (2018). Production, purification and utilization of biogas as fuel for internal combustion engine. *AIP Conference Proceedings, 1941*(020009), 1–11.
33. Hotta, S. K., Sahoo, N., & Mohanty, K. (2019). Comparative assessment of a spark ignition engine fueled with gasoline and raw biogas. *Renewable Energy, 134,* 1307–1319.
34. Jindal, M., Rosha, P., Mahla, S. K., & Dhir, A. (2015). Experimental investigation of performance and emissions characteristics of waste cooking oil biodiesel and n-butanol blends in a compression ignition engine. *RSC Advances, 5*(43), 33863–33868.
35. Heywood, J. B. (1988). *Internal combustion engine fundamentals.* New York: McGraw-Hill.
36. Kabir, M. M., Rajendran, K., Taherzadeh, M. J., & Sarvari, I. (2015). Experimental and economical evaluation of bioconversion of forest residues to biogas using organosolv pretreatment. *Bioresource Technology, 178,* 201–208.
37. Kacprzak, A., Krzystek, L., & Ledakowicz, S. (2010). Co-digestion of agricultural and industrial wastes. *Chemical Papers, 64*(2), 127–131.
38. Kadam, R., & Panwar, N. L. (2017). Recent advancement in biogas enrichment and its applications. *Renewable and Sustainable Energy Reviews, 73,* 892–903.
39. Kapdi, S. S., Vijay, V. K., Rajesh, S. K., & Prasad, R. (2005). Biogas scrubbing, compression and storage: Perspective and prospectus in Indian context. *Renewable Energy, 30*(8), 1195–1202.
40. Kapoor, R., Ghosh, P., Kumar, M., & Vijay, V. K. (2019). Evaluation of biogas upgrading technologies and future perspectives: A review. *Environmental Science and Pollution Research, 26,* 11631–21166.
41. Kougias, P. G., Treu, L., Benavente, D. P., Boe, K., Campanaro, S., & Angelidaki, I. (2017). Ex-situ biogas upgrading and enhancement in different reactor systems. *Bioresource Technology, 225,* 429–437.
42. Kummamuru, B. (2017). *Global bioenergy statistics*. World Bioenergy Association (WBA).
43. Lecker, B., Illi, L., Lemmer, A., & Oechsner, H. (2017). Biological hydrogen methanation—A review. *Bioresource Technology, 245,* 1220–1228.
44. Liu, Y., & Whitman, W. B. (2008). Metabolic, phylogenetic, and ecological diversity of the methanogenic archaea. *Annals of the New York Academy of Sciences, 1125,* 171–189.

45. Luo, G., & Angelidaki, I. (2013). Co-digestion of manure and whey for in situ biogas upgrading by the addition of H_2: Process performance and microbial insights. *Applied Microbiology and Biotechnology, 97,* 1373–1381.
46. Mahanta, P., Dewan, A., Saha, U. K., Kalita, P., Buragohain, B. (2005). Biogas digester: A discussion on factors affecting biogas production and field investigation of a novel duplex digester. *Journal of Solar Society of India (SESI) Journal, 15*(2), 1–12.
47. Mann, G., Schlegel, M., Schumann, R., & Sakalauskas, A. (2009). Biogas-conditioning with microalgae. *Agronomy Research, 7*(1), 33–38.
48. Mata-Alvarez, J., Mace, S., & Llabres, P. (2000). Anaerobic digestion of organic solid wastes. An overview of research achievements and perspectives. *Bioresource Technology, 74*(1), 3–16.
49. Mitzlaff, K. V. (1988). Engines for Biogas—Theory, Modification, Economic Operation, A publication of German Center for Development Technologies, GTZ-GATE, Germany.
50. Mohiuddin, K., & Park, S. (2019). Characteristics and fundamentals of particulates in diesel engine. In *Engine Exhaust Particulates. Energy, Environment, and Sustainability* (pp. 55–69).
51. Monnet, F. (2003, November). *An introduction to anaerobic digestion of organic waste.* Final report, Remade Scotland.
52. Mosier, N., Wyman, C., Dale, B., Elander, R., Lee, Y. Y., Holtzapple, M., & Ladisch, M. (2005). Features of promising technologies for pretreatment of lignocellulosic biomass. *Bioresource Technology*, 673–686.
53. Muñoz, R., Meier, L., Diaz, I., & Jeison, D. (2015). A review on the state-of-the art of physical/chemical and biological technologies for biogas upgrading. *Reviews in Environmental Science Bio Journal, 14*(4), 727–759.
54. Osorio, F., & Torres, J. C. (2009). Biogas purification from anaerobic digestion in a wastewater treatment plant for biofuel production. *Renewable Energy, 34,* 2164–2171.
55. Pagés-Díaz, J., Pereda, I., Taherzadeh, M. J., Sárvári-Horváth, I., & Lundin, M. (2014). Anaerobic co-digestion of solid slaughterhouse wastes with agro-residues: Synergistic and antagonistic interactions determined in batch digestion assays. *Chemical Engineering Journal, 245,* 89–98.
56. Parawira, W., Murto, M., Zvauya, R., & Mattiasson, B. (2004). Anaerobic batch digestion of solid potato waste alone and in combination with sugar beet leaves. *Renewable Energy, 29,* 1811–1823.
57. Patterson, T., Esteves, S., Dinsdale, R., & Guwy, A. (2011). An evaluation of the policy and techno-economic factors affecting the potential for biogas upgrading for transport fuel use in the UK. *Energy Policy, 39,* 1806–1816.
58. Persson, M. (2003). Evaluation of upgrading techniques for biogas [Internet] Lund School of Environmental Engineering. Available from https://www.sgc.se/document/Evaluation.pdf.
59. Petersson, A., & Wellinger, A. (2009). Biogas upgrading technologies, developments and innovations. IEA Bioenergy.
60. Pischinger, S., Rottmann, M., & Fricke, F. (2006). Future of Internal Combustion Engines. SAE 2006-21-0024.
61. Porpatham, E., Ramesh, A., & Nagalingam, B. (2008). Investigation on the effect of concentration of methane in biogas when used as a fuel for a spark ignition engine. *Fuel, 87*(8), 1651–1659.
62. Rachbauer, L., Voitl, G., Bochmann, G., & Fuchs, W. (2016). Biological biogas upgrading capacity of a hydrogenotrophic community in a trickle bed reactor. *Applied Energy, 180,* 483–490.
63. Ray, N. H. S., Mohanty, M. K., & Mohanty, R. C. (2016). Biogas Compression and Storage System for Cooking Applications in Rural Households. *International Journal of Renewable Energy Research, 6*(2), 593–598.
64. Ray, N. H. S., Mohanty, M. K., & Mohanty, R. C. (2013). Biogas as alternate fuel in diesel engines: A literature review. *IOSR Journal of Mechanical and Civil Engineering, 9*(1), 23–28.
65. Ryckebosch, E., Drouillon, M., & Vervaeren, H. (2011). Techniques for transformation of biogas to biomethane. *Biomass Bioenergy, 35*(5), 1633–1645.

66. Singh, A. P., & Agarwal, A. K. (2018). Low-temperature combustion: An advanced technology for internal combustion engines. *Advances in internal combustion engine research. Energy, environment, and sustainability* (pp. 9–41).
67. Singh, H. N., & Layek, A. (2019). An exposition on the results of utilizing biogas as an alternative fuel on the attributes of internal combustion engines. *International Journal of Renewable Energy Research, 9*(3), 1249–1259.
68. Steinhauser, A. (2008). *Biogas from waste and renewable resources, dieter doublein.* Wiley-VCH.
69. Sun, Q., Li, H., Yan, J., Liu, L., Yu, Z., & Yu, X. (2015). Selection of appropriate biogas upgrading technology-a review of biogas cleaning, upgrading and utilisation. *Renewable and Sustainable Energy Reviews, 51,* 521–532.
70. Tagliabue, M., Farrusseng, D., Valencia, S., Aguado, S., Ravon, U., Rizzo, C., et al. (2009). Natural gas treating by selective adsorption: Material science and chemical engineering interplay. *Chemical Engineering Journal, 155*(3), 553–566.
71. Taherzadeh, M., & Karimi, K. (2008). Pretreatment of lignocellulosic wastes to improve ethanol and biogas production: A review. *International Journal of Molecular Sciences, 9*(9), 1621–1651.
72. Tippayawong, N., & Thanompongchart, P. (2010). Biogas quality upgrade by simultaneous removal of CO_2 and H_2S in a packed column reactor. *Energy, 35,* 4531–4535.
73. Viyaj, K. V., Chandra, R., Subbarao, P. M. V., & Kapid, S. S. (2006). Biogas purification and Bottling into CNG Cylinders: Producing Bio-CNG from Biomass for Rural Automotive Applications. A paper presentation at The 2nd Joint International Conference on Sustainable Energy and Environment (SEE) on 21–23 November, Bangkok, Thailand.
74. Wang, W., Xie, L., Luo, G., Zhou, Q., & Angelidaki, I. (2013). Performance and microbial community analysis of the anaerobic reactor with coke oven gas biomethanation and in situ biogas upgrading. *Bioresource Technology, 146,* 234–239.
75. Weiland, P. (2010). Biogas production: Current state and perspectives. *Applied Microbiology and Biotechnology, 85,* 849–860.
76. Wellinger, A., & Lindberg, A. (1999). Biogas upgrading and utilization. *IEA Bioenergy, Task 24: Energy from biological conversion of organic wastes* (pp. 1–19).
77. Yadav, D., Barbora, L., Bora, D., Mitra, S., Rangan, L., & Mahanta, P. (2017). An assessment of duckweed as a potential lignocellulosic feedstock for biogas production. *International Biodeterioration & Biodegradation, 119,* 253–259.
78. Yang, B., & Wyman, C. E. (2008). Pretreatment: the key to unlocking low-cost cellulosic ethanol. *Biofuels, Bioproducts and Biorefining, 2*(1), 26–40.
79. Yeh, J. T., & Pennline, H. W. (2001). Study of CO_2 absorption and desorption in a packed column. *Energy & Fuels, 15*(2), 274–278.
80. Yun, Y. M., Sung, S., Kang, S., Kim, M. S., & Kim, D. H. (2017). Enrichment of hydrogenotrophic methanogens by means of gas recycle and its application in biogas upgrading. *Energy, 135,* 294–302.
81. Zhao, Q., Leonhardt, E., MacConnell, C., Frear, C., & Chen, S. (2010). *Purification technologies for biogas generated by anaerobic digestion.* CSANR Research Report.
82. Zheng, Y., Zhao, J., Xu, F., & Li, Y. (2014). Pretreatment of lignocellulosic biomass for enhanced biogas production. *Progress in Energy and Combustion Science*, 35–53.

A Comprehensive Study on Utilization of Producer Gas as IC Engine Fuel

Debarshi Baruah, Pankaj Kalita, and Vijayanand Suryakant Moholkar

List of Abbreviations

IPCC	Intergovernmental Panel on Climate Change
GTL	Gas-to-liquid
FT	Fischer–Tropsch
CI	Compression ignition
SI	Spark ignition
IC	Internal combustion
DI	Direct injected
IDI	Indirect injected
BTDC	Before top dead center
VCR	Variable compression ratio
HOME	Honge oil methyl ester
BE5	Honge oil methyl ester + 5% bioethanol
BE10	Honge oil methyl ester + 10% bioethanol
BE15	Honge oil methyl ester + 15% bioethanol
RBOME	Rice bran oil methyl ester
PG	Producer gas
CFB	Circulating fluidized bed
PID	Proportional integrative and derivative
LHV	Lower heating value
CR	Compression ratio

D. Baruah · P. Kalita (✉) · V. S. Moholkar
Centre for Energy, Indian Institute of Technology Guwahati, Guwahati, Assam, India
e-mail: pankajk@iitg.ac.in

V. S. Moholkar
Department of Chemical Engineering, Indian Institute of Technology Guwahati, Guwahati, Assam, India

A. P. Singh et al. (eds.), *Alternative Fuels and Advanced Combustion Techniques as Sustainable Solutions for Internal Combustion Engines*, Energy, Environment, and Sustainability, https://doi.org/10.1007/978-981-16-1513-9_6

SFC	Specific fuel consumption
AGR	Air–gas regulator
IMEP	Indicated mean effective pressure
AER	Air excess rate
BTE	Brake thermal efficiency
BHP	Brake horse power
NG	Natural gas
PAH	Polycyclic aromatic hydrocarbons
MNRE	Ministry of New and Renewable Energy

1 Introduction

The world is currently facing tremendous pressure to shift from fossil fuels to renewables. The reason for this is basically twofold. Firstly, the rampant exploitation of nature's reserves by mankind has led to a sharp decline of fossil fuels further available for extraction. It is uncertain how long these reserves are going to last and some projections for the future show alarming results. Shafiee and Topal [1] in their widely discussed research have estimated that considering a continuation of consumption of fossil fuels at the rate as in 2006, the reserves of oil, gas and coal will approximately last till the years 2046, 2076 and 2206, respectively. This implies that with the rising demand for sustainable energy and dwindling sources of fossil fuels, we have to look for alternate renewable resources. The second important reason for the imperative shift toward renewable energy is the environmental concern related to pollution and global warming. The increasing usage of fossil fuels in the last few decades has resulted in dangerously high levels of pollutants in the atmosphere. One of the major greenhouse gases CO_2 had a concentration level of 377.4 ppm by volume in the atmosphere in 2004, and the same value crossed the 400 ppm mark by September 2017, whereas CO_2 in the atmosphere is considered safe at a concentration level of 350 ppm [2]. Due to the increase in the levels of greenhouse gases in the atmosphere, the global temperature has risen by 0.6 °C in the last century and as per the Intergovernmental Panel on Climate Change (IPCC) projections, till 2100 increase in the global temperature is most likely to be over 2 °C [3]. As a result of this climate change, the world will witness catastrophic problems like a rise in sea level, wildfires, killer cyclones and extreme weather [2].

Hence, the future ahead calls for wide-scale deployment of renewable energy to control this climate change and to meet the ever-increasing global energy demand. Among the various options of renewable energy, biomass gasification is a promising technology, especially because of its simplicity and versatility. This chapter chiefly presents the various aspects of biomass gasification concerning its application in internal combustion engines.

2 Biomass Gasification

2.1 History

The first usages of gasification technology were recorded in both France and England toward the end of the eighteenth century. Many parts of England by 1850 used lighting systems by 'town gas' derived from the gasification of coal and biomass. Toward 1920, this technology was also used in the USA as cooking and lighting fuel provided to the communities by 'gasworks.' In World War I, small gasifiers were used to run vehicles, boats, trains and electric generators. World War II ushered in a phase of much higher usage of the small biomass gasifiers, due to the dearth of supply of petroleum fuels, and by 1943 approximately 8,20,000 of such gasifiers were being used worldwide [4]. The need for gasification technology was diminished after the end of the war and availability of cheap fuel. However, the need for this technology came again with the oil embargo of 1973 and by 2000, the importance of biomass gasification was felt globally owing to the unrest in oil-producing countries and issues related to climate change [5].

2.2 Fundamentals of Biomass Gasification

Biomass gasification involves partial oxidation of biomass at temperatures up to 1000 °C inside a reactor called the gasifier. The resultant gas from this process is called producer gas consisting primarily of combustible gases like carbon monoxide, hydrogen and traces of methane along with other unwanted by-products like tar and dust [6]. The general composition of producer gas from gasification of wood was given by Puig-Arnavat et al. [7]. They stated that hydrogen, carbon dioxide, carbon monoxide, methane and nitrogen concentrations lie in the ranges of 12–20%, 9–15%, 17–22%, 2–3% and 50–54%, respectively. They also estimated that the heating value of the gas lies between 5 and 5.9 MJ/Nm^3. The gas quality largely depends on the feedstock of the gasifier. For example, producer gas from coal gasification, having a heating value of 25 MJ/kg, will have higher energy content than that obtained by gasification of rice straw which has a heating value of 14.5 MJ/kg [8].

2.3 Types of Biomass Gasifiers

The reactors used for biomass gasification are broadly classified into fixed-bed, fluidized-bed and entrained-bed gasifiers, based on the movement of the feedstock material with respect to the gasifying agent. In fixed-bed gasifiers, there is almost no movement of the bed of feedstock in comparison to the gasifying agent. Fixed-bed gasifiers are again subdivided into updraft, downdraft and cross-draft gasifiers based

on positions of air intake and gas outlet. In a fluidized bed, the bed materials are in particulate form and are constantly in motion but relative to the motion of the gasifying agent. Fluidized-bed gasifiers are mainly of two types, bubbling fluidized bed and circulating fluidized bed, classified on the basis of the state of fluidization of the bed particles dependent largely on the velocity of the gasifying agent inside the gasifier. Entrained flow gasifiers are those in which the feedstock flow is entrained together with the flow of the gasifying agent, and there is no difference of motion between the two [9]. All the types of gasifiers discussed here are shown in Fig. 1.

2.4 Processes Inside the Gasifier

As shown in Fig. 1b, the reactor can be divided into four distinct zones, (i) drying zone, (ii) pyrolysis zone, (iii) combustion zone and (iv) reduction zone. The drying zone, with a temperature of around 150 °C, is where the feedstock releases its moisture content. The pyrolysis zone has temperatures in the range of 150–700 °C, and here the volatile matters are released leaving behind char. In between temperatures of 700–1500 °C, the fuel oxidizes in the combustion zone with the release of heat. Finally, the products of combustion are reduced to form producer gas by endothermic reactions in the reduction zone at a temperature range of 800–1100 °C [11]. The major reactions inside the gasifier leading to the formation of producer gas are given below [9]:

$$\text{Water gas reaction: } C + H_2 \rightarrow H_2 + CO \; (-131.38\,\text{kJ mol}^{-1}) \tag{1}$$

$$\text{Boudouardreaction: } CO_2 + C \rightarrow 2CO \; (-172.58\,\text{kJ mol}^{-1}) \tag{2}$$

$$\text{Shift Conversion: } CO + H_2O \rightarrow CO_2 + H_2 \; (-41.98\,\text{kJ mol}^{-1}) \tag{3}$$

$$\text{Methanation: } C + 2H_2 \rightarrow CH_4 \; (+74.90\,\text{kJ mol}^{-1}) \tag{4}$$

2.5 Utilization of Producer Gas

The advantage of producer gas is that it is highly versatile and is suitable for a large variety of applications. The major applications of producer gas are enlisted below:

i. ***Thermal applications***: As discussed before, there is historical evidence of producer gas being used for lighting and cooking. Biomass gasification based producer gas can be used to cater to the thermal needs, both in households and industries. For example, Sutar et al. [12] used small biomass gasifiers for

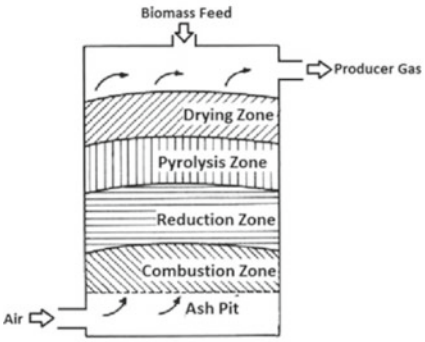

(a) Updraft

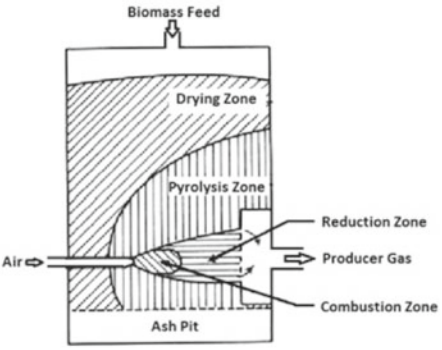

(c) Cross-draft

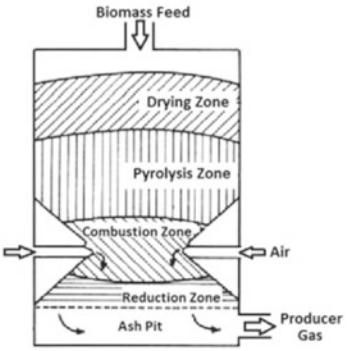

(b) Downdraft

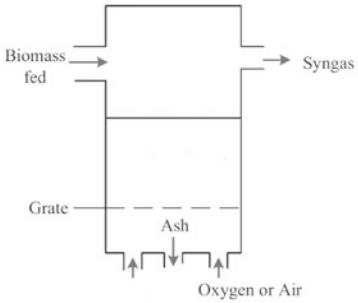

(d) Bubbling fluidized bed

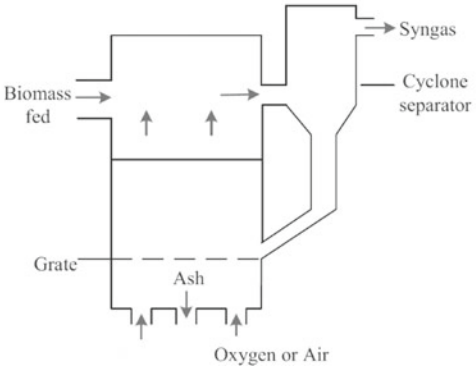

(e) Circulating fluidized bed

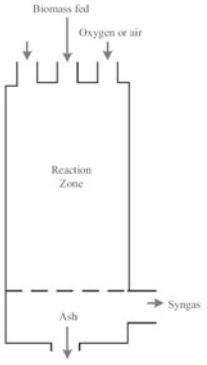

(f) Entrained flow

Fig. 1 Different types of biomass gasifiers [9, 10]

cooking, while Tippayawong et al. [13] utilized cashew nutshell gasification in a cashew nut processing industry.

ii. ***Liquid fuel production***: Producer gas acts as the precursor for gas-to-liquid (GTL) fuels by Fischer–Tropsch synthesis. Boerrigter et al. [14] have successfully demonstrated the operation of biomass gasification-based Fischer–Tropsch (FT) systems to produce 'green fuels'.

iii. ***IC engine operation***: Producer gas can be used to operate both CI and SI engines, and the same has been discussed in detail in the next section of this chapter.

3 Use of Producer Gas in IC Engines

As discussed earlier, the use of producer gas to run vehicular engines has been practiced since World War I. The biomass gasifier generated producer gas, however, needs to be pre-treated before use in engines. Prior to the introduction into the engine, the gas needs to be cleaned and conditioned. This is because the producer gas generated from the biomass gasifier contains impurities and particulate matter, and also the temperature of the gas at the exit from the gasifier is very high. Figure 2 shows a typical engine-gasifier setup with necessary filters and scrubber. The gasifier shown in the figure is typically a downdraft gasifier and immediately on exit from the gasifier the producer gas is introduced to a wet scrubber where water is drizzled on the incoming gas. As a result, the gas is cooled resulting in condensation of a part of the tars, which is washed away with the water along with ash particles. The coarse filter filled with absorbing materials like sawdust, rice husk, etc. is placed after the scrubber. These materials help in capturing tars, particulate matter and moisture. The fine filter further downstream containing layers of fabric or cloth inside takes care of more intensive cleaning of the gas. The flare bypasses a small amount of the gas to be lighted up to visibly monitor the quality of the gas. A blower (not in the figure) may also be introduced in the stream to create suction and maintain a steady gas pressure at the engine inlet as there will be a pressure drop at each of the filters. After passing through such a typical arrangement, the producer gas is finally let into the engine for utilization.

Producer gas has the suitability of being used in both spark ignition (SI) and compression ignition (CI) engines. Many researchers indicate favorable results of utilizing producer gas for fueling both SI and CI engines. The same has been discussed in detail in the following sections.

3.1 Producer Gas in CI Engines

The use of producer gas in diesel-powered engines is quite simple and requires no major engine modification. The producer gas, after proper pre-treatment, is allowed

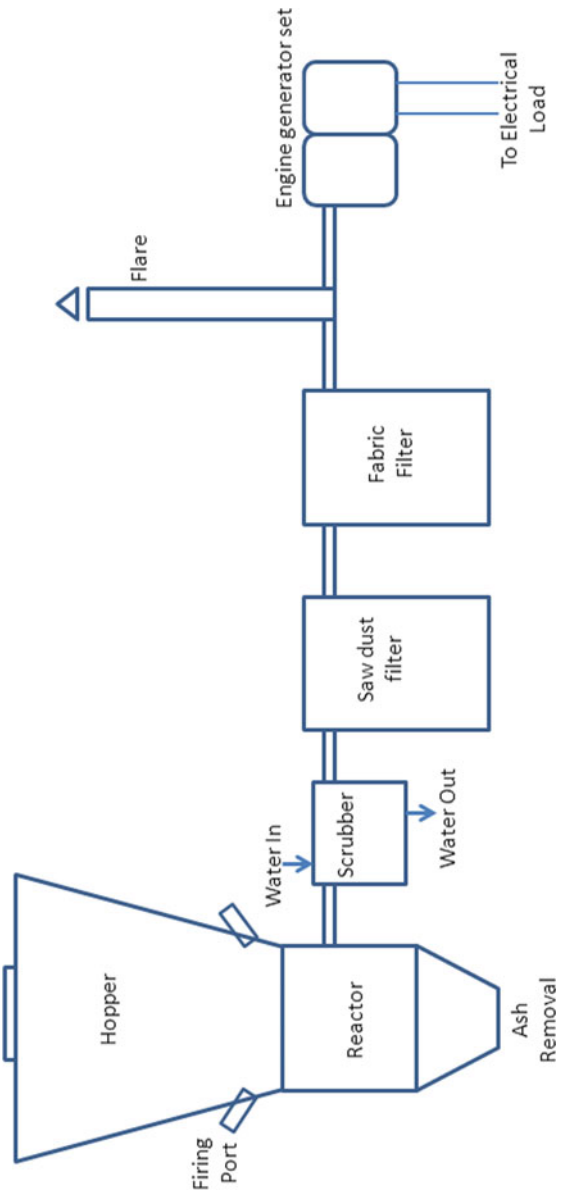

Fig. 2 Schematic of a typical engine-gasifier setup

into the diesel engine along with air through the air intake manifold. This fuel–air mixture input results in a lesser requirement of diesel injection for the necessary combustion and power generation. As a result, up to 80–90% diesel replacement by producer gas can be achieved. However, diesel in CI engines cannot be completely replaced by producer gas. Initially, 100% diesel is required to start the engine and to sustain the operation on dual-fuel mode; a part of diesel is constantly required.

Early researches on the utilization of producer gas for CI engine operation are seen from the last century, few of which have been discussed here. In 1981, Ortiz-Cañavate et al. [15] compared operating characteristics of a 34-kW diesel engine run on single-fuel mode with the same engine run on dual-fuel modes, with low-energy gas from gasification of densified solid waste and synthetic biogas. The low-energy gas, after filtration and cooling, was fed to the diesel engine through a mixing chamber, and the synthetic biogas was fed to the engine by using a carburetor. The requirement of diesel in both the dual-fuel modes was reduced to 15–24%. They reported that the power output in the dual-fuel modes was 86% with biogas and 71% with the low-energy gas, as compared to 100% of rated power with normal diesel operation. Vyarawalla et al. [16] in 1984 designed and built a 9 kW biomass gasifier of downdraft type for water-pumping and power generation applications. The gasifier was put to a field trial of around 1000 h using sawmill waste, cotton stalk and toor stalk as feed. They achieved a diesel saving of up to 75% utilizing producer gas in dual-fuel mode. They also reported that no problems of the engine were developed due to the usage of the producer gas during the trial. They concluded that the technology in its current state can be applied for rural applications. Parikh et al. [17] used a downdraft-type biomass gasifier with Subabool wood (Leucaena leucocephala) feed for running two types of diesel engines, direct injected (DI) and indirect injected (IDI). They found that the volume of the cooling–cleaning system is an important parameter in determining the level of diesel replacement along with the power capacity under dual-fuel mode. They reported an increase of diesel substitution from 68 to 80% at 80% of rated load and maximum power capacity from 3.7 to 4.5 kW by alteration in the volume of the gas cooling–cleaning system. They established that CO emissions are increased, more at part loads, while smoke levels are reduced under this dual-fuel operation. CO increases primarily due to improper combustion of the pre-mixed air–fuel mixture inside the cylinder. They achieved 80–90% diesel replacement on input energy basis in the DI as well as the IDI engine with producer gas. The dual-fueled DI engine showed high exhaust gas temperatures indicating delayed burning, whereas IDI engine exhaust temperatures remained practically unchanged for diesel and dual-fuel operation. They concluded that this is because of a higher level of turbulence in the combustion chamber of the IDI engine, which is desirable for rapid combustion in dual-fuel mode. Manes et al. [18] operated a 13 kVA diesel engine-generator set on dual-fuel mode with producer gas from a downdraft gasifier fed with wood, maize cobs and cotton sticks. They found that the brake thermal efficiency was lesser in dual-fuel mode due to slower combustion of producer gas. They also noted that the exhaust gas temperature was higher compared to that of the engine run on diesel alone. This was due to the higher energy input required with producer gas which led to an increase of temperature of the combustion chamber. The maximum diesel

substitution achieved was 74.5% at 80% of the rated load. The limitation of the load must be due to the inability of engines to run on rated capacity when operated with producer gas in dual-fuel mode. The engine failed after 50 h of operation due to tar and carbon deposits.

A sizeable volume of researches in this area can be seen in the last two decades, owing to the energy crisis and environmental concerns. In 2001, Bhattacharya et al. [19] conducted experiments on a multi-stage hybrid gasifier and diesel engine system using coconut shell-charcoal feed. The lowest tar content found in this hybrid gasification was 28 mg Nm^{-3}. An efficiency of 14.7% was obtained from the engine-generator system at a maximum electrical power output of 11.44 kWe. The energy input from producer gas was 81% of the total for this maximum output. The electrical power output of the system when running on dual-fuel mode reduces to 79% of that when the system is run on solely diesel. Uma et al. [20] in 2004 compared the emission characteristics of a biomass gasifier-based electricity generation system in diesel alone and dual-fuel modes. They found a diesel replacement rate ranging between 67 and 86% in dual-fuel mode. They observed that emissions of NO_x and SO_2 were reduced in dual-fuel mode as compared to solo-diesel operation. In dual-fuel mode, NO_x decreases due to lower flame temperatures, whereas SO_2 decreases due to lower sulfur content in the biomass feed. However, the CO emission was higher at all load conditions for dual-fuel, which they attributed to a number of factors like low calorific value gas, lower adiabatic flame temperatures and reduced mean effective pressures. Ramadhas et al. [21] analyzed the performance of a biomass gasifier-CI engine system by operating the engine at various gas–air input ratios and at varying loads. They used coir pith and wood chips as gasifier feed and they observed better results in engine efficiency and diesel savings with wood-feeding as compared to coir pith. The engine in dual-fuel mode could operate at only 50–60% of maximum load condition, and also the CO emission is higher compared to single-fuel mode. Lekpradit et al. [22] studied the effect of the advancement of injection timing on a dual-fuel diesel engine operated with producer gas. The factory set diesel injection timing of 12° before top dead center (bTDC) was increased to 17° bTDC. The advantages they achieved by this were lower CO emission, higher brake thermal efficiency, higher diesel replacement rate and lower specific energy consumption for the same power by the dual-fuel engine. This is primarily because of the enhancement of mixing time of diesel fuel with air-producer gas in the combustion chamber leading to better combustion characteristics. The only disadvantage they observed with injection timing advancement was an increase in the NO_x emissions which is due to elevated combustion temperatures. The performance and emission characteristics of a biomass gasifier-diesel engine setup in dual-fuel condition with supercharged intake and premixed intake were compared by Hassan et al. [23]. Using supercharged (compressed) air-producer gas mixture at 200 kPa, they found that the brake thermal efficiency improved by 15% than that of conventional premixed dual-fuel. The diesel replacement rate for premixed dual-fuel ranged between 48.3 and 62.2%, whereas the same for supercharged dual-fuel was 52.8–68.2%. With supercharging, combustion efficiency increases, and CO emission decreases as compared to premixed dual-fuel operation. Specific energy consumption also improved in supercharged condition.

The improvement in all the mentioned parameters with supercharging can be mainly attributed to the increase in air intake into the combustion chamber which ensures efficient combustion in dual-fuel mode. Shrivastava et al. [24] investigated the performance and emission of a CI Engine coupled with a biomass gasifier running in dual-fuel mode. They fed wood chips and mustard oil cakes obtained from a mustard seed oil expeller unit, in the ratio of 7:3, in the gasifier. They introduced producer gas through the inlet manifold of the dual-fuel engine at flow rates of 4 lpm, 6 lpm, and 8 lpm, respectively. Their complete findings are shown in Table 1. They concluded that the producer gas flow rate of 4 lpm with diesel in the dual-fuel operation gave the best engine performance and lowest tail-pipe emissions among all flow rates.

In recent research by Sharma and Kaushal [25], the operation of a variable compression ratio (VCR) CI engine utilizing producer gas derived from walnut shells was analyzed. They experimented with varying compression ratios (CR) of 12, 14, 16 and 18, respectively, for both diesel and dual-fuel mode at different values of brake power (0, 0.86, 1.72, 2.56 and 3.44 kW). A maximum diesel replacement of 58.18% was obtained at CR value of 18 for dual-fuel mode. Maximum brake

Table 1 Experimental performance and emission of 4.4 kW diesel engine with different producer gas (PG) flow rates [24]

Parameters	Fueling of the engine			
	Only diesel	Diesel + 4 lpm PG	Diesel + 6 lpm PG	Diesel + 8 lpm PG
Maximum brake thermal efficiency (%)	27.5	26	25	24.5
Brake-specific energy consumption (approx. value at full load) (MJ/kWh)	12.8	13.5	14	15
Exhaust gas temperature (at full load) (°C)	330	365	378	388
CO emission (approx. value at full load) (vol%)	0.019	0.022	0.024	0.029
HC emission (approx. value at full load) (ppm)	11.5	13.5	17.4	20.9
NO emission (approx. value at full load) (ppm)	428	350	288	230
Smoke density (approx. value at full load) (%)	22.5	25.5	27.8	32.2

thermal efficiencies in mono-fuel and dual-fuel modes were 25.63% and 21.61%, respectively. At 3.44 kW brake power, NO_x emission was 16.09–45.23% more in solo-diesel operation compared to dual-fuel operation. However, at the same power, CO emission showed a rise of 62.21–72.53% in dual-fuel mode compared to mono fuel mode.

Certain works show that the CI engine can be run on dual-fuel mode utilizing producer gas along with green fuels making it a renewable source of power completely independent from fossil fuels. Yaliwal et al. [26] experimented on a dual-fuel engine fueled with biomass gasifier generated producer gas and Honge oil methyl ester (HOME) with bioethanol blends. They used three blends for the engine operation, HOME + 5% bioethanol (BE5), HOME + 10% bioethanol (BE10) and HOME + 15% bioethanol (BE15). The best result was obtained from BE5-Producer gas operation, as compared to operation with producer gas and other blends or producer gas and plain HOME. With this optimum fuel blend, brake thermal efficiency increased up to 4–9%, HC and CO decreased while NO_x marginally increased. Nataraja et al. [27] utilized rice bran oil methyl ester (RBOME) and coconut shell-derived producer gas in a dual-fuel CI engine and also studied the effect of turbocharging. They observed that the turbocharged dual-fuel engine could operate at up to 90% of the rated load, whereas the normally aspirated dual-fuel engine could operate at up to 80% load. Turbocharging helped in the improvement of the performance of the dual-fuel engine at higher loads with maximum brake thermal efficiency of 22.5% and also reduced emissions of smoke, HC and CO by 10–25% as compared to the normally aspirated dual-fuel engine. Nayak and Mishra [28] studied the emission characteristics of a dual-fuel engine operated with Jojoba biodiesel and preheated Jojoba oil blends along with producer gas derived from the gasification of coir pith. The best results were obtained for 20% biodiesel blend on a volumetric basis with producer gas, at 8 kW loading condition and equivalent diesel saving of 80.6% was achieved. Lower NO_x, whereas higher CO, CO_2 and HC was observed in dual-fuel mode operation with producer gas as compared to that of single-fuel mode for all pilot fuels. This is due to inefficient combustion inside the engine when producer gas is introduced with air. Though such researchers have proved the suitability of CI engine operation with biodiesel and producer gas in dual-fuel mode, the possibility of continuous operation for longer duration without breakdown needs to be ascertained.

3.2 Producer Gas in SI Engines

Unlike CI engines, customization may be required for SI engines to be operated with producer gas. The SI engines can be run on 100% producer gas, but engine modifications are required. Researchers have suggested advancement of ignition timing, use of higher compression ratio, use of specialized air–gas regulators, etc. to run SI engines on producer gas. Ignition timing advancement is required due to lower flame speed, while a high compression ratio is required to increase the energy density of the low heating value gas. Shashikantha et al. [29], in 1994, developed a simulation

model of a 15 kWe SI engine converted from a diesel engine. They simulated the engine to operate on wood-derived producer gas of heating value 6–7 MJ/Nm^3. They used a reduced compression ratio of 11.5 and an ignition timing of 35° before top dead center (bTDC). The engine efficiency obtained from this simulation was in the range of 28–32%. Sridhar et al. [30] experimented on a multi-cylinder SI engine modified from a 28 kW commercial diesel engine using varying compression ratios from 11.5 to 17. They obtained the best performance of the engine at the highest compression ratio with maximum brake power with an overall efficiency of 21%. They also observed that the maximum de-rating of power of the engine was 16% and reduction in overall efficiency was 32.5% in the gas mode in comparison to that with diesel operation at the same compression ratios. A rice-husk-fueled CFB gasifier with a gas engine array, as shown in Fig. 3, was studied for a total power generation of 1 MW at a rice mill in China by Yin et al. [31]. They found the suitable operating temperatures of the CFB gasifier in the range of 700–850 °C and optimum performance of the system at a loading of over 800 kW. They estimated an overall efficiency of 17% of the complete system with a gasifier efficiency of 65%. They also calculated the economics of the system and found that the payback period was lesser than two years.

Pushp and Mande [32] used a proportional integrative and derivative (PID) governor mechanism for the operation of a producer gas-based SI engine on varying loads. For field testing, they converted a CI engine into a 100% producer gas SI engine by replacing the injector with a spark plug, machining the piston crown to facilitate fast burning and advancement of ignition timing to 24°–26° bTDC for obtaining maximum brake torque. Using the PID controller, the engine was able to cope with sudden fluctuations of the load to deliver a steady output frequency of 50 $\pm$ 1 Hz. Ulfvik et al. [33] compared the efficiency, emissions and performance of a gas engine operation on producer gas with that of natural gas. They observed that maximum loading possible for the engine decreases with producer gas operation as compared to natural gas operation. The advantage of producer gas operation they found over natural gas operation was that the engine was more stable over a higher range of air–fuel equivalence ratio (λ), and also the emissions of NO_x and HC were lower, though CO emission was on the higher side. Szwaja et al. [34] operated a gas engine on municipal sewage sludge-derived producer gas enriched with methane in ratios ranging from 0 to 60% by volume. This enrichment was required because of the low quality of the gas (LHV < 4.5 MJ/Nm^3) which resulted in the occurrence of frequent misfiring. They obtained optimum gas mixing at 40% methane with 60% producer gas where the LHV increases by 37% compared to only producer gas, and the engine operates smoothly with the least possible emissions. They also found that there is no significant effect on exhaust emissions or performance of the engine with methane enrichment higher than 40%. Homdoung et al. [35] analyzed the performance and emissions of a small CI engine converted to SI and operated on producer gas. For their experiments, they used varying loads, compression ratios and ignition timings in the engine. The maximum brake power for the engine was obtained at CR of 14. The optimum values of brake thermal efficiency and the specific energy consumption were obtained at CR 14. At a higher CR of 17, engine knock was observed to begin.

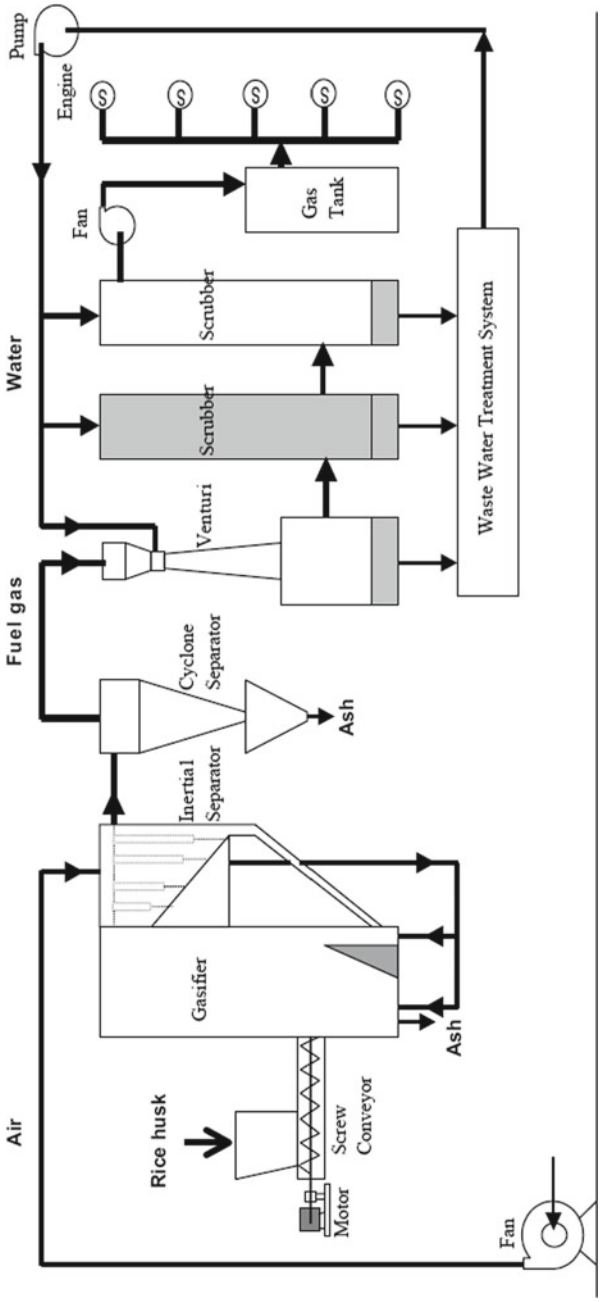

Fig. 3 Schematic of CFB gasifier with gas engine power generation studied by Yin et al. [31]

At all conditions, CO emission of the producer gas engine was found to be higher than its equivalent diesel engine, but less than that by gasoline operation by 2–6%. Indrawan et al. [36] conducted experiments on a commercial 10 kW natural gas engine modified to operate on producer gas supplied from a specialized downdraft gasifier with a cyclonic combustion chamber fed with switchgrass. The maximum power output of 5 kW was achieved with producer gas operation with an electrical efficiency of 21.3% and specific fuel consumption (SFC) of 1.9 kg/kWh, whereas the same engine running with natural gas gave the highest output of 9 kW with 22.7% electrical efficiency and 0.3 kg/kWh SFC. The CO, HC, NO_x and SO_2 emissions with producer gas as fuel were lower than that of natural gas operation at all loads. The CO emissions were lower with producer gas as it is partly hydrogen which combusts to form water molecules. SO_2 was also lower with producer gas due to a low amount of sulfur in feedstock as compared to natural gas. Lower NO_x with producer gas can be attributed to lower flame temperatures, whereas HC is lower due to the presence of unbound hydrogen in producer gas as compared to CH_4 in natural gas.

Babu et al. [37] utilized an air–gas regulator (AGR) for the running of a 2.2 kW producer gas engine. The regulator is required for the stability of the engine under conditions of varying load and gas composition. For their experiments, they used artificial producer gas from calibrated bottles as per the composition of typical biomass generated producer gas. With customization and adaptation of the air–gas regulator for the engine operation, they obtained a brake power output of 1.87 kW with peak in-cylinder pressure of 33 bar with producer gas, whereas the same was 2.2 kW at 38 bar, respectively, with gasoline operation. In very recent research, Naryanto et al. [38] investigated the working of a twin-cylinder Kawasaki FD750 engine with producer gas obtained from the gasification of wood pellets in an open-top downdraft gasifier. They concluded from their experiments that with an increase in air excess rate (AER), which is at leaner air–gas mixtures, indicated mean effective pressure (IMEP) inside the engine decreased. They also suggested the requirement of higher compression ratios for producer gas operation.

All the research works discussed in Sects. 3.1 and 3.2 of this chapter have been summarized in Table 2.

4 Problems Associated with Producer Gas Operation in Engines

In spite of the viability of the utilization of producer gas from biomass in engines as a renewable fuel, there are inherent problems of producer gas that must be addressed. A few of these major issues are discussed in the section below.

Table 2 Utilization of biomass gasification based producer gas for engine operation

Investigator (s)	System description	Gasifier feed	Experimental conditions	Research findings
Ortiz-Cañavate et al. [15]	34-kW diesel engine with batch-fed, downdraft gasifier and alternately, carburetted synthetic biogas	• Densified solid waste	• Single-fuel mode • Two dual-fuel modes • Pilot fuel diesel in each dual-fuel modes	• Diesel substitution of 76–85% achieved with both dual-fuel modes • Power output was 30 kW with biogas and 25 kW with low-energy gas, both dual-fuel mode, as compared to full 34 kW with only diesel
Vyarawalla et al. [16]	9 kW downdraft biomass gasifier with equivalent CI engine	• Sawmill waste • Cotton stalk • Toor stalk	• Dual-fuel mode • Pilot fuel diesel	• Field trial of around 1000 h without any engine problems • Achieved a diesel substitution of up to 75%
Parikh et al. [17]	Downdraft, open-top gasifier with 3.7 kW DI and 4.4 kW IDI engines	• Subabool wood	• Dual-fuel mode • Pilot fuel diesel	• 80–90% diesel replacement achieved in both DI and IDI engines • The design/volume of cooling-cleaning system has major influence on operation of engine-gasifier system • IDI engine more suitable for dual-fuel mode compared to DI engine due to higher turbulence in combustion chamber

(continued)

Table 2 (continued)

Investigator (s)	System description	Gasifier feed	Experimental conditions	Research findings
Manes et al. [18]	10 kW downdraft gasifier connected to diesel engine of 10.4 kW coupled with 13 kVA electric generator	• Wood • Maize cobs • Cotton sticks	• Dual-fuel mode • Pilot fuel diesel	• Highest diesel replacement achieved was 74.5% when engine at 80% load • Brake thermal efficiency decreases and exhaust gas temperature increases in dual-fuel operation
Bhattacharya et al. [19]	Multi-stage hybrid biomass–charcoal gasifier with 36 kW 3-cylinder DI engine	• Coconut shell and charcoal	• Single-fuel mode • Dual-fuel mode • Pilot fuel diesel	• Multi-stage hybrid gasifier produced low tar content gas • Diesel replacement of 81% achieved at maximum power output of 11.44 kW
Uma et al. [20]	Throat less, closed-top downdraft gasifier with direct injected six-cylinder 77.2 kW engine	• Keekar wood	• Single-fuel mode • Dual-fuel mode • Pilot fuel diesel	• Obtained 67–86% diesel replacement rate • NO_x and SO_2 emissions lesser in dual-fuel mode • CO emission higher in dual in dual-fuel mode

(continued)

Table 2 (continued)

Investigator (s)	System description	Gasifier feed	Experimental conditions	Research findings
Ramadhas et al. [21]	Downdraft gasifier connected to 5.5 kW single-cylinder CI engine	• Wood chips • Coir pith	• Dual-fuel mode • Pilot fuel diesel	• Wood chips generated gas gives higher diesel savings compared to that of coir pith • Brake thermal efficiency also higher while using wood chips in dual-fuel mode • Only 50–60% of maximum load condition of the engine could be achieved in dual-fuel condition
Lekpradit et al. [22]	50 kg/hr downdraft gasifier with 4-cylinder 50 kW dual-fuel engine	• Wood	• Dual-fuel mode • Standard injection timing • Advanced injection timing • Pilot fuel diesel	• Standard diesel timing of 12° bTDC increased by 5° • Thermal efficiency, fuel substitution, specific fuel consumption and emission improve on advancement of injection timing • NO_x emission increase on advanced injection timing

(continued)

Table 2 (continued)

Investigator (s)	System description	Gasifier feed	Experimental conditions	Research findings
Hassan et al. [23]	70 kgh^{-1} downdraft gasifier connected to single-cylinder (DI) 4.9 kW diesel engine	• Biomass fuel	• Dual-fuel mode • Premixed air-gas intake • Supercharged air–gas intake • Pilot fuel diesel	• Brake thermal efficiency increases by 15% for supercharged dual-fuel compared to premixed dual-fuel • Higher diesel displacement and reduction in specific energy consumption observed in supercharged engine • CO emission from supercharged dual-fuel decreased as compared to premixed dual-fuel operation
Shrivastava et al. [24]	Downdraft gasifier with single-cylinder (DI) 4.4 kW diesel engine	• Wood chips + mustard oil cakes in ratio of 7:3	• Dual-fuel mode • Varying gas flow rates • Pilot fuel diesel	• Best performance obtained at producer gas inlet rate of 4 lpm in the dual-fuel engine • Only 5.45% reduction in brake thermal efficiency gas flow rate of 4 lpm at full load compared to solo-diesel operation • NO emission is reduced by 18.60% at the optimum gas inlet

(continued)

Table 2 (continued)

Investigator (s)	System description	Gasifier feed	Experimental conditions	Research findings
Sharma and Kaushal [25]	Downdraft gasifier with VCR CI engine of 3.5 kW	• Walnut shells	• Single-fuel mode • Dual-fuel mode • Varying compression ratio • Different brake power • Pilot fuel diesel	• Highest diesel substitution of 58.18% achieved at CR value of 18 for dual-fuel operation • 25.63% and 21.61% were highest values of brake thermal efficiency in mono fuel and dual modes, respectively • NO_x reduces while CO increases in PG + diesel operation as compared to only diesel
Yaliwal et al. [26]	Downdraft gasifier with 5.2 kW single-cylinder CI engine (DI)	• Babool wood	• Dual-fuel mode • Pilot fuel plain biodiesel (HOME) and its blends with bioethanol (BE)	• Best results obtained in dual-fuel mode with producer gas and HOME + 5% bioethanol (BE-5) • Brake thermal efficiency increased up to 4–9% in BE-5 with PG compared to all other fuel combinations • With BE-5 and PG operation, HC and CO decreased in emission, but NOx marginally increased

(continued)

Table 2 (continued)

Investigator (s)	System description	Gasifier feed	Experimental conditions	Research findings
Nataraja et al. [27]	Downdraft gasifier fitted to a single-cylinder CI engine	• Coconut shell	• Dual-fuel mode • With turbocharging • Without turbocharging • Pilot fuel rice bran oil biodiesel	• Turbocharging allowed operation at higher loading (up to 90%) compared to normal aspiration • BTE under optimized and turbocharged condition increased by 4.24% with biodiesel as pilot fuel • Lower CO and HC emissions but higher NO_x emission with turbocharging
Nayak and Mishra [28]	Downdraft gasifier with 14 HP 2-cylinder CI engine	• Coir pith	• Dual-fuel mode • Pilot fuel blends of Jojoba biodiesel	• Optimum operation of dual-fuel engine obtained with B20 blend of Jojoba biodiesel and PG • Diesel replacement of 80.6% achieved with this blend • NO_x decreases, but CO, CO_2 and HC increases in dual-fuel mode in comparison to that of single-fuel mode
Shashikantha et al. [29]	Biomass gasifier fueled 15 kWe SI engine converted from a diesel engine	• Wood	• 100% gas mode • Simulation model	• CR and ignition timing used are 11.5 and 35° bTDC, respectively • Simulation showed engine efficiency of 28–32%

(continued)

Table 2 (continued)

Investigator (s)	System description	Gasifier feed	Experimental conditions	Research findings
Sridhar et al. [30]	Open-top downdraft gasifier connected to 28 kW multi-cylinder VCR SI-engine coupled with 25 kVA alternator	• Casuarina wood	• 100% gas mode • Varying compression ratios • Optimized ignition timing advance	• Changing CR from 11.5 to 17, best engine performance with 100% PG obtained at 17 • At 17 CR, maximum output and highest overall efficiency were obtained as 17:5 kWe and 21%, respectively • Overall efficiency declined by 32.5% with PG as compared to diesel mode at equivalent CR
Yin et al. [31]	1500 kg h^{-1}CFB gasifier connected with 5 parallel SI gas engines of 200 kW each	• Rice husk	• 100% gas mode	• Optimum performance at gasifier temperature 700–850 °C and connected load >800 kW • Total system efficiency 17% at gasifier efficiency of 65% • Economic evaluation shows payback period <2 years
Pushp and Mande [32]	Downdraft gasifier with a three-cylinder SI engine converted from 28 BHP CI engine	• Charcoal	• 100% gas mode • Fluctuating loads	• CI engine converted to 100% PG SI by installing spark plugs in place of injectors, customizing combustion chamber and advancing ignition to 24°–26° bTDC • With PID governor, engine managed to deliver output frequency of 50 ± 1 Hz even at instantaneous fluctuations of load

(continued)

Table 2 (continued)

Investigator (s)	System description	Gasifier feed	Experimental conditions	Research findings
Ulfvik et al. [33]	The Viking gasifier (efficiency 93%) connected to a customized single-cylinder gas engine	• Wood chips	• 100% gas mode • PG operation • NG operation	• Maximum load 19 bar of IMEP for NG, whereas 12 bar for PG • PG better lean burning fuel compared to NG • NO_x and HC emissions decreases with PG, but CO increases
Szwaja et al. [34]	Sludge gasifier connected with a 16 kW/1500 rpm gas engine	• Sewage sludge	• 100% gas mode • PG + fuel	• Sludge gasification based PG operation of engine causes inefficient combustion and misfiring • These issues resolved by enriching PG with an optimum of 40% CH_4
Homdoung et al. [35]	Downdraft gasifier with a 3.2 kW producer gas engine converted from diesel engine	• Longan wood charcoal	• 100% gas mode • Varying CR • Varying load • Varying ignition timing	• Best CR for PG operation found to be 14 • Maximum brake power and optimum BSFC were 3.17 kW and 0.74 kg/kWh, respectively • Highest brake thermal efficiency obtained was 23.9% • CO emission with PG higher than diesel in equivalent engine, but lesser in similar gasoline engine

(continued)

Table 2 (continued)

Investigator (s)	System description	Gasifier feed	Experimental conditions	Research findings
Indrawan et al. [36]	Downdraft gasifier with a cyclonic combustion chamber connected to 10 kW natural gas engine modified to run on producer gas	• Switchgrass	• 100% gas mode • PG operation • NG operation	• Electrical efficiency and SFC in PG operation are 21.3% and 1.9 kg/kWh, respectively • Electrical efficiency and SFC with NG operation are 22.7% and 0.3 kg/kWh, respectively • CO, HC, NOx and SO_2 emissions lower with PG compared to NG
Babu et al. [37]	Bottled producer gas to run 2.2 kW single-cylinder PG engine	–	• 100% gas mode • PG operation • NG operation • Air-gas regulation	• Regulator important for operating stability of the engine under varying conditions • Maximum brake power with PG was 1.87 kW and that with NG was 2.2 kW
Naryanto et al. [38]	Open-top downdraft gasifier to run a 0.75 L V-twin gas engine	• Wood pellets	• 100% gas mode • Producer gas operation	• IMEP decreases with increase in AER • Higher CR desirable for PG operation of SI engine

4.1 Tar Content

Tar presence in biomass gasification-based producer gas is one of the major deterrents in the use of the gas in IC engines. Milne et al. [39], in their widely popular report on biomass gasifier tars, provide a definition of tar as primarily aromatic hydrocarbons that are formed in the gasification process and condense in the gasifier itself or further downstream. Elliot [40] proposed a scheme of formation of tars wherein the transition is a function of temperature as shown in Fig. 4. In this scheme, the primary compounds pass through phases of phenolic hydrocarbons to final polycyclic aromatic hydrocarbons (PAHs) which largely constitute tars.

The presence of tar in producer gas makes it highly unsuitable for IC engine utilization. Operation of engine with tar containing producer gas causes clogging and fouling in valves, combustion chamber and other pathways due to condensation of tar. Manes et al. [18] attempted the operation of a CI engine with producer gas without a proper gas cleaning system. As a result, there were tar deposits inside the cylinder and on the piston head, and the valves along with piston rings were stuck with tar. Finally, the engine seized after only 50 h of operation. Thus, it is evident that working with tar-laden producer gas, an engine will require a high amount of maintenance and in most severe cases, will cause complete failure of the engine. To prevent such occurrence, the tar content in producer gas must be brought down to acceptable levels before its introduction into an IC engine. Thapa et al. [41] on the basis of their study of other researchers suggested tar content of 0.01–0.1 g/Nm^3 or lower in producer gas for favorable IC engine operation.

To lower the tar content of producer gas, many tar removal techniques are employed which are broadly classified into primary and secondary methods. The measures taken inside the gasifier itself are called primary, whereas the treatment methods used downstream from the gasifier are called secondary methods. The primary methods mainly involve optimization of operating parameters, utilization of bed additive/catalyst and modifications in the gasifier design [42]. There are mainly three ways for secondary treatment of tar, which are physical methods, catalytic cracking and thermal cracking. Physical methods are again divided into wet gas and hot gas treatment. The equipment used for wet gas cleaning includes spray towers, packed column scrubbers, OLGA, etc., whereas cyclone separators, electrostatic precipitators, ceramic filters, fabric filters, etc. are used for dry cleaning. Catalytic cracking involves the use of catalysts like zeolite, dolomite, olivine, etc. Thermal cracking gives good results in tar removal but is energy-intensive. Anis and Zainal [43] in their review of tar reduction methods stated that a secondary measure should compulsorily be applied for tar removal from producer gas, whereas primary

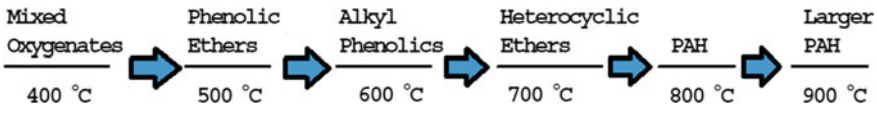

Fig. 4 Schematic of maturation of tars [40]

measures may be optionally used for optimization. The removal of tar from producer gas is itself a huge area of research. However, the discussion in this section is kept brief owing to the constraints of this chapter.

4.2 Presence of Ash

Other than tar, gas generated from a biomass gasifier has other unwanted components that create problems in the engine. Ash formed in the process flows out in particulate form with the gas which may cause problems in the engine. Hence, filtration units downstream of the gasifier capture such particulate matter along with tars. However, a high amount of such impurities in the producer gas will result in a greater need for frequent maintenance of the filtration units. Livingstone [44] had stated that the concentration of particulate matter in the gas should be within 2–6 g/m^3 in a properly designed gasifier.

4.3 De-rating of Engine

With the operation of commercially available engines (both CI and SI) on producer gas, the rated capacity of the engine can never be achieved. Hence, a certain percentage of de-rating is always present in all the comparative studies of producer gas operation versus fossil fuel operation of engines. Sridhar et al. [30] observed a maximum de-rating of the power output of 16% in producer gas operation of a modified SI engine as compared to its original diesel operation at equivalent compression ratios. They attributed this de-rating to the swirl-type combustion chamber designed for diesel fuel which results in higher heat loss to the cylinder walls. Ramadhas et al. [21] found that a de-rating of 40–50% occurs in a CI engine on dual-fuel mode with producer gas when compared to the maximum capacity with only diesel. They cited the reason for this de-rating to be the increased intake of the low calorific value gas containing certain pre-combusted components which decrease the oxygen supply inside the engine for proper combustion. They suggested the selection of a higher capacity engine than required when planning for dual-fuel operation with producer gas.

4.4 CO Emissions

Though the other emissions like NO_x, HC, SO_x, etc. decrease with the operation of engines with producer gas either on dual-fuel or single-fuel mode, many researchers have reported an increase in CO in the emissions [20, 25, 28, 33]. Uma et al. [20] attributed this to the low heating value of gas, low adiabatic flame temperatures and

Table 3 Corrective measures for problems associated with producer gas utilization in IC engines

Problem	Reason(s)	Corrective measure(s)
Tar formation	Formation of higher hydrocarbons with temperature rise	• Primary methods – Optimization of operating parameters – Use of bed additive or catalyst – Gasifier design modification • Secondary methods – Physical methods like spray towers, packed column scrubbers, cyclone separators, electrostatic precipitators, ceramic filters, fabric filters, etc. – Catalytic cracking – Thermal cracking
Ash and particulates	Formed during the gasification process and flow downstream with the gas	• Use of filters, scrubbers, cyclone separators, electrostatic precipitators, etc. • Improvement of gasifier design
Engine de-rating	Low calorific value of producer gas	• Improvement of combustion chamber design • Supercharging
CO emission	Incomplete combustion	• Utilization of producer gas specialized engines

low mean effective pressures. This leads to incomplete combustion in the engine resulting in an increase of CO emission. They recommended the design and development of specialized engines for producer gas rather than modifying petroleum fuel-based engines for the same.

The challenges to the utilization of producer gas as an IC engine fuel and their corrective measures as discussed in this section have been presented in Table 3.

5 Biomass Gasification for Decentralized Power Generation

Biomass gasification is a mature technology and a promising option for decentralized power generation, especially in a country like India where the majority of the population is agrarian. According to Ministry of New and Renewable Energy (MNRE, Government of India), estimated surplus biomass in India, including agriculture and forest residues, is approximately 120–150 million metric tonnes per annum which corresponds to a total bioenergy potential of around 18,000 MW [45]. With such a huge availability of biomass for energy conversion, biomass gasification should be one of the foremost technologies taken into consideration. In the case study of rural electrification of a small village of Hosahalli in Southern India by biomass

gasification, Ravindranath [46] has shown that such systems are technologically and economically feasible for decentralized power generation. He added that such systems provide advantages like the promotion of biomass generation locally for energy, employment generation, community independence, carbon sequestration and reduction of emissions. Buragohain et al. [47] too analyzed the suitability of biomass gasification for power generation in the context of the Indian perspective. They stated that the capital cost of grid extension to remote locations, high amount of transmission losses and low demand due to small isolated populations are the major factors deterring rural electrification in India. In such a situation, they advocated the deployment of biomass gasifiers for serving the purpose, citing the arguments that the technology is well established, easy to install/operate, environmentally clean, and additionally, there are socio-economic benefits of manpower development and industry generation. Nouni et al. [48] in 2007 conducted a financial analysis of different configurations of biomass gasifier-based power generation for decentralized use. They estimated that the cost of 100% producer gas-based biomass gasification power generation systems was higher than that of dual-fuel provisioned biomass gasification power generation systems by almost double. They felt that 100% producer gas-based biomass gasification power generation systems can be made to compete with equivalent dual-fuel systems only when the price of such systems was lowered by manufacturers. On analysis of dual-fuel biomass gasification power generation systems up to 40 kW, they obtained the minimum levelized unit cost of electricity at a system capacity of 20 kW. They expressed the need for government intervention through suitable loans and subsidies to make this technology economically favorable for decentralized generation.

To understand how the sizing of a biomass gasifier-engine system for decentralized power generation can be done, we can take the help of a small numerical problem. Let us consider a biomass gasifier required to run a CI engine to generate 350 kW of power. Assume that the engine operates in the dual-fuel mode with 85% diesel replacement. How to calculate the biomass feeding rate to the gasifier if the efficiency of the engine is 35% and the calorific value of biomass is 17 MJ/kg? Let us also assume that the efficiency of the gasifier is 75%.

The solution to this is simple.

- Calculating input power to the engine = 350 kW ÷ 0.35 = 1000 kW.
- 85% of this power is provided by producer gas which is = 1000 kW × 0.85 = 850 kW.
- To provide 850 kW of power from the gasifier, input power of biomass to the gasifier required = 850 kW ÷ 0.75 = 1133.33 kW or 1133.33 kJ/s.
- Therefore, the amount of biomass of CV = 17 MJ/kg required to provide this input power = 1133.33 kJ/s ÷ 17,000 kJ/kg = 0.066 kg/s or 240 kg/h, which is the required answer.

6 Conclusions

Biomass gasification is a technology more than two centuries old, but since the last few decades, the world has taken to research and deployment of this technology with renewed zeal. The option for biomass conversion to energy via gasification is an attractive one, mainly due to the applicability of producer gas to a large variety of applications. The operability of producer gas in both CI and SI engines has been widely discussed and researched. CI engines require almost no modification to run on producer gas on dual-fuel mode and can achieve up to around 90% diesel replacement on an input energy basis. SI engine on the other hand may require modifications in ignition timing, compression ratio, etc. to run on 100% producer gas. There are issues of tar, ash and capacity de-rating associated with producer gas operation of IC engines, but still, biomass gasification-based power generation is a promising solution to the lack of electrification in remote rural locations, especially in a bio-diverse country like India. In this context, policies from the government supporting such project implementation are the need of the hour. Citing the concluding line of Sharma [49], '*Technology has shown the way to lighting up rural India, now it is only an enabling policy environment that can ensure that the lights do not go off*.'

References

1. Shafiee, S., & Topal, E. (2009). When will fossil fuel reserves be diminished? *Energy policy, 37*(1), 181–189. https://doi.org/10.1016/j.enpol.2008.08.016.
2. Das, D., Kalita, P., & Roy, O. (2018). Flat plate hybrid photovoltaic-thermal (PV/T) system: A review on design and development. *Renewable and Sustainable Energy Reviews, 84,* 111–130. https://doi.org/10.1016/j.rser.2018.01.002.
3. Raftery, A. E., Zimmer, A., Frierson, D. M., Startz, R., & Liu, P. (2017). Less than 2 C warming by 2100 unlikely. *Nature Climate Change, 7*(9), 637–641.
4. Reed, T. B. (1985). Principles and technology of biomass gasification. *Advances in solar energy* (pp. 125–174). US: Springer.
5. Basu, P. (2010). *Biomass gasification and pyrolysis: Practical design and theory*. UK: Elsevier Inc./Academic Press.
6. Rajvanshi, A. K. (1986). Biomass gasification. *Alternative Energy in Agriculture, 2*(4), 82–102.
7. Puig-Arnavat, M., Bruno, J. C., & Coronas, A. (2010). Review and analysis of biomass gasification models. *Renewable and Sustainable Energy Reviews, 14*(9), 2841–2851. https://doi.org/10.1016/j.rser.2010.07.030.
8. Saikia, M., Bhowmik, R., Baruah, D., Dutta, B., & Baruah, D. C. (2013). Prospect of bioenergy substitution in tea industries of North East India. *IJMER, 3*(3), 1272–1278.
9. Kalita, P., & Baruah, D. (2018). Investigation of biomass gasifier product gas composition and its characterization. In *Coal and biomass gasification* (pp. 115–149). Singapore: Springer. https://doi.org/10.1007/978-981-10-7335-9_5.
10. Samiran, N. A., Jaafar, M. N., Ng, J. H., Lam, S. S., & Chong, C. T. (2016). Progress in biomass gasification technique—With focus on Malaysian palm biomass for syngas production. *Renewable and Sustainable Energy Reviews, 62,* 1047–1062. https://doi.org/10.1016/j.rser.2016.04.049.
11. Basu, P. (2006). *Combustion and gasification in fluidized beds*. London: Taylor and Francis Group/CRC Press.

12. Sutar, K. B., Kohli, S., & Ravi, M. R. (2017). Design, development and testing of small downdraft gasifiers for domestic cookstoves. *Energy, 124,* 447–460. https://doi.org/10.1016/j.energy.2017.02.076.
13. Tippayawong, N., Chaichana, C., Promwangkwa, A., & Rerkkriangkrai, P. (2011). Gasification of cashew nut shells for thermal application in local food processing factory. *Energy for Sustainable Development, 15*(1), 69–72. https://doi.org/10.1016/j.esd.2010.10.001.
14. Boerrigter, H., Calis, H. P., Slort, D. J., & Bodenstaff, H. (2004). Gas cleaning for integrated biomass gasification (BG) and Fischer-Tropsch (FT) systems; experimental demonstration of two BG-FT systems. Acknowledgement/Preface, p. 51.
15. Ortiz-Cañavate, J., Vigil, S. A., Goss, J. R., & Tchobanoglous, G. (1981). Comparison of operating characteristics of a 34-kW diesel engine fueled with low-energy gas, biogas, and diesel fuel. *Biotechnology and Bioengineering Symposium, United States, 11,* 225–236.
16. Vyarawalla, F., Parikh, P. P., Dak, H. C., & Jain, B. C. (1984). Utilisation of biomass for motive power generation—Gasifier engine system. *Biomass, 5*(3), 227–242.
17. Parikh, P. P., Bhave, A. G., & Kapse, D. V. (1989). Study of thermal and emission performance of small gasifier-dual-fuel engine systems. *Biomass, 19*(1–2), 75–97.
18. Manes, G. S., Khurane, H. K., Singh, S., & Jain, A. K. (1994). Performance evaluation of diesel engine using producer gas-diesel mixture as fuel. *Agricultural Engineering Today, 18*(1–2), 18–25.
19. Bhattacharya, S. C., Hla, S. S., & Pham, H. L. (2001). A study on a multi-stage hybrid gasifier-engine system. *Biomass and Bioenergy, 21*(6), 445–460. https://doi.org/10.1016/S0961-9534(01)00048-4.
20. Uma, R., Kandpal, T. C., & Kishore, V. V. N. (2004). Emission characteristics of an electricity generation system in diesel alone and dual fuel modes. *Biomass and Bioenergy, 27*(2), 195–203. https://doi.org/10.1016/j.biombioe.2004.01.003.
21. Ramadhas, A. S., Jayaraj, S., & Muraleedharan, C. (2006). Power generation using coir-pith and wood derived producer gas in diesel engines. *Fuel Processing Technology, 87*(10), 849–853. https://doi.org/10.1016/j.fuproc.2005.06.003.
22. Lekpradit, T., Tongorn, S., Nipattummakul, N., & Kerdsuwan, S. (2008). Study on advanced injection timing on a dual-fuel diesel engine with producer gas from a down-draft gasifier for power generation. *J Met Mater Miner, 18*(2), 169–173.
23. Hassan, S., Nor, F. M., Zainal, Z. A., & Miskam, M. A. (2011). Performance and emission characteristics of supercharged biomass producer gas-diesel dual fuel engine. *Journal of Applied Sciences, 11*(9), 1606–1611. https://doi.org/10.3923/jas.2011.1606.1611.
24. Shrivastava, V., Jha, A. K., Wamankar, A. K., & Murugan, S. (2013). Performance and emission studies of a CI engine coupled with gasifier running in dual fuel mode. *Procedia Engineering, 51,* 600–608.
25. Sharma, M., & Kaushal, R. (2020). Performance and emission analysis of a dual fuel variable compression ratio (VCR) CI engine utilizing producer gas derived from walnut shells. *Energy, 192,*. https://doi.org/10.1016/j.energy.2019.116725.
26. Yaliwal, V. S., Banapurmath, N. R., Tewari, P. G., & Adaganti, S. Y. (2014). Fuel efficiency improvement of a dual-fuel engine fuelled with Honge oil methyl ester (HOME)–bioethanol and producer gas. *International Journal of Sustainable Engineering, 7*(3), 269–282. https://doi.org/10.1080/19397038.2013.843038.
27. Nataraja, K. M., Banapurmath, N. R., Yaliwal, V. S., Manavendra, G., Akshay, P. M., & Kulkarni, C. (2015). Effect of turbo charging on the performance of dual fuel (DF) engine operated on rice bran oil methyl ester (RBOME) and coconut shell derived producer gas induction. *Journal of Petroleum & Environmental Biotechnology, 6*(3), 1. https://doi.org/10.4172/2157-7463.1000216.
28. Nayak, S. K., & Mishra, P. C. (2017). Analysis of a diesel engine fuelled with jojoba blend and coir pith producer gas. *International Journal of Automotive and Mechanical Engineering, 14*, 4675–4689. https://doi.org/10.15282/ijame.14.4.2017.7.0368.
29. Shashikantha, Klose W., & Parikh, P. P. (1994). Development of a 15 kWe spark ignition producer gas engine and some investigations of its in-cylinder processes. *Renewable Energy, 5*(5–8), 835–837. https://doi.org/10.1016/0960-1481(94)90100-7.

30. Sridhar, G., Paul, P. J., & Mukunda, H. S. (2001). Biomass derived producer gas as a reciprocating engine fuel—An experimental analysis. *Biomass and Bioenergy, 21*(1), 61–72. https://doi.org/10.1016/S0961-9534(01)00014-9.
31. Yin, X. L., Wu, C. Z., Zheng, S. P., & Chen, Y. (2002). Design and operation of a CFB gasification and power generation system for rice husk. *Biomass and Bioenergy, 23*(3), 181–187. https://doi.org/10.1016/S0961-9534(02)00042-9.
32. Pushp, M., & Mande, S. (2008). Development of 100% producer gas engine and field testing with pid governor mechanism for variable load operation. SAE Technical Paper, 2008-28-0035. https://doi.org/10.4271/2008-28-0035.
33. Ulfvik, J., Achilles, M., Tuner, M., Johansson, B., Ahrenfeldt, J., Schauer, F. X., et al. (2011). SI gas engine: Evaluation of engine performance, efficiency and emissions comparing producer gas and natural gas. *SAE International Journal of Engines, 4*(1), 1202–1209. https://doi.org/10.4271/2011-01-0916.
34. Szwaja, S., Kovacs, V. B., Bereczky, A., & Penninger, A. (2013). Sewage sludge producer gas enriched with methane as a fuel to a spark ignited engine. *Fuel Processing Technology, 110,* 160–166. https://doi.org/10.1016/j.fuproc.2012.12.008.
35. Homdoung, N., Tippayawong, N., & Dussadee, N. (2015). Performance and emissions of a modified small engine operated on producer gas. *Energy Conversion and Management, 94,* 286–292. https://doi.org/10.1016/j.enconman.2015.01.078.
36. Indrawan, N., Thapa, S., Bhoi, P. R., Huhnke, R. L., & Kumar, A. (2017). Engine power generation and emission performance of syngas generated from low-density biomass. *Energy Conversion and Management, 148,* 593–603. https://doi.org/10.1016/j.enconman.2017.05.066.
37. Babu, M. S., Clement, S., & Rajan, N. K. (2019). Adaptation of air-gas regulator for small capacity producer gas engine. *Energy Procedia, 156,* 435–441. https://doi.org/10.1016/j.egypro.2018.11.091.
38. Naryanto, R. F., Enomoto, H., Anh, V. C., Fukadu, K., Iwai, S., & Noda, R. (2020). Investigation of producer gas biomass gasification on reciprocated internal combustion engine. *IOP Conference Series: Earth and Environmental Science, 460,*. https://doi.org/10.1088/1755-1315/460/1/012016.
39. Milne, T. A., Evans, R. J., & Abatzaglou, N. (1998). *Biomass gasifier "Tars": Their nature, formation, and conversion.* Golden, CO (US): National Renewable Energy Laboratory.
40. Elliott, D. C. (1988). Relation of reaction time and temperature to chemical composition of pyrolysis oils. In E. J. Soltes, & T. A. Milne (Eds), *Pyrolysis oils from biomass, ACS symposium series*, (Vol. 376, pp. 55–65). Denver, CO(US). https://doi.org/10.1021/bk-1988-0376.ch006.
41. Thapa, S., Bhoi, P. R., Kumar, A., & Huhnke, R. L. (2017). Effects of syngas cooling and biomass filter medium on tar removal. *Energies, 10*(3), 349. https://doi.org/10.3390/en10030349.
42. Devi, L., Ptasinski, K. J., & Janssen, F. J. (2003). A review of the primary measures for tar elimination in biomass gasification processes. *Biomass and Bioenergy, 24*(2), 125–140. https://doi.org/10.1016/S0961-9534(02)00102-2.
43. Anis, S., & Zainal, Z. A. (2011). Tar reduction in biomass producer gas via mechanical, catalytic and thermal methods: A review. *Renewable and Sustainable Energy Reviews, 15*(5), 2355–2377. https://doi.org/10.1016/j.rser.2011.02.018.
44. Livingston, W. R. (2007). *Biomass ash characteristics and behaviour in combustion, gasification and pyrolysis systems.*, Report UK: Doosan Babcock Energy Limited.
45. Bio Energy, Ministry of New and Renewable Energy, Government of India. https://mnre.gov.in/bio-energy/current-status.
46. Ravindranath, N. H. (1993). Biomass gasification: Environmentally sound technology for decentralized power generation, a case study from India. *Biomass and Bioenergy, 4*(1), 49–60. https://doi.org/10.1016/0961-9534(93)90026-Z.
47. Buragohain, B., Mahanta, P., & Moholkar, V. S. (2010). Biomass gasification for decentralized power generation: The Indian perspective. *Renewable and Sustainable Energy Reviews, 14*(1), 73–92. https://doi.org/10.1016/j.rser.2009.07.034.

48. Nouni, M. R., Mullick, S. C., & Kandpal, T. C. (2007). Biomass gasifier projects for decentralized power supply in India: A financial evaluation. *Energy Policy, 35*(2), 1373–1385. https://doi.org/10.1016/j.enpol.2006.03.016.
49. Sharma, D. C. (2007). Transforming rural lives through decentralized green power. *Futures, 39*(5), 583–596. https://doi.org/10.1016/j.futures.2006.10.008.

Experimental Investigation of Unmodified Diesel Engine on Performance, Combustion and Emission with Various Proportions of Jatropha Biofuel in Diesel

Dhinesh Balasubramanian, Amudhan Rajarajan, Ramalingam Krishnamoorthy, and Tran Dang Quoc

Nomenclature

ASTM	American Society for Testing Materials
CI	Compression ignition
CO	Carbon monoxide
HC	Hydrocarbon
CO_2	Carbon dioxide
NO_x	Oxides of nitrogen
HRR	Heat release rate
J20	20% transesterified Jatropha oil and 80% diesel in volume
J40	40% transesterified Jatropha oil and 60% diesel in volume
J60	60% transesterified Jatropha oil and 40% diesel in volume
J80	80% transesterified Jatropha oil and 20% diesel in volume
J100	100% volume of transesterified Jatropha oil in volume

D. Balasubramanian (✉)
Department of Mechanical Engineering, Mepco Schlenk Engineering College, Sivakasi, Tamil Nadu, India

Mechanical Engineering, Faculty of Engineering, Khon Kaen University, Khon Kaen, Thailand

Center for Alternative Energy Research and Development, Khon Kaen University, Khon Kaen, Thailand

A. Rajarajan · R. Krishnamoorthy
Department of Mechanical Engineering, CK College of Engineering and Technology, Cuddalore, Tamil Nadu, India

T. D. Quoc
School of Transportation Engineering, Hanoi University of Science and Technology, Hanoi, Vietnam

A. P. Singh et al. (eds.), *Alternative Fuels and Advanced Combustion Techniques as Sustainable Solutions for Internal Combustion Engines*, Energy, Environment, and Sustainability, https://doi.org/10.1007/978-981-16-1513-9_7

1 Introduction

The compression ignition engine is used for an extensive range of applications in the transportation division, and it also has applications in agricultural and power generation sectors due to its higher thermal efficiency. But due to fossil fuel depletion, researchers all over the world are impelled to develop an alternative fuel source that has comparable properties with diesel oil. Biogas, vegetable oils and methanol have been considered as alternative fuels for diesel. The previous experimental studies suggested that esterified vegetable oil has been recognized as the best alternative for diesel [1–3]. It also has a higher cetane number, calorific value and latent heat of vaporization compared with diesel. Table 1 shows the various vegetable oil biodiesel fuels whose chemical properties are closer to those of diesel. The availability, plantation and extraction of oil from seeds or crops do not pose a problem. The vegetable oils have the advantage of being biodegradable, non-toxic and pollution-free. The oils extracted from seeds or plants can simply be transesterified to produce biodiesel. Pure vegetable oil also has the potential to run a diesel engine restricted to lower viscosity [4, 5].

For better combustion and performance, the viscosity of vegetable oil is decreased by the transesterification process. During this process, the viscosity of the biodiesel gets reduced and turns equivalent to diesel [10–14]. The effect of viscosity will influence combustion, performance and emissions through fuel droplets, vaporization and atomization. Some researchers have reported that preheated oils also lead to better performance and emission characteristics [15–19]. It has been observed that preheating gives better emissions of HC, CO and particulate matter emissions due to the reduction of viscosity. It has also been noted that for higher compression ratios, biodiesel improves performance. In recent years, biodiesel has achieved significant consideration as an alternative renewable fuel. Biodiesel has several advantages over other petroleum products. Recent researches have shown that exhaust gases have less

Table 1 Property of various biodiesels

Property	Diesel	Cottonseed biodiesel	Jatropha biodiesel	Neem biodiesel	Palm biodiesel	Soybean biodiesel	Sunflower biodiesel
Calorific value (MJ/kg)	41–45.9	40.32	42	40.1	40.39	39.76	40.56
Cetane number	45–55	51.2	46–70	51	50–65	40–53	49–52
Kinematic viscosity at 40 °C (cSt)	2.5–5.7	4	3.7–5.8	7.2	4.5	4.08	4.5
Relative density	0.82–0.867	0.874	0.878–0.885	0.87	0.87	0.885	0.878
References	[1]	[6]	[1]	[7]	[8]	[8]	[9]

unburned hydrocarbon, particulate matter, carbon monoxide and sulfur levels while using biodiesel as a fuel. But the oxides of nitrogen have increased. Nowadays, to reduce smoke and NO_x with improved performance, considerable research is going on with water emulsion fuel, EGR and SCR.

Priyabrata Pradhan [20] investigated on the impact of Jatropha on the performance, emission and combustion on CI engine and reported that Jatropha biodiesel had a marginal decrease in brake thermal efficiency compared with mineral diesel, and it also had a reduction in CO_2, HC and NO_x and increased in CO emissions. Anand et al. [21] investigated the Jatropha biodiesel for injection pressure that ranges from 200 bar and 250 bar on diesel engine.

It was reported that there was a negligible decrease in BTE and a rise in emissions of emissions for Jatropha blends. Higher density, viscosity and molecular weight make it challenging to atomize the biodiesel at low temperatures and the low loads, causing more CO emissions. A significant cause for the lower CO emissions at high loads from the combustion of biodiesel is the inbuilt oxygen content, which makes the burning of biodiesel more complete when the engine works at higher loads.

Nabi et al. [22] investigated the influence of cottonseed oil on single-cylinder water-cooled, four-stroke, DI diesel engines. It was noted that preferred biodiesel resulted in lower CO, particulate matter, smoke and higher NO_x emissions than diesel at all load conditions. At full load condition, it also resulted, in B10, in lower smoke emission and particulate matter by 14 and 24% to mineral diesel. Blend B30 showed that the CO emissions decreased by 24% and increased NO_x emissions of 10%, and it was owing to the existence of oxygen in their molecular structure. Cottonseed blend has slightly lower thermal efficiency than mineral diesel due to its more moderate calorific content. However, higher density, higher volatility and higher viscosity might be the reasons for its reduction in its efficiency. Table 2 shows the study of various biodiesel fuels and their performance, emission and combustion characteristics.

From Table 1, it can be observed that properties such as calorific value, cetane number, kinematic viscosity and relative density of Jatropha oil are highly relative to mineral diesel compared to other biofuels. So these properties will influence in better performance, combustion and emission characteristics of Jatropha diesel blend used as fuel in the CI engine. The government of India launched the biofuel mission in 2003 to develop the Jatropha biodiesel industry. The planning commission reported that 13.4 million hectares of land available for Jatropha plantation [31]. Jatropha is an off-seasonal crop. So it can be cultivated at a slack agricultural season.

From the literature analysis, it can be perceived that only very limited researches have investigated in the field of Jatropha biodiesel with preheating of oil using the engine exhaust. In the current investigation, raw Jatropha oil was transformed into biodiesel using the transesterification process and converted into the fuel of various proportions on a volume basis. And during its operation in the engine, it was preheated with the engine exhaust for the betterment of engine behavior. The chemical and the physical properties of the fuel models have been analyzed on ASTM biodiesel standards. The objective of the present investigation was to determine the extent to which biodiesel blending could improve the combustion and emission characteristics

Table 2 Effect of biodiesel usage in diesel engine

Investigator	Biodiesel type	Engine type	Test conditions	Engine characteristics						
				Performance		Combustion		Emission		
				BTE	BSFC	HRR	ICP	CO	HC	NO_x
Tarbet et al. [23]	Eucalyptus oil	Single cylinder, four stroke, direct ignition, CR:18:1, 4.5 kW power	Varying load at 1500 RPM	⇩	⇧	⇩	⇧	⇧	⇧	⇩
Rehman et al. [1]	Jatropha oil	Single cylinder, four stroke, direct ignition, CR:17.5, RP:7.4 kW	Varying load at 1500 RPM	⇩	⇧	–	–	⇧	⇧	⇧
Gogoi et al. [24]	Korach seed oil methyl ester (KSOME)	Single cylinder, four stroke, direct ignition, CR:12-18, RP:3.5 kW	Varying load at 1500 RPM	⇩	⇧	⇩	⇩	–	–	–
Lenin et al. [25]	Mahua oil methyl ester	Single cylinder, four stroke, direct ignition, CR:17.5, RP:5.2 kW	Varying load at 1500 RPM	⇩	⇧	⇩	⇩	⇧	⇩	⇧
Agarwal et al. [26]	Karanja oil	Single cylinder, four stroke, direct ignition, CR:17.5, RP:7.4 kW	Varying load at 1500 RPM	⇩	⇧	⇩	⇩	⇩	⇩	⇧
Nithyananda et al. [27]	Neem and mixed Pongamia coconut methyl esters	Single cylinder, four stroke, direct ignition, CR:16.5:1, RP:3.75 kW	Varying load at 1500 RPM	⇩	⇧	–	–	–	–	–

(continued)

Table 2 (continued)

Investigator	Biodiesel type	Engine type	Test conditions	Engine characteristics						
				Performance		Combustion		Emission		
				BTE	BSFC	HRR	ICP	CO	HC	NO_x
Anand et al. [21]	Turpentine oil	Single cylinder, four stroke, direct ignition, CR:17.5, RP:5.2 kW	Varying load at 1500 RPM	⇩	⇧	⇩	⇩	⇩	⇩	⇩
Sajid et al. [28]	Mustard Biodiesel (MB)	Four cylinders, four stroke, direct ignition, CR: 21:1	Varying load at 1500 RPM	⇩	⇧	–	–	⇩	⇩	⇧
Nalgundwar et al. [29]	Palm and Jatropha	Single cylinder, four stroke, direct ignition, CR:17.5, RP:5.2 kW	Varying load at 1500 RPM	⇧	⇧	–	–	⇩	⇩	⇧
Kakati and Gogoi [30]	Kultura fruit seed oil	Single cylinder, four stroke, direct ignition, CR:18:1, RP:3.5 kW	Varying load at 1500 RPM	⇧	⇩	–	–	⇩	⇩	⇧

⇧—increase/high; ⇩—decrease/low; CR—compression ratio; DI—direct ignition; RP—rated power; rpm—revolution per minute

without sacrificing its performance in an unmodified diesel engine. For that purpose, the experiment was conducted with a biodiesel blend in an unmodified diesel engine at all load conditions. The performance characteristics such as BTE, BSFC and emission characteristics such as CO_2, CO, HC, NO_x and smoke opacity were measured for Jatropha biodiesel and compared with mineral diesel. The combustion features such as rate of heat release and peak in-cylinder pressure graphs were constructed against the crank angle to find the effectiveness of combustion.

2 Materials and Methods

2.1 Jatropha

Jatropha is one of the flowering plants in the spurge family, & it is also called Euphorbiaceae. The Jatropha fruits are yellow color, and their dried seeds are black in color and oval in shape. The oil extracted from the seeds is golden yellow in color and fragrance-free. Jatropha has usually been used in basket creation and dye production. It had origin from tropical America and also many portions of the jungles in Africa [32, 33]. It is a drought-resistant, permanent plant, grown-up to fifty years, and it grows on any kind of soil. It has a yield of about 1 kg per square meter per year [34]. The toxin is the only drawback in it. In World War II, it was used as biodiesel for engines [35, 36]. In Jatropha seed oil, phorbol esters are considered toxic. The phorbol esters are destroyed by chemical refining (degumming, neutralization, silica/bleaching, mild deodorization) and physical refining (stripping at 240° and vacuum). The Jatropha seeds oil is highly viscous used in the manufacture of soap and candles. In cosmetics production, it is used as a diesel/paraffin additional or extender [37, 38]. It has significant inferences for fixing the demand for rural energy usage and also exploring useful substitutes for fossil fuels to reduce greenhouse gas addition in the atmosphere. Figure 1 shows the jatropha plant and its fruit.

2.2 Biodiesel Preparation Process—Transesterificaton

The energy content of the vegetable oils is similar to that of diesel. The vegetable oils cannot be used as fuels in unmodified diesel engines as they are too viscous due to their high molar mass. Triglycerides react with methanol in the presence of a catalyst to form glycerol, and methyl ester is called biodiesel, and the same is shown in Fig. 2. Vegetable oil can be converted into a usable fuel, known as biodiesel, in a transesterification reaction. The triglycerides in Jatropha oil react with methanol, which is one of the alcohols, in the existence of a strong base such as sodium hydroxide to produce glycerol and Jatropha methyl ester, which is also known as Jatropha biodiesel. The chemical reaction between them is shown in Fig. 3.

Fig. 1 Jatropha plant

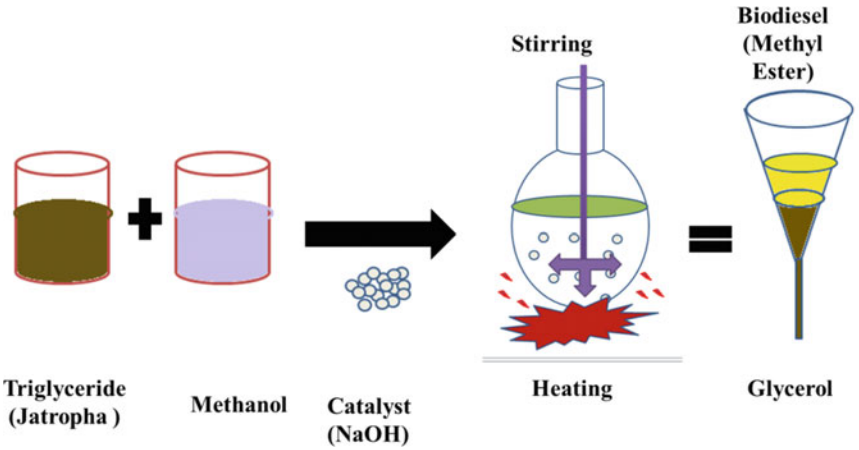

Fig. 2 Transesterification process

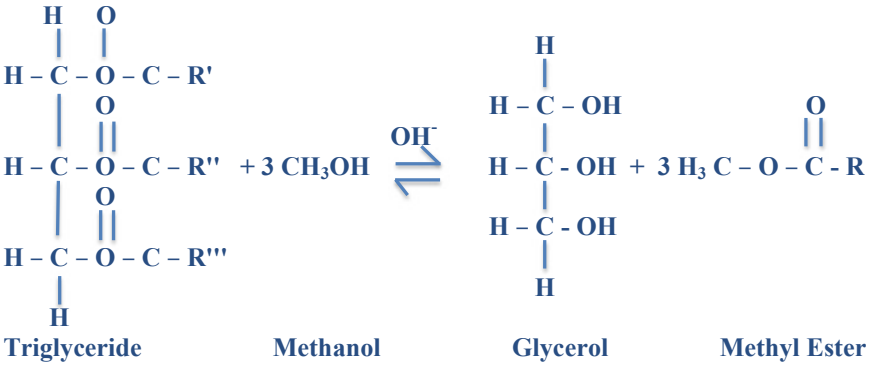

Fig. 3 Transesterification reaction

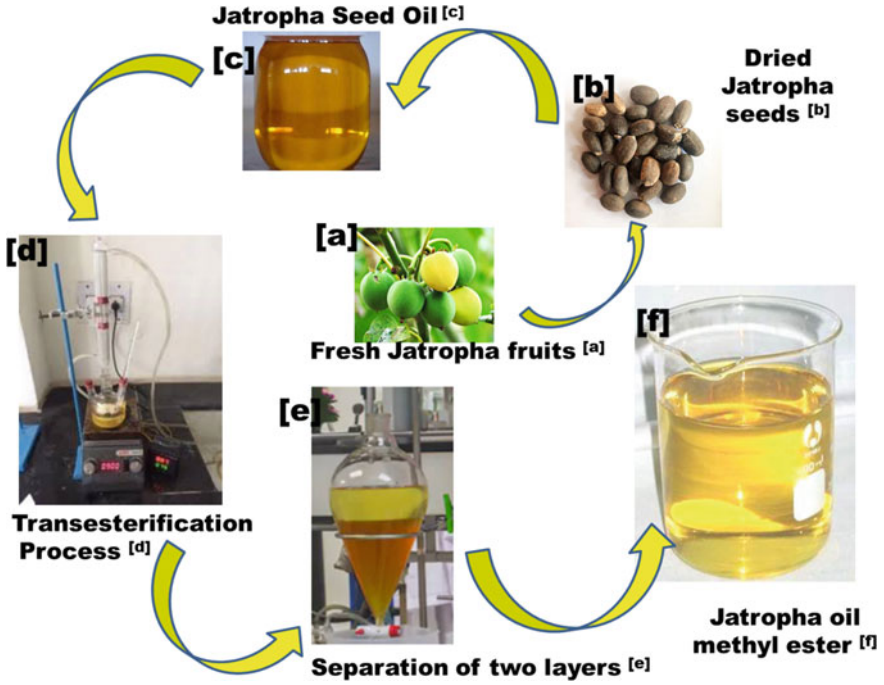

Fig. 4 Process of Jatropha biodiesel production

Table 3 Weight composition of Jatropha oil

Fatty acid	Weight composition %
Linoleic 18:2	30.8
Oleic 18:1	46.3
Palmitic 16:0	14.5
Stearic 18:0	6.9
Linolenic 18:3	0.2
Palmitoleic 16:1	0.7
Unrecognized components	0.3
Arachidic 20:0	0.3

In this reaction, an excess of alcohol is used to drive the position of equilibrium to the right in favor of the products. The three alkyl ester molecules produced have similar energy content to the triglyceride but are less viscous due to their lower molar mass, and they are suitable for use in diesel engines.

Biodiesel is much less toxic and more biodegradable than regular diesel. In the industrial sector, the alkali-catalyzed transesterification process is followed for mass production [39, 40]. The whole process, which contains the conversion of

Jatropha seeds into Jatropha biofuel, is as shown in Fig. 4. Table 3 shows the weight composition of fatty acid [41].

2.3 Experimental Setup

A water-cooled, single-cylinder and four-stroke direct-injection compression engine with a compression ratio of 17.5:1 and power of 5.2 kW run at a speed of 1500 rpm was used for the present research work. The high viscosity is the major drawback of using Jatropha oil in an unmodified compression ignition engine. So, it is imperative to reduce the fuel viscosity before its use in the engine. Its higher viscosity is reduced by preheating the Jatropha biodiesel up to 90 °C by the heat exchanger, which utilizes the heat from exhaust gases that pass through it. Its viscosity is also reduced by blending with diesel. Experiments were conducted on various proportions of Jatropha biodiesel blend (J20, J40, J60, J80 and J100) and mineral diesel. The properties of diesel and Jatropha blends at 90 °C were measured, as given in Table 4 and other technical specifications of the engine used for this work are given in Table 5.

The performance, combustion and emission of the Jatropha oil with diesel in various proportions were measured. The eddy current dynamometer was used for multiple loading conditions. The schematic experimental setup for our investigation is shown in Fig. 5.

The Jatropha and diesel oils were filled in separate fuel tanks, which are our major components. The heat exchanger, exhaust gas analyzer, smoke meter, dynamometer and data acquisition system were also used as main components. The engine was started with diesel first and then with Jatropha oil for the purpose of warm-up. It also reduced deposits and cold-starting problems in the fuel line and injection system. The

Table 4 Properties of Jatropha blends and diesel

Fuel used	Kimematic viscosity	Calorific value	Flash point	Density	Cetane number
Unit	(mm^2/s)	(MJ/kg)	(°C)	(kg/l)	–
Apparatus utilized	Redwood viscometer	Bomb calorimeter	Pensky–Martens	Hydrometer	Ignition quality tester
Apparatus standard	ASTM D445	ASTM D240	ASTM D93	ASTM D941	ASTM D613
J20	4.2	43.1	79	0.868	54.17
J40	4.5	42.8	92	0.876	54.53
J60	4.8	42.3	110	0.889	54.65
J80	5	41.5	131	0.908	55.62
J100	5.3	40.2	168	0.939	56.88
Diesel	2.71	44.8	70	0.836	54

Table 5 Specifications of the engine

Engine specifications	Manufacturer Kirloskar Ltd., India
Engine type	Single cylinder, four stroke, direct injection, vertical, water cooled and constant speed
Rated power	5.2 kW
Speed	1500 RPM
Bore/Stroke	102/ 116 (mm)
Compression ratio	17.5:1
Displacement volume in cylinder	0.9481 mm^3
Injection pressure	210 bar
Injection timing	26° before top dead center
Brake mean effective pressure at 1500 RPM	6.34 kg/cm^2

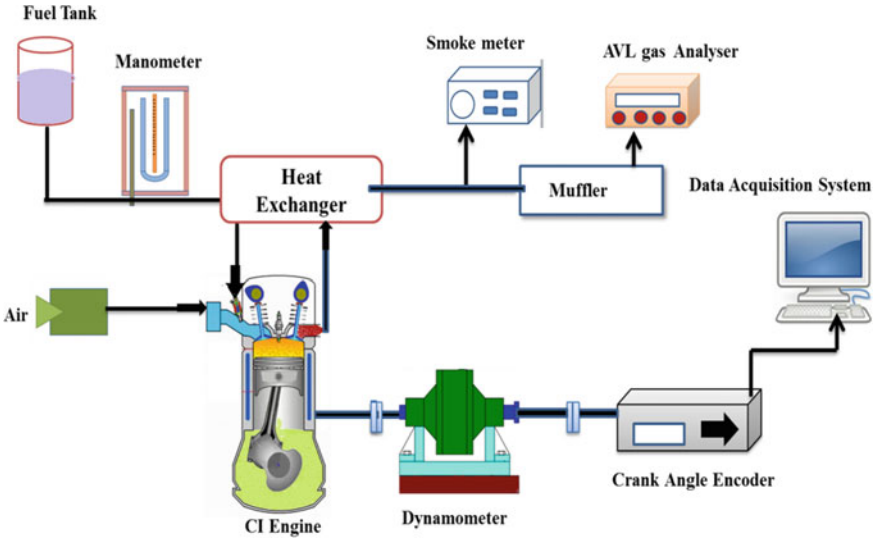

Fig. 5 Schematic diagram of the engine setup

voltage and the current spent by the load were measured by voltmeter and ammeter. The exhaust gas composition was measured using an exhaust gas analyzer. Figure 5 represents the schematic diagram of the experimental setup test rig.

The physical, thermal and chemical properties of the Jatropha and diesel are given in Table 4. Jatropha oil has a high pour point, density and cloud point compared with diesel. The fire and flash points are higher for Jatropha oil than diesel and make it safe to use. Increased carbon deposit is due to the higher carbon content

from the Jatropha oil. The emissions and combustion properties are enhanced by the existence of oxygen, but the calorific value of the Jatropha oil decreases. The Jatropha oil has around 80% calorific value compared with diesel. Higher viscosity in Jatropha oil is the main issue of its use as a fuel in the diesel engine. In this experimental examination, viscosity was minimized by preheating and blending the Jatropha oil with diesel. The viscosity of Jatropha oil was maintained at 90 °C in this investigation because, at this temperature, it had a relative viscosity closer to diesel. Hence, Jatropha must be heated up to 90 °C before its injection into the engine to attain fuel properties close to diesel. Viscosity decrease depends upon its concentration of the combination.

2.4 Analysis of Uncertainty

The range of error in the experimental results represents the uncertainty analysis. It arises due to multiple factors such as instrument selection, condition, calibration, environment, reading, observation and test procedure. The experiments were performed thrice to minimize the effect of errors in the results. The uncertainty of various measuring units is given in Table 6. The uncertainty percentage was calculated by the square root of the sum of squares of the uncertainty values of brake power, brake specific fuel consumption, brake thermal efficiency, total fuel consumption, carbon monoxide, hydrocarbon, oxides of nitrogen, smoke, temperature and pressure [42].

Table 6 Experimental uncertainty of various measuring units

Parameter	Methodology of measuring	Accuracy	Errors (±)
Load	Strain gauge load cell	±10 N	±0.2
Temperature	Thermocouple	±1 °C	±0.15
Pressure	Magnetic pickup principle	±0.1 kg	±0.1
Engine speed	Magnetic pickup principle	±10 rpm	±0.1
Fuel flow measurement	Volumetric measurement	±0.1 cc	±1
Crank angle encoder	Magnetic pickup principle	±1°	±0.2
Time	Stopwatch	±0.1 s	±0.2
Manometer deflection	Balancing of the column of liquid	±1 mm	±1
CO	NDIR technique	±0.02 vol%	±0.2
HC	NDIR technique	±10 ppm	±0.1
NO_x	NDIR technique	±12 ppm	±0.2
Smoke	NDIR technique	±1 HSU	±1

$$\text{Total uncertainty} = \sqrt{\begin{array}{l}(\text{BP uncertainty})^2 + (\text{BFSC uncertainty})^2 + (\text{BTE uncertainty})^2 \\ +(\text{TFC uncertainty})^2 + (\text{CO uncertainty})^2 + (\text{HC uncertainty})^2 \\ +(\text{NO}_x \text{ uncertainty})^2 + (\text{Smoke uncertainty})^2 + (\text{EGT uncertainty})^2 \\ +(\text{Press uncertainty})^2\end{array}}$$

$$= \sqrt{\begin{array}{l}(0.2)^2 + (1)^2 + (1)^2 + (1)^2 + (0.2)^2 + (0.1)^2 + (0.2)^2 + (1)^2 \\ +(0.15)^2 + (1)^2\end{array}}$$

$$= \pm 2.26\%$$

±2.26% was calculated as uncertainty values for the current experimental setup. The experimental uncertainty of various measuring units is given in Table 6.

3 Results and Discussion

3.1 Analysis of Performance Characteristics

3.1.1 Brake Thermal Efficiency (BTE)

The BTE of Jatropha oil and diesel blends increases with increases in engine load, as presented in Fig. 6. It is witnessed that the calorific value of Jatropha oil is lesser than that of diesel oil. As a result of increasing the proportion of Jatropha biodiesel in blend decreases, the calorific value is proportional, which affects in increased BSFC, and it reduces BTE. BTE of Jatropha blends lower than that of diesel. However, BTE of J20 stays very nearer to diesel, and all other combinations have lesser BTE

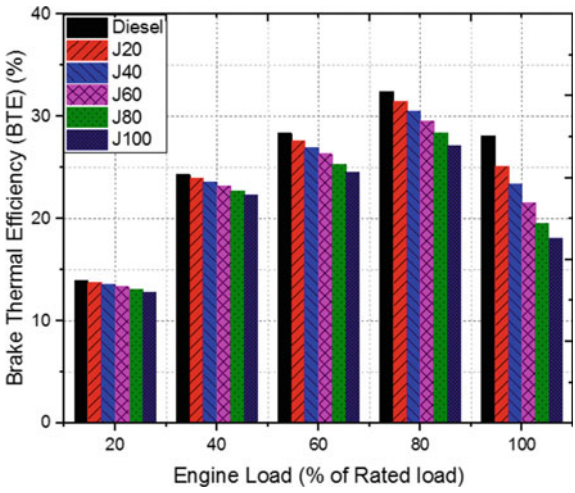

Fig. 6 Thermal efficiency versus engine load

compared with J20 and mineral diesel. The combustion characteristics of the fuel molecules were increased by the presence of oxygen content in the biodiesel.

The higher viscosity and reduced volatility of the Jatropha biodiesel oil affect the atomization and combustion characteristics [43]. Therefore, BTE was found to be lesser for higher blend concentrations related to diesel. The BTEs of diesel and its blends were found increased with increases in load, but it tended to decrease with further increase in peak load. The maximum BTE of 31.1% was attained for J20, while for diesel, it was 32.5% at 80% of its full load condition.

3.1.2 Brake Specific Fuel Consumption (BSFC)

Brake specific fuel consumption has been found to increase with a higher proportion of Jatropha biodiesel in the blend-related diesel in the various engine load range (Fig. 7). It is owing to the collective effects of the fuel density, viscosity and heating value of the blends. BSFC has increased owing to the high density of the Jatropha biodiesel oil blends based on its proportion levels. The higher bulk modulus has resulted in higher fuel discharge for the same value in BSFC. The usage of a low percentage of Jatropha biodiesel in diesel has resulted in lesser BSFC compared with diesel in all loads. The low BTE for J100 could be owing to lower calorific value and an increase in fuel consumption as related to J20. However, on the whole, by running the engine with Jatropha biodiesel, BSFC is always higher than the biodiesel as well as diesel.

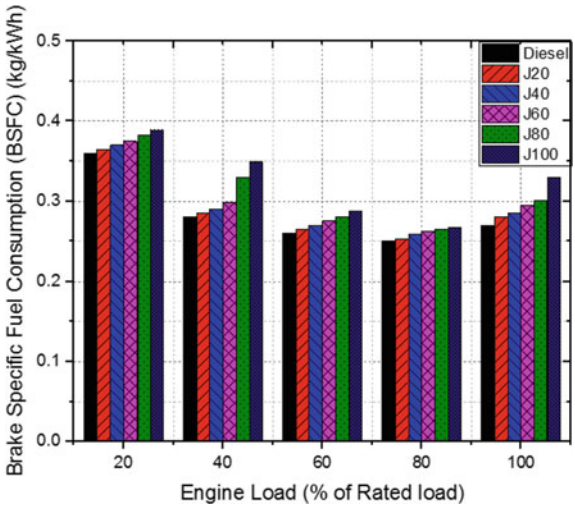

Fig. 7 Brake specific fuel consumption versus engine load

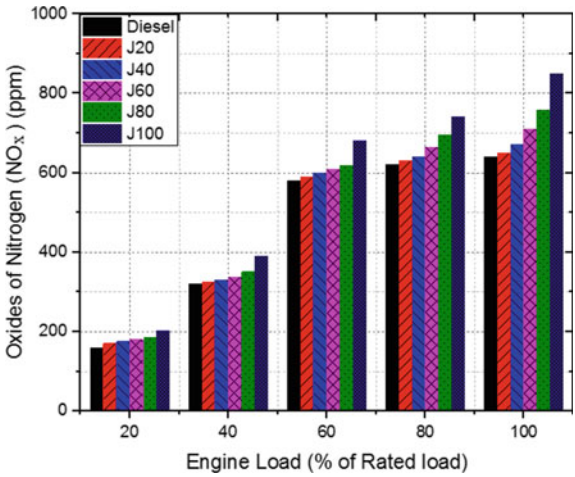

Fig. 8 Oxides of nitrogen (NO_x) versus engine load

3.2 Analysis of Emission Characteristics

3.2.1 Emissions of Nitrogen Oxides (NO_x)

NO_x emission is a highly harmful gaseous emission compared with other engine exhaust emissions. Hence, its reduction in an engine has always been one of the key aims of engine researchers all over the world. The NO_x emissions of diesel fuel were related to various proportions of Jatropha biodiesel at different loads as shown in Fig. 8. It is observed that the emission of oxides of nitrogen increases with increases in load for all fuels. It is also observed that if the amount of Jatropha in the blend increases, then emissions of NO_x also increase. This increase is due to Jatropha oil being an oxygenated fuel and that leads to improved combustion, and therefore, higher combustion temperature is attained. The higher temperature promotes NO_x formation. The NO_x emissions have increased enormously between 40 and 60% of the rated load for all blends and mineral diesel. However, the emissions of NO_x of blend J20 are nearer to diesel compared with others.

3.2.2 Carbon Monoxide

The development of CO emission mainly depends upon the physical and chemical properties of the fuel used. Figure 9 shows that the engine discharges lesser CO for Jatropha blends when related to diesel. When the proportion of Jatropha biodiesel in the blend increases, the percentage of emission of CO decreases. But all Jatropha blends are far below the percentage of CO emissions than that of mineral diesel. The decrease in CO emission of Jatropha blend is due to the high cetane number and oxygen present in the molecular structure of Jatropha oil, and it supplies the necessary oxygen to convert CO to CO_2 when combustion takes place. Kumar et al.

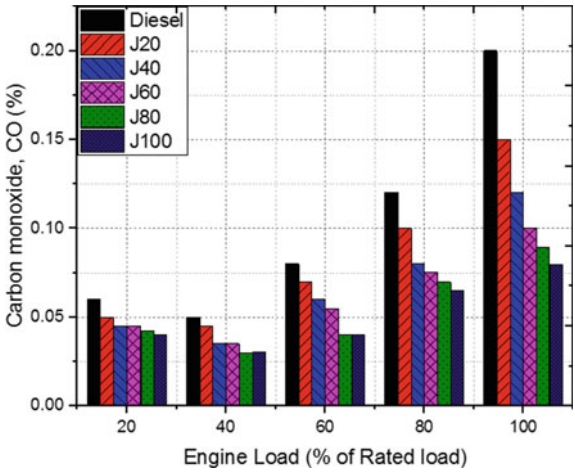

Fig. 9 Carbon monoxide (CO) versus engine load

[44], in his investigation, reported that an increase in cetane number, there was a reduction in ignition delay, increased the injection pressure, thereby making the fuel particles finer, giving lower CO emissions. The emissions of CO for all blends are closer to those of diesel at 20% and 40% of the rated load. But the variation increases as 0.2% for diesel and 0.08% for J100 at full load conditions.

3.2.3 Hydrocarbon

The HC emission variation for various proportions of blends is shown in Fig. 10. It is observed that for diesel and Jatropha blends, the HC emissions are showing a

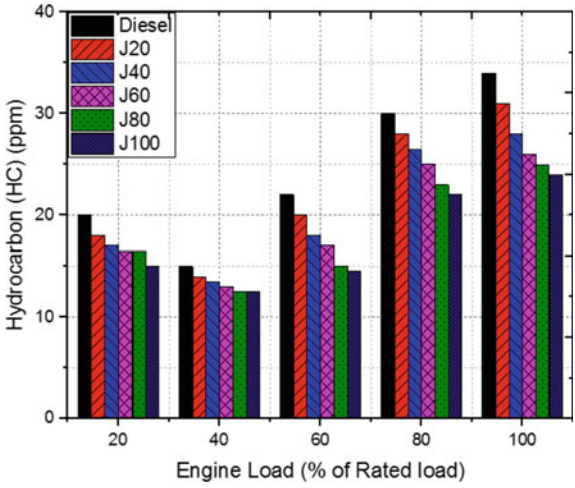

Fig. 10 Hydrocarbon versus engine load

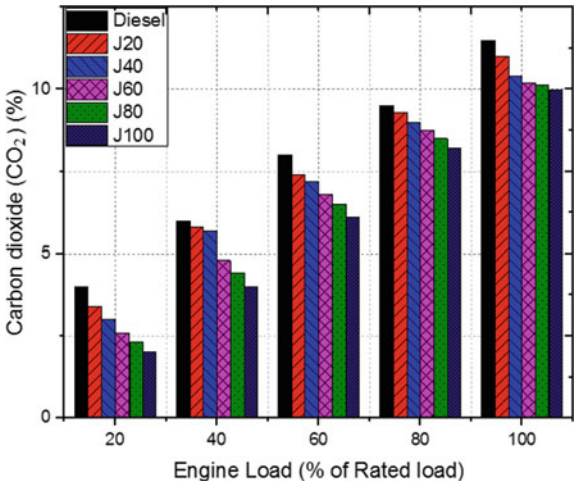

Fig. 11 Carbon dioxide (CO_2) versus engine load

decreasing trend first up to 40% of its load and then increasing trend with increasing load. It is owing to the existence of a rich fuel mixture at higher loads. It is witnessed that an increasing proportion of Jatropha in the blend decreases HC emissions. It is due to the presence of oxygen in the Jatropha oil, and the higher combustion temperature promotes the oxidation of HC. Elango and Senthilkumar [45] concluded that the effect of viscosity increased the HC emissions level of the blend at higher load conditions. The emissions of HC for all Jatropha blends are closer to those of diesel at 40% rated load as the emission values are 15% for diesel and 12.5% for J100. However, the variations of HC are maximum at its full load condition as the emissions values are 34.2% for diesel and 24.4% for J100.

3.2.4 Carbon Dioxide

The emission intensities of CO_2 for various proportions of biodiesel and diesel is shown in Fig. 11. At full load conditions, the CO_2 emissions for diesel, J20, J40, J60, J80 and J100 are found to be 11.5%, 11.01%, 10.4%, 10.21%, 10.15% and 10.11%, respectively. It is shown that the CO_2 emission of Jatropha blends is less than that of diesel at all load conditions. It may be pointed out that Jatropha blends contain lower carbon content than diesel. The Jatropha oil contains more oxygen content, which is also one of the reasons for lower CO_2 emissions of Jatropha blend compared with diesel.

3.2.5 Smoke Density

The emissions of smoke opacity with the varying load are shown in Fig. 12. It indicates that as Jatropha biodiesel concentration increases, the smoke opacity also

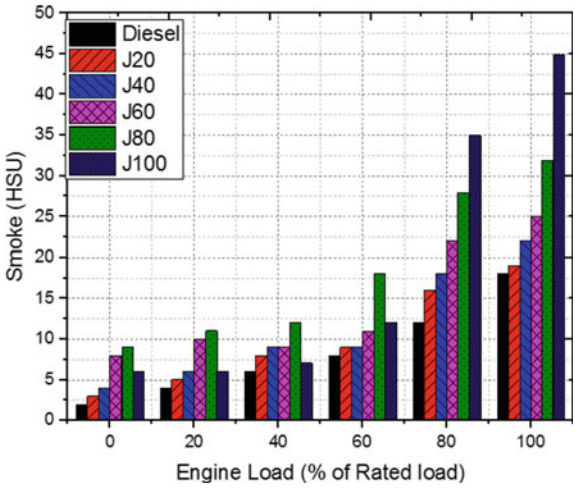

Fig. 12 Smoke versus engine load

increases irrespective of the load condition. At full load conditions, the smoke opacity for diesel, J20, J40, J60, J80 and J100 are found to be 18.2, 19.1, 22.4, 25.2, 32.7 and 45.1 HSU, respectively. It is owing to reduced volatility and improper mixing of fuel droplets with air because of the higher viscosity of the Jatropha blends. At full load condition, the value of the smoke density of Jatropha biodiesel J100 is two times the value of diesel at the same load condition. The NO_x and smoke emissions are controlled by combustion treatments (exhaust gas recirculation, emulsified biodiesel), exhaust after treatments (selective catalytic reduction, lean NO_x traps) and fuel treatments (fuel additives) [46].

3.3 Analysis of Combustion Characteristics

3.3.1 Heat Release Rate Versus Crank Angle

The heat release rates (HRR) versus crank angle for all Jatropha blends and diesel at full loading conditions are shown in Fig. 13. HRR attains negative value at the beginning of the combustion due to the vaporization of the fuel. After the start of the combustion phase (SOC), HRR turns into positive. All the proportions of Jatropha blends have almost identical combustion as mineral diesel at all stages, such as ignition delay, premixed combustion and diffusion combustion.

From Fig. 13, it is witnessed that at full engine load condition, combustion starts earlier for Jatropha blends. At the time of fuel injection, thermal cracking happens due to high cylinder temperature. It leads to shorter ignition delay for Jatropha blend compared to diesel. At the premixed combustion stage, the HRR is greater for diesel due to its high volatility and improved air–fuel mixing characteristics. It is also because of the longer ignition delay, which leads to a large amount of fuel addition.

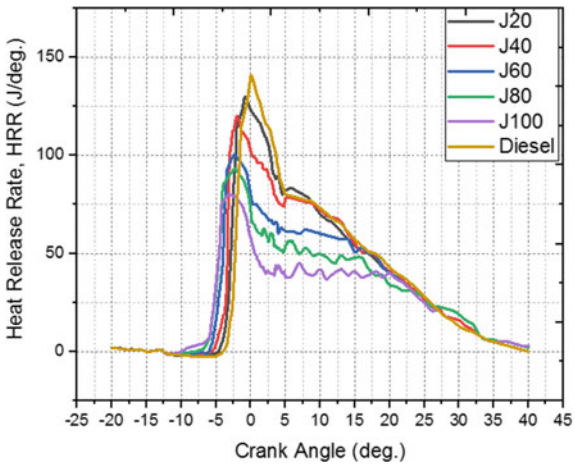

Fig. 13 Heat release rate versus crank angle

At diffusion combustion, Jatropha blends have high HRR in higher load conditions. The higher HRR for mineral diesel is 145.1 J/degree, and for J100, it is 76.3 J/degree, which is two times that of mineral diesel. However, the combustion duration for diesel is less than that of Jatropha blends.

3.3.2 In-Cylinder Pressure Versus Crank Angle

The variations of cylinder pressure for the crank angle for diesel and Jatropha blends J20, J40, J60, J80 and J100 at full engine loads are shown in Fig. 14. From these figures, it is observed that cylinder pressure rates are almost comparable with diesel for all fuel blends at low engine load conditions.

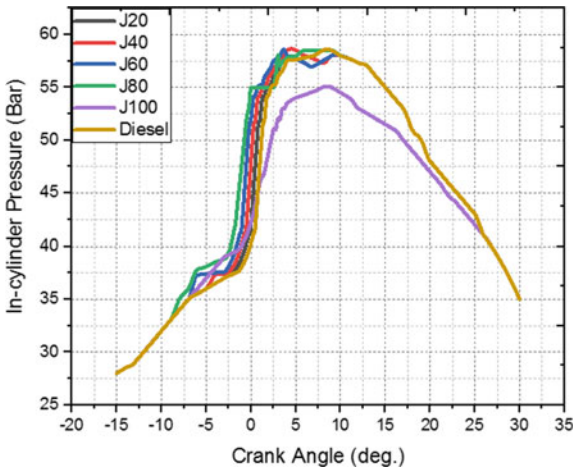

Fig. 14 In-cylinder pressure versus crank angle

At higher load conditions, Jatropha blends have earlier pressure rise than diesel, and mineral diesel had higher peak pressure. The Jatropha blends had initial combustion compared to diesel, and the pressure rise rate is slower for Jatropha blends at full load conditions. Hence, it is due to the slower burning characteristics. The starting point of combustion for all fuels gets advanced as the engine load is increased. The combustion starts earlier for Jatropha blends. It is because of shorter ignition delay and partly due to advanced injection timing and also due to higher density and higher bulk modulus of Jatropha oil. It is due to the complex and pre-flame chemical reaction at high temperature. In the high cylinder temperature existing during fuel injection, Jatropha attained thermal cracking, and it leads to formation of lighter compounds [26]. Therefore, it causes in earlier ignition and shorter ignition delay for Jatropha blend compared to diesel.

Jatropha blend J40 has higher peak pressure of 58.5 bar, and it is higher compared with all blends and diesel. J100 has a peak pressure of 54.2 bar, and it is lower compared with all blends and mineral diesel.

3.3.3 Exhaust Gas Temperature

The influence of BTE and BSFC was reflected in exhaust gas temperature as well. The exhaust gas temperature with blends having a higher proportion of biodiesel blend was higher than that of diesel at greater loads, as shown in Fig. 15. When biodiesel concentration was increased, the exhaust gas temperature rose by a small value. Upon using 100% Jatropha oil, a higher value of exhaust gas temperature was obtained, which indicated more loss of energy. Elango et al. suggested that combustion is delayed for the blends, and more of the heat is released during mixing controlled combustion phase in which higher amount of heat goes with exhaust gas [45]. Hence, exhaust gas temperatures are higher. The EGT improved with an increase in load for

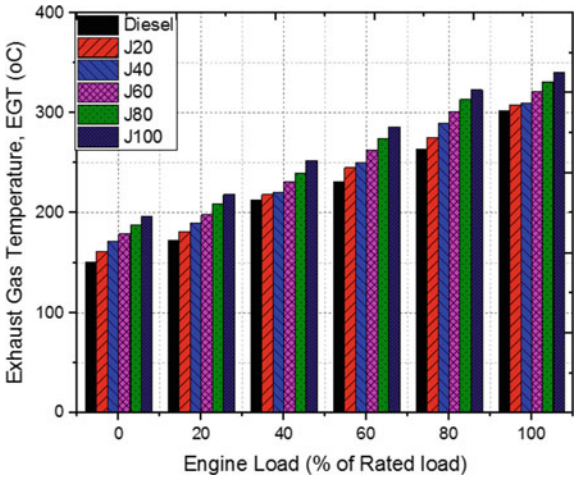

Fig. 15 Exhaust gas temperature versus engine load

all blends. The rise in EGT with load was evident, and it showed that more fuel was required to take additional capacity. EGT is a sign of the range of conversion of heat into work, which occurs inside the cylinder. It was found that EGT for various fuel blends at different load conditions were almost identical. EGT increased with a rise in power for all fuel blends. As the biodiesel fuel concentration was improved, the exhaust gas temperature also got enhanced. The highest exhaust gas temperature was 340 °C at higher power for J100.

4 Conclusion

The principal objective of the current investigation was to measure the performance, combustion and emission characteristics of the compression ignition engine fueled with various proportions of Jatropha blends with diesel and mineral diesel. Accordingly, an experimental investigation was conducted. The investigation revealed that if the viscosity of Jatropha could be nearer to diesel, it would give better performance and emission characteristics. Hence, the viscosity of the Jatropha oil was reduced by the transesterification process and then by blending it with diesel with a preheating technique from the exhaust gas.

- The experimentation was conducted for raw diesel and various proportions of Jatropha diesel blends (J20, J40, J60, J80 and J100) at different load conditions and constant speed (1500 rpm).
- Brake thermal efficiency (BTE) decreased as Jatropha concentration in the blend increased. In contrast, maximum brake thermal efficiency of 31.1% was achieved for J20, while for diesel, it was 32.5% at full load conditions. At the same time, the brake specific fuel consumption (BSFC) and exhaust gas temperature were higher for Jatropha biodiesel blends than for diesel.
- Jatropha blends had higher peak pressure at lower loads, and mineral diesel had higher peak pressure at higher loads. NO_x and smoke emissions were higher than diesel for Jatropha blends because of reduced volatility and higher viscosity of mixtures. In contrast, the emissions CO, HC and CO_2 were lower for Jatropha blends than for diesel due to low carbon content, high oxygen content and high cetane number of biodiesel.

From the detailed experimental investigation on performance, combustion and emission on Jatropha biodiesel, it could be inferred that J20 was the best alternative fuel, and it gave better efficiency and emissions similar to those of diesel. And hence, it can be directly used in the CI engine without any engine modification.

Acknowledgements The authors would like to convey their heartfelt thanks to Dr. S. Saravanan, Principal, CK College of Engineering and Technology, Cuddalore, for encouraging this research work and to the authorities of Mepco Schlenk Engineering College, Sivakasi, for their support.

Declaration of Competing Interest
The authors announce that they have no recognized competing financial interests or personal relationships that could have seemed to influence the work described in this article.

References

1. Rehman, A., Phalke, D. R., & Pandey, R. (2011). Alternative fuel for gas turbine: Esterified jatropha oil–diesel blend. *Renewable Energy, 36*(10), 2635–2640.
2. Balasubramanian, D., Kamaraj, S., & Krishnamoorthy, R. (2020). *Synthesis of biodiesel from waste cooking oil by alkali doped calcinated waste egg shell powder catalyst and optimization of process parameters to improve biodiesel conversion* (No. 2020-01-0341). SAE Technical Paper.
3. Kaisan, M. U., Abubakar, S., Ashok, B., Balasubramanian, D., Narayan, S., Grujic, I., & Stojanovic, N. (2018). Comparative analyses of biodiesel produced from jatropha and neem seed oil using a gas chromatography–mass spectroscopy technique. *Biofuels*, 1–12.
4. Mat, S. C., Idroas, M. Y., Hamid, M. F., & Zainal, Z. A. (2018). Performance and emissions of straight vegetable oils and its blends as a fuel in a diesel engine: A review. *Renewable and Sustainable Energy Reviews, 82,* 808–823.
5. EL-Seesy, A. I., He, Z., Hassan, H., & Balasubramanian, D. (2020). Improvement of combustion and emission characteristics of a diesel engine working with diesel/jojoba oil blends and butanol additive. *Fuel, 279*, 118433.
6. Gautam, A., & Agarwal, A. K. (2013). Experimental investigations of comparative performance, emission and combustion characteristics of a cottonseed biodiesel-fueled four-stroke locomotive diesel engine. *International Journal of Engine Research, 14*(4), 354–372.
7. Ali, M. H., Mashud, M., Rubel, M. R., & Ahmad, R. H. (2013). Biodiesel from neem oil as an alternative fuel for diesel engines. *Procedia Engineering, 56,* 625–630.
8. da Silva, M. A. V., Ferreira, B. L. G., da Costa Marques, L. G., Murta, A. L. S., & de Freitas, M. A. V. (2017). Comparative study of NO_x emissions of biodiesel-diesel blends from soybean, palm, and waste frying oils using methyl and ethyl transesterification routes. *Fuel, 194,* 144–156.
9. Leung, D. Y., Wu, X., & Leung, M. K. H. (2010). A review on biodiesel production using catalyzed transesterification. *Applied Energy, 87*(4), 1083–1095.
10. Sahoo, P. K., Das, L. M., Babu, M. K. G., Arora, P., Singh, V. P., Kumar, N. R., et al. (2009). Comparative evaluation of performance and emission characteristics of Jatropha, karanja, and polanga based biodiesel as fuel in a tractor engine. *Fuel, 88*(9), 1698–1707.
11. Gog, A., Roman, M., Toşa, M., Paizs, C., & Irimie, F. D. (2012). Biodiesel production using enzymatic transesterification–current state and perspectives. *Renewable Energy, 39*(1), 10–16.
12. Lee, A. F., Bennett, J. A., Manayil, J. C., & Wilson, K. (2014). Heterogeneous catalysis for sustainable biodiesel production via esterification and transesterification. *Chemical Society Reviews, 43*(22), 7887–7916.
13. Kouzu, M., & Hidaka, J. S. (2012). Transesterification of vegetable oil into biodiesel catalyzed by CaO: A review. *Fuel, 93,* 1–12.
14. Ramalingam, K., Balasubramanian, D., Chellakumar, P. J. T. J. S., Padmanaban, J., Murugesan, P., & Xuan, T. (2020). An assessment on production and engine characterization of a novel environment-friendly fuel. *Fuel, 279,*.

15. Lingesan, S., Annamalai, K., Parthasarathy, M., Ramalingam, K. M., Dhinesh, B., & Lalvani, J. I. J. (2018). Production of Garcinia gummi-gutta methyl ester (GGME) as a potential alternative feedstock for existing unmodified DI diesel engine: Combustion, performance, and emission characteristics. *Journal of Testing and Evaluation, 46*(6), 2661–2678.
16. Khalid, A., Tajuddin, A. S. A., Jaat, N., Manshoor, B., Zaman, I., Hadi, S. A. A., et al. (2017). Performance and emissions of a diesel engine fuelled with preheated biodiesel fuel derived from crude palm, Jatropha, and waste cooking oils. *International Journal of Automotive and Mechanical Engineering, 14,* 4273–4284.
17. Chauhan, B. S., Kumar, N., Du Jun, Y., & Lee, K. B. (2010). Performance and emission study of preheated Jatropha oil on a medium-capacity diesel engine. *Energy, 35*(6), 2484–2492.
18. Hazar, H., & Aydin, H. (2010). Performance and emission evaluation of a CI engine fueled with preheated raw rapeseed oil (RRO)–diesel blends. *Applied Energy, 87*(3), 786–790.
19. Jeyakumar, N., Narayanasamy, B., Balasubramanian, D., & Viswanathan, K. (2020). Characterization and effect of Moringa Oleifera Lam. antioxidant additive on the storage stability of Jatropha biodiesel. *Fuel*, *281*, 118614.
20. Pradhan, P., Raheman, H., & Padhee, D. (2014). Combustion and performance of a diesel engine with preheated Jatropha curcas oil using waste heat from the exhaust gas. *Fuel, 115,* 527–533.
21. Anand, B. P., Saravanan, C. G., & Srinivasan, C. A. (2010). Performance and exhaust emission of turpentine oil powered direct injection diesel engine. *Renewable Energy, 35*(6), 1179–1184.
22. Nabi, M. N., Akhter, M. S., & Shahadat, M. M. Z. (2006). Improvement of engine emissions with conventional diesel fuel and diesel–biodiesel blends. *Bioresource Technology, 97*(3), 372–378.
23. Tarabet, L., Loubar, K., Lounici, M. S., Khiari, K., Belmrabet, T., & Tazerout, M. (2014). Experimental investigation of DI diesel engine operating with eucalyptus biodiesel/natural gas under dual fuel mode. *Fuel, 133,* 129–138.
24. Gogoi, T. K., & Baruah, D. C. (2011). The use of Korach seed oil methyl ester blends as fuel in a diesel engine. *Applied Energy, 88*(8), 2713–2725.
25. Haiter, L. A., Ravi, R., Arumugham, S., & Thyagarajan, K. (2012). Performance, emission, and combustion evaluation of diesel engines using methyl esters of Mahua oil. *International Journal of Environmental Sciences*, *3*(1), 639–649.
26. Agarwal, A. K., & Dhar, A. (2013). Experimental investigations of performance, emission, and combustion characteristics of Karanja oil blends fuelled the DICI engine. *Renewable Energy, 52,* 283–291.
27. Nithyananda, B. S., Anand, A., & Prakash, G. V. N. (2013). Experimental investigation of neem and mixed Pongamia-coconut methyl esters as biodiesel on CI engine. *International Journal of Mechanical Engineering & Technology, 4,* 232–242.
28. Sanjid, A., Masjuki, H. H., Kalam, M. A., Abedin, M. J., & Rahman, S. A. (2014). Experimental investigation of mustard biodiesel blend properties, performance, exhaust emission, and noise in an unmodified diesel engine. *APCBEE Procedia, 10,* 149–153.
29. Nalgundwar, A., Paul, B., & Sharma, S. K. (2016). Comparison of performance and emissions characteristics of DI CI engine fueled with dual biodiesel blends of palm and Jatropha. *Fuel, 173,* 172–179.
30. Kakati, J., & Gogoi, T. K. (2016). Biodiesel production from Kutkura (Meyna Spinosa Roxb. Ex.) fruit seed oil: Its characterization and engine performance evaluation with 10 and 20% blends. *Energy Conversion and Management, 121,* 152–161.
31. Datta, A., & Mandal, B. K. (2014). Use of Jatropha biodiesel as a future sustainable fuel. *Energy Technology & Policy, 1*(1), 8–14.
32. Buyukkaya, E. (2010). Effects of biodiesel on a DI diesel engine performance, emission, and combustion characteristics. *Fuel*, *89*(10), 3099–3105.
33. Silitonga, A. S., Ong, H. C., Mahlia, T. M. I., Masjuki, H. H., & Chong, W. T. (2014). Biodiesel conversion from high FFA crude jatropha curcas, Calophyllum inophyllum, and Ceiba pentandra oil. *Energy Procedia, 61,* 480–483.
34. Henning, R. K. (1994). Fighting desertification by integrated utilisation of the Jatropha plant. www.Jatropha.org.

35. Xiao, J., Zhang, H., & Niu, L. (2015). Effect of detoxification on conformational and functional properties of Jatropha curcas proteins. *International Journal of Food Properties, 18*(7), 1524–1534.
36. Rani, C., Kajla, S., Pal, M., Poonia, A. K., & Kharb, P. (2013). Jatropha curcas: A potential source for biofuel production. *Renewable Energy Sources and Their Applications, 155*.
37. Silitonga, A. S., Atabani, A. E., Mahlia, T. M. I., Masjuki, H. H., Badruddin, I. A., & Mekhilef, S. (2011). A review of the prospect of Jatropha curcas for biodiesel in Indonesia. *Renewable and Sustainable Energy Reviews, 15*(8), 3733–3756.
38. Kim, H., & Choi, B. (2010). The effect of biodiesel and bioethanol blended diesel fuel on nanoparticles and exhaust emissions from the CRDI diesel engine. *Renewable Energy, 35*(1), 157–163.
39. Padhi, S. K. (2010). *Preparation and characterization of biodiesel from non-edible oils* (Doctoral dissertation).
40. Ahmed, W., Nazar, M. F., Ali, S. D., Rana, U. A., & Khan, S. U. D. (2015). Detailed investigation of optimized alkali catalyzed transesterification of Jatropha oil for biodiesel production. *Journal of Energy Chemistry, 24*(3), 331–336.
41. Kawakami, K., Oda, Y., & Takahashi, R. (2011). Application of a Burkholderia cepacialipase-immobilized silica monolith to batch and continuous biodiesel production with a stoichiometric mixture of methanol and crude Jatropha oil. *Biotechnology for Biofuels, 4*(1), 42.
42. Karthickeyan, V., Thiyagarajan, S., Ashok, B., Geo, V. E., & Azad, A. K. (2020). Experimental investigation of pomegranate oil methyl ester in ceramic coated engine at different operating condition in direct injection diesel engine with energy and exergy analysis. *Energy Conversion and Management, 205,*.
43. Özener, O., Yüksek, L., Ergenç, A. T., & Özkan, M. (2014). Effects of soybean biodiesel on a DI diesel engine performance, emission, and combustion characteristics. *Fuel, 115,* 875–883.
44. Kumar, P., Sharma, M. P., & Dwivedi, G. (2014). Impact of biodiesel on combustion, performance, and exhaust emissions of diesel engines. *Journal of Integrated Science and Technology, 2*(2), 57–63.
45. Elango, T., & Senthilkumar, T. (2011). Combustion and emission characteristics of a diesel engine fuelled with jatropha and diesel oil blends. *Thermal Science, 15*(4), 1205–1214.
46. Jeevahan, J., Mageshwaran, G., Joseph, G. B., Raj, R. D., & Kannan, R. T. (2017). Various strategies for reducing No_x emissions of biodiesel fuel used in conventional diesel engines: A review. *Chemical Engineering Communications, 204*(10), 1202–1223.

Characterization of Single-Cylinder DI Diesel Engine Fueled with Waste Cooking Oil Biofuel/Diesel Blends

Dhinesh Balasubramanian, P. V. Inbanaathan, S. K. Gugulothu, and Marcin Noga

Nomenclature

BTE	Brake thermal efficiency (%)
BSEC	Brake-specific energy consumption (kJ/kWhr)
BSFC	Brake-specific fuel consumption (kg/kWhr)
WCO	Waste cooking oil
DI	Direct injection
CI	Compression ignition
ASTM	American Standards for Testing and Materials
NO_x	Oxides of nitrogen (ppm)
CO	Carbon mono-oxide (vol%)
HC	Hydrocarbon (ppm)
CO_2	Carbon dioxide (vol%)
GCMS	Gas chromatography–mass spectroscopy method

D. Balasubramanian (✉) · P. V. Inbanaathan
Department of Mechanical Engineering, Mepco Schlenk Engineering College, Sivakasi, Tamil Nadu, India

D. Balasubramanian
Center for Alternative Energy Research and Development, Khon Kaen University, Khon Kaen, Thailand

Mechanical Engineering Division, Faculty of Engineering, Khon Kaen University, Khon Kaen, Thailand

S. K. Gugulothu
Department of Mechanical Engineering, National Institute of Technology Andhra Pradesh, Tadepalligudem, Andhra Pradesh-534 101, India

M. Noga
Institute of Automobiles and Internal Combustion Engines, Cracow University of Technology, Kraków, Poland

A. P. Singh et al. (eds.), *Alternative Fuels and Advanced Combustion Techniques as Sustainable Solutions for Internal Combustion Engines*, Energy, Environment, and Sustainability, https://doi.org/10.1007/978-981-16-1513-9_8

CHRR	Cumulative heat release rate (kJ)
NHRR	Net heat release rate (J/deg)
CP	Cylinder pressure (bar)
dP/dθ	Rate of pressure rise
MFB	Mass burn fraction
SOC	Start of combustion
EOC	End of combustion
D100	Diesel fuel
WCO10	10% WCO biofuel and 90% diesel
WCO20	20% WCO biofuel and 80% diesel
WCO30	30% WCO biofuel and 70% diesel
WCO40	40% WCO biofuel and 60% diesel
WCO50	50% WCO biofuel and 50% diesel
WCO100	100% WCO biofuel

1 Introduction

Nowadays, worldwide, diesel engines are used in most of the transport applications when compared to gasoline engines, since it delivers high power, lesser maintenance cost and increased range of torque. Due to modernization and an increase in population, usage of vehicles has been raised, thus leading to global warming and depletion of fossil fuels. Bio-derived fuels from various feedstocks serve as an alternative, which would help our community to attain the United Nation suggested sustainable development goals. Many researchers are involved in the extraction of bio-derived fuels from various vegetable and non-vegetable oils as an alternative energy source for the diesel engine [2].

There is a very little research on sustainable non-edible vegetable oil utilization in substituting the diesel oil. Also, utilization of pure vegetable oils to produce biofuel is not practical and economical, since it is the primary resource for many food industries [14]. Waste cooking oil (WCO) usage could importantly reduce the cost in the production of biofuel to about 2 times lesser than the biofuel from vegetable oils [9]. Also, the disposal of WCO from various food industries could be reduced with the usage of WCO as an alternative fuel in CI engine [17]. More amount of edible oil consumption led to the larger production of WCO. Many countries, such as the USA, Canada, Japan, Malaysia and Europe, produce 10, 0.135, 0.4–0.6, 0.5 and 0.7–1.0 million tons of WCO per year, respectively. Highly populated countries such as China and India produce 4.5 and 2 million tons of WCO per year, respectively [32]. Draining WCO into sewage and digging into landfills has been banned in many countries [16]. So, the depleting diesel can be easily replaced by economic WCO, leading to a sustainable future.

The usage of WCO directly in diesel engines could cause various difficulties such as blocking of fuel filters, injector coking, carbon deposits formation inside the

cylinder and increase in wear of the engine. To overcome the above criterion, WCO would be heated which would also result in increased performance characteristics of the engine [28]. In this study, esterified WCO is used as an alternate fuel in a CI engine that possesses similar physio-chemical properties to the diesel oil [25]. The higher viscosity of WCO affects fuel spray characterization and atomization leading to the rise in the size of the fuel droplets [19]. A common method used worldwide is transesterification in which the viscosity of WCO can be decreased, thus making it suitable for the usage in diesel engines [11].

Ashok et al. [6] utilized a constant speed CI engine to conduct experiments using WCO blended with base diesel. With respect to the experimental assessment, the authors concluded a decreased amount of NO_x emission with the usage of biodiesel and also saved 10% consumption of diesel fuel. Devendra Singh et al. [30] has observed decreased BTE and increased BSFC with WCO blends in a diesel engine. All types of WCO blends emitted increased NO_x and reduced HC and CO emissions. Muralidharan et al. [23] utilized WCO blended with diesel fuel of 80, 60, 40 and 20% by volume in a CI engine. The experimental plots pointed out that the exhaust temperature for WCO blends was increased in comparison with diesel. Also, WCO with a 20% volume in diesel fuel performed better in terms of emission and combustion characterization. Yuan Chung Lin et al. [20] conducted various tests on a single-cylinder CI engine using WCO blend with diesel of 30, 20 and 5% in volume, respectively. They found that BSFC was higher for WCO blends since calorific value of WCO was lesser than diesel fuel. Also, lower WCO blends performed better in both combustion and emission characteristics. Rasim Behcet et al. [10] found transesterification as a suitable method to reduce the viscosity of WCO biodiesel. In their research, WCO was blended with diesel fuel by 25% on volume. Various experiments were carried out in the diesel engine at varying the load conditions. They found that for the B25 blend, BSFC increased by 5.69%, and BTE decreased by 4.72% in comparison with the base diesel. Sanli et al. [27] produced two different types of biodiesels using ethanol and methanol from waste fry oil. Experiments were done in a CI engine at three different speeds (1700, 1400 and 1100 rpm) using B100 and B20 blend fuels. BTE and BSFC of prepared biodiesel blends from both the alcohols were better than the diesel fuel. In comparison with biodiesel from both the esters, ethyl ester biodiesel performed better than the methyl ester biodiesel. Mittelbach et al. [21] utilized methyl ester obtained from waste fry oil to investigate various emissions at the exhaust in CI engine. The decrease in CO emission, increase in NO_x emission and lower economy of fuel were observed using waste fry oil methyl ester. From the above literature work, it was found that BTE decreases and BSFC increases with the increase in brake power due to the usage of lower WCO blends as a fuel in diesel engines. In terms of emission characteristics, HC and CO emission decreases, while NO_x emission increases with the usage of lower WCO blends replacing the base diesel fuel. The reason behind was due to decreased viscosity and density of the lower WCO blends and calorific value nearer to the diesel fuel (Table 1).

From the detailed literature, it is evident that WCO blends suit diesel engines reducing various emissions like CO, HC, CO_2 and smoke along with increased NO_x. To control NO_x emission, various exhaust treatment methods can be used. Thus, in

Table 1 Characterization of diesel and WCO biofuels in diesel engines

Fuel used	Engine specification	Performance	Combustion	Emission	Optimum fuel and % EGR	References
D100, WCO20, WCO40, WCO60, and WCO100	Kirloskar single cylinder, DI, 4S, RO—4.4 kW @ 1500 rpm, IP—200 bar, IT—23° bTDC	BTE—Down BSFC—Up	HRR—Down CP—Up	NO_x—Up Smoke—Down HC—Down CO—Down	WCO20	[24]
D100, B10, B20, and B30	DEUTZ F1L511, DI, 4S, RO—5.775 kW @ 1500 rpm, CR 17.5:1, IT—24° bTDC	BTE—Down BSFC—Up Air–fuel ratio—Down	–	NO_x—Up Smoke—Down HC—Down CO—Down CO_2—Up EGT—Up	B10	[1]
D100, WCO10, WCO20, and WCO100	Kirloskar single cylinder, DI, 4S, RO—3.7 kW @ 1500 rpm, CR—17.5:1, IT—23° bTDC, IP—220 bar	BTE—Down BSFC—Up	CP—Down	PM—Up HC—Up NO_x—Down	WCO10	[5]

IT—injection timing, RO—rated output, CR—compression ratio, 4S—fourstroke, IP—injection pressure, PM—particulate matter, Up—increases, Down—decreases

this research work, WCO biofuel is prepared using the transesterification method, and the fuel properties of the prepared blends were studied using ASTM standards. The prepared WCO biofuel is mixed with diesel in volume proportions such as 100%, 50%, 40%, 30%, 20% and 10%, respectively. The emission, performance and combustion characterization for various test fuels have been studied in a DI diesel engine. Depending upon the experimental characterization, a suitable blend ratio is selected for the WCO biofuel. Thus, optimization has been done in terms of volume proportion that has to be blended with base diesel.

2 Materials and Methods

2.1 Engine Setup

A four-stroke, water-cooled, single-cylinder, DI diesel engine was utilized for the present investigation. Figure 1 depicts the diagrammatic representation of the test

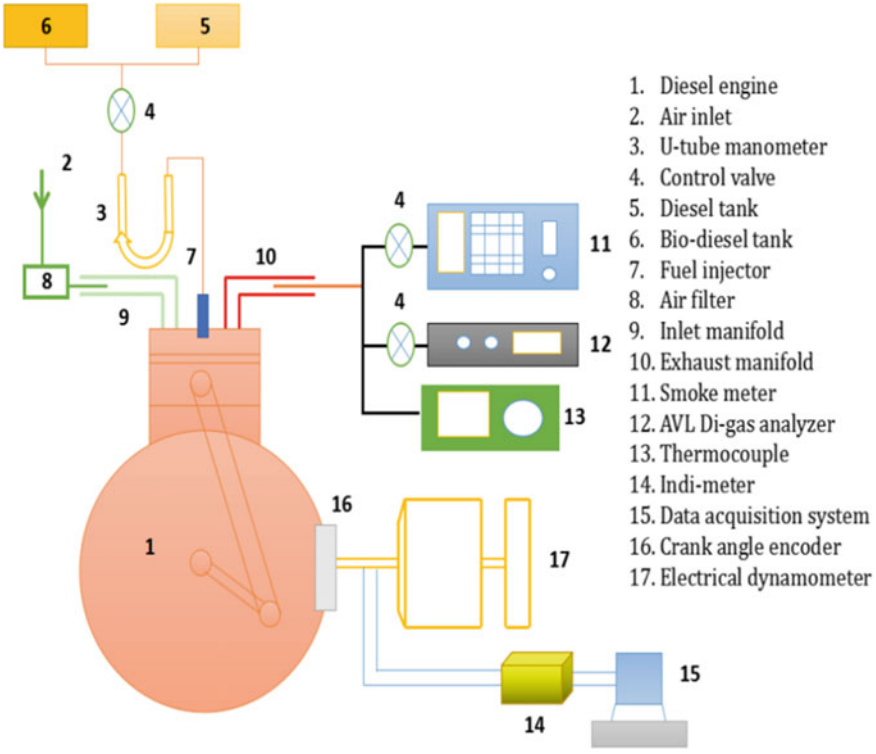

Fig. 1 Diagrammatic representation of engine setup

Table 2 Engine specifications

Parameter	Specification
Make and model	TV1 Kirloskar diesel engine
Maximum rating	3.5 kW @ 1500 rpm
No. of strokes	Four
No of cylinders	One
Bore diameter	87.5 mm
Injection system	Direct injection
Orifice diameter	20 mm
Stroke length	110 mm
Connecting rod length	234 mm
Co-efficient of discharge	0.6
Compression ratio	17:5:1
Injection pressure	220 bar
Capacity	661 cc
Dynamometer arm length	185 mm
Aspiration	Natural
Cooling system	Water-cooled
Governing	Mechanical
Injection timing	23° bTDC

engine setup along with the instruments used for experimental analysis. Table 2 represents the test engine specifications. To determine test engine characteristics, various instruments used along with uncertainties and errors predicted using a separate method [22] are represented in Table 3.

2.2 Preparation of WCO Biofuel

In this research work, WCO raw oil was collected from the households in the region of Virudhunagar District, Tamil Nadu, India. The collected raw oil was used mostly to fry various snack items. A transesterification setup was used to convert this raw WCO oil into usable biofuel. The steps taken to obtained pure biofuel are shown in Fig. 2. The first step involved was to filter the raw oil using a solid strainer. Then, the oil is heated to around 110 °C for 10 min, which would eliminate the suspended water particles present in the filtered WCO. An ultrasonicator reactor bath maintained at 60 °C was used to heat and stir the filtered WCO by adding a 20% volume of methanol and 1% volume of KOH. A constant stirring at 1100 rpm for 15 min was done in a separate vessel. The mixture obtained was made to settle down in a separation funnel for 1.5 h. The fatty acids in the crude biodiesel obtained reacts with potassium or sodium catalyst forming soaps and impurities of glycerin.

Table 3 Instruments used for measurement

Instruments used with model	Measuring parameter	Measuring range	Accuracy	Errors
TMEC10 technomech Eddy current dynamometer	Torque	10 BHP @ 1500–5000 rpm	±0.25	±0.2
EUREKA model PG5 rotameter	Air flow	25–250 lph	±1	±1
KISTLER pressure sensor	Pressure	0–200 bar	±0.75	±0.1
AVL 437 smoke-meter	Smoke	0–100%	±1	±1%
AVL DI GAS 444 N analyzer	NO_x	0–2000 ppm	±5	±1.15%
	HC	0–20,000 ppm	±3	±1.1%
	CO	0–15 vol%	±0.013	±0.9%
	O_2	0–25 vol%	±0.025	±0.8%
	CO_2	0–20 vol%	±0.15	±1.05%

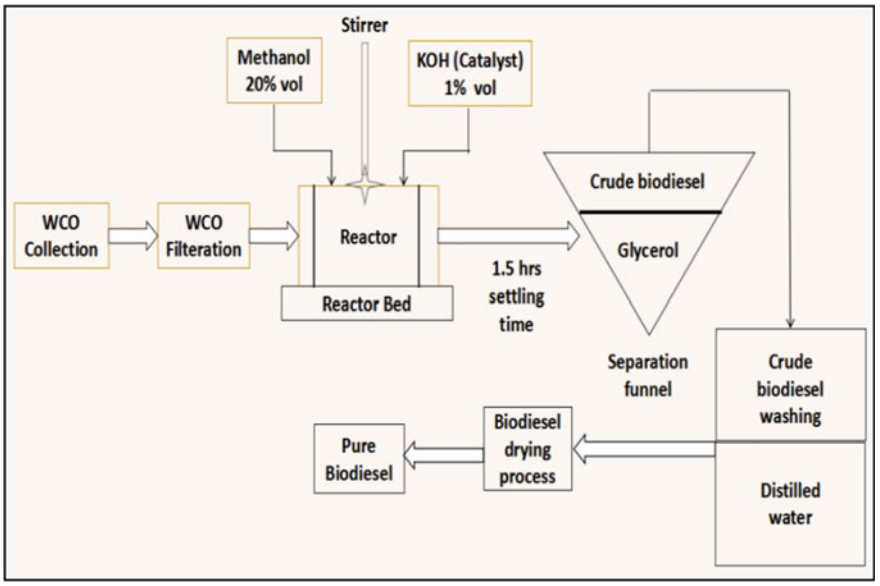

Fig. 2 Biofuel production

These formations would lead to problems on fuel and storage and operation of the engine. Therefore, these are removed by washing the obtained crude biodiesel with distilled water. After the waster washing is completed, the obtained fuel is then dried to remove the small traces of water particles in the biodiesel. Five different blends, namely WCO50, WCO40, WCO30, WCO20 and WCO10, were prepared by using

WCO and diesel oil on volume basis, respectively. The analysis was made on all the five prepared blends & WCO biofuel and compared concerning diesel oil. The chemical and physical properties of the test fuels which were obtained using different methods of standards are depicted in Table 4. The author has given more detailed description in his previous study [7] about the GCMS of WCO and WCO biofuel, and so, it is not explained now in a detailed manner.

2.3 Test Method Used

The experiments were conducted at 100%, 75%, 50%, 25% and no-load conditions of the test engine at brake mean effective pressure (BMEP) of 4.1, 3.1, 2.0, 1.0 and 0 bar, respectively. The brake power of the engine at which the experiments are performed was 3.4, 2.6, 1.7, 0.9 and 0 kW, respectively. The lubricating oil temperature was kept between 65 and 85 °C. The injection timing and pressure were set at 24° CA bTDC and 220 bar which was kept idle throughout the study. The room temperature was maintained at 27 °C and 1 atmospheric pressure to maintain the reliability in the readings. Before observing the experimental values, for each blend, the engine was made to run for 10 min with the selected fuel, and its exhaust gas temperature was maintained at a constant level. To plot graphs for performance and emission, every test done was repeated thrice, and only, their values of average were taken to maintain the repeatability. Table 5 represents the design matrix of test fuels used along with their blending percentage.

3 Results and Discussions

3.1 Characteristics of Performances

3.1.1 Variation in BTE

Figure 3 depicts the brake thermal efficiency (BTE) comparison for WCO biofuel, diesel and prepared test blends with the rise in brake power. Many researchers [18–5] on using different proportions of WCO blends found that increasing the brake power of the engine increases BTE. And the same results agree well with the present research work. While comparing the trend with respect to blends, BTE decreases when the blending percentage of WCO with diesel fuel increases. At 100% load conditions, BTE obtained is 29.44, 24.9, 26.04, 26.51, 27.13, 27.17 and 27.75 percentage for D100, WCO100, WCO50, WCO40, WCO30, WCO20 and WCO10, respectively. The main reason behind this trend was because of an increase in the percentage of blends of WCO biofuel. It can be stated as a result of lowered calorific value and increased density and viscosity. Due to the increased density and viscosity of the

Table 4 Determination of test fuel property

S. No.	Fuel property	D100	WCO10	WCO20	WCO30	WCO40	WCO50	WCO100	ASTM test standard
1	Kinematic viscosity @ 40 °C (cSt)	2.31	2.01	2.14	2.42	2.77	3.11	4.07	D445
2	Density (kg/m^3)	829	815	820	832	837	844	875	D4052
3	Lower heating value (MJ/kg)	43.8	42.35	41.45	40.92	40.09	38.92	36.12	D240
4	Flash point (°C)	71	78	88	102	127	159	186	D93

Table 5 Summary of test fuels, blends and conditions

Fuel No.	Test fuel												Short form of fuel
	Diesel, vol%						WCO, vol%						
	100%	90%	80%	70%	60%	50%	10%	20%	30%	40%	50%	100%	
1	√												D100
2		√					√						WCO10
3			√					√					WCO20
4				√					√				WCO30
5					√					√			WCO40
6						√					√		WCO50
7												√	WCO100

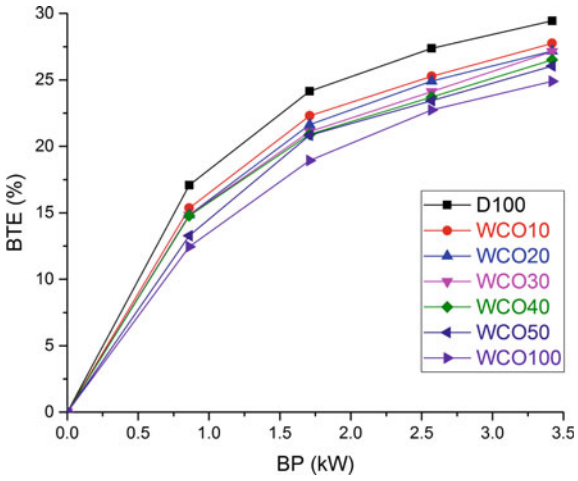

Fig. 3 Brake Power versus brake thermal efficiency

WCO biofuel, the size of the fuel droplets was bigger during the spray injection. Thus, the fuel atomization was affected ultimately reducing the efficiency of combustion. Because of the reduced combustion, BTE decreases for WCO biofuel, and it blends [13]. The percentage reduction for BTE at higher load conditions is 6.09, 8.34, 8.52, 11.07, 13.08 and 18.26% for WCO10, WCO20, WCO30, WCO40, WCO50 and WCO100, respectively, in comparison with respect to base diesel. At all load conditions, WCO10 blend fuel showed only a mild decrease in BTE as compared with diesel oil.

3.1.2 Variation in BSFC

Figure 4 represents BSFC comparison for WCO biofuel, diesel and prepared test blends along with the rise in brake power. BSFC drops with the rise in brake power

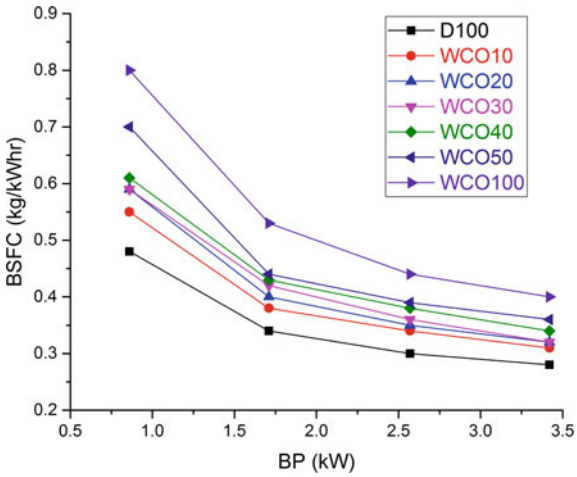

Fig. 4 Brake power versus brake-specific fuel consumption

for all test fuels. The measurement of BSFC at full load condition was 0.28, 0.40, 0.36, 0.34, 0.32, 0.32 and 0.31 kg/kWhr for D100, WCO100, WCO50, WCO40, WCO30, WCO20 and WCO10, respectively. As the blend percentage is increasing with WCO biofuel, BSFC increases at all the load conditions in comparison with base diesel. Higher density and lower heating value for increasing WCO blends consumed excess mass of fuel to provide a similar power output in comparison with diesel fuel. Less difference in fuel consumed at higher loads and wide difference at lower loads was understood clearly from Fig. 4. The main reason would be the induction of air–fuel mixture inside the cylinder which was lean at high load condition, which consumed lesser fuel than diesel [5].

3.1.3 Variation in BSEC

Figure 5 depicts BSEC comparison for WCO biofuel, diesel and prepared test blends with the rise in brake power. BSEC was calculated using calorific value, brake power and total fuel consumption of the fuel, and it indicates the energy obtained from the fuel burned per hour for the brake power. Many researchers [18–5] used different proportions of WCO blends found that the BSEC decreases with respect to rise in brake power for every type of test fuels. It indicates the energy obtained from the fuel burned per hour for the brake power. While comparing the trend with respect to blends, BSEC increases when the blending percentage of WCO with diesel fuel increases. At 100% load conditions, BSEC obtained is 12.23, 14.46, 13.83, 13.58, 13.27, 13.25 and 12.97 MJ/kWhr for D100, WCO100, WCO50, WCO40, WCO30, WCO20 and WCO10, respectively. BSEC comparison is essential since the fuels with different heating values are tested. Combined attribution of higher density, viscosity and lower heating value was the reason behind this trend. The density and viscosity of the fuel affect the brake power obtained which ultimately varies the

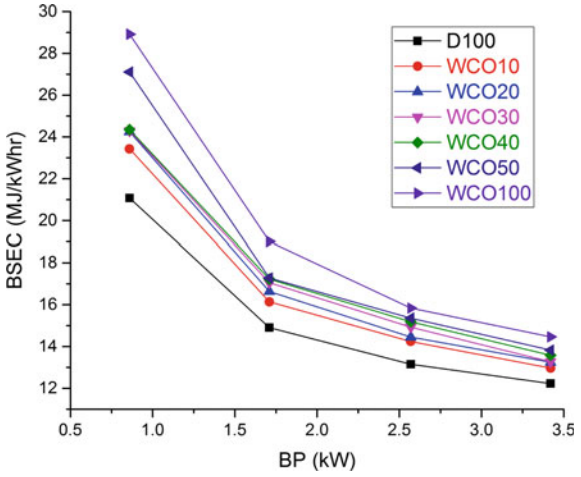

Fig. 5 Brake power versus brake-specific energy consumption

BSEC. The higher BSEC for WCO biofuel was due to variations in turbulence level leading to increased cycle by cycle variations in combustion at the early stages of the combustion process [31, 3]. A minimum rise in BSEC of about 6.09% at higher load was attributed to WCO10 biofuel, while a maximum of 37.19% at lower load was attributed to WCO100 biofuel.

3.2 Characteristics of Various Emissions

3.2.1 Variation in CO Emission

Figure 6 depicts the emission values of CO for diesel, WCO biofuel and prepared WCO blends with the increase in brake power. Many researchers [18–5] have seen a general trend in which the emission values rise steeply at high loads, while it was low in the case of lower and part-load conditions. At high load conditions, the air–fuel ratio becomes rich which decreases the quantity of air available for combustion to take place, thus creating a lower flame temperature. Also, the engine speed is higher because of which there will less time available for the combustion to take place inside the cylinder [29]. Increasing the blending percentage of WCO blend at lower and medium load conditions showed very slight differences in CO emission. These differences showed a trend of a decrease in emission values. With respect to increase in engine speed, CO emission increases because of the rise in air–fuel ratio along with the increase in specific fuel consumption. More amount of fuel–air mixture gets trapped in the clearance volume close to the cylinder walls inside the cylinder, thus leading to higher CO emissions at higher load conditions [27, 12]. Thus, a maximum reduction of 16.67% was observed for WCO100 fuel in comparison with diesel fuel. At 100% load condition, CO emissions obtained are 1.07, 1.05, 0.98, 0.91, 0.89, 0.83

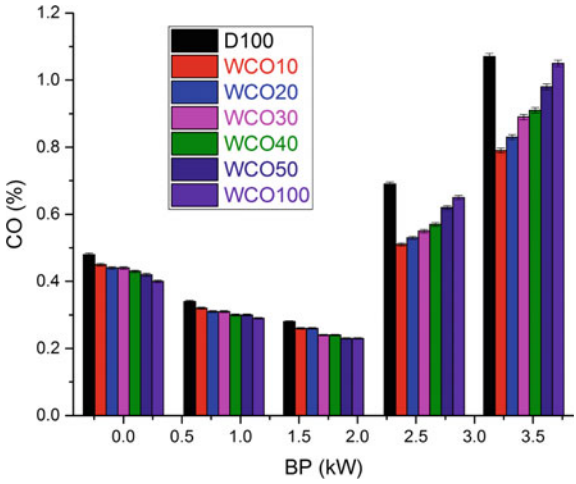

Fig. 6 Brake power versus CO emission

and 0.79% volume for D100, WCO100, WCO50, WCO40, WCO30, WCO20 and WCO10, respectively. In comparison with higher WCO blend fuels, WCO10 blend fuel showed better results. Rich air–fuel mixture in case of higher WCO blends has plenty of oxygen which quenches the flame, thereby reducing the flame temperature, thus increasing the CO emissions at higher load conditions [27]. Thus, a maximum reduction of 26.17% was obtained for WCO10 blend fuel in comparison with diesel fuel.

3.2.2 Variation in HC Emission

Figure 7 depicts the emission values of HC for diesel, WCO biofuel and its prepared blends with respect to rise in brake power. Initially, at lower and part-load conditions, HC emissions decrease, and then, it rises for 100% load condition. Excess mass of fuel was injected to produce required power output at higher loads leading to incomplete combustion. WCO blends follow a similar way of HC emissions at various loads on the par with diesel fuel. At 100% load condition, HC emissions obtained are 77, 106, 101, 94, 86, 74 and 71 ppm for D100, WCO100, WCO50, WCO40, WCO30, WCO20 and WCO10, respectively. HC emissions increase for higher WCO blends. The reason would be attributed to the increased oxygen availability, which would have quenched the amount of fuel–air mixture leading to incomplete combustion, while WCO10 and WCO20 biofuel blends stood out with a decrease in HC emissions in comparison with all the other test fuels. The reason would be the density and viscosity of the blend fuels, which are lesser than diesel and all the other test fuels. Though both the fuels show lesser calorific value, the correct quantity of O_2 availability enhanced the combustion inside the combustion chamber [8, 4]. A maximum reduction of about 10.71% was obtained for WCO10 blend at lower load in comparison with the base diesel fuel.

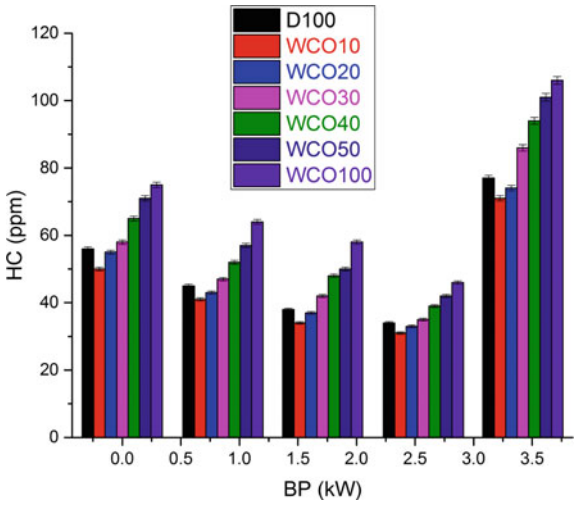

Fig. 7 Brake power versus HC emission

3.2.3 Variation in NO_x Emission

Figure 8 shows the trade-off for NO_x emission values of WCO biofuel, diesel and its prepared blends with respect to rise in brake power. The NO_x trend seen by many researchers [18–5] depicts that it increases with the rise in load for all the types of test fuels. Flame temperature rises inside the cylinder because of the quick reaction rate. At 100% load condition, NO_x emissions obtained are 910, 827, 842, 863, 887, 921 and 934 ppm for D100, WCO100, WCO50, WCO40, WCO30, WCO20 and WCO10, respectively. At all the load conditions, NO_x emission increased for WCO10 and WCO20, while it decreases for all other WCO blends as comparing with the diesel.

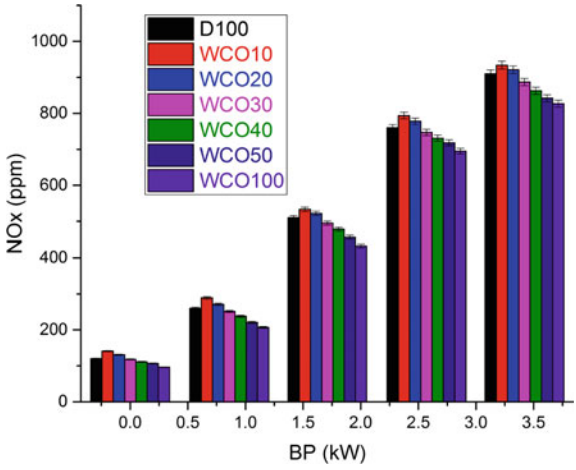

Fig. 8 Brake power versus NO_x emission

Higher HRR and CP for WCO10 and WCO20 blends enabled complete combustion, producing peak temperature inside the combustion chamber.

In contrast, the other WCO blend types released lesser HRR and showed increased CP. An agglomeration effect was created by the excess oxygen availability in higher WCO blends which released lesser cumulative heat release rate and showed reduced cylinder pressure inside the combustion chamber, thus quenching the flame and reducing the flame temperature. Lower heating value of the WCO fuel increased the latent heat of evaporation producing a cooling effect ultimately affecting the NO_x emissions. A maximum rise of about 17.5% of NO_x was observed in WCO10 blend at lower load, while a maximum reduction of about 20% was obtained for WCO100 biofuel in comparison with base diesel fuel. The increase in NO_x emissions can be controlled by various strategies such as injection retardation, modifying the nozzle injector, varying compression ratio, exhaust gas recirculation, water emulsification and selective catalytic reduction.

3.2.4 Variation in Smoke Emission

Figure 9 represents the comparison of smoke emission values of diesel, WCO biofuel and its prepared test fuels with an increase in brake power. Many researchers [17–5] showed similar trends in which smoke emission increases with the rise in brake power for every test fuels. Higher equivalence ratio and increased amount of fuel injection at higher loads would be the major factor. At 100% load condition, smoke opacities are 90.4, 84.1, 84.9, 86.4, 87.8, 89.1 and 90.2% and at 50% load, smoke opacities are 32.8, 40.2, 37.8, 35.4, 33.7, 32.9 and 30.2% for D100, WCO100, WCO50, WCO40, WCO30, WCO20 and WCO10, respectively. As WCO blend percentage increases, smoke increases at lower and part loads, while it decreases at higher load conditions. At lower and part loads, as the air–fuel mixture being lean, fuel molecules undergo

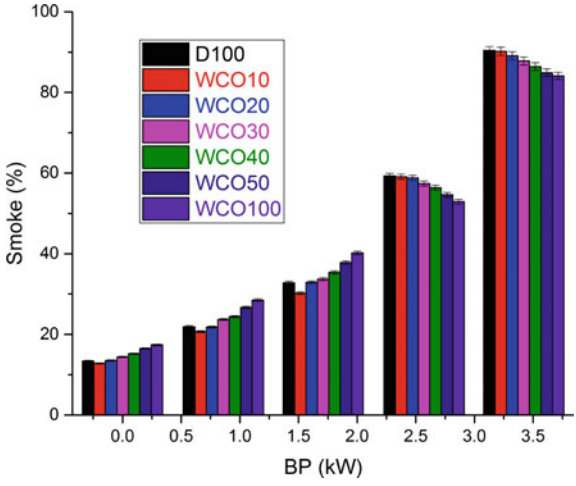

Fig. 9 Brake power versus smoke emission

pyrolysis reaction to form carbon particles at the earlier stage of combustion. In this lean flame region, the presence of oxygen in WCO biofuel burns the carbon particles completely. The rich air–fuel mixture at high loads, increased fuel injection before ignition, earlier completion of the combustion process, longer ignition delay periods and increased residence time reduced the smoke emission at higher load conditions [26]. A maximum reduction of 7.93% was observed for WCO10 blend fuel at part-load condition, while a maximum increase of about 30.14% was obtained for WCO100 biofuel at the same load. WCO10 blend fuel seemed to be performed well with a decrease in smoke emission at all the load conditions in comparison with diesel. The other higher WCO blends performed poorly in terms of emission of smoke values at lower and part-load conditions.

3.2.5 Variation in CO_2 Emission

Figure 10 depicts the trade-off between CO_2 emission values of diesel, WCO biofuel and prepared blends with the rise in brake power. CO_2 emission rises as the load increases for all the test fuels, which were also noticed by a researcher showing a similar trend [1]. Excess mass of fuel inducted inside the cylinder would be the major factor. Increasing the blending percentage of WCO increases CO_2 emission except at higher loads. At high load conditions, oxygen availability in higher WCO blends quenches the flame, thus reducing the formation of CO_2. At 100% load condition, CO_2 emission obtained is 12.51, 11.75, 11.97, 12.18, 12.24, 12.31 and 12.41% volume and at part load condition, 7.1, 8.1, 7.79, 7.48, 7.28, 7.07 and 6.91% for D100, WCO100, WCO50, WCO40, WCO30, WCO20 and WCO10, respectively. WCO10 blend fuel performed better at all the load conditions in comparison with base diesel fuel. But comparing WCO10 with its higher blends, at higher load conditions, the

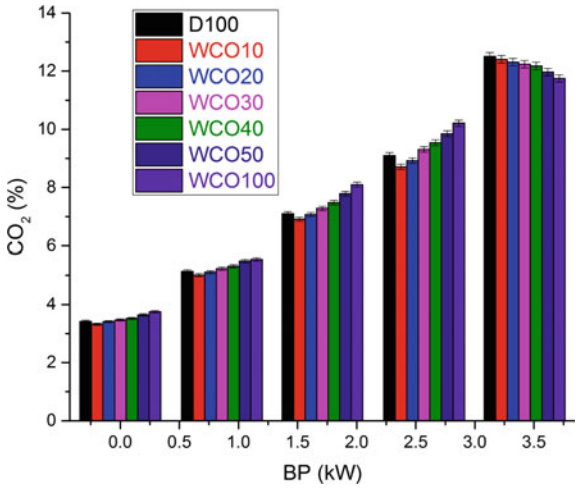

Fig. 10 Brake power versus CO_2 emission

percentage reduction in CO_2 was less. Because at high loads, WCO10 blend fuel has less oxygen content preventing the flame quenching, ultimately increasing CO_2 emission values. A maximum reduction of about 4.29% was obtained for WCO10 blend fuel at part load condition, while the maximum rise of 14.08% for WCO100 biofuel was observed at the same load condition.

3.3 Combustion Characteristics

3.3.1 Rate of Pressure Rise and Cylinder Pressure

Figure 11 represents the cylinder pressure (CP) variation with the crank angle for WCO biofuel, diesel and prepared blends at 100% load condition. CP is characterized by the capability of burning of fuel and mixing of air with fuel [15]. The obtained peak cylinder pressure values are 54.08, 53.66, 53.86, 53.74, 54.85, 54.02 and 54.89 bar at an 8° crank angle for D100, WCO100, WCO50, WCO40, WCO30, WCO20 and WCO10, respectively. As discussed in the NO_x section, the trend showed that WCO10 blend fuel exhibits higher cylinder pressure in comparison with all the other types of test fuels. A similar pattern was followed by every WCO blend fuels on the par with diesel fuel. So, WCO biofuel would be best suitable for the test engine.

Figure 12 represents the pressure rise rate plotted against the crank angle in degrees for WCO biofuel, prepared test blends and diesel fuel. The reason for the plotting of $dP/d\theta$ curve was to find out SOC and EOC inside the engine. The rate of pressure rise would be higher at the SOC inside the cylinder. The graph clearly shows the start

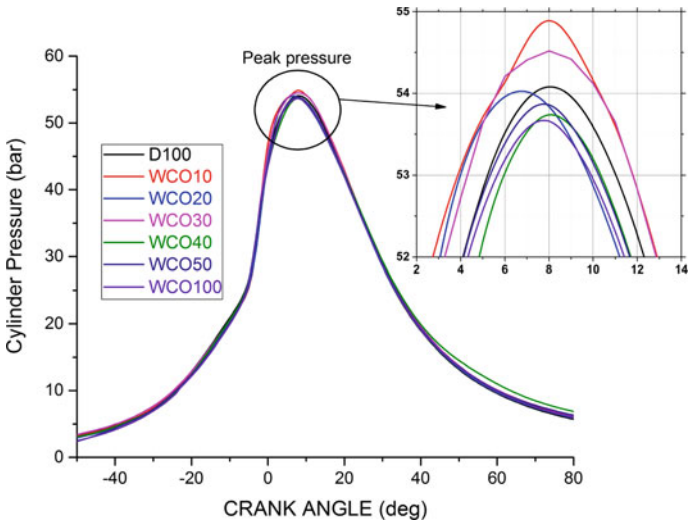

Fig. 11 Crank angle versus in-cylinder pressure

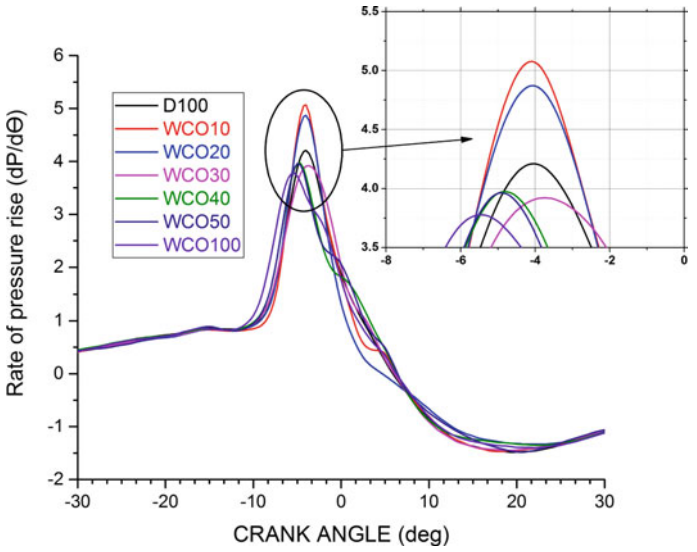

Fig. 12 Crank angle versus pressure rise rate

of combustion occurring at −4° for D100, WCO10, WCO20 and WCO30 while −5° for WCO40, WCO50 and WCO100 fuels, respectively. At fuller load condition, the maximum values of pressure rise rate obtained are 4.21, 3.72, 3.96, 3.96, 3.91, 4.87 and 5.07 for D100, WCO100, WCO50, WCO40, WCO30, WCO20 and WCO10, respectively. From the above values, WCO10 blend fuel had a higher rate of pressure rise in comparison with any type of test fuel considered. The reason behind that would be better-premixed combustion of fuel causing more amount of pressure rise in the earlier stage of combustion. The other blend fuels have a low pressure which can be attributed to the delay period of ignition being longer causing the fuel to unburn at the premixed stage of combustion.

3.3.2 Cumulative and Net Heat Release Rate

Figure 13 represents NHRR variation with the degrees of crank angle for WCO biofuel, diesel and all WCO blends at 100% load condition. NHRR graph clearly explains various combustion parameters such as the ignition delay period, SOC, SOI and the peak HRR. This graph also shows the differences that occur at both the premixed and diffusive stages of combustion [18]. Both the stages are depicted clearly in Fig. 13. There were few negative values initially before the premixed stage, which represents the evaporation of fuel. At 100% load condition, NHRR obtained is 39.06, 34.83, 35.07, 34.37, 41.44, 40.43 and 46.99 kJ/deg for D100, WCO100, WCO50, WCO40, WCO30, WCO20 and WCO10, respectively. A similar trend was exhibited for every WCO blends on the par with diesel fuel. WCO100, D100 and higher WCO

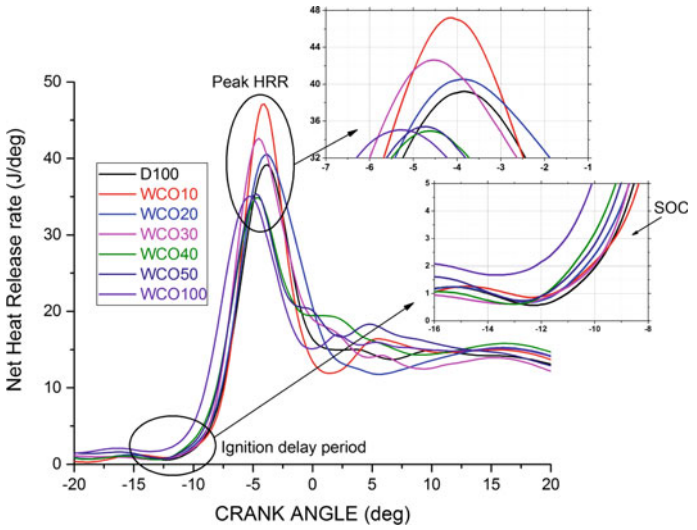

Fig. 13 Crank angle versus net heat release rate

blends exhibited lower NHRR because, in all these fuels, ignitions occur faster due to shorter ignition delay period. WCO10 blend fuel had better NHRR due to its sufficient O_2 content, which helped the diesel to burn fully. Longer ignition delay period could also be a reason behind better NHRR, thus increasing the combustion temperature causing the release of more NO_x in the case of WCO10 blend fuel. Better burning of fuel at the diffusive stage of combustion was because of air–fuel mixing being better, leading to complete combustion.

Figure 14 represents CHRR variation with the crank angle for WCO biofuel, diesel and all WCO blends at 100% load condition. This graph shows an S-type of the characteristic curve. CHRR means a total sum of the instantaneous HRR inside the combustion chamber. CHRR curve shows a slow start in the curve and increases suddenly peaking at a point and then again decreases slowly. Every type of WCO blend, along with WCO biofuel, follows a similar trend as that of diesel fuel. The peak values of CHRR obtained at various crank angle degrees are depicted clearly in Fig. 14. Except for WCO10 blend fuel, all the other WCO blend fuels showed CHRR around 1–1.2 kJ at 88–98° crank angle, which was better than diesel fuel. The reason is because of increased O_2 content helping them to release more amount of heat. But still WCO10 showed higher CHRR, since the flame developed in diffusive phase was quenched beyond 90° crank angle. WCO10 blend fuel showed a maximum CHRR of 1.37 kJ at a 130° crank angle. The reason is due to the correct required quantity of oxygen available to burn the remaining diesel fuel increased the release of heat, enabling complete combustion.

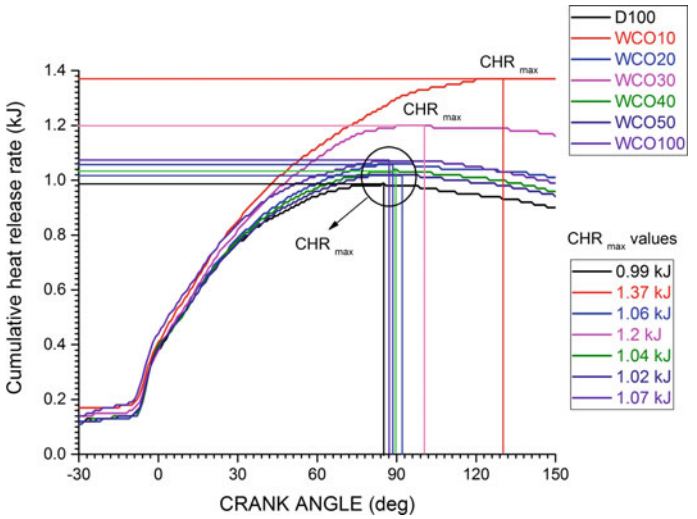

Fig. 14 Crank angle versus cumulative heat release rate

3.3.3 Mass Burn Fraction

Figure 15 shows the variation in mass burn fraction (MFB) with the degrees of crank angle for WCO biofuel, diesel and all prepared blend fuels. MFB can be calculated

MFB	D100	WCO10	WCO20	WCO30	WCO40	WCO50	WCO100
SOC	-17	-18	-17	-16	-17	-15	-18
EOC	46	54	65	62	65	68	62
MFB5%	-5.65	-5.48	-5.21	-5.61	-5.63	-5.4	-6.52
MFB10%	-4.31	-4.3	-3.86	-4.3	-4.2	-3.88	-5.03
MFB50%	6.9	7.24	9.97	7.92	11.79	11.64	9.29
MFB90%	30.79	35.02	42.09	39.82	48.08	48.01	40.92

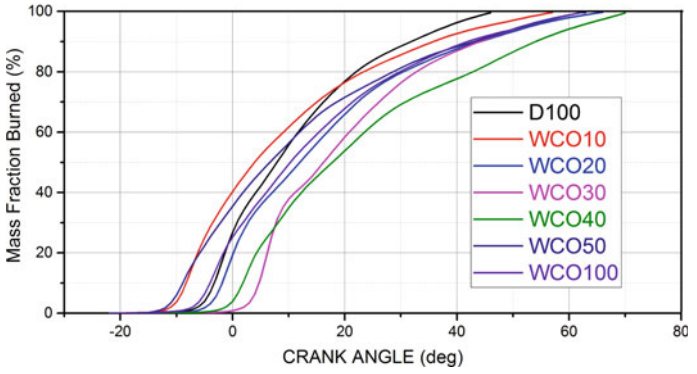

Fig. 15 Crank angle versus mass burn fraction

by the ratio of CHRR to the content of energy obtained through the charge trapped inside the cylinder. It is always better to compare MFB for different calorific value fuels to determine the actual performance of the test fuels. Similar to the CHRR curve, MFB also follows an S-type of the characteristic curve. The initial stage of the curve represents the burning of air and fuel mixture (SOC), which peaks at the middle and decreases to zero at EOC. SOC and EOC represent the start and end of the combustion process. Here, MFB for 5, 10, 50 and 90% were compared for all types of test fuels. From Fig. 15, it is evident that there are no major differences in MFB at 5, 10, and 50% for all the types of test fuels. MFB for 90% shows major differences in which diesel has minimal duration when compared it all the other WCO blend fuels. WCO10 performed well in terms of burning duration in comparison with its higher WCO blend types and WCO biofuel.

4 Conclusion

In the present study, the transesterification method was used to obtain WCO biofuel. Its physio-chemical properties were determined using ASTM standards. The obtained biofuel was blended with diesel fuel in different proportions like 10, 20, 30, 40 and 50% in volume, respectively. A four-stroke, single-cylinder, direct-injection CI engine fitted with an electrical dynamometer was utilized to investigate the characteristics of emission, performance and combustion using the prepared test fuels. The following conclusions were drawn from the current research work:

- Concerning BTE, WCO10 blend fuel performed better showed the lowest reduction of 6.09% at 100% load condition in comparison with diesel. The reason would be due to LHV of the fuel. But it showed a rise of about 10.29, 6.18, 4.49, 2.24 and 2.08% for WCO100, WCO50, WCO40, WCO30 and WCO20, respectively.
- At all load conditions, the WCO10 blend showed increased BSFC with a maximum of 14.96% in comparison with diesel at no-load condition. But the same fuel blend showed a maximum reduction in BSFC of 44.71, 25.89, 9.78, 7.28 and 5.73% at the same load for WCO100, WCO50, WCO40, WCO30 and WCO20, respectively. A similar variation was seen in the case of BSEC with slight changes in percentage variation
- WCO10 blend exhibited high NHRR, CHRR, cylinder pressure and pressure rise rate in comparison with the test fuels. The required amount of oxygen available in the WCO10 blend was sufficient to increase the flame temperature inside the cylinder, thus increasing the cylinder pressure and heat released inside the combustion chamber.
- At full load condition, MFB for diesel was lesser any other type of test fuel. Though not much difference was found at 5, 10 and 50% MFB, a wide difference was seen in the case of 90% MFB. Very less burning duration was obtained for diesel fuel, while only WCO10 blend fuel only has a closer relationship with the diesel fuel.

- Regarding emission values, the WCO10 blend performed well within the case of HC, CO, smoke and CO_2. A maximum reduction of 10.71% HC, 26.17% CO, 7.93% smoke, and 4.29% CO_2, while an increase in NO_x with a maximum of about 17.5% was observed in comparison with the base diesel fuel. The reason would be due to complete combustion occurring inside the combustion chamber.

From the current research work, it can be concluded that WCO10 blend fuel would be an optimum fuel to enhance emission (except NO_x), combustion and performance parameters of a direct-injection CI engine. The future scope of the present work would be to use various treatment techniques to reduce NO_x emission values.

Acknowledgements The authors would like to thank and acknowledge the management of Mepco Schlenk Engineering College for encouraging and providing the experimental facilities throughout the research work.

Conflicts of Interest The authors declare that they have no known competing for financial interests or personal relationships that could have appeared to influence the work reported in this paper.

References

1. Abed, K. A., El Morsi, A. K., Sayed, M. M., El Shaib, A. A., & Gad, M. S. (2018). Effect of waste cooking-oil biodiesel on performance and exhaust emissions of a diesel engine. *Egyptian Journal of Petroleum, 27,* 985–989.
2. Agarwal, A. K. (2007). Biofuels (alcohols and biodiesel) applications as fuels for internal combustion engines. *Progress in Energy and Combustion Science, 33,* 231–277.
3. Agarwal, A. K., et al. (Eds.) *Biofuels, green energy and technology*. https://doi.org/10.1007/978-981-10-3791-7_1.
4. Agarwal A. K., et al. (Eds.) *Engine exhaust particulates, energy, environment, and sustainability*. https://doi.org/10.1007/978-981-13-3299-9_1.
5. Al-Dawody, M. F., Jazie, A. A., & Abbas, H. A. (2019). Experimental and simulation study for the effect of waste cooking oil methyl ester blended with diesel fuel on the performance and emissions of diesel engine. *Alexandria Engineering Journal, 58*, 9–17.
6. Ashok, Y., Onkar, S. (2012). Investigations on diesel engine performance based on jatropha, karanja and neem biodiesels. *Proceedings of the Institution of Mechanical Engineers, Part A: Journal of Power and Energy, 226*(5), 674–681.
7. Balasubramanian, D., Kamaraj, S., & Krishnamoorthy, R. (2020). Synthesis of biofuel from waste cooking oil by alkali doped calcinated waste egg shell powder catalyst and optimization of process parameters to improve biofuel conversion (No. 2020-01-0341) SAE Technical Paper.
8. Balasubramanian, D., Venugopal, I. P., & Viswanathan, K. (2019). Characteristics investigation on DI diesel engine with nano-particles as an additive in lemon grass oil (No. 2019-28-0081). SAE Technical Paper.
9. Balat, M. (2011). Potential alternatives to edible oils for biodiesel production e a review of current work. *Energy Conversion and Management, 52,* 1479.
10. Behcet, Rasim, Yumrutas, Recep, & Oktay, Hasan. (2014). Effects of fuels produced from fish and cooking-oils on performance and emissions of a diesel engine. *Energy, 71,* 645–655.
11. Buyukkaya, E., Benli, S., Karaaslan, S., & Guru, M. (2013). Effects of trout-oil methyl ester on a diesel engine performance and emission characteristics. *Energy Conversion and Management, 69*, 41–48.

12. De, S., et al. (Eds.) *Coal and biomass gasification, energy, environment, and sustainability*. https://doi.org/10.1007/978-981-10-7335-9_1.
13. Dhanasekaran, R., Ganesan, S., Rajesh Kumar, B., & Saravanan, S. (2019). Utilization of waste cooking oil in a light-duty DI diesel engine for cleaner emissions using bio-derived propanol. *Fuel, 235*, 832–837.
14. Dogan, T. H. (2016). The testing of the effects of cooking conditions on the quality of biodiesel produced from waste cooking oils. *Renewable Energy, 94,* 466–473.
15. Inbanaathan, P. V., Dhinesh, B., & Tamilarasan, U. (2020). Experimental investigation of performance and emission characteristics of diesel blended with palm methyl ester along with alumina nano-additive using D.I. diesel engine. In S. Ghosh, R. Sen, H. Chanakya, & A. Pariatamby (Eds.), *Bioresource utilization and bioprocess.* Singapore: Springer.
16. Kalam, M. A., Masjuki, H. H., Jayed, M. H., & Liaquat, A. M. (2011). Emission and performance characteristics of an indirect ignition diesel engine fuelled with waste cooking oil. *Energy, 36*(1), 397–402. https://doi.org/10.1016/j.energy.2010.10.026.
17. Karacan, S., & Cagatay, M. T. (2017). Transesterification of waste cooking oil into biodiesel using aspen HYSYS. *International Journal of Scientific Research in Science and Technology, 3*(3), 83–87.
18. Karthickeyan, V., Dhinesh, B., & Balamurugan, P. (2020). Effect of compression ratio on combustion, performance and emission characteristics of DI diesel engine with orange oil methyl ester. In S. Ghosh, R. Sen, H. Chanakya, & A. Pariatamby (Eds.), *Bioresource utilization and bioprocess.* Singapore: Springer.
19. Kent Hoekman, S. (2012). Review of biofuel composition, properties, and specifications. *Renewable and Sustainable Energy Reviews, 16*, 143–169.
20. Lin, Yuan-Chung, Hsu, Kuo-Hsiang, & Chen, Chung-Bang. (2011). Experimental investigation of the performance and emissions of a heavy-duty diesel engine fueled with waste cooking-oil biodiesel/ultra-low sulfur diesel blends. *Energy, 36,* 241–248.
21. Mittelbach, M., & Tritthart, P. (1988). Diesel fuels derived from vegetable oils, III. Emission tests using methyl esters of used frying oil. *Journal of the American Oil Chemists' Society, 65*(7), 1185–1187.
22. Moffat, R. J. (1985). Using uncertainty analysis in the planning of an experiment. *Journal of Fluids Engineering, 107*(2), 173–178.
23. Muralidharan, K., & Vasudevan, D. (2011). Performance, emission and combustion characteristics of a variable compression ratio engine using methyl esters of waste cooking-oil and diesel blends. *Applied Energy, 88,* 3959–3968.
24. Nantha Gopal, K., Pal, A., Sharma, S., Samanchi, C., Sathyanarayanan, K., & Elango, T. (2014). Investigation of emissions and combustion characteristics of a CI engine fueled with waste cooking oil methyl ester and diesel blends. *Alexandria Engineering Journal, 53*, 281–287.
25. Oner, C., & Altun, S. (2009). biofuel production from inedible animal tallow and an experimental investigation of its use as alternative fuel in a direct injection diesel engine. *Applied Energy, 86,* 2114–2120.
26. Puhan, S., & Nagarajan, G. (2008). Effect of biodiesel unsaturated fatty acid on combustion characteristics of a DI compression ignition engine. SAE Technical Paper 2008-28-0041. https://doi.org/10.4271/2008-28-0041.
27. Sanli, H., Canakci, M., Alptekin, E., Turkcan, A., & Ozsezen, A. N. (2015). Effects of waste frying oil based methyl and ethyl ester biodiesel fuels on the performance, combustion and emission characteristics of a DI diesel engine. *Fuel, 159,* 179–187.
28. Senthil Kumar, M., & Jaikumar, M. (2014). A comprehensive study on performance, emission and combustion behavior of a compression ignition engine fuelled with WCO (waste cooking oil) emulsion as fuel. *Journal of the Energy Institute, 87*(3), 263–271. https://doi.org/10.1016/j.joei.2014.03.001.
29. Senthur Prabu, S., Asokan, M. A., Roy, R., Francis, S., & Sreelekh, M. K. (2017). Performance, combustion and emission characteristics of diesel engine fuelled with waste cooking oil biodiesel or diesel blends with additives. *Energy*. https://doi.org/10.1016/j.energy.2017.01.119.

30. Singh, D., Singal, S. K., Garg, M. O., Maiti, P., Mishra, S., & Ghosh, P. K. (2015). Transient performance and emission characteristics of a heavy-duty diesel engine fuelled with microalga Chlorella variabilis and Jatropha curcas biofuels. *Energy Conversion and Management, 106*, 892–900.
31. Wasiu, S., Aziz R. A., & Megat, P. (2018). Brake specific energy consumption (BSEC) and emission characteristics of the direct injection spark ignition engine fuelled by hydrogen enriched compressed natural gas at various air-fuel ratios. *International Journal of Applied Engineering Research, 13*(1), 677–683. ISSN 0973-4562.
32. Xue, J. (2013). Combustion characteristics, engine performances and emissions of waste edible oil biodiesel in diesel engine. *Renewable and Sustainable Energy Reviews, 23,* 350–365.

Effect of 1,4-Dioxane Emulsified Fuel on Diesel Engine Performance and Emission Operating with Varying Injection Timing

Vigneswaran Rajendran, Dhinesh Balasubramanian, Akash Deep, and Sunil Kumar Mahla

1 Introduction

Global energy requirements, limited availability of fossil resources, environmental pollution and future sustainability goals have urged the research community to search for suitable alternative energy sources. Diesel powertrains are dominating and widely utilized in on-road, off-road, marine and stationary sectors due to their immense thermal efficiency, long-lasting nature and more dependability [2]. Parallelly, the significant issues that come up with diesel powertrains are emissions, huge consumption of fuel and adverse health issues [22]. Many replacements have been investigated for diesel powertrains like biodiesel, alcohols, emulsion, nanofuels, etc. along with minor adjustments like combustion bowl geometry, injection timing, pressure and compression ratio [10, 11, 18, 28]. Diesel/water emulsion fuel with additives as a suitable alternative is being tried nowadays by the research community [27].

Lin and Wang [14] investigated the diesel powertrain with two types of emulsion fuels. From their studies, they identified that CO and brake-specific fuel consumption (BSFC) increased for the alternative fuels due to quenching of fuels with the presence

V. Rajendran (✉)
Department of Mechanical Engineering, Sri Sairam Institute of Technology, Chennai, India

D. Balasubramanian
Department of Mechanical Engineering, Mepco Schlenk Engineering College, Sivakasi, India

Mechanical Engineering, Faculty of Engineering, Khon Kaen University, Khon Kaen, Thailand

Center for Alternative Energy Research and Development, Khon Kaen University, Khon Kaen, Thailand

A. Deep
School of Mechanical Engineering, Lovely Professional University, Jalandhar, Punjab, India

S. K. Mahla
Department of Mechanical Engineering, IKG Punjab Technical University, Kapurthala, India

A. P. Singh et al. (eds.), *Alternative Fuels and Advanced Combustion Techniques as Sustainable Solutions for Internal Combustion Engines*, Energy, Environment, and Sustainability, https://doi.org/10.1007/978-981-16-1513-9_9

of water. However, smoke and NO_x reduced due to microrange explosion and low chamber temperature. Further, CO, BSFC, NO_x and smoke decreased by mixing 5% of diglyme to emulsion fuels on the effect of enhanced burning characteristics. Baskar and Kumar [5] conducted the engine performance test with emulsion fuel and oxygen-enriched air (OEA). The enrichment was done up to 27% of oxygen. Apart from their conclusions, the BTE increased for both emulsion fuel and OEA fuel on a par with neat diesel. While combining OEA with emulsion, the cylinder pressure and heat release rate (HRR) were higher. Similarly, NO_x and HC levels were reduced by incorporating the OEA.

Basha and Anand [4] incorporated the alumina nanoparticles with emulsion fuel up to a maximum of 50 ppm. From the results, the BTE, combustion duration, maximum pressure rise, CO, HC and BSFC increased for the emulsion fuels. Ignition delay, smoke, exhaust gas temperature (EGT) and NO_x could be reduced for the emulsion fuel. CO, HC and BSFC decreased on adding nanoadditive to the emulsion fuel due to reduced delay period. Vellaiyan and Amirthagadeswaran [26] tested the nanoblended emulsion fuel and compared the results with plain diesel. Except for NO_x, the parameters like ignition delay (ID), CO and HC rose for the emulsion fuel. It could be attributed to low in-cylinder temperature and quenching of mixture due to the presence of water in the emulsion fuel. The above emissions could be reduced by adding 50 ppm and 100 ppm of zinc oxide nanoadditives to emulsion fuel. The stability of nanoemulsion fuel was reduced with an increasing level of nanoadditives. From the above literature, incorporation of nanoparticles always reduces the exhaust emission of emulsion fuels.

Ramalingam et al. [20] experimented on the engine attributes with 5 ml and 10 ml of 1,4-dioxane together with Annona biodiesel (A20). From their results, the brake thermal efficiency was found to have increased by 6.48% for 1,4-dioxane blended A20-10 ml fuel. HC, CO, NO_x and smoke were reduced with A20-1,4-dioxane blended fuel. This was reasoned out with excess oxygen and the presence of 1,4-dioxane which improved the engine attributes and reduced the emissions.

Vedharaj et al. [25] presented their research with 1,4-dioxane blended kapok biodiesel (B25). They prepared two blended fuels which contained 0.5% and 1% of 1,4-dioxane in B25 blends (B25-0.5 and B25-1%). The output exhibited that adding 1,4-dioxane to B25, increased the BTE up to 5.7% for B25-1% blended fuel which was due to enhanced fuel properties. HC, CO, NO_x and smoke emissions were sharply decreasing for the B25-1% fuel due to the rise in the ignition and cold flow properties. Sendilvelan and Sundar [23] tested the blended fuel contains diesel and 1,4-dioxane. Five sample fuel blends were prepared with 10%, 20%, 30%, 40% and 50% 1,4-dioxane, respectively, with diesel. From their results, the BSEC and smoke were reducing for B10 (90% diesel: 10% 1,4-dioxane) fuel blend when compare to other blends due to heating value and inbuilt oxygen content of 1,4-dioxane in the mixture. Also, BTE and NO_x were increased for B10 fuel due to improved oxidation and rich zones of oxygen. A similar improvement was achieved by Savariraj et al. [21] with 1,4-dioxane and their respective base fuel blends. Having reviewed the above literature, 1,4-dioxane was chosen for further investigations and incorporated with emulsion fuel.

Ashok et al. [3] experimented on the engine with Calophyllum Inophyllum Methyl Ester (CIME-100%) fuel, three injection timings of 21°, 23° and 27° bTDC, and exhaust gas recirculation (EGR). Retarding the timing to 21° bTDC greatly diminished the NO_x emission. When advancing the timing to 23° and 25° bTDC, BTE and BSFC improved due to huge physical delay and resulted in enhanced mixing between air and fuel. CO, HC and smoke greatly reduced with advancing the injection timing due to air entrainment and its subsequent burning rate. Natarajan et al. [16] experimented with algae biodiesel along with retarding and advancing the injection timing. They chose 19° and 21° bTDC being considered as retarded timing. 25° and 27° bTDC were portrayed as advanced injection timings. The results showed that BTE had risen by 5.7% due to the huge delay period. CO, HC and smoke decreased by 81.25%, 30% and 26.39%, respectively, at 27° bTDC due to prolonged injection timing and subsequent amplified mixing and burning. During retardation, the NO_x emission decreased by 28% due to the low temperature in the combustion chamber. Deep et al. [9] inspected the engine with three different injection pressures and injection timings. During their study, the injection timing was fixed as 21°, 23° and 25° bTDC. The various pressures were 200, 250 and 300 bar with B20 (castor oil) fuel. From the results, it was evident that advancing injection timing greatly increased the ignition delay and combustion duration. Also, smoke reduced for the advanced timings. However, at advanced timings, the NO_x emission greatly increased due to the accumulation of more heat in the chamber. Pal et al. [17] studied the engine that ran on pyrolyzed plastic oil. Also, the test was carried out with retarded and advanced injection timings. During advancing, the parameters such as BTE, NO_x increased. CO, HC and smoke reduced due to the delay period variation. When retarding the injection timing, except NO_x, all the parameters dropped due to less residence time. Damodharan et al. [8] had chosen three dissimilar injection timings, namely 21°, 23° and 25° bTDC. The engine was run with waste pyrolysis oil (WPO) and varying percentage of EGR. From their investigations, they reported that at 25° bTDC injecting timing and running with 10% EGR, the WPO fuel was identified to be a better fuel. Also, the BTE, CO, HC, smoke and BSFC could be improved when the engine was run with advanced injection timing due to intensified ignition.

Wang et al. [29] experimented with pumpkin seed oil methyl ester (PSOME). Also, three engine modifications, namely compression ratio, injection pressure and injection timing, were incorporated. The injection timing was altered from 19° to 25° bTDC in steps of 2° crank angle. The results projected that at advanced injection timing say 25° bTDC, the BTE rose due to the delay period and complete burning. Also, CO, HC, BSFC, smoke and PM were drastically decreasing due to enhanced mixing and burning characteristics. However, NO_x emission at 25° bTDC stayed higher due to peak temperature and pressure at an advanced position. Shameer and Ramesh [24] provided wide reviews for engine modifications such as injection timing and nozzle opening pressure. They concluded from their reviews that advancing the injection timing had a positive impact on in-cylinder pressure, peak cycle pressure, HRR, ignition delay and combustion duration due to the availability of residence time. On the other side of the review, retarding the timing provided diminished magnitude on in-cylinder pressure, HRR, cycle pressure and delay period. This could be ascribed

to less preparation time. Karthic et al. [13] researched the diesel powertrain with *Syzygium cumini* biodiesel. They also incorporated the injection parameters during their testing process. While operating with higher injection timing and injection pressures, the combustion and BTE got boosted. Simultaneously CO, HC and smoke emissions got reduced. This was reasoned out with enhanced powertrain attributes by operation conditions. Also, they revealed that when the engine was run with SCO fuel operating on advanced injection conditions, the operating cost decreased by 33% on a par with standard operating conditions.

Ganapathy et al. [12] tested biodiesel fuel with varying parameters like injection timing, speed and torque. While considering the timing variations, the engine was set to operate with 5° retarded and advanced positions from the original equipment manufacturers (OEM) settings. They concluded while advancing the timing the BTE increased, and emissions like HC, CO, smoke and BSFC decreased. This could be due to improved preparation between air–fuel and time available. On retarding the timing, an opposite trend was attained due to a lower mixing rate. From the above literature, modification of injection timing was found to be a promising operating factor that affected engine attributes, emission and combustion. This positive essence was considered and incorporated into this work. Initially, DWSD fuel was prepared, the prepared fuel was tested with advanced and retarded injection timings, and the outputs were compared with diesel.

2 Methods and Materials

From the deep survey, it can be confidently stated that 1,4-dioxane could be a promising additive to maximize the engine attributes and reduce emissions. In this regard, 10% of 1.4-dioxane was blended with diesel, water and surfactant to form DWSD fuel, which has a composition of [79.8% diesel + 10% water + 0.2 surfactant + 10% 1.4-dioxane]. The firmness of the emulsion fuel was kept and tested at normal room temperature, and it was found to last 44 days. The properties of diesel and DWSD are shown in Table 1. The fuel preparation is indicated in Fig. 1.

Table 1 Physio-chemical property of test fuels

Property	Diesel [27]	DWSD [27]
Density in kg/m^3	820	826
Kinematic viscosity in cSt	2.9	2.92
Calorific value in MJ/kg	44.12	44.10
Flash point in °C	65	77
Cetane number	47	50.5

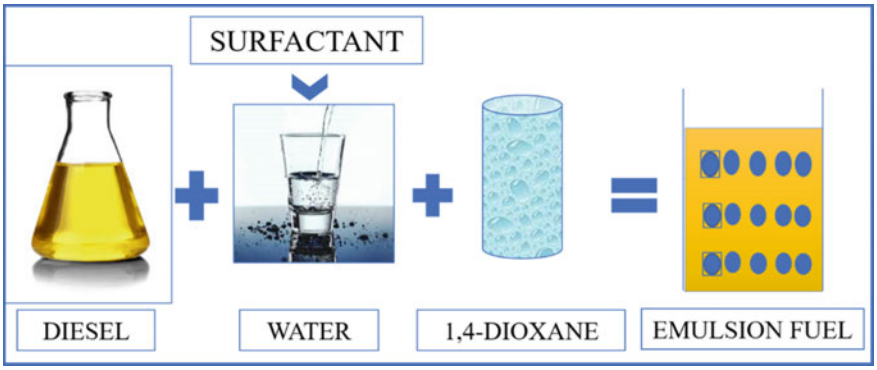

Fig. 1 Pictorial representation of fuel preparation process

3 Experimental Setup

For this investigation, a mono cylinder, agro-based CI engine, was chosen to study the parameters like performance, combustion and emission characteristics. The specification of the powertrain is shown in Table 2. The experimental setup is represented in Fig. 2. The engine can develop a maximum output of 5.2 kW at a consistent speed of 1500 rpm. An eddy current dynamometer of 2450 rpm with 20 kW capacity was integrated with the powertrain to test efficiency. Load of the engine was altered by passing the current through the eddy current dynamometer. Five loading conditions such as 20%, 40%, 60%, 80% and 100% were chosen for this study. The powertrain was equipped with hemispherical bowl and MICO fuel pump. Exhaust gases were measured using an AVL gas analyzer. Smoke emission was measured using AVL 437C meter. The crank position and in-cylinder pressure were noted with a crank angle encoder and a piezoelectric transducer. The pressure data was acquired

Table 2 Specification of the engine

Make and type of engine	Kirloskar, single cylinder direct injection diesel engine with water-cooled [27]
Bore and stroke	87.5 mm and 110 mm
Type of combustion chamber	Hemispherical
Capacity of the engine	661 cc
Rated power	5.2 kW
Rated speed	1500 rpm
Injection timing	23° BTDC
Injection pressure	200 bar
No of nozzle holes	Three
Nozzle hole diameter	0.3 mm

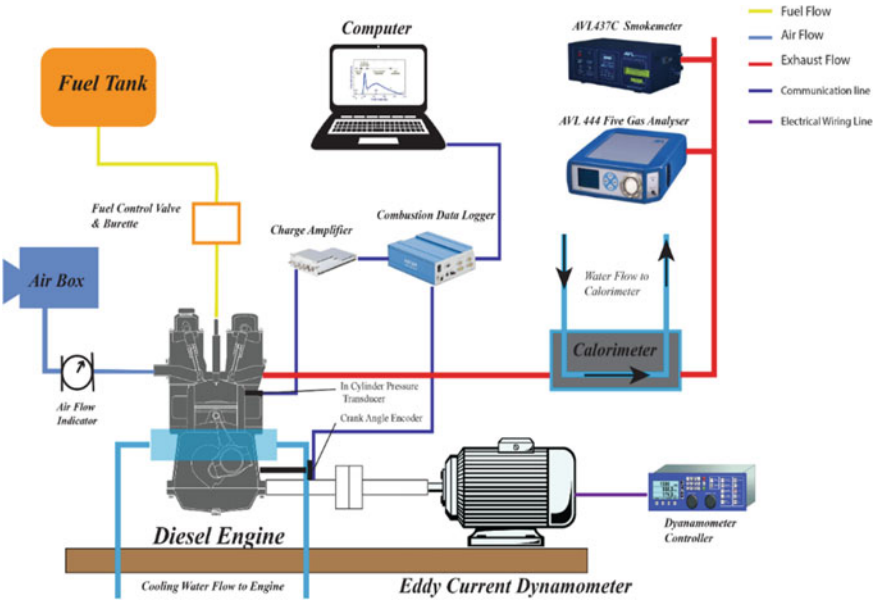

Fig. 2 Layout of experimental setup

for 100 number of cycles, and the average was plotted against crank angle. All the combustion data was recorded using the Indwin software (Version 2.2). Initially, the powertrain was operated with diesel fuel for about 30 min to maintain a steady running condition. After an initial warm-up period, oil and water temperatures were noted to ensure its compatibility. The experiments were performed five times, and the average was considered for the comparisons. To vary the injection timing, the number of shims in the fuel pump was varied. This was achieved by incorporating or removing the shims in the pump. To obtain a minimal error, an uncertainty analysis was carried out on testing. So many factors cause errors like observation, environment, calibration of equipment, etc. The uncertainty was performed by the square root formula for the parameters considered. The total percentage uncertainty for the current investigation was

$$
\begin{aligned}
&= \sqrt{[(U_{\text{Load}})^2 + (U_{\text{Power}})^2 + (U_{\text{BTE}})^2 + (U_{\text{BSEC}})^2 + (U_{\text{HC}})^2} \\
&\quad + (U_{\text{CO}})^2 + \left(U_{\text{NO}_x}\right)^2 + (U_{\text{Smoke}})^2 \\
&= \sqrt{[(0.4)^2 + (0.2)^2 + (0.6)^2 + (0.7)^2 + (0.2)^2 + (0.2)^2 + (0.2)^2 + (0.5)^2} \\
&= 1.19\%
\end{aligned}
$$

4 Results and Discussion

4.1 BP Versus BTE

Figure 3 presents the deviations in BTE for the non-identical injection timings to brake power for the fuels like diesel and DWSD. The outcomes from the experiments were compared with diesel at normal pressure and injection timing of 200 bar and 23° bTDC. The injection pressure was kept constant at 200 bar through the whole experiment. The BTE values for DWSD-27°, DWSD-23°, DWSD-19° bTDC, and diesel were 32.7%, 32.32%, 28.01% and 30.06%, respectively, at peak loads. Similarly, at low loads, the BTE values for the above fuels were 12.99, 12.86, 12.1 and 12.7%. The variation of BTE at low loads were minimum due to lack of oxygen content at lower operating conditions. The raise in BTE for DWSD fuel at 27° bTDC was reasoned out with the huge amount of vaporized fuel which accumulated in the chamber was burned which released quick HRR, drastic rise in pressure and temperature in the chamber, cetane number of DWSD fuel, which led to rising in BTE [2]. The drop in BTE at DWSD-19° bTDC was ascribed to less residence time and poor air/fuel mixing [19]. At 23° injection timing, the BTE of diesel and DWSD fuel improved on a par with a 19° crank angle due to improvement in the burning process. The drop in BTE for DWSD-19° bTDC was 6.82% on a par with diesel, and the percentage rises for DWSD-23° and DWSD-27° were 7% and 8.07% on a par with diesel at normal injection timing. When comparing diesel and DWSD fuel at 23° injection timing, the BTE has been increased. This could be attributed to improved cetane number, and micro-explosion of water molecules at higher temperatures may lead to improved BTE of DWSD fuels.

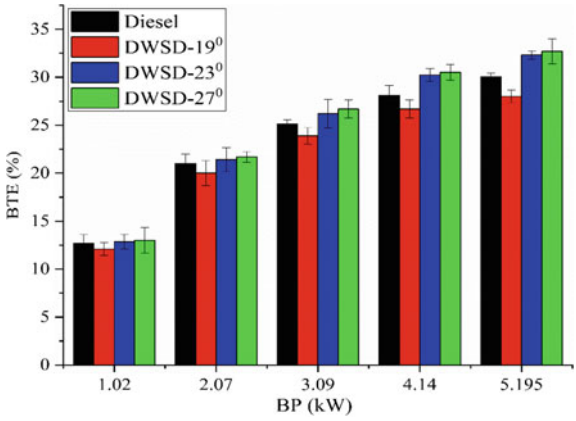

Fig. 3 Brake power versus brake thermal efficiency

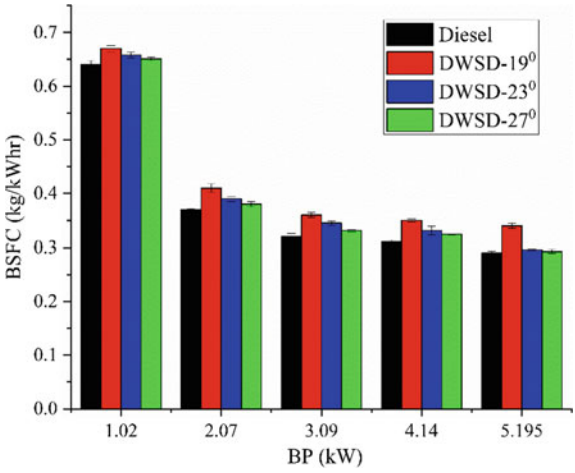

Fig. 4 Brake power versus brake-specific fuel consumption

4.2 BP Versus BSFC

Figure 4 explains the variations in BSFC against brake power for the diesel at 23° crank angle and DWSD fuels at 19°, 23° and 27° crank angles. At top loads, diesel had least BSFC with 0.29 kg/kWh. For DWSD fuels at 19°, 23° and 27° crank angles, the BSFC values were 0.34, 0.296 and 0.293 kg/kWh, respectively. At part loads (say 60%), the variation of BSFC for DWSD fuel at 19°, 23° and 27° crank angles were higher, viz. 11.11%, 7.245 and 3.32%, respectively, with diesel. This could be attributed by lower calorific value of DWSD fuel which rises the BSFC at part loads. While comparing diesel and DWSD fuels at standard injection timing (Say 23° bTDC), the BSFC was higher for DWSD fuel. This may be ascertained to lower calorific value and absorption of latent heat due to the presence of water content in the fuel mixture which leads to increases the BSFC. For fuel DWSD-19° crank angle, the BSFC was maximum throughout the cycle analysis. This was due to less time for air/fuel mixing and improper burning. Hence, a higher quantity of fuel was consumed in the retarded injection timing [15]. DWSD fuel at 27° bTDC gave lower BSFC on a par with 19° and 23° crank angles. This could be ascribed to the productive utilization of fuel during burning near to top dead center which significantly improved the vaporization process in the combustion chamber [1]. Hence the BSFC was lower.

4.3 BP Versus CO

Figure 5 portrays the CO emissions for fuels like diesel and DWSD fuels at 19°, 23° and 27° crank angles. The levels of CO emissions for diesel at 23° bTDC, DWSD-19°, 23°, 27° bTDC were 0.18%, 0.2%, 0.17% and 0.16% by volume at top loads. Normally, CO formation is related to improper burning and insufficient

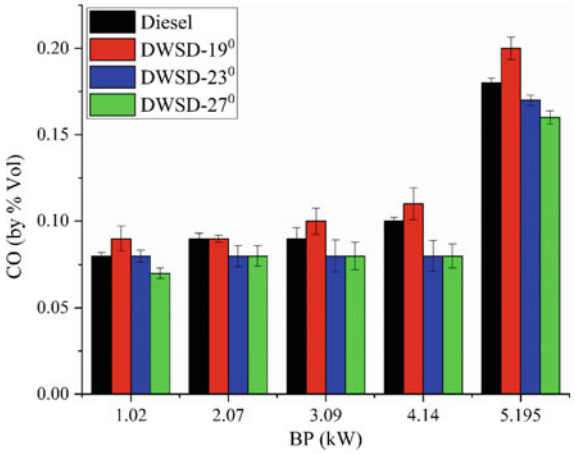

Fig. 5 Brake power versus carbon monoxide emission

temperature inside the chamber. The CO emission for DWSD-19° fuel increased by 10% compared with diesel and was found to be higher throughout the testing process. It could be reasoned out due to lower in-cylinder temperature, which rose the CO emissions [14]. At 23° bTDC, the CO level was low due to enhanced air/fuel mixing, longer delay period and more time available for rapid mixing [2]. Diesel fuel got lower CO emission on a par with DWSD-19° injection timing. It could be reasoned out due to base diesel properties and operating with standard timing. At low and part loads for DWSD-19° fuel, the CO emission has been increased due to improper combustion. At 23° bTDC and 27° bTDC, the CO emission for DWSD fuel were reduced to 11.11% on par with diesel due to improved air augmentation in the cylinder. On comparing diesel and DWSD fuel at standard timing, the CO emission was reducing for DWSD fuel which could be ascertained by the inbuilt oxygen molecule in 1,4-dioxane which enhances the oxidation rate.

4.4 BP Versus HC

The levels of HC for diesel at 23° bTDC, DWSD-19°, DWSD-23° and DWSD-27° crank angles with respect to brake power are shown in Fig. 6. HC emission genesis is linked to wetting, misfire and rich fuel zones. The values of HC emission for the fuels such as diesel, DWSD-19°, DWSD-23° and DWSD-27° bTDC were 120 ppm, 136 ppm, 82 ppm and 75 ppm at top loads. Compared to diesel fuel, the HC emission for DWSD-19° was higher by 11.76%. This was attributed to the retardation of injection timing that led to a short delay period, which caused under mixing of fuel, that increased HC emissions [12]. Advancing the injection timing from 23° to 27° bTDC enhanced the burning rate and reduced the HC emissions. At 27° bTDC, it looked to be very low HC emission on a par with all the fuels and the other injection timings. It was due to prolonged physical delay and a rise in burning temperature,

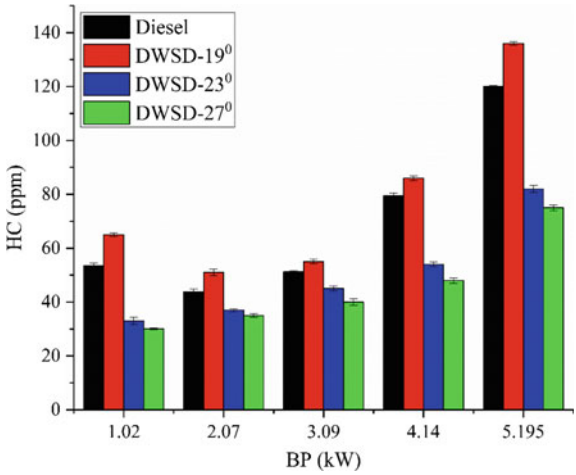

Fig. 6 Brake power versus hydrocarbon emission

which reduced the HC emissions [3]. At low and part loads, for DWSD-19° fuel the HC emission was higher due to lower calorific value of DWSD fuel. At 23° bTDC and 27° bTDC, the HC emission for DWSD fuel was decreased due to time enough available for preparing the fuel for combustion. While equating DWSD fuel with diesel in standard operating conditions, the HC emission was decreased due to presence of 1,4-dioxane and the split of water molecules which boost the evaporation rate.

4.5 BP Versus NO_x

Figure 7 illustrates the NO_x emission for the DWSD and diesel fuel with varying injection timing. From the graph, it is evident that DWSD-19° fuel exhibits lower values of NO_x. This can be ascribed to low in-cylinder heat, which leads to reduce the oxidation process [7]. Over and above 23° bTDC, due to improved burning rate, the NO_x emission increases for both diesel and DWSD-23° bTDC. For DWSD-27° bTDC, the NO_x level is very high when compared with all the other injection timings in the cycle and also with diesel fuel. This may be attributed to increased preparation time and its subsequent mixing rate, which accelerates the oxidation and combustion, leading to rise in the temperature and further elevates the NO*x* emissions [13]. The levels of NO_x emissions are 1112, 790, 831 and 1215 ppm, respectively, for the fuels, viz. diesel @ 23°, DWSD-19°, DWSD-23° and DWSD-27° bTDC at apex loads. A similar trend was observed at lower and part loads. On comparing diesel and DWSD fuels at normal running condition of 23° bTDC, NO_x emission for DWSD fuel was lower. It may be attributed to in-cylinder temperature has been grasped by the existing water molecules.

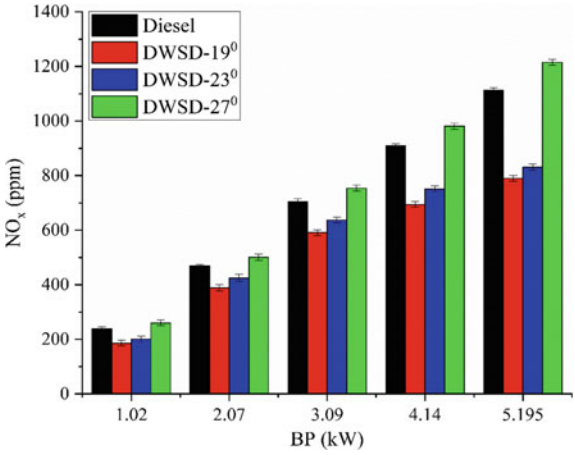

Fig. 7 Brake power versus oxides of nitrogen emission

4.6 BP Versus Smoke

The ranges of smoke emission with brake power for diesel, DWSD-19°, DWSD-23° and DWSD-27°, are shown in Fig. 8. Smoke emission is a carbonaceous solid soot particle that forms due to incomplete burning of fuel. For the fuel DWSD-19°, the smoke opacity is huge on a par with all the other timings and diesel fuel. This is due to the shorter duration to release the heat energy and also earlier diffusion burning occurring, which leads to more considerable smoke being attained [9]. When advancing the injection timing, almost maximum energy is liberated in the premixed burning region, and hence lower emission of smoke is produced [16]. The ranges of smoke emission gained are 77.6, 86, 56 and 52 HSU for the fuels, viz. diesel, DWSD-19°, DWSD-23° and DWSD-27°, respectively, at peak engine loads. At low

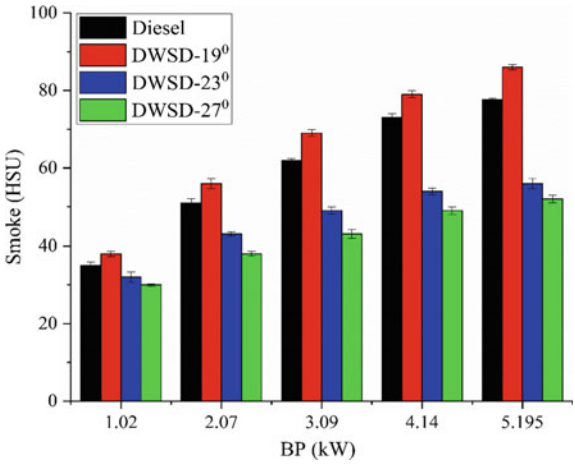

Fig. 8 Brake power versus smoke emission

loads, the smoke emission was 35, 38, 32 and 30 HSU and the deviation is minimum. At part loads, the smoke values were 62, 69, 49 and 43 HSU, and the variation is quite higher. Above 100 degree temperature, the water content in the DWSD fuel mixture at part loads will start vaporizing and burning takes place, and further reduction of smoke was achieved. When equating diesel and DWSD fuel at normal timing, the smoke value is less for DWSD fuel on par with diesel. It could be attributed to the effect of micro-explosion and the existence of 1,4-dioxane which reduces the smoke level.

4.7 Cylinder Pressure Versus Crank Angle

The emergence of burning in diesel powertrain is significant by feeling the deviations in gas pressures. The growth of pressure is determined by the amount of fuel consumed in the premixed region. The in-cylinder pressure versus crank angle for the fuels such as diesel and DWSD is presented in Fig. 9. At DWSD-27° bTDC, the pressure was high through the whole testing process due to the combined effect of vaporization, improved rate of mixing and delay period [22]. On the other hand, with DWSD-19° bTDC, the cylinder pressure decreased when compared with all the different injection timings and also with diesel fuel. It could be ascribed to reduced evaporation rate, less preparation time and a lower range of injection timing [9]. When compared with DWSD-19°, diesel fuel has a slight increase in in-cylinder pressure due to natural properties of diesel fuel and 23° bTDC injection timing.

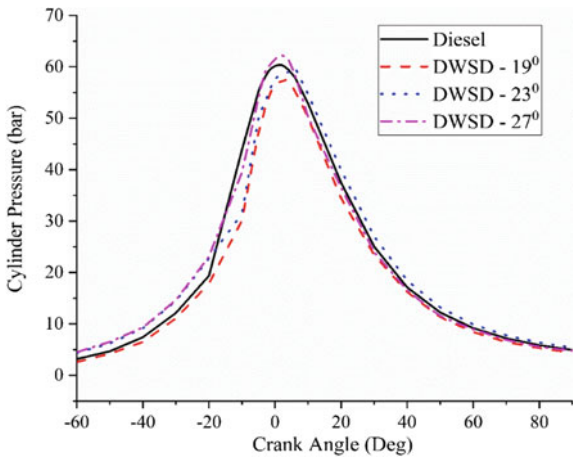

Fig. 9 In-cylinder pressure versus crank angle

4.8 Heat Release Rate and Cumulative Heat Release Rate

The investigation to calculate the burning rate of fuel should be possible by computing the HRR and its aggregate. HRR is nothing but the rate of energy liberated when the fuel burns during the combustion. Figures 10 and 11 present the HRR and its cumulative for the diesel, DWSD-19°, DWSD-23° and DWSD-27° fuels. The HRR and the CHRR for DWSD-19° were low on a par with other timings and diesel fuel. It could be ascertained by the presence of 10% water and 19° bTDC injection timing resulting in diminished burning rate [13]. At DWSD-27° bTDC timing, the HRR and the CHRR accomplished were more significant on a par with all the other fuels and timings. This was attributed to turbulent atomization and its subsequent blending between air/fuel and a rise in BTE, which are the basis for the escalation in HRR and

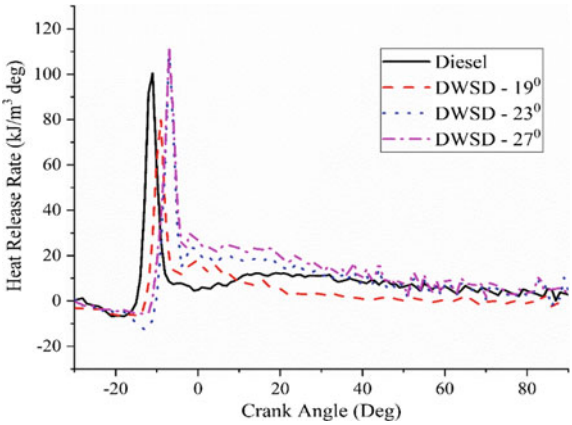

Fig. 10 Heat release rate versus crank angle

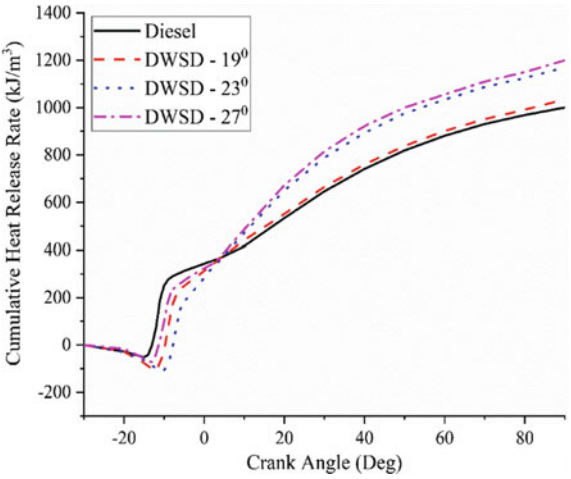

Fig. 11 Cumulative heat release rate versus crank angle

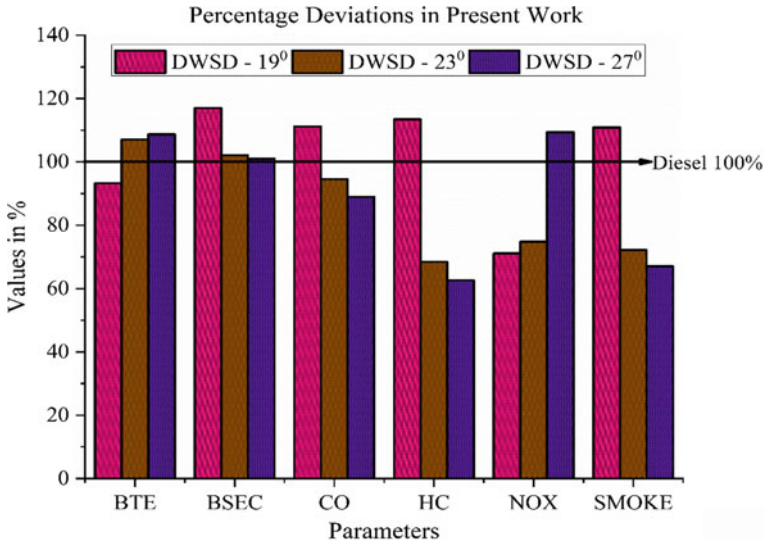

Fig. 12 Percentage deviations in present work

CHRR [6]. Accumulation of rich zones of fuel may suppress the CHRR for diesel fuel, and it was very low on a par with other timings and fuels.

4.9 Deviation for the Current Work

Figure 12 represents the whole deviations attained in the present study. The diesel fuel performance is depicted as 100%, and it is specified as a horizontal line in the figure. The fluctuations of engine attributes for the DWSD fuel with their respective timings are equated with diesel fuel at normal operating timing.

5 Conclusions

Deviating the injection timings and blending of multifaceted additive to emulsion fuel was examined constructively as alternate elements for diesel powertrain. Having reviewed the literature and present situations, it is concluded that water-based emulsified fuel can act as a satisfactory fuel that can reduce the use of pure diesel. Integrating emulsion fuel with varying injection timing has given possible solutions for the reduction of emissions besides favorable engine attributes. The ensuing results were attained while operating the powertrain with emulsion and different injection timings:

- The firmness of the DWSD emulsified fuel has reached up to 44 days.
- BTE of DWSD-27° bTDC has raised to 8.07% when compared with diesel fuel due to enhanced residence time.
- The BSEC of DWSD-27° bTDC decreases by 13.8% on a par with 19° crank angle.
- CO, HC and smoke emissions have been dramatically curtailed by 11%, 37.5% and 32.98, respectively, at higher injection timing compared with diesel fuel due to improved burning characteristics.
- The NOx emission for fuel DWSD-19° and DWSD-23° crank angles are lower by 28.9% and 25.2% when compared with diesel fuel. However, for DWSD-27° fuel the NO_x emission holds maximum throughout the testing.
- HRR and its net HRR, gas pressure for the DWSD fuel at advanced injection timing have increased on a par with diesel fuel due to a considerable delay period.

Overall, DWSD fuel with advanced injection timing of 27° crank angle may be considered as a suitable fuel in terms of enhanced performance and reduced emissions.

Acknowledgements The authors sincerely thank the Department of Mechanical Engineering, Sri Sai Ram Institute of Technology, for providing the support to conduct the experimental work.

Declaration of Interests
The authors declare that they have no known competing financial interests or personal relationships that could have appeared to influence the work reported in this paper.

References

1. Agarwal, A. K., Dhar, A., Gupta, J. G., Kim, W. I., Choi, K., Lee, C. S., & Park, S. (2015). Effect of fuel injection pressure and injection timing of Karanja biodiesel blends on fuel spray, engine performance, emissions and combustion characteristics. *Energy Conversion and Management, 91,* 302–314.
2. Agarwal, A. K., Srivastava, D. K., Dhar, A., Maurya, R. K., Shukla, P. C., & Singh, A. P. (2013). Effect of fuel injection timing and pressure on combustion, emissions and performance characteristics of a single cylinder diesel engine. *Fuel, 111,* 374–383.
3. Ashok, B., Nanthagopal, K., Raj, R. T. K., Bhasker, J. P., & Vignesh, D. S. (2017). Influence of injection timing and exhaust gas recirculation of a *Calophyllum inophyllum* methyl ester fuelled CI engine. *Fuel Processing Technology, 167,* 18–30.
4. Basha, J. S., & Anand, R. B. (2012). Effects of nanoparticle additive in the water–diesel emulsion fuel on the performance, emission and combustion characteristics of a diesel engine. *International Journal of Vehicle Design, 59*(2), 164.
5. Baskar, P., & Kumar, A. S. (2017). Experimental investigation on performance characteristics of a diesel engine using diesel-water emulsion with oxygen enriched air. *Alexandria Engineering Journal, 56*(1), 137–146.
6. Bragadeshwaran, A., Kasianantham, N., Kaisan, M. U., Reddy, D. M. S., Aravind, K. M., Paul, N., & Chungath, T. (2019). Influence of injection timing and exhaust gas recirculation (EGR) rate on lemon peel oil–fuelled CI engine. *Environmental Science and Pollution Research, 26*(21), 21890–21904.

7. Channappagoudra, M., Ramesh, K., & Manavendra, G. (2020). Effect of injection timing on modified direct injection diesel engine performance operated with dairy scum biodiesel and bio-CNG. *Renewable Energy, 147,* 1019–1032.
8. Damodharan, D., Sathiyagnanam, A. P., Rana, D., Kumar, B. R., & Saravanan, S. (2018). Combined influence of injection timing and EGR on combustion, performance and emissions of DI diesel engine fueled with neat waste plastic oil. *Energy Conversion and Management, 161,* 294–305.
9. Deep, A., Sandhu, S. S., & Chander, S. (2017). Experimental investigations on the influence of fuel injection timing and pressure on single cylinder CI engine fueled with 20% blend of castor biodiesel in diesel. *Fuel, 210,* 15–22.
10. Dhinesh, B., Annamalai, M., Lalvani, I. J., & Annamalai, K. (2017). Studies on the influence of combustion bowl modification for the operation of *Cymbopogon flexuosus* biofuel based diesel blends in a DI diesel engine. *Applied Thermal Engineering, 112,* 627–637.
11. Dhinesh, B., Raj, Y. M. A., Kalaiselvan, C., & Krishnamoorthy, R. (2018). A numerical and experimental assessment of a coated diesel engine powered by high-performance nano biofuel. *Energy Conversion and Management, 171,* 815–824.
12. Ganapathy, T., Gakkhar, R. P., & Murugesan, K. (2011). Influence of injection timing on performance, combustion and emission characteristics of Jatropha biodiesel engine. *Applied Energy, 88*(12), 4376–4386.
13. Karthic, S. V., Kumar, M. S., Nataraj, G., & Pradeep, P. (2020). An assessment on injection pressure and timing to reduce emissions on diesel engine powered by renewable fuel. *Journal of Cleaner Production, 255,* 120186.
14. Lin, C. Y., & Wang, K. H. (2004). Effects of a combustion improver on diesel engine performance and emission characteristics when using three-phase emulsions as an alternative fuel. *Energy & Fuels, 18*(2), 477–484.
15. Mohan, B., Yang, W., Raman, V., Sivasankaralingam, V., & Chou, S. K. (2014). Optimization of biodiesel fueled engine to meet emission standards through varying nozzle opening pressure and static injection timing. *Applied Energy, 130,* 450–457.
16. Natarajan, S., Trasy, K. A., Srihari, N., & Raja, S. (2017). Effects of injection timing on CI engine fuelled with algae oil blend with Taguchi technique. *Energy Procedia, 105,* 1043–1050.
17. Pal, S., Chintala, V., Sharma, A. K., Ghodke, P., Kumar, S., & Kumar, P. (2019). Effect of injection timing on performance and emission characteristics of single cylinder diesel engine running on blends of diesel and waste plastic fuels. *Materials Today Proceedings, 17,* 209–215.
18. Rahman, S. A., Masjuki, H. H., Kalam, M. A., Sanjid, A., & Abedin, M. J. (2014). Assessment of emission and performance of compression ignition engine with varying injection timing. *Renewable and Sustainable Energy Reviews, 35,* 221–230.
19. Rajesh, S., Kulkarni, B. M., Banapurmath, N. R., & Kumarappa, S. (2018). Effect of injection parameters on performance and emission characteristics of a CRDi diesel engine fuelled with acid oil biodiesel–ethanol blended fuels. *Biofuels, 9*(3), 353–367.
20. Ramalingam, S., Rajendran, S., & Ganesan, P. (2016). Improving the performance is better and emission reductions from Annona biodiesel operated diesel engine using 1, 4-dioxane fuel additive. *Fuel, 185,* 804–809.
21. Savariraj, S., Ganapathy, T., & Saravanan, C. G. (2013). Characterization of the DI diesel engine powered by mango seed oil methyl ester with fuel additive. *European Journal of Applied Engineering and Scientific Research, 2*(4), 44–50.
22. Saxena, M. R., & Maurya, R. K. (2017). Effect of premixing ratio, injection timing and compression ratio on nano particle emissions from dual fuel non-road compression ignition engine fueled with gasoline/methanol (port injection) and diesel (direct injection). *Fuel, 203,* 894–914.
23. Sendilvelan, S., & Sundar, R. (2017). Implementation of dioxane and diesel fuel blends to reduce emission and to improve performance of the compression ignition engine. *Journal of Engineering Science and Technology, 12*(11), 3092–3101.
24. Shameer, P. M., & Ramesh, K. (2018). Assessment on the consequences of injection timing and injection pressure on combustion characteristics of sustainable biodiesel fuelled engine. *Renewable and Sustainable Energy Reviews, 81,* 45–61.

25. Vedharaj, S., Vallinayagam, R., Yang, W. M., Chou, S. K., & Lee, P. S. (2014). Effect of adding 1,4-dioxane with kapok biodiesel on the characteristics of a diesel engine. *Applied Energy, 136,* 1166–1173.
26. Vellaiyan, S., & Amirthagadeswaran, K. S. (2016). Zinc oxide incorporated water-in-diesel emulsion fuel: Formulation, particle size measurement, and emission characteristics assessment. *Petroleum Science and Technology, 34*(2), 114–122.
27. Vigneswaran, R., Annamalai, K., Dhinesh, B., & Krishnamoorthy, R. (2018). Experimental investigation of unmodified diesel engine performance, combustion and emission with multipurpose additive along with water-in-diesel emulsion fuel. *Energy Conversion and Management, 172,* 370–380.
28. Wamankar, A. K., Satapathy, A. K., & Murugan, S. (2015). Experimental investigation of the effect of compression ratio, injection timing and pressure in a DI (direct injection) diesel engine running on carbon black-water-diesel emulsion. *Energy, 93,* 511–520.
29. Wang, S., Karthickeyan, V., Sivakumar, E., & Lakshmikandan, M. (2020). Experimental investigation on pumpkin seed oil methyl ester blend in diesel engine with various injection pressure, injection timing and compression ratio. *Fuel, 264,* 116868.

Advanced Combustion and Engine Technologies

Advanced Ignition System to Extend the Lean Limit Operation of Spark-Ignited (SI) Engines—A Review

S. Vedharaj

1 Introduction

For the past few decades, emission regulation and fuel economy have been the driving force behind the advancements in internal combustion (IC) engines [1]. To meet the stringent emission regulations and to satisfy customer requirements, modern spark-ignition (SI) engines are equipped with direct fuel injection system, efficient turbocharging system and integrated fast response electronic system [2–4]. Recent technological advancements with SI engine include engine downsizing and lean combustion [5, 6]. Both these concepts are envisaged as future engine technology as they produce higher efficiency and lower emission levels. Engine downsizing is the concept of using a small-volume engine to produce the power generated by large-volume engine. This is accomplished by inducting air into the combustion chamber at a higher pressure. As a result, the pressure at the time of ignition is higher than the naturally aspirated SI engines, which increases the breakdown voltage requirement. This affects the durability of the conventional ignition system [7]. Lean combustion is the phenomenon of combusting the fuel in an oxygen-rich environment (i.e., with excess air) or fuel-deprived condition (i.e., exhaust gas recirculation). Though lean combustion increases the engine efficiency, there are few difficulties like engine misfire, combustion instability and low flame speed [8, 9]. These drawbacks are due to the inefficacy of the conventional ignition system with lean combustion. The increase in in-cylinder pressure at the time of ignition and lean air/fuel mixture in the combustion chamber challenges the durability and ignition ability of the conventional ignition system.

S. Vedharaj (✉)
Department of Mechanical Engineering, National Institute of Technology, Tiruchirappalli, Tamil Nadu, India
e-mail: vedha@nitt.edu

A. P. Singh et al. (eds.), *Alternative Fuels and Advanced Combustion Techniques as Sustainable Solutions for Internal Combustion Engines*, Energy, Environment, and Sustainability, https://doi.org/10.1007/978-981-16-1513-9_10

It is well understood that the improvements in engine subsystem have led to a substantial increase in engine efficiency [10]. However, there is not much improvement in the ignition system, and the current trend mandates the development of advanced ignition system for future SI engine. Thus, a highly efficient advanced ignition system for lean burn and down-sized SI engine increases the engine efficiency and reduces engine out emissions. In the recent times, many research works are carried out to ascertain the capability of the advanced ignition systems like laser ignition (LI), turbulent jet ignition (TJI), radio-frequency corona ignition (RFCI) and microwave-assisted spark-ignition (MASI) system in SI engines [11–14]. This chapter provides a brief outline about the principle of operation, fundamental understanding, engine characteristics, advantages, limitations and future challenges of these advanced ignition systems.

2 Lean Combustion—A High Efficiency Concept

2.1 Definition of Lean Combustion

Stoichiometric air–fuel ratio is defined as the ideal air–fuel mixture required for complete combustion of the fuel [15]. The value will be different for different fuels as the amount of air required for complete combustion of each fuel varies. Hence, equivalence ratio (Φ) and lambda (λ) are the two commonly used normalized terms which provides appropriate comparison between different fuels. Lambda refers to the ratio of actual air–fuel ratio to stoichiometric air–fuel ratio. Lambda is the inverse of equivalence ratio as described in Eq. 1. Based on the values of lambda, the air–fuel mixture is categorized as either rich mixture ($\lambda < 1$ and $\Phi > 1$) or lean mixture ($\lambda > 1$ and $\Phi < 1$) [15].

$$\lambda = \frac{1}{\Phi} = \frac{(A/F)_{\text{Actual}}}{(A/F)_{\text{Stoichiometric}}} \tag{1}$$

Lean combustion occurs, when fuel-deficient or oxygen-rich condition prevails inside the combustion chamber. In case of exhaust gas recirculation, the inlet air is diluted with exhaust gases and fuel-deficient condition prevails inside the combustion chamber which can also be termed as lean combustion. The major difference is the diluent type, with EGR inert gases like CO_2, H_2O and N_2 act as diluent, whereas with excess air, inert N_2 acts as diluent.

2.2 Thermodynamic Efficiency of SI Engine

Engine efficiency is the product of combustion, thermodynamic, gas exchange and mechanical efficiency [16]. With the advancement in engine subsystems, it is possible to maximize the combustion, gas exchange and mechanical efficiencies. However, the improvement in the thermodynamic efficiency depends on the thermodynamic cycle of the SI engine (Otto cycle), and the thermodynamic efficiency is defined as,

$$\eta_{\text{thermodynamic}} = 1 - \frac{1}{r^{\gamma-1}} \tag{2}$$

where r is the engine compression ratio and γ is the specific heat ratio of the working medium.

Ideally, the thermodynamic efficiency depends on compression ratio and specific heat ratio of the working medium, and it increases with an increase in engine compression ratio. However, the increase in compression ratio is limited by knocking phenomenon and heat transfer losses. The ideal compression ratio for SI engine is 8–12 [15]. In order to increase the thermodynamic efficiency of the engine, many engine researchers increased the compression ratio of SI engine beyond the theoretical limit by adopting the Miller or Atkinson cycle [17]. Herein, the effective compression ratio is reduced by late closure of intake valve, and thus, the expansion ratio is higher than the compression ratio resulting in higher efficiency.

Few researchers are also adopting high specific heat ratio gases (like Argon), as working medium for IC engines to increase the thermodynamic efficiency [18]. Theoretically, the engine with Argon as working medium and hydrogen as a fuel is capable of achieving higher efficiency with zero-emission levels. However, there are many practical difficulties [18–20] associated with this engine: (1) Argon as working medium increases the in-cylinder temperature to a higher level at the end of the compression stroke; (2) to reduce the in-cylinder temperature, the engine has to be operated at lower compression ratio; (3) As argon is a noble gas, it has to be recycled, and hence, closed-cycle engine operation is preferred; (4) to recycle argon, the combustion products (i.e., H_2O) have to be separated at the end of each cycle. All these practical obstacles limit the commercial development of argon engine.

2.3 Lean-Burn SI Engines

In a commercial SI engine, air is the working medium and fuels like gasoline, methanol and ethanol are used. The specific heat ratio of methanol, ethanol and iso-octane (a surrogate of gasoline) are 1.12, 1.13 and 1.05, respectively, whereas that of air is 1.4 [21]. Henceforth, lean-burn SI engine operated with excess air increases the specific heat ratio of the air–fuel mixture inside the combustion chamber resulting in higher thermodynamic efficiency. Thus, the benefits of specific heat ratio on engine efficiency can be obtained in production SI engines by adopting lean-burn SI engine.

Ever since the invention of IC engine, lean combustion holds an advantage of lower fuel consumption and emissions. For nearly a century, stoichiometric operation of SI engine is preferred over lean operation owing to the stable combustion and efficient use of after-treatment systems (three-way catalytic converter) [9]. However, in the current scenario, the effect of stringent emission regulations and requirement of high-efficiency engines have led to the development of advanced lean-burn SI engine.

In a lean-burn SI engine, the fuel is combusted in an oxygen rich environment, and hence, efficient combustion of the air–fuel mixture occurs resulting in higher combustion efficiency and lower hydrocarbon (HC) and carbon monoxide (CO) emission. The combustion generated heat is observed by the excess air in lean-burn SI engine, thereby reducing the overall in-cylinder temperature. This results in reduced heat transfer losses and lower nitrogen oxide (NO_X) emission. Hence, the combined effect of higher specific heat ratio, higher combustion efficiency and lower in-cylinder temperature increases the engine efficiency and reduces the engine-out emission in lean-burn SI engine. Further, lean-burn SI engine eliminates the throttling losses associated with SI engine by effectively managing the required air–fuel mixture in the combustion chamber for different engine operating conditions. Lean mixtures are less susceptible to knocking condition, and thus, engine compression ratio can be increased for lean-burn SI engine, which in turn increases the thermodynamic efficiency of the engine as well as results in better combustion characteristics.

Though lean-burn SI engine improves the engine efficiency, the practical limitations associated with it include lower reaction rates, reduced flame speed, flame instability and extinction [8, 9]. It is well understood that the flame speed of air–fuel mixtures decreases with the increase in dilution [22] and the flame doesn't propagate when the generated flame kernel size is less than the critical value, resulting in partial burn or engine misfire. Thus, the probability of misfire increases with increase in dilution levels [23]. The lean-burn SI engines with conventional ignition system has the limitation of lower ignition energy and slower combustion rate. However, lean-burn SI engines hold a promise for future engine developments with the advancement in ignition technology and electronic systems.

2.4 Advanced Ignition System for Lean-Burn SI Engines

Initially, lean air–fuel mixtures are combusted by increasing the voltage and energy supplied to the conventional SI system [9]. However, the higher voltage generates greater reliability problems like higher secondary voltage breakdown, plug erosion, electrode degradation and frequent replacements of spark plugs [24]. Multiple spark plugs and spark plugs with multiple electrodes are also examined for lean-burn SI engines [25–27]. Positioning multiple spark plugs in a single cylinder provides an advantage of multiple ignition sites which compensates for the lower flame speed associated with lean mixtures. Further, the maximum flame propagation distance is also reduced with multiple spark plugs resulting in stable combustion. Two or

more flame kernels are being developed with multiple electrode spark plug, and this volumetrically increases the ignition area resulting in increased flame speed and better combustion characteristics.

In addition to the developments with conventional SI system, few researchers have also adopted other advanced ignitions system for lean-burn SI engines which includes high-energy spark plugs, plasma jet igniter, rail plug igniter, laser ignition (LI), turbulent jet ignition (TJI), radio-frequency corona ignition (RFCI) and microwave-assisted spark-ignition (MASI) system [8–11, 27–30]. The major objective of these systems is to increase the ignition energy and generate multi-point ignition which increase the combustion rate.

The plasma generation by these advanced ignition systems can be classified as either thermal plasma or non-thermal plasma generation [13, 31–33]. In thermal plasma, the electrons, ions and neutrals are in thermal equilibrium caused by dynamic energy exchange through collisions. The electrons and neutrals are at higher temperature in thermal plasmas, and thus, high amount of heat transfer losses and thermal damages to electrodes are apparent. However, in non-thermal plasmas, the energy transferred to the electrons increases the reaction kinetics without causing larger increase in temperature. The applied electromagnetic field transfers the energy to the free electrons and excites it to higher energy levels. The excited electrons initiate the ionization of gas molecules resulting in the generation of electron avalanche. These electrons can dissociate the gas molecules into reactive radicals which accelerate the combustion reaction rates. These energized electrons and activated molecules require lower activation energy and accelerate chemical kinetics. Non-thermal plasma can be achieved with much lower energy input than thermal plasma. Further, the heat transfer losses and thermal damages can also be avoided with non-thermal plasma generation. However, collision theory prescribes that at higher pressures, non-thermal plasma effects are vanished due to high-frequency collision resulting in rapid heat transfer from electrons to gas molecules. Conventional SI and TJI generate thermal plasma, whereas RFCI and MASI result in non-thermal plasma generation. The detailed information of certain widely accepted advanced ignition system is discussed in the below sections.

3 Laser Ignition (LI)

In 1978, LI was first introduced in IC engines and showed superior combustion characteristics than SI engine [34]. At that time, spark plug was widely preferred for engine operation due to its better performance, simple operation and lower cost. In recent times, modern SI engines are operated with lean air–fuel mixtures to meet the stringent emission regulations. It is well known that the ignition capability of conventional spark plugs is limited for lean mixtures, and thus, LI can be adopted as an efficient alternate ignition system for future engines.

3.1 Principle of Operation

A convex lens focuses the laser beam to a small spot, and the laser beam energy is concentrated at the focal point where a localized plasma is generated if the energy intensity is above the threshold value. The plasma formation with LI system is shown in Fig. 1, and herein, the laser beam is directed from right to left. Laser beam interacts with the combustible mixture by four different mechanisms to initiate the ignition process, and they are (1) thermal ignition, (2) photochemical ignition, (3) resonant breakdown ignition and (4) non-resonant breakdown ignition [7, 11, 36, 37].

- Thermal ignition is performed by targeting a low-energy, long-wavelength laser beam into the combustible mixture mixed with suitable absorbing target species. These target species absorb the incident laser beam, and the kinetic energy of them at molecular level is increased. The energy absorbed by these target species is transferred to the combustible mixture leading to autoignition.
- Photochemical ignition takes place when a high-energy photon is used to breakdown the gas molecules into highly ionized particles which reacts with surrounding gas molecules. This process directly reacts with gases in the combustible mixture and uses radiation at ultraviolet wavelengths or higher range. Photochemical ignition is adopted for combustible mixtures which are at low pressure, near flammable limits and capable of generating a large number of reactive radicals.
- In laser-induced resonant breakdown, initially, the gas molecules are dissociated by the non-resonant multi-photon ionization. The dissociated molecules are then ionized by resonant photo-ionization process. The seed electrons formed by resonant photo-ionization process gain energy through inverse Bremsstrahlung photon absorption process and can cause breakdown by electron cascade process.
- The non-resonant breakdown is initiated with multi-photon ionization of gas molecules, which liberates electrons. The liberated electrons have a tendency to absorb more photons from the laser beam, thereby increasing their kinetic energy.

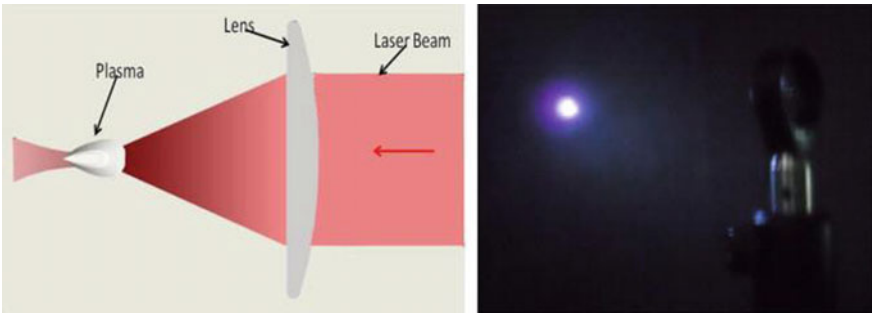

Fig. 1 Plasma formation with the laser ignition system. Laser beam is directed from right to left in this system [35]

These electrons collide with other gas molecules and ionize them, promoting electron avalanche and subsequent breakdown of the gas molecules. Initial electron generation by multi-photon ionization is unlikely to happen as the laser beam intensity in the focal region is lower than the ionization energy required for gas molecules. Hence, the impurities (like dust, aerosol and soot particles) present in the combustible mixtures absorb the laser energy and generate high temperature locally. This consequently produces free electrons leading to electron avalanche. As of now, the non-resonant breakdown is the commonly used laser ignition technique in engine studies, since it has a choice of selecting suitable laser wavelength and is easy to implement. It is also known as laser-induced spark ignition.

3.2 Fundamental Study

A fundamental study on the flame kernel characterization with the LI system was carried out by Srivastava et al. [38] in a constant-volume combustion chamber. The experiments were conducted at a chamber pressure and temperature of 10 bar and 373 K, respectively, and the flame kernel development has been visualized by a shadowgraphy technique using a CMOS high-speed camera. Figures 2 and 3 show the flame kernel development images for natural gas–air mixtures at $\lambda = 1.2$ and $\lambda = 1.6$, where the laser beam enters from right to left. The flame kernel images showed two stages of development. In the early stage, the flame kernel develops radially into a toroidal shape, and later, a front lobe is formed which propagates toward the incoming laser beam for $\lambda = 1.2$. However, the front lobe formation for lean mixtures ($\lambda = 1.6$) exists only during the initial period and disappears after 1 ms. The phenomenon of front lobe formation is unique with LI system, and the reason is that the preheated air–fuel mixture readily ignites and propagates faster than the cold air–fuel mixture. The preheated air–fuel mixture is formed in the region between the

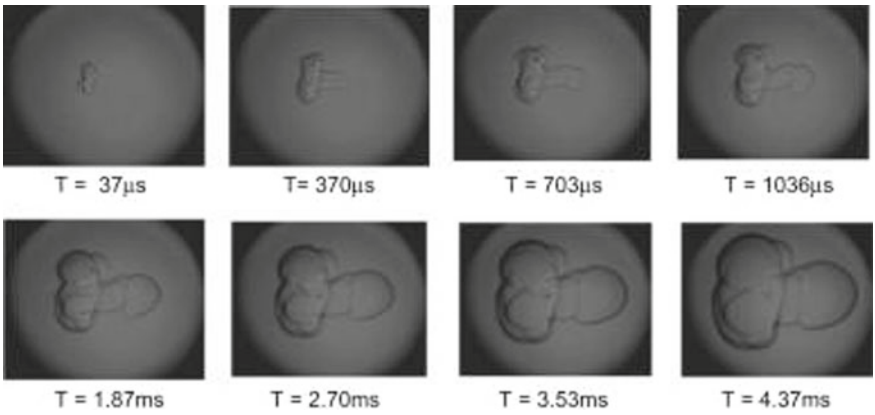

Fig. 2 Flame kernel development images for natural gas–air mixtures at $\lambda = 1.2$ [38]

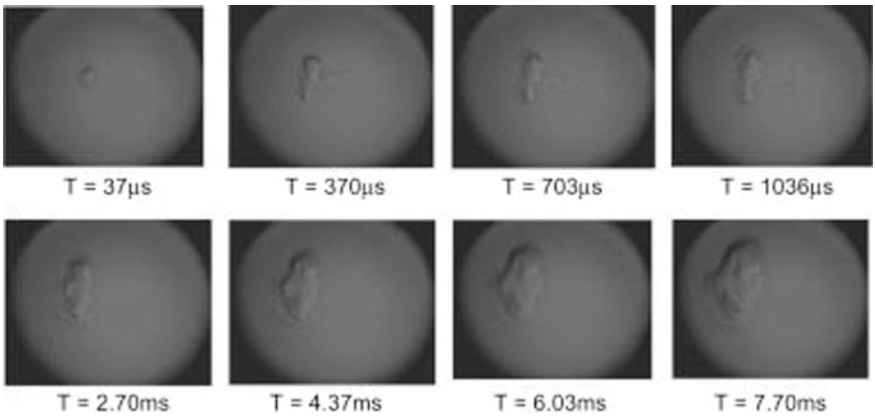

Fig. 3 Flame kernel development images for natural gas–air mixtures at $\lambda = 1.6$ [38]

optical window and the focal point (i.e., ignition point) where the laser beam passes through and heat the gaseous medium.

The effect of focal length of a converging lens, beam quality, focal spot size, equivalence ratio and wavelength on ignition characteristics of LI system was explored [39, 40]. Three different converging lenses of 200, 150 and 100 mm focal length were used to understand the effect of focal length. The minimum ignition energy requirement shows an increasing trend with the increase in focal length of the lenses, whereas the energy density shows a decreasing trend. The focal spot size depends on various parameters like wavelength, beam quality and focal length. The diameter of the focal spot size increases with increase in focal length, and it decreases with decrease in beam quality factor (M^2). From the pressure–time history, the combustion duration is observed to be shorter for 150 mm focal length lens, and the effect is more prominent with lean mixtures. An optimum balance between the energy density and focal spot size is obtained with 150 mm focal length lens resulting in shorter combustion duration. The minimum ignition energy requirement for LI is observed to be lower at stoichiometric condition, and lean mixtures require higher ignition energy similar to the conventional SI system. 100% ignition probability is achieved for gasoline–air mixture in an equivalence ratio range of 0.8–1.6, whereas misfire occurred at other lean and rich conditions. To ignite same equivalence ratio mixtures with same ignition probability, the incident energy requirement is more for longer wavelength laser beams than shorter wavelength laser beams.

3.3 Laser-Induced Cavity Ignition

One major drawback with the LI system is that only a portion of incident energy is absorbed by the gaseous medium near the focal point, and the remaining energy is

lost. The unabsorbed laser beam passes through the focal point, into the combustion chamber. Laser-induced cavity ignition [41, 42] effectively minimizes the energy losses, wherein the incident laser energy is absorbed on the surface of the conical cavity, and the remaining energy is reflected. The reflected laser beam undergoes multiple reflections inside the conical cavity and is directed toward the apex of the conical cavity. Thus, all the incident energy is effectively trapped by the conical cavity, and the principle of operation is depicted in Fig. 4. The reflection of the incident laser beam has led to the development of the breakdown channel along the central axis of the conical cavity. The gaseous medium inside the conical cavity is heated by the incident laser energy and the reflected laser beams, and finally, the heated reacting gas is ejected from the conical cavity in the form of a jet.

Figure 5 shows the flame kernel development for a laser-induced cavity ignition captured using shadowgraphy technique, and here, the direction of laser is from left to right. The single-shot laser beam was irradiated on the conical cavity, and it heats the methane–air mixture in that region. After 2 ms, the hot burnt gas was ejected from

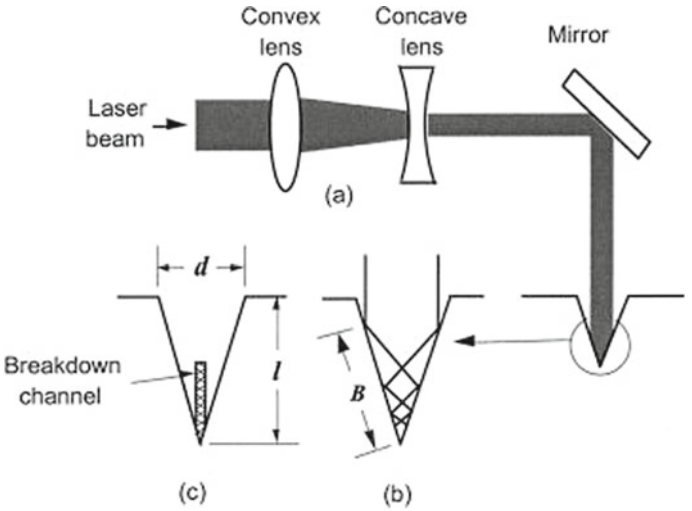

Fig. 4 Laser-induced cavity ignition **a** principle of operation **b** multiple reflection of laser beam in the conical cavity **c** formation of breakdown channel in the central axis [41]

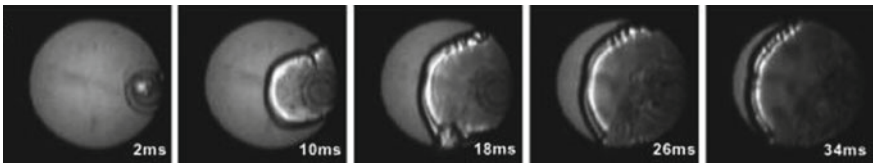

Fig. 5 Flame kernel development images for a laser-induced cavity ignition. Laser beam is directed from left to right [42]

the cavity as seen from Fig. 5. The flame propagates toward the unburnt methane–air mixture, and the flame front has a relatively smooth surface. The overall features of flame kernel development for laser-induced cavity ignition look similar to a typical flame from a conventional spark plug.

3.4 Multi-point Laser Ignition

Multi-point ignition improves the combustion characteristics of lean-burn engine by reducing the flame propagation distance which in turn results in shorter combustion duration. Earlier, many researchers have adopted multiple spark plugs in a single cylinder to achieve lean combustion in SI engines [9]. A maximum of 12 spark plugs have been installed in a single cylinder [43], and the combustion duration is reduced by 50%. Considering the practical difficulties with multiple spark plugs installation, twin spark ignition has been widely accepted [44]. Laser ignition provides an advantage of inducing multi-point ignition with a single laser plug. Multi-point laser ignition is achieved from a single laser beam by various techniques like beam splitting, combination of conical cavities, dual head laser and phase controlling technique [11].

Figure 6 shows the principle of two-point and three-point laser ignition system. The setup consists of two conical cavities: One cavity is located on the wall opposite to the optical window (second cavity), and another cavity is located adjacent to the optical window, and it has an opening near the apex region (first cavity) [45]. The first cavity is attached to the wall where the optical window is placed by means of a small cylindrical chamber. The cylindrical region between the window and the cavity acts as a pre-chamber.

The laser beam passes through a combination of convex and concave lens, and an unfocused parallel laser beam is targeted into the first cavity. The incident laser beam is partially irradiated by the conical cavity surface, and the remaining non-irradiated beam, which passes through the opening near the apex of the first cavity, is targeted into the second cavity. The breakdown of air–fuel mixture happens in the two cavities leading to a two-point laser ignition, as shown in Fig. 6a. Three-point laser ignition is generated with the same setup. The laser beam is focused by a convex lens, and when it passes through the first cavity, part of the laser beam is irradiated generating laser-induced cavity ignition. The remaining non-irradiated beam is focused at the center of the combustion chamber, generating a laser-induced spark ignition. After this, the unutilized laser beam is targeted on the second cavity leading to a laser-induced cavity ignition as depicted in Fig. 6b.

Figure 7 shows the flame kernel development for two-point and three-point ignition by shadowgraphy technique. Both in two-point and three-point ignitions, the flame kernel development from the first cavity is delayed compared to the second cavity. This can be attributed to the pre-chamber associated with the first cavity. The flame kernel initially grows inside the pre-chamber before ejecting the burnt flame jet into the main chamber. However, it could be observed that the jet penetration speed

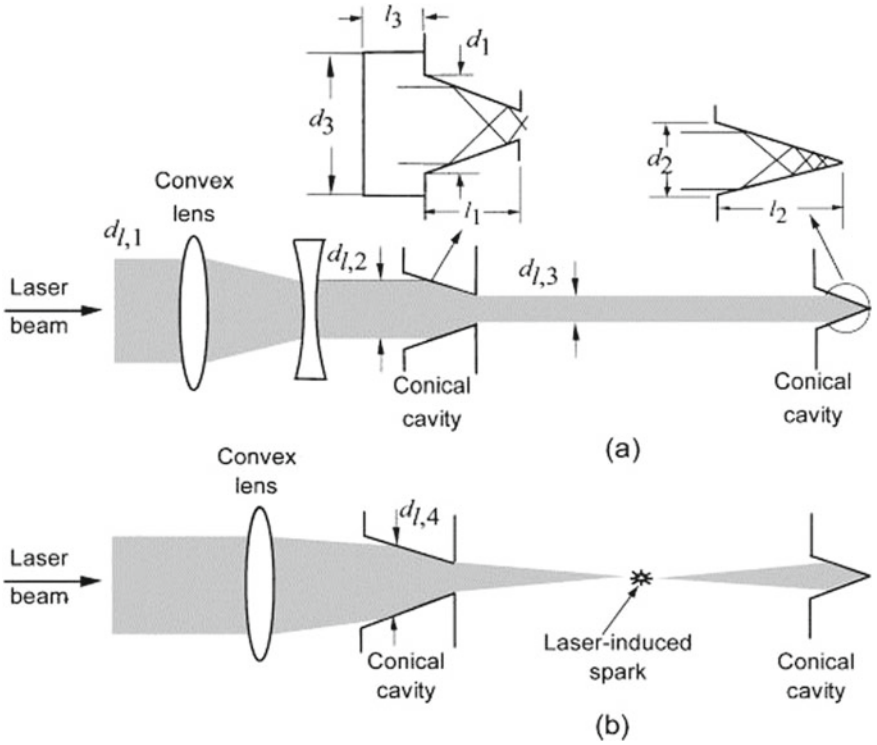

Fig. 6 Principle of multi-point laser ignition: **a** two-point laser ignition and **b** three-point laser ignition [45]

is faster in the first cavity after the initial delay period. The flame kernel development from the first cavity is slower for three-point ignition compared to two-point ignition. This can be attributed to the smaller irradiated surface area of the first cavity as a focused beam is employed in three-point ignition. The laser-induced spark ignition in the three-point laser ignition shows the typical LI flame kernel shape with a frontal lobe.

Figure 8 shows the flame initiation period (i.e., the start of combustion) and total combustion time (i.e., combustion duration) as a function of initial chamber pressure for different ignition modes. Here, two-point laser ignition is generated by a single laser beam where one is laser-induced spark ignition and the other is laser-induced cavity ignition [46]. Early start of combustion and shorter combustion duration is observed for two-point laser ignition when compared to laser-induced spark ignition and laser-induced cavity ignition. Multi-point ignition phenomenon reduces the flame travel distance, and thereby, significant reduction in combustion duration is observed. Further, it can also be noted that the threshold breakdown intensity is indirectly proportional to in-cylinder pressure for LI engine, whereas it is directly proportional to in-cylinder pressure for the SI engine. The threshold breakdown

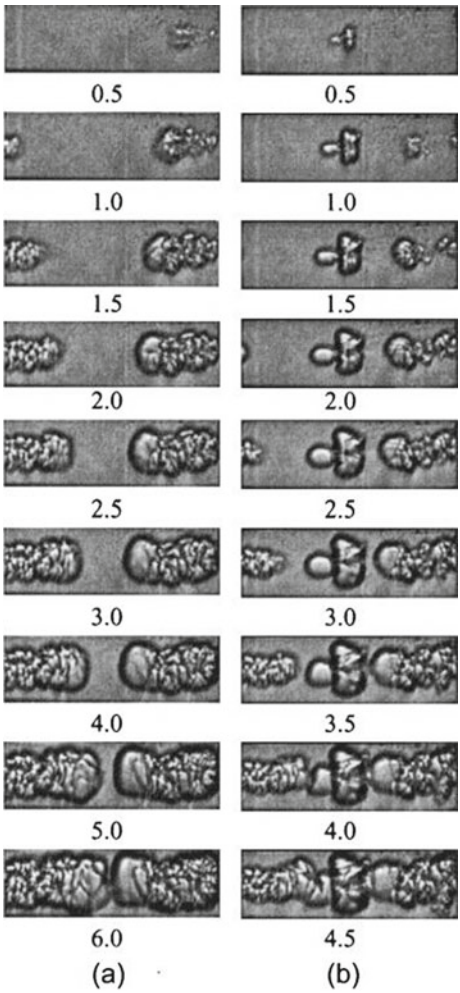

Fig. 7 Flame kernel development images for **a** two-point and **b** three-point laser ignition system. The numerical value below each image indicates time in milliseconds [45]

intensity is decreased with an increase in in-cylinder pressure in LI engine, and this dependence is strong with shorter wavelength and weak with longer wavelength laser beams.

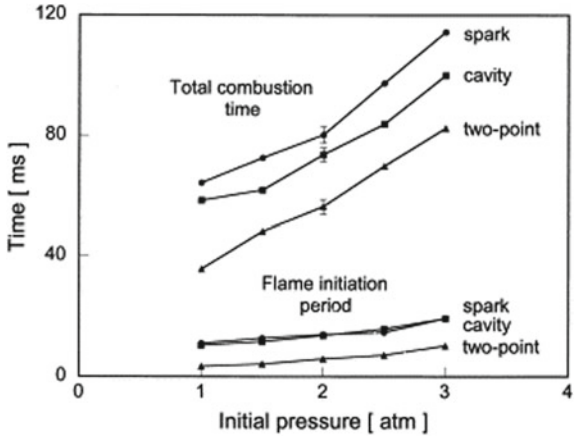

Fig. 8 Flame characteristics for spark, cavity and two-point laser ignition [46]

3.5 LI Engine Characteristics

The conventional SI system can be replaced with LI system without any further modification to other engine subsystems. The performance characteristics for LI engine are found to be superior to SI engine at all engine load and speed conditions. The maximum in-cylinder pressure, pressure rise rate and heat release rate are noted to be higher for LI engine [35, 47]. However, the difference between the maximum in-cylinder pressure observed in LI engine and SI engine is higher for lean mixtures, whereas the difference decreases with a decrease in lambda as evident for Fig. 9.

Early start of combustion (defined as the crank angle at which 10% mass of fuel burnt) and shorter combustion duration (defined as the difference between crank angle at which 90 and 10% mass of fuel burnt) were observed for LI engine in comparison with SI engine [35]. The temperature and pressure at the plasma generated by the laser beam are in the order of 10^6 K, and 10^3 bar, respectively whereas that of spark plug is in the order of 10^4 K and 10^2 bar. Further, the energy transfer rate in plasma region is in terms of a nanosecond for laser ignition whereas it is in millisecond for spark ignition. Thus, higher temperature, pressure and energy transfer rate resulted in early start of combustion and shorter combustion duration for LI system. The difference between the combustion duration in LI and SI engine increased with the increase in dilution levels. Further, the combustion is observed to be smooth and stable even for lean mixtures in LI engine [48].

The coefficient of variance for engine indicated mean effective pressure (COV_{IMEP}) with respect to various lambda conditions at different compression ratios for LI engine is shown in Fig. 10. COV_{IMEP} increases with the increase in lambda, and the combustion becomes unstable with frequent misfires for lean mixtures ($\lambda >$ 1.6). It is well known that COV_{IMEP} affects the combustion stability and vehicle drivability, and hence, it has to be maintained within acceptable limit for smooth engine operation [49]. For a similar COV_{IMEP}, the lean limit operation of compressed natural gas in LI engine is extended from $\lambda = 1.62$–1.76 by increasing the compression ratio

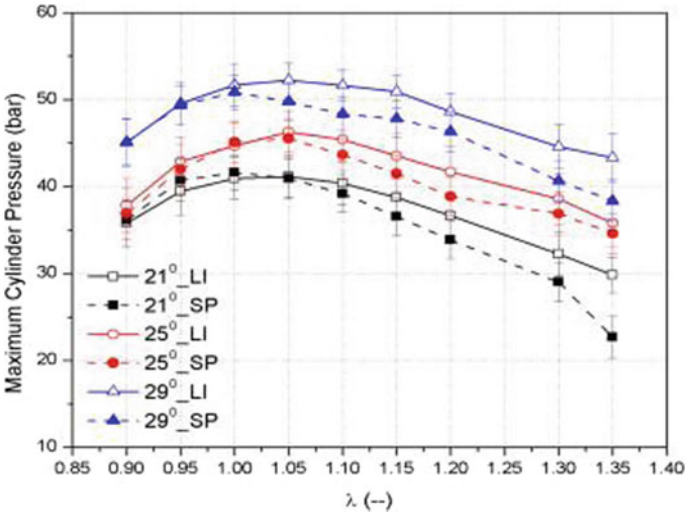

Fig. 9 Maximum in-cylinder pressure obtained in LI and SI engine at various lambda conditions and different ignition timings [35]

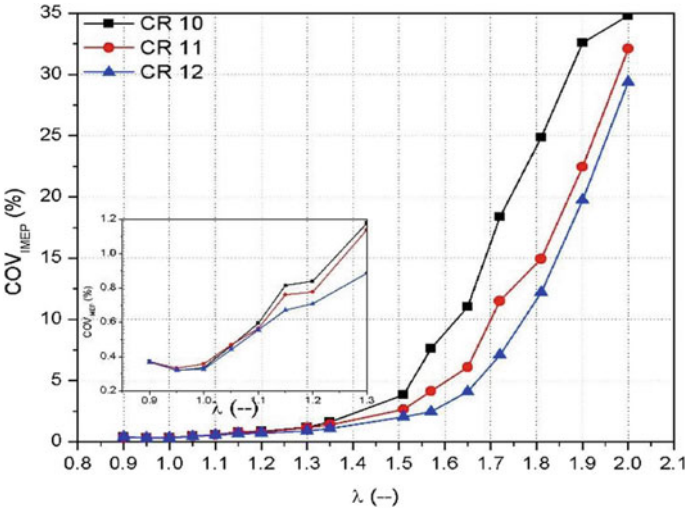

Fig. 10 Combustion stability of LI engine at various lambda conditions [49]

from 10 to 12. The combined effect of higher compression ratio and laser ignition energy improved the overall engine characteristics for lean mixtures.

At stoichiometric conditions ($\lambda = 1$), reduction in BSFC and CO emission with higher NO_X emission is observed for LI engine when compared to SI engine. However, a substantial reduction in BSFC, combustion duration and CO emission is

noted for LI engine at lean conditions ($\lambda = 1.25$), whereas THC and NO_X emission increased. As the combustion duration is shortened, the fuel oxidation time is reduced resulting in higher THC emissions. Further, the sharp increase in the pressure rise rate attributed to the increased NO_X emission [48]. With increase in dilution, the NO_X emission is observed to be lower in many research studies [7]. Thus the extension of lean limit in SI engines with smooth and stable combustion is possible with laser ignition systems. However, the installation cost and system complexity has to be reduced for the adoption of LI systems in future engine technology.

In SI engine, suitable air–fuel mixture has to be maintained near the spark plug region to develop a stable flame kernel, whereas these conditions are not applicable for LI engine. Laser ignition provides the flexibility in optimizing the ignition location and ignition energy for lean combustion. The ignition location is modified by a special laser plug arrangement [50]. In this setup, the combustion chamber window is screwed separately to the cylinder head, and the focusing lens can be altered by a separate screw. The distance between the focusing lens and the window can be altered to vary the ignition location. Higher brake thermal efficiency (BTE), lower brake-specific fuel consumption (BSFC), early start of combustion and shorter combustion duration are observed when the ignition location is at central spot [50, 51]. This may be due to the shift in the flame kernel from the metallic surface to inside region of the combustion chamber resulting in reduced heat loss, faster flame kernel growth and reduced flame propagation distance.

Laser irradiance is an important parameter in ascertaining the combustion characteristics in LI engine and is defined as the ratio of laser power to the focal spot area [52]. Higher irradiance resulted in shorter ignition delay, higher in-cylinder pressure and higher heat release rate. However, there is a threshold irradiance level for the given focal volume, and when incident laser energy is beyond the threshold value, there is no substantial improvement in the combustion process. Increased laser input energy showed lower cycle-to-cycle variations and stable combustion for lean mixtures. Therefore, the maximum possible incident laser energy has to be provided to achieve stable combustion and better engine performance. The amount of incident laser energy transferred to the combustion chamber is affected by the deposits in the optical window. A clean window with the transmissivity of 86% is reduced to 57% after 2 h and to 33% after 30 h of engine operation [50]. Therefore, the incident energy of laser beam targeted on the focal point decreases, resulting in an engine misfire. A comparison of the energy adsorbed by SI and LI systems reveals that the frequency of laser beam is higher than the plasma frequency, and thus, laser energy is strongly adsorbed by the gases in the focal point, whereas the frequency of electrical spark is lower than the plasma frequency, and thus, spark energy is adsorbed only by a thin layer near the plasma surface. In LI engine, generated plasma acts as a good absorber of incident laser energy.

A comparative study of two-point and single-point laser ignition in LI engine was carried out by maintaining the same total incident laser energy for both the conditions [53]. An optical system was developed with a spatial light modulator (SLM) to deliver multi-beam patterns without clipping. More stable combustion and higher engine power output were observed for two-point ignition than single-point

ignition, and the difference is higher at lean mixtures. Two-point ignition reduced the probability of engine misfire, and stable combustion is achieved for lean mixtures. The lean limit operation is extended to Lambda of 1.45 with two-point ignition, whereas with the conventional SI system, the lean limit is observed to be 1.2.

3.6 Advantages

From the literature review with LI engine, it can be concluded that LI system has potential to substantially improve the combustion process for even lean mixtures. LI system provides the flexibility to modify ignition location by either using a converging lens of suitable focal length or moving the position of the converging lens inside the plug [50, 51]. This modification is practically not possible with conventional SI system. As ignition location can be moved in the LI system, the plasma can be placed at an optimum location inside the combustion chamber to reduce heat loss to metallic surfaces like electrodes and cylinder walls. Further, the maximum flame propagation distance is also reduced, resulting in a shorter combustion duration [7]. LI system is electrode free, and there is no possibility of electrode erosion and surface ignition, as observed in the conventional SI system [11]. Thus, the lifetime of laser plug is expected to be longer. LI system provides precise control over ignition timing, and ignition energy could also be varied [36]. High-energy laser beams can provide stable combustion for lean air–fuel mixtures without any misfires. Contrary to the conventional SI system, multi-point LI is possible without any practical difficulties, and it produces higher combustion pressure with shorter combustion duration [11]. Hence, multi-point LI system is best suited for lean air–fuel mixtures where slower combustion is a concern.

3.7 Limitations and Future Challenges

Only a portion of the incident laser energy is being absorbed by the gases near the focal point, and the remaining portion of incident energy is unutilized [41]. Hence, research on increasing the energy efficiency of incident laser beam by multi-point laser ignition with a higher number of ignition sites has to be carried out. Propagation of a laser beam into the combustion chamber through cylinder head is a significant barrier [11].

Laser beam is introduced into the engine by any one of the following methods: open beam paths, optical fiber delivery and compact laser sources [7, 11]. Most of the researchers have adopted open beam path technique which uses lenses or mirrors to focus the laser beam into an engine. However, this method is not suitable for commercial engine applications as the extreme engine operating condition (high temperature and vibrations) may result in misalignment of laser beam [54]. Considering the practical difficulties in delivering the laser beam, optical fiber cables were adopted for

commercial engine applications. Herein, the laser source can be placed away from the engine, thereby protecting it from the heat and vibration issues. The optical fiber cable facilitates closed beam transportation and requires minimal installation space. Various types of optical fiber cables were experimented and compared [11]. Though the laser beam delivery through optical fiber cable is attractive, there are few technical challenges like decrease in transmission due to fiber bending, engine vibrations affecting the laser beam divergence angle and space for large sized laser source in commercial vehicles which need to be addressed [54]. Research on the development of a robust, low-cost, highly efficient compact laser ignition system that can easily fit in the engine similar to the conventional spark plug is required. In the past decade, research on various diode-pumped laser spark plugs was being explored at large scale [48]. This compact system consists of laser plug (similar to spark plug), pumping diode and optical fiber cables, and pump pulse is transported from the diode through the conventional optical fiber cables.

Optical window employed in the laser plug has to be robust as it has to withstand higher pressure and temperature generated during the combustion process. Unclean optical window affects the transmissivity of laser beam resulting in reduced beam intensity and engine misfire [50]. New methods for self-cleaning of optical window need to be addressed. The cost involved in developing a LI system is quite high [37]. Hence, research on low-cost, compact and high-energy LI system with efficient methods to deliver laser beam into combustion chamber needs to be accelerated.

4 Turbulent Jet Ignition (TJI)

The turbulent jet ignition (TJI), also known as pre-chamber spark ignition, was adopted in SI engines in early twentieth century with two-stroke Ricardo Dolphin engine [8]. However, it was not widely used in commercial SI engine at that time due to the requirement of additional mechanical components and increased cost. In recent times, there are more research on TJI engines [14, 55], and with the advancement in engine subsystem and fast response electronics, the development of TJI engines for lean combustion looks promising.

4.1 Principle of Operation

Turbulent jet ignition is envisioned as an efficient ignition system for lean combustion. Herein, the lean air–fuel mixture is inducted into the main combustion chamber through the intake port, and a rich mixture is made available in the pre-chamber, equipped with a fuel injector and spark plug [8]. The rich mixture in the pre-chamber is ignited by the spark plug, and combustion is initiated in the pre-chamber. With the increase in pressure, the flames and partially burnt air–fuel mixture are forced out of the pre-chamber through nozzle holes into the main chamber [8, 14]. The flame jet

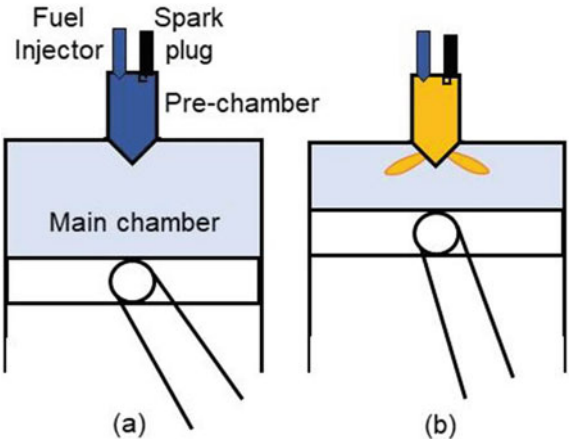

Fig. 11 **a** Schematic of turbulent jet ignition (TJI) engine with pre-chamber and main chamber **b** flame jet ejecting out of the pre-chamber to ignite main chamber mixtures

and partially burnt air–fuel mixture ignite the lean mixture in the main chamber as depicted in Fig. 11.

Turbulent jet ignition is categorized as a homogeneous or stratified charge based on the mixture present in the pre-chamber. In homogeneous TJI, there is no secondary fuel injector installed in the pre-chamber, and the fuel is injected either in the intake port (port-fuel injection) or inside the main chamber (direct injection). Herein, the air–fuel mixture from the main chamber enters the pre-chamber through the nozzle holes, and the air–fuel ratio is the same in both the chambers. With stratified charge TJI, secondary fuel injection is triggered to have a rich mixture in pre-chamber, and the lean mixture is inducted into the main chamber through the intake port. The volume of pre-chamber is maintained relatively small (less than 3% of the clearance volume) in most of the studies [8], and thus, rich mixture in pre-chamber does not affect the overall fuel consumption. Further, the stratified mixture preparation in pre-chamber and main chamber results in a reliable and stable ignition system for lean combustion with better engine characteristics.

4.2 Fundamental Studies

A fundamental understanding on the flame jet ejected from the pre-chamber in a TJI system has to be established [56]. Figure 12 shows the development of a flame jet ejected from the homogenous and stratified TJI system with single and dual orifice configurations. The pre-chamber mixture is maintained near stoichiometric ($\lambda = 1.06$), whereas the main chamber is filled with lean mixtures ($\lambda = 3.30$) for stratified TJI system. However, lean mixture ($\lambda = 3.00$) is fully occupied in both pre-chamber and main chamber for homogeneous TJI system. For a dual orifice stratified TJI system, two narrow flame jets travel at a faster rate and reach the combustion chamber wall. The fluid flow directs the flame toward the unburnt fuel in the bottom where

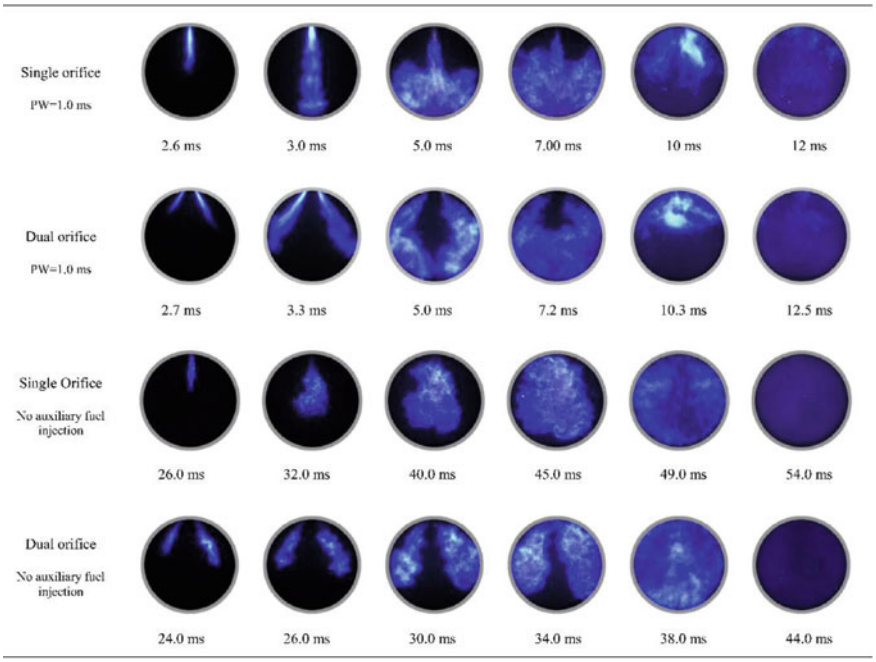

Fig. 12 Flame jet ejected from the homogenous and stratified TJI system with single and dual orifice configurations [56]

both the flame jet meets and entrains the unburned fuel–air mixture. Combustion happens within this flow field, and flame front propagates toward the unburnt fuel–air mixture in the top region where autoignition of end gas happens as seen from the bright spots in the combustion images.

A comparison between the performance of SI and homogenous TJI system reveals that shorter ignition delay, shorter combustion duration and slightly higher peak in-cylinder pressure are observed for TJI system [57]. The flame initiation period in homogeneous TJI system is almost an order of magnitude higher than stratified TJI system as evident from Fig. 12. This implies that the existence of rich/stoichiometric mixture inside the pre-chamber initiates early combustion, and the flame jet ejected from the pre-chamber travels at a faster rate resulting in shorter combustion duration [56]. It is well understood that the overall combustion characteristics of TJI system are influenced by the existence of pre-chamber, and it is also sensitive to the mixture fraction present in the pre-chamber.

Nozzle orifice is crucial in TJI system as the fuel–air mixture enters the pre-chamber through the orifice before ignition, and after combustion, the flame jet velocity and distribution of ignition sites are determined by the nozzle orifice [58]. With homogeneous TJI system, a smaller diameter nozzle hole is preferred for lean combustion as it generates a faster and more turbulent flame jet to ignite the lean mixtures in main chamber. However, for near stoichiometric air–fuel mixture, a

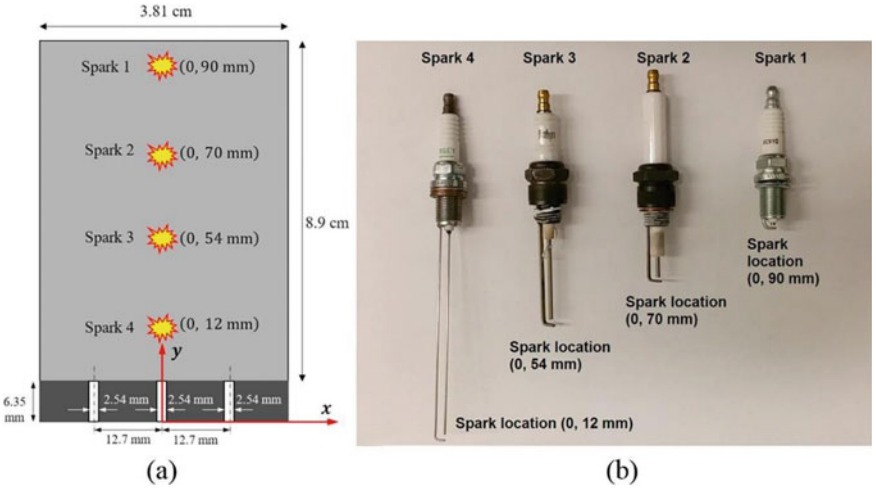

Fig. 13 **a** Schematic of pre-chamber showing different ignitions **b** photographic view of four spark plugs with different electrode configurations [59]

nozzle with maximum number of orifices resulted in faster combustion rates as it produces spatially distributed ignition locations. The flame jet velocity decreases with increase in nozzle orifice diameter and increase in dilution levels. Further, the turbulent jet does not have enough time to be fully developed and considered as an intermediate flow field.

The effect of modifying the ignition location in the pre-chamber on the combustion characteristics of the main chamber was analyzed [59]. Four different spark plugs with different ignition locations are employed, and the details are shown in Fig. 13. Spark 4 is located near to the nozzle orifice whereas spark 1 is placed far away from the nozzle orifice. The mixtures in pre-chamber were at stoichiometric condition whereas the mixtures in the main chamber were near the lean limit ($\Phi < 0.5$). The pre-chamber has three straight nozzle orifices and is separated from the main chamber by a thin aluminum diaphragm (~25 μm), which is ruptured during the combustion process.

Shorter ignition delay is observed for the spark plug located near the nozzle orifice, and it increases with the increase in ignition location. Figure 14 shows the regime diagram for different spark locations and pre-chamber equivalence ratio. Based on the flame jet behavior, pre-chamber is categorized into four different regions corresponding to the four different ignition locations [59]. For ignition in spark 4 region, the flame jet behaved as a laminar or slightly turbulent for all the pre-chamber equivalence ratio conditions as the ignition happens near to the nozzle hole. In this case, the flame jet is ejected from all the three holes of the pre-chamber. For ignition in spark 1 region, the flame jet from the side holes ignited the main chamber mixture for all the pre-chamber equivalence ratio conditions, and the same jet behavior is noted for the ignition in spark 2 region and pre-chamber equivalence ratio range of

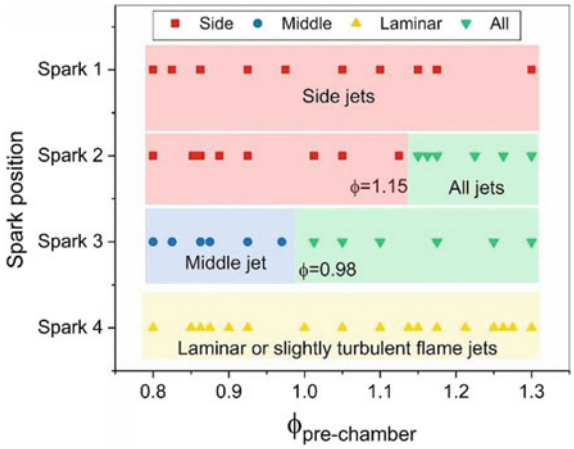

Fig. 14 Regime diagram for different spark locations and pre-chamber equivalence ratio conditions [59]

0.8–1.15. However, for rich mixtures ($\Phi = 1.15$–1.3), the flame jet is ejected from all the nozzle holes. For ignition in spark 3 region, the ignition of main chamber mixture is initiated by the flame jet from the middle hole till $\Phi = 0.98$, and beyond that, at rich mixture conditions ($\Phi = 0.98$–1.3), the flame is ejected from all the three holes.

4.3 TJI Engine Characteristics

A compact pre-chamber is installed in the spark plug region of the cylinder head, and it accommodates a fuel injector and a spark plug. The lean limit extension of TJI engine is explored with gasoline–air mixtures [60]. Gasoline is injected in the inlet port, while propane is directly injected into the pre-chamber to generate a rich gasoline and propane mixture. It is observed that the lean limit is extended from $\lambda = 1.4$ with SI engine to $\lambda = 2.1$ with TJI engine. As higher dilution levels were achieved with stable combustion, improvement in fuel consumption and net indicated thermal efficiency was reported [60, 61]. The improvement in efficiency may be attributed to the improved combustion with distributed ignition and reduced heat transfer losses. The ignition delay and combustion duration are observed to be shorter for TJI than SI engine except for very rich mixtures. This may be due to the large number of active radicals in the flame jet ejected from the pre-chamber resulting in distributed multiple ignitions in the main chamber.

In TJI system, combustion is initiated in the pre-chamber, and the flame jet reaches the main chamber to ignite the lean air–fuel mixture. Henceforth, the overall in-cylinder temperature is noted to be lower than the conventional SI engine resulting in lower NO_X emission. As the mixture in the pre-chamber is rich, only small amount of NO_X is formed due to lack of oxygen content. The flame jet interacts with the cool mixture in the main chamber and promotes rapid quenching of NO_X formation

reactions. Lower CO emission and higher HC emission have been observed with most of the pre-chamber studies [8]. This may be due to increased surface area with pre-chamber, lower in-cylinder temperature quenching the oxidation reactions, and also, some mixtures in main chamber get accumulated in crevice regions. Further research is required to identify the measures to reduce HC emission with TJI engine. Though extreme lean condition with stable combustion is achieved with TJI engines, the lean limit extension of TJI system is restricted in such a way that NO_X emission is lower while maintaining lower CO and HC emissions [14]. Several researchers have studied the effect on pre-chamber geometric conditions on engine-out emissions. It is observed that NO_X emission decreases with increase in pre-chamber volume, whereas little change is noted with HC and CO emission [62]. Further, the indicated NO_X, HC and CO emission increased with the increase in nozzle diameter. Better mixing of flame jet and burnt gases with the lean mixture in the main chamber is evident for smaller nozzle hole diameter resulting in lower engine-out emissions [62].

The possibility of further extending the lean limit of gasoline–air mixtures with TJI engine has been experimented by optimizing the parameters associated with the spark plug [63]. Unlike conventional SI engine, TJI engine is unaffected by the changes with spark plug type, electrode gap, orientation and location of the spark plug. However, the variation of spark plug depth showed small improvement in TJI engine. Flush-mounted spark plug does not allow any residual gases to be trapped inside the pre-chamber. When the spark plug depth was increased, small amount of residual gases was trapped near the spark plug electrode region. It is hard to scavenge the residual gases from this region, and hence, it is proposed to eliminate this dead volume in the TJI system by proper mounting of spark plug. Reducing the trapped residual gases resulted in slight increase in the lean limit extension ($\lambda = 2.14$). Most of the TJI engine studies reported a significant reduction in NO_X emission, due to the lower in-cylinder temperature encountered in the main chamber [8, 14]. Further, higher HC emission and lower CO emission are observed for TJI system. The excess air aids in complete oxidation of CO to CO_2, whereas the entrainment of air–fuel mixtures in the squish regions and high heat transfer rate to walls resulted in higher HC emissions.

The ignition energy requirement is much lower for TJI system in the lambda range of 1–1.8 with excellent combustion stability [64]. This provides an advantage of using small size ignition coil and spark plugs for TJI system resulting in improved component life, reduce cost and compact packaging. As TJI engine provides stable combustion with lean mixture, the engine compression ratio can be increased without knocking. It was predicted that TJI engine with a high compression ratio would result in 45% indicated efficiency, which is higher than the peak thermal efficiency of HCCI engine (~43%) [61].

4.4 Advantages

TJI engine has several advantages when compared to the conventional SI engine. The lean limit operation with TJI engine can be extended to higher dilution level as achieved with HCCI combustion mode [61]. TJI engine produces multiple and distributed ignition sites in the main chamber to rapidly consume the air–fuel mixture with minimal cycle-to-cycle variation (i.e., stable combustion) [14]. Further, TJI engine also provides an opportunity to increase the compression ratio from the baseline SI condition as the knocking tendency can be reduced with the faster burn rate [8]. Throttling losses associated with the part-load operation of SI engine can be eliminated by TJI engine [64]. The engine load conditions are varied by switching from lean-burn to stoichiometric condition in TJI system, and thus, the throttling losses can be eliminated, resulting in higher engine efficiency [8, 14]. TJI engine provides a flexibility to operate at all load ranges without any complex hardware systems unlike other low-temperature combustion technologies like homogeneous charge compression ignition (HCCI) and partially premixed combustion (PPC).

4.5 Limitations and Future Challenges

With the increasing demand for highly efficient powertrain with near zero emission, TJI technology has a greater role on the future engine technologies. The major limitation and technical challenge associated with TJI system are the fuel injection into the pre-chamber. Research on new fuel injector has to be initiated, and the injector should be capable of injecting the fuel into the small volume effectively without any fuel deposition on the chamber surfaces. Installing pre-chamber in the cylinder head is highly complicated due to the space constraints, and hence, the design parameters of pre-chamber have to be optimized to produce a compact pre-chamber for TJI engine. Computational research on TJI engine has to be initiated to better optimize the geometrical parameters of the pre-chamber like volume, nozzle orifice diameter, length of the orifice, number of nozzle orifices and mixture fraction for better combustion characteristics. These research shall provide the fundamental understanding on the influence of different parameters on TJI system and its combustion characteristics at low cost and shorter time. Though higher efficiency and lower emission levels are achieved with TJI engine, HC emission is observed to be higher due to the increase in surface area with the addition of pre-chamber. Future research should focus on methods to reduce HC emission without much compromise in the engine efficiency.

5 Radio Frequency Based Corona Ignition (RFCI)

Radio frequency based corona ignition system (RFCI) consists of a series resonant circuit with a coil and capacitor. The system converts the low voltage input into a high voltage output at the igniter tips to generate corona [65]. RFCI system has the capability to promote the ignition process due to its high discharge energy and large ignition volume. Thus, many researchers are keen on developing this system for future combustion engines.

5.1 Principle of Operation

RFCI system comprises of a series resonant R-L-C circuit (i.e., resistance–inductance–capacitance circuit) and is depicted in Fig. 15. RFCI system consists of an electronic system and an igniter assembly [66, 67]. The electronic system provides high-frequency power to the igniter assembly for generating corona inside the combustion chamber based on ECU data. The inductor and resistance combination amplifies received low voltage to required high voltage. The plug installed in the engine cylinder head contributes to the majority of the capacitance in the igniter assembly. Unlike conventional spark plug, there is no ground electrode in the corona igniter. The electrode (i.e., firing tip) in the igniter has one or more sharp tips from which the corona formation takes place.

When high voltage is applied to corona igniter, the free electrons are accelerated and collide with the gas molecules. The ionization process occurs when the kinetic energy of the electrons is higher than the ionizing energy of gas molecules. This results in the production of electron avalanche leading to the electrical breakdown of gases. The high frequency associated with the RFCI system limits the energized ions

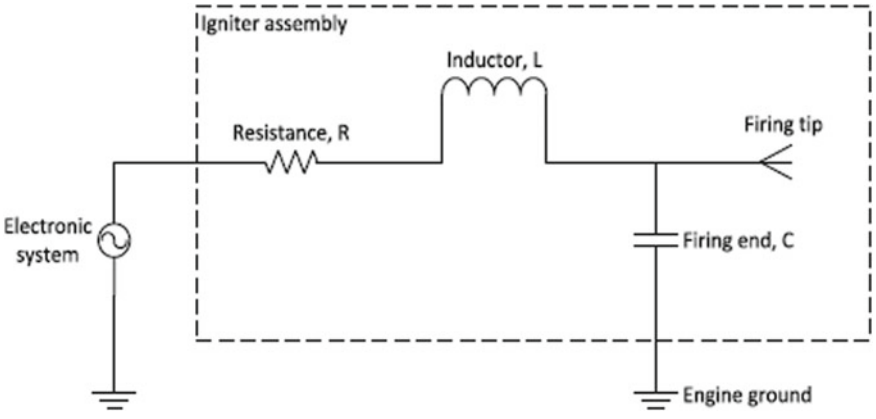

Fig. 15 Electric circuit of radio frequency-based corona igniter [66]

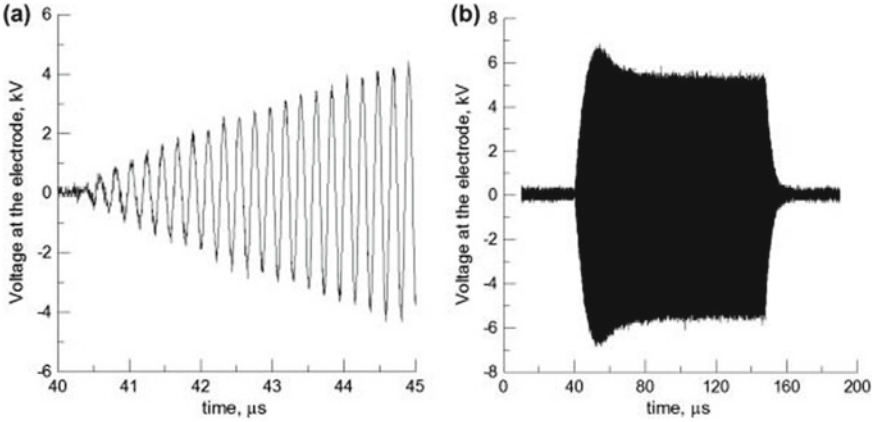

Fig. 16 Electrode voltage for RFCI system with an input voltage of 100 V and excitation frequency of 4.967 MHz at $\Phi = 0.6$ [67]

and electrons near the electrode region. A typical electrode voltage of the corona igniter is shown in Fig. 16. During the initial transient period, the electrode voltage increases, and once the breakdown conditions are attained, the discharge is generated, and the voltage drops to nearly zero.

5.2 Fundamental Studies

A fundamental understanding on the supply voltage, corona duration and excitation frequency of RFCI system on the ignition characteristics is essential. It is observed that the supply voltage and corona duration of RFCI system have a significant effect during the early stage of combustion, whereas the flame propagation is independent of the supplied source after 5% mass of fuel burnt [28]. The supply voltage influences the size, length and number of streamers emerging from the plug, which in turn affects the initial flame growth rate and combustion stability. The maximum supply voltage without causing arching event results in a higher initial flame growth rate, whereas the low supply voltage results in a smaller number of flame kernel development, causing combustion instability [28].

Increasing the corona duration supports early flame development; however, beyond a specific limit, there is no improvement in combustion [28]. Lower corona duration results in a smaller number of flame kernel development and may lead to engine misfire or combustion instability. The average corona size decreased with an increase in pressure and temperature of the combustion chamber [68].

5.3 RFCI Engine Characteristics

Figure 17 shows the single- and five-electrode configurations of RFCI system for engine application. The electrode tips are sharp with RFCI system than the conventional SI system to generate strong electric field corona discharge. Five-electrode RFCI system showed poor engine performance compared to a single-electrode RFCI system due to higher heat losses and reduced energy transfer efficiency at lean conditions [67, 68]. A single-electrode RFCI system showed a 2–5% increase in engine efficiency than conventional SI system due to faster flame speed.

The flame development characteristics in RFCI system and conventional SI system were compared in an optical engine fueled by methane and methane/hydrogen mixtures [69]. With corona igniter, the lean limit is extended from $\lambda = 1.5$–1.65 for methane, from $\lambda = 1.9$–2.0 for methane/hydrogen mixture and from $\lambda = 1.4$–1.65 for gasoline [70]. Ignition delay is observed to be shorter with RFCI system, whereas there is no considerable change in the combustion duration between SI and RFCI systems. The reduction in ignition delay is reported to be more than 50% for most of the studies with RFCI system when compared to the SI system [67, 69–71]. During the initial flame development, the flame speed is about four times higher for RFCI system than SI system. The efficiency of RFCI engine is slightly increased than SI engine due to early ignition and higher initial flame speed [72].

Figure 18 shows the flame front evolution in RFCI and SI optical engine for both methane and methane hydrogen mixtures. The flame development is faster in RFCI engine than SI engine for both the fuel–air mixtures. By the time SI-induced flames start to propagate, RFCI-induced flame occupies half of the combustion chamber [69]. In SI engine, the flame is initiated by the plasma generated at the electrode gap and develop as a spherical flame front. Corona ignition is volumetric, and initially, four independent flame fronts were developed rapidly, resulting in higher flame speed. Then, these four flame fronts coalesce and develops gradually reducing the flame speed.

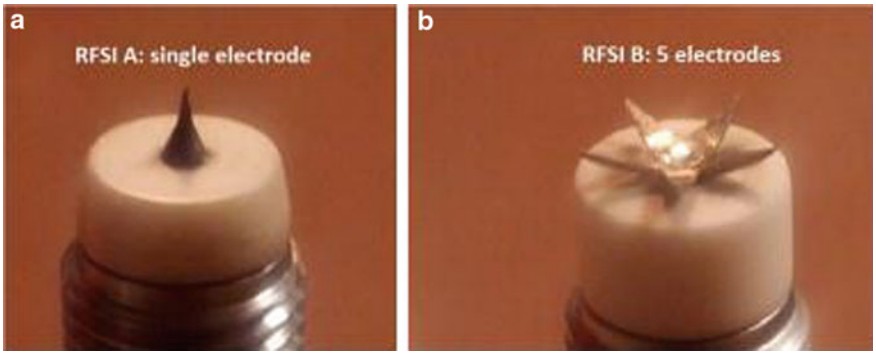

Fig. 17 **a** Single and **b** five-electrode configuration of RFCI system [67]

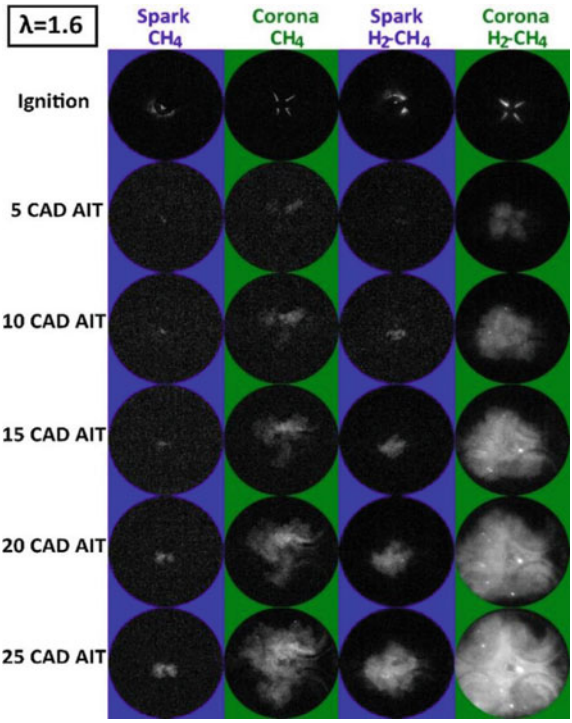

Fig. 18 Flame front evolution in RFCI and SI optical engine for both methane and methane–hydrogen mixtures [69]

The EGR compatibility limit is extended from 27% in SI engine to 32% in RFCI engine [71]. Low cycle-to-cycle variation, increased engine efficiency and stable combustion are observed with RFCI engine when compared to SI engine. The increase in engine efficiency with RFCI engine is attributed to the faster combustion rate. Further, efficiency of RFCI engine increased with the reduction in the equivalence ratio. There is no improvement with HC and CO emissions in RFCI engine compared to SI engine at same operating conditions [72]. However, it is possible to achieve lower HC and CO emissions with RFCI engine by exploiting the potential of lean engine operation. At lean condition, SI engine reported increase in HC and CO emission due to partial burning or misfiring, whereas the combustion is stable with RFCI engine and thus resulting in lower HC and CO emission [67]. NO_X emission in RFCI engine is higher than SI engine due to faster combustion and higher in-cylinder pressure.

5.4 Advantages

RFCI system generates large ignition volume, and hence, the ignition spot is not limited by electrode gap as in conventional SI systems. Further, multiple flame

fronts and faster flame kernel development are observed with RFCI system. RFCI system promotes initial flame development, lean limit extension and improved flame stability [72]. As there is no ground electrode in RFCI system, the heat loss to the electrode is minimized, improving the overall engine performance [28]. Other significant advantages of the RFCI system are better combustion control and continuous energy delivery. Energy consumption per discharge volume is significantly lower with RFCI system which makes it more efficient to ignite lean air–fuel mixtures than conventional SI system [68].

5.5 Limitations and Future Challenges

The major limitation of RFCI system is arcing. Arc is formed when a metal surface is placed near to the streamers (corona discharge) [65]. In RFCI system, the duration and intensity of the arc are not sufficient to ignite air–fuel mixture in the combustion chamber, and hence, this condition causes engine misfire [73]. Further, arcing may lead to excessive wear of the sharp igniter tip. Development of streamers in the igniter tip is highly influenced by several parameters like gas density, supply voltage and in-cylinder thermal and chemical processes. Increase in gas density suppresses corona formation, and sudden variation of in-cylinder conditions causes difficulties in control [28]. The input energy required by RFCI system is in order of magnitude higher than conventional SI systems [74]. The input energy requirement is increased with the increase in pressure at the ignition point and dilution levels. This is a challenge for the current automotive electrical system.

6 Microwave-Assisted Spark Ignition (MASI)

Plasma-assisted combustion is one of the promising technologies for the future combustion engines. Plasma generation can be accomplished with pulsed laser, radio frequency waves or microwave. Compared to other methods, plasma generation by microwave is much easier, requires less power and cost effective. Hence, many research works are carried out to access the performance of this ignition system under robust conditions.

6.1 Principle of Operation

Microwave-assisted spark-ignition (MASI) system consists of a conventional spark plug and a mixing unit which comprises of high voltage and microwave transmission lines. Initially, the plasma is triggered by the spark plug as like the conventional SI system. The generated spark is enhanced volumetrically by the microwaves supplied

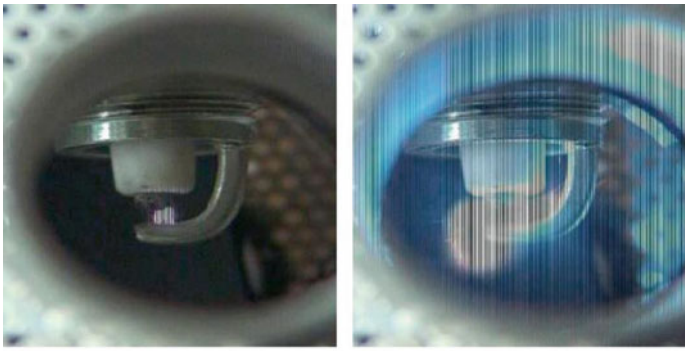

Fig. 19 Flame kernel development in conventional SI and MASI engines [75]

at higher frequency [75], as seen from Fig. 19. The microwaves transmit the energy to the free electrons in the region near to the spark plug. The energized electrons collide with the gas molecules through inelastic collision and generates ions and radicals in that region. High concentration of radicals reduces the ignition delay and triggers faster chemical kinetic reactions [32]. The ignition coil and microwave system are synchronized such that there is no delay in spark generation and spark exposure to microwaves. The microwave system cannot produce a breakdown process on its own, and it can only volumetrically enhance the generated spark.

6.2 Fundamental Studies

Figure 20 shows the variation of flame speed to the flame kernel size for SI and MASI system at an equivalence ratio of 0.7. These data are derived from the combustion images obtained through schlieren imaging technique. It is clear that the minimum flame size required for successful combustion increased with an increase in dilution [75], and the estimated critical flame size for $\Phi = 0.7$ is shown as a black circular dot in Fig. 20. The microwave accelerates the initial flame kernel development, and the critical flame size is achieved quickly. It could be seen that the spark only condition and spark with lower microwave energy (0.1 ms) do not result in successful combustion as the flame extinguished before reaching critical flame size.

Figure 21 shows the lean limit extension with MASI engine across different chamber pressure conditions. It is observed that the lean limit is extended by 10% in lean limit side and 15% in rich limit side with MASI. For MASI system, larger flame kernel size and increased flame speed are evident. This observation is due to the deposition of microwave energy to the free electrons present near the flame kernel resulting in enhanced chemical kinetic reactions [13]. The flame kernel surface is smooth for SI system, while wrinkled flame structure is evident for MASI system,

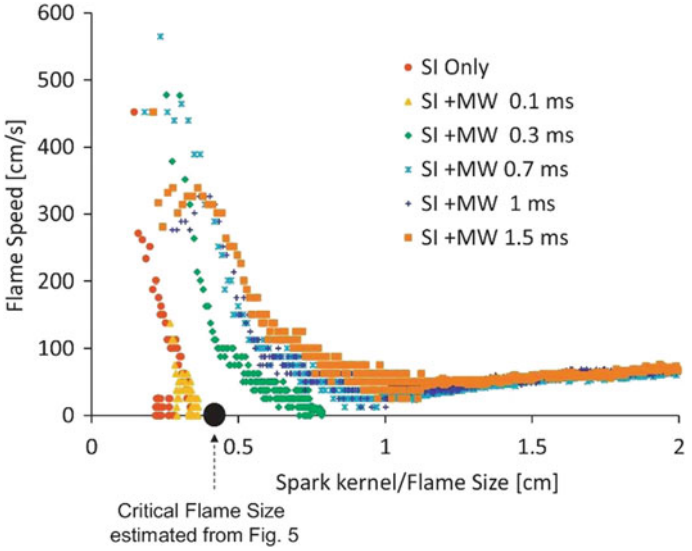

Fig. 20 Variation of flame speed with respect to flame size for SI and MASI system at an equivalence ratio of 0.7 [75]

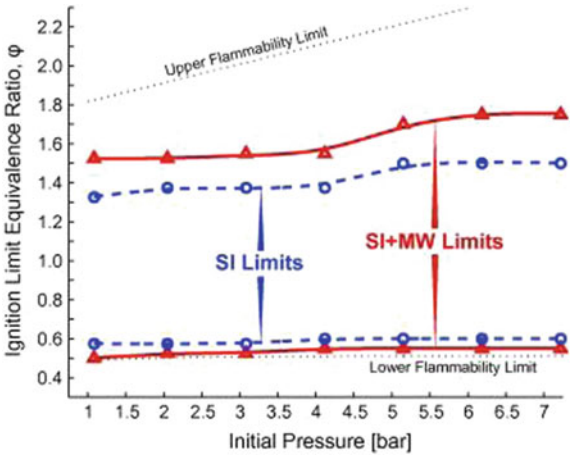

Fig. 21 Lean limit extension of MASI engine compared to SI engine [13]

and this is caused by the application of microwave electric field near the spark plug region.

The effect of initial chamber pressure on the flame kernel development is depicted in Fig. 22. The flame kernel size is noted to be higher for MASI system than SI system, and the difference is more prominent at lower chamber pressure. Flame kernel size decreased with an increase in the initial chamber pressure for both SI and MASI systems. The mean free path of the energized electrons is reduced with an increase in

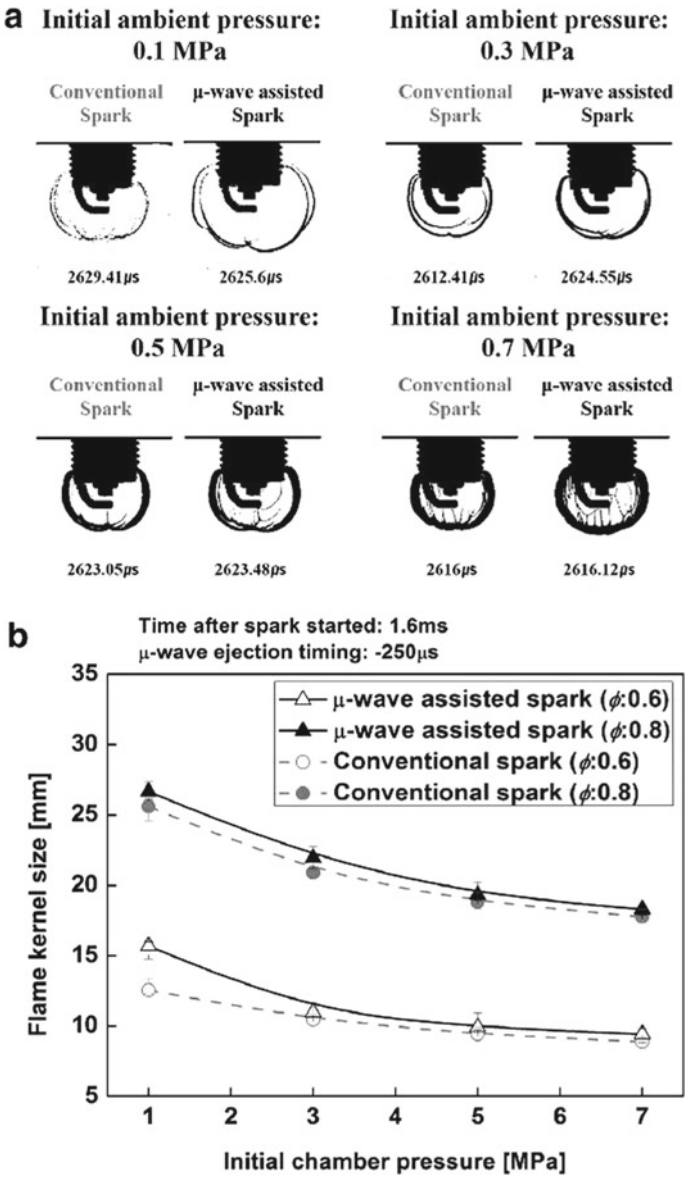

Fig. 22 Comparison of spark generated by MASI and SI system for different initial chamber pressures [33]

chamber pressure (increased gas density). This frequent collision between electron and gas molecules results in less degree of electron acceleration, and thus, the flame enhancement is not prominent in higher chamber pressures [33]. For lean mixtures, MASI system produces a flame kernel easily even at higher in-cylinder pressure, and the combustion is noted to be stable [76, 77]. Early start of combustion and larger initial flame kernel are associated with MASI system. The intensity of OH radicals is observed to be higher for MASI system, which implies that combustion is improved by the non-thermal kinetic mechanism.

6.3 MASI Engine Characteristics

Fuel efficiency and initial combustion period is improved with MASI engine when compared to conventional SI engine [29]. Further, the cycle-to-cycle variation is also decreased, and stable combustion is achieved for lean mixtures with MASI engine. MASI showed shorter combustion duration, higher peak in-cylinder pressure and higher heat release rate in a direct-injection gasoline engine [78]. The lean limit is extended from 1.28 for SI engine to 1.57 for MASI engine. Figure 23 shows the engine characteristics for different ignition conditions at the maximum efficiency point. All the engine parameters are optimized to obtain the best engine operating point, and it observed at $\lambda = 1.286$ for SI and $\lambda = 1.387$ for MASI engine. Engine operation with MASI system is superior to the SI system when the microwave ignition energy is higher than 260 mJ.

The ignition characteristics improved with the increase in microwave energy input, however, diminishing behavior was noted in a single-cylinder engine [32]. The microwave input energy is increased from 0 to 900 mJ/cycle, and stable combustion with improved engine characteristics was observed. However, increasing the microwave input energy from 900 to 1640 mJ/cycle showed no further improvement in engine characteristics. Stable combustion of lean air–fuel mixtures with reduced CO and NO_X emission is observed for MASI engines [32, 76].

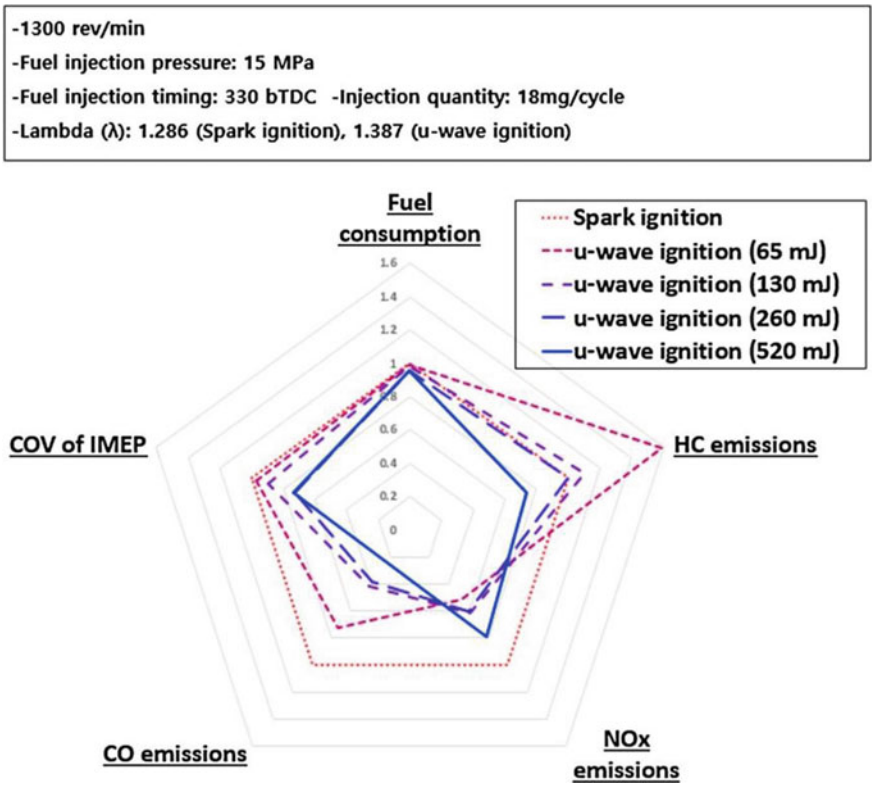

Fig. 23 Engine performance and emission characteristics at the maximum fuel efficiency point for SI and MASI engine [78]

6.4 Advantages

Early start of combustion and faster initial flame development enables extension of lean limit of MASI engine. Stable combustion of lean air–fuel mixture with low cycle-to-cycle variation is achieved with MASI engine. Lean-burn MASI engine results in lower fuel consumption, increased engine efficiency and lower CO and NO_X emissions.

6.5 Limitations

The enhancement in flame development vanishes at higher in-cylinder pressure, and thus, improvement with the combustion characteristics of MASI engine is marginal at same engine operating condition. In order to achieve better combustion characteristics with MASI engine, high-frequency and high-energy microwaves are required.

However, this will have an effect on the overall engine efficiency. The transmission of microwave into the combustion chamber encounters losses. The total microwave coupling efficiency is observed to be less than 20%, and methods to improve the coupling efficiency have to be analyzed. Further research on energy-efficient methods to achieve effective MASI at higher in-cylinder pressure is required. The research aimed to overcome the drawbacks associated with MASI system increases the commercial viability of MASI engine in the near future.

7 Summary

The extensive review of the advanced ignition systems like laser ignition, turbulent jet ignition, radio frequency-based corona ignition and microwave-assisted spark ignition reveals that the lean limit extension is possible with stable combustion. A comparison of these advanced ignition systems with conventional spark ignition reveals that there is not much improvement in the engine characteristics with these ignition systems at stoichiometric conditions. Table 1 compares the engine characteristics of different advanced ignition system at their best operating point with conventional SI engine at stoichiometric condition. From the summary, it is clear that the maximum possible lean limit extension is achieved with TJI system.

Development of optimized pre-chamber and fuel induction methodology for pre-chamber will boost the commercialization of TJI system in passenger vehicles.

Table 1 A comparison of the engine characteristics of different advanced ignition systems at their best operating point with conventional SI engine at stoichiometric condition ($\lambda = 1$)

Parameters	LI [7]	TJI [8]	RFCI [69]	MASI [78]
Lambda	Maximum: 1.8	Maximum: 2.1 Optimum: 1.8	Maximum: 1.65	Maximum: 1.57 Optimum: 1.387
Start of combustion	Early	Early	Early	Early
Combustion duration	Shorter	Shorter	No improvement	Shorter
Flame speed	No improvement	Faster	Faster	Faster
COV_{IMEP}	Lower	Lower	Lower	Lower
Peak in-cylinder pressure	Slightly higher	Higher	Slightly lower	Slightly higher
Heat release rate	Slightly higher	Higher	Slightly lower	Slightly higher
BSFC	Slightly lower	Lower	Slightly lower	Slightly lower
BTE	Slightly higher	Higher	Slightly higher	Slightly higher
HC emission	Slightly lower	Slightly higher	Lower	Lower
CO emissions	Slightly lower	Lower	Lower	Lower
NO_X emission	Lower	Lower	Higher	Lower

Electrode less ignition is realized with LI system where the ignition location and ignition energy can be optimized for better engine characteristics. Laser spark ignition, laser cavity ignition and multi-point laser ignition (combination) are the three different LI techniques employed to support lean combustion. The development of low cost, energy-efficient multi-point laser ignition system with higher number of ignition locations can be incorporated in future IC engine. The volumetric ignition with RFCI and MASI system shows a faster initial flame kernel development which will lead to complete combustion without any misfire when compared to delayed flame kernel development.

Multi-point ignition is accomplished with TJI and LI system whereas volumetric ignition is achieved with RFCI and MASI systems. Thus, on the performance front, these advanced ignition systems are best suited for future engine technologies. However, the high energy requirement of LI, RFCI and MASI system challenges the current automotive electrical systems and TJI system demands an effective technology to maintain rich mixture in pre-chamber in actual engine conditions. Hence, to address the limitation imposed by these ignition systems, more computational and application-oriented research has to be carried out in the near future.

It is well known that lean-burn SI engine results in higher engine efficiency and lower engine-out emissions. However, the lean limit extension is limited in conventional SI engine by considering the durability and ignition ability of spark plug. The engines equipped with these advanced ignition systems showed better engine characteristics with stable combustion at lean conditions owing to the increased flame speed and distributed ignition sites. Higher engine efficiency, lower fuel consumption, lower NO_X, CO and HC emissions are observed for lean burn engines with advanced ignition systems. With the increasing global concern on energy and environment, these lean burn engines equipped with advanced ignition systems along with hybrid vehicle technology will have greater prospects in the near future.

Acknowledgements This work is supported by the project funded by Science and Engineering Research Board (SERB), Department of Science and Technology, Government of India, under Early Career Research Award scheme (Project Number: ECR/2018/001078).

References

1. Atabani, A. E., Badruddin, I. A., Mekhilef, S., & Silitonga, A. S. (2011) A review on global fuel economy standards, labels and technologies in the transportation sector. *Renewable and Sustainable Energy Reviews.*
2. Zhao, F., Lai, M. C., & Harrington, D. L. (1999). Automotive spark-ignited direct-injection gasoline engines. *Progress in Energy and Combustion Science*. https://doi.org/10.1016/S0360-1285(99)00004-0.
3. Petitjean, D., Bernardini, L., Middlemass, C., & Shahed, S. M. (2004). Advanced gasoline engine turbocharging technology for fuel economy improvements. SAE Technical Papers.
4. Ashok, B., Denis Ashok, S., & Ramesh Kumar, C. (2016). A review on control system architecture of a SI engine management system. *Annual Reviews in Control*.

5. Leduc, P., Dubar, B., Ranini, A., & Monnier, G. (2003). Downsizing of gasoline engine: An efficient way to reduce CO_2 emissions. *Oil & Gas Science and Technology*. https://doi.org/10.2516/ogst:2003008.
6. Ran, Z., Hariharan, D., Lawler, B., & Mamalis, S. (2019). Experimental study of lean spark ignition combustion using gasoline, ethanol, natural gas, and syngas. *Fuel*. https://doi.org/10.1016/j.fuel.2018.08.054.
7. Morsy, M. H. (2012). Review and recent developments of laser ignition for internal combustion engines applications. *Renewable and Sustainable Energy Reviews, 16,* 4849–4875. https://doi.org/10.1016/j.rser.2012.04.038.
8. Toulson, E., Schock, H. J., & Attard, W. P. (2010). A review of pre-chamber initiated jet ignition combustion systems. SAE Technical Papers. https://doi.org/10.4271/2010-01-2263
9. Dale, J. D., Checkela, M. D., & Smyb, P. R. (1997). Application of high energy ignition systems to engines. *Progress in Energy and Combustion Science, 23,* 379–398.
10. Kalghatgi, G. T. (2015). Developments in internal combustion engines and implications for combustion science and future transport fuels. *Proceedings of the Combustion Institute*. https://doi.org/10.1016/j.proci.2014.10.002.
11. Patane, P., & Nandgaonkar, M. (2020). Review: Multipoint laser ignition system and its applications to IC engines. *Optics & Laser Technology, 130,* 106305. https://doi.org/10.1016/j.optlastec.2020.106305.
12. Cruccolini, V., Discepoli, G., Cimarello, A., et al. (2020). Lean combustion analysis using a corona discharge igniter in an optical engine fueled with methane and a hydrogen-methane blend. *Fuel, 259*, 116290. https://doi.org/10.1016/j.fuel.2019.116290.
13. Wolk, B., DeFilippo, A., Chen, J. Y., et al. (2013). Enhancement of flame development by microwave-assisted spark ignition in constant volume combustion chamber. *Combustion and Flame, 160,* 1225–1234. https://doi.org/10.1016/j.combustflame.2013.02.004.
14. Alvarez, C. E. C., Couto, G. E., Roso, V. R., et al. (2018). A review of prechamber ignition systems as lean combustion technology for SI engines. *Applied Thermal Engineering, 128,* 107–120. https://doi.org/10.1016/j.applthermaleng.2017.08.118.
15. Heywood, J. B. (2018). *Internal combustion engine fundamentals* (2nd ed.).
16. Bhavani Shankar, V. S., Johansson, B., & Andersson, A. (2018). Double compression expansion engine: A parametric study on a high-efficiency engine concept. SAE Technical Papers.
17. Zhao, J. (2017). Research and application of over-expansion cycle (Atkinson and Miller) engines—A review. *Applied Energy*.
18. Killingsworth, N. J., Rapp, V. H., Flowers, D. L., et al. (2011). Increased efficiency in SI engine with air replaced by oxygen in argon mixture. *Proceedings of the Combustion Institute*. https://doi.org/10.1016/j.proci.2010.07.035.
19. Aznar, M. S., Chorou, F., Chen, J. Y., et al. (2018). Experimental and numerical investigation of the argon power cycle. In *ASME 2018 Internal Combustion Engine Division Fall Technical Conference*, ICEF 2018.
20. Mohammed, A. M., Masurier, J. B., Elkhazraji, A., et al. (2019). A path towards high efficiency using argon in an HCCI engine. SAE Technical Papers.
21. Germane, G. J., Wood, C. G., & Hess, C. C. (1983). Lean combustion in spark-ignited internal combustion engines—A review. SAE Technical Papers. https://doi.org/10.4271/831694
22. Vagelopoulos, C. M., & Egolfopoulos, F. N. (1998). Direct experimental determination of laminar flame speeds. In *Symposium (International) on Combustion.*
23. Endo, T., Kuwamoto, K., Kim, W., et al. (2018). Comparative study of laser ignition and spark-plug ignition in high-speed flows. *Combustion and Flame, 191,* 408–416. https://doi.org/10.1016/j.combustflame.2018.01.029.
24. Bisetto, F., Toniolo, J., & Menezes, R. (2006). Spark plugs for multi-fuel vehicles. SAE Technical Papers.
25. Davis, G. W., Bouboulis, J., & Heil, E. (1999). The effect of a multiple spark discharge ignition system and spark plug electrode configuration on cold starting of a dedicated E85 fueled vehicle. SAE Technical Papers.

26. Chen, W., Madison, D., Dice, P., et al. (2013). Impact of ignition energy phasing and spark gap on combustion in a homogenous direct injection gasoline SI engine near the EGR limit. SAE Technical Papers.
27. Abdel-Rehim, A. A. (2013). Impact of spark plug number of ground electrodes on engine stability. *Ain Shams Engineering Journal*. https://doi.org/10.1016/j.asej.2012.09.006.
28. Cimarello, A., Cruccolini, V., Discepoli, G., et al. (2018). Combustion behavior of an RF corona ignition system with different control strategies. SAE Technical Papers, April 1–19, 2018. https://doi.org/10.4271/2018-01-1132.
29. Nishiyama, A., & Ikeda, Y. (2012). Improvement of lean limit and fuel consumption using microwave plasma ignition technology. SAE Technical Papers. https://doi.org/10.4271/2012-01-1139.
30. Edwards, C. F., Stewart, H. E., & Oppenheim, A. K. (1985). A photographic study of plasma ignition systems. SAE Technical Papers. https://doi.org/10.4271/850077.
31. Ju, Y., & Sun, W. (2015). Plasma assisted combustion: Dynamics and chemistry. *Progress in Energy and Combustion Science*.
32. Defilippo, A., Saxena, S., Rapp, V., et al. (2011). Extending the lean stability limits of gasoline using a microwave-assisted spark plug. SAE 2011 World Congress and Exhibition. https://doi.org/10.4271/2011-01-0663.
33. Hwang, J., Bae, C., Park, J., et al. (2016). Microwave-assisted plasma ignition in a constant volume combustion chamber. *Combustion and Flame, 167,* 86–96. https://doi.org/10.1016/j.combustflame.2016.02.023.
34. Dale, J. D., Smy, P. R., & Clements, R. M. (1978). Laser ignited internal combustion engine—An experimental study. SAE Technical Papers.
35. Srivastava, D. K., & Agarwal, A. K. (2014). Comparative experimental evaluation of performance, combustion and emissions of laser ignition with conventional spark plug in a compressed natural gas fuelled single cylinder engine. *Fuel, 123,* 113–122. https://doi.org/10.1016/j.fuel.2014.01.046.
36. Phuoc, T. X. (2006). Laser-induced spark ignition fundamental and applications. *Optics and Lasers in Engineering, 44,* 351–397. https://doi.org/10.1016/j.optlaseng.2005.03.008.
37. Ronney, P. D. (1994). Laser versus conventional ignition of flames. *Optical Engineering, 33,* 510. https://doi.org/10.1117/12.152237.
38. Srivastava, D. K., Dharamshi, K., & Agarwal, A. K. (2011). Flame kernel characterization of laser ignition of natural gas–air mixture in a constant volume combustion chamber. *Optics and Lasers in Engineering, 49,* 1201–1209. https://doi.org/10.1016/j.optlaseng.2011.04.015.
39. Xu, C., Fang, D., Luo, Q., et al. (2014). A comparative study of laser ignition and spark ignition with gasoline-air mixtures. *Optics & Laser Technology, 64,* 343–351. https://doi.org/10.1016/j.optlastec.2014.05.009.
40. Srivastava, D. K., Wintner, E., & Agarwal, A. K. (2014). Effect of focal size on the laser ignition of compressed natural gas-air mixture. *Optics and Lasers in Engineering, 58,* 67–79. https://doi.org/10.1016/j.optlaseng.2014.01.023.
41. Morsy, M. H., Ko, Y. S., & Chung, S. H. (1999). Laser-induced ignition using a conical cavity in CH_4-air mixtures. *Combustion and Flame, 119,* 473–482. https://doi.org/10.1016/S0010-2180(99)00060-7.
42. Ryu, S. K., Won, S. H., & Chung, S. H. (2009). Laser-induced multi-point ignition with single-shot laser using conical cavities and prechamber with jet holes. *Proceedings of the Combustion Institute, 32*(II), 3189–3196. https://doi.org/10.1016/j.proci.2008.05.080.
43. Nakamura, N., Baika, T., & Shibata, Y. (1985). Multipoint spark ignition for lean combustion. SAE Technical Papers. https://doi.org/10.4271/852092.
44. Ramtilak, A., Joseph, A., Sivakumar, G., & Bhat, S. S. (2005). Digital twin spark ignition for improved fuel economy and emissions on four stroke engines. SAE Technical Papers.
45. Morsy, M. H., & Chung, S. H. (2003). Laser-induced multi-point ignition with a single-shot laser using two conical cavities for hydrogen/air mixture. *Experimental Thermal and Fluid Science, 27,* 491–497. https://doi.org/10.1016/S0894-1777(02)00252-2.

46. Morsy, M. H., Ko, Y. S., Chung, S. H., & Cho, P. (2001). Laser-induced two-point ignition of premixture with a single-shot laser. *Combustion and Flame.* https://doi.org/10.1016/S0010-2180(00)00218-2.
47. Pal, A., & Agarwal, A. K. (2015). Comparative study of laser ignition and conventional electrical spark ignition systems in a hydrogen fuelled engine. *International Journal of Hydrogen Energy, 40,* 2386–2395. https://doi.org/10.1016/j.ijhydene.2014.12.030.
48. Pavel, N., Chiriac, R., Birtas, A., et al. (2019). On the improvement by laser ignition of the performances of a passenger car gasoline engine. *Optics Express.* https://doi.org/10.1364/oe.27.00a385.
49. Srivastava, D. K., & Agarwal, A. K. (2018). Combustion characteristics of a variable compression ratio laser-plasma ignited compressed natural gas engine. *Fuel, 214,* 322–329. https://doi.org/10.1016/j.fuel.2017.10.012.
50. Graf, J., Weinrotter, M., Kopecek, H., & Wintnen, E. (2004). Laser ignition, optics and contamination of optics in an I.C. Engine. In *Proceedings of the 2004 Fall Technical Conference of the ASME Internal Combustion Engine Division.*
51. Srivastava, D., & Agarwal, A. K. (2013). Laser ignition of single cylinder engine and effects of ignition location. SAE Technical Papers 2. https://doi.org/10.4271/2013-01-1631.
52. Srivastava, D. K., Wintner, E., & Agarwal, A. K. (2014). Effect of laser pulse energy on the laser ignition of compressed natural gas fueled engine. *Optical Engineering*. https://doi.org/10.1117/1.oe.53.5.056120.
53. Kuang, Z., Lyon, E., Cheng, H., et al. (2017). Multi-location laser ignition using a spatial light modulator towards improving automotive gasoline engine performance. *Optics and Lasers in Engineering, 90,* 275–283. https://doi.org/10.1016/j.optlaseng.2016.10.024.
54. Pavel, N., Bärwinkel, M., Heinz, P., et al. (2018). Laser ignition—Spark plug development and application in reciprocating engines. *Progress in Quantum Electronics.*
55. Toulson, E., Watson, H. C., & Attard, W. P. (2007). The lean limit and emissions at near-idle for a gasoline HAJI system with alternative pre-chamber fuels. SAE Technical Paper, September 2007. https://doi.org/10.4271/2007-24-0120.
56. Gentz, G., Gholamisheeri, M., & Toulson, E. (2017). A study of a turbulent jet ignition system fueled with iso-octane: Pressure trace analysis and combustion visualization. *Applied Energy, 189,* 385–394. https://doi.org/10.1016/j.apenergy.2016.12.055.
57. Wu, H., Wang, L., Wang, X., et al. (2018). The effect of turbulent jet induced by pre-chamber sparkplug on combustion characteristics of hydrogen-air pre-mixture. *International Journal of Hydrogen Energy, 43,* 8116–8126. https://doi.org/10.1016/j.ijhydene.2018.02.155.
58. Gentz, G., Thelen, B., Gholamisheeri, M., et al. (2015). A study of the influence of orifice diameter on a turbulent jet ignition system through combustion visualization and performance characterization in a rapid compression machine. *Applied Thermal Engineering, 81,* 399–411. https://doi.org/10.1016/j.applthermaleng.2015.02.026.
59. Biswas, S., & Qiao, L. (2018). Ignition of ultra-lean premixed H_2/air using multiple hot turbulent jets generated by pre-chamber combustion. *Applied Thermal Engineering, 132,* 102–114. https://doi.org/10.1016/j.applthermaleng.2017.11.073.
60. Attard, W. P., Fraser, N., Parsons, P., & Toulson, E. (2010). A turbulent jet ignition pre-chamber combustion system for large fuel economy improvements in a modern vehicle powertrain. SAE Technical Papers, 3, 20–37. https://doi.org/10.4271/2010-01-1457.
61. Attard, W. P., & Parsons, P. (2010). A normally aspirated spark initiated combustion system capable of high load, high efficiency and near Zero NO_x emissions in a modern vehicle powertrain. *SAE International Journal of Engines, 3,* 269–287. https://doi.org/10.4271/2010-01-2196.
62. Wall, J. C., & Heywood, J. B. (1978). The influence of operating variables and prechamber size on combustion in a prechamber stratified-charge engine. SAE Technical Papers.
63. Attard, W. P., & Parsons, P. (2010). Flame kernel development for a spark initiated pre-chamber combustion system capable of high load, high efficiency and near zero NO_x emissions. *SAE International Journal of Engines.* https://doi.org/10.4271/2010-01-2260.

64. Attard, W. P., Kohn, J., & Parsons, P. (2010). Ignition energy development for a spark initiated combustion system capable of high load, high efficiency and near zero NO_x emissions. SAE Technical Papers, 3, 481–496. https://doi.org/10.4271/2010-32-0088.
65. Bonazza, T. J., Vanvoorhies, K. L., & Smith, J. E. (1992). RF plasma ignition system concept for lean burn internal combustion engines. SAE Technical Papers. https://doi.org/10.4271/929416.
66. Burrows, J., & Mixell, K. (2017). Analytical and experimental optimization of the advanced corona ignition system. In *Ignition systems for gasoline engines.*
67. Mariani, A., & Foucher, F. (2014). Radio frequency spark plug: An ignition system for modern internal combustion engines. *Applied Energy, 122,* 151–161. https://doi.org/10.1016/j.apenergy.2014.02.009.
68. Hampe, C., Kubach, H., Spicher, U., et al. (2013). Investigations of ignition processes using high frequency ignition. SAE Technical Papers 2. https://doi.org/10.4271/2013-01-1633.
69. Cruccolini, V., Discepoli, G., Cimarello, A., et al. (2020). Lean combustion analysis using a corona discharge igniter in an optical engine fueled with methane and a hydrogen-methane blend. *Fuel, 259.* https://doi.org/10.1016/j.fuel.2019.116290.
70. Cimarello, A., Grimaldi, C. N., Mariani, F., Battistoni, M., & Dal Re, M. (2017). Analysis of RF corona ignition in lean operating conditions using an optical access engine. Author, co-author (Do NOT enter this information). It will be pulled from participant tab in. SAE 1–22. https://doi.org/10.4271/2017-01-0673.Copyright.
71. Marko, F., König, G., Schöffler, T., et al. (2017). Comparative optical and thermodynamic investigations of high frequency corona- and spark-ignition on a CV natural gas research engine operated with charge dilution by exhaust gas recirculation. In *Ignition systems for gasoline engines.*
72. Mariani, A., Foucher, F., & Moreau, B. (2013). The effects of a radio frequency ignition system on the efficiency and the exhaust emissions of a spark-ignition engine. SAE Technical Papers 6. https://doi.org/10.4271/2013-24-0053.
73. Mazacioglu, A., Gross, M. C., Kern, J., & Sick, V. (2019). Infrared borescopic characterization of corona and conventional ignition for lean/dilute combustion in heavy-duty natural-gas engines. *Proceedings of the Combustion Institute, 37,* 4993–5001. https://doi.org/10.1016/j.proci.2018.06.060.
74. Pineda, D. I., Wolk, B., Chen, J. Y., & Dibble, R. W. (2016). Application of corona discharge ignition in a boosted direct-injection single cylinder gasoline engine: Effects on combustion phasing, fuel consumption, and emissions. *SAE International Journal of Engines, 9,* 1970–1988. https://doi.org/10.4271/2016-01-9045.
75. Padala, S., Nishiyama, A., & Ikeda, Y. (2017). Flame size measurements of premixed propane-air mixtures ignited by microwave-enhanced plasma. *Proceedings of the Combustion Institute, 36,* 4113–4119. https://doi.org/10.1016/j.proci.2016.06.168.
76. Ikeda, Y., Nishiyama, A., Katano, H., et al. (2009). Research and development of microwave plasma combustion engine (Part II: Engine performance of plasma combustion engine). SAE Technical Papers. https://doi.org/10.4271/2009-01-1049.
77. Ikeda, Y., Nishiyama, A., Wachi, Y., & Kaneko, M. (2009). Research and development of microwave plasma combustion engine (Part I: Concept of plasma combustion and plasma generation technique). SAE Technical Papers.
78. Hwang, J., Kim, W., Bae, C., et al. (2017). Application of a novel microwave-assisted plasma ignition system in a direct injection gasoline engine. *Applied Energy, 205,* 562–576. https://doi.org/10.1016/j.apenergy.2017.07.129.

Dimensionless Quantities in Pre-chamber Turbulent Jet Ignition of Premixed Methane/Air

Sayan Biswas

Abbreviations

.

α	Thermal diffusivity
$\mathbb{D}$	Diffusion coefficient
ρ	Density
ϕ	Equivalence ratio
μ	Dynamic viscosity
ν	Kinematic viscosity
λ	Heat conductivity
δ	Flame thickness
Δ	Difference
$\dot{\omega}$	Rate of production
A	Area
ACI	Advanced compression ignition
BEV	Battery-electric vehicles
c_p	Specific heat capacity
d	Nozzle diameter
Da	Damköhler number
DI	Direct injection
FWHM	Full width half maximum
GHG	Greenhouse gas
h_0	Heat of formation
H	Atomic hydrogen

S. Biswas (✉)
University of Minnesota Twin Cities, Minneapolis, MN 55455, USA
e-mail: biswas@umn.edu

A. P. Singh et al. (eds.), *Alternative Fuels and Advanced Combustion Techniques as Sustainable Solutions for Internal Combustion Engines*, Energy, Environment, and Sustainability, https://doi.org/10.1007/978-981-16-1513-9_11

HO_2	Hydroperoxyl radical
J	Jet momentum
l	Integral length scale
L/D	Pre-chamber length-to-diameter ratio
LTHR	Low-temperature heat release
$\dot{m}$	Mass flow rate
$\dot{m}/A$	Mass flux
NO_x	Oxides of nitrogen
O	Atomic oxygen
O_3	Ozone
OH	Hydroxyl radical
p	Pressure
p_0	Thermodynamics pressure
p_1	Hydrodynamic pressure
PLIF	Planar laser-induced fluorescence
PM	Particulate matter
Pr	Prandtl number
Re	Reynolds number
R	Alkyl radical
RO_2	Alkylperoxy radical
ROOH	Alkylperoxide radical
RGF	Residual gas fraction
SACI	Spark-assisted compression ignition
Sc	Schmidt number
SI	Spark-ignited
s_L	Laminar flame speed
T	Temperature
t	Time
TDC	Top dead center
TI	Turbulent intensity
TJI	Turbulent jet ignition
$\vec{u}$	Velocity field
UHC	Unburned hydrocarbon
u'	Fluctuating component of velocity
V_d	Diffusion velocity
Y	Mass fraction

Superscripts

$\widetilde{A}$	Dimensionless variables

Subscripts

chemical	Chemical
cr	Critical
d	Diffusion
flame	Flame
fluid	Fluid
i	Initial
int	Integral
*i*th	Species number
lam	Laminar
main	Main chamber
pre	Pre-chamber
turb	Turbulent

1 Introduction

Future automotive efficiency gains will require the transition of spark-ignited (SI) gasoline engine combustion toward more challenging lean/dilute regimes [1]. A viable strategy for lean-burn SI engines is downsized boosted operation. A downsized engine employs smaller combustion volume instead of a larger combustion chamber, keeping the overall engine power fixed by adding a forced aspiration device for intake boosting such as turbocharger or supercharger and direct-injection (DI) technology. Downsizing offers comparable performance to a much larger engine while reduces carbon emissions, losses due to throttling, wall heat transfer and friction at low-to-moderate engine load [2–4]. Likewise, intake boosting provides high torque but also incurs losses via the usage of turbochargers [5]. Even though lean burn can significantly improve engine efficiency by a combination of increased charge-specific heat ratios [6], reduced heat transfer and throttling losses [7], it requires some level of fuel stratification by a late cycle second injection to stabilize combustion which raises undesirable oxides of nitrogen (NO_x) and particulate matter (PM) emissions [8].

Advanced compression ignition (ACI) strategy is an alternate method that offers improved efficiency via a higher compression ratio and reduced throttling losses. However, maintaining stable, knock-free combustion across the entire load-speed map proved to be extremely challenging. Mixed-mode operation strategies, where ACI can be utilized for part-load and boosted SI for high power-density conditions, have also been explored [9]. An ACI variant, spark-assisted compression ignition (SACI) technique, has shown promises by eliminated knocking and provided stable combustion at low load by limiting the compression ratio below 14 [10–13]. However, at low-speed, low-load conditions to ensure sufficient mixture reactivity and maintain stable combustion, either charge heating or mixture stratification by

second DI becomes indispensable. This again negates the purpose of lean burn and its advantages.

A novel, robust ignition system is the key to achieve stable lean burn. The major challenge in lean operation is partial burn or misfires that lead to higher cycle-to-cycle variation, reduced efficiency and increased unburned hydrocarbon (UHC) emissions [14, 15]. Turbulent jet ignition (TJI), a simple yet powerful lean-burn strategy, uses turbulent hot jets generated by burning stoichiometric or slightly fuel-rich mixtures in a small separate chamber with orifices/nozzles at the end called pre-chamber, to ignite a main chamber filled with lean fuel/air mixtures. A typical pre-chamber volume is 0.1–5% of the main chamber with nozzle diameters ranging from 0.1–10 mm. Compared to conventional point-source spark ignition, TJI produces multiple ignition sites on the surface of the hot jet distributed over a larger area that enables higher ignition probability, stronger ignition kernels and shorter burn duration.

The physics of TJI is extremely complicated due to the intricate coupling between turbulence and chemistry. Ignition depends on numerous spatially and temporally varying thermophysical and geometric parameters such as system pressure, temperature, thermal and mass diffusivity of reactants, the concentration of radicals and actives species (O, OH, HO2, O3, etc.), pre-chamber geometry, nozzle size, shape, orientation, numbers, etc. For example, atomic oxygen (O) produced by pre-chamber combustion advances low-temperature heat release (LTHR) reactions via atomic hydrogen (H) abstraction, $RH + O \rightarrow R + OH$. In high-density, low-temperature conditions such as those found near the top dead center (TDC), the produced alkyl radical, R, combines with O_2 to form alkylperoxy radicals, $R + O_2 \rightarrow RO_2$. The RO_2 continues fuel H abstraction: $RO_2 + RH \rightarrow ROOH + R$. Alklyperoxide (ROOH) is then decomposed into alkyloxy radicals (RO) and OH to become a sustainable source of LTHR radicals [16]. The pre-chamber design can differ widely depending on the type of engine, fuel and the purpose of the operation. A pre-chamber optimized for a specific engine condition can be far away from optimum at a different operating point. Hence, it is critical to understand the fundamentals of TJI, ignition mechanisms and associated processes.

Nearly all experimental studies of TJI were dedicated to explore the typical characteristics and performance of the TJI system compared to conventional spark focusing on specific applications or operating conditions. These studies can be classified into two groups, (1) TJI in production or research engines, e.g., lean-burn extension, natural gas TJI operation, active versus passive pre-chamber, performance and emissions measurements, etc. (2) TJI in stand-alone experimental vessels with or without optical accessibility. Only a handful of studies in the latter group investigated the fundamentals of TJI. Ghoniem et al. [17], Pitt et al. [18] and Yamaguchi et al. [19] were among the earliest researchers to explore TJI physics. Chen observed that the turbulent length scales and eddies created by the hot jet play a vital role in the ignition. Pitt showed that TJI exhibits shorter ignition delay and faster burning compared to conventional spark. Through a series of experiments, Yamaguchi examined the effect of nozzle diameter on jet behavior and ignition pattern. Over the last two decades, advancement in laser diagnostics and high-speed optical imaging has enabled a better understanding of the TJI physics. Sadanandan et al. [20] employed

high-speed laser schlieren and OH planar laser-induced fluorescence (PLIF) to investigate the ignition process. Gholamisheeri et al. [21], Toulson et al. [22] explored the combustion stability, lean limit performance and emissions characteristics of different pre-chamber fuels using an optically accessible rapid compression machine. Shah et al. [23, 24] found the critical pre-chamber to main chamber volume ratio beyond which the TJI loses its effectiveness in a heavy-duty natural gas engine. Biswas [25–31] investigated different TJI ignition mechanisms, the effect of jet interactions and impingement and critical non-dimensional numbers associated with TJI. Validi and Jaberi [32] performed direct numerical simulations (DNS) to demonstrate how the existence of a high-energy hot turbulent jet filled with combustion products differs from a non-reacting jet in terms of flow structures and mixing statistics. Li et al. [33] carried out TJI experiments using multiple nozzles in a large bore constant-volume vessel filled with methane/air mixtures and found that TJI by propagating flame jets became dominant with increase in initial pressures. Wang et al. [34] examined the OH mass fraction distribution along the hot turbulent jet and identified three regions within the jet—extinction region, just-igniting region and combustion region. These studies illustrate that a complete utilization of the immense potential of TJI requires a comprehensive understanding of the fundamentals. An in-depth understanding of the TJI would help translate the knowledge obtained in the laboratory to real-world production engines.

The present study investigates the fundamental processes and non-dimensional numbers associated with TJI and how this knowledge can be leveraged to build a scalable TJI system. Experiments were carried out in a custom-build, optically accessible, dual-chamber TJI system for lean ($\phi = 0.55 - 0.95$) methane/air. The characteristics and behavior of two distinct types of TJI mechanisms are discussed. The effect of four key parameters—initial pressure, nozzle diameter, pre-chamber equivalence ratio and pre-chamber volume—is carefully examined. An in-depth discussion of various competing pre-chamber processes on TJI highlights the necessity of non-dimensionalization. Through simple analytical observation, two major non-dimensional numbers—Reynolds and Damköhler—were identified. Correlations were developed to separate different TJI mechanisms based on the non-dimensional analysis. Finally, the crucial factors and challenges in developing a scalable TJI system are addressed. The purpose of this study is to provide insights and guidelines on TJI fundamentals to enable the design and optimization of an efficient and reliable pre-chamber system.

2 Governing Non-dimensional Equations

The non-dimensional governing equations for compressible, reacting flow are explored to identify the non-dimensional numbers associated with TJI. Table 1 shows the dimensional and non-dimensional form of conversation equations—continuity, momentum, energy, species and ideal gas law. Appropriate reference variables are used for non-dimensionalization. The detailed derivation of the non-dimensional

Table 1 Governing equations for compressible, reacting flow in dimensional and non-dimensional form

Equation	Dimensional form	Non-dimensional form	
Continuity	$\frac{\partial \rho}{\partial t} + u.\nabla\rho = \rho\nabla.u$	$\widetilde{\nabla}.\widetilde{\vec{u}} = \frac{1}{\mathrm{Re\,Pr}}\widetilde{\nabla}^2\widetilde{T} + \mathrm{Da}\sum_{i=1}^{N}\frac{\widetilde{h}_i^0}{\widetilde{T}}\dot{\widetilde{\omega}}_i'$	(1)
Momentum	$\rho\left(\frac{\partial \vec{u}}{\partial t} + \vec{u}.\nabla\vec{u}\right) =$ $-\nabla p_1 + \nabla.\mu\left(\nabla\vec{u} + \vec{u}^{\mathrm{T}} - \frac{2}{3}(\nabla.\vec{u})\mathbb{I}\right)$	$\frac{\partial \widetilde{\vec{u}}}{\partial \widetilde{t}} + \widetilde{\vec{u}}.\widetilde{\nabla}\widetilde{\vec{u}} =$ $-\frac{1}{\widetilde{\rho}}\widetilde{\nabla}\widetilde{p}_1 + \frac{\tilde{\nu}}{\mathrm{Re}}\left(\widetilde{\nabla}^2\widetilde{\vec{u}} + \frac{1}{3}\widetilde{\nabla}\left(\widetilde{\nabla}.\widetilde{\vec{u}}\right)\right)$	(2)
Energy	$\rho c_p\left(\frac{\partial T}{\partial t} + \vec{u}.\nabla T\right) = \nabla.\lambda T +$ $\sum_{i=1}^{N} h_i^0\,\dot{\omega}_i - \nabla.\rho T\sum_{i=1}^{N} c_{p,i}Y_iV_i +$ $\frac{\partial p_0}{\partial t}$	$\frac{\partial \widetilde{T}}{\partial \widetilde{t}} + \widetilde{\vec{u}}.\widetilde{\nabla}\widetilde{T} =$ $\frac{\tilde{\alpha}}{\mathrm{Re\,Pr}}\widetilde{\nabla}^2\widetilde{T} + \mathrm{Da}\sum_{i=1}^{N}\widetilde{h}_i^0\,\dot{\widetilde{\omega}}_i'$	(3)
Species	$\rho\left(\frac{\partial Y_i}{\partial t} + \vec{u}.\nabla Y_i\right) =$ $-\nabla.\rho Y_iV_{di} + \dot{\omega}_i \;\; i = 1, 2, \ldots, N$	$\frac{\partial \widetilde{Y}_i}{\partial \widetilde{t}} + \widetilde{\vec{u}}.\widetilde{\nabla}\widetilde{Y}_i =$ $\frac{\widetilde{\mathbb{D}}}{\mathrm{Re\,Sc}}\widetilde{\nabla}^2\widetilde{Y}_i + \mathrm{Da}\,\dot{\widetilde{\omega}}_i' \;\; i = 1, 2, \ldots, N$	(4)
Ideal gas	$p = \rho\mathrm{R}T$	$1 = \tilde{\rho}\widetilde{T}$	(5)

equations can be found in [35, 36] and hence is not elaborated here. The first set of equations in Table 1 describes these conversation equations in the dimensional form where $\vec{u}$ is velocity field, T is temperature, Y is mass fraction, p_0 is thermodynamics pressure, p_1 is hydrodynamic pressure, V_d is diffusion velocity, ρ is density, h^0 is the heat of formation, $\dot{\omega}$ is the rate of production, μ is dynamic viscosity, λ is heat conductivity, c_p is specific heat capacity, subscript i denotes ith species. Non-dimensional equivalence of each equation in the dimensional form is written next to it. All non-dimensional variables are denoted using $\widetilde{A}$ tildes. The additional quantities introduced in the non-dimensional form are kinematic viscosity, ν, thermal diffusivity, α and diffusion coefficient, $\mathbb{D}$.

Four non-dimensional numbers emerge from the non-dimensionalization—Reynolds number, Re, Prandtl number, Pr, Schmidt number, Sc and Damköhler number, Da. For the sake of simplicity, detailed species transport was neglected, and a global, single-step reaction mechanism was considered. This implies that all species have an identical binary diffusion coefficient, specific heat capacity and molecular weight. Moreover, all dynamic transport coefficients, μ, λ, c_p, and $\rho\mathbb{D}$ are assumed to be independent of temperature, and kinematic transport coefficients, α, $\mathbb{D}$ and ν, are directly proportional to the temperature. This suggests that $\tilde{\alpha} = \widetilde{\mathbb{D}} = \tilde{\nu} = \widetilde{T}$. Hence, we can further assume unity Schmidt ($\mathrm{Sc} = \tilde{\nu}/\widetilde{\mathbb{D}}$) and Prandtl ($\mathrm{Pr} = \tilde{\nu}/\tilde{\alpha}$) number. So, the remainder two non-dimensional numbers are Reynolds number and Damköhler number.

$$\mathrm{Re} = \frac{\rho u d}{\mu} \tag{6}$$

$$\mathrm{Da} = \frac{t_\mathrm{fluid}}{t_\mathrm{chemical}} = \frac{s_\mathrm{L} l_\mathrm{int}}{u'\delta_\mathrm{flame}} \tag{7}$$

where d is characteristic length scale (nozzle diameter), t is time, s_L is laminar flame speed, l_{int} is integral length scale, u' is fluctuating component of velocity, δ_{flame} is flame thickness, t_{fluid} is the fluid timescale, and $t_{chemical}$ is the chemical timescale. s_L and δ_{flame} were estimated using Chemkin [37] Premix module. Full width half maximum (FWHM) of CH concentration was considered as the laminar flame thickness. The fluctuating component of velocity was determined using $u' = \overline{\vec{u}}.TI$, where TI is the turbulent intensity, and $\overline{A}$ denotes the mean. Reynolds number-dependent empirical correlations [38] are used to calculate the turbulent intensity of the reacting jet. Integral length scale was estimated using correlations for compressible round jets [39, 40].

3 Experimental Methods

All experiments were performed in a custom-made, optically accessible, dual-chamber–pre-chamber and main chamber configuration. The detailed description of the experimental apparatus can be found in [25, 26]. Hence, for readers' interest, only a brief description is presented here. A cylindrical (diameter 38.1 mm, length 88.9 mm) stainless steel (SS316) pre-chamber was placed on top of a rectangular (length 304.8 mm, 152.4 mm × 152.4 mm cross section) carbon steel (C-1144) main chamber connected by a nozzle of diameters ranging from 0.5 to 10 mm ($d = 0.5$, 0.75, 1, 1.5, 2, 2.5, 3, 4, 5, 7, 10 mm). The schematic of the experimental setup is shown in Fig. 1. Four different pre-chamber volumes of 3.5, 5, 10 and 100 cc were used to produce pre-chamber to main chamber volume ratio of 0.07, 0.1, 0.2 and 2%, respectively. A 25-micron thick aluminum diaphragm, scored at the center for easy and repeatable rupture, was employed to prevent mixing between pre-chamber and main chamber mixtures of dissimilar equivalence ratio. The diaphragm was replaced after every test. Industrial grade methane (purity 99.99%) was mixed with air upstream before introducing the premixed mixture to the test chambers. Note the typical molar concentration of methane in natural gas ranges between 87 and 98%. The pre-chamber was kept stoichiometric unless otherwise stated. The main chamber equivalence ratio was varied from nearly stoichiometric ($\phi = 0.95$) to the lean limit. The fuel/air mixture in both the chambers was heated using built-in heating cartridges (Omega HDC001-series) to 500 K. The pre-chamber mixture was ignited using a resistive-type Iridium Bosch spark plug driven by a custom-made capacitor discharge ignition (CDI) coil capable of delivering 90 mJ of energy per pulse.

To visualize main chamber ignition and flame propagation, four optical UV grade quartz (type GE124) windows (height 139.7 mm, width 88.9 mm, thickness 19.05 mm) were installed in the main chamber body. Note that the dual-chamber configuration shown in Fig. 1, only the main chamber was optically accessible. The front and back viewing windows enabled direct infrared and OH*/CH* chemiluminescence imaging. Two orthogonally installed side windows allowed a z-type schlieren imaging of the ignition and flame propagation inside the main chamber. Two Kulite XTEL-190 high-temperature piezoelectric pressure transducers were used to

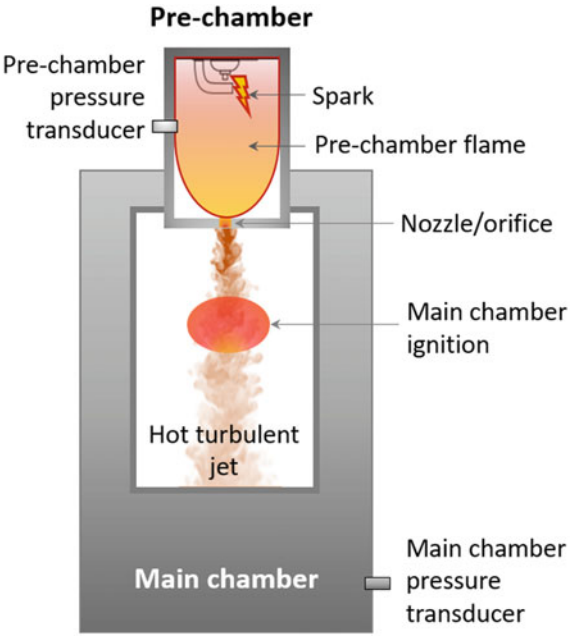

Fig. 1 Schematic of the TJI experimental setup

measure the pre-chamber and main chamber pressure. The pressure data was post-processed to obtain the pre-chamber mass flow rate and jet velocity. Two K-type thermocouples were positioned at the top and bottom of the chamber to monitor the mixture temperature to minimize the effect of natural convection in the 304.8-mm-tall main chamber. A thick polymer insulation jacket was wrapped around the apparatus to reduce heat loss. After each test, both the chambers were filled up and vacuum purged using desiccated bottled air to assure no residual stays from the previous test. In engine operation, the residual gas fraction (RGF) plays a key role in stabilizing combustion via increased charge temperature. In the present study, the RGF was zero.

4 Results and Discussion

The results and discussion are divided into four sections. The first section discusses the behavior and characteristics of different types of TJI mechanisms. The second section talks about the effects of various thermodynamic and geometric parameters on TJI. The third section examines key pre-chamber processes and correlations based on non-dimensional numbers associated with TJI. The concluding section explores the possibility and potential challenges to build a scalable TJI system in production engines.

4.1 Types of Ignition Mechanisms

Based on the presence of active radicals in the pre-chamber jet, two distinct TJI mechanisms exist, (a) jet (reacted jet) ignition and (b) flame (reacting jet) ignition [25, 27]. Simultaneous high-speed schlieren and OH* chemiluminescence imaging was used to classify jet and flame ignition mechanisms. The high-speed OH* imaging identified the presence of radicals in the turbulent jet. When the pre-chamber flame passed through a nozzle diameter that was too small, the active radicals such as O, OH*, CH* extinguished due to surface quenching of chain branching reactions and wall heat losses. Deprived of the active radicals, the pre-chamber turbulent jet contained only hot combustion products. Hence, the main chamber ignition relied on the mixing dynamics and heat transfer characteristics of the turbulent hot jet with the main chamber fuel/air mixture. The velocity of the turbulent jet was an important parameter in the jet ignition mechanism. A higher jet velocity ensured mixing but provided too little time for chemistry to occur in the main chamber. On the other hand, a jet too slow did not guarantee satisfactory mixing. Hence, the velocity of the turbulent jet had to be within a suitable range to warrant mixing as well as chemical reactions and heat transfer to occur between the jet and the main chamber fuel/air mixture. Since the jet velocity and temperature decayed and shear layer mixing increased at jet downstream, ignition in the main chamber never occurred too close or far away from the pre-chamber nozzle. Instead, the main chamber ignition always initiated from the side of the jet (i.e., mixing shear layer) at a downstream distance of 8–12 times the diameter of the nozzle [27, 28, 31]. Unlike the jet ignition, flame ignition occurred when active radicals of the pre-chamber flame survived wall quenching and aerodynamic stretch. Reaction flame fronts exposed to a highly turbulent flow field experience aerodynamic stretching imposed by the fluctuating nonuniform local velocities. The flame surface gets wrinkled and convoluted due to applied stretch and could extinct if the stretch is higher than the critical extinction stretch. The turbulent reacting jet consisted of radicals and flamelets. Flamelet concept assumes that the reaction zone is exceptionally thin and could be embedded within turbulent eddies such that each flamelet experiences a laminar flow. Turbulent jet filled with such flamelets-containing radicals in the reaction or post-reaction regimes is the source of flame ignition. Hence, flame ignition primarily was a radical-driven ignition phenomenon. The active radicals in the hot jet initiated the first hydrogen abstraction, and chain initiation reactions and the hot pre-chamber combustion products helped sustain these reactions.

Two different TJI mechanisms—jet ignition and flame ignition—show distinct ignition characteristics and early flame kernel behavior. Figure 2 illustrates the pre-chamber (dashed line) and main chamber (solid line) pressure history of jet and flame ignition of lean methane/air at 1 bar, 500 K. The pre-chamber was kept stoichiometric for the conditions shown in Fig. 2. A 25-μ thick aluminum diaphragm was placed between the pre-chamber and the main chamber to prevent mixing between the chambers kept at dissimilar equivalence ratios. Hence, the pre-chamber pressure profiles of jet and flame ignition are nearly identical.

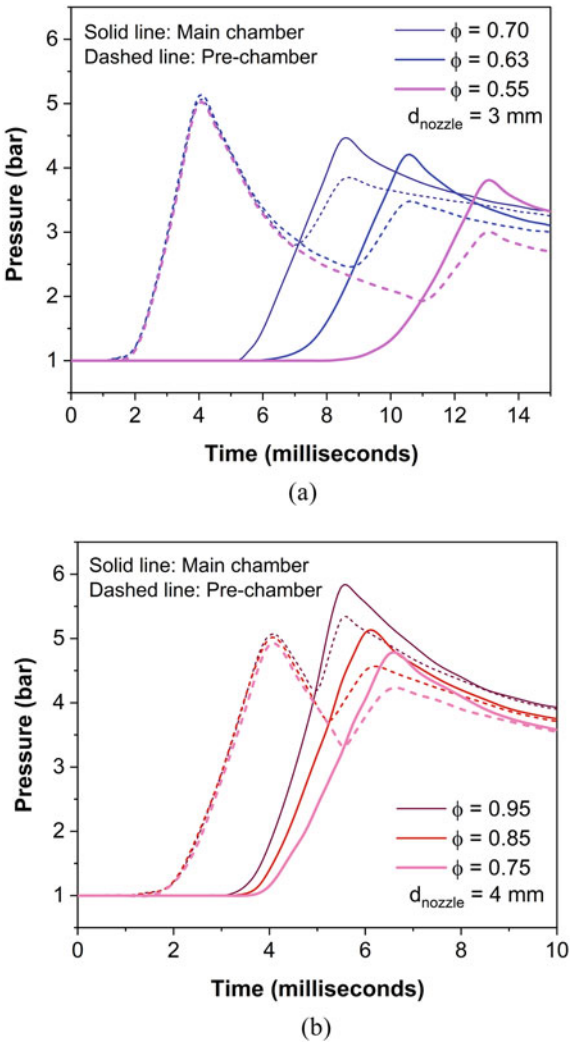

Fig. 2 Pressure history of the pre-chamber and main chamber for **a** jet ignition and **b** flame ignition of methane/air at 1 bar, 500 K

It is evident from Fig. 2 that compared to the jet ignition, flame ignition occurred at a higher equivalence ratio and for larger nozzle diameter. For an identical pre-chamber volume and thermodynamic conditions, flame with greater equivalence ratio had a higher adiabatic flame temperature and was likely to survive the excessive stretch and wall heat losses through a larger diameter nozzle. The flame passing behavior through the nozzle can be explained, estimating quenching distance. The quenching distance is the minimum separation distance between two surfaces, beyond which a flame cannot pass. The quenching distance of stoichiometric methane/air at 1 bar, 500 K, is 3.31 mm [41]. Since the nozzle diameter of 4 mm was larger than the quenching distance of the pre-chamber flame, the flame passed through the nozzle and entered

the main chamber in the form of a turbulent jet filled with radicals and flamelets. However, nozzle diameter of 3 mm was smaller than the quenching distance of the pre-chamber flame that led to flame extinction, and the ignition mechanism switched to jet ignition.

Jet ignition produced a longer ignition delay compared to flame ignition. For jet ignition, the turbulent hot jet had to wait for a favorable ignition condition to arise in terms of velocity, temperature and mixing. Note that the jet ignition always occurred by a decelerating turbulent jet. This would be discussed in detail in Sect. 4.2. For all the conditions presented in this study, the range of ignition delays for jet and flame ignition was 6.7–20 and 0.45–8.1 ms, respectively.

Another key performance metric for TJI was combustion repeatability. Each experiment was repeated five times to estimate the test to test variability by comparing ignition delay, ignition location and 10, 50 and 80% burn times. The results demonstrate (not shown here) that flame ignition was extremely repeatable with less than 2% test to test variability. However, jet ignition showed a noteworthy variability between tests, especially at the lean limit [28]. This could be a limiting factor that requires further attention while implementing TJI in engines.

4.2 Thermophysical and Geometric Parameters on TJI

There are several thermophysical and geometric parameters that influence TJI mechanisms. Table 2 lists different parameters and their effect on TJI processes. While the effect of some of these parameters can be understood intuitively, but for most cases, the intertwined effects possess significant difficulty toward a parametric understanding of TJI. For example, with the increase in initial pressure, quenching distance goes down, which helps the pre-chamber flame to pass through the nozzle leading to a flame ignition. However, increased pressure also reduces flame thickness, making the flame extremely susceptible to the aerodynamic stretch and hence weaker. Also, the reaction rates and turbulence–chemistry interactions add further complicacy to predict TJI behavior at elevated pressures.

In this study, the effect of four key TJI parameters—nozzle diameter, initial pressure, pre-chamber volume and pre-chamber equivalence ratio, has been discussed in detail. Figure 3 shows a map of TJI outcomes as a function of nozzle diameter and initial pressure for methane/air at 500 K, $\phi_{\text{pre}} = 1$, $\phi_{\text{main}} = 0.75$. The gray region represents non-ignition cases, while the blue and red regimes represent jet and flame ignition cases, respectively. Figure 3 indicates that at 1 bar initial pressure, nozzle diameter of 1.5 mm or smaller did not result in ignition. However, the 1.5 mm diameter nozzle was able to ignite at a slightly higher pressure of 1.5 bar. For a fixed nozzle diameter, with an increase in pressure, the TJI mechanism shifts from jet to flame ignition. The 1.5 mm nozzle initiated the main chamber ignition via jet ignition mechanism for a range of pressures 1.5–4 bars. However, at 5 bar, the main chamber ignition mechanism shifted from jet to flame ignition. Above a nozzle diameter of 4 mm, all TJI was via flame ignition.

Table 2 Key thermophysical and geometric parameters and their effects on TJI mechanisms

Thermophysical parameters	
Initial pressure, p_i	Quenching distance decreases (flame thickness decreases) with increasing pressure allowing the flame to pass through smaller orifice without quenching, $p_i \downarrow$ jet ignition, $p_i \uparrow$ flame ignition
Initial temperature, T_i	Higher initial charge temperature (below autoignition limit) adds to the cost of intake heating but leads to stable combustion
Pre-chamber equivalence ratio, ϕ_{pre}	For active (direct fueling) pre-chamber, near stoichiometric ϕ_{pre} has higher adiabatic flame temperature, suitable for flame ignition. ϕ_{pre} controls the flame strength and TJI mechanisms to a certain extent
Main chamber equivalence ratio, ϕ_{main}	Decreasing ϕ_{main} reduces ignition probability in the main chamber; however, it does not affect the ignition mechanism
Turbulence intensity	Higher turbulent intensity enhances mixing, favorable for TJI. Excessive turbulence can also inhibit reactions and increases undesirable effects such as flame stretch
Residual gas fraction (RGF)	RGF plays a vital role in engine operation [11, 12]. A higher RGF leads to increased charge temperature but also makes the pre-chamber lean and difficult to ignite
Geometric parameters	
Nozzle diameter, d	Smaller diameter nozzle imposes a higher stretch rate and excessive wall heat losses; hence, flame extinction becomes more likely. $d \downarrow$ jet ignition, $d \uparrow$ flame ignition
Pre-chamber spark location	The pre-chamber spark location affects the pre-chamber flame behavior. Ignition pattern and delay times can vary based on the spark location
Pre-chamber volume, length-to-diameter (L/D) ratio, volume to area ratio	These parameters contribute to total heat release, wall heat losses and the shape of the pre-chamber flame. The heat release to heat loss ratio is lower for a pre-chamber with a smaller volume. L/D ratio controls the pre-chamber flame front shape [26, 42, 43]
Pre-chamber to main chamber volume ratio, V_{pre}/V_{main}	V_{pre}/V_{main} for TJI can vary between 0.1 and 5% [23, 44]. A smaller ratio limits the operating range of TJI, and a larger ratio becomes unpractical due to space constraints in the engine

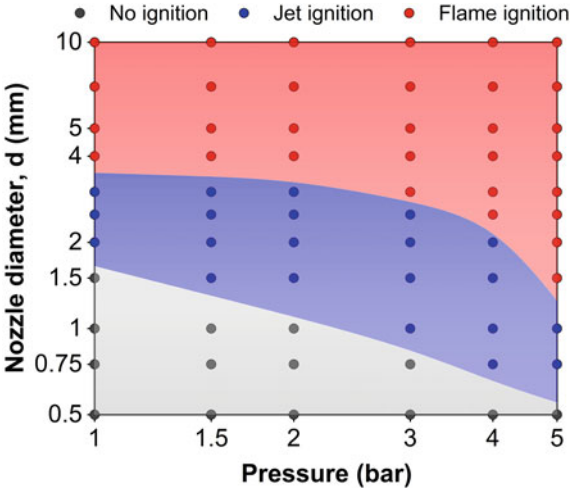

Fig. 3 Effect of nozzle diameter and initial pressure on TJI mechanisms of methane/air

Figure 4 illustrates the effect of nozzle diameter and pre-chamber equivalence ratio on different TJI mechanisms of methane/air at 500 K, $P_i = 2$ bar, $\phi_{main} = 0.75$. Note that the current study employed an active (externally fueled) pre-chamber to independently vary the pre-chamber equivalence ratio. In a passive pre-chamber, controlling and monitoring the temporal and spatial variation of the pre-chamber equivalence ratio would add further challenges.

As expected, for a fixed ϕ_{pre}, increasing the nozzle diameter shifted the TJI mechanism from jet ignition toward flame ignition. With a nozzle diameter above 7 mm, TJI mechanisms became insensitive to the pre-chamber equivalence ratio. Furthermore, Fig. 4 exemplifies an interesting and somewhat intuitive behavior of a pre-chamber.

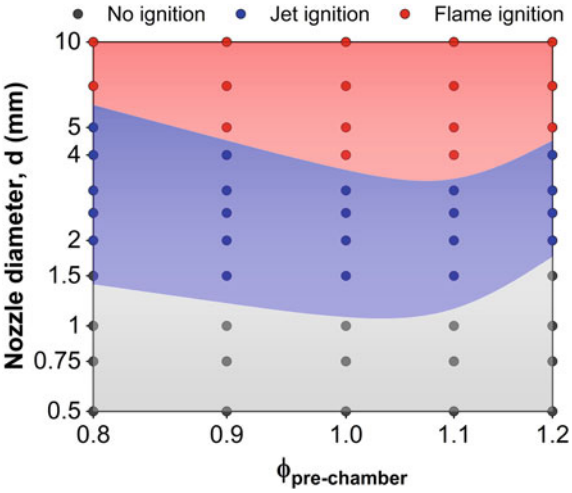

Fig. 4 Effect of nozzle diameter and pre-chamber equivalence ratio on TJI mechanisms of methane/air

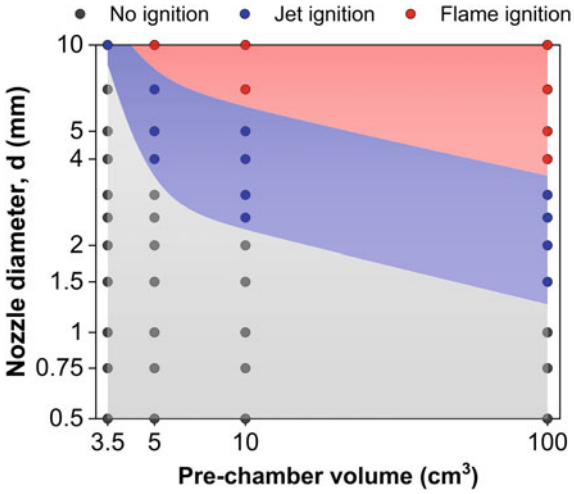

Fig. 5 Effect of nozzle diameter and pre-chamber volume on TJI mechanisms of methane/air

The optimum value of ϕ_{pre} lied between $1.0 < \phi_{pre}|_{optimum} < 1.1$. For methane, the peak adiabatic flame temperature and laminar flame speed occur in a slightly rich mixture than stoichiometric. Hence, a slightly rich pre-chamber flame could sustain greater heat losses and aerodynamic stretch.

Figure 5 shows the effect of pre-chamber volume and nozzle diameter on TJI mechanisms of methane/air at 500 K, $P_i = 2$ bar, $\phi_{pre} = 1$, $\phi_{main} = 0.75$. Note that the 100 cc pre-chamber was 2% of the main chamber volume. Hence, 10, 5 and 2.5 cc pre-chambers were 0.2, 0.1 and 0.07% of the main chamber volume, respectively. The idea behind using such small pre-chambers was to find the minimum pre-chamber to main chamber volume ratio that could lead to successful TJI. The only successful ignition by the 3.5 cc (pre-chamber volume 0.07% of the main chamber) pre-chamber was via jet ignition mechanism for the largest nozzle diameter of 10 mm. The 3.5 cc pre-chamber volume was too small to contain enough energy for TJI and suffered high wall heat losses. The pre-chamber volumes of 5 and 10 cc (pre-chamber volume 0.1 and 0.2% of the main chamber, respectively) were progressively better than one another but failed to ignite below a nozzle diameter of 2 mm. 100 cc (pre-chamber volume 0.1% of the main chamber) pre-chamber volume was the best among the other pre-chambers in terms of ignitability. Hence, a 100 cc pre-chamber was chosen to use throughout this study. For a fixed pre-chamber volume, with an increase in nozzle diameter, the TJI mechanism shifted from jet to flame ignition.

4.3 Non-dimensional Numbers in TJI

As discussed in Sect. 2, the two key non-dimensional numbers associated with TJI of premixed methane/air are Reynolds and Damköhler number. Note that the Lewis

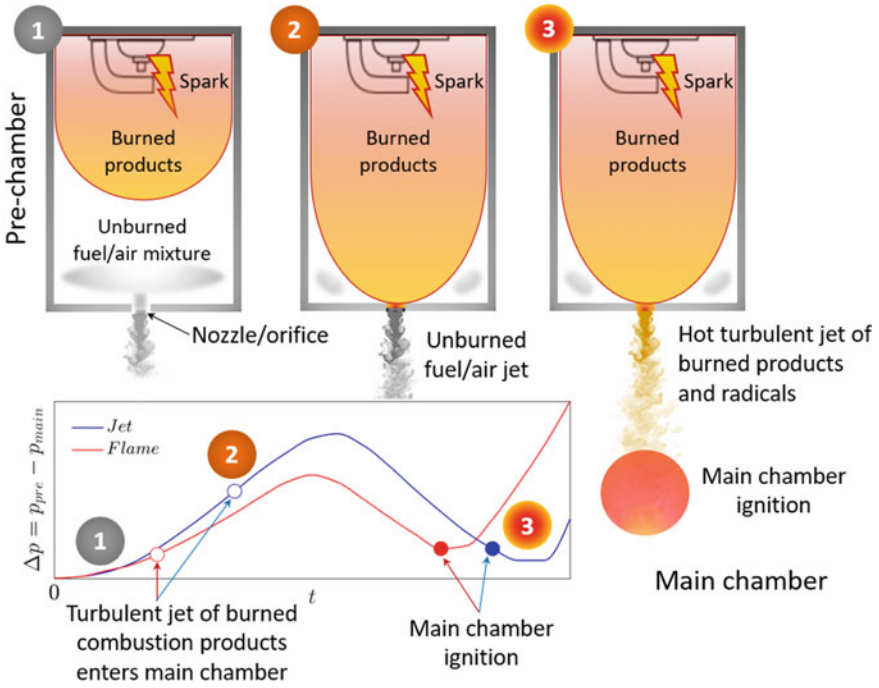

Fig. 6 Schematic of the three key instances in TJI and their occurrence on the pre-chamber pressure differential, $\Delta p = p_{\text{pre}} - p_{\text{main}}$, profile

number, which is defined as the ratio of the Schmidt and the Prandtl number, of methane is close to unity for the range of equivalence ratio, $\phi = 0.55-0.95$, discussed in the present study. However, for other fuels such as hydrogen and propane, the Lewis number is much lower and great than unity, respectively. For a mixture with non-unity Lewis number, the Lewis number effect could play a vital role in influencing the thermal and mass diffusion of the turbulent jet products into the lean premixed main chamber mixtures. Reynolds and Damköhler number provide an excellent tool to identify different TJI mechanisms, ignition regimes and predict ignition characteristics. However, these two numbers vary within the turbulent hot jet, both spatially and temporally. Experimentally, it was extremely challenging to measure quantities associated with these two non-dimensional numbers such as velocity, turbulent intensity, length scales, flame thickness, kinematic viscosity, within the entire jet throughout its lifetime. The author would argue that the complete knowledge of spatially and temporally resolved pre-chamber jet is unnecessary except for a handful of key moments in the jet lifetime. To understand the key instances and critical locations of the pre-chamber jet, it is imperative to have a comprehensive understanding of the physical processes happening in TJI.

Figure 6 illustrates the three key instances in TJI. These key instances are also marked on the time evolution plot of the pressure differential between the pre-chamber and main chamber, $\Delta p = p_{\text{pre}} - p_{\text{main}}$. At $t = 0$, the spark ignited the quiescent pre-chamber fuel/air mixture. As the hemispherical flame started to propagate inside the pre-chamber, it pushed out the unburned pre-chamber fuel/air through the nozzle. The 'instance $1'$ represented the event when the pre-chamber started issuing an unburned fuel/air jet. However, as the pre-chamber flame propagated further, the burned combustion products reached the nozzle, and at 'instance $2'$, the unburned fuel/air jet suddenly switched into a turbulent jet comprised of hot burned products that might or might not contain active radicals. The open markers on the pressure differential curve indicate the 'instance 2.' Subsequently, the pre-chamber hot jet of burned combustion products kept going until they ignited the main chamber mixture. The 'instance $3'$ indicates the main chamber ignition and is denoted by closed/filled markers on the pressure differential plot in Fig. 6.

Time evolution of eight important parameters and scalars associated with TJI, namely pre-chamber pressure differential, Δp, density, ρ, mean velocity, u, temperature, T, mass flow rate, $\dot{m} = \rho u A$, mass flux, $\dot{m}/A = \rho u$, jet momentum, $J = \rho u^2 A$, and reaction rate, $\dot{\omega}$, were estimated at the nozzle exit for a representative jet, and flame ignition cases are illustrated in Fig. 7. The pre-chamber pressure differential increased as the pre-chamber combustion progressed in time and then started to decline due to the wall heat losses and in the form of a turbulent hot jet. The density at the nozzle exit dropped suddenly since the density of the burned product was nearly an order of magnitude lower than the unburned fuel/air mixture. The sharp discontinuity in the pre-chamber pressure affected several other parameters,

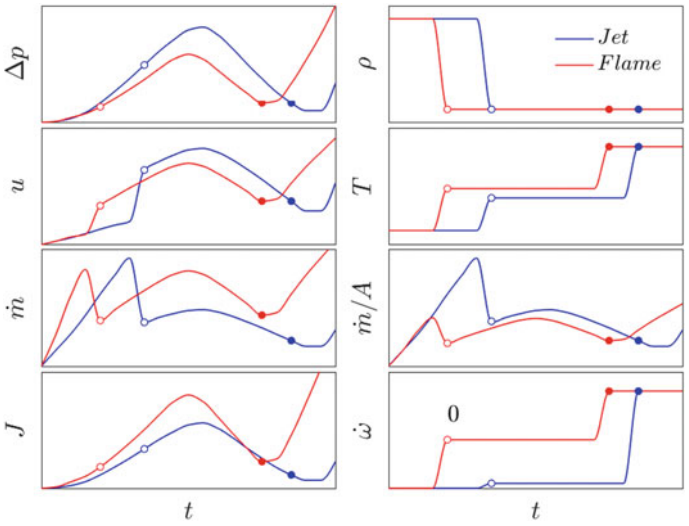

Fig. 7 Time evolution of key parameters and scalars associated with TJI. Open markers denote the transition from unburned to burned. Closed markers indicate ignition in the main chamber

including velocity, mass flow and reaction rates. The jet velocity at the nozzle exit $u \propto \sqrt{\Delta p/\rho}$ increased, and mass flow rate $\dot{m} = \rho u A$ dropped abruptly. Over time, the jet velocity reached the maximum and then started to drop. The main chamber ignition occurred when the jet velocity was declining, i.e., decelerating. TJI always occurred by a decelerating jet. The main chamber ignition created a pressure rise that led to backflow into the pre-chamber.

The temperature jumped twice—as the pre-chamber combustion products started flowing into the main chamber and as the main chamber ignited. Note that the nozzle flow area of flame ignition was twice compared to the jet ignition resulted in a higher mass flow rate for flame ignition. However, the mass flux $\rho u = \dot{m}/A$ (independent of the flow area) of the burned products from jet and flame ignition was comparable. Like the temperature, the reaction rate increased twice. The first increase in the reaction rate was more noticeable for flame ignition due to the presence of active radicals. The second jump in the reaction rate happened due to the main chamber ignition. For both the ignition mechanisms, the jet momentum during the main chamber ignition was much lower than its peak value. This observation was consistent for all the experiments performed in this study.

The competing effect of mixing and chemistry was difficult and, at times, nearly impossible to separate by examining the physical quantities and scalars for every single test condition. Hence, the focus of the present study was to find correlations among the non-dimensional numbers associated with different types of TJI mechanisms. Figure 8 exemplifies one ignition and two non-ignition test cases to explain the concept of critical Reynolds and Damköhler number associated with TJI. For every test condition, a pair of critical Reynolds number, $\mathrm{Re_{cr}}$, and Damköhler number, $\mathrm{Da_{cr}}$, needed to be satisfied for TJI to occur. For successful TJI, the jet Reynolds and

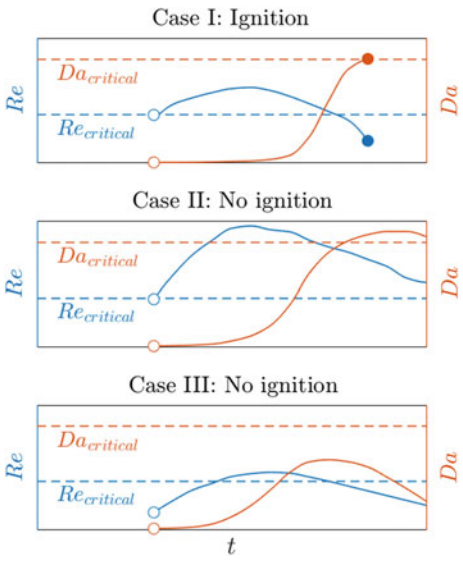

Fig. 8 Critical Reynolds and Damköhler number for typical ignition and non-ignition cases

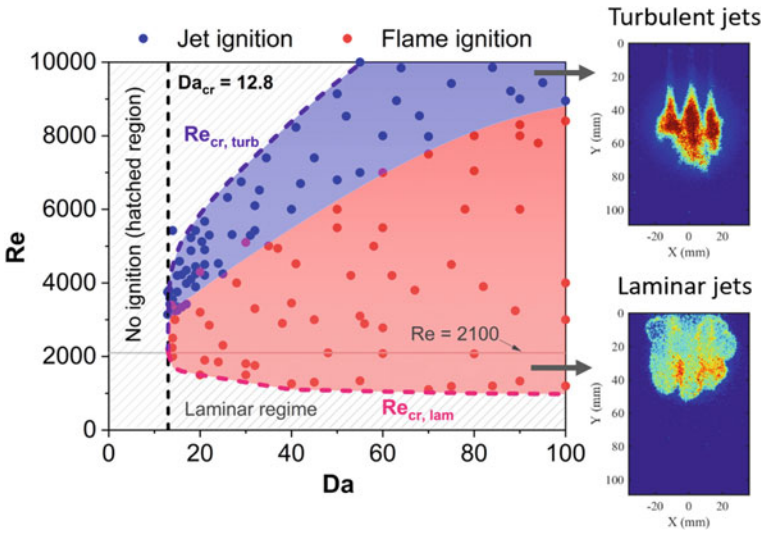

Fig. 9 Critical Reynolds and Damköhler numbers in TJI

Damköhler numbers must follow $Re \leq Re_{cr}$ and $Da \geq Da_{cr}$. The fulfillment of these two criteria resulted in the ignition, as shown in Case I. However, one of the two criteria was not satisfied for Case II and III. Case II illustrates that a strongly reacting jet with extremely high velocity was able to exceed the Da_{cr}, but failed to satisfy $Re < Re_{cr}$. Case III represents a situation with a moderate velocity, weakly reacting jet that was able to achieve $Re < Re_{cr}$, but failed to attain $Da > Da_{cr}$. Hence, ignition did not occur for Case II and III.

All successful TJI outcomes are plotted on a Re versus Da diagram, as shown in Fig. 9. The Reynolds and Damköhler numbers were estimated at the onset of the main chamber ignition (denoted by closed markers in Figs. 7 and 8). Jet and flame ignition occupied two separate regimes in this diagram with negligible overlap. Note that the horizontal line of $Re = 2100$ separates the laminar and transitional/turbulent regimes. Two representative images of TJI by laminar and turbulent jets are shown in the inset of Fig. 9. The ignition characteristics by laminar flame jets were very different than by a turbulent reacting/reacted jet. As soon as the laminar flame jets entered the main chamber, it immediately ignited the mixture, and a finger-shaped, laminar looking flame front propagation was observed. Further details of such laminar TJI can be found in [26].

The interesting and practical part of the Re–Da diagram is the transitional/turbulent region, where the most TJI cases fall. It is evident from Fig. 9 that the jets responsible for successful flame ignition possessed a lesser Re. An increase in Re extinguished the reactions when the flame passed through the nozzle due to an increased flame stretch and heat losses, which shifted the TJI mechanism from flame to jet ignition.

TJI never happened for a Damköhler number less than 12.8 for methane/air, as shown by the black vertical dashed line. Hence, Da = 12.8 is considered as the critical Damköhler number. However, two critical Reynolds numbers can be estimated based on the laminar or transitional/turbulent jet. Unlike Da_{cr}, the Re_{cr} depends on the system. Equations 8–10 correlates the critical Reynolds number as a function of Damköhler number.

$$Da_{cr} \geq 12.8 \tag{8}$$

$$Re_{cr,turb} \leq 1554(Da - 7.2)^{0.493} \tag{9}$$

$$Re_{cr,lam} \geq 973 + 1487 \exp\left(-\frac{Da}{18.7}\right) + 6.1 \exp\left(-\frac{Da}{0.46}\right) \tag{10}$$

For successful ignition by a turbulent reacting/reacted jet, both the correlations for Da_{cr} and Re_{cr} (Eqs. 8 and 9) must be met simultaneously.

4.4 Scalability Aspect of TJI

Pre-chamber TJI poses a viable alternative to conventional spark ignition by extending the lean limit and improving combustion efficiency while reducing emission. So far, most studies on TJI have demonstrated its superiority over the spark ignition at a handful of discretely selected operating points. However, to emerge as a viable and extensive substitute for the existing ignition system, TJI must demonstrate robustness and scalability. The scalability of an ignition system depends on the size and type of the engine, e.g., large bore natural gas, heavy-duty diesel, the light-duty gasoline engine, etc. Once the pre-chamber is optimized for a few chosen operating points of a certain engine type, the major question remains—How is the performance and scalability of a TJI system over the engine's entire load/speed map?

Figure 10 shows the ignition and non-ignition regimes of a pre-chamber TJI system on a pressure versus residence time plot. The residence time is the time delay between the main chamber ignition and the first instance of the turbulent jet with pre-chamber combustion products entering the main chamber. Typical engine speed and load values are also added to Fig. 10. TJI was successfully elsewhere except two corners of the load/speed map—high-speed, low load and low-speed, high load, highlighted in gray. At a higher rpm, too short of available cycle time for the compete burn was difficult for TJI. Similarly, achieving a high load at a lower speed was challenging using a TJI system. Additional strategies are required to overcome these problems, such as for low-load, high-speed conditions, increasing charge reactivity via fuel additives enabling end-gas autoignition, usage of fuel-rich active pre-chamber to shorten ignition delays via charge stratification, intake heating

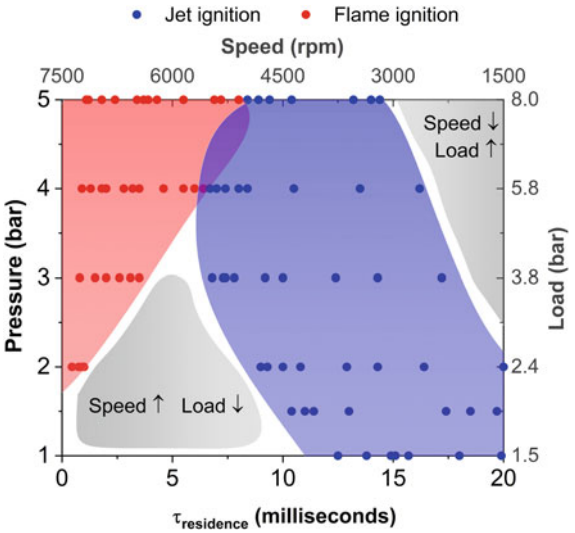

Fig. 10 Ignition and non-ignition regimes of a TJI system on a pressure versus residence time map. A typical engine load/speed information is added to illustrate the scalability aspect of TJI

and throttling. For low-speed, high-load conditions, split fueling, intake boosting to achieve high load via enhanced energy density, spark advance, etc.

Combined with advanced combustion strategies, TJI has the capacity to serve as a scalable alternative ignition system to modern internal combustion engines. Noteworthy progress has been made exploring the TJI fundamentals. Conclusively, the TJI system should be considered for both light-duty and heavy-duty engine applications.

5 Conclusions

The present study discussed the fundamental processes involved in TJI and their effects on distinct types of ignition mechanisms. The influence of major thermophysical and geometric parameters on TJI mechanisms was discussed in detail. Ignition correlations based on two key non-dimensional numbers were proposed. Finally, the scalability of the TJI system was examined. Major findings are as follows:

- Active radicals played a key role in determining TJI mechanisms. Depending on the radical concentration in the turbulent jet, ignition could occur either via (a) flame ignition (reacting jet)—a turbulent jet full of radicals such as O, OH, CH* and flamelets or (b) jet ignition—a turbulent jet deprived of any active radicals consisted of pre-chamber combustion products only. For an extremely narrow range of operating conditions, TJI could happen via a laminar flame jet.
- The temperature, velocity, density, mass flux, momentum and reaction rates of the pre-chamber turbulent jet varied spatially and temporally. However, the ignition always initiated by the decelerating part of the transient jet, where the jet momentum was much lower compared to its peak value.

- Four key parameters associated with TJI—nozzle diameter, initial pressure, pre-chamber volume and pre-chamber equivalence ratio—significantly impacted the ignition behavior and mechanisms. The effect of nozzle diameter was strongly dependent on the initial pressure. For a fixed pressure, increasing the nozzle diameter shifted the ignition mechanism from jet to flame ignition. For the same nozzle diameter, higher initial pressure led to flame ignition. The minimum nozzle diameter for successful TJI was 0.75 mm. Compared to other pre-chamber volumes, a pre-chamber volume of 100 cc that created a pre-chamber to main chamber volume ratio of 2% had the greatest likelihood of ignition. A pre-chamber equivalence ratio between 1 and 1.1 was optimum for methane/air.
- Reynolds number and Damköhler number were two key non-dimensional numbers governing the ignition probability and mechanisms. The critical Damköhler number for methane/air was 12.8. The critical Reynolds number was a function of the Damköhler number. For successful TJI, both the criteria for critical Reynolds and Damköhler number must be satisfied simultaneously.

Pre-chamber TJI emerges as a practical substitute to conventional spark ignition, offering extended lean limit, improved combustion efficiency and reduced emission. TJI has the potential to be a scalable system. However, two difficult ignition regimes exist—low-speed, high-load and high-speed, low-load conditions. Additional combustion strategies coupled with TJI could overcome regimes with difficult ignitability. The present study provides fundamental knowledge on TJI that would enable pre-chamber optimization for future internal combustion engines.

Acknowledgements The author would like to thank Dr. Isaac Ekoto, Dr. Prashant Rai, Dr. Dario Lopez Pintor and Dr. Gerald Genz from Sandia National Laboratories, Dr. Riccardo Scarcelli and Dr. Ashish Shah from Argonne National Laboratory and Dr. Li Qiao from Purdue University for helpful discussions related to turbulent jet ignition. Partial financial support was provided by Caterpillar, Inc.

References

1. Dunn-Rankin, D. (2008). *Lean combustion: Technology and control* (xi, 261 p., 8 p. of plates.). Amsterdam; Boston: Academic Press.
2. Gheorghiu, V. (2012). Ultra-downsizing of internal combustion engines. In A. Subic, J. Wellnitz, M. Leary, & L. Koopmans (Eds.), *Sustainable automotive technologies.* Berlin: Springer.
3. Lecointe, B., & Monnier, G. (2003). Downsizing a gasoline engine using turbocharging with direct injection. SAE Technical Paper 2003-01-0542.
4. Agarwal, A. K., Gupta, J. G., Sharma, N., & Singh, A. P. (Eds.). (2019).*Advanced engine diagnostics. Energy, Environment, and Sustainability*. Singapore: Springer.
5. Kellermayr, G., Schutting, E., & Mitterecker, H. (2019). Turbocharging of engines with low cylinder numbers: A thermodynamic consideration. *Automotive and Engine Technology, 4*, 153–167.

6. Ceviz, M. A., & Kaymaz, I. (2005). Temperature and air–fuel ratio dependent specific heat ratio functions for lean burned and unburned mixture. *Energy Conversion and Management, 46,* 2387–2404.
7. Zhao, L., & Wang, D. (2020). Combined effects of cooled EGR and air dilution on butanol-gasoline TGDI engine operation, efficiency, gaseous, and PM emissions. *ACS Omega, 5*(12), 6556–6565.
8. Agarwal, R. A., Agarwal, A. K., Gupta, T., & Sharma, N. (Eds.). (2019). *Pollutants from energy sources. Energy, Environment, and Sustainability*. Singapore: Springer.
9. Dec, J. E. (2009). Advanced compression-ignition engines—Understanding the in-cylinder processes. *Proceedings of the Combustion Institute, 32*(2), 2727–2742.
10. Weinrotter, M., Wintner, E., Iskra, K., Neger, T., Olofsson, J., Seyfried, H., Aldén, M., Lackner, M., Winter, F., Vressner, A, Hultqvist, A., & Johansson, B. (2005). Optical diagnostics of laser-induced and spark plug assisted HCCI combustion. SAE Technical Paper 2005-01-0129.
11. Biswas, S., & Ekoto, I. (2019). Detailed investigation into the effect of ozone addition on spark assisted compression ignition engine performance and emissions characteristics. SAE Technical Paper 2019-01-0966.
12. Biswas, S., & Ekoto, I. (2019). Spark assisted compression ignition engine with stratified charge combustion and ozone addition. JSAE 20199089.
13. Biswas, S., & Ekoto, I. (2019). Ozone added spark assisted compression ignition. In A. P. Singh, N. Sharma, R. A. Agarwal, & A. K. Agarwal (Eds.), *Advanced combustion techniques and engine technologies for the automotive sector*. Singapore: Springer.
14. Rapp, V., Killingsworth, N., Therkelsen, P., & Evans, R. (2016). *Lean-burn internal combustion engines* (pp. 111–146).
15. Shurpali, N., Agarwal, A. K., & Srivastava, V. K. (Eds.). (2019). *Greenhouse gas emissions: Challenges, technologies and solutions. Energy, Environment, and Sustainability*. Singapore: Springer.
16. Zádor, J., Taatjes, C. A., & Fernandes, R. X. (2011). Kinetics of elementary reactions in low-temperature autoignition chemistry. *Progress in Energy and Combustion Science, 37*(4), 371–421.
17. Ghoniem, A. F., Oppenheim, A. K., & Chen, D. Y. (1983). *Experimental and theoretical study of combustion jet ignition*. California University.
18. Pitt, P. L., Ridley, J. D., & Clemilnts, R. M. (2007). An ignition system for ultra lean mixtures. *Combustion Science and Technology, 35*(5–6), 277–285.
19. Yamaguchi, S., Ohiwa, N., & Hasegawa, T. (1985). Ignition and burning process in a divided chamber bomb. *Combustion and Flame, 59*(2), 177–187.
20. Sadanandan, R., Markus, D., Schießl, R., Maas, U., Olofsson, J., Seyfried, H., et al. (2007). Detailed investigation of ignition by hot gas jets. *Proceedings of the Combustion Institute, 31*(1), 719–726.
21. Gholamisheeri, M., Thelen, B. C., Gentz, G. R., Wichman, I. S., & Toulson, E. (2016). Rapid compression machine study of a premixed, variable inlet density and flow rate, confined turbulent jet. *Combustion and Flame, 169,* 321–332.
22. Toulson, E., Huisjen, A., Chen, X., Squibb, C., Zhu, G., Schock, H., & Attard, W. P. (2012). Visualization of propane and natural gas spark ignition and turbulent jet ignition combustion. *SAE International Journal of Engines, 5*(4), 1821–1835.
23. Shah, A., Tunestal, P., & Johansson, B. (2015). Effect of pre-chamber volume and nozzle diameter on pre-chamber ignition in heavy duty natural gas engines 1.
24. Shah, A., Tunestål, P., & Johansson, B. (2015). CFD simulations of pre-chamber jets mixing characteristics in a heavy duty natural gas engine. SAE Technical Paper 2015-01-1890.
25. Biswas, S., Tanvir, S., Wang, H., & Qiao, L. (2016). On ignition mechanisms of premixed CH_4/air and H_2/air using a hot turbulent jet generated by pre-chamber combustion. *Applied Thermal Engineering, 106,* 925–937.
26. Biswas, S., & Qiao, L. (2018). Ignition of ultra-lean premixed H_2/air using multiple hot turbulent jets generated by pre-chamber combustion. *Applied Thermal Engineering, 132*(5), 102–114.

27. Biswas, S. (2018). *Physics of turbulent jet ignition: Mechanisms and dynamics of ultra-lean combustion* (1st ed.). Berlin: Springer.
28. Biswas, S., & Qiao, L. (2018). Combustion instabilities of ultra-lean premixed H_2/air mixtures by pre-chamber turbulent jet ignition. *Journal of Propulsion and Power*.
29. Biswas, S., & Qiao, L. (2018). Ignition of ultra-lean premixed hydrogen/air by an impinging hot jet. *Applied Energy, 228,* 954–964.
30. Biswas, S., & Qiao, L. (2017). A numerical investigation of ignition of ultra-lean premixed H_2/air mixtures by pre-chamber supersonic hot jet. *SAE International Journal of Engines, 10*(5), 2231–2247.
31. Biswas, S., & Qiao, L. (2016). Prechamber hot jet ignition of ultra-lean H_2/air mixtures: Effect of supersonic jets and combustion instability. *SAE International Journal of Engines, 9*(3).
32. Validi, A., & Jaberi, F. (2018). Numerical study of turbulent jet ignition in a lean premixed configuration. *Flow, Turbulence and Combustion, 100,* 197–224.
33. Li, X., Zhang, W., Huang, Z., Ju, D., Huang, L., Feng, M., et al. (2019). Pre-chamber turbulent jet ignition of methane/air mixtures with multiple orifices in a large bore constant volume chamber: Effect of air-fuel equivalence ratio and premixed pressure. *Frontiers in Energy, 13,* 483–493.
34. Wang, N., Liu, J., Chang, W. L., & Lee, C. (2018). A numerical study of the combustion and jet characteristics of a hydrogen fueled turbulent hot-jet ignition (THJI) chamber. *International Journal of Hydrogen Energy, 43*(45), 21102–21113.
35. Kundu, P. K., Cohen, I. M., & Dowling, D. R. (2012). *Fluid mechanics* (5th ed., xxvi, 891 p). Waltham, MA: Academic Press.
36. White, F. (2015). *Fluid mechanics*. New York: McGraw-Hill Education.
37. (2013). *Reaction design*. Reaction Workbench 15131 San Diego.
38. Crane Co. Engineering Division. (1957). *Flow of fluids through valves, fittings, and pipe*. Crane Company Technical Paper 1957. Chicago: Crane Co.
39. Debonis, J. R., & Scott, J. N. (2002). Large-Eddy simulation of a turbulent compressible round jet. *AIAA Journal, 40*(7), 1346–1354.
40. Uzun, A., & Hussaini, M. Y. (2007). Investigation of high frequency noise generation in the near-nozzle region of a jet using large eddy simulation. *Theoretical and Computational Fluid Dynamics, 21*(4), 291–321.
41. Law, C. K. (2006). *Combustion physics* (xviii, 722 p). Cambridge; New York: Cambridge University Press.
42. Xiao, H., Wang, Q., Shen, X., Guo, S., & Sun, J. (2013). An experimental study of distorted tulip flame formation in a closed duct. *Combustion and Flame, 160*(9), 1725–1728.
43. Ponizy, B., Claverie, A., & Veyssière, B. (2014). Tulip flame—The mechanism of flame front inversion. *Combustion and Flame, 161*(12), 3051–3062.
44. Attard, W. (2012). *Turbulent jet ignition pre-chamber combustion system for spark ignition engines*. MAHLE Powertrain LLC: US 20120103302 A1.

Lean-Burn Combustion in Direct-Injection Spark-Ignition Engines

Ankur Kalwar and Avinash Kumar Agarwal

1 Introduction

Advancements in automotive industry have focussed on attaining key objectives such as high thermal efficiency, high power output, lower fuel consumption, lower exhaust emissions and superior driving comfort. Spark-ignition (SI) engines have undergone many technological transitions in order to meet the market requirements as well as emission legislations [1, 2]. As the number of vehicles on the road is increasing at a significant pace, vehicular exhaust emissions have become a significant contributor to the air pollution. In order to curb deterioration of air quality, governments across the world have implemented strict emissions limits on the transport vehicles and have revised them periodically. Simultaneously, the demand for crude oil imports has increased continuously due to its limited reserves and increasing fuel requirement. This has put the burden on the pockets of individuals due to higher fuel prices.

This changing scenario eliminated the use of carburetor as a fuel induction system from passenger cars in 1980s. However, lower segment two-wheelers still use carburetor due to economic reasons. Introduction to electronically controlled port fuel injection (PFI) system provided solution for the limitations of carburetor. Inefficiency in the responsiveness to maintain the stoichiometric air–fuel ratio at variable engine operating conditions is a major bottleneck of carburetor for meeting fuel economy and emission norms. Engine response to varying throttle position also gets improved in PFI systems. Although PFI system has improved the engine performance in many aspects compared to the carburetor, still it has its own limitations. Further advancements in SI engine technology led to emergence of GDI engine technology. GDI engines started powering passenger cars since 2000s. and substantial technical advancements have been done subsequently [3–5].

A. Kalwar · A. K. Agarwal (✉)
Engine Research Laboratory, Indian Institute of Technology Kanpur, Kanpur 208016, India
e-mail: akag@iitk.ac.in

A. P. Singh et al. (eds.), *Alternative Fuels and Advanced Combustion Techniques as Sustainable Solutions for Internal Combustion Engines*, Energy, Environment, and Sustainability, https://doi.org/10.1007/978-981-16-1513-9_12

Direct injection technology in gasoline engines seems very promising from fuel economy point of view. Although, gasoline engines with direct injection technology have entered the market in the late 1990s, their acceptance among the customers was very low compared to diesel engines. Main reason behind it was the inability to meet the expectation regarding fuel economy as compared to diesel engines. The designs that were employed in those engines were having wall-guided or air-guided type combustion systems. Their operating range for stratified mode operation was very limited. Hence, practically they could not achieve the desired fuel economy benefits on-road [6, 7]. This limitation of restricted operating window for stratified charge operation and installation of sophisticated exhaust gas after-treatment system due to lean combustion led to several automobile manufacturers going for homogeneously charged stoichiometric GDI engines. Although GDI engines with homogeneous stoichiometric mixtures have their own advantages along with the use of conventional three-way catalytic converter (TWC) as the only after-treatment devices, the expected reduction in fuel consumption has not been achieved so far [8].

With the advancements in fuel injection technology and as an outcome of intensive research and development work, spray-guided combustion system (second-generation GDI) was implemented and introduced in the market in 2006 by BMW and Mercedes-Benz. With this, it became possible to operate the engine at lean equivalence ratios in a wide operating range. The fuel saving of roughly between 10 to 20% was achieved compared to PFI engines and stoichiometric operations [7, 9]. Further reduction in fuel consumption was achieved by employing supercharging and downsizing measures.

The advantage of high thermal efficiency from lean mixture combustion in direct injection engine can be understood by the thermodynamic analysis of the Otto cycle [10]. With the direct injection of gasoline, improvement in thermal efficiency and fuel consumption are achieved due to throttle-free operation, especially at part-load conditions. Use of lean mixture in stratified mode operation further enhances the fuel efficiency of the engine. Considering the assumptions of Otto cycle, neglecting losses from the fuel conversion, the thermal efficiency is only dependent on the engine's compression ratio (r) and isentropic exponent (k). Higher values of r and k can be used for producing the highest possible efficiency. Injecting the fuel directly decreases the sensible enthalpy of the charge in the cylinder because of latent heat of vaporization and resulting evaporative cooling. This reduces the cylinder charge temperature at the end of compression. As a result, the knocking tendency is reduced when compared to PFI engines. Thus, compression ratio can be increased by taking advantage of improved knock resistance. With increase in compression ratio between 1.5 and 2 units, fuel consumption can be reduced by ~3%. Another factor is increasing the isentropic coefficient of mixture, which is possible by utilizing the lean mixture, as shown in Fig. 1. The maximum value of k can be close to 1.4 (pure air).

Other major features of GDI are as follows:

- Lean combustion results in lower heat loss from the combustion chamber, thereby improves the thermal efficiency.

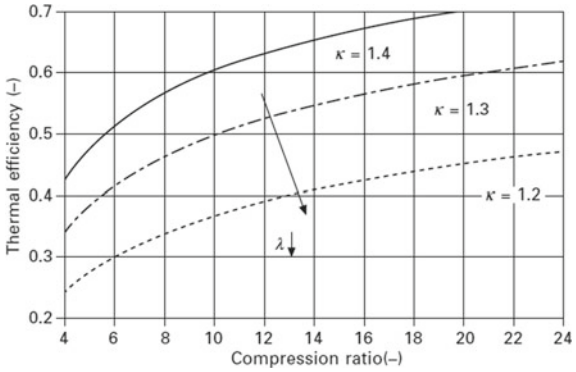

Fig. 1 Thermal efficiency as a function of k and r for a constant-volume process [11]

- Greater power output due to higher volumetric efficiency and lower carbon monoxide (CO) and carbon dioxide (CO_2) emissions.
- Injection in expansion stroke made fast heating of catalyst possible.
- Better dynamic response of fuel–air mixture control and drive comfort.

However, apart from these benefits, combustion stability of lean stratified mixture is highly compromised due to formation of non-repeatable mixture. Further, stratified mixture combustion faces issue of high particulate, NO_x and HC emissions. These issues are discussed in great details in the forthcoming sections. At this point, let us understand possible ways of mixture formation, their operating ranges and combustion systems designs for achieving stratification of charge.

1.1 Mixture Formation in GDI Engines

There are basically two modes in which mixture formation is implemented in a GDI engine, (i) stratified mode and (ii) homogeneous mode, as shown in Fig. 2. In **stratified mode**, gasoline is injected late in the compression stroke such that rich air–fuel charge gets accumulated near the spark plug and locations far from spark plug are generally occupied by lean mixture. Overall equivalence ratio is always on the leaner side in this mode. The air–fuel ratio of the engine can reach up to 100 with the fully unthrottled operation; however, air–fuel ratio in the range of 30–40 is maintained with slight throttle so that a large fraction of exhaust gas recirculation (EGR) can be introduced. In **homogeneous mode**, fuel is injected early during the intake stroke for homogeneous mixture preparation. The engine is operated in slightly rich or stoichiometric conditions so that high-load and speed demands can be catered. In medium load conditions or during switching from stratified to homogeneous mode, **homogeneous lean mode** is operated where homogeneous mixture is utilized with

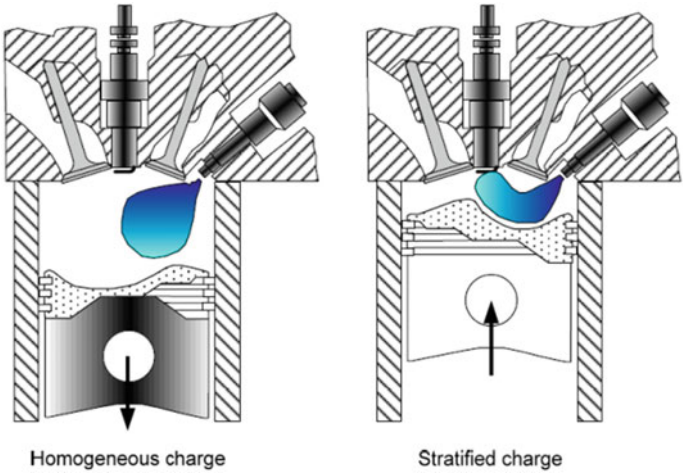

Fig. 2 Homogeneous and stratified charge formation [2]

lean charge condition. This is done to further improve the fuel economy [12]. Air–fuel ratio in the range of 20–25 is being operated in this mode.

During homogeneous mode, different load demands are catered by throttling, while in stratified mode, engine operates in unthrottled condition and fuel quantity is adjusted to meet different load requirements [13]. As a result of direct injection and unthrottled operation, dynamic engine response characteristics are affected positively. When there is a sudden change from part load to full load, air in the intake system should be filled in and allowed to build higher pressure. In unthrottled stratified operation, higher intake pressure of air is always available; hence, faster torque response can be achieved.

1.2 Mode Switching in GDI Engines

GDI engine switches between different modes of operation depending upon the load and speed conditions. There are four modes based on their operating window as shown in Fig. 3.

- Stratified charge mode having overall lean mixture: for low-load and speed conditions.
- Homogeneous lean mode: for medium load and speed conditions.
- Homogeneous stoichiometric mode: for high-load and speed conditions.
- Homogeneous stratified mode: for high-load-low-speed conditions.

Electronic control unit (ECU) switches among these operating modes based on the engine requirements by controlling the fuel injection timing and quantity. Hence,

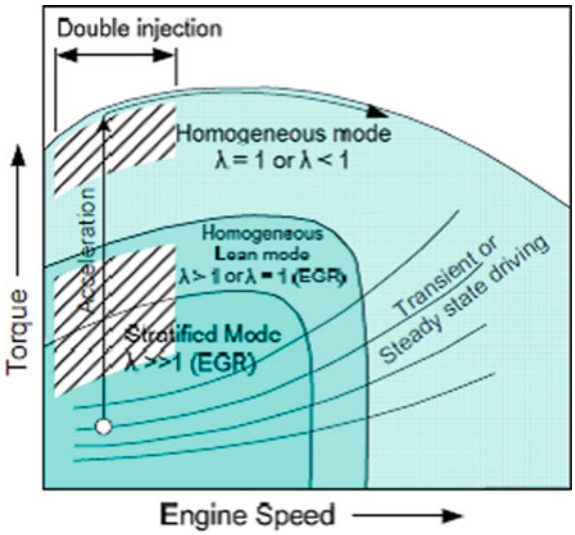

Fig. 3 Different operating modes in GDI engine based on load and speed conditions [14]

it alters the air–fuel ratio of the charge. In **stratified charge mode**, only low-load and speed requirements can be fulfilled, without any acceleration. Running the mixture lean results in increased NO_x emissions, and thus, stratified mode is accompanied by EGR to limit the NO_x emission. At higher engine speed, stratification of the mixture cannot be sustained due to increase in the in-cylinder turbulence. Hence, at high-speed and load conditions or during acceleration, **homogeneous mode** is used for high torque and power output. Stoichiometric mixture caters to the need of high power output and low emissions. In this, stoichiometric fuel quantity is injected during the intake stroke to provide sufficient time for the formation of homogeneous charge. EGR activation is not required due to low NO_x emissions.

During transition from stratified to homogeneous mode, engine operates at **homogeneous lean mode**. This mode covers medium load and speed requirements. In this mode, fuel is injected early in the intake stroke and mixture is generally lean or stoichiometric. EGR is activated in this region to control NO_x emissions. Fourth operating mode is **homogeneous stratified mode**, which is applied when the engine runs under low-speed-high-load conditions. When large fuel quantity is injected for stratification, it results in richer mixture presence in some pockets, which increases soot emission. Therefore, split injection is opted in which large fraction of total injected fuel is injected during intake stroke for the formation of overall lean homogeneous mixture and remaining fuel is injected during the compression just before spark, in order to form stratified mixture. This mode is used during accelerating while transitioning from stratified to homogeneous mode at low speed conditions. Double injection is implemented for reducing the soot emissions as well as fuel consumption. Additionally, there are high chances of knocking at low speed-high-load conditions due to increased combustion duration and high temperature. Double injection also

helps in reducing the knocking tendency. It can be also used in rapid activation of the catalyst [2].

1.3 Combustion Systems Designs

There are three types of combustion system designs used for generating stratification of charge in direct-injection spark-ignition (DISI) engine, namely wall-guided, air-guided and spray-guided. These are basically defined and distinguished on the basis of formation of ignitable charge near the spark plug at the time of ignition, as shown in Fig. 4. All three systems utilize different ways of transporting fuel spray close to the spark plug [15].

- **Wall-Guided Combustion System**: Most of the first-generation direct-injection gasoline engines were having wall-guided combustion system. This system used a special shape piston to transport the mixture up to the spark plug. The side-mounted injector inducts the fuel spray over the piston crown and directs it toward the spark plug. Air flow motion (swirl or tumble) also supports the transportation of the mixture. Major disadvantage in this combustion system is the wetting of piston crown due to spray impingement, which produces fuel deposits and hydrocarbon (HC) emissions. This issue is not only pronounced during the cold start, but also during normal engine operation. Moreover, during low to medium load operation, fuel injection quantity has to be increased, for which advancing of fuel injection timing is required to achieve optimum ignition timing. In that case, there are chances of spilling of fuel spray over the piston crown and entering into squish gap. This may also lead to emissions of unburnt HCs. Furthermore, as the fuel injection timing is dependent on piston position and desirable in-cylinder flow pattern is also dependent on engine speed, hence coordination of injection and ignition timing is difficult to achieve over wide speed/ load range. Hence, realizing the potential of GDI engine to minimize the fuel consumption with the wall-guided system is quite challenging.

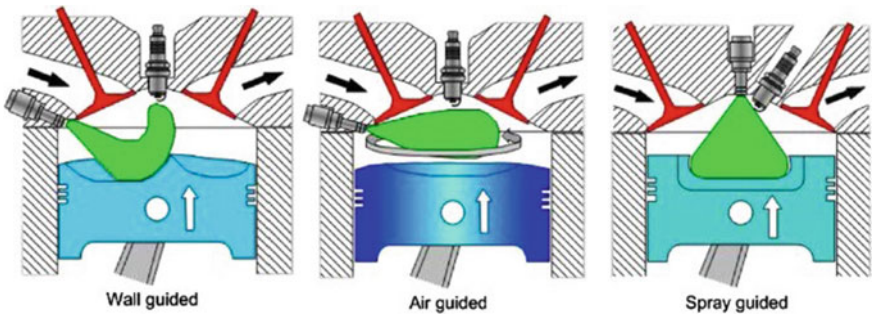

Fig. 4 Different combustion systems designed for stratified operation [16]

- **Air-Guided Combustion System**: In this system, air flow guides the injected fuel spray, which remains concentrated near the spark plug. This system aims at preventing the contact of fuel spray with the walls of the combustion chamber. Hence, as compared to wall-guided system, the chances of HC emissions are reduced with air-guided system. However, the specific charge movement is used to mix the fuel spray with intake air. Large-scale air motion and appropriately shaped piston crown are used for generating the specific charge movement. In both wall-guided and air-guided systems, injector is located far from the spark plug, mounted at the side of the cylinder. Large-scale air motion (swirl or tumble) is created with specific design of inlet port or using tumble flap, respectively [16]. However, it is very important to maintain the required in-cylinder flow over varying operating conditions. Modifications for creating swirl or tumble flow required for this operation decreases the volumetric efficiency and hence the performance of the engine. These systems are also referred as first-generation GDI systems.
  Volkswagen had used combination of both wall-guided and air-guided systems in its direct-injection combustion system. This system was efficient in homogeneous as well as stratified modes. Moreover, it was less prone to cyclic variations of air motion. It was achieved with the help of two bowls of the piston. Fuel bowl on intake side and air bowl on the exhaust side were used to guide the fuel to the spark plug via incoming air. Air-guided subsystem employed tumble flow with the help of specially designed inlet ports [17, 18].
- **Spray-Guided Combustion System**: Modern-age GDI engine uses spray-guided combustion system. In this system, injector is located near spark plug so that fuel is injected in the vicinity of spark plug. It employs highly efficient piezo-injector for fuel injection. The position of spark plug is determined optimally with respect to injection plume so that correct mixture formation takes place near the spark plug for a wide operating range. The performance of this system is highly dependent on the injection characteristics. Moreover, it should be ensured that highly lean mixtures having steep gradients of stratification present at the edge of spray plume are ignited properly.

Considering the special characteristics of this system, few points require particular attention [11]:

- Injector coking: Coking at the nozzle due to deposit formation adversely affects the spray plume characteristics.
- Spray pattern tolerances: Changes in the spray pattern due to varying operating conditions or manufacturing tolerances negatively affect the combustion. Hence, reproducibility of spray pattern is important.
- Fouling of spark plug: Fouling of spark plug can result in misfire.
- Thermal shock at spark plug: Contact of liquid fuel with hot spark plug reduces the temperature of spark plug rapidly and acts as thermal shock. Thus, robust ignition system should be employed.
- Fuel injection timing: Fuel injection is done shortly before ignition happens. Therefore, fuel injection timing and ignition timing are closely related for

achieving good performance at wide speed/load conditions. Usually at retarded injection timings, higher fuel injection pressure (FIP) is used.

- Engine speed: Engine speed significantly controls the in-cylinder flow and mixture formation. Hence, it plays a critical role in optimizing the controlling parameters for successful engine operation.

In contrast to wall/air-guided system, wetting of piston and cylinder liner is significantly reduced in this case. It results in minimizing HC emissions. With spray-guided system, primary breakup of fuel spray improves and the presence of compact mixture cloud results in faster fuel conversion efficiency. Further, this system reinforces similarities with ideal constant-volume process. Additionally, there is no compulsion for swirl or tumble flow in spray-guided combustion system. Here, designing of inlet ports can be done as filling channels to get optimized performance. Its other advantages include extension of operating range in stratified mode, better fuel economy, centrally mounted injector leading to superior mixture formation control, less sensitivity to cyclic and cylinder-to-cylinder variations. However, reliability of spark plug due to fouling and poor robustness due to high sensitivity toward injection and ignition timing are some of its drawbacks [19]. Mercedes-Benz developed stratified-charged GDI engine which uses spray-guided combustion system. Piezo-injection technology used in this system enabled multiple injections in a fraction of second apart. It improved the lean-burn limit over the extended operating range, hence allowing superior control on the mixture formation and improving the fuel efficiency [20].

2 Combustion, Performance and Emission Characteristics of Lean Mixtures in DISI Engine

Spray dynamics and mixture preparation play a critical role in successful operation of stratified mode GDI engine. Spray droplet dynamics depend on the interactions between inertial and surface tension forces. Spray interactions with in-cylinder air flow affects the mixture quality, which govern the combustion and emission characteristics of the engine. As already discussed in the previous subsections, wall-guided combustion system suffers from the issue of wall film formation. Hence, there are chances that spray droplets, when interacting with hot piston surface, may result in splashing, rebounding and fuel deposition. In addition, heat transfer from piston wall to fuel droplets or film deposited over it results in secondary evaporation. This is further dependent on the temperature of the wall and surrounding gas properties such as pressure, temperature and velocity [21, 22]. These processes of droplet impact, wall impingement, secondary evaporation and heat transfer are influenced by the fuel injection timing. Therefore, injection timing is a critical parameter to be optimized for proper mixture formation at any operating condition. Complex nature of air and fuel dynamics in the cylinder for a wall-guided system has to be well understood

Table 1 Experimental operating parameters [24]

	SOI (°BTDC)	SOS (°BTDC)	A/F	P_{inj} (MPa)	IMEP (bar)	CoV_{IMEP} (%)
Stoichiometric charge (s)	307	19	14.7	15	10.75	1.35
Overall lean charge (L1)	70	13	21.5	6	7.30	2.31
Overall lean charge (L2)	70	23	21.5	6	7.31	2.13
Overall lean charge (L3)	70	13	21.5	20	7.24	1.65
Overall lean charge (L4)	70	23	21.5	20	7.17	1.36

in order to optimize the fuel economy, combustion stability and exhaust emissions, within the flammability window of injection timings.

Bonatesta et al. [23] clarified that even early fuel injection in homogeneous mode could not achieve complete fuel evaporation and proper air–fuel mixing with this combustion system. Part-load condition and high load-low speed ranges were most likely resulting in spray impingement. This led to high number of nucleation mode particles formation. In a study by Costa et al. [24], four cases of lean-burn combustion were investigated experimentally and numerically and were compared with the homogeneous stoichiometric combustion. A four-cylinder turbocharged GDI engine with wall-guided configuration was used for conducting these experiments. The operating parameters for one homogeneous case (S1) and four lean-burn cases (L1 to L4) are defined in Table 1.

It was reported that with late injection to achieve mixture stratification, gasoline evaporation rate decreased and formation of pollutants also increased. Mixture inhomogeneity affected the combustion development, leading to asymmetric flame development, as shown in Fig. 5. It also resulted in undesired auto-ignition of the charge. However, they stated that late injection combustion improved upon increasing FIP and advancing ignition timings. It improved the power output, lowered the cyclic variability and soot and CO emissions, although nitrous oxide (NO) emission remained unaffected. Local enrichment of fuel caused by late injection resulted in incomplete combustion and formation of pollutants, as shown in Fig. 6.

In another study performed by Su et al. [25], different injection timings for stratified combustion in wall-guided GDI engine were investigated experimentally. Further, numerical studies were conducted to analyze the equivalence ratio distribution and fuel–air mixing characteristics. They mentioned that inappropriate equivalence ratio distribution was mainly responsible for poor burning characteristics. Late injection at 48° bTDC resulted in a finitely rich mixture concentration with steep gradients around the spark plug, which was difficult to ignite; thereby, it increased the misfires. On the other hand, early injection at 78° bTDC led to comparatively homogeneous but lean mixture surrounding the spark plug. Slower burning speed

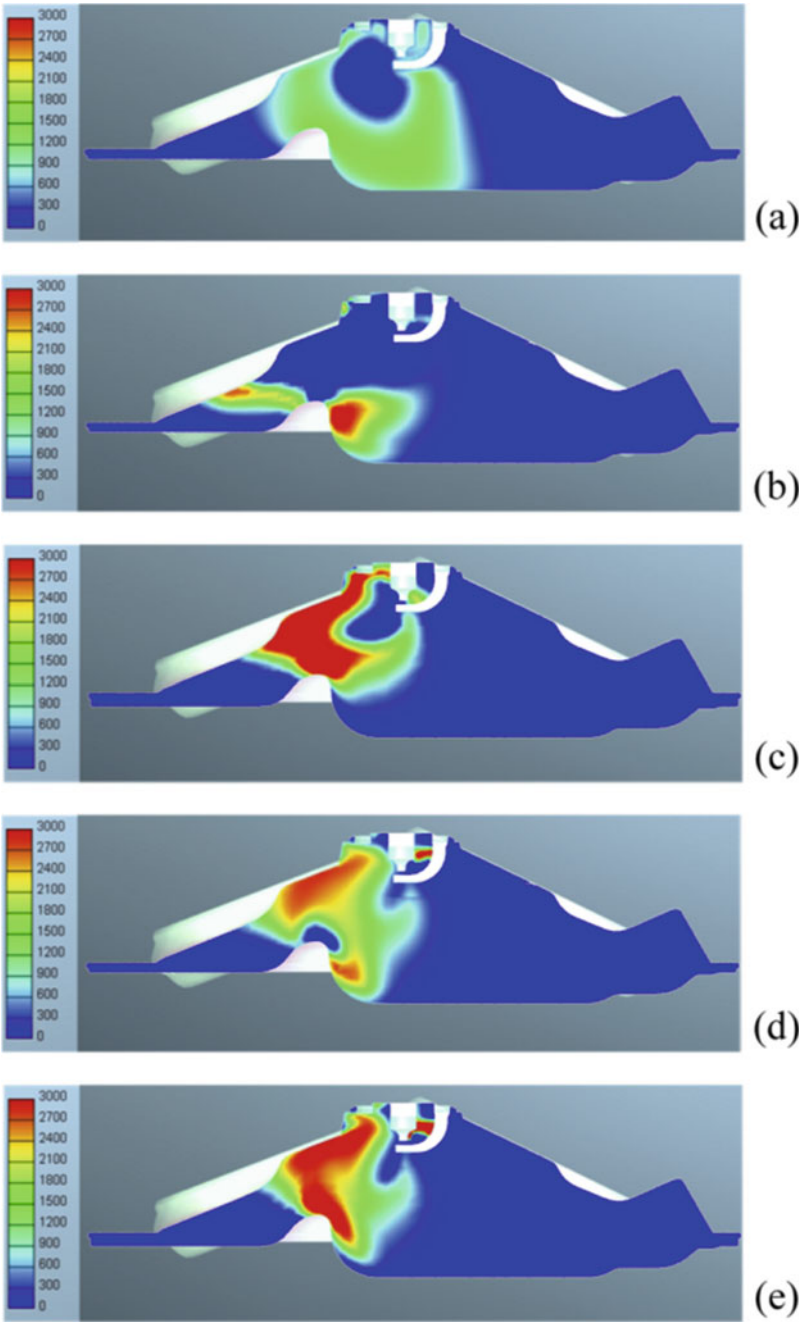

Fig. 5 Flame surface density 15° after SOS case **a** S; case **b** L1, **c** L2, **d** L3 and **e** L4 [24]

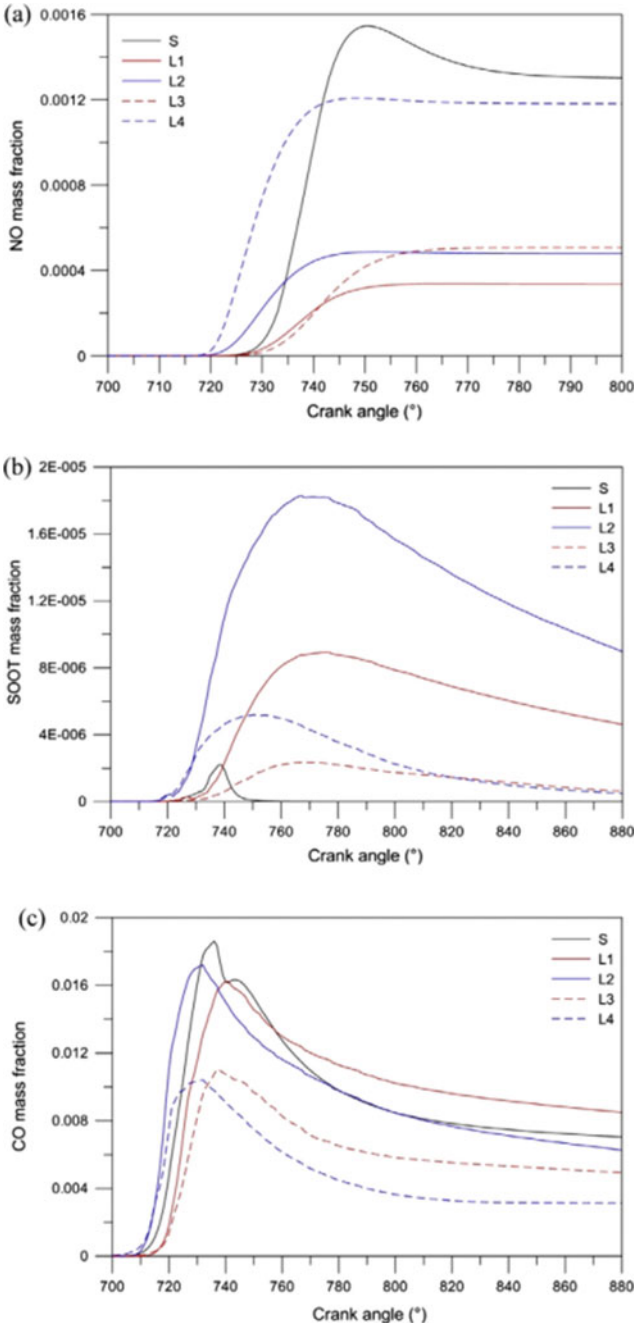

Fig. 6 Pollutants formation in all 5 cases [24]

of lean mixture also increased the cyclic variations in combustion. However, for same fuel injection quantity and spark timing, stratified charge produced 10% higher indicated mean effective pressure (IMEP) as compared to homogeneous charge with little sacrifice in combustion stability. In a study [26] involving optical characterization of stratified and homogeneous mixture for stoichiometric combustion in the wall-guided GDI engine, flame propagation in homogeneous mode was found to be in spherical shape, while in stratified mode, flame propagated in asymmetrical manner having elongation toward the injector. Evolution of flame in terms of propagation direction and speed was directly affected by the presence of rich mixture over the piston bowl below the injector. This further controlled the flame stability and coefficient of variance (COV). The flame speed was faster in stratified mixture during early combustion phase which increased further for homogeneous mixture. The flames in stratified mode were more luminous and diffusive in nature than the homogenous mode. Further, higher values of in-cylinder pressure and heat release were obtained in the stratified mode.

Spray-guided combustion system possess very narrow range of injection timing for ignitable mixture conditions. Also, it is important to maintain the spray targeting such that it does not impact other surfaces such as inlet valves and spark plug; otherwise, it would give rise to diffusion flames. However, it further depends on the injection timings, geometric constraints, air flow, etc. Proper coordination of injection and ignition timing is required to achieve stable combustion. It has to be maintained that spray does not over-dilutes and still mixes to an extent that does not cause excessive soot emissions. There are three ways in which mixture can be ignited, namely ignition at the start of spray, middle of spray and the end of spray. Ignition at the end of spray provides sufficient time for premixing of charge, and hence, it lowers soot formation. Park et al. [27] studied stratified lean combustion in a GDI engine, employed with spray-guided combustion system. It was employed with outward opening piezo-type GDI injector. They demonstrated the effect of injection parameters like fuel injection timing and FIP on the fuel economy, combustion stability and emissions characteristics. Further, the optimized injection and ignition timings were studied with application of EGR. For leaner combustion having $\lambda = 2$ or higher, fuel consumption was minimum for injection, and ignition timing was set to 40° bTDC, as the combustion efficiency was very sensitive to injection and ignition timings. The application of higher FIP of 200 bar extended the flammability limit to ultra-lean mixtures ($\lambda \sim 3$). However, the smoke did not reduce with increasing FIP to 200 bar, due to spray impingement. They suggested that applying EGR with optimum ignition timing was more effective in reducing NO_x and HC emissions than retarding the ignition timing.

In another study [28], flame characterization, combustion and emission investigations on a spray-guided direct-injection spark-ignition (DISI) engine under lean-burn condition were conducted. They reported 23% improvement in fuel economy, while COV of IMEP was under 4%, with advanced ignition timing and delayed injection timing, as compared to stoichiometric combustion. Further, they were able to realize stable combustion with $\lambda = 4$, however, NO_x and HC emissions were reportedly higher due to rich fuel–air mixture combustion and spray impingement. They also

reported diffusive and highly luminous flames in case of stratified mixture due to fuel impingement on the spark plug electrodes. They suggested two-stage injection for stable combustion and lower fuel consumption, but NO_x and particulate matter (PM) could only be controlled by after-treatment devices.

Lean-burn GDI engines are very unpopular for their higher emissions of ultra-fine particles, which are beyond the emission limits prescribed by EURO-VI standards. In one such study, researchers [29] investigated particulate emission characteristics at different lean-burn conditions in a spray-guided GDI engine. Particulate mass concentration was found to decrease with increasing engine load due to increased soot oxidation. They mentioned that the fuel film caused by spray impingement over the piston wall was major reason behind high nucleation mode particles (<50 nm). Further, particle collision frequency in diffusion flames was lower for GDI engine than a diesel engine, which mainly led to increase in size of particles. Significantly higher amount of particulate concentration was observed at excess air ratio of 1.5, which was stated to be because of transition from premixed flames to diffusion flames. Further, increase of PM beyond $\lambda = 2$ was reported due to action of higher ambient pressure and lower combustion temperature.

3 Limitations of Combustion Stability

3.1 Misfire and Partial-Burn Cycles

Lean-burn mixtures suffer from major limitations of frequent misfire, and partial-burn cycles due to which it results in relatively lower engine performance and higher emissions. It is very important to investigate the causes and understand the mechanism behind its occurrence, in order to improve combustion stability and minimize cyclic variations in lean-burn combustion. Several studies have been performed for investigating different parameters responsible for misfire in SI engines. It has been investigated in various studies using optical diagnostics [4, 30] and computational studies [31] that misfire are strongly correlated with the presence of lean mixtures near spark plug. Abnormal spark phenomenon like low spark energies, low spark duration, surface spark and spark extinguishment were also reported to be the cause of misfire [32, 33]. Furthermore, variations in local flow velocity in the vicinity of spark plug can disturb the spark motion; resulting in misfire [34]. These studies clearly suggest that it would be wrong to state any universal reason for the misfire event. In order to study the impact of several factors simultaneously, Peterson et al. [35] performed the experiments in which simultaneous imaging of fuel distribution and flow field was done using planar laser-induced florescence (PLIF), particle image velocimetry (PIV) and Mie scattering to analyze its effect on flame kernel evolution. Spray-guided stratified combustion engine operating at idling condition was considered for the study for stable combustion operation with rare occurrence of partial-burn cycles and misfires. Different dilution levels of N_2 (0–26% v/v) were

used to explore the effect of EGR on the combustion stability. Distinctive characteristics of early flame kernel development for well-burning (WB), poor-burning (PB) and misfire (MF) cycles were studied. Further, the quantitative measurements helped in understanding the mechanism impeding the growth of flames. Spark energy measurements revealed that ignition energy was sufficiently available and had no impact on the nature of cycles. Hence, it indicated that variation in spark energy was an inherent cause for poor-burning cycles. Moreover, the ensemble values of equivalence ratio and velocity of poor burning cycles at the time of spark were within the distribution of adequately burning cycles. Hence, in order to deeply understand distinctive features of WB, PB and MF cycles, spatial and temporal distribution of fuel, flow velocity and flame propagation were further investigated.

For WB cycles, flame kernel propagated toward the direction of expired spray plume passing close to the spark plug electrode. The flame kernel was able to consume the charge rapidly and remained in contact with the flammable mixture, while propagating toward the piston bowl. Early propagation of flame was not affected by dilution ratio; however, the later phases exhibited slower flame propagation for dilute mixtures. For PB cycles, the enflamed region was smaller than WB cycles. The flame kernel did not propagate rapidly into the piston bowl and lagged behind flammable charge. Later interactions of flame kernel with the charge available at the piston bowl could not sustain the combustion as the mixture became leaner with time, which resulted in partial combustion of fuel–air mixture. Misfire cycles did not show significant growth in flame kernel development. The flame was initiated in all cycles; however, it remained primarily near the spark plug and the size of kernel was smaller than that of WB and PB cycles. The presence of surrounding lean mixture around the flame kernel was not sufficient for propagation of flames. Indeed, it did not reach the flammable mixture often. Hence, as flame further travelled, the size of kernel continued to shrink, resulting in flame extinction. Figure 7 showed early flame development characteristics for WB, PB and MF cycles for non-diluted charge.

It was also found that strong convective flow velocities were responsible for the misfire cycles. The strong upward flow field directed the already formed flame kernel in the direction opposite to the region of fuel–air charge availability, as shown in Fig. 8. The reason for the motion was the fuel cloud struck at the side of the piston bowl during compression; hence, a reverse flow field was created in the upward direction. This strong upward flow directed the kernel in an opposite direction, away from the fuel cloud present beneath the spark plug. The kernel continued to travel in lean mixture until the fuel-rich charge reached the spark plug. Eventually, the flame began to consume the flammable charge, but due to longer mixing time, the fuel–air mixture became leaner and could not sustain the flame growth. Hence, as an overall conclusion, the mechanism reported behind the occurrence of partial-burn and misfire cycles was the low flame propagation speed due to presence of lean mixture in the surrounding, dilution of the charge and upward flow velocities that impeded the movement of kernel toward the flammable mixture.

In another study carried out by Zeng et al. [36] on spray-guided stratified GDI engine, it was observed that in-cylinder motion generated due to intake and compression stroke during engine operation at 2000 rpm was strong enough to cause cyclic

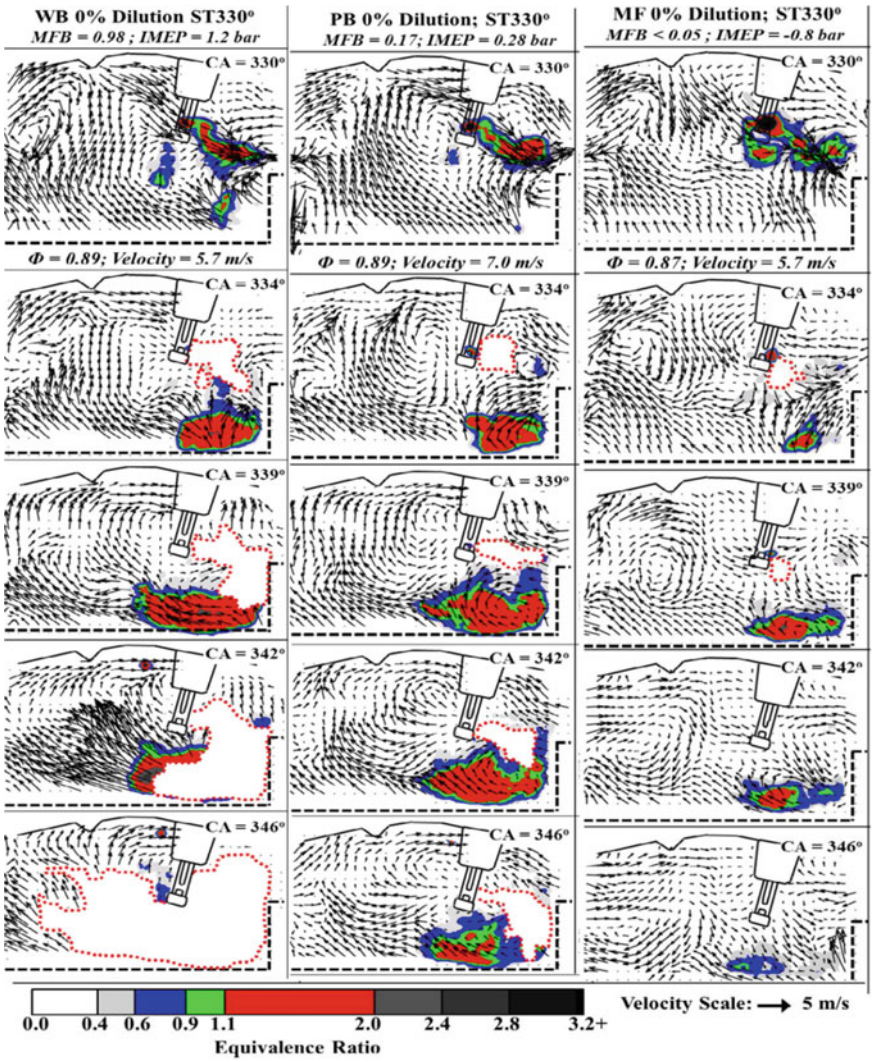

Fig. 7 Flame images for 0% dilution show lesser flame development for MF cycles as compared to WB and PB cycles [35]

variations in the combustion characteristics, when EGR was applied. After analyzing all the variations of the flow/ spray interaction, it was divided into two types, on the basis of which, likelihood of partial-burn cycle could be predicted. The first-type characterized the in-cylinder air flow in proper direction before the start of fuel injection, along with higher collapsed spray leading to strong flow/ spray interaction. The higher kinetic energy of flow during injection resulted in fast combustion in the early phase. This increased the chances of complete combustion even for EGR operated cycles.

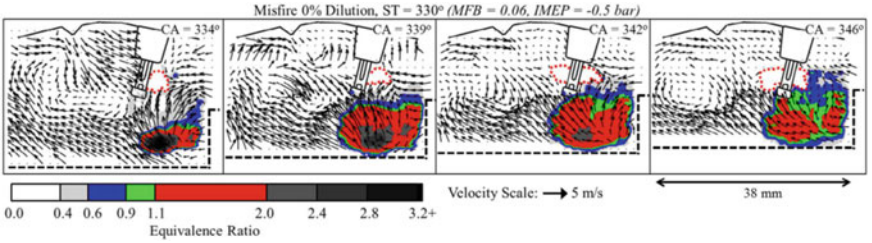

Fig. 8 Flame propagation for MF cycles shows upward movement of flame kernel due to strong convective flow [35]

The other type was specified by improper flow direction before fuel injection with less collapsed spray leading to lower flow energy during mixing. During this kind of interaction, ~30% partial-burn cycles were reported when operated with EGR. Hence, weak flow during fuel injection was considered to be a major contributing factor for the occurrence of partial-burn cycles. In addition, it was observed that the flame development for partial-burn cycles with EGR was weak and variable in nature. However, without EGR, flames developed were repeatable in nature, irrespective of the type of flow/ spray interaction.

3.2 Cyclic Variability

Direct-injection SI engines are more prone to cyclic variations in the in-cylinder flow and fuel–air mixing, which affected the flame development and hence combustion characteristics of the engine. This can be justified by variations in the IMEP from cycle to cycle, which was represented by the coefficient of variance (COV) of IMEP. It has been shown that turbulence level of in-cylinder flow and rate of early flame growth are the dominant factors responsible for cyclic variability in the combustion characteristics of the engine [37]. Fast early flame growth and MBT ignition timing region resulted in lower COV of IMEP [38]. In addition, flow field around the spark plug influences the spark behavior and may result in cycle-to-cycle variations in spark development. Various phenomena related to spark discharge process such as shortening and stretching of spark channel were affected by near-by flow [39]. Therefore, consideration of spark discharge process is required for studying cycle-to-cycle variation (CCV) in SI engines. Minimum ignition energy and critical flame radius is required for sustained flame propagation. Moreover, these requirements increased with increasing Lewis number, which is generally higher for lean mixtures (greater than unity) [40]. Therefore, lean mixtures face difficulty in ignition. Indeed, CCV becomes more pronounced in stratified combustion mode, in which late injections are employed. Proper mixture formation and gas flow are very critical for combustion of stratified mixture. Intake manifold and cylinder head are designed to create large-scale rotating flow structures (tumble), which constitute major fraction

of kinetic energy of the flow. The dimension of these flow structures are limited by the size of the combustion chamber [41]. However, these large-scale flows are highly three-dimensional and turbulent in nature. At the end of the compression stroke, tumble flow motion becomes unstable and results in 'tumble breakdown' [42], where flow energy gets transferred into turbulence at small scales. The origin of the cyclic variations can be tracked by determining the in-cylinder flow evolution backward in time [43]. Additionally, in-cylinder pressure analysis in combination with time-resolved spatial evolution of flow field, fuel air mixing and flame kernel propagation can provide comprehensive understanding of combustion performance of the engine [44].

In the study performed by Stiehl et al. [45], impact of cyclic variations of the in-cylinder flows on spray evolution in a spray-guided stratified DISI engine was investigated. Time-resolved PIV within the tumble plane and Mie scattering techniques were used for conducting these experiments. Stratification of the mixture was obtained by employing triple injection strategy. The spray pattern for first injection showed good repeatability; however, it varied significantly for the second injection for different cycles. The study reported good correlation between the fluctuations in the spray pattern of second injection with the flow induced by initial spray/air interactions. This flow structure was directed in an upward direction (flow 1) opposing the developing spray from the second injection. It is shown in Fig. 9.

In further development of this work [43], tracking the flow backwards before the first injection revealed CCV in the vortex location of large tumble flow within the central tumble plane. This resulted in variations in tumble flow near the piston, which had major impact on the structure of second injection spray. Out-of-plane flow was reported to be the probable reason for the cyclic variability of this near piston flow.

The subsequent extension of this work [46] aimed at investigating the origin of out-of-plane flow and assessing its influence on the combustion performance of engine. By applying time-resolved PIV in two parallel planes, three-dimensional flow characteristics were obtained. Central tumble plane passing through the injector and

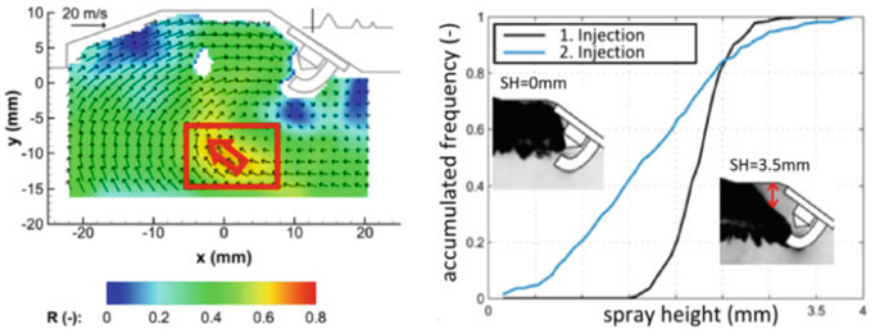

Fig. 9 (Left) Flow field at 40° bTDC showing high correlation values for upward flow over piston, (Right) Accumulated frequency showing large variation in spray height for the second injection [46]

spark plug was considered to be the first plane, and mid-valve plane passing through pair of intake exhaust was considered to be the second plane. Velocity–velocity correlation analysis revealed strong macroscopic convective movements from areas below the valves toward the central tumble plane. This led to velocity component directing out of plane, which influenced the central tumble flow. These were mainly generated as a result of geometric constraints. Figure 10 showed the illustration, where streamlines of tumble flow originating from mid-valve planes were merging with streamlines of central tumble flow, leading to occurrence of Flow 1.

Furthermore, influence of CCV in flow on combustion was studied by IMEP-velocity correlation. They observed that flow in particular regions resulted in higher values of IMEP with lower fluctuations due to favorable early flame growth. Region 1, located above the piston (similar to flow 1), constituted negative correlation, while region 2 near cylinder head held positive correlation. Hence, high momentum flow in region 2 with low momentum flow in region 1 led to better combustion performance with less cyclic variations. Figure 11 shows the respective flow regimes. These studies were useful for improving the engine geometry during the engine design process.

The authors also investigated the impact of cyclic variations on the in-cylinder flows and early flame development in a lean homogeneous DISI engine [47]. They employed high-speed PIV scanning using acousto-optical deflector (AOD) to measure 3D flow field. Flow imaging was done simultaneously at central tumble plane and two mid-valve planes, along with spark and combustion characterization. Variations in the in-cylinder flows were created with the help of tumble flap incorporated in the intake manifold. It was observed that fully open intake manifold (TF0) resulted in curved tumble vortex trajectory. Bending of the tumble axis and decentering of vortex centers resulted in higher variability of flow field. On the other hand,

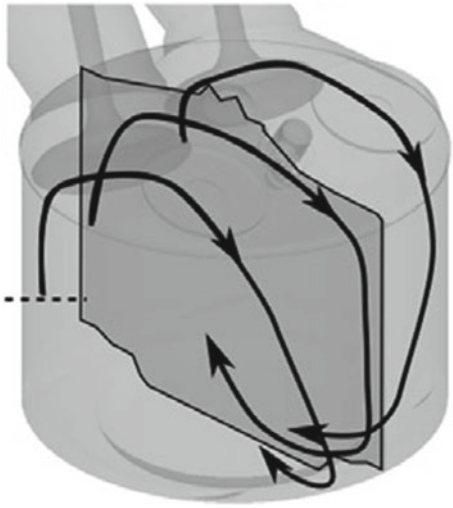

Fig. 10 Representation of streamlines showing out-of-plane flow at mid-valve planes [46]

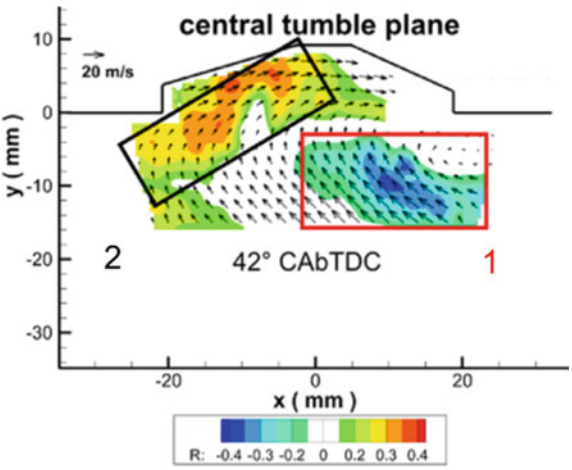

Fig. 11 Map showing correlation between IMEP and flow field in central plane at 42° bTDC [46]

partial-opened tumble flap (TF35) enhanced the overall velocity of flow. It resulted in central alignment of vortex centers in the central tumble plane. Hence, vortex center trajectory was maintained straight in the middle of cylinder during the compression. Figure 12 shows the above-mentioned phenomenon.

Further study included analysis of flow structure around the spark plug, whose higher variability was observed to be a major reason for CCV in case of TF0. Although large fluctuations of flow around the spark plug were also reported for TF35, their orientation favored reduction in the CCV in spark x-location (center of gravity of enflamed region). A good agreement of correlation was seen between the spark x-location and the early flame development. Rapid flame growth and reduced combustion duration were achieved with the flow favoring the movement of kernel growth toward center of the cylinder, as shown in Fig. 13. The analysis helped in better understanding of the interactions of large-scale flow structures with the ignition processes that led to combustion CCV. In another study [48], the authors reported reduction in combustion variability by employing swirl-flow through intake manifold modifications. However, gasoline vapor imaging revealed that fuel–air mixture turned asymmetric and non-uniform toward the end of the compression stroke, which resulted in higher soot emissions.

4 Strategies to Improve Combustion Stability, Operating Range and Emissions

In order to extract the advantages of higher thermal efficiency from lean-burn SI engine, its operational limit to higher excess air ratio has to be extended. However, increasing the lean limit leads to other issues such as combustion instability, misfires

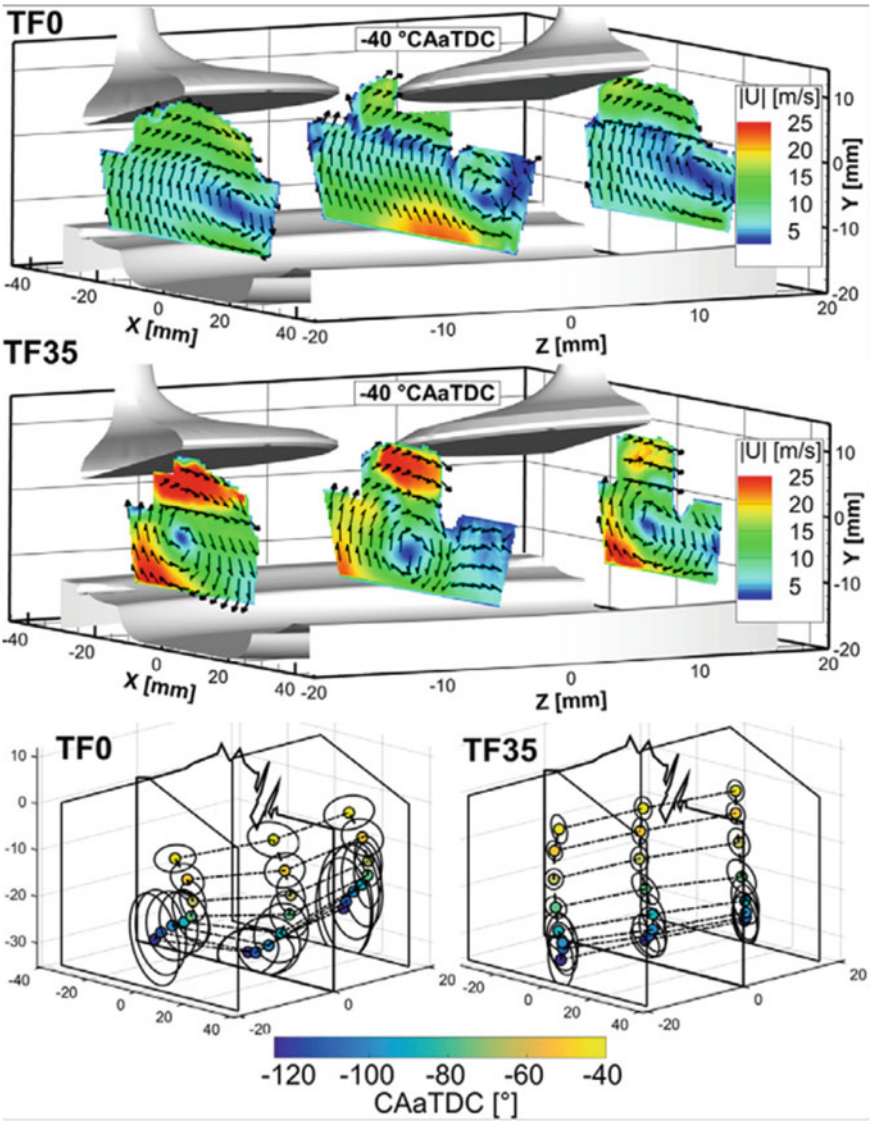

Fig. 12 Top: Flow field prior ignition. Bottom: Tumble flow straightens the tumble vortex trajectory during compression, ellipsis shows the two-sigma isoline of the CCV at the tumble center [47]

and partial burn, which results in CCV of engine combustion and performance. All these issues become prominent due to lower flame speed in lean mixtures. Nevertheless, various studies [49, 50] were performed to increase the lean-burn limit for further improvement in the thermal efficiency of the engine. Additionally, it has been suggested that repression of cyclic variations in early phase of combustion is

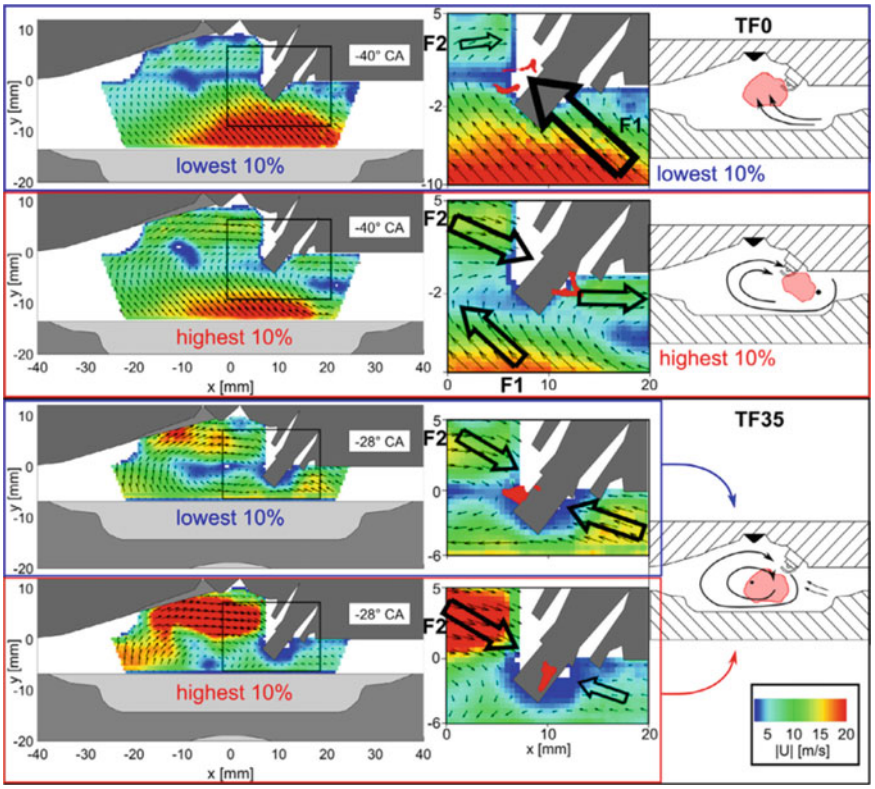

Fig. 13 Left and middle column: flow field prior to ignition with respect to. x-position of spark plug. Right column: flame kernel evolution [47]

extremely important for overall combustion stability in a cycle [51, 52]. This section describes the effect of various operating parameters to improve the combustion stability, extend the operating range and to reduce exhaust emissions from lean-burn combustion engines.

4.1 Effect of Ignition Parameters

Many researchers investigated the effect of ignition parameters on combustion stability and the ways to improve it. Aleiferis et al. [51] mentioned that short time interval within spark discharge could be detrimental to the quality of cycle. Although improvement in lean combustion has been seen by utilizing higher in-cylinder turbulence of the air flow, which are intensified by mainly tumble flows [53, 54], however high energy ignition system were also adopted for reliable combustion of lean mixtures [55]. In one such study [56], the authors extended the stable lean

operation upto $\lambda = 1.8$ with the application of high spark discharge energy using 10 ignition coils. In another experiment involving methane-air mixture [57], it was inferred that enhanced ignition energy was required for lean mixture combustion as long as turbulence level of flow was sufficient to propagate flames in lean conditions.

There were also many studies, which involved modifications of the conventional inductive ignition system that were suitable for operating lean mixtures. Investigations related to spark plug electrode gap revealed that EGR tolerances could be increased by using large gap plugs [58]. Alger et al. [59] studied the use of multi-coil discharge with dual coil offset (DCO) ignition system. It was observed that continuous discharge by operating the coils alternately enhance the burn rate and stability during combustion. In another study [60], authors found that multiple discharge strategy was more efficient in transfer of energy from spark plug coil, when compared to single discharge. Further, maintaining constant discharge current level for certain period results in restricting the discharge blow-off and hence improve the lean-burn limit [39]. Some studies [39, 61] observed that overlapping multiple flame kernels produced due to re-striking and short-circuiting of spark result in successful flame propagation. Shiraishi et al. [62] reported that formation of large flame kernel due to stretching of spark channel inhibited the cyclic variability of combustion. In a study performed by Tsubai et al. [63], inductive ignition system was customized with 20 ignition coils in order to increase the ignition energy. Discharge ignition energy delivered in the cylinder was increased by increasing the discharge interval. At discharge interval of 0.4 ms, the cyclic variations in combustion were minimum, which resulted in operational excess air ratio of $\lambda = 2.1$. The study suggested that longer discharge interval with lower discharge current could result in proper combustion of lean mixtures. Further flame kernel development was promoted by spark channel elongation and occurrence of spark-shortening phenomenon. Chen et al. [64] demonstrated the use of multi-claw spark plug and high ignition energy in combating the cyclic variations in combustion and increasing the early flame development. The above-mentioned studies suggested that optimization of spark characteristics has potential to improve ignition of lean mixtures in SI engines.

4.2 Effect of Nozzle Design

Three basic types of nozzles are popular for gasoline direct-injector applications, namely swirl nozzle, multi-hole nozzle and outward-opening nozzle. The multi-hole and swirl nozzles are both inward opening nozzles. These are classified on the basis of spray structure they produce, as shown in Fig. 14.

Swirl nozzle employs swirl generator upstream to create swirl motion in the injected spray. They bear high flexible spray characteristics, along with good atomization quality. Moreover, they have high resistance toward contamination and are relatively economical. They produce hollow conical spray, where FIP determines the cone angle. These are not used for spray-guided combustion system, as they influence the spray location with respect to the spark plug. They are considered most suitable

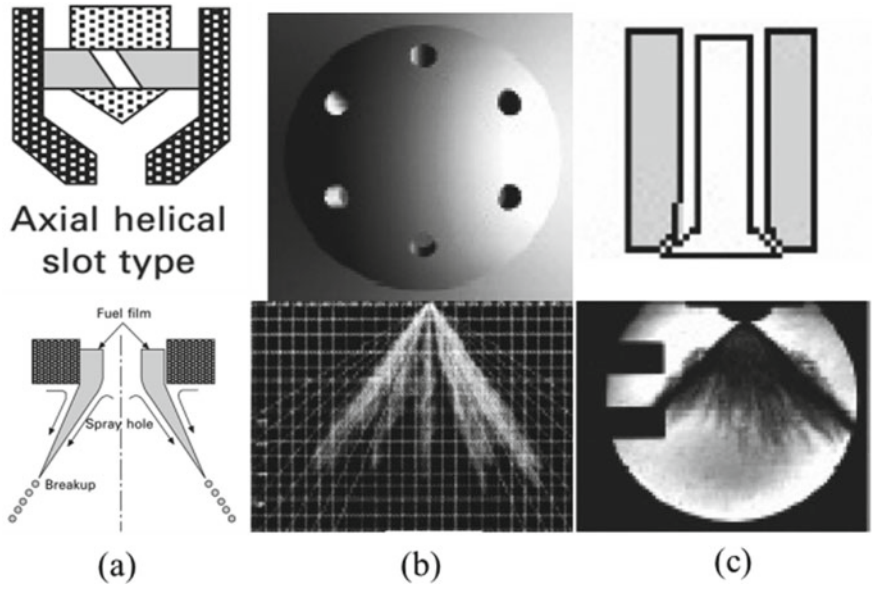

Fig. 14 Spray structures from (**a**) swirl, (**b**) multi-hole and (**c**) outward-opening nozzle [65]

for homogeneous GDI application and stratified GDI operation with wall-guided configuration.

In multi-hole nozzle, the spray plumes create spray configuration having several fuel-enriched zones with surrounding lean mixture zones. Further, it results in partial homogeneous mixture due to inadequate atomization capabilities. The hole pattern and orientation of nozzles result in uniform spread of flame front in combustion chamber and exhibit the best engine performance. Large number of holes is generally suitable for lean-burn operation. However, spray penetration characteristics lead to wall-wetting issues, resulting in high HC and soot emissions. Multi-hole injectors provide benefits in terms of cost and ease of production.

In comparison to swirl nozzle, outward opening nozzle produces hollow conical spray that is less affected by the back pressure [66]. The piezo-control actuation system used with outward opening nozzle enables multiple injections with precise control over the injected mass, hence makes it far superior than solenoid actuated system [67]. Spark plug is normally located at the boundary of spray envelope. These are considered most suitable for spray-guided stratified engine operation due to low sensitivity of spray profile. Further, these injectors are known to generate high turbulence and superior mixture preparation [66, 68].

4.3 Effect of Fuel Injection Parameters

Stratified combustion mode of GDI engine is heavily dependent on fuel injection timing for proper mixture preparation. Initial models of stratified GDI engines were mainly wall-/air-guided type, which utilized internal flow for stratification of fuel–air mixture. However, the internal flows are very susceptible to engine operating conditions and variables such as speed and valve timing [69]. On the other hand, spray-guided engines exhibit comparatively stable operation as the mixture is prepared using spray momentum. Spray-guided engines are designed with narrow spacing concept between the injector and the spark plug, where spark plug is positioned slightly eccentric. Therefore, its stratification capabilities are relatively better than wall-guided type [70]. Though it has its own complexity due to short-mixing length and limited time available for mixture preparation. Unfavorable mixture formation could lead to unstable combustion. Considering this aspect, fuel injection timing is essentially a very important operational parameter for successful engine combustion. It has been found in earlier studies that injection timing has a very narrow range for stable stratified operation in spray-guided configuration and is limited by misfire. Further, fuel injection in the middle of the operable injection timing window results in minimum fuel consumption and cyclic variations [71, 72]. Fuel injection timings also have major influence on the engine emissions. Retarding the fuel injection timing reportedly increased soot emissions and decreased NO_x emissions [72, 73].

In a study done by Oh et al. [74], optical diagnostics tools were employed along with metal engine testing to investigate the effect of injection timing on stratified combustion in a spray-guided DISI engine. They performed the experiments at low speed for fixed fuel injection quantity, with an excess air ratio of 2.8. The optimized spark timings were used for different fuel injection timings. The combustion efficiency was found to be higher in the middle of the narrow injection timing window and lower at both advanced and retarded timings. They mentioned that early fuel injection during comparatively lower ambient pressure resulted in higher spray penetration, which would have resulted in slightly lean homogeneous mixture, rather than the stratified mixture. Due to spread of overall lean mixture widely in the cylinder, chances of incomplete combustion increased, and this was identified by over-mixing effect [75]. On the other hand, injecting fuel with retarded timings resulted in lower spray penetration and stagnant spray due to higher ambient pressure. Hence, in this condition, the presence of locally rich fuel zones due to insufficient mixing further resulted in incomplete combustion and was identified by under-mixing effect [76]. Advanced fuel injection resulted in premixed combustion with blue flames having low luminosity, while retarded fuel injection led to diffusion controlled flames having high luminosity. Higher IMEP values were reported for retarded fuel injection timing. Further, NO_x emissions decreased and smoke increased with retarded fuel injection timings, as shown in Fig. 15. Combustion phasing varied due to retarded injection timing was found critical for these observations.

Since the mixture preparation is realized in very short time in stratified mode combustion, PM emissions are observed in significant amounts, which are higher than

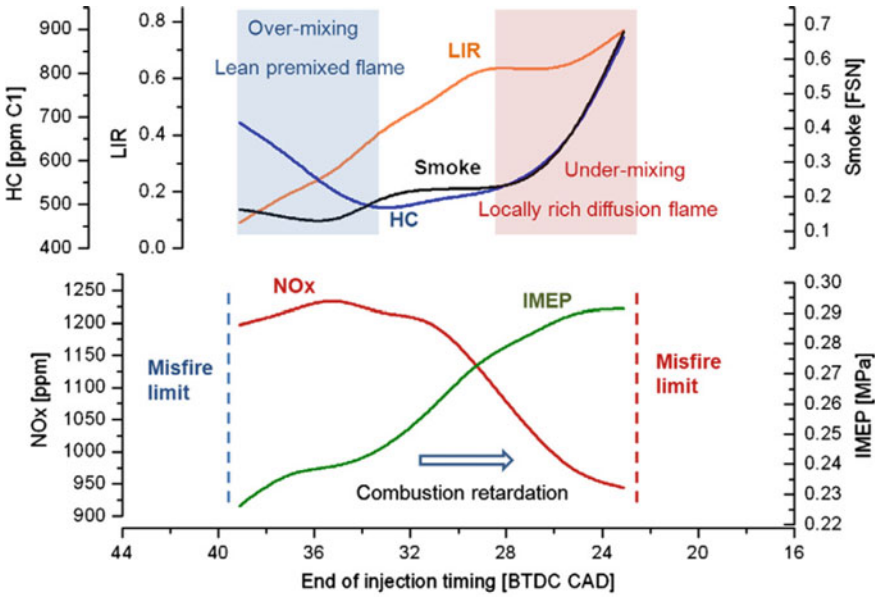

Fig. 15 Emission and combustion parameters for different fuel injection timings [74]

EURO-6 emission limits [77]. Many studies have explored split-injection strategy and considered it as a viable option [78, 79]. Though it is also being used to increase the exhaust gas temperature to reduce the warm-up time of catalyst, in addition, it has resulted in considerable reduction in both HC and particulate emissions along with higher fuel economy benefits and improved quality of charge stratification at part-load conditions [80, 81].

Homogeneously-stratified lean mode operation is particularly of interest to many researchers. In this strategy, first injection is done during the intake stroke to develop homogeneous lean mixture as a base and the second injection is done later during the compression stroke to form stratified mixture over the uniformly lean mixture [82]. Surrounding lean mixture near the cylinder walls stabilizes the combustion and improves the operating limit of engine running with stratified mixture. The number of injections can vary depending on the engine operating point. In one such study performed by Costa et. al. [83], benefits of split-injection under lean operation were demonstrated by experiments and simulations. They used single cylinder wall-guided GDI engine operating at 2000 rpm with excess air ratio of 1.1. Comparison of split injection was made with the single injection as the baseline, achieved by injecting full fuel quantity at 300° bTDC. Results from the study revealed that higher rate of heat release could be obtained with proper selection of spark advance and second injection timing. Timing for second injection was suggested to be just after the closing of inlet valve for optimized performance and lower emissions, as shown in Fig. 16. It also highlighted reduction in cycle-to-cycle variations.

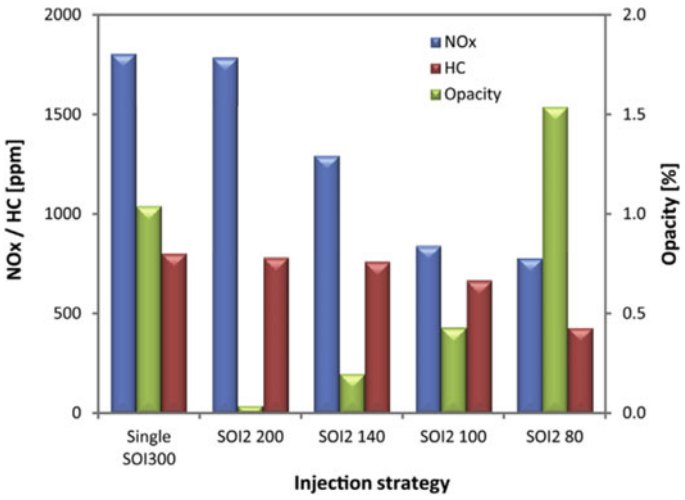

Fig. 16 Emission characteristics for single injection and split-injection for different second injection timings [83]

4.4 Influence of EGR

With growing demand for fuel efficient and downsized high-performance engines, turbocharged GDI engines are becoming increasingly popular. However, their high power density increases the tendency of knocking and NO_x emissions [84]. Hence, EGR is applied in addition to other techniques for limiting the NO_x emissions. Since GDI engine mostly operates under lean conditions, where TWC is non-functional, EGR is used as a primary measure to control the NO_x emissions [27, 85]. In addition, EGR application reduces the throttling losses at part-load conditions as higher throttle opening is required to raise the trapped charge density so that similar torque and power characteristics can be maintained as when no EGR is used. EGR application with respect to different operating modes of GDI engine has already been discussed in the earlier section. Higher EGR application has its own associated limitations such as deteriorated mixture quality, low flame speed, increased HC emissions and high combustion instability [86]. Therefore, a good EGR system having dynamic response capabilities is essential to meet the desired charge quality, while transition from one operating mode to another mode is essential.

Further, EGR stratification can be a possible solution to limit these difficulties. By employing it, EGR can be kept separated from the fresh air in the cylinder; therefore, minimum presence of residual gases around the spark plug can lead to improved flame propagation. However, realizing stratification of EGR in such a complex flow structure in the cylinder is quite challenging. Figure 17 shows various possibilities of obtaining EGR stratification as lateral, axial and radial stratification. Radial stratification can be sustained for a longer time at the end of compression; therefore, it is considered as a most viable method [87, 88].

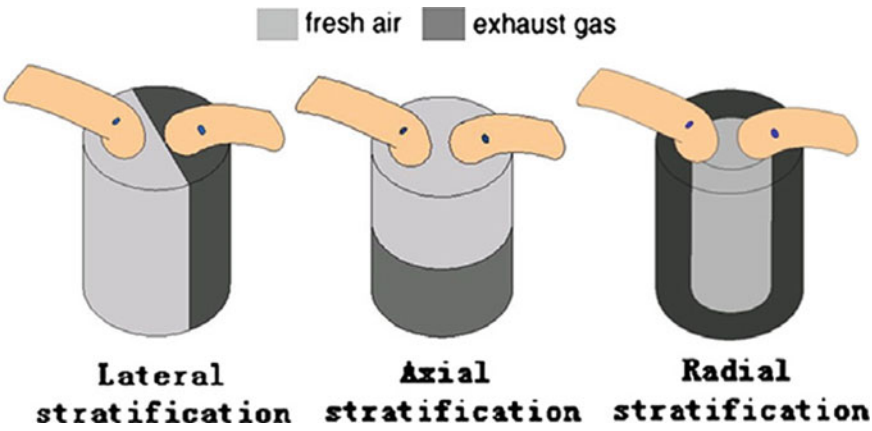

Fig. 17 Different modes of EGR stratification [86]

Practically, studies involving hot EGR have reported lower COV of IMEP, better fuel–air mixing, enhanced flame propagation and lower HC emissions compared to cooled EGR application [89]. However, cooled EGR is most effective in controlling NO_x emissions. Further cooling of exhaust gas maintains the volumetric efficiency of engine at higher level. Hence, cooled EGR is used more extensively in downsized DISI engines.

4.5 Effect of Alternative Fuels

Gaseous fuels: As it is discussed already that the combustion of lean mixtures in gasoline engine suffers from a major limitation of deteriorated combustion stability. Moreover, use of exhaust gas after-treatment devices such as LNT and SCR is unavoidable as TWC alone cannot be used under lean combustion conditions. Use of hydrogen is seen as a potential alternative, which can overcome the barrier of limited utilization of lean combustion in the SI engines. Properties such as higher adiabatic flame speed, diffusion coefficient and flammability limit of hydrogen compared to gasoline favors the improvement in combustion stability and hence increases the thermal efficiency of engine operating under lean conditions [90, 91]. However, its lower energy density and heating value compared to gasoline, along with the challenges of its on-board storage, make the utilization of H_2 difficult [92].

Results from several studies [93, 94] have shown that hydrogen addition has resulted in positive effects on the combustion characteristics. Kim et al. [95] investigated the effect of H_2 addition in turbocharged four-cylinder wall-guided GDI engine at different air–fuel ratios. H_2 was introduced in the front of intercooler sharing 0, 1, 3 and 5% of energy. Major findings of the study were that the combustion phasing advanced with hydrogen addition under all conditions; however, later

phase of combustion was realized with longer duration for part-to-high load conditions. Hydrogen addition resulted in significant reduction in cylinder-to-cylinder and cycle-to-cycle variations, especially at lean combustion conditions. Further, indicated thermal efficiency improved by ~7.7% under lean conditions. Its carbon-deficient feature reduced the HC, CO and CO_2 emissions and resulted in more complete combustion. However, H_2 addition increased the NO_x emissions due to its higher adiabatic flame temperature. Ji et al. [96] investigated the effect of H_2 addition on the split injection mode of DISI engine under lean operation. They observed that addition of H_2 weaken the variations in combustion characteristics caused due to varying second injection timing, which were otherwise very significant without H_2.

Researchers also explored the performance of direct injection of H_2 in gasoline engine [97–99]. Direct injection of H_2 results in formation of rich H_2 cloud near the spark plug, and its wide flammability limit helps in easier combustion of lean gasoline mixtures, while avoiding the limitations of low energy density and back fire. Du et al. [92] explored this by suitable modifications in GDI engine to achieve direct injection of H_2 and port injection of gasoline. The percentage of H_2 addition was varied from 0 to 11% of the incoming air flow rate, and the excess air ratio was kept between 1 and 1.5. It was observed that increasing the H_2 quantity decreased the combustion duration and increased mean effective pressure, rate of pressure rise and exhaust gas temperature. HC and CO emissions reportedly reduced, while NO_x emissions increased. Further, direct injection of H_2 eliminated the problem of lower volumetric efficiency; hence, higher power output was obtained. Additionally, stable combustion at excess air ratio of 1.5 could be achieved, which improved the thermal efficiency of the engine. He et al. [98] reported significant reduction of particulate number of accumulation mode particles with H_2 addition as compared to conventional GDI operation. Similar observations were reported by other researchers also [96, 99]. Yu et al. [100] achieved extension of lean-burn limit and reduction of cyclic variations with application of H_2. The above-mentioned studies suggested that small fraction of H_2 addition could improve overall performance of lean combustion gasoline engines.

Liquid fuels: Ethanol has been considered as a potential alternative fuel for SI engines from many years. Ethanol utilization has increased over the years because of its many favorable properties such as high latent heat of vaporization, high octane number, oxygen content, fast adiabatic flame speed and wide flammability limit. Various studies have reported improved knock limiting characteristics [101], reduced HC and CO emissions [102] and improved lean-burn performance [103] of ethanol. Some studies have investigated the influence of ethanol on lean-burn performance of port fueled SI engines. Only slight increase of 0.2 in the lean limit and 2% reduction in COV of IMEP was reported [104].

Many previous studies have utilized ethanol in blended form with gasoline and indeed, obtained improved thermal efficiency and lower emissions at specific operating conditions [105, 106]. However, this strategy could not fully exploit ethanol's potential at different operating conditions as ethanol/gasoline ratio for optimal performance varies with operating conditions [107]. Therefore, incomplete vehicle coverage, difficult cold start [108], phase separation problem and lack of lubricity

[109] were some of the limitations of this strategy. On the contrary, dual-fuel injection strategy provided the benefit of altering individual fuel quantities according to the requirements of operating conditions. Zhuang et al. [110] performed dual-fuel injection study by employing ethanol direct injection (EDI) with gasoline port injection (GPI). GPI was done to achieve homogeneous gasoline–air mixture, while EDI resulted in ignitable ethanol mixture near the spark plug. Ethanol direct injection improved the stability of lean mixture because of its higher flame speed. Further, late direct injection of ethanol (LEDI) preserved the charge-cooling effect as the time for heat transfer from the walls to gases gets considerably reduced. However, mixture quality gets compromised due to less time availability [111]. Although higher volatility of ethanol than gasoline may improve the mixture homogeneity [112]. From the results, they found that higher extension of lean limit was possible with early DI as compared to late DI of ethanol. EEDI achieved maximum excess air ratio upto 1.29. Further, higher IMEP, lower value of COV of IMEP and reduced emissions were reported with EEDI. Due to poor mixture quality, LEDI could raise the lean limit slightly above the stoichiometric condition. However, higher energy ratio of ethanol (48%) reduced the IMEP and increased the HC and CO emissions compared to energy ratio of 24%, irrespective of fuel injection timing. In another study [26], the researchers compared bio-ethanol and gasoline behavior in the engine operation. A DISI engine was equipped with wall-guided combustion system. Optical analysis revealed that spray behavior of gasoline was more sensitive than ethanol toward the in-cylinder flow. Ethanol usage improved the combustion stability and reduced the particulates and unburnt HC emissions. Further, it resulted in higher combustion speed and peak in-cylinder pressure than gasoline in both homogeneous and stratified combustion modes. Ethanol flames were obtained with less bright spots than gasoline flames, hence were associated with lower soot levels.

Butanol is also utilized as an alternative fuel in SI engines due to its properties close to gasoline. Investigations revealed improved engine performance with use of butanol. Addition of butanol to gasoline has reported reduction in combustion duration and particulate number emissions [113, 114]. Further, in a study on PFI engine with butanol–gasoline blends, improved combustion stability under lean conditions was observed [115]. Aleiferis et al. [116] reported higher laminar flame speed of butanol than gasoline. Utilization of butanol in dual-fuel injection mode was also explored. The fuel injection strategy affected the distribution of different fuels in the engine combustion chamber; hence, it influenced mixture preparation at the time of spark and eventually the combustion process. He et al. [117] performed experiments by employing port injection of butanol/gasoline and direct injection of butanol/gasoline. They reported that IMEP values were higher for $\lambda = 1.3$ compared to $\lambda = 1$ at constant spark timing, when port injection of n-butanol and direct injection of gasoline was done. Further, increase in n-butanol fraction increased the IMEP and thermal efficiency of both lean and stoichiometric conditions. Hence, these studies suggested that there is a scope of eliminating the limitations of lean combustion in DISI engines by optimizing different operational parameters such as ignition, fuel injection, charge control and addition of alternate fuels such as hydrogen and primary alcohols.

5 Conclusion and Way-Forward

Lean-burn combustion in DISI engines is a very promising technology in meeting the stringent requirements of today's automotive industry. Their excellent fuel economy expectation requires enhancement of thermal efficiency of the engine, which in a way favors the government policy of efficient utilization of energy. This is of utmost importance for human beings and for protection of the environment. Along with homogeneous mode operation of GDI engine, which features high torque and power characteristics, GDI engine technology stands at par with other automotive technologies, in catering to the needs of potential users. However, lean mixture combustion and stratified combustion mode of GDI engine face the challenge of limited operating range, high combustion variability and exhaust emissions. The lean-burn combustion in DISI engine has been discussed in great detail with an elaborate explanation of different operating modes and combustion system designs. Second-generation spray-guided combustion systems offer various advantages in terms of superior mixture stratification, improved fuel/air mixing, low sensitivity of spray and combustion characteristics, extended operating range and lower HC and soot emissions, in comparison to first-generation wall-/air-guided combustion system. Various case studies involving diagnosis of in-cylinder flows, spray–air interactions and early flame kernel development using optical and computational tools were discussed to understand the causes for occurrence of misfire and poor-burning cycles, which result in combustion variability, loss of efficiency and increased emissions from lean-burn operation. Tracing the 3D flow field revealed that cycle-to-cycle variations in air flow motion, turbulence level and fuel–air mixture distribution at the time of ignition were mainly responsible for combustion variability of the engine. Moreover, the presence of lean mixture around the spark plug at the time of ignition, dilution of fresh air due to EGR and movement of flame kernel away from the flammable mixture due to strong convective velocities were the main mechanisms behind misfire and poor-burning cycles. Use of large-scale tumble and swirl motion helped in limiting the cyclic variations of flow field in the combustion chamber and improving the combustion stability. Next section included strategies and effects of different operating parameters for combating these limitations and improving the overall performance of lean-burn operation in DISI engines. Employing high ignition discharge energy was successful in improving lean-burn limits. In addition, multiple spark discharge enabled greater flame development in lean mixtures. The effects of various fuel injection parameters were also discussed, which were most crucial in determining the engine performance. Based on different types of nozzle designs, piezo-actuated outward opening nozzle was considered to be most suitable for stratified engine operation in spray-guided configuration. Its features of excellent spray characteristics, precise control over the injected fuel quantity, ability of dynamic response and low sensitivity toward the variations in flow behavior contribute to improving stratified combustion. Further, effect of injection timing and multiple-injection strategies were discussed. Role of multiple-injection strategy in extending the operating limit from high load-low speed condition was explained. Finally, utilization of gaseous and liquid alternative fuels in blended

or dual-fuel injection mode in DISI engine was also discussed. Several studies justified that addition of hydrogen, which significantly reduced the cyclic combustion variability in lean combustion DISI engines, however, increased NO_x emissions was its major limitation. Use of primary alcohols resulted in faster flame propagation and lower soot and NO_x emissions, which improved overall lean-burn performance. Hence, it is clear that further improvement in stratified and lean engine operation is possible if these operating parameters are optimized according to engine driving demand. Realizing the mixtures with desired air–fuel ratio to achieve complete oxidation of gasoline at different operating conditions is itself a challenging task, which requires sophisticated feedback control system. Application of high precision sensors is therefore needed for operating wide range of advanced actuators to control EGR dosage, inlet and exhaust valve timing, etc. Moreover, utilization of high pressure fuel injection system for adequate atomization and spray characteristics suited optimally to specific combustion chamber design is needed.

References

1. Stone, R. (1999). *Introduction to internal combustion engines.* London: Macmillan.
2. Çelik, M. B., & Ozdalyan, B. (2010). Gasoline direct injection. *Fuel Injection.*
3. Zhao, F., Lai, M. C., & Harrington, D. L. (1999). Automotive spark-ignited direct-injection gasoline engines. *Progress in Energy and Combustion Science, 25*(5), 437–562.
4. Smith, J. D., & Sick, V. (2006). *A multi-variable high-speed imaging study of ignition instabilities in a spray-guided direct-injected spark-ignition engine.* SAE Technical Paper.
5. Kalwar, A., & Agarwal, A. K. (2020). *Overview, advancements and challenges in gasoline direct injection engine technology. In advanced combustion techniques and engine technologies for the automotive sector 2020* (pp. 111–147). Singapore: Springer.
6. Fröhlich, K., Borgmann, K., & Liebl, J. (2003). *Potenziale zukünftiger Verbrauchstechnologien, 24.* Vienna: Internationalen Wiener Motorensymposium.
7. Wirth, M., Zimmermann, D., Friedfeldt, R., Caine, J., Schamel, A., Storch, A., Ries-Müller, K., Pilgram G., Ortmann, R., Wuerfel, G., & Gerhardt, J. (2003). The next generation of gasoline direct injection increased consumption potential with optimized system costs/The next generation of gasoline direct injection: improved fuel economy and optimized system cost. In *12. Aachen Colloquium Vehicle and Engine Technology*, 6-8. October 2003 2003 (Vol. 1).
8. Schnittger, W., Königstein, A., Pritze, S., Pöpperl, M., Rothenberger, P., & Samstag, M. (2003). 2.2 Direct Ecotec. *MTZ worldwide, 64*(12), 2–7.
9. Lückert, P., Frey, J., Kemmier, R., Schaupp, U., Vent, G., & Waltner, A. (2005). Kunden-und zukunftsorientierte Technologien am Ottomotor–heute und morgen. na; 2005 April 28.
10. Heywood, J. B. (1988). *Internal combustion engine fundamentals.* New York: McGraw-Hill.
11. Spicher, U., & Heidenreich, T. (2010). Stratified-charge combustion in direct injection gasoline engines. In *Advanced Direct Injection Combustion Engine Technologies and Development 2010 January 1* (pp. 20–44). Woodhead Publishing.
12. Kume, T., Iwamoto, Y., Iida, K., Murakami, M., Akishino, K., & Ando, H. (1996). Combustion control technologies for direct injection SI engine. *SAE Transactions., 1,* 704–717.
13. Spicher, U., Kölmel, A., Kubach, H., & Töpfer, G. (2000). *Combustion in spark ignition engines with direct injection.* SAE Technical Paper; 2000 Mar 6.
14. Sharma, N., & Agarwal, A. K. (2018). Gasoline direct injection engines and particulate emissions. In *Air Pollution and Control 2018* (pp. 87–105). Singapore: Springer.

15. Ortmann, R., Arndt, S., Raimann, J., Grzeszik, R., & Würfel, G. (2001). Methods and analysis of fuel injection, mixture preparation and charge stratification in different direct injected SI engines. *SAE Technical Paper 2001 March 5*.
16. Baumgarten, C. (2006, September 28). *Mixture formation in internal combustion engines*. Springer Science & Business Media.
17. Stefan, S. (2004). Optical diagnostics on FSI transparent engine. In FISITA World Automotive Congress, Barcelona 2004 (pp. 23–27).
18. Anon, V. A. (2002). Bosch Motronic MED7 Gasoline Direct Injection. *Volkswagen Self-Study Program, 253*.
19. Cathcart, G., & Railton, D. (2001). Improving robustness of spray guided DI combustion systems: The air-assisted approach. In *JSAE Spring Convention 2001* (Vol. 20015360).
20. https://www.greencarcongress.com/2006/02/mercedesbenz_pr.html.
21. Ashgriz, N., (Ed.). (2011, February, 18). *Handbook of atomization and sprays: Theory and applications*. Springer Science & Business Media.
22. Moreira, A. L., Moita, A. S., & Panao, M. R. (2010). Advances and challenges in explaining fuel spray impingement: How much of single droplet impact research is useful? *Progress in Energy and Combustion Science., 36*(5), 554–580.
23. Bonatesta, F., Chiappetta, E., & La Rocca, A. (2014). Part-load particulate matter from a GDI engine and the connection with combustion characteristics. *Applied Energy, 1*(124), 366–376.
24. Costa, M., Catapano, F., Sementa, P., Sorge, U., & Vaglieco, B. M. (2016). Mixture preparation and combustion in a GDI engine under stoichiometric or lean charge: An experimental and numerical study on an optically accessible engine. *Applied Energy, 15*(180), 86–103.
25. Su, Y. H., & Kuo, T. F. (2019). CFD-assisted analysis of the characteristics of stratified-charge combustion inside a wall-guided gasoline direct injection engine. *Energy, 15*(175), 151–164.
26. Sementa, P., Vaglieco, B. M., & Catapano, F. (2012). Thermodynamic and optical characterizations of a high performance GDI engine operating in homogeneous and stratified charge mixture conditions fueled with gasoline and bio-ethanol. *Fuel, 1*(96), 204–219.
27. Park, C., Kim, S., Kim, H., & Moriyoshi, Y. (2012). Stratified lean combustion characteristics of a spray-guided combustion system in a gasoline direct injection engine. *Energy, 41*(1), 401–407.
28. Park, C. W., Oh, H. C., Kim, S. D., Kim, H. S., Lee, S. Y., & Bae, C. S. (2014). Evaluation and visualization of stratified ultra-lean combustion characteristics in a spray-guided type gasoline direct-injection engine. *International Journal of Automotive Technology, 15*(4), 525–533.
29. Park, C., Lee, S., & Yi, U. (2016). Effects of engine operating conditions on particle emissions of lean-burn gasoline direct-injection engine. *Energy, 15*(115), 1148–1155.
30. Smith, J. D., & Sick, V. (2005). Crank-angle resolved imaging of fuel distribution, ignition and combustion in a direct-injection spark-ignition engine. *SAE Transactions, 1,* 1575–1585.
31. Goryntsev, D., Sadiki, A., & Janicka, J. (2013). Analysis of misfire processes in realistic direct injection spark ignition engine using multi-cycle large eddy simulation. *Proceedings of the Combustion Institute, 34*(2), 2969–2976.
32. Hamai, K., Kawajiri, H., Ishizuka, T., & Nakai, M. (1988). Combustion fluctuation mechanism involving cycle-to-cycle spark ignition variation due to gas flow motion in SI engines. In *Symposium (International) on Combustion 1988 January 1* (Vol. 21, No. 1, pp. 505–512). Elsevier.
33. Fansler, T. D., Drake, M. C., Düwel, I., Zimmermann, F. P. (2006). Fuel-spray and spark-plug interactions in a spray-guided direct-injection gasoline engine. In *Proceedings of the 7th International Symposium on Internal Combustion Diagnostics. Baden-Baden, Germany 2006 May 18* (pp. 81–97).
34. Fansler, T. D., Drake, M. C., & Böhm, B. (2008). High-speed Mie-scattering diagnostics for spray-guided gasoline engine development. In *W: 8th International Symposium on Combustion Diagnostic, Baden-Baden 2008 January 10*.
35. Peterson, B., Reuss, D. L., & Sick, V. (2014). On the ignition and flame development in a spray-guided direct-injection spark-ignition engine. *Combustion and Flame, 161*(1), 240–255.

36. Zeng, W., Sjöberg, M., & Reuss, D. L. (2015). Combined effects of flow/spray interactions and EGR on combustion variability for a stratified DISI engine. *Proceedings of the Combustion Institute, 35*(3), 2907–2914.
37. Sjerić, M., Kozarac, D., & Tatschl, R. (2015). Modelling of early flame kernel growth towards a better understanding of cyclic combustion variability in SI engines. *Energy Conversion and Management, 1*(103), 895–909.
38. Brown, A. G., Stone, C. R., & Beckwith, P. (1996 February 1). *Cycle-by-cycle variations in spark ignition engine combustion-Part I: Flame speed and combustion measurements and a simplified turbulent combustion model*. SAE Technical Paper.
39. Hayashi, N., Sugiura, A., Abe, Y., & Suzuki, K. (2017). Development of ignition technology for dilute combustion engines. *SAE International Journal of Engines, 10*(3), 984–994.
40. Kelley, A. P., Jomaas, G., & Law, C. K. (2009). Critical radius for sustained propagation of spark-ignited spherical flames. *Combustion and Flame, 156*(5), 1006–1013.
41. Freudenhammer, D., Peterson, B., Ding, C. P., Boehm, B., & Grundmann, S. (2015). The influence of cylinder head geometry variations on the volumetric intake flow captured by magnetic resonance velocimetry. *SAE International Journal of Engines, 8*(4), 1826–1836.
42. Lumley, J. L. (2001). Early work on fluid mechanics in the IC engine. *Annual Review of Fluid Mechanics, 33*(1), 319–338.
43. Stiehl, R., Bode, J., Schorr, J., Krüger, C., Dreizler, A., & Böhm, B. (2016). Influence of intake geometry variations on in-cylinder flow and flow-spray interactions in a stratified DISI engine captured by time-resolved PIV. *International Journal of Engine Research* (published online 2016). https://doi.org/10.1177/1468087416633541.
44. Sick, V., Drake, M. C., & Fansler, T. D. (2010). High-speed imaging for direct-injection gasoline engine research and development. *Experiments in Fluids, 49*(4), 937–947.
45. Stiehl, R., Schorr, J., Krüger, C., Dreizler, A., & Böhm, B. (2013). In-cylinder flow and fuel spray interactions in a stratified spray-guided gasoline engine investigated by high-speed laser imaging techniques. *Flow, Turbulence and Combustion, 91*(3), 431–450.
46. Bode, J., Schorr, J., Krüger, C., Dreizler, A., & Böhm, B. (2017). Influence of three-dimensional in-cylinder flows on cycle-to-cycle variations in a fired stratified DISI engine measured by time-resolved dual-plane PIV. *Proceedings of the Combustion Institute, 36*(3), 3477–3485.
47. Bode, J., Schorr, J., Krüger, C., Dreizler, A., & Böhm, B. (2019). Influence of the in-cylinder flow on cycle-to-cycle variations in lean combustion DISI engines measured by high-speed scanning-PIV. *Proceedings of the Combustion Institute, 37*(4), 4929–4936.
48. Zeng, W., Sjöberg, M., Reuss, D. L., & Hu, Z. (2017). High-speed PIV, spray, combustion luminosity, and infrared fuel-vapor imaging for probing tumble-flow-induced asymmetry of gasoline distribution in a spray-guided stratified-charge DISI engine. *Proceedings of the Combustion Institute, 36*(3), 3459–3466.
49. Nakata, K., Nogawa, S., Takahashi, D., Yoshihara, Y., Kumagai, A., & Suzuki, T. (2016). Engine technologies for achieving 45% thermal efficiency of SI engine. *SAE International Journal of Engines, 9*(1), 179–192.
50. Sjöberg, M., & Zeng, W. (2016). Combined effects of fuel and dilution type on efficiency gains of lean well-mixed DISI engine operation with enhanced ignition and intake heating for enabling mixed-mode combustion. *SAE International Journal of Engines, 9*(2), 750–767.
51. Aleiferis, P. G., Taylor, A. M., Whitelaw, J. H., Ishii, K., & Urata, Y. (2000). Cyclic variations of initial flame kernel growth in a Honda VTEC-E lean-burn spark-ignition engine. *SAE Transactions, 1,* 1340–1380.
52. Masouleh, M. G., Keskinen, K., Kaario, O., Kahila, H., Wright, Y. M., & Vuorinen, V. (2018). Flow and thermal field effects on cycle-to-cycle variation of combustion: scale-resolving simulation in a spark ignited simplified engine configuration. *Applied Energy, 15*(230), 486–505.
53. Jung, D., Sasaki, K., Sugata, K., Matsuda, M., Yokomori, & T., Iida, N. (2017 March 28). *Combined effects of spark discharge pattern and tumble level on cycle-to-cycle variations of combustion at lean limits of SI engine operation.* SAE Technical Paper; 2017.

54. Lee, B., Oh, H., Han, S., Woo, S., & Son, J. (2017, October, 8). *Development of high efficiency gasoline engine with thermal efficiency over 42%.* SAE Technical Paper.
55. Dale, J. D., Checkel, M. D., & Smy, P. R. (1997). Application of high energy ignition systems to engines. *Progress in Energy and Combustion Science, 23*(5–6), 379–398.
56. Jung, D., Sasaki, K., & Iida, N. (2017). Effects of increased spark discharge energy and enhanced in-cylinder turbulence level on lean limits and cycle-to-cycle variations of combustion for SI engine operation. *Applied Energy, 1*(205), 1467–1477.
57. Shy, S. S., Liu, C. C., & Shih, W. T. (2010). Ignition transition in turbulent premixed combustion. *Combustion and Flame, 157*(2), 341–350.
58. Chen, W., Madison, D., Dice, P., Naber, J., Chen, B., Miers, S., Czekala, M., Glugla, C., Qu, Q., & Huberts, G. (2013, April 8). *Impact of ignition energy phasing and spark gap on combustion in a homogenous direct injection gasoline si engine near the egr limit*. SAE Technical Paper.
59. Alger, T., Gingrich, J., Mangold, B., & Roberts, C. (2011). A continuous discharge ignition system for EGR limit extension in SI engines. *SAE International Journal of Engines, 4*(1), 677–692.
60. Yu, X., Yu S, Yang, Z., Tan, Q., Ives, M., Li, L., Liu, M., & Zheng, M. (2017, March 28). *Improvement on energy efficiency of the spark ignition system.* SAE Technical Paper.
61. Zhang, A., Cung, K., Lee, S. Y., Naber, J., Huberts, G., Czekala, M., & Qu, Q. (2013). The impact of spark discharge pattern on flame initiation in a turbulent lean and dilute mixture in a pressurized combustion vessel. *SAE International Journal of Engines, 6*(1), 435–446.
62. Shiraishi, T., Teraji, A., & Moriyoshi, Y. (2016). The effects of ignition environment and discharge waveform characteristics on spark channel formation and relationship between the discharge parameters and the EGR combustion limit. *SAE International Journal of Engines, 9*(1), 171–178.
63. Tsuboi, S., Miyokawa, S., Matsuda, M., Yokomori, T., & Iida, N. (2019). Influence of spark discharge characteristics on ignition and combustion process and the lean operation limit in a spark ignition engine. *Applied Energy, 15*(250), 617–632.
64. Chen, L., Wei, H., Zhang, R., Pan, J., Zhou, L., & Feng, D. (2019). Effects of spark plug type and ignition energy on combustion performance in an optical SI engine fueled with methane. *Applied Thermal Engineering, 5*(148), 188–195.
65. Zhao, H. (2010, January 1). Overview of gasoline direct injection engines. In *Advanced Direct Injection Combustion Engine Technologies and Development* (pp. 1–19). Woodhead Publishing.
66. Skogsberg, M., Dahlander, P., & Denbratt, I. (2007, April 16). *Spray shape and atomization quality of an outward-opening piezo gasoline DI injector*. SAE Technical Paper.
67. Schwarz, C., Schünemann, E., Durst, B., Fischer, J., & Witt, A. (2006, April 3). *Potentials of the spray-guided BMW DI combustion system*. SAE Technical Paper.
68. Merdes, N., Enderle, C., Vent, G., & Weller, R. (2011). The new turbocharged four-cylinder gasoline engine by Mercedes-Benz. *MTZ Worldwide eMagazine., 72*(12), 16–23.
69. Stevens, E., & Steeper, R. (2001). Piston wetting in an optical DISI engine: Fuel films, pool fires, and soot generation. *SAE Transactions, 1,* 1287–1294.
70. VanDerWege, B. A., Han, Z., Iyer, C. O., Muñoz, R. H., & Yi, J. (2003). Development and analysis of a spray-guided DISI combustion system concept. *SAE Transactions, 1,* 2135–2153.
71. Szekely, G. A., & Alkidas, A. C. (2005). Combustion characteristics of a spray-guided direct-injection stratified-charge engine with a high-squish piston. *SAE Transactions, 1,* 1310–1326.
72. Oh, H., Bae, C., & Min, K. (2010). Spray and combustion characteristics of ethanol blended gasoline in a spray guided DISI engine under lean stratified operation. *SAE International Journal of Engines, 3*(2), 213–222.
73. Hemdal, S., Andersson, M., Dahlander, P., Ochoterena, R., & Denbratt, I. (2011). In-cylinder soot imaging and emissions of stratified combustion in a spark-ignited spray-guided direct-injection gasoline engine. *International Journal of Engine Research, 12*(6), 549–563.
74. Oh, H., & Bae, C. (2013). Effects of the injection timing on spray and combustion characteristics in a spray-guided DISI engine under lean-stratified operation. *Fuel, 1*(107), 225–235.

75. Petersen, B., Miles, P., & Ekoto, I. (2010). Optical investigation of UHC and CO sources from biodiesel blends in a light-duty diesel engine operating in a partially premixed combustion regime. *SAE International Journal of Fuels and Lubricants, 3*(1), 414–434.
76. Heywood, J. B. (1988). *Internal combustion engine fundamentals*. Mcgrawhill.
77. Choi, K., Kim, J., Myung, C. L., Lee, M., Kwon, S., Lee, Y., & Park, S. (2012). Effect of the mixture preparation on the nanoparticle characteristics of gasoline direct-injection vehicles. *Proceedings of the Institution of Mechanical Engineers, Part D: Journal of Automobile Engineering, 226*(11), 1514–1524.
78. Li, T., Nishida, K., Zhang, Y., & Hiroyasu, H. (2007). Effect of split injection on stratified charge formation of direct injection spark ignition engines. *International Journal of Engine Research., 8*(2), 205–219.
79. Li, T., Nishida, K., Zhang, Y., Onoe, T., & Hiroyau, H. (2005). Enhancement of stratified charge for DISI engines through split injection. *JSME International Journal Series B Fluids and Thermal Engineering., 48*(4), 687–694.
80. Oh, H., Bae, C., Park, J., & Jeon, J. (2011, September 11) Effect of the multiple injection on stratified combustion characteristics in a spray-guided DISI engine. *SAE Technical Pape.*
81. Costa, M., Sorge, U., & Allocca, L. (2012). Increasing energy efficiency of a gasoline direct injection engine through optimal synchronization of single or double injection strategies. *Energy Conversion and Management, 1*(60), 77–86.
82. Song, J., Kim, T., Jang, J., & Park, S. (2015). Effects of the injection strategy on the mixture formation and combustion characteristics in a DISI (direct injection spark ignition) optical engine. *Energy, 15*(93), 1758–1768.
83. Costa, M., Sorge, U., Merola, S., Irimescu, A., La Villetta, M., & Rocco, V. (2016). Split injection in a homogeneous stratified gasoline direct injection engine for high combustion efficiency and low pollutants emission. *Energy, 15*(117), 405–415.
84. Fontana, G., & Galloni, E. (2010). Experimental analysis of a spark-ignition engine using exhaust gas recycle at WOT operation. *Applied Energy, 87*(7), 2187–2193.
85. Bai, Y. L., Wang, Z., & Wang, J. X. (2010). Part-load characteristics of direct injection spark ignition engine using exhaust gas trap. *Applied Energy, 87*(8), 2640–2646.
86. Wei, H., Zhu, T., Shu, G., Tan, L., & Wang, Y. (2012). Gasoline engine exhaust gas recirculation–a review. *Applied Energy, 1*(99), 534–544.
87. Xu, M., Chen, G., Daniels, C., & Dong, M. (2000). Numerical study on swirl-type high-dilution stratified EGR combustion system. *SAE Transactions, 1,* 1689–1699.
88. Dong, M., Chen, G., Xu, M., & Daniels, C. (2002). A preliminary CFD investigation of in-cylinder stratified EGR for spark ignition engines. *SAE Transactions, 1,* 767–778.
89. Toulson, E., Watson, H.C., Attard, W.P. (2007, August 5). *The effects of hot and cool EGR with hydrogen assisted jet ignition.* SAE Technical Paper.
90. Karim, G. A. (2003). Hydrogen as a spark ignition engine fuel. *International Journal of Hydrogen Energy, 28*(5), 569–577.
91. Ji, C., & Wang, S. (2009). Effect of hydrogen addition on combustion and emissions performance of a spark ignition gasoline engine at lean conditions. *International Journal of Hydrogen Energy, 34*(18), 7823–7834.
92. Du, Y., Yu, X., Wang, J., Wu, H., Dong, W., & Gu, J. (2016). Research on combustion and emission characteristics of a lean burn gasoline engine with hydrogen direct-injection. *International Journal of Hydrogen Energy, 41*(4), 3240–3248.
93. Wang, S., Ji, C., Zhang, B., & Liu, X. (2014). Lean burn performance of a hydrogen-blended gasoline engine at the wide open throttle condition. *Applied Energy, 31*(136), 43–50.
94. Kim, J., Chun, K. M., Song, S., Baek, H. K., & Lee, S. W. (215, September 1). *Effect of hydrogen as an additive on lean limit and emissions of a turbo gasoline direct injection engine*. SAE Technical Paper.
95. Kim, J., Chun, K. M., Song, S., Baek, H. K., & Lee, S. W. (2018). Hydrogen effects on the combustion stability, performance and emissions of a turbo gasoline direct injection engine in various air/fuel ratios. *Applied Energy, 15*(228), 1353–1361.

96. Ji, C., Cong, X., Wang, S., Shi, L., Su, T., & Wang, D. (2018). Performance of a hydrogen-blended gasoline direct injection engine under various second gasoline direct injection timings. *Energy Conversion and Management, 1*(171), 1704–1711.
97. Yu, X., Li, G., Dong, W., Shang, Z., Guo, Z., Li, Y., et al. (2020). Numerical study on effects of hydrogen direct injection on hydrogen mixture distribution, combustion and emissions of a gasoline/hydrogen SI engine under lean burn condition. *International Journal of Hydrogen Energy, 45*(3), 2341–2350.
98. He, F., Li, S., Yu, X., Du, Y., Zuo, X., Dong, W., et al. (2018). Comparison study and synthetic evaluation of combined injection in a spark ignition engine with hydrogen-blended at lean burn condition. *Energy, 15*(157), 1053–1062.
99. Niu, R., Yu, X., Du, Y., Xie, H., Wu, H., & Sun, Y. (2016). Effect of hydrogen proportion on lean burn performance of a dual fuel SI engine using hydrogen direct-injection. *Fuel, 15*(186), 792–799.
100. Yu, X., Wu, H., Du, Y., Tang, Y., Liu, L., & Niu, R. (2016). Research on cycle-by-cycle variations of an SI engine with hydrogen direct injection under lean burn conditions. *Applied Thermal Engineering, 25*(109), 569–581.
101. Costa, R. C., & Sodré, J. R. (2011). Compression ratio effects on an ethanol/gasoline fuelled engine performance. *Applied Thermal Engineering, 31*(2–3), 278–283.
102. He, B. Q., Wang, J. X., Hao, J. M., Yan, X. G., & Xiao, J. H. (2003). A study on emission characteristics of an EFI engine with ethanol blended gasoline fuels. *Atmospheric Environment, 37*(7), 949–957.
103. Germane, G. J,. Wood, C. G., & Hess, C. C. (1983, October, 31). Lean combustion in spark-ignited internal combustion engines-a review. *SAE Technical Paper*.
104. Wei, M., Wang, Y., & Reh, L. (2002). Experimental investigation of the prevaporized premixed (vpl) combustion process for liquid fuel lean combustion. *Chemical Engineering and Processing: Process Intensification, 41*(2), 157–164.
105. Ikoma, T., Abe, S., Sonoda, Y., Suzuki, H., Suzuki, Y., & Basaki, M. (2006, April 3). Development of V-6 3.5-liter engine adopting new direct injection system. SAE Technical Paper.
106. Cohn, D.R., Bromberg, L., & Heywood, J. B. (2008, January 1). Inventors; Massachusetts Institute of Technology, assignee. Fuel management system for variable ethanol octane enhancement of gasoline engines. United States patent US 7,314,033.
107. Hsieh, W. D., Chen, R. H., Wu, T. L., & Lin, T. H. (2002). Engine performance and pollutant emission of an SI engine using ethanol–gasoline blended fuels. *Atmospheric Environment., 36*(3), 403–410.
108. Chen, R. H., Chiang, L. B., Chen, C. N., & Lin, T. H. (2011). Cold-start emissions of an SI engine using ethanol–gasoline blended fuel. *Applied Thermal Engineering, 31*(8–9), 1463–1467.
109. Kabasin, D., Hoyer, K., Kazour, J., Lamers, R., & Hurter, T. (2009). Heated injectors for ethanol cold starts. *SAE International Journal of Fuels and Lubricants., 2*(1), 172–179.
110. Zhuang, Y., & Hong, G. (2014). Effects of direct injection timing of ethanol fuel on engine knock and lean burn in a port injection gasoline engine. *Fuel, 1*(135), 27–37.
111. Hemdal, S., Denbratt, I., Dahlander, P., & Wärnberg, J. (2009). Stratified cold start sprays of gasoline-ethanol blends. *SAE International Journal of Fuels and Lubricants, 2*(1), 683–696.
112. Dunn-Rankin, D., (Ed.). (2011, July 28). *Lean combustion: Technology and control* Academic Press.
113. Zhang, Z., Wang, T., Jia, M., Wei, Q., Meng, X., & Shu, G. (2014). Combustion and particle number emissions of a direct injection spark ignition engine operating on ethanol/gasoline and n-butanol/gasoline blends with exhaust gas recirculation. *Fuel, 15*(130), 177–188.
114. Lattimore, T., Herreros, J. M., Xu, H., & Shuai, S. (2016). Investigation of compression ratio and fuel effect on combustion and PM emissions in a DISI engine. *Fuel, 1*(169), 68–78.
115. Dernotte, J., Mounaïm-Rousselle, C., Halter, F., & Seers, P. (2010). Evaluation of butanol–gasoline blends in a port fuel-injection, spark-ignition engine. *Oil & Gas Science and Technology-Revue De l'Institut Français Du Pétrole, 65*(2), 345–351.

116. Aleiferis, P. G., & Behringer, M. K. (2015). Flame front analysis of ethanol, butanol, iso-octane and gasoline in a spark-ignition engine using laser tomography and integral length scale measurements. *Combustion and Flame, 162*(12), 4533–4552.
117. He, B. Q., Chen, X., Lin, C. L., & Zhao, H. (2016). Combustion characteristics of a gasoline engine with independent intake port injection and direct injection systems for n-butanol and gasoline. *Energy Conversion and Management, 15*(124), 556–565.

Potential of Gasoline Compression Ignition Combustion for Heavy-Duty Applications in Internal Combustion Engines

Harsimran Singh, Utkarsha Sonawane, Ashutosh Jena, and Avinash Kumar Agarwal

Abbreviations

CI	Compression ignition
SI	Spark ignition
LOF	Low octane fuel
HDV	Heavy-duty vehicle
PRF	Primary reference fuel
HCCI	Homogenous charge compression ignition
PM	Particulate matter
NO_x	Oxides of nitrogen
RCCI	Reactivity controlled compression ignition
EGR	Exhaust gas recirculation
HC	Hydrocarbon
PRF	Primary reference fuel
RON	Research octane number
CN	Cetane number
CO	Carbon monoxide
CA	Crank angle
bTDC	Before top dead center
aTDC	After top dead center
PRR	Pressure rise rate
GSA	Global sensitivity analysis
FIP	Fuel injection pressure
IVCT	Intake valve closing time

H. Singh · U. Sonawane · A. Jena · A. K. Agarwal (✉)
Engine Research Laboratory, Department of Mechanical Engineering, Indian Institute of Technology Kanpur, Kanpur 208016, India
e-mail: akag@iitk.ac.in

A. P. Singh et al. (eds.), *Alternative Fuels and Advanced Combustion Techniques as Sustainable Solutions for Internal Combustion Engines*, Energy, Environment, and Sustainability, https://doi.org/10.1007/978-981-16-1513-9_13

TDC	Top dead center
BTE	Brake thermal efficiency
WTW	Well-to-wheel
PCCI	Premixed charge compression ignition
CR	Compression ratio
PFS	Partial fuel stratification
MFS	Medium fuel stratification
HFS	Heavy fuel stratification
LTC	Low-temperature combustion
aHRR	Apparent heat release rate
dB	Decibel
DPF	Diesel particulate filter
TWC	Three-way catalyst
SOI	Start of injection
FIP	Fuel injection pressure
MPRR	Maximum pressure rise rate
GPF	Gasoline particulate filter
HFR	Hydraulic fluid rates
HCB	Hydrogenated catalytic biodiesel
FN	Flow number
EID	Engine ignition delay
BTE	Break thermal efficiency

1 Introduction

Transport sector is by-and-large powered by IC engines, and petroleum-based liquid fuels provide ~95% of transport propulsion energy. By 2040, it is expected that the world population will rise to 9.1 billion from 7.3 billion at present. This will lead to economic expansion, and transportation-related energy demand will climb up by 25%. Liquid fuels became an appropriate choice for the transport sector because of higher volumetric energy density (~3100 and 800 times more as compared to hydrogen and natural gas at NTP), secure storage and transport and availability [1]. The global demand for fossil fuels in transport sector is huge and increasing day-by-day. Gasoline demand will flatten as the average fuel economy for modern passenger cars would improve from 30 miles per gallon to 50 miles per gallon in next one decade. By 2040 diesel demand will grow by ~30% to meet heavy-duty trucking and marine requirements [2]. In 2018, ~26% of global transport sector was supported by heavy-duty vehicles. Global count of heavy-duty vehicles by 2025 is predicted to be ~507 million and will rise to ~790 million by 2040 [3]. In India, road transportation is an attractive and flexible mode to transfer goods and making it available at door step. In present scenario, heavy-duty vehicles make a major contribution to the air pollution including ~66 and ~58% to PM and NO_x emissions even though their

numbers are a quarter of total commercial vehicles plying on the roads. CI engines are more efficient; however; they emit more NO_x and PM emissions compared to their SI engine counterparts. Further, simultaneous reduction in PM and NO_x emissions is challenging for CI engines. These emissions adversely affect human health and the environment; e.g., PM inhalation causes health problems such as asthma, heart and lung ailments. NO_x is a poisonous gas that produces atmospheric smog. Black carbon from diesel vehicles has a tendency to trap 16 times more heat, which makes it a more severe threatening agent than carbon dioxide. To control NO_x and PM emissions from vehicles, various advanced exhaust control devices have been developed. However, they add to system complexity and overall cost of the engine.

Health and environmental concerns have motivated researchers to develop LTC strategies such as GCI, HCCI, PCCI and RCCI. These advanced combustion technologies intend to take advantage of both SI and CI engines and reduce PM and NO_x emissions simultaneously. Conventional diesel combustion with PM and NO_x islands is shown in Fig. 1. More EGR can be used to reduce in-cylinder temperature as well as oxygen content. This leads to reduction in NO_x emissions but oxidation of soot decreases, leading to higher PM emission. This phenomenon is known as PM-NO_x trade-off. LTC strategies ensure lower NO_x emissions due to lower adiabatic flame temperature.

Gasoline-fueled CI engines suffer from longer ignition delay compared to diesel-fueled engines, primarily because of lower cetane number of gasoline. Longer ignition delay means more time for the formation of air–fuel mixture, which leads to superior combustion. Implementation of GCI technology is expected to lower the capital investment in refinery processes with an overall reduction in GHG footprint. GCI has already caught the attention of automotive sector since the last decade. However, there is not a significant research effort reported for its heavy-duty application, which is challenging but a necessity for the future. Therefore, the main objective

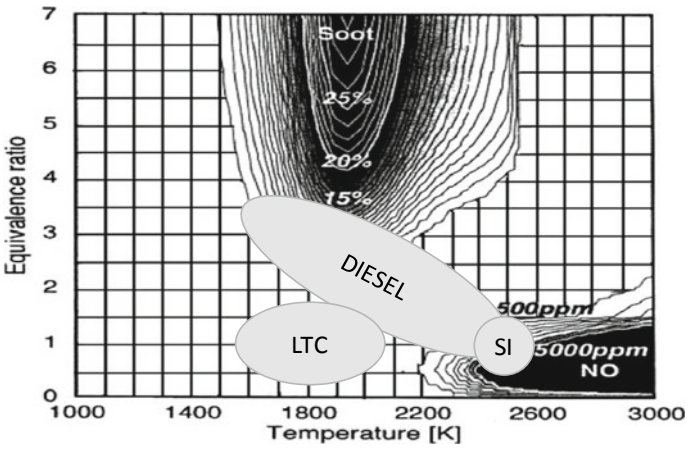

Fig. 1 NO_x islands and working regimes of CI, SI and LTC technique (Adapted from [4])

of this chapter is to explore potential of GCI for heavy-duty CI engines. The chapter starts with an overview and working principle of GCI technology, followed by brief on challenges in heavy-duty applications. Various challenges and their possible solutions are discussed in detail, which add significant value to this chapter. Overall, this chapter provides state of the art about research opportunities associated with the practical implementation of GCI.

2 Overview of GCI Combustion Technology

2.1 Principle of GCI Combustion Technology

GCI is an advanced combustion technology having potential for higher thermal efficiency, and lower exhaust emissions without any major modifications in conventional CI engines. In this technique, CI engine is fueled with gasoline-like fuels instead of diesel. Longer ignition delay of gasoline-like fuels (higher RON than diesel) allows more time for the mixture formation before combustion. It can operate in between fully homogenous combustion like HCCI mode to conventional diffusion combustion like CI mode at different engine loads. At low engine loads, gasoline-like fuel is injected during the intake stroke or at the start of the compression stroke and forms a homogenous mixture, whereas the fuel is injected directly into the cylinder near TDC at high engine loads. Figure 2 provides an idea about the fuel stratification level of GCI with respect to other combustion technologies.

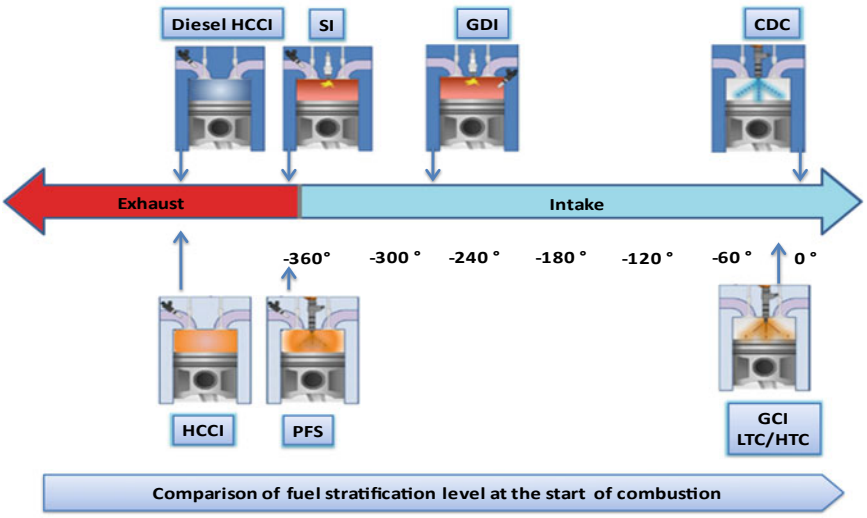

Fig. 2 Fuel stratification spectrum for GCI and other combustion technologies (Adapted from [5])

2.2 Naphtha as a GCI Fuel

Petroleum products like gasoline and diesel are derived from fractional distillation and refinery processes of the crude oil (Fig. 3). Kalghatgi and Johansson [6] in their research concluded that in the near future, energy demand of the transport sector would continue to be fulfilled by petroleum-derived fuels. The demand for diesel in comparison to gasoline would increase at a higher rate, which would lead to a proportional increase in the quantity of low octane components during extraction. Presently, they are processed and blended to increase the octane rating of gasoline. However, reduced demand for gasoline and more than sufficient availability of low octane fractions may create an oversupply and imbalance in availability of petroleum products. Author therefore used the word 'homeless hydrocarbons' to address this waste fraction because these certainly would not be used for production of gasoline in near future. It is expected that the volume of low octane fraction will grow up to 23 quadrillions BTUs by 2040. Now the obvious question, which comes to mind is, where will this large volume of low octane fractions get consumed? What will be the market for low octane fraction? The answer to all these questions is offered by the GCI technology. This low octane gasoline is called 'naphtha,' which can be used with little or no upgrading after desulphurization. It will be readily available in majority of oil refineries as a by-product during fractional distillation process.

Conventional gasoline is more volatile and has a higher octane rating than diesel. Now the question is, what would be the optimum fuel for GCI? Several studies showed that the optimum range of RON for GCI fuel lies within 70–80. Hildingsson et al. [8] concluded that GCI could operate efficiently on low-grade gasoline-like fuels having RON of ~75 to 85. Jiang et al. [9] tested gasoline surrogates PRF 90, 80, 70 and 60

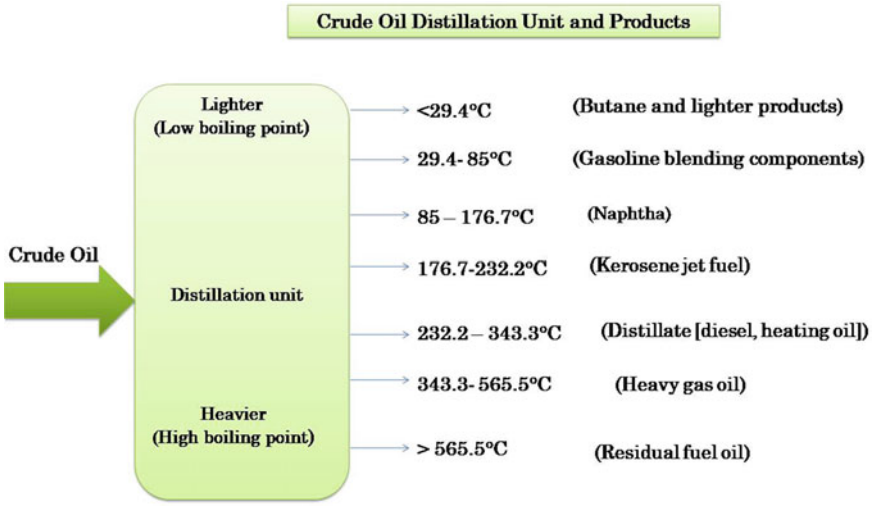

Fig. 3 Typical petroleum refining process (Adapted from [7])

in GCI mode, and their results showed that by controlling the fuel octane number and air intake conditions; the indicated thermal efficiency of PRF70 was even higher than 47% at medium loads in GCI mode. Yang et al. [10] suggested that the RON of ~70 was more appropriate when gasoline was used in a CI engine. Wang et al. [11] numerically investigated the effect of different octane ratings on combustion and emission characteristics of CI engine. They found that PRF70 achieved higher thermal efficiency while maintaining a lower maximum pressure rise rate. It also reduced HC and CO emissions with similar PM and NO_x emissions compared to PRF92. The high octane rating of gasoline resisted auto-ignition due to presence of small branches or cyclic HCs with high bond strength. Naphtha has a complex structure of hydrocarbon molecules having carbon atoms in between 5 and 11. Typically, ~30% of crude oil constitutes of naphtha. Lu et al. [12] performed WTW analysis of the GHG emissions on GCI engines fueled with low octane gasoline. Results showed that WTW GHG emissions for LOF were (12.8 g CO_2 –eq/MJ) lower than gasoline (14.8 CO_2 –eq/MJ) and diesel (13.5 CO_2 –eq/MJ). This showed that LOF followed footpaths of lesser energy-intensive processes. Also, WTW fossil energy usage on per mile basis for LOF was 18% and 6% lower than SI and CI engine-powered vehicles, respectively. Naphtha is the least processed refinery product, which is cheaper and emits much less GHG emissions during production. Hence, it has a larger potential to penetrate the market and act as a competitor for diesel. It shows similar properties as gasoline [13]. Typical properties of diesel, gasoline and naphtha are listed in Table 1.

Chang et al. [15] used naphtha as fuel for CI engines having a CR of 19 in their work and observed lower smoke emission compared to diesel-fueled CI engine. A possible reason may be prolonged ignition delay, which form superior mixture. In a similar study, Wang et al. [16] reported that NO_x emissions could be controlled by adding moderate EGR during combustion. Readily available market fuels can fuel GCI engine. However, in long-term, customized fuels need to be developed for sustainable transport sector. Many researchers used gasoline or gasoline–diesel blends as a low octane fuel for experimental evaluation of GCI. Gasoline and diesel blends can match the required fuel specifications for GCI. Mao et al. [17] investigated multiple injection strategies for heavy-duty diesel engines fueled by gasoline, and

Table 1 Fuel properties of diesel, gasoline and naphtha [14]

Item	Diesel	Gasoline	Naphtha
Cetane number (CN)	52.8	–	31–41
Research octane number (RON)	–	92–98	65.5
Liquid density (kg/m^3)	0.82	0.72–0.78	0.758
Low heating value (MJ/kg)	42.5	43.4	43.99
Kinetic viscosity (at 313 K) (cSt)	2.6–4.1	0.37–0.44	–
Auto-ignition temperature (K)	508	578	498
Boiling point at 1 atm (K)	450–643	299.5–498.5	299.7–421.9

results were compared with baseline diesel. It was found that pilot injection provided better control over combustion and also lowered the emissions. Zou et al. [18] experimentally investigated a single cylinder CI engine for heavy-duty GCI experiments using gasoline as fuel. They studied the influence of intake valve closing timing, two pulse fuel injection and fuel injection pressure on combustion and exhaust emissions at high engine loads. Paz et al. [19] investigated the performance and emission characteristics of heavy-duty engines at high loads and reported that gasoline-fueled engines showed 2° CA longer ignition delay and lower PM emissions. GCI showed pathway to improve PM-NO_x trade-off in CI engines without any reduction in efficiency. GCI technology can potentially downsize the exhaust gas after-treatment devices, hence reduce the cost and complexity.

2.3 GCI Operation Modes

Fuel stratification level depends on the engine operating condition in GCI and can be controlled by fuel injection strategy. Level of fuel stratification affects auto-ignition, combustion phasing, combustion noise and stability and emissions. Therefore, GCI is advantageous in terms of combustion stability for a wider range of operations compared to HCCI. Depending upon the level of fuel stratification, GCI is classified into three major categories as follows (Fig. 4).

In partial fuel stratification (PFS), port fuel injection or early direct injection of the majority of fuel in the intake stroke creates a homogenous charge. During the compression stroke, the main injection creates slight fuel stratification and auto-ignite the entire homogenous charge with an overall reduction in PM and NO_x emissions. All injections in medium fuel stratification (MFS) strategy take place during compression stroke only. The main injection takes place near the TDC and acts as a trigger for combustion. MFS improves the charge stratification by reducing the quantity of premixed fuel, whereas high fuel stratification (HFS) uses the highest level of fuel stratification by eliminating pre-injection of fuel and having a direct injection near TDC. HFS needs higher FIP compared to PFS and MFS. For gasoline-like fuels having high volatility and high resistance to auto-ignition, FIP required for HFS is still lower than what is required for diesel PCCI.

2.4 GCI Versus Other LTC Technologies

As discussed previously, LTC has a few challenges that need to be resolved. Presently, HCCI and PCCI can work under low-to-medium loads, but it is difficult to extend their application to high engine loads [21]. Heavy-duty engines used for experimental evaluation of GCI resulted in lower emissions with higher thermal efficiency compared to HCCI/PCCI [22]. In HCCI strategy, air–fuel mixture is premixed and auto-ignited by increasing the temperature during compression stroke. Premixed charge lowers

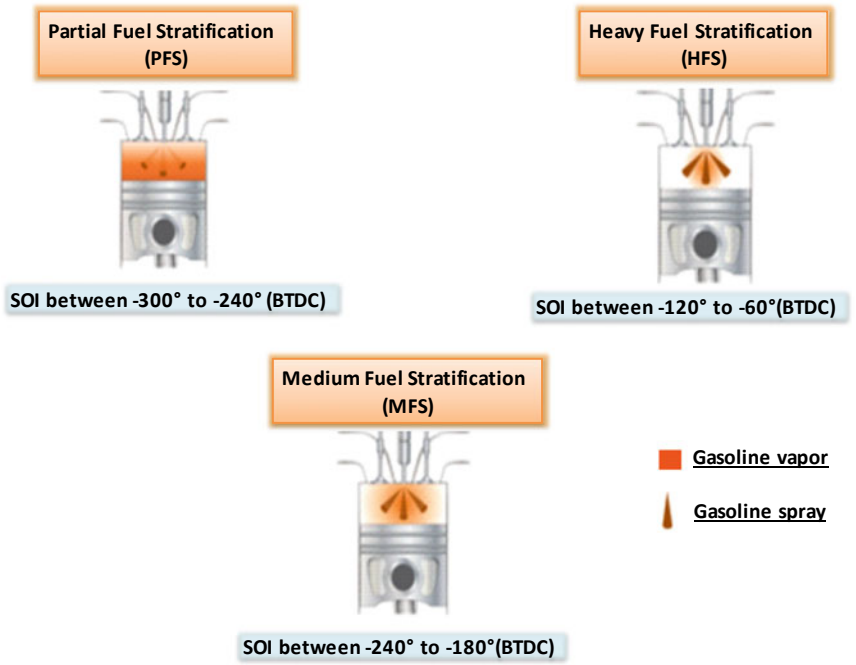

Fig. 4 Classification of GCI operation modes based on fuel stratification levels (Adapted from [20])

the in-cylinder temperature and formation of local fuel-rich zones. High pressure rise rate and unstable operation at high loads remain the main challenges associated with HCCI strategy. However, GCI can resolve issues related to HCCI, owing to superior control over combustion. RCCI is yet another promising strategy to obtain high BTE and comply with stringent emission norms. In this strategy, high reactivity fuel such as diesel is directly injected into the combustion chamber with a port fuel injection of low reactivity fuel like gasoline, alcohol, etc. High reactivity fuel is used to trigger ignition in the combustion chamber. RCCI needs two fuel injection systems, leading to system complexity and additional cost compared to other LTC modes. It emits more CO and HC emissions at lower engine loads. PCCI strategy offers more stable combustion than HCCI mode. It has more mixture formation time compared to conventional CI mode. Ignition of PCCI is same as that of HCCI mode, but it emits lesser CO and HC.

GCI technology may overcome many of the shortcomings of other LTC techniques without substantial design modifications. It also reduces WTW cost of the vehicle in addition to significant reduction in PM and NO_x emissions. GCI uses gasoline-like fuels, which are available in surplus and cheaper. Since GCI engine uses fuels having high volatility, there is no need of using a high-pressure fuel injection systems. Zhang et al. [23] found that the total particle number concentration could be reduced by

~90% by adding 50% gasoline in baseline diesel, along with lower NO_x emissions and higher BTE. Gasoline-diesel blends offer benefits in the combustion process by reducing emissions. RCCI mode emits lower NO_x and engine noise, while higher CO and PM emissions are observed compared to GCI mode. Also, RCCI is sensitive to initial temperature and has a lower fuel economy [24]. Noh et al. [25] studied combustion and performance in CI engines using bio-ethanol as fuel. They found that GCI is one of the advanced combustion technologies capable of overcoming the issues of the LTC technologies. GCI does not require high EGR to resolve problems with high engine load. Moderate EGR can be useful in reducing the NO_x emissions. It has some challenges associated with practical implementation in heavy-duty vehicles. Apart from high CO and HC emissions, it has cold-starting issues, combustion noise issues at medium-to-high load engine conditions and combustion instability at low loads.

3 Major Challenges of GCI Technology

Figure 5 lists the major challenges of GCI technology implementation in heavy-duty CI engines.

3.1 High HC and CO Emissions

One of the major concerns of GCI technology is high HC and CO emissions. CO is a poisonous gas that replaces oxygen from the blood upon human exposure and can be fatal at higher concentrations. Its exposure can trigger heart problems. HC is

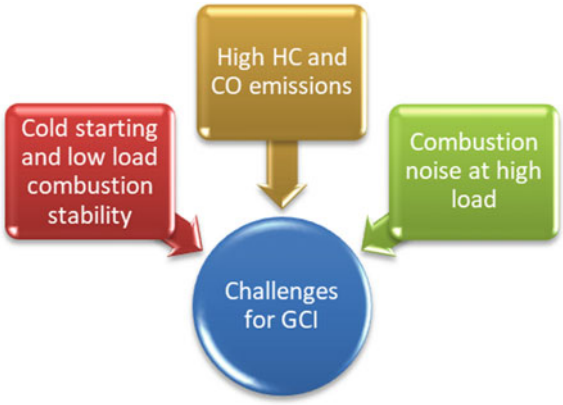

Fig. 5 Major challenges of GCI technology

mostly relatively harmless themselves but helps in formation of photochemical smog in the atmosphere. Yang et al. [26] experimented with a modified six-cylinder engine having CR of 16:1 and displacement volume of 1.08 L per cylinder. Lubricating agent H4140 (1000 ppm) was mixed with gasoline (RON 93) to avoid the failure of the fuel injection equipments. Emission investigations were performed by varying the pilot injection timing (−30° to −70° CA aTDC) with an interval of 15° CA and split ratio of 20 to 80% with 10% interval. In Fig. 6, variations in CO emission values are shown as a function of pilot injection timing and the split ratio. CO emissions were dramatically different before −50° CA aTDC. As the pilot timing advanced to − 50° CA aTDC, the fuel injected undergoes longer ignition delay before the start of combustion (SOC). It leads to formation of further lean air–fuel mixture. This hindered the conversion of CO to CO_2 because of lower combustion temperature. However, split ratio had very little effect on the variation of CO before −50° CA ATDC pilot injection. On the other hand, as the pilot injection was retarded from − 50° CA aTDC, CO values showed variation with split ratio and attained minima at 50%. As split ratio was increased from 50%, more fuel quantity was injected in pilot injection, which again led to the formation of locally lean mixture and low combustion temperature. Thus, higher CO values were recorded because of incomplete oxidation of CO to CO_2. Figure 6 also illustrates the dependence of THC upon the pilot injection timing monotonically. For early split injection, the in-cylinder gas densities were low as the engine was still in the compression stroke and the piston was moving upwards. Thus, pilot fuel injection was likely to have caused spray impingement on the combustion chamber wall surfaces and then entered into crevices because of less hindrance offered by low-density in-cylinder gas. This led to partial flame quenching, which was responsible for unburnt HCs. Indicated thermal efficiency of ~44 to 45% was recorded over the entire range.

Zou et al. [18] experimented on a modified six-cylinder engine with an active cylinder (CR 17:1). Effect of intake valve closing time (IVCT) delay on regulated emissions was studied, and results are shown in Fig. 7.

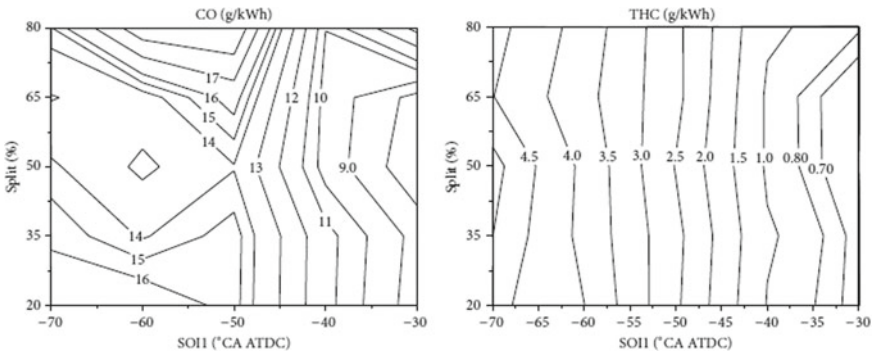

Fig. 6 Variation of CO and HC as a function of pilot injection timing and split ratio [26]

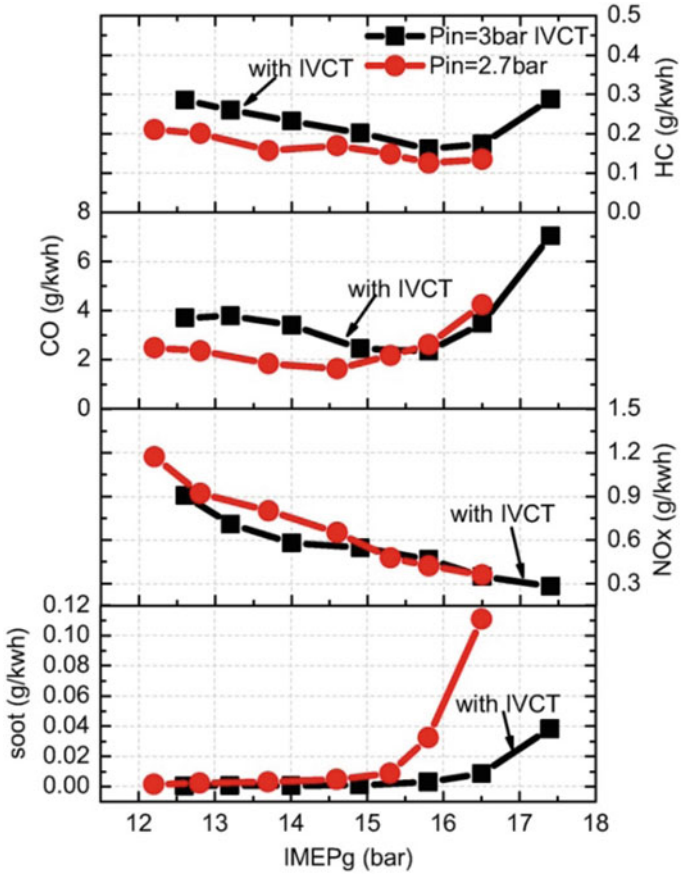

Fig. 7 With/without IVCT effect on HC, CO, NO_x, soot as a function of IMEP [18]

With delay in IVCT, the effective CR and temperature can be reduced during the compression stroke. With IVCT, rise in UHC's and CO emissions were observed. Due to reduction in average combustion temperature, oxidation of CO and HC decreased. Also, under high-load conditions, as IMEP was increased, in-cylinder oxygen concentration decreased, which increased the unburned HC and CO emissions. IVCT greatly affected engine thermal efficiency by reducing the heat transfer loss, which increased by 2.4 to 52.3% under high loads at 16.5 bar IMEP. Wang et al. [27] investigated emissions from different gasoline-like fuels by changing the fuel rail pressure from 20 MPa to 100 MPa in steps of 20 MPa. Figure 8 showed that gasoline-like fuels emitted higher CO and HC emissions compared to baseline diesel. Higher values of fuel injection pressure resulted in well-atomized spray, which assisted the formation of over-lean air–fuel mixture pockets. As explained earlier, over-lean mixture is difficult to burn hence gives rise to emissions. Also, as injection pressure increases, spray penetration length also increases, leading to wall

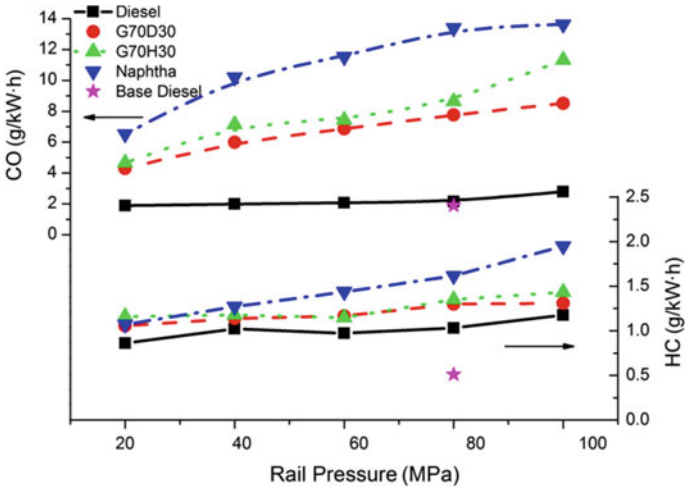

Fig. 8 CO and HC emissions as a function of fuel rail pressure for different test fuels [27]

wetting and partial flame quenching. This may be a possible reason for higher HC emissions. Naphtha showed longer ignition delay and yielded the highest emissions because of over-mixing. In addition, 30% diesel blending in gasoline (G70D30, gasoline 70% and diesel 30% on volume basis) lowered the overall fuel volatility. This formed lesser leaner air–fuel mixtures as compared to G70H30 (gasoline 70% and n-heptane 30% on volume basis) and naphtha.

GCI emits higher HC and CO emissions compared to conventional CI mode. However, with the help of an oxidation catalyst, it is easier to control HC and CO emissions downstream of the engine as compared to NO_x because exhaust in GCI contains trivial amount of oxygen in the engine exhaust. Oxidation catalysts use platinum, palladium or both in order to increase the rate of reaction between oxygen, unburned hydrocarbons and carbon monoxide in the exhaust. This reaction would normally proceed slowly. Catalyst effectiveness depends on its temperature, the air–fuel ratio of the mixture and on several other factors. During cold starting, oxidation of CO and HC does not take place because exhaust temperature is generally not enough to activate the oxidation catalyst. Post-injection of small fuel quantity during exhaust stroke is one possible way to increase the exhaust gas temperature and activate catalyst in early stages. However, this strategy will certainly hit ISFC value. The reason being that post-injection does not contribute to engine power output, but it is only used to raise the exhaust gas temperature. Application of GCI will change the primary focus of the exhaust gas after-treatment devices, i.e., toward the control of HC and CO emissions rather than control of soot and NO_x emissions. However, in GCI, soot emissions over the entire load range are lower in comparison to CI engines. Hence, GPF (similar to DPF) is less soaked at low loads and regenerates itself at high loads because of high exhaust gas temperature. Therefore, CO and HC

emission control with after-treatment devices is one of the effective ways to tackle GCI emissions. Other methods have also been discussed in Sect. (4.1).

3.2 Cold Starting and Low-Load Combustion Stability

Other major challenges for GCI technology include low-load combustion stability and cold-starting issues. These are major reasons because of which the automotive industry has not been able to commercialize this technology thus far. Even the proposers of GCI engine technology, Prof. Gautam Kalghatgi and Prof. Bengt Johansson [6] in their research mentioned the need for further improvement in tackling cold-starting problems. Unburned mixture reactivity, heat aggregation rate and initial thermodynamic state are the prominent factors that affect the firing of GCI engine greatly. Researchers across the globe proposed various strategies to overcome these issues; however, the problems are not fully solved yet. Different strategies such as intake air pre-heating, split fuel injection strategies, negative valve overlap, installation of a glow plug and fuel reforming have been proposed and explored, but cold starting still remains as an unresolved issue. Intake boosting and intake air preheating can easily go with heavy-duty vehicles due to high exhaust kinetic energy. Yao et al. [28] proposed a method to overcome cold-starting and low-load combustion stability issues. This method included switching to GCI mode after starting the engine in conventional mode for a short period. This conventional mode could be either SI or CI combustion mode. For SI combustion mode, additional equipment are required, which include spark plugs, ignition coils, etc., which certainly make engine more complex. Since all modern vehicles are controlled by a microcomputer called 'electronic control unit' (ECU), additional maps for optimizing spark timing and fuel injection timing need to be developed. This would lead to application of more advanced, flexible and more expensive ECU. If the engine initially runs in conventional CI mode, a separate high capacity and expensive fuel supply system would be required. As mentioned earlier, fuel injection pressure in GCI mode is much lower than diesel vehicles. Thus, one would eventually miss a potential advantage of GCI, which is ability to use cheaper and low capacity fuel induction system**.**

NVO is an operating strategy that improves combustion during cold starting. It also extends low-load working regime via trapping of residual gases because of earlier closure of exhaust valve. Residual gases are recompressed, and a fraction of cycle's fuel can be injected to accelerate the engine warm-up. Borgqvist et al. [29] and Hunicz [30] performed experiments and extended low load limit to 0.19 MPa and 0.14 MPa, respectively, while using NVO strategy. Vallinayagam et al. [31] extended the load limit of CI engine fueled with gasoline using a fuel with 91RON and NVO. Researchers explored three-valve overlap cases, which are shown in Fig. 9.

Two modes of combustion, i.e., HCCI and PPC, were successfully achieved by setting SOI as 180° bTDC and 30° bTDC, respectively. HCCI mode achieved slightly lowered IMEP compared to PPC mode at the cost of a reduction in the indicated thermal efficiency. At 30 CAD NVO condition, net indicated efficiency dropped to

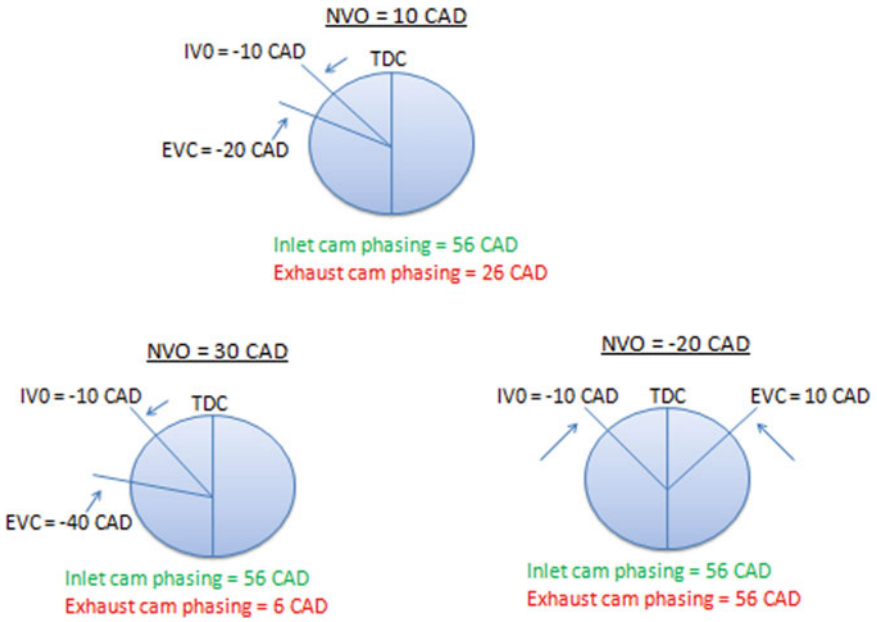

Fig. 9 Valve overlap cases explored for GCI experiments (Adapted from [31])

~18% to achieve the lowest IMEP of 1 bar. Apart from this, net indicated efficiency increased as load increased because of reduction in heat losses. As compared to HCCI, PPC mode attained maximum efficiency of ~33% because of formation of stratified mixture. However, heated intake air was supplied as ignition support at low-load conditions. Soot concentration was almost zero in HCCI mode for all NVO cases. However, soot concentration slightly increased in PPC mode after 2 bar IMEP because of rich mixture formation, as the load increased. As compared to nearly zero NO_x emission levels in HCCI mode at low load (IMEP = 1 bar), PPC mode showed nearly 100 ppm NO_x emissions, which were way higher than HCCI mode but lower than CI mode. At low loads with 30 CAD NVO case, PPC mode exhibited lower CO emission compared to HCCI mode (6500 ppm). CO formation mainly depends on the oxygen concentration and in-cylinder temperature, which act as a catalyst in the oxidation process from CO to CO_2. Stratified mixture favored an increase in temperature, which was not possible in HCCI mode. Also, over-lean mixture gets into the crevices, resulting in incomplete combustion, lower combustion efficiency and increased HC emissions. At IMEP of 1 bar with 30 CAD NVO, HCCI mode recorded 2875 ppm as compared to PPC mode with 1950 ppm. This was attributed to the fact that fuel spray directly targeted the piston top (with 30 CAD BTDC injection) rather than crevices and hence formed stratified mixture. Zhou et al. [32] also evaluated NVO strategy to enhance the low-load combustion stability and cold firing capacity of GCI engine. As shown in Fig. 10a, NVO strategy resulted in the lowest IMEP, low COV and most advanced CA_{50} because of highest reactivity of unburned mixture

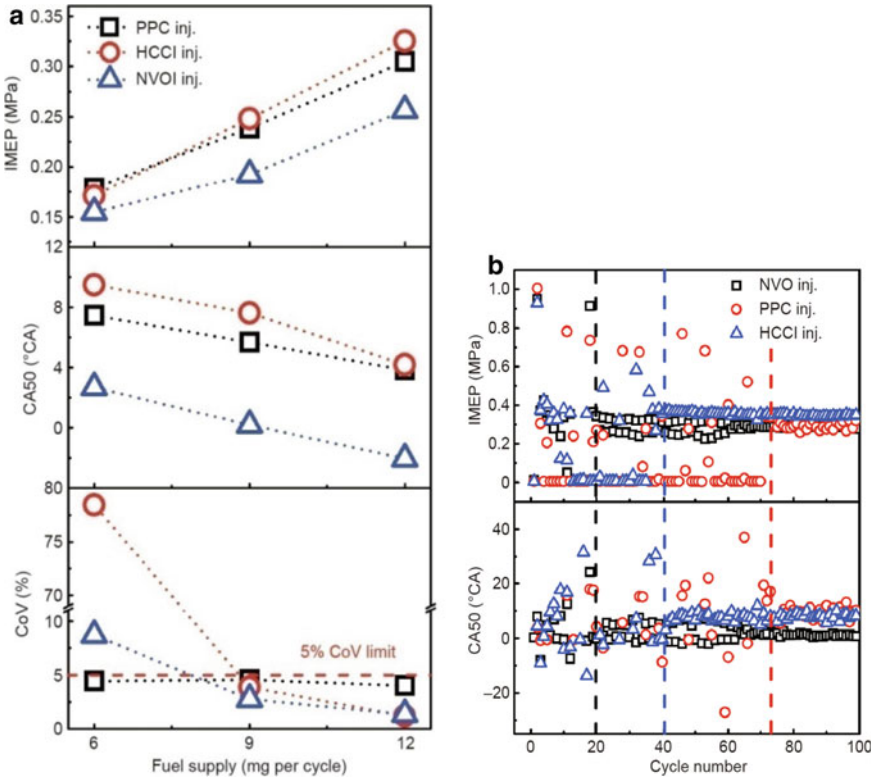

Fig. 10 **a** IMEP, CA_{50}, and CoV with different fuel supplies, **b** IMEP and CA_{50} changing trajectories for three different fuel injection strategies [32]

from previous combustion stroke. This makes it an appropriate strategy for engine warm-up. The pressure and HRR profiles of NVO and HCCI mode were almost similar (not shown here) with the difference being early combustion phasing in NVO because of the presence of highly reactive mixture with shorter ignition delay. Amazingly, NVO strategy showed stable combustion, with COV much lower than 5% and CA_{50} near the TDC when coolant temperature decreased to room temperature. NVO strategy takes minimum time in starting the engine compared to other strategies. NVO takes about 20 cycles (~3 s) at 800 RPM to stabilize the combustion compared to 40 cycles in the HCCI mode (Fig. 10b).

According to Lawler et al. [33], installation of glow plug in the combustion chamber could be another way to warm up the in-cylinder ambient air during cold-starting phase. Glow plug can widen the temperature distribution via unequal heating of charge, which leads to prolonged combustion duration. However, the installation of glow plug has disadvantage of consumption of electric energy, which in some cases lowers the engine efficiency by ~1.4% to 2.5% at low loads. Thus, NVO strategy in conjunction with heated intake has huge potential to extend the low load limit in GCI

mode. However, indicated efficiency drops significantly at low loads. Split fuel injection such as double or triple injections showed promising improvements in indicated efficiency at low loads. Heated intake air is compulsory when the engine coolant is cold. However, the supply of warm air during the intake stroke is not possible for on-road vehicles. Hence, to counter this effect, fuel supply must be sufficient to prevent misfiring. However, analyzing the effect of glow plug position (centrally or side-mounted) along with different in-cylinder swirl spread is still not an explored area in tackling cold start issue in GCI combustion. Particular emphasis must be given to explore its potential on cold-starting issues in GCI mode.

3.3 Combustion Noise at High Load

Vehicle noise not only lowers the ride comfort but also easily stresses out driver, causes agitation, fatigue and distraction. In general, for heavy-duty diesel engines under high-load conditions, magnitude of noise associated with cylinder pressure rise is approximately 20 dB. This noise mainly comes from low-frequency noise of internal combustion engine. In GCI mode, high-pressure rise rate and heat release rate under high-load condition still need refinement because they contribute the most to high engine noise issue. Split fuel injection strategy targets the root cause and diminishes the combustion noise to a great extent. Goyal et al. [34] performed a noise study by varying the first injection proportion for fuels with different ignition quality. Figure 11 shows PRR, which starts decreasing with the increase in the first injection proportion because of an increase in mixture homogeneity. Thus, GCI combustion with split fuel injection strategy can control noise without breaching noise regulations, while maintaining efficiency of ~50%.

Chang et al. [13] compared combustion noise for three different nozzles. Surprisingly, combustion sound level (CSL) for all injectors significantly increased with engine load. Specifically, for HFR520 injector having the largest nozzle diameter 0.141 mm, CSL was 6 dB more than baseline diesel value despite lower HC and

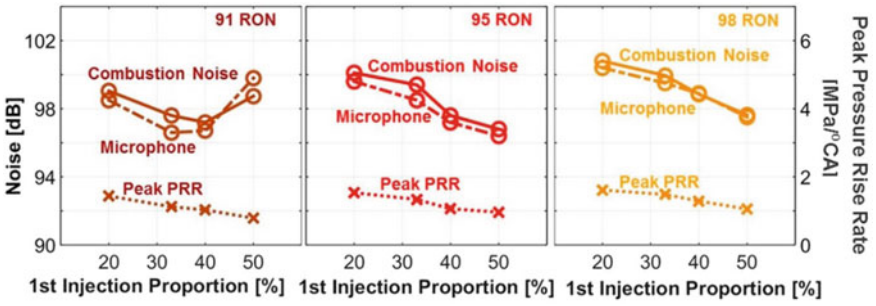

Fig. 11 Measured engine noise, combustion noise and PRR for various fuel ignition qualities and varying first injection proportions [34]

smoke emissions and superior indicated efficiency. This was because of an increase in PRR. Torregrosa et al. [35] observed that the oxygen concentration in the intake stroke has a great impact on the combustion noise. For all injection timings and fuels tested, combustion noise diminished when the oxygen concentration reduced because of the introduction of EGR. Reduction in burning velocity, longer ignition delay and shifting of combustion event toward TDC helped reduce the combustion noise level along with reduction in intake oxygen concentration. However, the above-mentioned strategies can be applied to the combustion chamber only. What if the noise level from a vehicle is still high even with the application of above-mentioned strategies? A suitable muffler can effectively control the noise, especially from heavy-duty vehicles. Most mufflers are passive devices that route the exhaust gases through the chambers and perforated tubes in order to filter the acoustic frequency vibrations without hindering the gas flow. However, traditional passive filters work well only for middle- and high-frequency noise. On the other hand, active mufflers use multiple vibrating panels (essentially speakers), which are driven by microprocessor signals. Microprocessor monitors the acoustic frequencies propagating in the exhaust pipe and generates sound from a speaker, which is out of phase (destructive interference) with the noise generated by the engine. Same principle is used in the noise-canceling headphones. Only difference being that the microphones and speakers used in the automobile exhaust system must be powerful enough to withstand intense heat and corrosive environment of the engine exhaust. The advantage of an active noise cancelation system is that they are relatively light, compact, reduce the length of the exhaust pipe and save additional weight and material costs. Zhu et al. [36] observed that traditional muffler has poor noise reduction characteristics below 150 Hz. Loud buzz from heavy-duty vehicles is found mainly in this frequency band. Results showed that a semi-active muffler device is far superior to traditional muffler in a low-frequency band below 150 Hz. Roughly, all the noise within this range was successfully eliminated. On an average, transmission loss of ~33 and 12 dB was observed in semi-active and traditional muffler devices, respectively. Hence, the crux of this discussion is that along with control in fuel injection pressure, injectors with different cone angles and hole size can control noise levels at high loads. Also, retarded pilot injection can serve the purpose of reduction in noise level but at the expense of increased soot emission because of longer injection event. Mufflers have huge potential in reducing noise downstream of an engine. However, application and investigation of numerous muffler designs (e.g., reactive, absorptive) specifically in GCI heavy-duty engines is still an un-explored area.

4 Control Strategies to Overcome GCI Challenges

4.1 Effect of Injection Strategy

Fuel injection strategy has great potential to control GCI combustion, performance and tailpipe emissions. Multi-injection technology, also known as split fuel injection uses a minimum of two injection pulses to control the rate of pressure rise and heat release rate. Luxury automotive brands use up to seven injections in one engine cycle, which signifies the importance of injection events. Zhang et al. [24] conducted experiments on four-cylinder heavy-duty engines with CR of 18:1. Fuel blends of gasoline and HCB (20–40% v/v) were used to reduce the octane number of fuel and hence increased the ignition delay. Figure 12 shows the variations in CO and HC concentrations with respect to intake air temperature and HCB blending ratio. Interestingly, both species showed an almost similar trend. High intake air temperature and high HCB blending effectively reduced CO and HC emissions. As already discussed, the root cause of these emissions was low combustion temperature, and it was strongly affected by the equivalence ratio. An increase in intake air temperature resulted in a significant rise in combustion temperature, which improved the oxidation of CO and HC emissions; thus, reduction in emission levels was achieved.

Figure 13 shows the equivalence ratio and in-cylinder temperature variations for two HCB blending ratios (P_{GH} 0.1 and P_{GH} 0.5) with a fixed intake air temperature of 370 K for both cases. Equivalence ratio and combustion temperature increased as P_{GH} jumped from 0.1 to 0.5, resulting in reduced CO and HC emissions.

The effect of change in the start of pilot injection timing was also studied, as shown in Fig. 14. With the early pilot injection before −40° aTDC, especially for lower HCB blending ratio, CO emissions increased. The possible reason for such behavior may be the extent of fuel–air mixing before the auto-ignition. With early injection, because of large delay in ignition, over-lean mixture packets formed, which did not burn completely hence emitted CO. Researchers proposed a blending ratio of

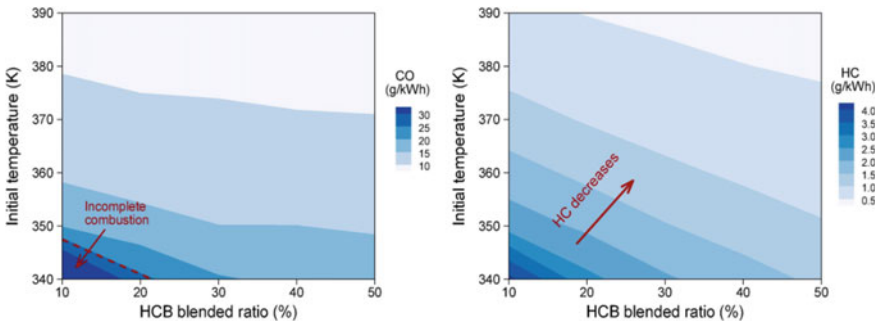

Fig. 12 Variations of CO and HC as a function of HCB blending ration and intake air temperature [24]

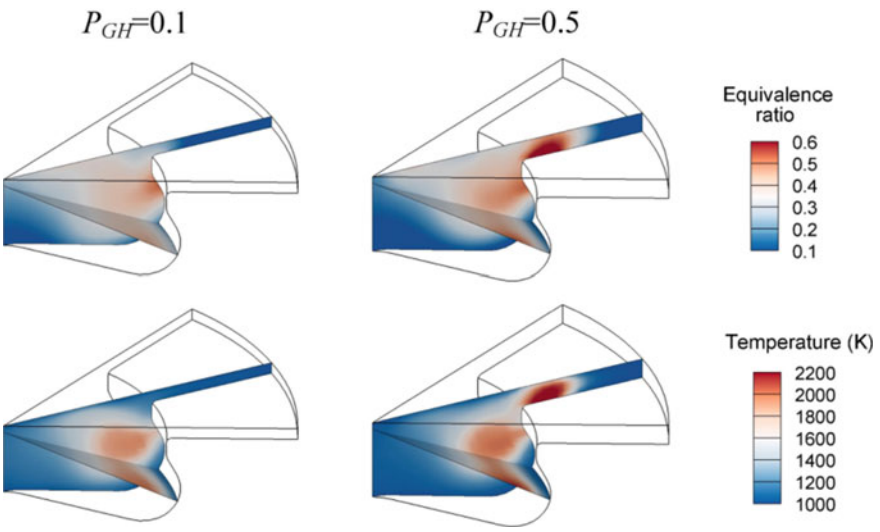

Fig. 13 In-cylinder variations of equivalence ratio and combustion temperature [24]

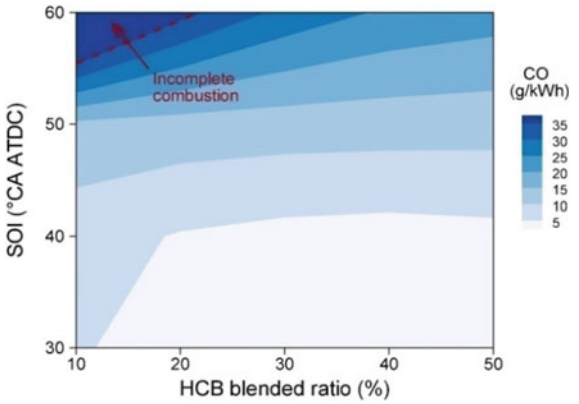

Fig. 14 Distribution of CO as a function of HCB blending ratio and pilot injection timing [24]

10–30% and pilot injection timing −60 to −50° CA aTDC for good fuel economy and to avoid combustion noise at high load.

Manente et al. [37] concluded that ~36% decrease in HC emissions was achieved due to lower piston and wall wetting, when pilot injection timing sweep was performed from 80° bTDC to 20° bTDC in steps of 20°. However, in the beginning, CO concentration decreased and then increased because of over mixing of the air–fuel mixture in early pilot injection and under-mixing (lack of O_2), respectively. For heavy-duty engines under high load, Zou et al. [18] found that the pilot injection ratio of 17.2% was optimum in controlling emissions under 0.98 g/kWh of HC and

10.2 g/kWh of CO. Pal et al. [38] performed a global sensitivity analysis (GSA) to figure out the relative effect of design parameters on the engine efficiency and emissions. A total of eleven design parameters were considered, such as EGR %, injection timing, intake air temperature and intake pressure injector configuration. These design parameters were varied within their defined range using Monte Carlo method, and 256 CFD simulations were performed with commercial CFD software CONVERGE. Six-cylinder heavy-duty engine with a CR of 17.3 fueled with gasoline was used to generate the experimental data. It was found that EGR fraction and intake air temperature affect CO and HC emissions to greater extent. With rise in intake air temperature, regions of lower equivalence ratio formed on a large scale near the cylinder head as compared to lower intake air temperature case. This favored lower UHC production as intake temperature was increased. A value of 0.025 g/kW-hr of HC emissions was recorded at 370 K. Thus, higher intake air temperature is advisable to limit UHC formation. The effect of EGR on CO emissions is discussed in the next section. Low-pressure rise rate along with stretched aHRR profile is possible with early pilot injection and late main injection near TDC, which directly reduced engine knocking tendency. Researchers found that thermal efficiency ranging from ~44 to 50% can be easily achieved with split injection strategy and heated intake air in GCI operation. Split percentage of ~40 to 50% is advisable to maintain high efficiency along with lower ISFC. However, injection timing should be select by keeping CA_{50}within a range of 5°–10° CA aTDC. Along with the effective injection strategy, exhaust after-treatment devices could be an alternative way to control high HC and CO emissions to meet emission regulations.

4.2 Exhaust Gas Recirculation

An effective method to achieve HCCI like low NO_x levels is to dilute the charge with exhaust products before the combustion starts. By increasing the magnitude of air–fuel mixing, the problem of combustion phasing control can be tackled, while meeting stringent emission norms. All LTC technologies mainly focus on controlling NO_x and PM emissions, primarily by reduction in the combustion temperature. Exhaust gas recirculation can be used to reduce combustion temperature in an effective way. The combustion products have a higher value of specific heat as compared to fresh air. By mixing a specific amount of exhaust in the fresh air, the mixture formed can absorb a large amount of heat without showing much increase in temperature and hence reduction in combustion temperature [39]. Hanson et al. [22] experimented on a 2.44 L heavy-duty CI engine with a CR of 16 fueled by gasoline having RON of 95.6. Lubricity agent called Infineum was added to eliminate the possibility of failure of the fuel injection systems because it was originally designed for diesel. Sweep in EGR levels were performed, starting from 0 to 45%. Combustion instability increased for EGR values beyond 45%. Initially, NO_x levels were high because of high combustion temperature and low PM numbers due to high PM oxidation rates. As EGR value increased up to 45%, a decreasing trend was observed for NO_x because

of continuous reduction in combustion temperature. On the other hand, PM values attended maxima and started decreasing after attaining constant values between 10 and 20% EGR. Increment in local equivalence ratio due to induction of charge with inferior oxygen content was responsible for increase in PM numbers. Higher levels of EGR also affect EID. According to researchers, increased ignition delay boost air–fuel mixing, which forms lower equivalence ratio regions and decreases PM levels. GCI requires ~20% lower EGR rate as compared to conventional diesel combustion in order to achieve lower ISFC. ISFC kept on improving as EGR increased and hit its minima of 172.5 g/KWh at 45% EGR. However, researcher suggested 40% EGR as an optimum value in their studies. Hanson et al. [22] also varied pilot injection quantity from 30 to 60% with fixed CA_{50} and main SOI 13° and −13° aTDC, respectively. Results showed that CO values were almost constant over the entire range of pilot percentage, which indicated that within a specific range of split ratio, CO emissions were unaffected. However, rise in HC emissions was noticeable. This increase can be due to more amount of fuel gets confined in rings as the pilot percentage was increased [40]. Manente et al. [41] performed experiments for heavy-duty engine under high-load conditions (8 bar IMEP) for different gasoline-like fuels. Results revealed that all the fuels showed greater than 50% thermal efficiency with a peak of 57%. Even with a higher EGR (>50%), combustion efficiency remained in the range of 95 to 99% as the load increased from 4 to 8 bar gross IMEP. At 4 bar IMEP due to high combustion efficiency (~99%), almost all the fuel gets burnt, thus lowering CO and HC emissions. The values kept on decreasing for higher load conditions at 1300 rpm. As discussed earlier in Sect. 4.1, Pal et al. [38] studied the effect on engine emissions and performance by varying eleven design parameters. Oxygen content reduced with high EGR fraction, resulting in the rise of CO emissions due to decrease in oxidation capacity. However, in general, EGR of 40% is advisable to control both CO and NO_x emissions. The temperature between 1500 and 2000 K was considered to be an optimum to control CO, NO_x, UHC simultaneously. Combustion temperature above 1500 K decreased CO and UHC emissions via providing suitable conditions for oxidation reaction, and temperatures below 2000 K avoid the formation of NO_x. For a heavy-duty vehicle lambda between 1.3 and 1.6 with EGR 45–55% limits the combustion temperature within the range specified above [42]. Reduction in NO_x emissions with exhaust gas after-treatment devices is quite effective but complicated method. Such devices usually operate in a narrow window of lambda. If trace amounts of oxygen content is left in the engine exhaust, the efficiency of these devices drastically drops from 90 to 20%. Thus, with efficient operation of EGR with proper lambda, NO_x, CO, UHC emissions can be reduced to a great extent.

4.3 Combustion Chamber Design

Modifications in combustion chamber design can also help tackle challenges of GCI technology in current scenario. Many researchers around the globe have tested various piston bowl geometries and injectors with different nozzle hole diameters.

Table 2 Specifications of nozzles used in the experiment [43]

Nozzle designation	Specifications
Nozzle 1	0.13 mm orifice diameter (standard for diesel)
Nozzle 2	0.13 mm orifice diameter(with increased FN via honing and designed for blended fuel)
Nozzle 3	0.17 mm orifice diameter (highest FN)

Higher HC and CO emissions at lower loads can be reduced by controlling the mixture strength via changing fuel injection pressure and injector nozzle geometries. Won et al. [43] evaluated three different nozzles having the same cone angle with different nozzle orifice diameters as shown in Table 2. Diesel (CN 56) and GD10 (90% v/v RON 95 gasoline and 10% v/v CN 56 diesel) were used for experiments. However, the experiments were not performed on the heavy-duty engine; yet, results were sufficient to provide an initial idea for an engine with high-load capacity.

Initially, SOI sweep at low load with the engine running at 1200 rpm was performed at constant FIP of 250 bar and pilot injection timing of 50° bTDC. Nozzles with large orifice diameter (high flow rates) show lesser HC and CO emissions as compared to other nozzles by avoiding formation of over-lean mixture pockets, which were difficult to burn. Because of shorter ignition delay in multiple injections, emissions were much lower compared to single injection. Researchers suggested that the use of high intake temperature to avoid higher CO and HC emissions in these conditions. ISFC in the presence of EGR (0–50%) for GD10 blend (~205 g/kWh) was lower than diesel (210 g/kWh) with all three nozzles. This was because heat release was confined closer to TDC and combustion products pushed the piston downwards with greater momentum, and hence, more power was produced compared to diesel. Also, combustion temperature and heat loss were less for GD10 blend, which contributed to higher power output. Thus, a low injection pressure and nozzles with higher flow rates can be used. This may avoid over mixing to lower HC and CO emissions at low-load conditions. However, fuel injection pressure should be sufficient to cause adequate atomization. Engine thermal efficiency decreased with a reduction in CR. However, superior NO_x /PM trade-off can be expected. Chang et al. [35] tested two nozzles with different HFRs and orifice diameters. Nozzle with comparatively large orifice diameters tends to form relatively richer fuel–air mixture, which resulting lower overall HC formation. As discussed earlier, over-lean mixture is always difficult to burn. For the same nozzle, engine with a higher CR produced fewer emissions than an engine with a lower CR because of higher in-cylinder temperature and pressure. However, CO emissions were similar for all cases, indicating that fuel bowl containment was almost similar. Viollet et al. [44] observed improvement in ISFC from 11.5 to 26% as CR increased from 12 to 14 for engine fueled with light naphtha. Kim et al. [45] tested five injector configurations (Table 3) to find their effect on emission and combustion characteristics. Gasoline was used for all experiments. Nozzles with narrow injection angles showed less CO and HC emissions as compared to other

Table 3 Specifications of different injectors used for experiments [45]

Injector	Number of holes	Injection angle (°)	Hole diameter (mm)
8H70	8	70	0.146
8H100	8	100	0.146
8H146	8	146	0.146
10H146	10	146	0.129
14H146	14	146	0.107

nozzles. This may have occurred because narrow injection angle nozzles form stratified mixture, because the whole fuel spray gets confined within the piston bowl. Due to formation of the spray boundary area, which used to be quite lean for wide-angle spray nozzles, this was prohibited in a narrow spray angle case.

Pei et al. [46] evaluated 14.9 L heavy-duty CI engine fueled with gasoline having RON of 80. They presented experimental baseline data for the combustion system design optimization of various parameters such as piston bowl geometry, injector spray and in-cylinder swirl motion. CONVERGE CFD software was used for the numerical study. A design software CASES was used to optimize various piston bowl geometries. Figure 15 depicts important design terms used to describe the piston bowl profile.

According to researchers, lip radius was one of the most important parameters, which affected the spray splitting and mixture formation in the combustion chamber. After running approximately 3000 CFD simulations in MIRA supercomputer, CASES successfully generated 256 optimized piston bowl geometry profiles. A 3D map was constructed for ISFC values with variations in lip radius and step curvatures. Interestingly, it was found that lip radius mainly affected ISFC values. Results suggested that as the lip radius increased, less interaction between the spray and bowl lip took place. Also, poor air utilization in the central bowl region was observed. However, the converse of the above statement was true. Four combinations of engine load and speed were used for testing selected profiles over the entire working range. A dimensionless number called ‘merit number’ was coined, which

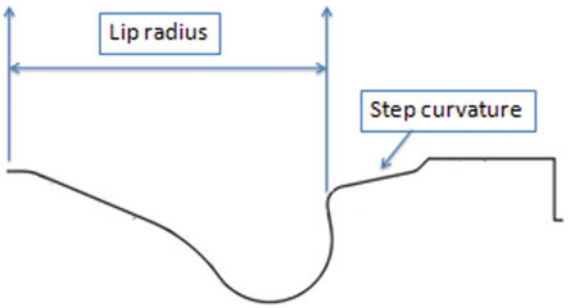

Fig. 15 Description of piston geometry (Adapted from [46])

represented the combined value of MPRR, NO_x, soot and ISFC value of baseline diesel. Based on results, previously selected designs showed higher merit number than baseline diesel, thus showing the best compromise between air utilization and losses due to heat transfer. An increase of 6.3% ISFC was recorded in optimized piston profile. This showed to what extent design considerations affect the GCI combustion. Overall, narrow injection nozzles along with split fuel injection strategy should be employed to reduce the spray penetration into the crevices, hence reducing HC and CO emissions. However, low fuel injection pressure can also serve the purpose of reducing liquid spray length but may cause poor fuel atomization. Various piston geometries with different combinations of bowl and piston diameter along with initial in-cylinder swirl ratios must be investigated in detail.

5 Summary

The future will see higher demand for diesel compared to gasoline. An abundance of cheap naphtha or low octane gasoline will be produced in the refineries, which could be potentially used in GCI engines. This served as the prime motivation for the evolution of GCI technology. It successfully eliminates high PM and NO_x formation problems, while maintaining comparable indicated thermal efficiency of CI engines. The main objective of this chapter was not only to explore the scope of GCI technology in heavy-duty vehicles, but also to identify possible solutions to various challenges, GCI technology faces. Significant reduction in PM levels can be achieved with successful implementation of GCI technology. Gasoline having RON in the range of 70–80 is considered to be an appropriate GCI combustion fuel. Blends of iso-octane and n-heptane can effectively mimic low octane gasoline-like fuel's physical and chemical properties in case of unavailability and it can be used for conducting research experiments. Combustion noise issues can be reduced via split fuel injections. Cold start and combustion instability at low loads can be scaled down via NVO and implementation of a glow plug. Reduction in indicted efficiency because of NVO can be controlled with a split fuel injection strategy. HC, CO and PM emissions can be mitigated effectively using emission control devices. An increase in the cost due to usage of emission control devices can be neutralized by deployment of cheaper and low-cost fuel injection systems. Injectors with lower injection angles should be preferred as they directly target the piston top and eliminate wall impingement problems, thus reducing HC and CO emissions. Globally, a few research laboratories are exploring GCI concept for heavy-duty engines. Effective research efforts for optimization of various influencing parameters will play an important role in addressing various challenges associated with GCI mode.

Particular emphasis must be given to areas like cylinder deactivation methods, opposed-piston concept, design of the muffler, glow plug implementation, piston design and in-cylinder flow dynamics to investigate their potential used in GCI technology engines. GCI technology implementation in IC engines needs further improvements and extensive research. It can be concluded that implementation of

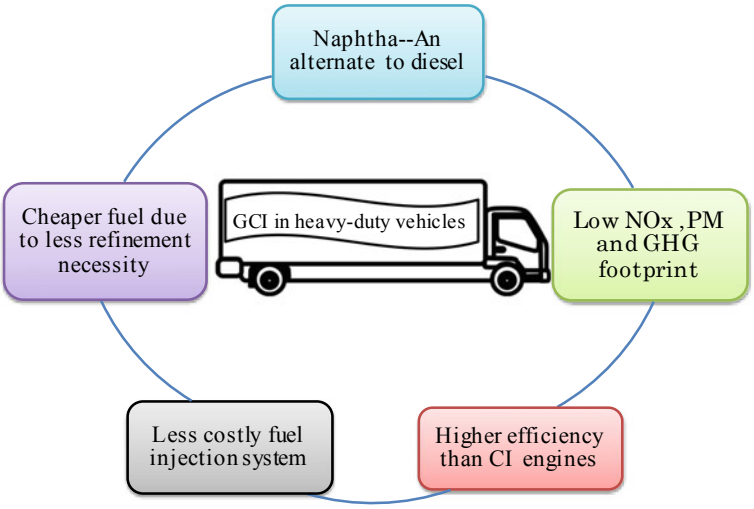

Fig. 16 Gasoline compression ignition-A relatively clean combustion technology for heavy-duty transport

GCI has the capability to create a new market for low octane gasoline in the near future. It is an efficient approach toward an environment-friendly, clean combustion technology for heavy-duty transport sector (Fig. 16).

References

1. Leach, F., Kalghatgi, G., Stone, R., & Miles, P. (2020). The scope for improving the efficiency and environmental impact of internal combustion engines. *Transportation Engineering*, 100005.
2. Mobil, E. (2013). The outlook for energy: A view to 2040. *Exxon Mobil, 6*.
3. World Economic Forum. (2016). Available from: https://www.weforum.org/agenda/2016/04/the-number-of-cars-worldwide-is-set-to-double-by-2040.
4. Agarwal, A. K., Singh, A. P., & Maurya, R. K. (2017). Evolution, challenges and path forward for low temperature combustion engines. *Progress in Energy and Combustion Science, 61,* 1–56.
5. Singh, A. P., & Agarwal, A. K. (2019). Characteristics of particulates emitted by ic engines using advanced combustion strategies. In *Advanced Engine Diagnostics* (pp. 57–71). Singapore: Springer. https://doi.org/10.1007/978-981-13-3275-3_4.
6. Kalghatgi, G., & Johansson, B. (2018). Gasoline compression ignition approach to efficient, clean and affordable future engines. *Proceedings of the Institution of Mechanical Engineers, Part D: Journal of Automobile Engineering, 232*(1), 118–138. https://doi.org/10.1177/0954407017694275.
7. U.S Energy Information Administration. (2019). Refining process. https://www.eia.gov/energyexplained/oil-and-petroleum-products/refining-crude-oil-the-refining-process.php.
8. Hildingsson, L., Kalghatgi, G., Tait, N., Johansson, B., & Harrison, A. (2009). Fuel octane effects in the partially premixed combustion regime in compression ignition engines (No. 2009–01–2648). SAE Technical Paper. https://doi.org/10.4271/2009-01-2648.

9. Jiang, C., Li, Z., Liu, G., Qian, Y., & Lu, X. (2019). Achieving high efficient gasoline compression ignition (GCI) combustion through the cooperative-control of fuel octane number and air intake conditions. *Fuel, 242*, 23–34.https://doi.org/10.1016/j.fuel.2019.01.032.
10. Yang, H., Shuai, S., Wang, Z., & Wang, J. (2013). Fuel octane effects on gasoline multiple premixed compression ignition (MPCI) mode. *Fuel, 103,* 373–379. https://doi.org/10.1016/j.fuel.2012.05.016.
11. Wang, H., Zhu, H., Ma, T., & Yao, M. (2020). Numerical investigation on low octane gasoline-like fuel compression ignition combustion at high load. *Fuel, 270*, 117532. https://doi.org/10.1016/j.fuel.2020.117532.
12. Lu, Z., Han, J., Wang, M., Cai, H., Sun, P., Dieffenthaler, D., Gordillo, V., Monfort, J.C., He, X., & Przesmitzki, S. (2016). Well-to-wheels analysis of the greenhouse gas emissions and energy use of vehicles with gasoline compression ignition engines on low octane gasoline-like fuel. *SAE International Journal of Fuels and Lubricants, 9*(3), 527–545. https://doi.org/10.4271/2016-01-2208.
13. Chang, J., Kalghatgi, G., Amer, A., Adomeit, P., Rohs, H., & Heuser, B. (2013). Vehicle demonstration of naphtha fuel achieving both high efficiency and drivability with EURO6 engine-out NOx emission. *SAE International Journal of Engines, 6*(1), 101–119. https://doi.org/10.4271/2013-01-0267.
14. Bae, C., & Kim, J. (2017). Alternative fuels for internal combustion engines. *Proceedings of the Combustion Institute, 36*(3), 3389–3413. https://doi.org/10.1016/j.proci.2016.09.009.
15. Chang, J., Kalghatgi, G., Amer, A., & Viollet, Y. (2012). Enabling high efficiency direct injection engine with naphtha fuel through partially premixed charge compression ignition combustion (No. 2012–01–0677). SAE Technical Paper. https://doi.org/10.4271/2012-01-0677.
16. Wang, B., Yang, H. Q., Shuai, S. J., Wang, Z., He, X., Xu, H. & Wang, J. (2013). Numerical resolution of multiple premixed compression ignition (MPCI) mode and partially premixed compression ignition (PPCI) mode for low octane gasoline (No. 2013–01–2631). SAE Technical Paper. https://doi.org/10.4271/2013-01-2631.
17. Mao, B., Chen, P., Liu, H., Zheng, Z., & Yao, M. (2018). Gasoline compression ignition operation on a multi-cylinder heavy duty diesel engine. *Fuel, 215,* 339–351. https://doi.org/10.1016/j.fuel.2017.09.020.
18. Zou, X., Liu, W., Lin, Z., Wu, B., & Su, W. (2018). An experimental investigation of the effects of fuel injection strategy on the efficiency and emissions of a heavy-duty engine at high load with gasoline compression ignition. *Fuel, 220*, 437–445. https://doi.org/10.1016/j.fuel.2018.02.035.
19. Paz, J., Staaden, D., & Kokjohn, S. (2018). Gasoline compression ignition operation of a heavy-duty engine at high load (No. 2018–01–0898). SAE Technical Paper. https://doi.org/10.4271/2018-01-0898.
20. Dempsey, A. B., Curran, S. J., & Wagner, R. M. (2016). A perspective on the range of gasoline compression ignition combustion strategies for high engine efficiency and low NOx and soot emissions: Effects of in-cylinder fuel stratification. *International Journal of Engine Research, 17*(8), 897–917. https://doi.org/10.1177/1468087415621805.
21. Zhao, F., Asmus, T. N., Assanis, D. N., Dec, J. E., Eng, J. A., & Najt, P. M. (2003). Homogeneous charge compression ignition (HCCI) engines (No. PT-94). SAE Technical Paper.
22. Hanson, R., Splitter, D., & Reitz, R. D. (2009). Operating a heavy-duty direct-injection compression-ignition engine with gasoline for low emissions (No. 2009–01–1442). SAE Technical Paper. https://doi.org/10.4271/2009-01-1442.
23. Zhang, F., Xu, H., Zhang, J., Tian, G., & Kalghatgi, G. (2011). Investigation into light duty dieseline fuelled partially-premixed compression ignition engine. *SAE International Journal of Engines, 4*(1), 2124–2134. https://doi.org/10.4271/2011-01-1411.
24. Zhang, Y., Zhan, L.,He, Z., Jia, M., Leng, X., Zhong, W., Qian, Y., & Lu, X. (2019). An investigation on gasoline compression ignition (GCI) combustion in a heavy-duty diesel engine using gasoline/hydrogenated catalytic biodiesel blends. *Applied Thermal Engineering, 160*, 113952. https://doi.org/10.1016/j.applthermaleng.2019.113952.

25. Noh, H. K., No, S. Y. (2017). Effect of bioethanol on combustion and emissions in advanced CI engines: HCCI, PPC and GCI mode–A review. *Applied Energy, 208*, 782–802. https://doi.org/10.1016/j.apenergy.2017.09.071.
26. Yang, B., Yao, M., Zheng, Z., & Yue, L. (2015). Experimental investigation of injection strategies on low temperature combustion fuelled with gasoline in a compression ignition engine. *Journal of Chemistry* https://doi.org/10.1155/2015/207248.
27. Wang, B., Wang, Z., Shuai, S., & Xu, H. (2015). Combustion and emission characteristics of Multiple Premixed Compression Ignition (MPCI) mode fuelled with different low octane gasolines. *Applied Energy, 160*, 769–776. https://doi.org/10.1016/j.apenergy.2015.01.115.
28. Yao, M., Zheng, Z., & Liu, H. (2009). Progress and recent trends in homogeneous charge compression ignition (HCCI) engines. *Progress in Energy and Combustion Science, 35*(5), 398–437. https://doi.org/10.1016/j.pecs.2009.05.001.
29. Borgqvist, P., Tunestal, P., & Johansson, B. (2013). Comparison of negative valve overlap (NVO) and rebreathing valve strategies on a gasoline PPC engine at low load and idle operating conditions. *SAE International Journal of Engines, 6*(1), 366–378. https://doi.org/10.4271/2013-01-0902.
30. Hunicz, J., (2014). An experimental study of negative valve overlaps injection effects and their impact on combustion in a gasoline HCCI engine. *Fuel, 117*, 236–250. https://doi.org/10.1016/j.fuel.2013.09.079.
31. Vallinayagam, R., AlRamadan, A. S., Vedharaj, S., An, Y., Sim, J., Chang, J., & Johansson, B. (2018). Low load limit extension for gasoline compression ignition using negative valve overlap strategy (No. 2018–01–0896). SAE Technical Paper. https://doi.org/10.4271/2018-01-0896.
32. Zhou, L., Hua, J., Wei, H., & Han, Y. (2019). An experimental investigation on low load combustion stability and cold-firing capacity of a gasoline compression ignition engine. *Engineering, 5*(3), 558–567. https://doi.org/10.1016/j.eng.2018.12.010.
33. Lawler, B., Lacey, J., Güralp, O., Najt, P., & Filipi, Z. (2018). HCCI combustion with an actively controlled glow plug: The effects on heat release, thermal stratification, efficiency, and emissions. *Applied Energy, 211*, 809–819. https://doi.org/10.1016/j.apenergy.2017.11.089.
34. Goyal, H., Kook, S., & Ikeda, Y. (2019). The influence of fuel ignition quality and first injection proportion on gasoline compression ignition (GCI) combustion in a small-bore engine. *Fuel, 235*, 1207–1215. https://doi.org/10.1016/j.fuel.2018.08.090.
35. Torregrosa, A. J., Broatch, A., Novella, R., Gomez-Soriano, J., & Mónico, L. F. (2017). Impact of gasoline and Diesel blends on combustion noise and pollutant emissions in Premixed Charge Compression Ignition engines. *Energy, 137,* 58–68. https://doi.org/10.1016/j.energy.2017.07.010.
36. Zhu, Y. W., Zhu, F. W., Zhang, Y. S., & Wei, Q. G. (2017). The research on semi-active muffler device of controlling the exhaust pipe's low-frequency noise. *Applied Acoustics, 116,* 9–13. https://doi.org/10.1016/j.apacoust.2016.09.011.
37. Manente, V., Johansson, B., & Tunestal, P. (2009). Partially premixed combustion at high load using gasoline and ethanol, a comparison with diesel (No. 2009–01–0944). SAE Technical Paper. https://doi.org/10.4271/2009-01-0944.
38. Pal, P., Probst, D., Pei, Y., Zhang, Y., Traver, M., Cleary, D., & Som, S. (2017). Numerical investigation of a gasoline-like fuel in a heavy-duty compression ignition engine using global sensitivity analysis. *SAE International Journal of Fuels and Lubricants, 10*(1), 56–68. https://doi.org/10.4271/2017-01-0578.
39. Heywood, J. B. (1988). *Internal combustion engine fundamentals.* New York: McGraw-Hill.
40. Salazar, V. M., & Ghandhi, J. B. (2009). Ring pack crevice effects on the hydrocarbon emissions from an air-cooled utility engine. *SAE International Journal of Engines, 1*(1), 1319–1331.
41. Manente, V., Johansson, B., Tunestal, P., & Cannella, W. (2010). Effects of different type of gasoline fuels on heavy duty partially premixed combustion. *SAE International Journal of Engines, 2*(2), 71–88.
42. Manente, V. (2010). Gasoline partially premixed combustion-an advanced internal combustion engine concept aimed to high efficiency, low emissions and low acoustic noise in the whole load range (Doctoral dissertation, Lund University).

43. Won, H. W., Peters, N., Tait, N., & Kalghatgi, G. (2012). Sufficiently premixed compression ignition of a gasoline-like fuel using three different nozzles in a diesel engine. *Proceedings of the Institution of Mechanical Engineers, Part D: Journal of Automobile Engineering, 226*(5), 698–708. https://doi.org/10.1177/0954407011423453.
44. Viollet, Y., Chang, J., & Kalghatgi, G. (2014). Compression ratio and derived cetane number effects on gasoline compression ignition engine running with naphtha fuels. *SAE International Journal of Fuels and Lubricants, 7*(2), 412–426. https://doi.org/10.4271/2014-01-1301.
45. Kim, K., Jung, Y., Kim, D., & Bae, C. (2016). Effect of injector configurations on combustion and emissions in a gasoline direct-injection compression ignition engine under low-load conditions. *International Journal of Engine Research, 17*(3), 316–330. https://doi.org/10.1177/1468087415573799.
46. Pei, Y., Pal, P., Zhang, Y., Traver, M., Cleary, D., Futterer, C., Brenner, M., Probst, D., & Som, S. (2019). CFD-guided combustion system optimization of a gasoline range fuel in a heavy-duty compression ignition engine using automatic piston geometry generation and a supercomputer. *SAE International Journal of Advances and Current Practices in Mobility, 1*(2019–01–0001), pp. 166–179. https://doi.org/10.4271/2019-01-0001.

Application of CFD in the Design of Reciprocating Engine for Light Commercial Vehicle Applications

D. Siva Krishna Reddy and Pankaj Kumar

1 Introduction

Automotive vehicles use reciprocating engines to generate the required power. Reciprocating engine is an internal combustion engine where a suitable hydrocarbon fuel burned inside the engine. The chemical energy of fuel converted into thermal energy and the process is known as combustion. The released thermal energy further converted into propulsive power with the help of reciprocating mechanism [1]. Thus, the foremost design criteria in the design of an automotive engine are to have lower fuel consumption with higher power delivery. The burned gas or exhaust gas is composed of carbon dioxide (CO_2), partially burned hydrocarbons (HC), carbon monoxide (CO), oxides of nitrogen (NO_X) and soot particulates [2]. These chemical components together are popularly known as emissions and are harmful to human's health. CO_2, HC, CO, NO_X contribute to greenhouse gases and soot particles create respiratory problems to humans [3]. In the last decade, concerns over these emissions have escalated and government regulating authorities impose a certain limit on the released emissions from the automobile engines. Meeting these emission limits is a challenging task as reducing emissions can increase fuel consumption. Thus, the central thrust in the design of an automotive engine is to have lowest fuel consumption with emissions as minimum as possible. It calls for a careful design of each component in the engine system.

Some of the critical components of the engine are (a) air intake system—it includes intake pipe and turbocharger, and controls air flow rate to the engine, (b) intake port geometry—determines flow and swirl coefficients, (c) intake and exhaust valve train—allows fresh air to enter into the engine and exhaust gas to leave from the

D. S. K. Reddy · P. Kumar (✉)
Department of Mechanical Engineering, College of Engineering and Technology, SRM Institute of Science and Technology, SRM Nagar, Kattankulathur, Chennai, TN, India
e-mail: pankajkr@srmist.edu.in

A. P. Singh et al. (eds.), *Alternative Fuels and Advanced Combustion Techniques as Sustainable Solutions for Internal Combustion Engines*, Energy, Environment, and Sustainability, https://doi.org/10.1007/978-981-16-1513-9_14

engine at pre-determined time instants, (d) piston bowl—affects fuel-air mixing, in-cylinder combustion and emission formation (e) fuel injector—controls the injection pressure and duration and (f) EGR cooler—influences the fresh air-EGR mixture temperature. Each component influences the performance of other component, and hence, combustion development is an inter-coupled activity. Combustion development for a diesel engine aims to choose optimal engine components that can lower emissions and lower fuel consumption for the desired vehicle performance.

Over the years, the automotive industry has developed guidelines to design an optimum engine. With the advancement of mathematical modeling of engine processes such as gas exchange process, in-cylinder combustion and engine heat transfer, simulation methods have a part of the engine design process. With the modern-day computational methods and resources, many combinations of engine components can be simulated to arrive at an optimum design for a given emission regulation and vehicle performance. This method can reduce number of physical prototypes required for the engine design, resulting in reduced product development time and cost. Simulation methods can be broadly divided into two categories: (1) one-dimensional thermodynamic performance simulation (1DTPS) and (2) three-dimensional computational fluid dynamics simulation (3DCFDS). In 1DTPS, one-dimensional gas dynamic equations are solved for intake and exhaust strokes [4]. Air flow rates to the engine can be obtained from these equations. For compression and expansion stokes, first law of thermodynamics in the crank angle domain is solved. The combustion of fuel is modeled in the context of one dimensional [5]. These calculations will provide power delivery from the engine. In 3DCFDS, species continuity equations, momentum and energy equations are solved to a specific engine component [6]. These methods provide net heat release, distribution of emission formation and heat transfer across the cylinder head and liner as a function of the crank angle. Hence, these are three-dimensional unsteady simulations.

The industry procedure to design an engine is to determine optimum stoke length, bore diameter, intake pipe length, exhaust pipe length, manifold volumes, intake and exhaust valve timings, valve lift profiles, turbocharger and injection parameters using 1DTPS. After this, preliminary dynamic response of the vehicle to acceleration is evaluated. Then, 3DCFDS will be used to design valves, combustion chamber, injector configuration parameters such as number of holes, spray cone angle and injection rate pattern, etc. The parameters such as flow and swirl coefficients of valves, heat transfer coefficients of critical surfaces and ignition delays need to be provided as input to the 1DTPS. These parameters can be obtained from benchmark data or existing old engine data. In the event of non-existence of data, 3DCFDS can be performed to obtain these parameters. Similarly, input data required for 3DCFDS such as air flow rates, valve timings and lift profiles can be obtained from 1DTPS. Thus, these two simulations are interlinked and depend on each other for inputs. Once the engine is designed from simulations, the physical prototype is tested on engine dynamometer. It is to prove the engine capacity to meet the required performance. In the physical testing, parameters such as nozzle protrusion length, rate shaping, injection strategies are further optimized to obtain the minimum fuel consumption and emissions.

The article discusses the application of 1DTPS and 3DCFDS to design of a naturally aspirated single-cylinder engine that powers a light commercial vehicle. The vehicle is intended to meet BS IV emission regulation. Intake pipe geometric parameters, i.e., length and diameter affect the volumetric efficiency of the engine, and optimization of these parameters with 1DTPS is presented. Measured volumetric efficiency data that supports the optimized intake pipe is discussed. A root cause analysis for the deviation between the predicted and measured volumetric efficiency of the optimized intake pipe is discussed. Engine-out emissions are predicted with 3DCFDS for two piston bowls, which have variations in the combustion chamber geometry. The reduction in brake-specific fuel consumption and emissions which are achieved with modified piston bowl are explained. The interlink between the combustion chamber geometry and emissions is discussed.

2 Methodology

In the present work, 1DTPS and 3DCFDS are performed using commercial softwares AVL BOOST and AVL FIRE, respectively. Governing equations, which are solved in the above softwares are presented below.

2.1 Governing Equations for 1DTPS/AVL BOOST

The air/gas flows in the intake/exhaust piping system are governed by Euler equations and are described below.

$$\frac{\partial U}{\partial t} + \frac{\partial F(U)}{\partial x} = S(U) \tag{1}$$

where $U = [\rho\ \rho u\ E\ \rho w_j]^{\mathrm{T}}$ is vector of state variables. Here ρ is the mixture density, u is velocity, E is total energy and w_j is mass fraction of species j. The total energy is summation of internal energy and kinetic energy and is given by $E = \rho CvT + 0.5\rho u^2$. C_v and T are mixture-specific heat at constant volume and temperature respectively. The flux vector F is given by

$$F = \begin{bmatrix} \rho \\ \rho u^2 + p \\ u(E + p) \\ \rho w_j u \end{bmatrix} \tag{2}$$

Here p is mixture pressure. The term $S(U)$ is source term, and it is given by

$$S(U) = S_A(F(U)) + S_R(U) \tag{3}$$

S_A is source term due to area change in intake and exhaust flow path. It is given by

$$S_A(F(U)) = -\frac{1}{A}\frac{\mathrm{d}A}{\mathrm{d}x}\left[F^{+}\begin{bmatrix}0\\-p\\0\\0\end{bmatrix}\right] \tag{4}$$

where A is area of the pipe at given x location. $S_R(U)$ is source term due to friction, wall heat transfer and chemical reactions. Specific expressions for these terms are given in AVL BOOST manual [7]. The above Euler equations represent system of coupled hyperbolic equations and can be solved using explicit time integration methods.

The thermodynamic state of the gas inside the cylinder is obtained by solving below equations.

$$\begin{aligned}\frac{\mathrm{d}(m_c e)}{\mathrm{d}t} = &-p_c\frac{\mathrm{d}V}{\mathrm{d}t} + \frac{\mathrm{d}Q_F}{\mathrm{d}t} - \sum\frac{\mathrm{d}Q_w}{\mathrm{d}t} - h_{BB}\frac{\mathrm{d}m_{BB}}{\mathrm{d}t} + \sum\frac{\mathrm{d}m_i}{\mathrm{d}t}h_i \\ &- \sum\frac{\mathrm{d}m_e}{\mathrm{d}t}h_e - q_{ev}f\frac{\mathrm{d}m_{ev}}{\mathrm{d}t}\end{aligned} \tag{5}$$

The above equation represents conservation of energy for the gas mixture inside the cylinder. The cylinder is considered as an open system, and the net mass inside cylinder (m_c) is given by

$$\frac{\mathrm{d}m_c}{\mathrm{d}t} = \sum\frac{\mathrm{d}m_i}{\mathrm{d}t} - \sum\frac{\mathrm{d}m_e}{\mathrm{d}t} - \sum\frac{\mathrm{d}m_{BB}}{\mathrm{d}t} + \frac{\mathrm{d}m_{ev}}{\mathrm{d}t} \tag{6}$$

where m_i is mass entering into the cylinder through inlet valve, m_e is mass leaving the cylinder through the exhaust valve, m_{BB} is mass of blow by gases and m_{ev} is mass of the fuel evaporated inside the cylinder. In Eq. 5, e is internal energy of air or gas, p_c is cylinder pressure, V is volume of the cylinder, Q_F is heat input by the fuel, Q_w is wall heat losses, h_{BB} is enthalpy of blow by gases, h_i and h_e are enthalpy of gases entering through intake valve and exhaust vales, respectively. The last term in Eq. 5 indicates heat interaction due to evaporation of fuel inside the cylinder. Note that all the terms in Eqs. 5 and 6 are time dependent.

Equations 1 and 5 are coupled through boundary conditions given by Engl and Rentrop [4]. Solution of Eq. 1 provides thermodynamic conditions of the gas upstream of the intake and exhaust valves. Solution of Eq. 5 gives thermodynamic state of the gas inside the cylinder. Using these conditions, gas flow rates through the intake valve (m_i) and exhaust valve (m_e) can be determined. Details of the 1D combustion models used in BOOST are given in Ref. [7].

2.2 Governing Equations for 3D CFDS/AVL FIRE

In 3DCFDS, conservation equations for mass, momentum and energy will be solved. To account for combustion, species continuity equations will be solved in addition to the above three equations. The above equations for turbulent flows are given in Ref. [6] and are reproduced here.

$$\frac{\partial \overline{\rho}}{\partial t} + \nabla . \overline{\rho} \tilde{\boldsymbol{u}} = 0 \tag{7}$$

$$\overline{\rho} \frac{\partial \tilde{\boldsymbol{u}}}{\partial t} + \overline{\rho} \tilde{\boldsymbol{u}} . \nabla \tilde{\boldsymbol{u}} = -\nabla \overline{p} + \nabla . \overline{\tau} - \nabla . \left(\overline{\rho} \widetilde{(\boldsymbol{u}' \boldsymbol{u}')} \right) \tag{8}$$

$$\overline{\rho} \frac{\partial \widetilde{Y}_k}{\partial t} + \overline{\rho} \tilde{\boldsymbol{u}} . \nabla \widetilde{Y}_k = -\nabla . \left(-\overline{\rho} \widetilde{(\boldsymbol{V}_k Y_k)} \right) + \nabla . \left(-\overline{\rho} \widetilde{(\boldsymbol{u}' Y_k)} \right) + \overline{\omega_k}, \quad k = 1, 2, \ldots., N \tag{9}$$

$$\overline{\rho} \frac{\partial \tilde{e}}{\partial t} + \overline{\rho} \tilde{\boldsymbol{u}} . \nabla \widetilde{e} = -\nabla . \tilde{\mathbf{q}} - \overline{(p \nabla . \mathbf{u})} + \overline{(\tau : \nabla \boldsymbol{u})} - . \left(\overline{\rho} \widetilde{(\mathbf{u}' e')} \right) \tag{10}$$

Equations (7), (8), (9) and (10) are Favre-averaged mixture continuity, mixture momentum, species continuity and mixture energy equations, respectively. Time-averaged flow quantities are represented by an overbar, and that of Favre-averaged flow quantities are given by the symbol tilde, "~". In the above equations, $\overline{\rho}$ is mixture density, $\tilde{\boldsymbol{u}}$ is velocity vector, $\overline{p}$ is pressure, $\overline{\tau}$ is shear stress, $\widetilde{(u'u')}$ is turbulent shear stress, $\overline{Y_k}$ is mass fraction of kth species, N is total number of species, $\overline{\boldsymbol{V}}$ is molecular diffusion velocity of the kth species, $\overline{\omega_k}$ is source term of kth species due to combustion chemical reactions and $\tilde{e}$ is total energy of the mixture. Closure for the above equations for turbulent chemically reacting flows is given in the work of Echekki and Mastorakos [6].

In the AVL FIRE software, k-ξ-f turbulence model is used to account for the turbulence effects. Extended coherent flame model (ECFM)-3Z [8] is used to compute the combustion. The diesel combustion is approximated by solving 11 species transport equations for the species, O_2, N_2, CO_2, CO, H_2, H_2O, O, H, N, OH and NO. Fuel spray is modeled using Lagrangian approach, and detailed validation study of spray model has been reported by Reddy et al. [9].

2.3 Experimental Setup

The performance of engine with different intake pipes and piston bowls is evaluated on a steady-state engine test bed. A schematic of the test bed is shown in Fig. 1. The test bed consists of an eddy current dynamometer with necessary controls. The engine is supplied with conditioned air. The test bed is instrumented with fuel, air

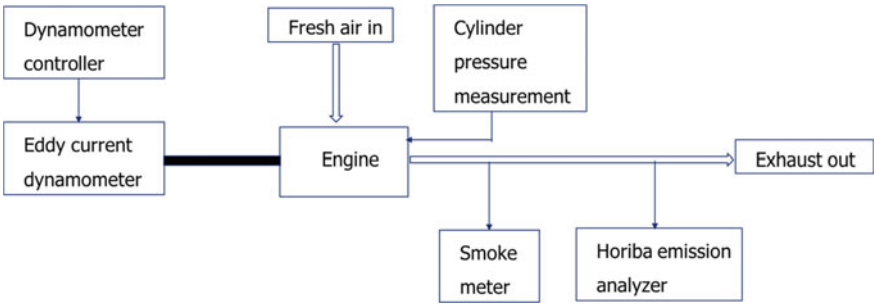

Fig. 1 Schematic of the engine test bed with necessary instrumentation

and emission measurement systems. Horiba emission analyzer is used to measure the emissions. Smoke of the exhaust gas is measured with AVL smoke meter. In-cylinder pressure is measured with fast response pressure sensors. Engine performance parameters such as torque, power, brake specific fuel consumption and air flow rates are measured at different engine speeds spanning from 1000 to 3600 RPM. With Horiba emission analyzer, exhaust emissions such as THC, CO and NO_X are measured. With the in-cylinder pressure measurement, instantaneous cylinder pressure, peak firing pressure and heat release rate and indicative mean effective pressure are obtained.

3 Results

3.1 Optimization of Intake Pipe

The pipe that connects air filter and engine is termed as intake pipe. For naturally aspirated engines, air breathing capacity or volumetric efficiency is a strong function of intake pipe length and diameter [1]. 1DTPS is performed to determine air flow rates of the engine as a function of length and diameter. Commercial software AVL BOOST is used for this purpose. Figure 2 shows contours of volumetric efficiency at 3600 RPM. Maximum volumetric efficiency of 93% is obtained for a combination of 36 mm diameter and 600 mm length. Similar data analysis is performed for the engine in the range of 1000–3600 RPM, with an interval of 200 RPM. It covers the entire engine operating speed range. In the medium-to-high speed range, the combination of 36 mm diameter and 600 mm length found to give maximum volumetric efficiency [10].

To understand the reasons for higher air flow rates with 600 mm pipe, pressure variations at the inlet port with respect to crank angle are analyzed. The pressure pulsations obtained from the simulations with 500 mm, 700 mm and 900 mm are shown in Fig. 3. The pipe length includes 100 mm of intake port length also. The diameter for the three pipes is 34.4 mm. Crank angle is non-dimensionalized, and

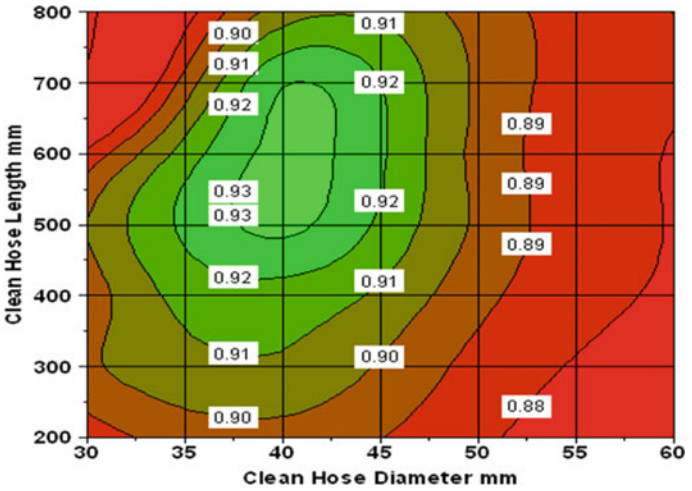

Fig. 2 Predicted volumetric efficiency as a function of diameter and length of intake pipe at engine speed of 3600 RPM

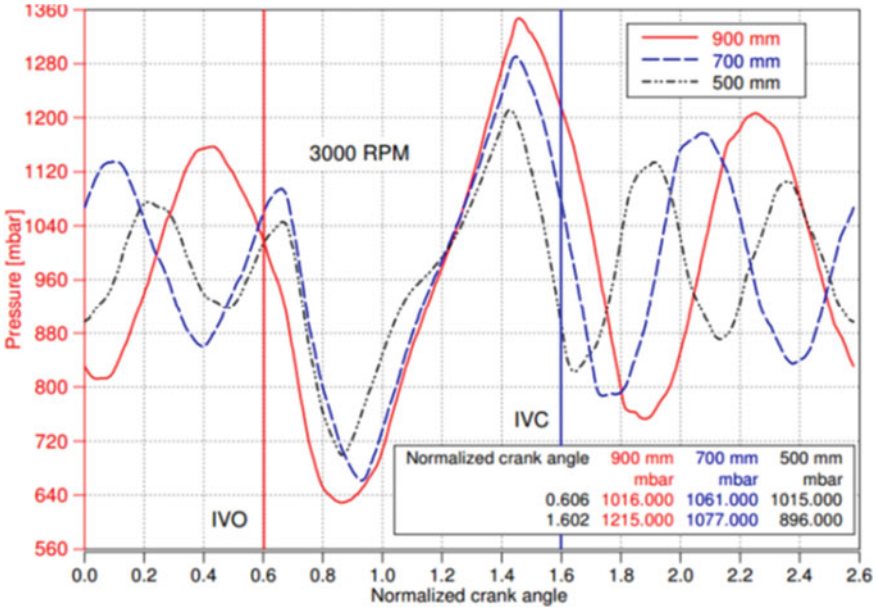

Fig. 3 Variation of pressure at the intake port as a function of crank angle for intake pipes of different length

the vertical lines 'IVO' and 'IVC' indicate intake valve open and intake valve close timings, respectively. During the intake valve open period, i.e., normalized crank angle (NCA) ranging from 0.6 to 1.6, there is a decrease in pressure for the three pipes until NCA 0.9, and with further increase in NCA pressure increases. As the intake valve opens, air rushes into the cylinder resulting in the decrease of pressure in the initial part of valve open period. As the intake valve closes, area available for the air to enter into cylinder diminishes. As a result, pressure builds up in the intake port, in the later part of the valve open duration. The increase in air pressure, enhances the stagnation pressure just upstream of the intake valve. This allows additional air flow, into the cylinder. This effect is known as ramming phenomena [1].

After IVC, the residual air mass in the intake port travels toward air filter due to its high pressure and momentum. After hitting air filter, air travels again toward to intake port. This sets up the pulsating flow in the intake pipe. The amplitude of these pressure pulsations will decay with respect to time due to viscous effects. If the intake valve opens, when the pressure pulse arrives at intake port, then higher amount of air flow can be expected. The pulse also suppresses the back flow of air from the cylinder when the intake valve opens. This effect is known as tunning. For the chosen three pipes in Fig. 3, 700 mm pipe has a higher pressure peak at IVC, and moderate pressure at IVC. Therefore, the tunning and ramming effects are dominant for 700 mm length, and resulted in higher air flow rates to the engine, compared to the other pipes. An in-depth analysis of pressure pulsations and their effect on air flow rates to the engine are reported by Manjunath et al. [11].

Air flow rates to the engine with intake pipes of different diameters and lengths are measured on steady-state engine dynamometer and are shown in Fig. 4. Testing was performed with polyvinyl chloride (PVC) pipes, and 36 mm diameter pipe was not available. Hence, pipe with diameter 34.4 mm, which is nearest to optimum diameter of 36 mm, was tested. Maximum air flow rates are observed for intake pipe with diameter of 44 mm and 380 mm length, and minimum air flow rates occurred for the combination of 34.4 mm and 600 mm. This is opposite to that observed in the numerical simulations. Simulated air flow rates for 34.4 mm diameter with 600 mm length are also shown in the figure. The deviation between prediction and measurement is negligible for speeds up to 2400 RPM, and beyond this, deviation increases as the speed of the engine increases. With none of the above combinations, the smoke limits for BS IV emission regulations at rated speed of 3600 RPM are achieved by the engine. This necessitated to perform a root cause analysis for this deviation and increase air flow rates at rated speed so that smoke limits as per the emission regulation can be achieved.

The PVC pipes used in the testing were not flexible; hence, flexible rubber hoses are used to join the PVC pipes at the air filter and engine ends. The rubber connectors are randomly chosen, and final configuration resulted in a shape similar as shown in Fig. 5. During the testing, the rubber hoses have bulged and the air flow has to undergo uneven variation in its diameter as it passes through the air filter outlet pipe, rubber connector and intake pipe. Similar conditions prevailed at junction of other end of intake pipe, rubber connector and engine inlet. As air passes through this system, it experiences abrupt changes in the diameter of flow path. There are

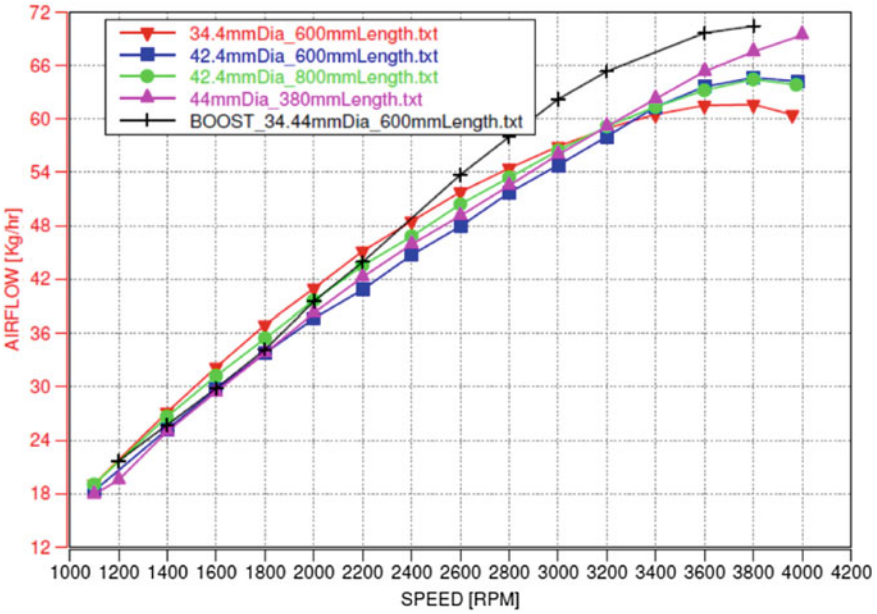

Fig. 4 Measured air flow rates to the engine with intake pipes of different diameter and length

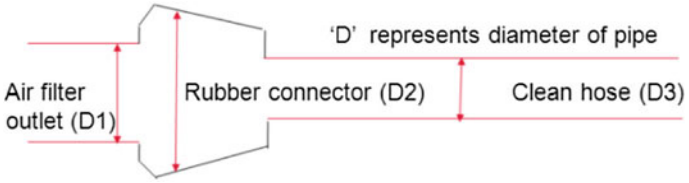

Fig. 5 Schematic of the flexible rubber hoses which are used to connect the air filter and intake pipe

sudden expansion and contraction at the junction of the rubber connector, air filter and clean hose. Flow separation occurs at these sudden contraction and expansion points and causes additional pressure losses. Flow separation also causes a reduction in the effective area available for air, to flow. It leads to enhanced pressure losses and lower air flow rates. Measured pressure drop across the intake pipe corroborated this fact. Further, pressure drop has increased non-monotonically with the speed of the engine. It is against 1DTPS results, which showed a linear increase in the pressure drop with the engine speed.

To avoid non-smooth variations in the diameter, rubber hoses are carefully selected and joined as shown in Fig. 6. During testing, this combination has not bulged, and there is a smooth variation in the diameter of the flow. Measured air flow rates with smooth rubber connectors are shown in Fig. 7. For comparison, BOOST predictions

Fig. 6 Schematic of the modified flexible rubber hoses

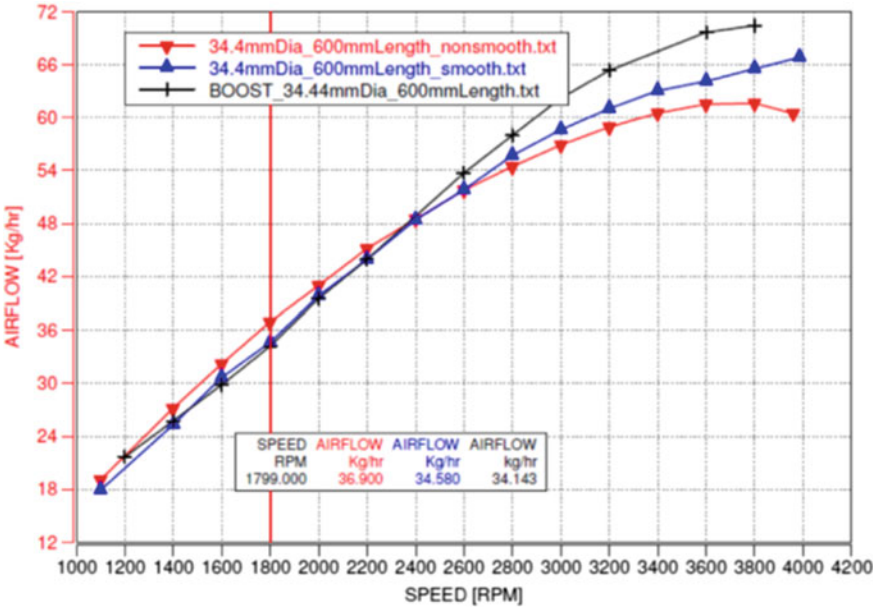

Fig. 7 Comparison of measured and predicted air flow rates for 34.4-mm-diameter and 600-mm-length intake pipe

and air flow rates with non-smooth connectors are also shown in the figure. There is an increase in air flow rates with smooth rubber connector from 2600 RPM onward. The enhancement in air flow rates at 3600 RPM is about 4%. Air flow rates are lower for speeds up to 2200 RPM compared to those obtained with non-smooth rubber connectors. The decrease in air flow rates is about 6.3% at engine speed of 1800 RPM. The comparison between BOOST predictions and air flow rates obtained with smooth rubber connectors is good up to 2400 RPM. Beyond this speed point, both curves continue to diverge. Maximum deviation is observed at 3600 RPM, and predicted air flow rates are higher by 7.92%. Note that air flow rates obtained with non-smooth rubber connectors are higher than those of BOOST predictions for engine speeds below 2200 RPM. Local pressure fluctuations at junction points would have increased the air flow rates. Similar trends were observed with the remaining intake ducts also [10].

Clearly, smooth rubber connectors deliver higher air flow rates compared to those of the non-smooth rubber connectors for speeds above 2400 RPM. The air flow rates

to the reciprocating engine are affected by many parameters such as instantaneous vacuum between cylinder and atmosphere, pressure drop across air filter, bends and valves, tunning effect and ramming phenomena. Tunning and ramming are net result of wave phenomena of air flow in the intake pipe [12]. For the chosen engine, 600 mm corresponds to tuned length for 3600 RPM. For speeds above 3000 RPM, ramming effect has significant effect on the engine's air flow rates. Now the interplay between air flow rates and rubber connectors can be summarized as follows.

Flow dynamics at the junction points of rubber connects is complicated, as flow separation and subsequent re-attachment are superimposed on a incoming pulsating flow. The pulsating nature of flow can amplify the surface pressure variations due to flow separation and re-attachments. The amount of these pressure variations will depend on diameter ratios, local turbulence levels, Reynolds number and engine speed. These local pressure perturbations at the junction point of engine side would have nullified the effect of ramming. As a result, air flow rates obtained with non-smooth rubber connectors are lower than those obtained with smooth rubber connector. As ramming is not a significant contributor to the air flow rates at low engine speeds, the difference in the measured air flow rates obtained with smooth and non-smooth rubber connectors is low. 3D CFD transient simulations need to be performed to gain some more insights into the effects of flow separation on the dynamics of gas flows and air flow rates to the engine.

3.1.1 Analysis of Air Flow Measurement System

For calibration activities of production engines, air flow rates will be measured with Sensyflow sensor, which has a long cylindrical pipe. The setup will be placed upstream of the air filter (see Fig. 8). A surge tank, whose volume is about 300 times the swept volume of the engine, will be used to reduce the effect of pulsations on the measurement. The surge tank will be placed between Sensyflow and air filter. The industry practice in the combustion and calibration development of the engine is that the Sensyflow device and associated surge tank will not affect the breathing capacity of the engine. There can be additional pulsations in the intake pipe due to considerable volume of Sensyflow device and its surge tank. Pressure drop across the surge tank can be significant. Hence, the air flow rates to engine can be different with this setup due to additional volume and pressure drop. Hence for a given engine speed, air flow rates with and with out Sensyflow setup will be different. The difference between these two is termed as disturbance error (E_d). A method to determine this disturbance error is proposed by Dwarshala et al. [10]. Their analysis indicated that the disturbance error is approximately zero for speeds below 2400 RPM. Beyond 2400 RPM, it has positive value and increases unevenly with the speed. Measured pressure drop across the Sensyflow device, and surge tank is in between 2 and 4 mbar in the entire speed range.

The disturbance error is negligible for speeds below 2400 RPM, in spite of having significant pressure drop across the surge tank and Sensyflow device. It suggests that the disturbance error is not due to the pressure drop, rather it is purely due to gas

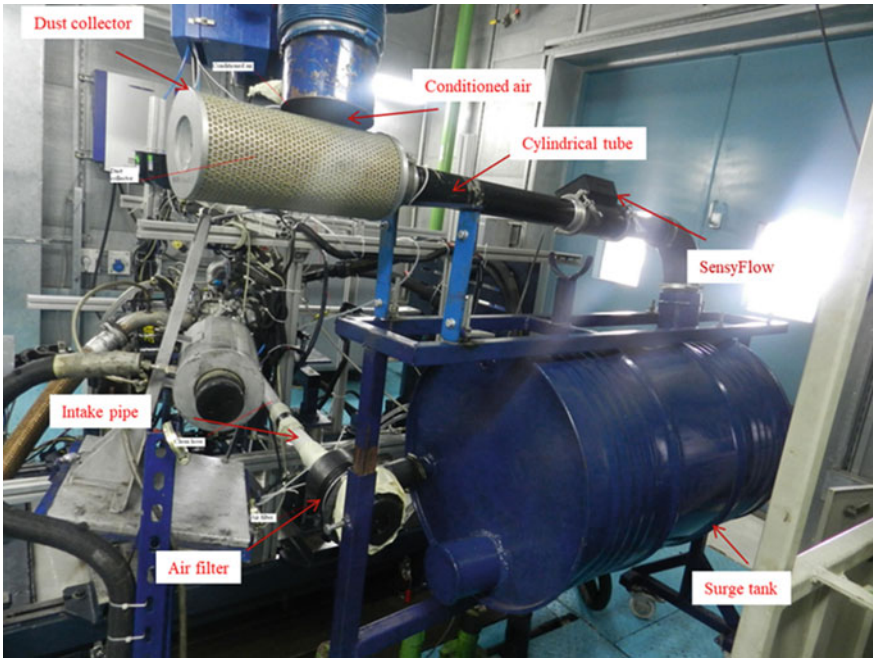

Fig. 8 Setup of Sensyflow and surge tank which are used to measure the air flow rates to the engine

dynamic effects. Corrected air flow rates obtained by accounting disturbance error are compared with BOOST predictions in Fig. 9. The comparison is good for speeds up to 3000 RPM, beyond which both data deviate. Based on this comparison, it can be concluded that intake system with Sensyflow and associated surge tank does not represent the true breathing capacity of the engine. The measurement system introduces errors. Similar conclusions were also given by Pesic et al. [13]. Hence when measured data is compared against 1DTPS predictions, disturbance error should be accounted.

3.1.2 Enhancing the Air Flow Rates to the Engine

For the production engines, PVC pipes cannot be used, and usually rubber hoses will be employed. The chosen air filter outlet outer diameter is 48 mm, and it is different from that of optimum diameter of 36 mm. The engine inlet inner and outer diameters are 36 and 38 mm, respectively. Hence, rubber hoses should be taper, with diameter reducing from 48 to 38 mm. A tapered section can be used to reduce the diameter smoothy so that pressure losses can be minimized. A schematic of such rubber intake hose is shown in Fig. 10. The part $L1$ is toward air filter whose diameter is 42 mm and part $L3$ is toward engine inlet whose diameter is 36 mm. $L1$ and $L3$ are constant diameter parts, whereas $L2$ is tapered part. Now lengths $L1$, $L2$ and $L3$ are further

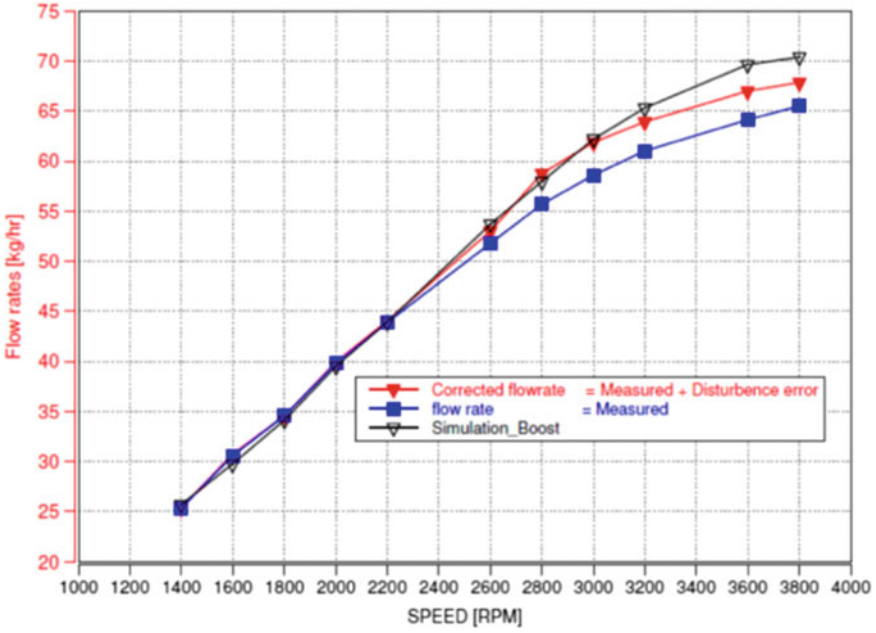

Fig. 9 Comparison of measured, corrected and predicted air flow rates for 34.4-mm and 600-mm-combination intake pipe

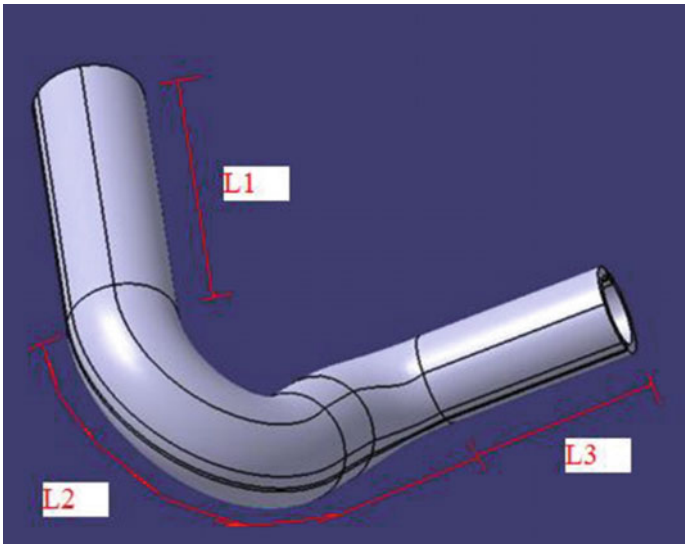

Fig. 10 A schematic of the rubber hose used to connect the air filter and engine inlet

Table 1 Lengths and diameters of parts $L1$, $L2$ and $L3$ for the configuration shown in Fig. 10

	$L1$	$D1$	$L2$	$L3$	$D3$
Intake pipe 1	159	48	71	103	38
Intake pipe 2	50	48	100	450	38
Intake pipe 3	50	48	100	450	36

All dimensions are in mm

optimized to get higher air flow rates. The 1DTPS indicated that air flow rates will be higher if $L3$ is larger than rest of the two parts. Three samples with different combinations of $L1$, $L2$, $L3$ are tested, and their dimensions are shown in Table 1. Intake pipe 2 is a Rapid Proto Type (RPT) sample, whereas other two are rubber hoses, which are production versions of the intake pipe. For intake pipes 2 and 3, the total length is 600 mm which is optimized length to have higher air flow rates, as per the preceding discussion.

Measured air flow rates obtained with the three intake pipes, as a function of the engine speed, are shown in Fig. 11. Maximum air flow rate is obtained at engine speed of 3600 RPM, with intake pipe 3. This value is used to non-dimensionalize the air flow rate of three intake pipes. In the entire speed range, intake pipe 3 delivers higher air flow rates. From 2400 RPM onward, Intake pipe 2 has higher air flow rates than that of intake pipe 1. Both the intake pipe 2 and 1 have approximately same air flow rates for speeds below 2400 RPM. At rated speed of 3600 RPM, air flow rate obtained with intake pipe 3 is 2.94% and 5.88% higher than those of intake pipe 2 and 1, respectively. Note that the geometric difference in intake pipes 2 and 3 are in the diameter of $L3$ part. Rest of all dimensions are identical. Therefore, measured air

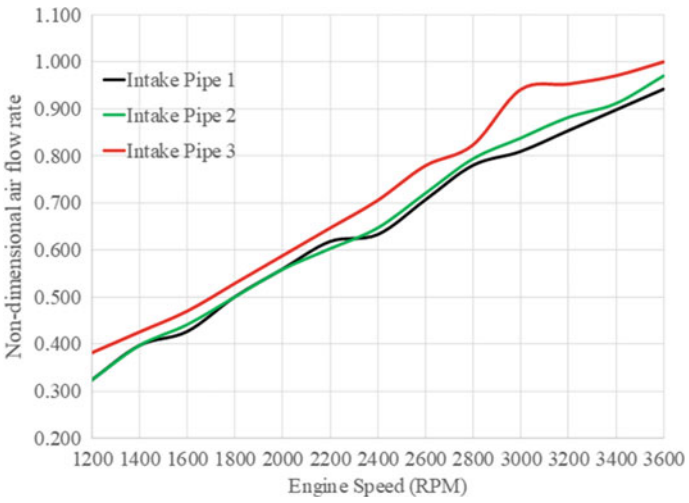

Fig. 11 Measured air flow rates to the engine with different tapered intake pipes

flow data indicates that, a change in diameter of 2 mm over a length of 450 mm has significant effect on air flow rates.

The thermodynamic simulations indicated that tuned length for speeds around 2000 RPM is above 900 mm length [10]. Therefore, as the length of intake pipe 2 is higher than that of intake pipe 1, it is expected to have higher air flow rates for intake pipe 2 compared to that of intake pipe 1 for the engine speeds around 2000 RPM. However, measured air flow rates are nearly the same for these two pipes.

But intake pipe 3 which has identical lengths of intake pipe 2 has higher air flow rates. The enhancement in air flow rates is majorly due change in the diameter for speeds around 2000 RPM. This indicates that for low speeds, diameter of the intake pipe has significant effect on breathing capacity of the engine. Air flow rates predicted from 1DTPS for the above three intake pipes have not differed significantly. This indicates a shortfall in the modeling of gas dynamics of the pulsating flow.

The changes in the air flow rates to the engine are expected to induce corresponding changes in the engine performance parameters and emissions. The tests are conducted for full load conditions with identical injection conditions for the three intake pipes. Figure 12 shows the comparison of brake-specific fuel consumption (BSFC) at full load condition in non-dimensional form. In the low speed range, the difference in BSFC is negligible. From 2800 to 3400 RPM, intake pipe 3 has lower BSFC. At 3000 RPM, BSFC of intake pipe 3 is 1.92% and 1.28% lower than that of intake pipe 1 and 2, respectively. Full load points in this speed range are part of emission test cycle for BS IV regulations. Hence, intake pipe 3 is expected to have higher mileage compared to rest of the two intake pipes. A comparison of exhaust smoke of the engine, with the three intake pipes, is shown in Fig. 13. The data is shown in non-dimensional form. Intake pipe 3 has lower smoke in the entire speed range except at

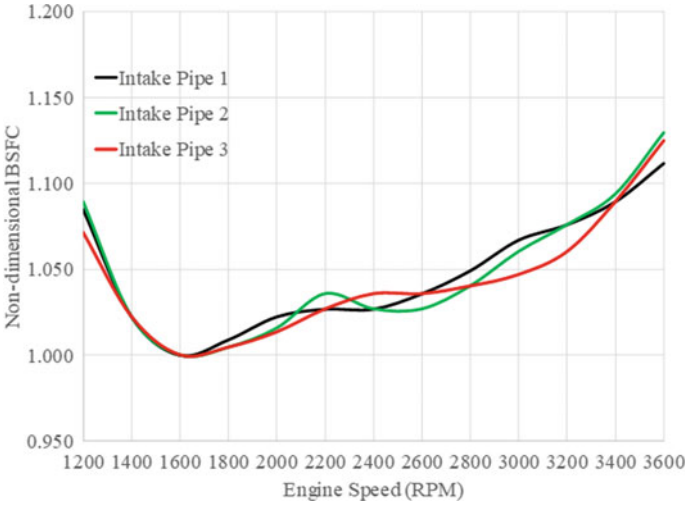

Fig. 12 Comparison of measured BSFC obtained with different tapered intake pipes

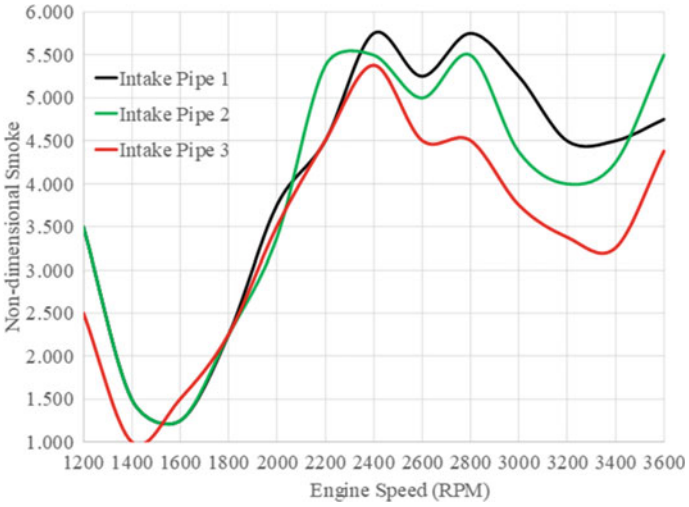

Fig. 13 Comparison of smoke emitted by the engine with different tapered intake pipes for full load condition

around 1600 RPM. The enhanced air flow has improved the mixing between fuel and air and resulted in lower smoke levels. The reduction is more significant in the high speed range. At 3000 RPM, maximum reduction in smoke is observed, and smoke values of intake pipe 3 are 40% and 17% lower than those of intake pipe 1 and 2, respectively. Similarly, smoke levels obtained with intake pipe 2 are lower than that of intake pipe 1 for speeds above 2400 RPM.

Non-dimensional total unburned hydrocarbon (THC) values of the exhaust are shown in Fig. 14. In the entire speed range, intake pipe 3 has lower THC than intake pipe 1, and maximum reduction occurs at 2400 RPM, and it is about 48%. Up to 3000 RPM, THC of intake pipe 2 is higher than that of intake pipe 3; beyond this speed, intake pipe 2 has lower THC values. Note that in this speed range, air flow rates with intake pipe 3 are higher. The intake pipe 3 is RPT sample, and it cannot be clamped to the engine inlet, similar to rest of other two pipes. Rubber connectors, similar to shown in Fig. 6, are used to join the intake pipe 3 on engine intake side and air filter side. There could be significant flow separation zones at the junction point of intake pipe and engine inlet. Flow perturbation from these junction points at high speeds would have reduced in-cylinder swirl and turbulence. It would have deteriorated the combustion, resulting in higher THC emissions for intake pipe 3. In the calibration trials of the engine also, it was observed that the air flow rates to the engine for speeds above 3500 RPM are highly sensitive to small geometric changes at the junction of engine inlet. Overall, the reduction in THC with intake pipe 3 is significant, and it is expected to reduce the loading on catalytic converter significantly.

A summary of the above intake pipe development work is given below. For naturally aspirated single- and multiple-cylinder engines, the intake pipe length and

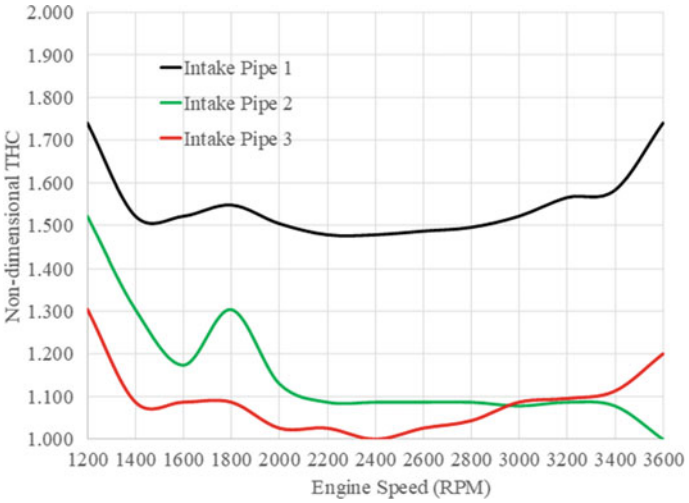

Fig. 14 Comparison of THC obtained with different tapered intake pipes for full load condition

diameter have a significant effect on the engine performance and emissions. 1DTPS provides some guidelines on choosing right combination of diameter and length. But the optimum dimensions which will give the highest air flow rates and the lowest BSFC and emissions can differ from that of predictions. Hence, a set of combinations derived from 1DTPS needs to be tested on engine dynamometer before freezing the design. Also the predicted air flow rates from 1DTPS and experiments may not match exactly due to measurement and disturbance errors, as explained above. These deviations need to be considered while finalizing the engine performance targets in the concept phase of engine product development.

3.2 Reducing the Emissions by Modifying the Combustion Chamber Geometry

The combustion chamber's geometric shape, i.e., piston bowl, plays a critical role in the combustion of a direct injection diesel engine. The critical combustion processes, such as the mixing between fuel and air, squish flow from the bowl when the piston is close to TDC; in-bowl swirl and turbulence are strongly influenced by the bowl shape [14]. An attempt was made to reduce the fuel consumption and emissions by modifying the combustion chamber geometry. Figure 15 shows the comparison of base and modified piston bowls. The base bowl is an existing design used in the preceding air flow optimization trials, and modified bowl is the proposed design to enhance engine performance and reduce emissions. The compression ratio of the engine with the two piston bowls is identical. The diameter and central pip height of the modified bowl are larger and lower respectively compared to those of the

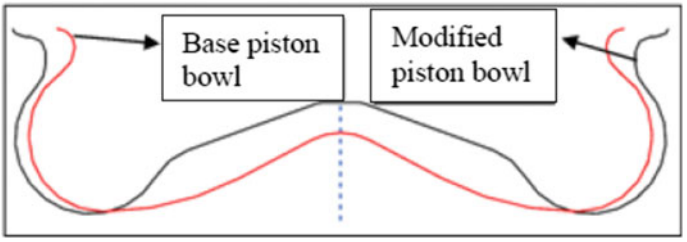

Fig. 15 Comparison of chosen two piston bowl shapes for comparative analysis of combustion performance

base bowl. The shape of base bowl is similar to that used in the Volvo cars, which are designed for Euro 5 emission regulations [15]. The modified bowl is similar to step-cone bowl used in Hyundai-Kia's 2.0 1 and 2.2 1 four-cylinder diesel engines [16].

Closed cycle simulations are performed from crank angles/crank angle at which intake valve closes and to crank angle at which exhaust valve opens. Simulations are performed for full load conditions at engine speeds of 1600 RPM and 3600 RPM. Simulation trials are performed with the same input conditions for injection parameters for both piston bowls. The time step used in the compression stroke is about 3 crank angels. By the time, simulation progress to fuel injection and subsequent combustion, the time step progressively reduced to 0.2 crank angels. A top view of the piston bowl surface with meshing is shown in Fig. 16a. A schematic of the mesh

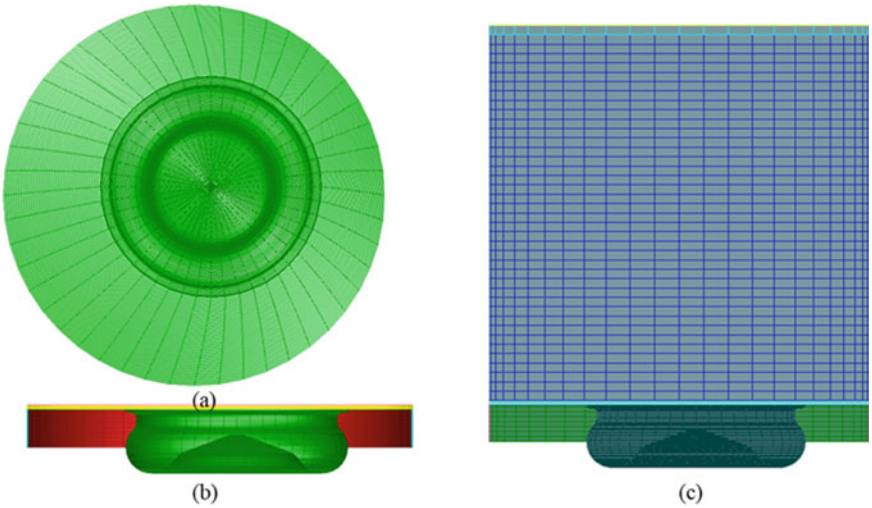

Fig. 16 Schematic of the computational mesh used for combustion simulation, **a** top view of the piston bowl surface, **b** side view, when the piston is at TDC, and **c** side view, when the piston is at BDC

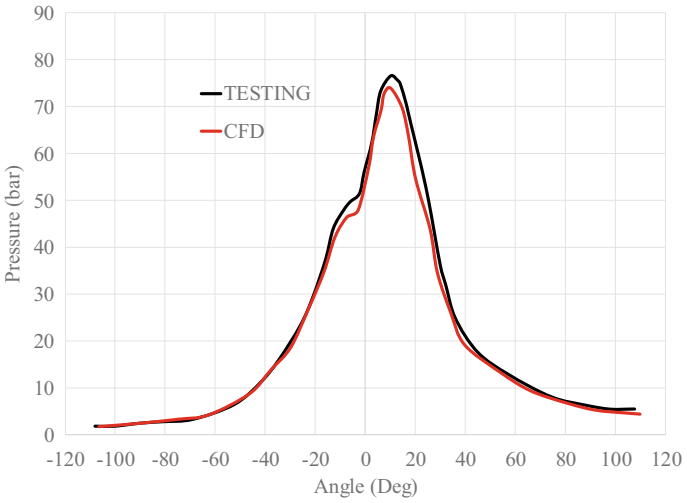

Fig. 17 Simulated and measured in-cylinder pressure at 1400 RPM obtained with base piston bowl. Firing TDC is located at 0°

when the piston is at TDC and BDC are shown in Fig. 16b, c, respectively. The computational domain has 1.2 lakh cells when piston is at TDC, and 4.75 lakh cells when piston is at BDC.

Initially predicted in-cylinder pressure and heat release rate from the base piston bowl are validated against experimental data. Figure 17 shows the comparison of cylinder pressure for 1400 RPM. The crank angle corresponding to peak firing pressure predicted well. In simulations and testing, this occurs close to 10° aTDC. There is a difference in the peak firing pressure, and deviation is about 4%. Heat release rates obtained from testing and simulations are shown in Fig. 18. In the simulations, heat release due to pre-injection of fuel at crank angle 7° bTDC has not captured. However, the initial part of the premixing phase, diffusion phase and after burning phase predicted well. Simulations predict a higher peak heat release rate, and the deviation from the test data is about 6.5%. Similar observations were made from the simulations at an engine speed of 3600 RPM. However, data is not presented here for the sake of brevity. A rigorous validation study has not performed, as the key objective is to determine relative performance between the two piston bowls. The predicted in-cylinder pressure and heat release rate for the modified bowl are given in the work of Shaik et al. [17]. The pattern of in-cylinder pressure and heat release rates with the modified bowl is similar to those of base piston bowl. The crank angles at which peak firing pressure and maximum heat release rate occur are nearly the same in both the bowls. However, these two parameters are higher with the modified bowl by 2.23% and 5.89%, respectively.

Figure 19 shows a comparison of equivalence ratio (ER) distribution over the piston bowl surface toward end of fuel injection (12° after TDC) at 1400 RPM. Red color regions represent fuel rich zones, on the other hand, blue color zones indicate

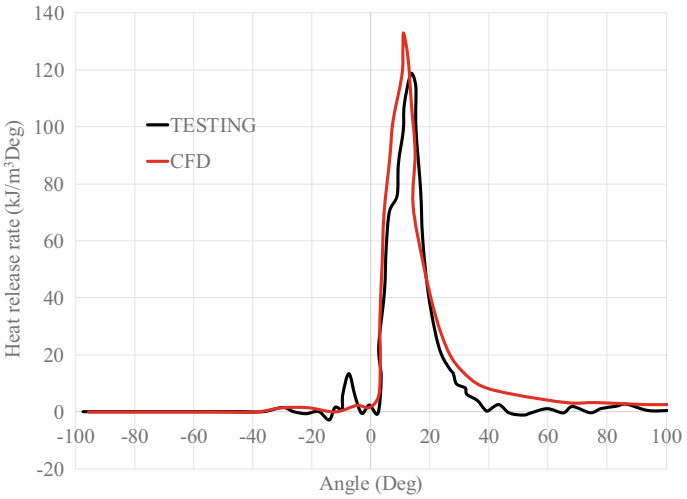

Fig. 18 Heat release rate pattern obtained from testing and simulation for engine speed of 1400 RPM with base piston bowl

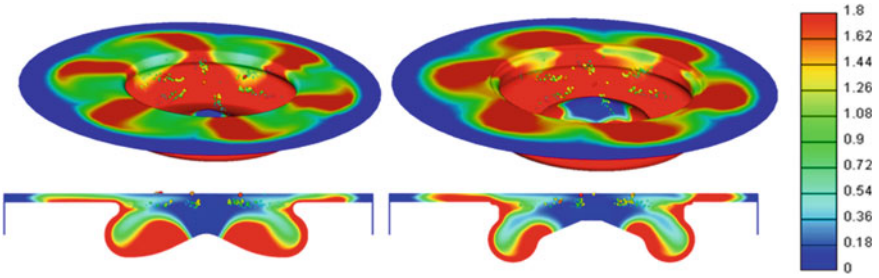

Fig. 19 Equivalence ratio distribution at the end of fuel injection (12° after TDC) for engine speed of 1400 RPM. Left side represents base piston bowl, and right side represents modified piston bowl. Top figures correspond to top view of the bowl surface, while bottom figures correspond to cut away planar section passing through the central axis of the piston bowl

air-rich zones or fuel lean regions. The transition zones from red to blue color indicate diffusion and mixing of fuel with air. The nozzle has six holes, and hence, six fuel sprays can be noticed. Deflection of spray due to in-bowl swirl can be clearly noticed for both the bowls. However, deflection of spray is relatively higher for the modified bowl. Spillage of the fuel beyond the bowl cavity is more for the modified bowl. Comparison of cut section view indicates that more amount of fuel is trapped inside the bowl for base design, and majority of this fuel is concentrated in the lobes. Fuel droplets emanated from the nozzle hole are shown in the figure. In case of base bowl, the droplets travel linearly with out much affected by the swirling motion. On the contrary, in the modified bowl, the droplets distorted quickly and vaporized quickly.

Hence when spray hit the bowl surface, a significant portion of the fuel would have evaporated.

The variation of average swirl and turbulent kinetic energy with respect to crank angle is similar for both bowls. However, significant deviation between the two curves is observed when the pistons are close to TDC. The maximum swirl and turbulent kinetic energy achieved with modified piston bowl are 4.5% and 12%, respectively, lower than that of base bowl. The angles at which maximum swirl and turbulent kinetic energy occur are approximately the same for both bowls. Figures pertaining to this data are not shown for the sake of brevity. The reduction in the swirl for the modified bowl is due to decreases bowl diameter, as reported in Ref. [12]. In spite of having lower swirl and turbulent kinetic energy, the modified bowl has better mixing between fuel and air. This is essentially due to changes in the central pip region.

Figure 20 compares the ER distribution at 12, 20 and 32 crank angle (CA) after TDC for the base and modified bowls. In the figure, the term 'ER' indicates equivalence ratio, and the subsequent number represents maximum value of 'ER' for the respective crank angle. For the base bowl, at 12° aTDC, maximum value of ER is about 3.6125. Significant amount of fuel is concentrated in bottom portion of the bowl lobes. The concentration of the fuel in the central pip region is not significant. As the piston moves downward, the distribution of ER is modified, and it can be noticed from the contours shown for 20° of piston position. The maximum ER decreased to 2.224. This indicates mixing between fuel and air, and the fuel–air mixture moved

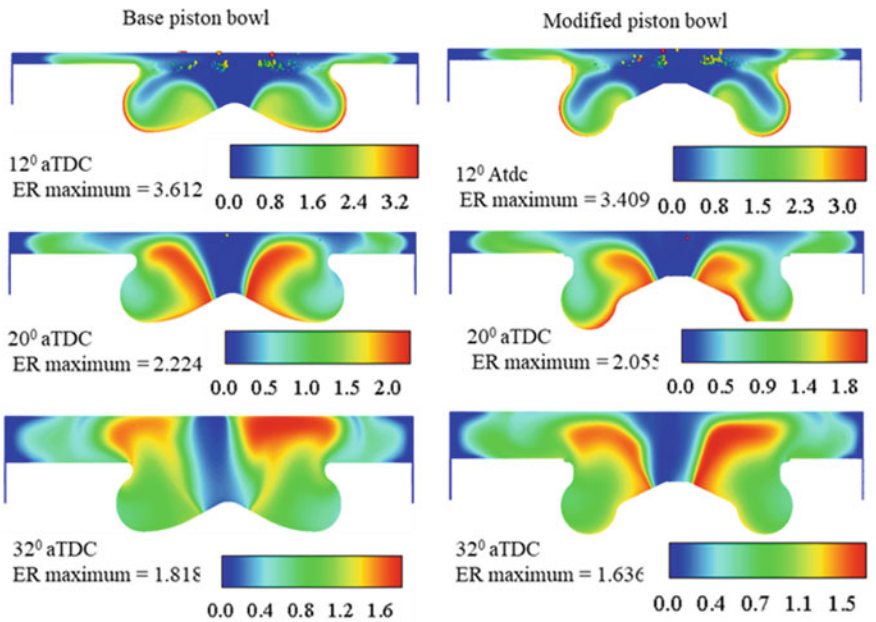

Fig. 20 Comparison of equivalence ratio at different crank angles during the combustion. Red color indicates higher ER values. Blue color indicates minimum value of zero

in the vertical direction. The fuel-rich zones migrated to neighborhood of central pip region. Layers of fuel-rich regions can be noticed from lob region to pip region. As the piston moves further downward, mixing between fuel and air enhances, and as a result, maximum ER decreases. At 32°, its value is 1.818. Also at this CA, piston bowl does not have fuel rich zones, and they convected upward and touched the cylinder head surface.

The maximum value of ER for the modified bowl at 12° aTDC is 3.409, and the fuel-rich region is confined to the near wall region in the two lobes. At 20° and 32° aTDC, the maximum ER is about 2.055 and 1.636, respectively. The distribution of fuel is relatively more uniform compared to that of the base bowl. The qualitative trends are nearly the same between the two bowls up to 32°. The fuel and air mixture does not hit the cylinder head surface in the modified bowl, which is opposite to that is observed for base bowl. However, there is a deflection of the mixture, which avoids the hitting the cylinder head surface. This has a drastic effect on emissions which is discussed in the subsequent sections. The reduction in maximum ER when the piston travels from 12° to 20°; 20° to 32° are 40% and 20%, respectively, for the modified bowl, where these numbers for base bowl are 38% and 18%, respectively. The faster is the reduction, better is the mixing. Therefore, mixing between fuel and air is better in the modified bowl.

The temperature distribution inside the combustion chamber at CA corresponding to 12°, 20° and 32° after TDC is shown in Fig. 21. For each crank angle, maximum

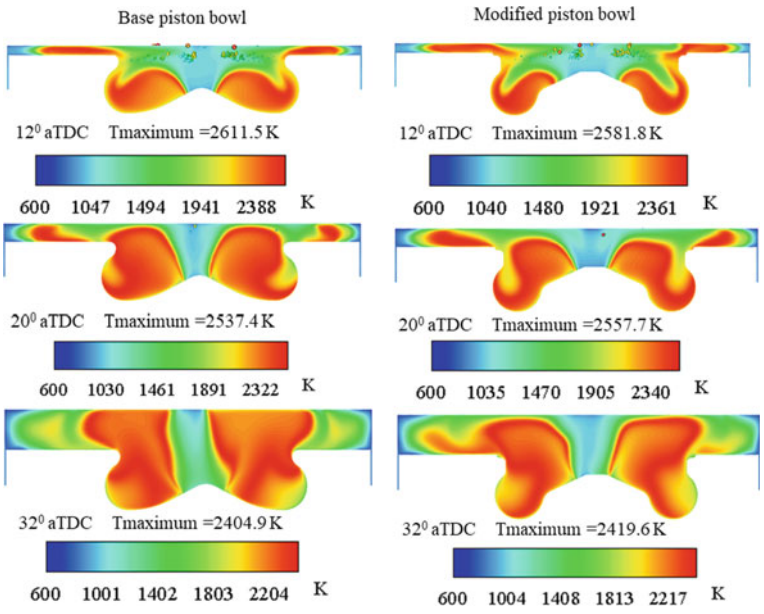

Fig. 21 Comparison of temperature distribution between base piton bowl and modified piston bowl at different crank angles during combustion

temperature in the combustion chamber is indicated. Higher temperatures in the bowl volume are due to combustion of fuel. At 12°, combustion occurred in the two lobes (for both bowls), and in the central pip region combustion has not occurred. There is a good amount of fuel burning above the top surface of piston for both the bowls. The maximum temperature is higher for base bowl. The pre-mixing phase of combustion ends at this crank angle (see Fig. 18). Hence, it can be said that in the pre-mixing phase of combustion, base bowl has higher gas temperatures. As the piston moves downward, the diffusion phase of combustion starts. As explained before, when the piston moves from 12° to 20°, the diffusion of fuel is more in the modified bowl. This leads to better combustion and results in higher temperatures in the modified bowl. Same trend can be observed for 32° CA position also. Note that in the base bowl, at this CA, the diffusion flames touch the cylinder head surface, on the other hand, for the modified bowl, diffusion flames deflect right side without touching the cylinder head surface. Overall, in the diffusion phase of combustion, the modified bowl has relatively higher temperatures.

Figure 22 shows a comparison of soot distribution for the two piston bowls. As discussed earlier in case of the base bowl, the fuel and air mixture touches cylinder

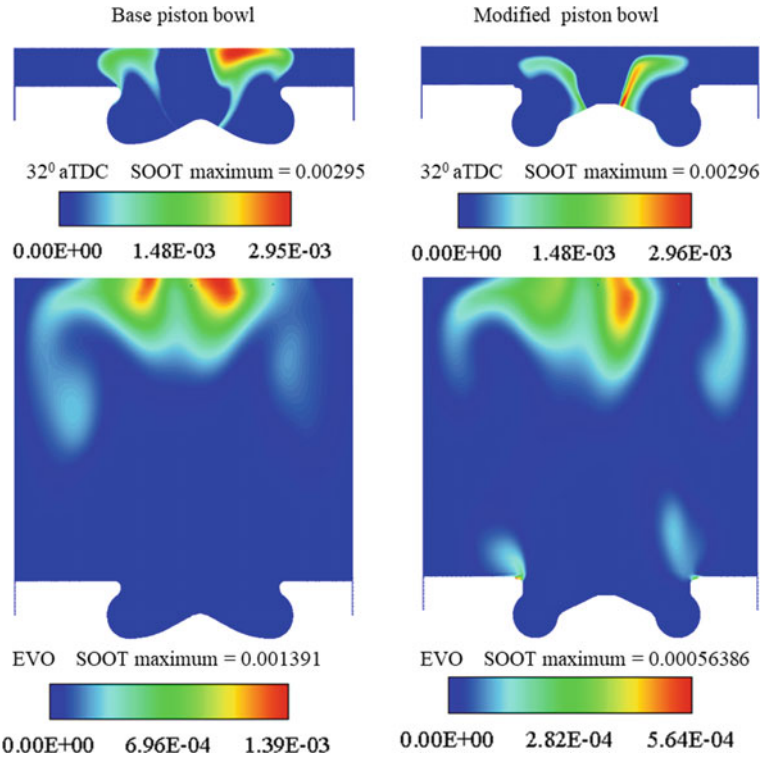

Fig. 22 Visualization of soot mass fraction distribution at two crank angles during the combustion. EVO refers to crank angle at which exhaust vale opens

head surface about 32° CA. As this surface has a relatively lower temperature, quenching of the flames occurs. Hence combustion ceases, and fuel particles will be converted into soot. So the accumulation of soot occurs in the neighborhood of cylinder head surface. On the other hand, accumulation of soot occur in the central pip region for modified bowl. At 32° CA, maximum mass fraction of soot particles is nearly same for both the bowls. However, soot is distributed over more area in the base bowl, indicating that accumulated mass of soot will be higher with the base bowl. When the piston reaches to CA corresponding to EVO, the maximum soot mass fraction in the modified bowl is considerably lower than that of the base bowl. As indicated earlier, gas temperature in the modified bowl from CA 20° to 32° is higher, and this promotes oxidation of soot to a larger extent than that can occur in the base bowl. As a result, there is a greater reduction in the soot mass fraction in the modified geometry, when the piston travels from CA 20° to 32°.

Soot reaction rate and mass fraction as a function of the CA obtained from simulations are shown in Fig. 23. A positive and negative reaction rate indicates formation and destruction (or burning) of soot particles, respectively. There is a sudden rise in the reaction rate at 2° aTDC for both piston bowls. Reaction rate attains maximum value in between 8° and 10°, and afterward it decreases. The maximum reaction rate obtained with the modified bowl is higher than that of the base bowl. Reaction rates attain a value of zero at about 14° aTDC. Hence from 2° to 14°, formation of soot occurs and results in accumulation of soot in the piston bowl. This leads to a rapid increase in mass fraction of soot as indicated in Fig. 23b. This portion of combustion represents pre-mixing phase. Beyond this crank angle, reaction rates are negative for both bowls, and this indicates the initiation of soot burning in the diffusion phase of combustion. For the base bowl, soot burning rate decreases at a faster rate than that of the modified bowl. For the base bowl, soot burning ceases at about CA of 32° aTDC, whereas for the modified bowl it occurs at 43° aTDC. As soot burning is initiated, reduction in mass fraction of soot occurs (see Fig. 23b). The reduction is more rapid in case of the modified bowl. From 100° aTDC onward soot mass fraction remains constant. However, at this CA, soot levels in the modified bowl are lower by 55%. Note that emission values at this crank angle represent engine out emissions. The higher soot burning rate for modified bowl is essentially due to higher temperatures in the diffusion phase of combustion, as discussed earlier. A similar inference from computed soot reaction rates is also given by Ganesh et al. [18].

Fuel distribution, soot reaction rate and associated soot mass fraction at 3600 RPM for both bowls are similar to those of 1600 RPM. Hence, modified bowl expected to have lower smoke levels in the majority of the engine operating speed. The trends of total unburned hydrocarbons and carbon monoxide are similar to those of soot. The region close to cylinder head surface found to have higher concentrations of these emissions at CA corresponding to EVO.

Comparison of the velocity flow field and streamlines in the two bowls is shown in Fig. 24. When the piston is at 14° CA, the recirculating motion of gas mixture can be noticed in the lobes of the bowl for both cases. However, modified bowl has a higher maximum velocity. In both the bowls, the central pip region is characterized by stagnant regions. For the base bowl, there is strong vortex toward left side of

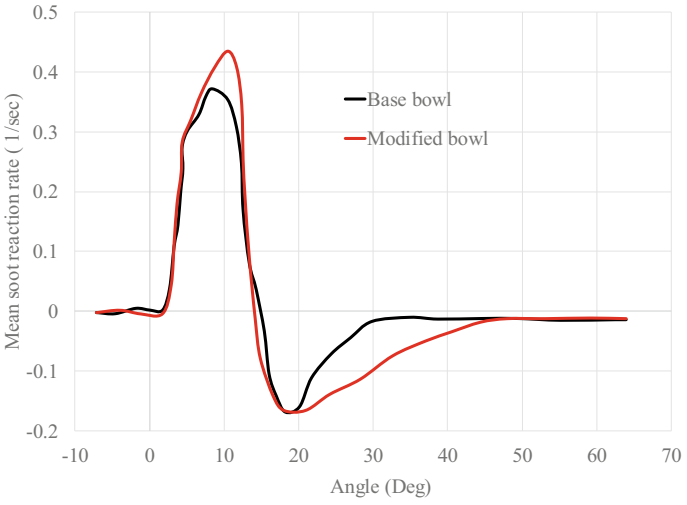

(a)

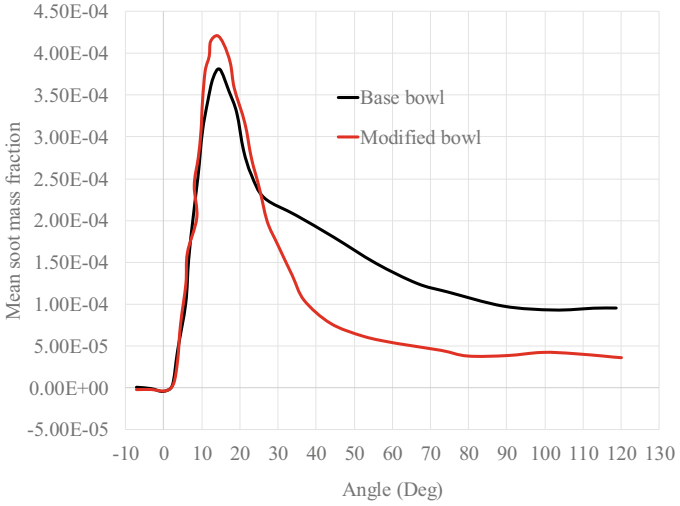

(b)

Fig. 23 Predicted averaged **a** soot reaction rate and **b** mass fraction as a function of crank angle. Firing TDC is at 0°

right lobe. This region is pointed by a red color line. Such strong vortex region is not observed in the modified bowl. As the piston moves downward, the recirculating flow in the lobes disappears, and gas mixture flows from the bowl to outside region of the bowl. This actually sets up squish flow. The presence of larger red color region

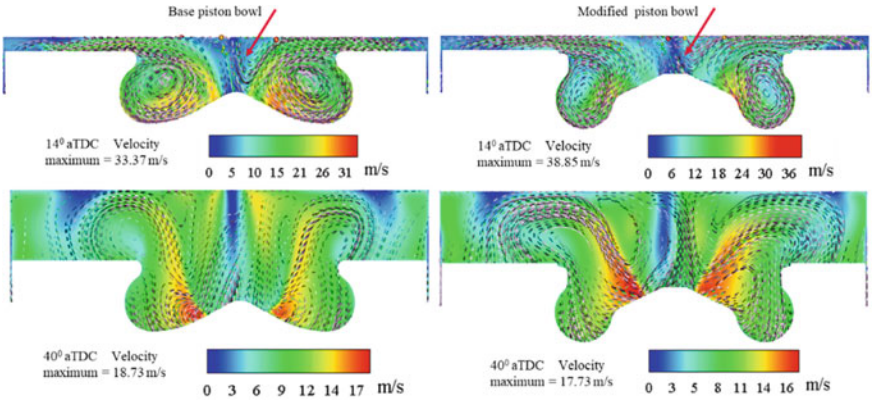

Fig. 24 Depiction of velocity flow field (flooded contours) and streamlines for the two piston bowls. Red color indicates maximum velocity regions

for the modified bowl at 40° indicates that the squish flow is more stronger. Due to this, the global flow deflects away from the cylinder head surface.

In case of base bowl, the resulting squish flow is not strong enough to dissipate the vortex or stagnant region that formed in the central pip region. As a result, gas mixture moves vertically upward, until it is blocked by cylinder head surface. Streamlines clearly indicate this pattern of flow. This impact region is actually source of emissions. Overall, the squish flow is better in the modified bowl, and it resulted in better combustion.

The pattern of predicted flow field in the piston bowls is similar to those reported by Andersson et al. [15]. A large vertical vortex is observed in the pip region of the base bowl. However for the conditions chosen by Andersson et al., the geometry of the optimized bowl is similar to that of the base bowl in the present investigation. The vertical vortex acted as a source for additional turbulence and enhanced mixing between air and fuel. However, the vertical vortex has not touched the cylinder head surface similar to that observed in the present work. This shows that flow fields and associated flow structures are very sensitive to engine operating conditions. A detailed measurement of velocity flow field, similar to that of Perini et al. [19], is required to accurately analyze the sensitivity of in-cylinder flow field to various engine operating conditions and geometry of piston bowl.

Next, The engine is tested with the two piston bowls, and injection parameters are further optimized for each bowl on steady-state engine dynamometer. The measured BSFC and smoke are shown in Fig. 25. The modified bowl has lower BSFC for the entire speed range compared to that of the base bowl. The reduction ranges from 1 to 3.5%. The maximum reduction is observed at an engine speed of 1800 RPM. The reduction in BSFC is essentially due to better combustion in the modified bowl, as described earlier. The smoke values are also lower for the modified bowl up to 3000 RPM. At 1800 RPM, maximum reduction is observed, and it is about 52%. The lower level of smoke is mainly due to faster burning of soot in the diffusion phase

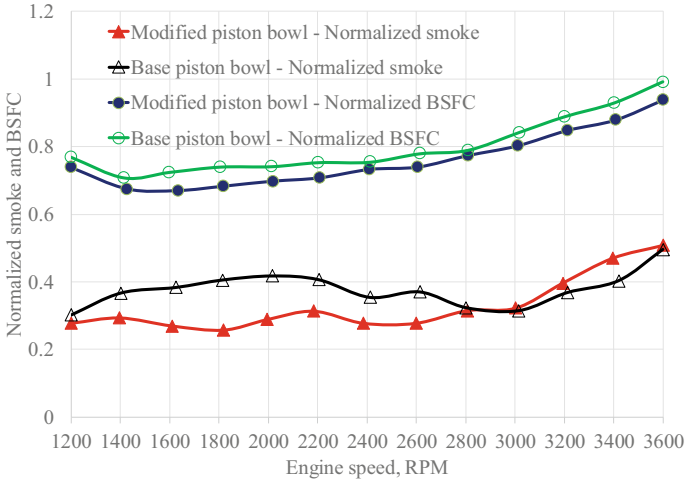

Fig. 25 Comparison of measured smoke and BSFC obtained from the both bowls as a function of the engine speed

of combustion. Similar trends in THC and CO emissions are observed. Overall, the modified bowl promoted complete combustion, to a extent greater than that of base bowl, and resulted in lowering the THC, CO and BSFC significantly.

In the concept phase of engine development, extensive combustion simulations are performed to investigate sensitivity of swirl ratio and other geometric parameters of piston bowl. All the simulations are performed taking base piston bowl shape as a reference. Some of the injection parameters are omitted from this study. In the physical prototype testing, engine-out emissions deviated too much from target values. This necessitated to modify the piston bowl design, which prolonged the product development time. The short fall in the concept phase combustion simulations probably due to the initial conditions chosen for the simulations. There is a mismatch in the air flow rates, injection pressure, etc. which are used in the simulations of concept phase and prototype testing phase. Hence for designing the piston bowl, initial conditions should be as accurate as possible. Also to arrive at best piston bowl geometry, a detailed optimization study, similar to that of Andersson et al. [15] and Idicheria and Diwakar [20] needs to be performed.

The combustion analysis presented in this work can be summarized as follows. The changes in the geometry of the piston bowl resulted in a better squish flow. This promoted better mixing and dissipated stagnant regions in central pip region. This leads to better BSFC and lower emissions. An excellent correlation between the CFD predictions and measurements is obtained.

4 Conclusions

Engine performance simulations are used to optimize the length and diameter of the intake pipe of the engine to have higher air flow rates. The optimized parameters found to be diameter of 36 mm and length of 600 mm. The higher air flow rate for this combination is due to the combined effect of tunning and ramming. In the initial testing, measured air flow rates found to be lower than those predicted from the simulations. The deviation found to be due to geometric discontinuities at the junction points of intake pipe and air filter; intake pipe and engine inlet. By minimizing the geometric discontinuity at these junction points with the usage of a smooth rubber connector, air flow rates are recovered. An analysis of the air flow measurement system is performed. It is observed that the volume of the measurement system alters the gas dynamics in the intake pipe and leads to changes in the air flow rate. The effects are negligible for low-speed engine operations, whereas for speeds above 2400 RPM, these effects will introduce significant errors in the measurement. The length of tapers sections in the intake pipe is further optimized. It found that optimum intake pipe has higher air flow rate for entire range of engine speed, and the enhancement at 3600 RPM is about 5.88%. The enhanced air flow rate resulted in decrease of brake-specific fuel consumption in the mid speed range. The maximum reduction found to be 1.92% at 3000 RPM. The maximum reduction in smoke also observed at this speed, and it is about 40%. A similar reduction in the total unburned hydrocarbons also observed.

3D CFD combustion simulations are performed on two piston bowls to asses their superior combustion performance. The modified bowl has better squish flow. This has enhanced the mixing between fuel and air in the diffusion phase of combustion. This resulted in elevated temperatures for the modified bowl. Due to this, soot burning also found to be higher, which has lead to lower soot levels. The reduction in smoke is about 55% at 1400 RPM. On engine steady-state dynamometer, the modified bowl found to have lower smoke for the majority range of engine speed. The maximum reduction is about 52% at engine speed of 1800 RPM. A similar reduction in total unburned hydrocarbons and carbon monoxide is also observed. For entire speed range, brake-specific fuel consumption is also lower with the modified bowl. The reduction ranges from 1 to 3.5%. Overall, simulations are effectively used to reduce fuel consumption and emissions of the engine, thereby making engine more energy efficient and greener.

References

1. Heywood, J. B. (2011). *Internal combustion engine fundamentals*. TATA McGraw-Hill Publications.
2. Bowman, C. T. (1975). Kinetics of pollutant formation and destruction in combustion. *Progress in Energy and Combustion Science, I,* 33–45.

3. Amann, C. A., & Siegla, D. C. (1982). Diesel particulates—What they are and why? *Aerosol Science and Technology, 1*, 73–101.
4. Engl, G., & Rentrop, P. (1992). Gas flow in a single cylinder internal combustion engine: A model and its numerical treatment. *International Journal of Numerical Methods in Heat and Fluid Flow, 2,* 63–78.
5. Wiebe, I. I. (1956). Semi-empirical expression for combustion rate in engines. In *Proceedings of Conference on Piston Engines* (pp. 185–191). USSR. Academy of Sciences.
6. Echekki, T., & Mastorakos. (2011). Turbulent combustion: Concepts, governing equations and modelling strategies. In *Turbulent combustion modelling* (Vol. 95, pp. 19–39). ISBN: 978-94-007-0411-4.
7. Theory, AVL BOOST manual, Version 2013.2. https://www.avl.com.
8. Mobasheri, R. (2015). Analysis of the ECFM-3Z combustion model for simulating the combustion process and emission characteristics in a HSDI diesel engine. *International Journal of Spray and Combustion Dynamics, 7*(4), 353–372.
9. Reddy, D. S. K., Bakshi, S., & Anand, T. N. C. (2016). Investigation of high pressure diesel spray characteristics with computational fluid dynamics approach. In *18th Annual Conference of Liquid Atomization and Spray Systems*, Asia, India, 6–9 November 2016, Paper No. ILASS-Asia-75.
10. Dwarshala, S., Ramadandi, P., Shaik, R., & Shankar, R. (2014). *Practical considerations in the airflow optimization of a single cylinder diesel engine.* SAE Technical Paper, 2014-01-1705. https://doi.org/10.4271/2014-01-1705.
11. Manjunath, C. R., Reddy, D. S. K., Rehan, S., & Padmavathi, R. (2014). *Analysis of pressure pulsations in the intake duct of a single cylinder diesel engine.* ASME Conference Paper FEDSM2014-21305.
12. Stone, C., & Etminan, Y. (1992). *Review of induction system design and a comparison between prediction and results from a single cylinder diesel engine.* SAE Technical Paper 921727. https://doi.org/10.4271/921727.
13. Pesic, R. B., Davinic, A. L., Petkovic, S. D., Taranovic, D. S., & Miloradovic, D. M. (2013). Aspects of volumetric efficiency measurement for reciprocating engines. *Thermal Science, 17*(1), 35–48.
14. Miles, P. C., & Andersson, O. (2016). A review of design considerations for light-duty diesel combustion systems. *International Journal of Engine Research, 17*(1), 6–15.
15. Andersson, O., Somhorst, J., Lindgren, R., Blom, R., & Ljungqvist, M. (2009). *Development of the Euro 5 combustion system for Volvo cars' 2.4.I diesel engine*. SAE paper 2009-01-1450.
16. Lee, E., Kwak, S., Kim, M., Joo, S., Chun, J., Pae, S., Yu, J., & Grimm, J. (2009). The new 2.0 l and 2.2 l four-cylinder diesel engine family of Hyundai-Kia. *MTZ Worldwide, 70*(10), 14–19.
17. Shaik, R., Kumar, A., Padmavathi, R., Jagan, G., Anshul, A., Ganguly, G., Dwarshala, K., & Ravishankar, S. (2015). *Computational and experimental investigations to improve performance, emissions and fuel efficiency of a single cylinder diesel engine.* SAE Technical Paper 2015-26-0099.
18. Ganesh, V., Deshpande, S., & Sreedhara, S. (2016). Numerical investigation of late injection strategy to achieve premixed charge compression ignition mode of operation. *International Journal of Engine Research, 17*(4), 469–478.
19. Perini, F., Zha, K., Busch, S., Kurtz, E., Peterson, R., Warey, A., & Reitz, R. (2018). Piston geometry effects in a light-duty, swirl-supported diesel engine: Flow structure characterization. *International Journal of Engine Research, 19*(10), 1079–1098.
20. Idicheria, C., & Diwakar, R. (2011). Design of an optimum combustion chamber across multiple speed/load points for a heavy-duty diesel engine: Analytical design and experimental validation. *International Journal of Engine Research, 12*(2), 123–143.

An Approach to Improve Smoke–Fuel Consumption Trade-Off Under Pilot Injection Mode in a Diesel Engine—Experimental and Numerical Study

Hiren Dave, Bharatkumar Sutaria, and Brijesh Patel

1 Introduction

To this day, diesel engine is the most efficient user of fossil fuel known to mankind and largely used in automotive sector, especially for heavy-duty commercial vehicles due to its high torque and power output. However, diesel engines are suffering from greater nitrogen oxides (NO_x) and soot emissions and reducing them simultaneously is a difficult task due to existing trade-off between them [1]. As the diesel engine is one of the major contributors of these NO_x and soot pollutants, emission regulation authorities from all over the world are making norms for these emissions more and more stringent in each revised regulation for reducing their impact on human health and environment. Achieving these stringent emission norms while maintaining good thermal efficiency have become a challenging task for the diesel engine manufacturers.

In pilot injection, some fuel is injected before main injection and is mainly used for lowering NO_x emissions from modern diesel engines. Combustion of this pre-injected (pilot) fuel creates enhanced thermodynamic conditions and reduces the ignition delay of main fuel by accelerating chemical and physical phenomena and leads to lowered NO_x emissions. Park et al. [2] reported that a reduction of NO_x emissions with pilot injection was mainly due to reduced peak heat release rate (HRR) compared to conventional single injection. Anand [3] investigated split injection along with cooled exhaust gas recirculation (EGR) using biodiesel obtained from waste frying oil. The study reported that split injection leads to simultaneous

H. Dave (✉)
U. V. Patel College of Engineering, Ganpat University, Kherva, Gujarat, India

B. Sutaria
S. V. National Institute of Technology, Surat, Gujarat, India

B. Patel
Gdhyana Sanshodhana Nagari Foundations, Vadodara, Gujarat, India

A. P. Singh et al. (eds.), *Alternative Fuels and Advanced Combustion Techniques as Sustainable Solutions for Internal Combustion Engines*, Energy, Environment, and Sustainability, https://doi.org/10.1007/978-981-16-1513-9_15

reduction of NO_x and soot emissions. Jeon and Park [4] investigated pilot injection mode using diesel and biodiesel fuels. Obtained results demonstrated that pilot injection results in significant reduction of brake-specific energy consumption (BSEC) compared to single injection for most of the pilot injection timings and pilot quantities under consideration. Moreover, the reduction in BSEC was much more significant for diesel fuel compared to biodiesel.

Dwell and pilot quantity are the most important parameters which affects overall combustion process. However, some recent studies have reported that dwell has greater impact on combustion process compared to pilot quantity [4–6]. Many earlier studies have reported the effects of dwell on combustion, performance and emission characteristics of diesel engine. All the literature reviewed here represents these effects with constant main injection timing. If start of pilot injection (SOPI) is too early and dwell becomes too long, specific fuel consumption (SFC) gets deteriorated as pilot fuel cannot be included with main combustion process [7]. Increasingly advanced SOPI results in lower soot emissions due to longer delay period of main fuel resulting in greater homogeneity of mixture and consequently in reduced diffusion combustion duration [8]. However, NO_x tends to increase with longer dwell [9–12] due to longer delay period of main fuel. If SOPI is retarded and the dwell becomes short enough, it results in improvement of SFC due better linking between pilot and main combustion events. Lee et al. [13] also confirmed that SOPI closer to main injection can attain significant reduction in SFC due to higher gas temperature. Li et al. [14] claimed improved thermal efficiency with shorter dwell between pilot and main injections for a given pilot quantity (10%). Results obtained from experimental as well as numerical simulation study proved that this was mainly attributed to better utilization of thermo-atmosphere (a high temperature zone created by burning of pilot fuel) by main fuel spray. Huang et al. [15] investigated pilot injection mode by using diesel as well as blends of diesel and pine oil. From the obtained results, authors concluded that in addition to improvement in thermal efficiency, smaller dwell also reduces the energy loss in terms of friction. Several other studies also claimed SFC improvement with shorter dwell [5, 12, 16–22]. Shorter dwell also resulted in reduced NO_x emissions due to shorter delay period of main injection fuel [8]. Unfortunately, retarded SOPI results in greater smoke emissions due to longer diffusion combustion duration of main fuel. This is primarily due to lesser fuel–air mixing time available due to shorter delay period of main fuel [8]. When pilot and main fuel injections are performed by the same fuel injector (which is the most general case), fuel is injected into the same region of combustion chamber by both the injections (especially for diesel engines without intake swirl). Therefore, liquid components of the main fuel interact with still burning pilot flame which reduces the mixing time available for main fuel with air and combustion takes place under locally rich conditions resulting in high levels of soot formation. Shorter dwell between two injections will aggravate this phenomenon and further augments the soot formation [23]. Similar phenomena were reported by Zhang [24] using optical observations. From the computational fluid dynamics (CFD) simulation results, Moiz et al. [25] confirmed that air entrainment upstream the main fuel spray reduces with retarded SOPI which leads to greater soot formation. Cheolwoong and Stephen [26] studied

pilot-main injection strategy by using a diesel engine with optical access. From OH chemiluminescence imaging, it was noticed that existence of more reactive pilot mixture near main fuel spray in case of shorter dwell apparently ignited main fuel through interactions between reactive pilot mixture and liquid components of main fuel spray jet. Similar relationship between dwell period and soot/smoke emissions was reported by several other researchers too [2, 4, 5, 11, 13, 16, 18, 20, 22, 27, 28]. However, Zhang [24] reported in his study that measures other than reduced pilot quantity and reduced dwell are needed for improved pilot combustion to reduce the smoke emissions further.

The study conducted from above literature summarizes that there exists a trade-off between smoke/soot emissions and brake-specific fuel consumption (BSFC) under pilot injection mode and reducing both of them simultaneously is a difficult task. This trade-off is named as '*smoke–BSFC trade-off*' in present work. This *smoke/soot–BSFC trade-off* has been reported by many earlier studies [13, 16, 18, 20, 22]. However, very few studies have focused on solution of this intrinsic issue. Few earlier studies suggested some solutions to reduce soot/smoke emissions alone (without focusing on BSFC) under pilot injection mode for a given dwell. Binde et al. [23] suggested to use separate fuel injector for injecting pilot and main fuel so that pilot and main injections get spatially separated and soot formation due to interactions between pilot flame and main fuel liquid components (spray interactions) reduces to a great extent. Sahoo et al. [29] suggested to use lower pilot quantity, but too small pilot fuel quantity might result in over lean mixture and pilot fuel may not ignite at all which will result in greater hydrocarbon (HC) emissions and fuel consumption penalties [30]. Dave et al. [31] suggested to reduce the nozzle hole diameter for reducing soot emissions under pilot injection mode. Yet another method is to increase the fuel injection pressure which was proposed by Park et al. [2], but upper values of injection pressure are restricted by limitations of the injection system. Moreover, increasing fuel injection pressure also increases power consumption by the fuel pump. It was confirmed in an earlier study that at excessively high injection pressure (~1500 bar), the increase in power consumption by fuel pump was greater than the increase in indicated power [32]. However, Li et al. [33] achieved simultaneous reduction of BSFC and soot emissions under pilot injection mode by using increased swirl rate (SR). Based on the results of experimental and numerical study, it was stated that higher swirl rate improves the air–fuel mixing process and shortens the combustion duration by accelerating progress of combustion process. At SR = 1, reduction of BSFC claimed was in the range of 1.1–2.01 g/kWh along with reduction of KL factor (a measure of soot particle concentration) as much as 34.9% compared to SR = 0. Therefore, it can be noticed that some significant measures are taken to reduce smoke/soot emissions under pilot injection mode in a diesel engine, but studies which focused on simultaneous reduction of smoke and BSFC are scarce. So, proposing a methodology other than increased SR (the only methodology proposed till date as per authors' knowledge) to reduce smoke and BSFC simultaneously under pilot injection mode would be a noteworthy contribution. In this backdrop, present work is aimed to propose a new methodology that can reduce smoke emissions and BSFC simultaneously under pilot injection mode.

It is believed that the intrinsic problem of *smoke–BSFC trade-off* existing under pilot injection mode can be resolved by another much simpler technique compared to method proposed earlier [33], which involves complex designing and higher cost of the intake system (intake ports, deflector, etc.) for generating swirling intake air flow. Therefore, another method to improve the *smoke–BSFC trade-off* existing under pilot injection mode is proposed in this work. In present study, this issue is addressed by reducing the injection duration of pilot fuel by using a fuel injector with increased number of nozzle holes. For a given fuel quantity and injection pressure, a fuel injector with increased number of nozzle holes results in lesser fuel injection duration compared to another fuel injector with less number of nozzle holes [34]. Therefore, soot formation due to spray interactions can be reduced to a considerable extent with an injector having increased number of nozzle holes. It was also conveyed in earlier studies that when the number of nozzle holes exceeds a certain threshold value, it resulted in very rich combustion zones and subsequent higher soot emissions due to overlapping of individual burning jet [35]. Therefore, the maximum number of nozzle holes is kept limited to only 6 in present study. In present work, experimental as well as numerical investigations have been carried out with an aim to improve the *smoke–BSFC trade-off* existing under pilot injection mode. Experiments were conducted using a single cylinder diesel engine equipped with electronic fuel injection kit. Initially, experiments were conducted with a 3-hole injector and similar experiments at equivalent pilot and main injection timings were repeated by replacing this 3-hole injector with a 6-hole injector of similar configuration. Results obtained by using these two different injectors were compared in terms of combustion and emission characteristics. Moreover, in order to explore the in-cylinder physical phenomena responsible for improving smoke–BSFC trade-off under pilot injection mode, numerical simulations were carried out using *Converge* 3-D CFD tool.

2 Experimental Setup and Procedure

2.1 Test Engine

A naturally aspirated, water cooled, direct injection (DI), single cylinder, 4-stroke Kirlosker TV1 diesel engine was used for the present work. Specifications of the test engine are listed in Table 1, and schematic diagram of experimental test setup is

Table 1 Specifications of the test engine

Compression ratio	17.5
Displacement (cc)	661.45
Bore (mm)	87.5
Stroke (mm)	110
Max. power (kW@rpm)	5.2@1500

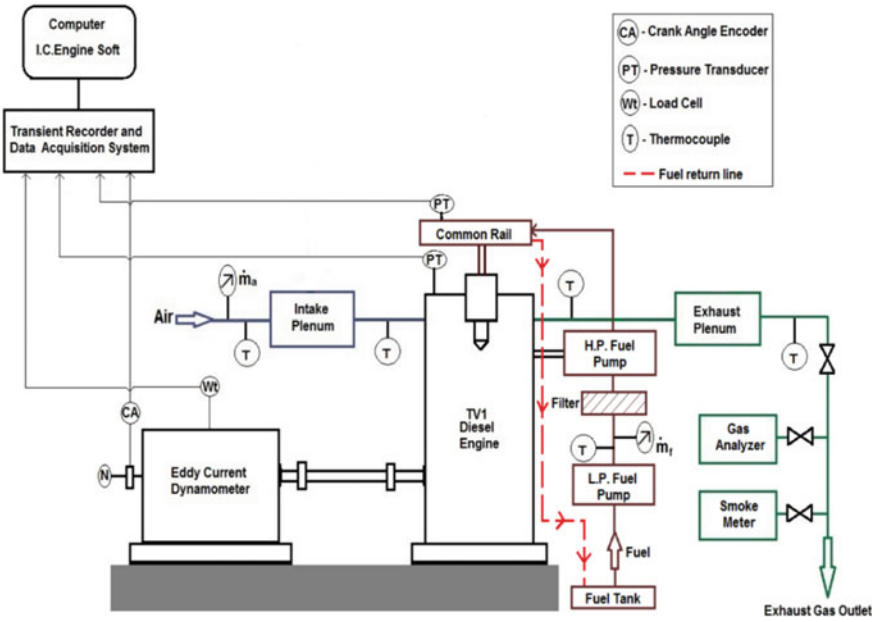

Fig. 1 Schematic diagram of experimental test setup

shown in Fig. 1. Entire test setup includes test engine, eddy current dynamometer, electronic fuel injection system, data acquisition system and emission measuring devices.

Base engine (Kirlosker TV1) uses mechanical injection system. This mechanical injection system was replaced by an electronic fuel injection system in order to perform pilot injection. An electronic fuel injection system attached to the test engine can perform up to four injections in a single cycle of engine operation with minimum 8° dwell. Further reduction in dwell was resulting in unacceptable cyclic variations. Minimum injection duration provided by the injection kit is 800 μs. When injection duration gets lower than this, injection system stops supply of fuel to the engine. This is one of the major limitations of the injection kit attached to the test engine. Maximum injection pressure provided by fuel injection system is 1200 bar. However, base engine having mechanical injection system uses injection pressure of 240 bar. Further details of experimental test setup, data acquisition system, injection system, fuel properties and uncertainty analysis can be found in authors' earlier work [36].

The fuel injector specifications of newly attached electronic injection system are listed in Table 2. Initially, two similar 6-hole solenoid fuel injectors were chosen, out of which three holes of one of the injectors were precisely laser welded to have a 3-hole injector of similar configuration as 6-hole injector.

Table 2 Fuel injector specifications

Code	No. of nozzle holes	Nominal hole diameter (mm)	Spray angle (°)
N03	3 (equally spaced)	0.120	135
N06	6 (equally spaced)	0.120	135

2.2 Experimental Test Conditions

All the experiments were conducted at 1500 rpm and 4.6 bar BMEP (~75% load). Single injection with 3-hole injector at −20° after top dead center (ATDC) is considered as a reference condition. This CA is representative of combination of highest IMEP and lowest BSFC for single injection strategy with 3-hole injector. Based on this, main injection timing was fixed at −20° ATDC throughout the study. Binde et al. [23] reported in their study that larger pilot quantity (at fixed pilot and main injection timings) results in greater soot formation due to more aggressive spray interactions. Based on this, a fixed pilot quantity of 40% of total fuel was chosen for all the pilot injection modes which led to significant rise of smoke emissions with closer pilot injections. Fuel injection pressure was fixed at 350 bar. While performing pilot injection with 6-hole injector under targeted operating conditions (1500 rpm and 75% load) with main injection timing of −20° ATDC (which is a sweet-spot injection timing), injection duration was getting lower than 800 μs. This is because injection duration is already lower in case of N06 compared to N03 case due to greater fuel flow rate offered by N06. If injection pressure is increased beyond 350 bar, it would further lead to further reduction in injection duration and injection duration will become lower than 800 μs which was resulting in fuel supply cutoff by the injection system. This is the reason for fixing injection pressure at 350 bar only in spite of much higher injection pressure offered by the injection system. However, this injection pressure is still higher compared to the injection pressure offered by the mechanical injection system attached to the base engine. Figure 2 shows the representative line diagram of the injection profiles for pilot injection mode with 3-hole injector (referred as N03) as well as with 6-hole injector (referred as N06) for comparison purpose.

As depicted in Fig. 2, fuel injection with N06 resulted in longer dwell between two injections compared to N03 for equal start of (pilot as well as main) injection timings and similar fuel injection quantities in percentage. This is mainly attributed to increased mass flow rate of fuel (per °CA) associated with N06 case due to increased number of nozzle holes which ultimately resulted in shorter injection duration. This can be understood more clearly from Table 3. As the aim of present work is to lower the disadvantage of increased smoke emissions associated with the benefit of improved SFC under close pilot injection condition, SOPI was varied from −39° ATDC to −43° ATDC with step size of 2°, which are correspond to dwell of 8° to 12°, respectively, for N03 case. Injection duration retrieved from data acquisition

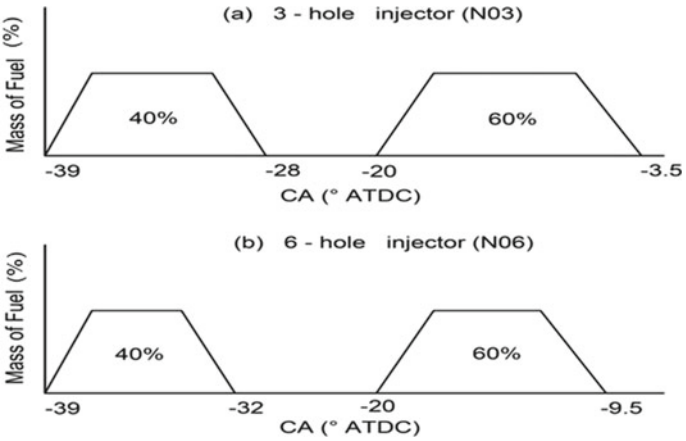

Fig. 2 Represenative line diagram of fuel injection profiles for pilot injection with **a** N03 and **b** N06

Table 3 Experimental operating conditions

Injection strategy	Pilot fuel quantity (%)	SOPI (° ATDC)		Main injection timing (° ATDC)	Dwell (° CA)	
		N03	N06		N03	N06
Single	0	–	–	−20	–	–
Pilot + Main	40	−39	−39	−20	8	12
Pilot + Main	40	−41	−41	−20	10	14
Pilot + Main	40	−43	−43	−20	12	16

system (in μs) was converted into °CA. While maintaining the main injection timing constant, SOPI was decided based on required dwell and duration for pilot injection. SOPI cannot be retarded beyond −39° ATDC which corresponds to the minimum dwell (8°) offered by the injection system for N03 case for a given main injection timing (−20° ATDC) and chosen pilot quantity (40%). Additionally, SOPI could not be advanced beyond −43° ATDC due to similar limitation of the injection system (injection duration was getting lower than 800 μs) because of increased pressure difference (ΔP) between injection pressure and in-cylinder pressure (at SOPI beyond −43° ATDC). Moreover, advancing SOPI beyond −43° ATDC resulted in severe spray wall impingement issues due to lower in-cylinder pressure leading to severe rise in HC emissions and fuel consumption penalties. Therefore, variation of SOPI was conducted from −39° ATDC to −43° ATDC with step size of 2°.

3 Results and Discussion

3.1 Results with N03

Initially, experiments were performed with N03.

3.1.1 Effect of Dwell on Combustion Characteristics

Effect of SOPI on net heat release rate (NHRR) traces has been discerned in Fig. 3. Most of the pilot fuel gets combusted in pre-mixed mode only, which produced much higher peaks of HRR compared to reference condition as shown in Fig. 3. This is because of less favorable in-cylinder conditions for autoignition of pilot fuel at the time of SOPI resulting in its longer delay period and almost all the pilot fuel burnt instantaneously. In-cylinder conditions are more favorable for autoignition when fuel injection took place in case of reference condition. So, fuel passed through a shorter delay period and most of the fuel got combusted in diffusion mode only.

More heightened peaks of HRR are observed with advanced SOPI due to longer delay period associated with them. On the contrary, earlier and lower pre-mixed peak of HRR for main injected fuel can be noticed from Fig. 3 with retarded SOPI as expected. This is because enhanced temperature and pressure produced inside the combustion chamber due to pilot fuel combustion are better to support the autoignition of main fuel with retarded SOPI as pilot fuel is injected closer to main injected

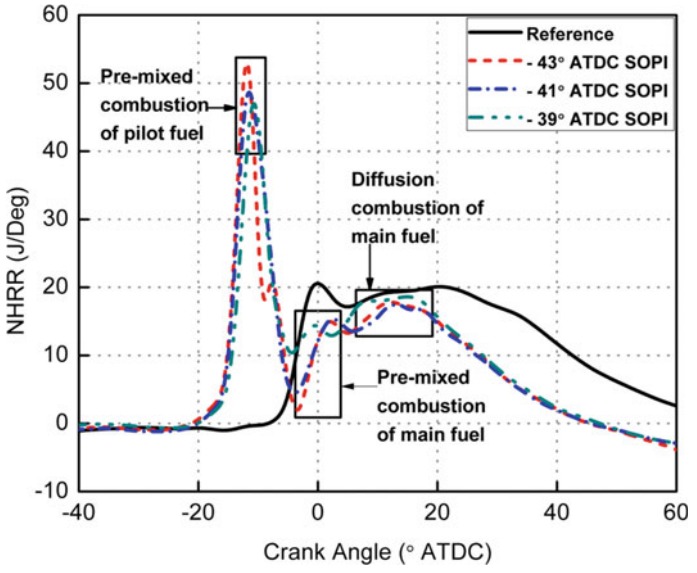

Fig. 3 Effect of SOPI on NHRR traces

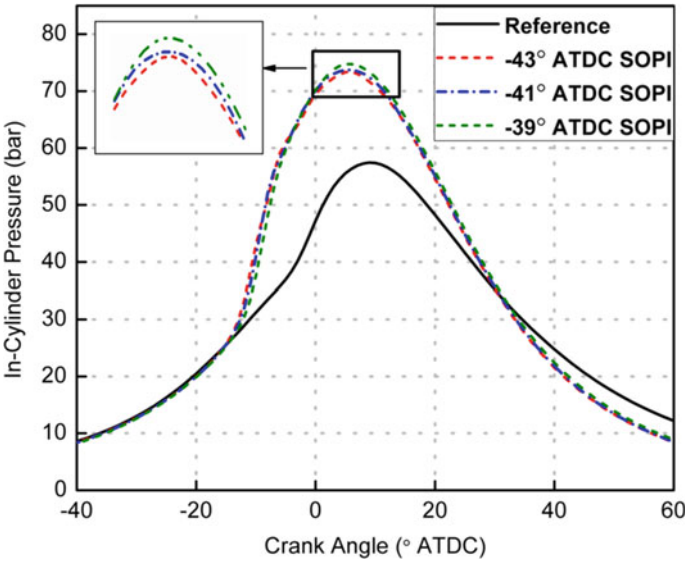

Fig. 4 Effect of SOPI on in-cylinder pressure traces

fuel. Diffusion combustion peak for main fuel increases with closer pilot injections due to shorter mixing time available for main fuel and combustion taking place in rich condition. Though higher HRR peak of diffusive combustion associated with SOPI at −43° ATDC compared to −41° ATDC, pilot injection timing cannot be explained by this phenomenon. Moreover, pilot injection results in much shorter combustion duration compared to single injection case. For example, combustion ceases (a CA where NHRR curve cuts the zero line) at 48° ATDC in case of pilot injection with −39° ATDC SOPI, while combustion process continues till 74° ATDC in case of single injection (not shown in Fig. 3).

Figure 4 represents the in-cylinder pressure traces of various injection strategies. Compared to single injection, pilot injection resulted in much higher combustion pressure irrespective of SOPI. This is because in case of single injection, there was no fuel injection before −20° ATDC. Earlier occurrence of peak pressure can be noticed with all pilot injection cases compared to single injection case from Fig. 4. This is attributed to shorter combustion duration associated with pilot injection as inferred from Figs. 3 and 4. In case of pilot injection, higher peak pressure is observed with retarded SOPI. This is due to greater impact of pilot combustion on main combustion event with retarded injection timing due to shortened dwell period. These trends of pressure traces are in-line with many earlier studies [4–6, 14, 37, 38].

Figure 5 represents the effect of variation of SOPI on MGT traces. Pilot injection produced much higher MGT compared to reference condition. This is due to thermo-atmosphere provided by the pilot combustion for main combustion [37]. During initial combustion stages, MGT is higher for −43° ATDC SOPI compared to other two pilot injection cases as inferred from Fig. 5. This is due to greater amount of heat released

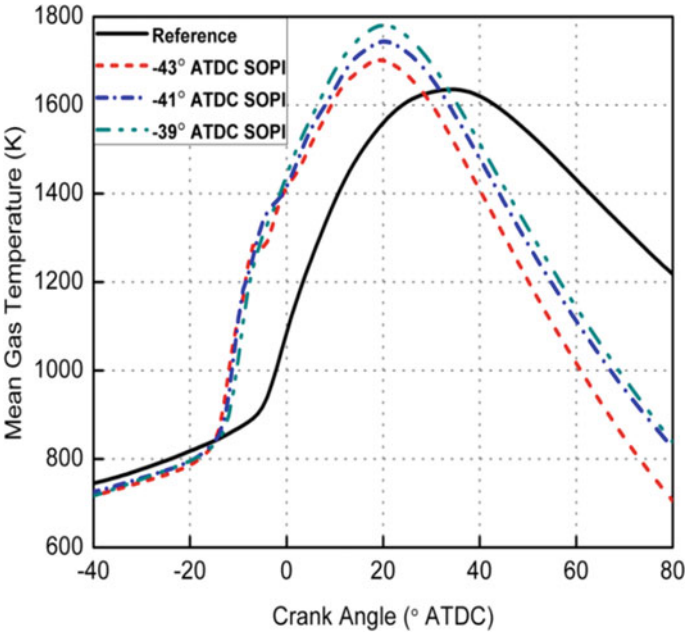

Fig. 5 Effect of SOPI on MGT traces

in pre-mixed combustion of pilot fuel after longer delay period in case of advanced SOPI (refer Fig. 3). However, peak MGT is higher in case of retarded SOPI as can be noticed from Fig. 5 which is mainly due to greater impact of pilot fuel on main combustion.

3.1.2 Effect of Dwell on Emissions and BSFC

Effect of variation of SOPI on emissions and BSFC is represented in Fig. 6. Values of emissions and BSFC for reference condition are given in Table 4 for comparison purpose.

For all the pilot injection cases, smoke emissions are quite lower compared to single injection mode (refer Fig. 6 and Table 4). For example, smoke emissions reduce by around 34% in case of pilot injection with −39° SOPI compared to that with reference condition. This is because single injection mode has longer as well as more dominant diffusion combustion phase as shown in Fig. 3 earlier, which facilitated more time for soot formation. As seen from the MGT traces in Fig. 5, much higher temperature is pertaining in later stages of expansion process in case of single injection compared to all the pilot injection modes, which is very beneficial for oxidation of the formed soot particles. In spite of this, higher exhaust smoke emissions in case of reference condition reveals that soot formation must be significantly larger compared to all the pilot injection cases. Additionally, combustion

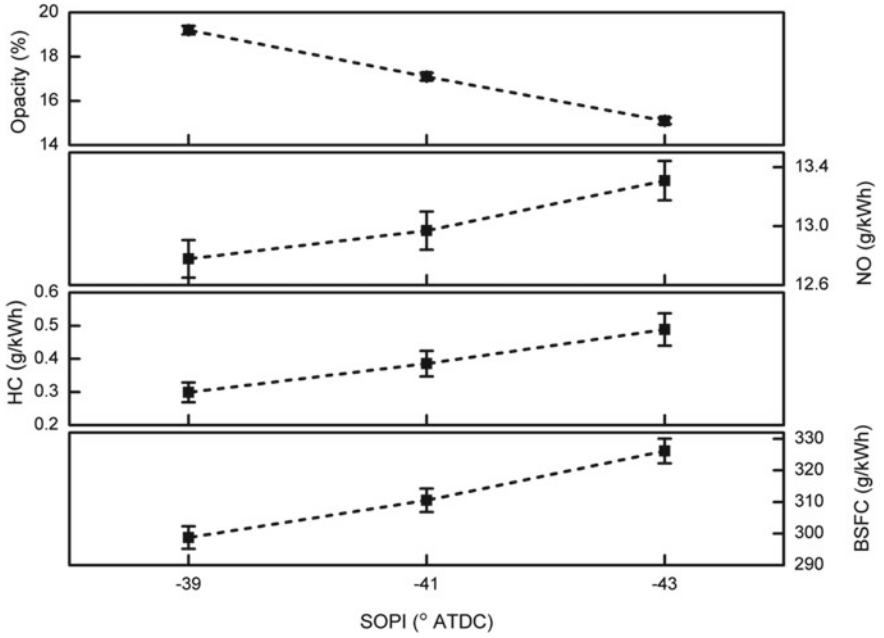

Fig. 6 Effect of SOPI on emissions and BSFC

Table 4 Emissions and BSFC for reference condition

Opacity (%)	NO (g/kWh)	HC (g/kWh)	BSFC (g/kWh)
28.9	3.83	0.45	314.52

duration is lesser for all the pilot injection cases compared to the reference condition as discussed earlier. This shorter combustion duration is likely to improve soot oxidation as formed soot particles have greater time to oxidize at higher temperature compared to conventional single injection. Smoke emissions increased by around 21% when SOPI is retarded from −43° ATDC to −39° ATDC. Increased smoke emissions with retarded SOPI are due to more aggressive spray interactions [39]. Adopting pilot injection mode has negative impact on NO emission (refer Fig. 6 and Table 4). NO emission increased by around 70% in case of pilot injection with −39° ATDC SOPI compared to that with reference condition. This is mainly due instantaneous burning of almost all the pilot fuel. It seemed to be that more advanced the SOPI, greater the NO emission. This is because of elongated delay period of earlier injected pilot fuel due to lower in-cylinder temperature and pressure conditions. The much-reported *NO-smoke emission trade-off* in a diesel engine can be noticed from Fig. 6. Also, the trade-off between BSFC and smoke emissions can be clearly seen at all the SOPI under consideration. When SOPI is retarded from −43° ATDC to −39° ATDC, BSFC reduced by 5.8%. Reduction in BSFC with closer pilot injections is due to accelerated main combustion event which is mainly attributed to greater impact

of pilot combustion on main injected fuel. Retarded SOPI (−39° ATDC and −41° ATDC) attained BSFC lower than single injection mode. This is mainly attributed to enhanced ambient conditions produced by burning of pilot fuel inside engine cylinder which caused quicker combustion of main injected fuel. Similar trends of BSFC were reported by Jeon and Park [4]. Increased HC emissions with advanced SOPI might be due increased possibility of wall wetting and loss of fuel in crevice and squish regions [40].

3.2 Results with N06

All the experiments conducted earlier with N03 were repeated with N06 at similar SOPI and under similar operating conditions. However, in this section, comparison of combustion characteristics is discussed for two extreme pilot injection cases only (i.e., −39° SOPI and −43° SOPI) to attain clear visualization.

3.2.1 Effect of Number of Nozzle Holes on Combustion Characteristics

Figure 7 represents the effect of number of nozzle holes on NHRR traces. Earlier and greater pre-mixed peak of HRR can be observed for pilot fuel in case of N06 compared to N03 case for both the SOPI (Fig. 7a). Pre-mixed peaks of main fuel are

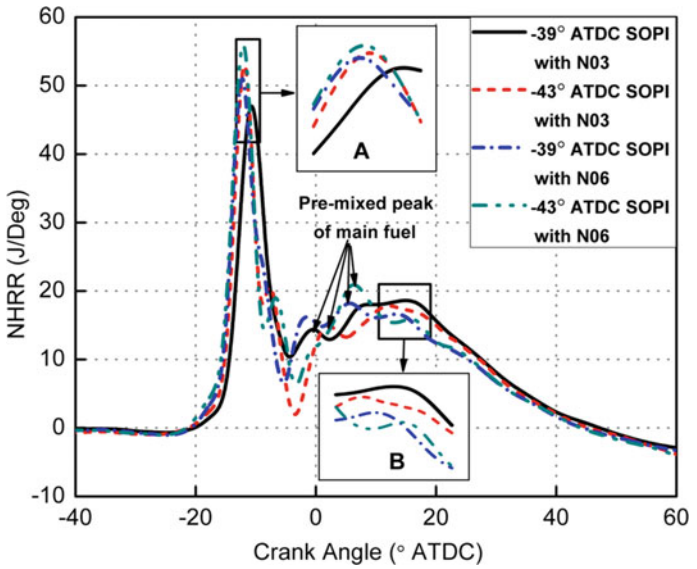

Fig. 7 Comparison of NHRR traces with N03 and N06

more delayed and of greater value in case of N06 than that of N03 case for similar SOPI as shown in Fig. 7. Reasonably lower diffusion combustion peaks as well as shorter diffusion combustion duration of main fuel in case of fuel injection with N06 for equivalent SOPI compared to N03 case can be noticed from Fig. 7b. These trends of NHRR traces with variation in number of nozzle holes are explained using numerical simulation results in Sect. 5.1.

The effect of number of nozzle holes on combustion pressure at similar SOPI has been portrayed in Fig. 8. Increased and retarded peak pressures associated with N06 case compared to N03 case at corresponding SOPI can be observed from Fig. 8. Moreover, rise of negative work (indicated by higher pressure before TDC) is almost negligible while rise in positive work (indicated by higher pressure after TDC) is quite significant in case of N06 compared to N03 case. This confirms improvement of combustion process with increased number of nozzle holes. As operating conditions are similar except number of nozzle holes, increased positive work in case of N06 compared to N03 case is strongly related to increased fuel flow rate (or shorter fuel injection duration) associated with additional number of nozzle holes. Similar results were obtained by Montgomery et al. [34].

Peak MGT is higher for a given SOPI with N06 case than that of N03 case as shown in Fig. 9, but fell more quickly, especially in case of −39° ATDC SOPI.

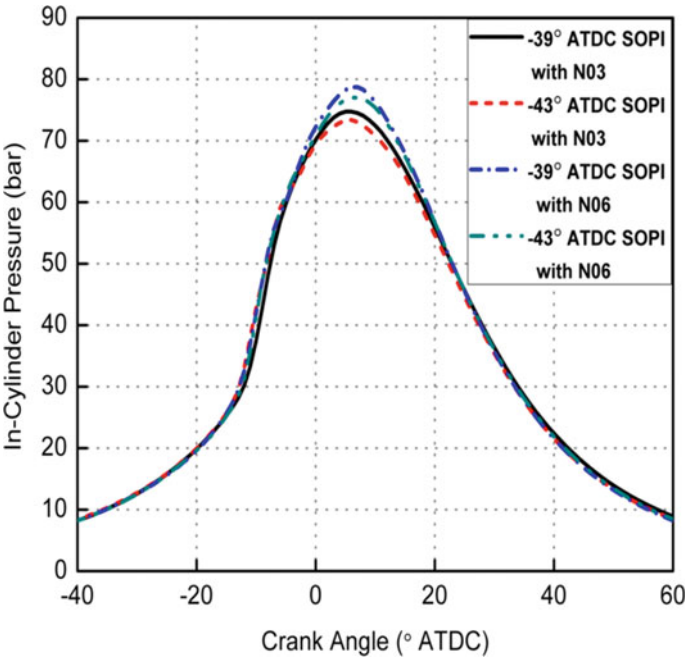

Fig. 8 Comparison of in-cylinder pressure traces with N03 and N06

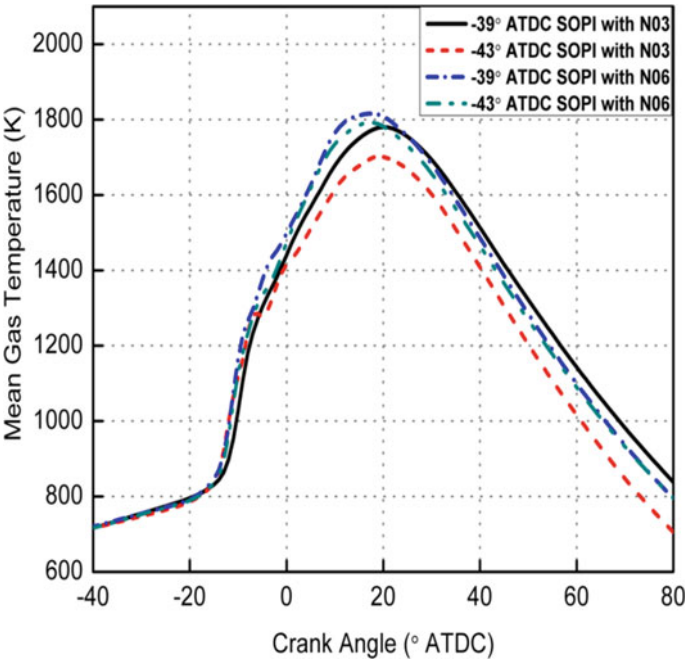

Fig. 9 Comparison of MGT traces with N03 and N06

3.2.2 Effect of Number of Nozzle Holes on Emissions and BSFC

Figure 10 represents the comparison of engine-out emissions and BSFC for two different injectors. Lower smoke emissions are exhausted in case of N06 compared to N03 case at all SOPI under consideration. Smoke emissions reduced by around 57% in case of N06 compared to that with N03 case at −39° SOPI, while this reduction is around 77% at −43° SOPI. Therefore, it can be said that smoke emissions reduce at a faster rate with advanced SOPI in case of N06 compared to that with N03 case. For a given SOPI, NO emission increases in case of N06 compared to N03 case at all the SOPI under consideration. NO emission increased by around 15% in case of N06 compared to N03 case at −39° ATDC pilot injection timing. Moreover, HC emissions as well as BSFC tend to reduce with increased number of nozzle holes. HC emissions as well as BSFC were reduced by 20.69% and 2.46%, respectively, in case of N06 compared to N03 case at −39° ATDC pilot injection timing. These trends of emissions and BSFC with variation of number of nozzle holes are explained using numerical simulation results in Sects. 5.1 and 5.2.

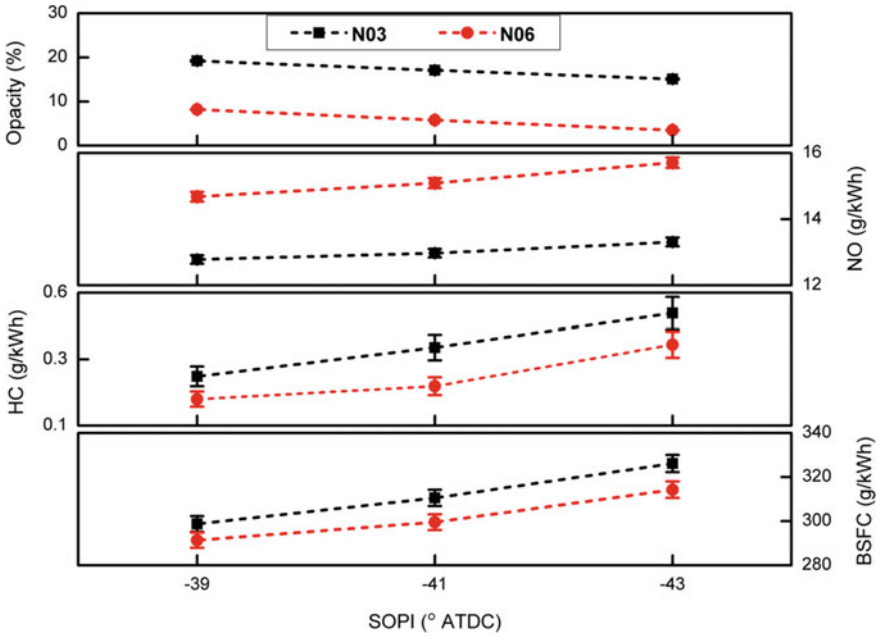

Fig. 10 Effect of number of nozzle holes on emissions and BSFC

4 Numerical Simulation

Numerical simulations are very useful for getting better insight into the in-cylinder physical phenomena affecting overall combustion process. Therefore, numerical simulations were performed using *Converge* 3-D CFD tool. Numerous earlier studies have explained effects of varying dwell period on diesel combustion and emissions characteristics by using various computational tools. Therefore, computational results explaining effects of varying dwell on diesel combustion process are not included in present work in order to conserve the space. Aim of the numerical simulations performed in present study is to explore the physical aspects of in-cylinder combustion process which are responsible for improving *smoke–BSFC trade-off* under pilot injection mode with increased number of nozzle holes. Hence, numerical simulation results of only two pilot injection cases, i.e., (i) −39° SOPI with N03 and (ii) −39° SOPI with N06, are discussed in present work. This is because highest smoke emissions as well as lowest BSFC are noticed at −39° SOPI for both N03 and N06 cases.

Two different sectors, i.e., 120° (1/3rd sector of engine geometry) and 60° (1/6th sector of engine geometry), were created for simulating experimental results of two selected pilot injection modes with N03 and N06, respectively, in order to save computational time and also due to symmetry of the combustion chamber geometry. Figures 11a, b represent 120° sector and 60° sector, respectively.

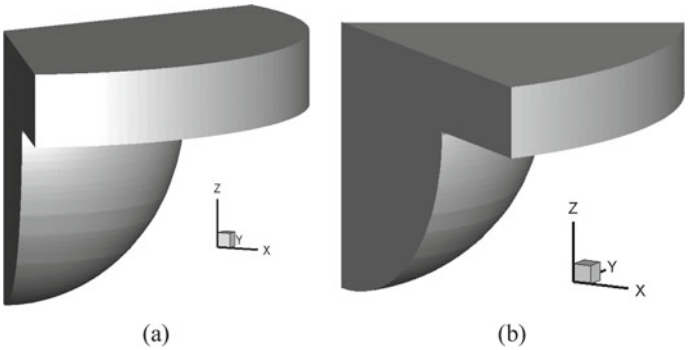

Fig. 11 **a** 120° sector and **b** 60° sector

Table 5 Details of model used for simulating combustion process and emissions

Process/Emission	Simulation model
Combustion	SAGE detailed chemistry model [41]
Turbulence	Re-normalization group (RNG) k-ε [42]
Spray breakup	Kelvin Helmholtz–Rayleigh Taylor (KH-RT) [43]
Spray droplet collision	Schmidt and Rutland [44]
Wall heat transfer	Han and Reitz [45]
Nitrogen oxides (NO_x)	Extended Zeldovich [46]
Soot formation	Hiroyasu [47]
Soot oxidation	Nagle–Strickland-Constable (NSC) model [48]

Closed cycle simulations from intake valve closing (−365° ATDC) to exhaust valve opening (145° ATDC) were performed for both the selected cases with base grid size of 1.4 mm. Grids were refined further at required places using *fixed embedding and adaptive mesh refinement* (*AMR*) techniques available in *Converge.* Values of coefficient of discharge (C_d) were 0.8 and 0.68 for N03 and N06, respectively. Models used for simulating various phenomena and emissions are listed in Table 5. A detailed description of numerical approach, chemical mechanism as well as models used for simulating various phenomena and emissions can be found in [36].

4.1 Code Validation

Figure 12a, b represents comparison of numerical in-cylinder pressure data with corresponding experimental data for two selective pilot injection cases with N03 and

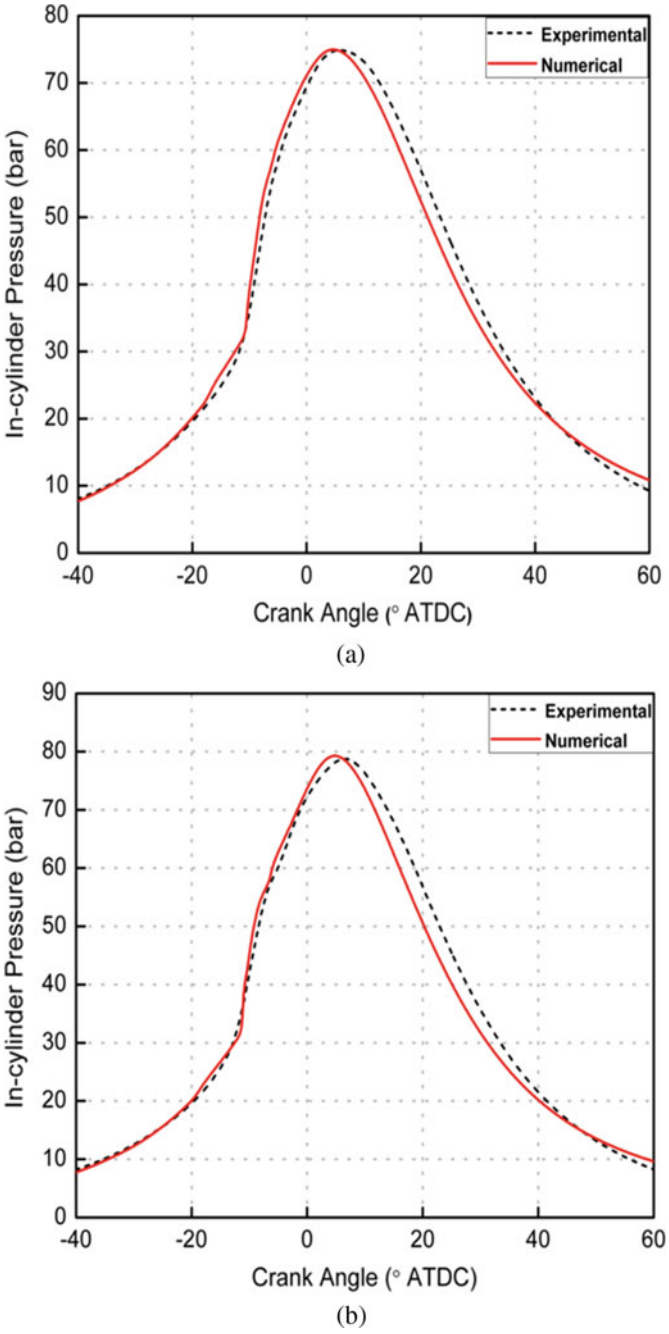

Fig. 12 Comparison of experimental and numerical in-cylinder pressure traces for two selected cases with **a** N03 and **b** N06

Table 6 Comparison of experimental and numerical emissions data

Pilot injection with −39° SOPI	NO (g/kWh) (Experimental)	NO (g/kWh) (Numerical)	Deviation (%)
N03	12.778	12.023	5.90
N06	14.678	15.325	4.22

N06, respectively. An acceptable match between experimental and numerical pressure data can be noticed from Fig. 12a, b. Moreover, a good agreement between experimental and numerical NO emission data can be observed from Table 6. Therefore, it can be said that combustion process is simulated.

5 Numerical Simulation Results and Discussion

As stated earlier, numerical simulation results which are helpful for explaining physical phenomenon responsible for improving *smoke–BSFC trade-off* under pilot injection mode with increased number of nozzle holes are only discussed in present work. Two pilot injection cases selected for this aim are: (i) pilot injection with −39° SOPI with N03 and (ii) pilot injection with −39° SOPI with N06.

5.1 Numerical Results for Combustion Parameters

Contours of temperature and equivalence ratio for selected pilot injection cases at similar CAs are represented in Fig. 13.

A high-temperature region (HTR) and a low-temperature region (LTR) can be noticed for both the selected cases from Fig. 13a. The presence of HTR is attributed to combustion of pre-injected pilot fuel which increased temperature inside combustion chamber and produced a significant rise in temperature. A low-temperature region is generated inside combustion chamber due to evaporation of main injected fuel which absorbed heat from high-temperature combustion gases. As observed from Fig. 13a, HTR is much greater and wider in case of N06 compared to N03 case. This can be explained as follows: for analogous SOPI, end of injection for pilot fuel is earlier in case of N06 compared to N03 case (refer Fig. 2). So, pilot fuel is injected in a lower temperature condition at the end of injection in case of N06. Therefore, pilot fuel passed through a longer physical delay period after getting injected inside the cylinder and burned more instantaneously in case of N06 compared to N03 case. This is why pre-mixed combustion peak of pilot fuel is higher in case of N06 compared to N03 case in Fig. 7a. This greater amount of heat released is responsible for producing wider and greater HTR inside the combustion chamber in case of N06 compared to N03 case (refer Fig. 13a). This faster (or more instantaneous) combustion of pilot fuel after longer delay period in case of N06 compared to N03 case is the main reason

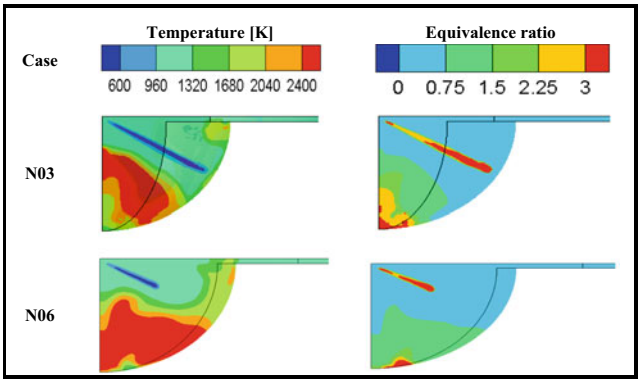

(a)

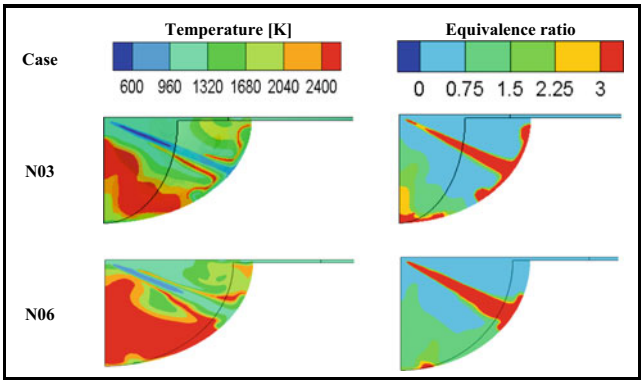

(b)

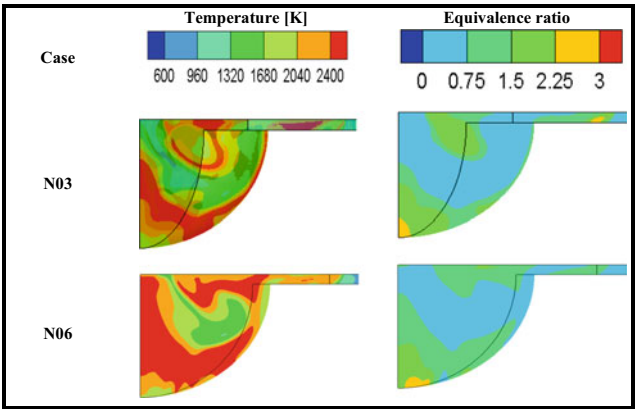

(c)

Fig. 13 In-cylinder temperature and equivalence ratio distribution for two selected cases at −39° SOPI at **a** −8° ATDC, **b** −5° ATDC and **c** 13° ATDC with N03 and N06

for getting earlier pre-mixed combustion peak of pilot fuel in Fig. 7a. Moreover, in case of −39° SOPI pilot injection mode, amount of total fuel (pilot + main) injected per cycle is 6.8% higher in case of N03 compared to N06 case for maintaining engine speed and load constant. Therefore, corresponding pilot (40%) as well as main fuel quantities (60%) and their injection durations are also larger in case of N03 compared to N06 case. Additionally, reduced fuel flow rate associated with N03 case further increases the injection duration of both pilot and main injections compared to N06 case. Therefore, both these factors (greater fuel mass per cycle and reduced fuel flow rate) ultimately led to greater pilot and main fuel injection duration in case of N03 compared to N06 case. Wider as well as greater HTR in case of N06 compared to N03 case in Fig. 13b confirms that more amount of pilot fuel got combusted in case of N06 compared to N03 case. Therefore, it can be said that combustion of pilot fuel progresses at faster rate in case of N06 compared to N03 case. Smaller LTR in case of N06 compared to N03 case at −5° ATDC proves that evaporation rate of main injected fuel is much faster in case of N06 compared to N03 case. Moreover, injected mass of pilot fuel per cycle (for similar pilot quantity in percentage) is greater in case of N03 compared to N06 as discussed earlier. In spite of this, the presence of smaller HTR proves that much more amount of pilot fuel is yet to be combusted and its combustion will be continued for longer duration in case of N03 compared to N06 case. The presence of smaller HTR and greater fuel mass per cycle in case of N03 compared to N06 led to longer delay period of main injected fuel. Additionally, delay period of main injected fuel is further elongated by slower evaporation rate of main fuel (evident by the presence of larger LTR) in case of N03. Moreover, injection duration of main fuel is larger in case of N03 compared to N06 case as stated earlier. So, combined effect of all these factors (slower progress of pilot fuel combustion, slower evaporation rate of main fuel, greater mass of main fuel and longer injection duration of main fuel) signifies that spray interactions will be continued for longer duration and therefore will become more severe in case of N03 compared to N06 case. However, these interactions continued for shorter duration due to faster combustion of pilot fuel (evident by greater and wider HTR at −5° ATDC), faster evaporation rate of main injected fuel (evident by presence of smaller LTR at −5° ATDC), smaller mass of main fuel and shorter injection duration of main fuel. Therefore, severity of spray interactions will be reduced significantly in case of N06 compared to N03 case. This increased severity of spray interactions in case of N03 reduced mixing time of main fuel with air and combustion took place under locally rich condition compared to N06 case. This is also evident by the presence of greater rich regions in equivalence ratio contours of Fig. 13b, c in case of N03 compared to N06 case. Similar phenomena were noticed by Zhang [24] also. Using optical observations, it was reported that if more pilot fuel exists at the time of commencement of main fuel injection, interference of pilot flame with main fuel spray causes poor mixing of main fuel and leads to the formation of greater rich regions inside the cylinder. This reduced mixing time of main fuel and air due to more aggressive interactions is responsible for getting lowered and earlier pre-mixed combustion peak (refer Fig. 7) as well as subsequent greater and delayed diffusion combustion peak (refer Fig. 7b) for main fuel in case of N03 compared to N06 case. Moreover, HTR grows at much

faster rate in case of N06 compared to N03 case which is evident of faster progress of combustion in case of N06. Lesser intensity of spray interactions in case of N06 compared to N03 case resulted in fewer rich regions in Fig. 13b, c. Few more rich regions can be observed in the squish area in case of N03 compared to N06 case from Fig. 13c. This further proves shorter delay period of main fuel and subsequent faster combustion process in case of N06 compared to N03 case which allowed lesser time for main fuel to approach the squish area. Improvement of BSFC in case of N06 compared to N03 case is attributed to this faster and improved (indicated by significant rise in positive work as well as peak pressure in Fig. 8) combustion process. This faster combustion process associated with N06 case is also responsible for lowering HC emissions in case of N06 compared to N03 case. This is because formed HC emissions in case of N06 have greater time to get oxidized at higher temperature compared to N03 case.

5.2 *Numerical Results for Emissions*

NO_x and soot emissions contours for selected pilot injection cases at similar CA (13° ATDC) are represented in Fig. 14. This CA is selected in order to correlate NO_x and soot emissions with in-cylinder temperature contours in Fig. 13c. Greater NO_x regions can be seen in case of N06 compared to N03 case as expected. This is because of more intense pre-mixed combustion of injected pilot fuel in case of N06 compared to N03 case (refer Fig. 7a). Moreover, distribution of peak temperature regions higher than 2000 K is also wider in case of N06 compared to N03 case (refer Fig. 13). Both these factors (longer pre-mixed combustion duration of pilot fuel and wider HTR distribution) led to higher NO_x emissions in case of N06 compared to N03 case.

Greater soot regions can be noticed from Fig. 14 in case of N03 compared to N06 case. This is because of more aggressive spray interactions in case of N03 compared

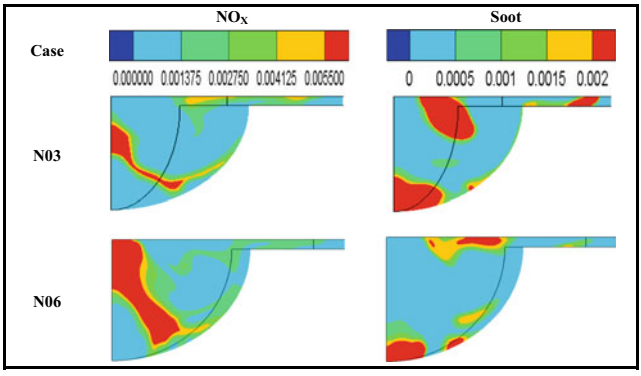

Fig. 14 NO_x and soot emissions for two selected cases at 13° ATDC with N03 and N06

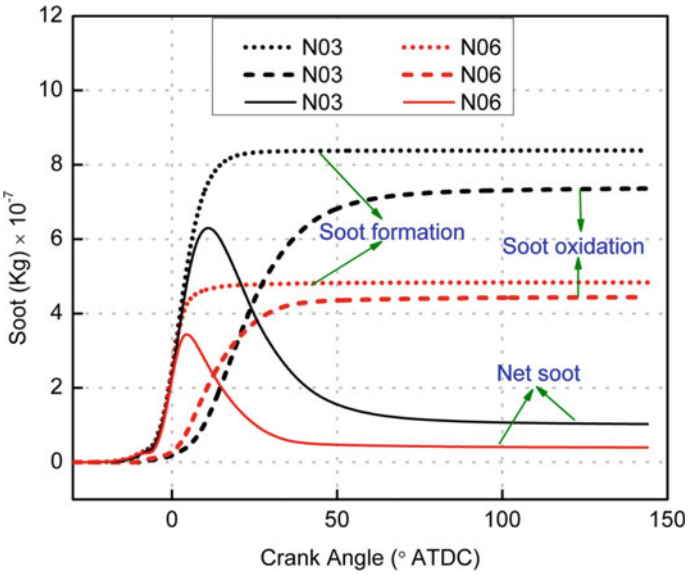

Fig. 15 Computed soot emissions for pilot injection mode at −39° SOPI with N03 and N06

to N06 case which reduced the mixing time of main fuel with air. Due to this more severe spray interactions, overall combustion of main injected fuel took place under locally rich condition (evident from greater rich regions in Fig. 13b, c) and led to larger soot formation in case of N03 compared to N06 case.

Independent investigation of soot formation and soot oxidation processes was carried out in order to investigate the prime reason of getting higher net smoke emissions under pilot injection mode with N03 case compared to N06 case. This is represented in Fig. 15.

Negligible soot formation in the earlier stages of combustion for both the cases reveals that pilot fuel burns with almost soot free mode. Hence, it can be said that most of the pilot fuel combusts in pre-mixed combustion mode only (as evident from NHRR traces in Fig. 7a) and prime source of soot emissions is the main injected fuel in case of pilot injection mode for both N03 and N06 cases. Soot formation stopped at 15° ATDC in case of N06 while it continued till 24° ATDC in case of N03. This is also evident from greater diffusion combustion peak and longer diffusion combustion duration of main fuel in case of N03 compared to N06 case from Fig. 7b. This longer and more dominant diffusion combustion period and subsequent greater soot formation duration in case of N03 is mainly attributed to spray interactions which continued for longer time in case of N03 compared to N06 case as discussed earlier. Soot oxidation continued for longer duration in case of N03 compared to N06 case as inferred from Fig. 15. This is mainly attributed to higher temperature pertaining in the later stage of combustion in case of N03 (refer Fig. 9) due to slower combustion process (evident by gradual growth of HTR in Fig. 13) compared to N06

case. In spite of this longer soot oxidation time, greater net soot emissions exhausted in case of N03 compared to N06 case proves that soot formation must be extensively larger in case of N03 compared to N06 case. Therefore, it can be said that greater soot formation due to more aggressive spray interactions is the prime reason for getting higher net soot emissions in case of N03 compared to N06 case.

6 Assessment of Results

Statistical comparison of various emissions and BSFC obtained with N03 and N06 case at closest SOPI (−39° ATDC) is represented in Table 7.

Smoke and HC emissions as well as BSFC are reduced in case of N06 as compared to N03 case, while NO emission is increased. However, percentage increase in NO emission is considerably lower than percentage reduction in smoke emissions at all the SOPI under consideration. This increased NO emission formation inside combustion chamber can be controlled by various in-cylinder measures like retardation of pilot as well as main injection timings, using optimized quantity of EGR, using optimized injection pressure, etc., as well as by using after treatment devices like selective catalytic reduction (SCR), lean NO_x traps (LNT), etc.

Simultaneous reduction of smoke emissions and BSFC in case of N06 compared to N03 case is the most important marking that can be made from Table 7. Additionally, in case of pilot injection with N06, SOPI can be retarded further to achieve additional improvement in BSFC with still lower or equivalent smoke emissions compared to N03 case. Therefore, intrinsic problem of increased smoke emissions coupled with benefit of lower BSFC under close pilot injection condition can be

Table 7 Comparison of various output parameters

Sr. No.	Injection condition	BSFC (g/kWh)	Opacity (%)	NO (g/kWh)	HC (g/kWh)
1	Pilot injection at -39° ATDC with N03	298.74	19.2	12.78	0.29
2	Pilot injection at -39° ATDC with N06	291.40	8.2	14.68	0.23
3	% change in N06 compared to N03	**2.46 (↓)**	**57.29 (↓)**	**14.87 (↑)**	**20.69 (↓)**

Percentage change in various performance parameters and emissions due to change in number of nozzle holes was highlighted with bold fonts just to highlight the significant change in these parameters when number of nozzle holes were changed from 3 to 6. Advantageous parts like reduction in smoke emissions (represented as opacity) and HC emissions as well as reduction in BSFC were highlighted with green fonts and disadvantageous part (increased NO emission) was highlighted with red color fonts

successfully resolved by using an injector with greater number of orifices. Moreover, reduction obtained in smoke emissions as well as in BSFC is quite higher by the proposed technique compared to reduction claimed by another method [33], particularly reduction in smoke emissions is much more significant.

In present study, maximum number of nozzle holes was restricted to 6 only. However, this study does not convey that 6 is the optimized number of nozzle holes in a fuel injector beyond which improvement in *smoke–BSFC trade-off* cannot not noticed. The objective of the presented work is not to define the optimized number of nozzle holes in terms of improving *smoke–BSFC trade-off*. The prime objective of the presented work is to define a *smoke–BSFC trade-off* in a diesel engine operating under pilot injection mode and to suggest a methodology to improve it.

7 Conclusions

Experimental as well as numerical studies were carried out with an aim of improving '*smoke–BSFC trade-off*' existing under pilot injection mode by using a fuel injector with greater number of nozzle holes. Two fuel injectors of similar configuration except number of nozzle holes, one with 3 holes and another with 6 holes, were used for present work.

For similar pilot injection and main injection timings, fuel injection with N06 resulted in substantial reduction in smoke emissions (about 57% and 77% at SOPI −39° ATDC and −43° ATDC, respectively) and comparatively smaller increase in NO emission (about 15% and 19% at SOPI −39° ATDC and −43° ATDC, respectively) compared to N03 case. Numerical results showed that spray interactions continued for longer duration in case of N03 compared N06 case. This is mainly attributed to lesser quantity of pilot fuel combusted before completion of main injection as well as longer main fuel injection duration associated with N03 case compared to N06 case. This in turn allowed more time for soot formation and found to be a prime reason for getting higher net smoke emissions in case of N03 compared to N06 case under similar pilot as well as main injection timings. Improved and quicker combustion process is one of the most beneficial effects obtained by using an injector with increased number of nozzle holes, which resulted from shorter injection duration. This in turn resulted in reduction of BSFC and HC emissions in case of N06 compared to N03 case.

Use of fuel injector with increased number of nozzle holes can be the pertinent solution of the inherent problem of increased smoke emissions coupled with the benefit of improved BSFC in case of closer pilot injection. Moreover, in case of pilot injection with N06, SOPI can be retarded further to achieve additional improvement in BSFC with still lower or equivalent smoke emissions compared to N03 case.

Acknowledgements Authors gently acknowledge the financial support provided by SVNIT, Surat, to conduct this research.

References

1. Shukla, P. C., Gupta, T., & Agarwal, A. K. (2018). Techniques to control emissions from a diesel engine. In *Air pollution and control* (pp. 57–72). Springer. https://doi.org/10.1007/978-981-10-7185-0_4.
2. Park, C., Kook, S., & Bae, C. (2004). *Effects of multiple injections in a HSDI diesel engine equipped with common rail injection system.* SAE Technical Paper 2004-01-0127. https://doi.org/10.4271/2004-01-0127.
3. Anand, R. (2018). Simultaneous control of oxides of nitrogen and soot in crdi diesel engine using split injection and cool EGR fueled with waste frying oil biodiesel and its blends. In *Air pollution and control* (pp. 11–44). Springer. https://doi.org/10.1007/978-981-10-7185-0_2.
4. Jeon, J., & Park, S. (2015). Effects of pilot injection strategies on the flame temperature and soot distributions in an optical CI engine fueled with biodiesel and conventional diesel. *Applied Energy, 160,* 581–591. https://doi.org/10.1016/j.apenergy.2015.09.075.
5. Huang, H., Wang, Q., Shi, C., Liu, Q., & Zhou, C. (2016). Comparative study of effects of pilot injection and fuel properties on low temperature combustion in diesel engine under a medium EGR rate. *Applied Energy, 179,* 1194–1208. https://doi.org/10.1016/j.apenergy.2016.07.093.
6. Zheng, Z., Yue, L., Liu, H., Zhu, Y., Zhong, X., & Yao, M. (2015). Effect of two-stage injection on combustion and emissions under high EGR rate on a diesel engine by fueling blends of diesel/gasoline, diesel/n-butanol, diesel/gasoline/n-butanol and pure diesel. *Energy Conversion and Management, 90,* 1–11. https://doi.org/10.1016/j.enconman.2014.11.011.
7. Liu, Y., & Reitz, R. D. (2005). *Optimizing HSDI diesel combustion and emissions using multiple injection strategies.* SAE Technical Paper 2005-01-0212. https://doi.org/10.4271/2005-01-0212.
8. Carlucci, P., Ficarella, A., & Laforgia, D. (2003). *Effects of pilot injection parameters on combustion for common rail diesel engines.* SAE Technical Paper 2003-01-0700. https://doi.org/10.1243/146808705X7301.
9. Shi, X. Y., Qiao, X. Q., Ni, J. M., Zheng, Y. Y., & Ye, N. Y. (2010). Study on the combustion and emission characteristics of a diesel engine with multi-injection modes based on experimental investigation and computational fluid dynamics modelling. *Proceedings of the Institution of Mechanical Engineers, Part D: Journal of Automobile Engineering, 224,* 1161–1176. https://doi.org/10.1243/09544070JAUTO1434.
10. Okude, K., Mori, K., Shiino, S., Yamada, K., & Matsumoto, Y. (2007). *Effects of multiple injections on diesel emission and combustion characteristics.* SAE Technical Paper 2007-01-4178. https://doi.org/10.4271/2007-01-4178.
11. Benajes, J., Molina, S., & García, J. M. (2001). *Influence of pre- and post-injection on the performance and pollutant emissions in a HD diesel engine.* SAE Technical Paper 2001-01-0526. https://doi.org/10.4271/2001-01-0526.
12. Ehleskog, R., Golovitchev, V., Denbratt, I., Andersson, S., & Rinaldini, C. A. (2006). *Experimental and numerical investigation of split injections at low load in an HDDI diesel engine equipped with a piezo injector*. SAE Technical Paper 2006-01-3433. https://doi.org/10.4271/2006-01-3433.
13. Lee, J., Hong, K., Choi, S., Yu, S., Choi, H., & Min, K. (2017). Comparison of the effects of multiple injection strategy on the emissions between moderate and heavy EGR rate conditions: Part 1-pilot injections. *Journal of Mechanical Science and Technology, 27,* 1135–1141. https://doi.org/10.1007/s12206-013-0220-x.
14. Li, X.-R., Yang, W., Zhao, L. M., & Liu, F.-S. (2017). The influence of pilot-main injection matching on DI diesel engine combustion using an endoscopic visualization system. *Fuel, 188,* 575–585. https://doi.org/10.1016/j.fuel.2016.10.069.
15. Huang, H., Huang, R., Guo, X., Pan, M., Teng, W., Chen, Y., & Li, Z. (2019). Effects of pine oil additive and pilot injection strategies on energy distribution, combustion and emissions in a diesel engine at low-load condition. *Applied Energy, 250,* 185–197. https://doi.org/10.1016/j.apenergy.2019.05.028.

16. Yun, H., Choi, K., & Lee, C. S. (2016). Effects of biobutanol and biobutanol–diesel blends on combustion and emission characteristics in a passenger car diesel engine with pilot injection strategies. *Energy Conversion and Management, 111,* 79–88. https://doi.org/10.1016/j.enconman.2015.12.017.
17. Ishikawa, N., Uekusa, T., Nakada, T., & Hariyoshi, R. (2004). *DI diesel emission control by optimized fuel injection.* SAE Technical Paper 2004-01-0117. https://doi.org/10.4271/2004-01-0117.
18. Chen, S. K. (2000). *Simultaneous reduction of NO_x and particulate emissions by using multiple injections in a small diesel engine.* SAE Technical Paper 2000-01-3084. https://doi.org/10.4271/2000-01-3084.
19. Carlucci, P., Ficarella, A., & Laforgia, D. (2005). Effects on combustion and emissions of early and pilot fuel injections in diesel engines. *International Journal of Engine Research, 6,* 43–60. https://doi.org/10.1243/146808705X7301.
20. Park, S., Kim, H. J., Shin, D. H., & Lee, J. T. (2018). Effects of various split injection strategies on combustion and emissions characteristics in a single-cylinder diesel engine. *Applied Thermal Engineering, 140,* 422–431. https://doi.org/10.1016/j.applthermaleng.2018.05.025.
21. Liu, B., Cheng, X., Liu, J., & Pu, H. (2018). Experimental investigation of injection strategies on particle emission characteristics of partially-premixed low temperature combustion mode. *Applied Thermal Engineering, 141,* 90–100. https://doi.org/10.1016/j.applthermaleng.2018.05.066.
22. Huang, H., Zhu, Z., Zhu, J., Lv, D., Pan, Y., Wei, H., & Teng, W. (2019). Experimental and numerical study of pre-injection effects on diesel-n-butanol blends combustion. *Applied Energy, 249,* 377–391. https://doi.org/10.1016/j.apenergy.2019.04.163.
23. Binde, A., Busch, S., Velji, A., & Wagner, U. (2012). Soot and NO_x reduction by spatially separated pilot injection. *SAE International Journal of Engines, 5,* 1242–1259. https://doi.org/10.4271/2012-01-1159.
24. Zhang, L. (1999). *A study of pilot injection in a DI diesel engine.* SAE Technical Paper 1999-01-3493. https://doi.org/10.4271/1999-01-3493.
25. Moiz, A. A., Ameen, M. M., Lee, S. Y., & Som, S. (2016). Study of soot production for double injections of n-dodecane in CI engine-like conditions. *Combustion and Flame, 173,* 123–131. https://doi.org/10.1016/j.combustflame.2016.08.005.
26. Cheolwoong, P., & Stephen, B. (2017). The influence of pilot injection on high-temperature ignition processes and early flame structure in a high-speed direct injection diesel engine. *International Journal of Engine Research, 6,* 668–681. https://doi.org/10.1177/1468087417728630.
27. Hotta, Y., Inayoshi, M., Nakakita, K., Fujiwara, K., & Sakata, I. (2005). *Achieving lower exhaust emissions and better performance in an HSDI diesel engine with multiple injection.* SAE Technical Paper 2005-01-0928. https://doi.org/10.4271/2005-01-0928.
28. Herfatmanesh, M. R., Lu, P., Attar, M. A., & Zhao, H. (2013). Experimental investigation into the effects of two-stage injection on fuel injection quantity, combustion and emissions in a high-speed optical common rail diesel engine. *Fuel, 109,* 137–147. https://doi.org/10.1016/j.fuel.2013.01.013.
29. Sahoo, D., Miles, P. C., Trost, J., & Leipertz, A. (2013). The impact of fuel mass, injection pressure, ambient temperature, and swirl ratio on the mixture preparation of a pilot injection. *SAE International Journal of Engines, 6,* 1716–1730. https://doi.org/10.4271/2013-24-0061.
30. Qi, D., Leick, M., Liu, Y., & Lee, C. F. (2011). Effect of EGR and injection timing on combustion and emission characteristics of split injection strategy DI-diesel engine fueled with biodiesel. *Fuel, 90,* 1884–1891. https://doi.org/10.1016/j.fuel.2011.01.016.
31. Dave, H., Sutaria, B., & Patel, B. (2020). Influence of nozzle hole diameter on combustion and emission characteristics of diesel engine under pilot injection mode. *IOP Conference Series: Materials Science and Engineering, 810,* 012041. https://doi.org/10.1088/1757-899x/810/1/012041.
32. Badami, M., Nuccio, P., & Trucco, G. (1999). *Influence of injection pressure on the performance of a DI diesel engine with a common rail fuel injection system.* SAE Technical Paper 1999-01-0193. https://doi.org/10.4271/1999-01-0193.

33. Li, X., Zhou, H., Zhao, L. M., Su, L., Xu, H., & Liu, F. (2016). Effect of split injections coupled with swirl on combustion performance in DI diesel engines. *Energy Conversion and Management, 129,* 180–188. https://doi.org/10.1016/j.enconman.2016.09.011.
34. Montgomery, D. T., Chan, M., Chang, C. T., Farrell, P. V., & Reitz, R. D. (1996). *Effect of injector nozzle hole size and number on spray characteristics and the performance of a heavy duty D.I. diesel engine*. SAE Technical Paper 962002. https://doi.org/10.4271/962002.
35. Hielscher, K., Brauer, M., & Baar, R. (2016). Reduction of soot emissions in diesel engines due to increased air utilization by new spray hole configurations. *Automotive and Engine Technology, 1,* 69–79. https://doi.org/10.1007/s41104-016-0010-4.
36. Hiren, D., Bharatkumar, S., & Brijesh, P. (2019). Effect of pilot quantity on combustion and emission characteristics of a single-cylinder diesel engine under fixed dwell condition: Experimental and numerical study. *Clean Technologies and Environmental Policy, 21,* 905–921. https://doi.org/10.1007/s10098-019-01680-6.
37. Li, X., Gao, H., Zhao, L., Zhang, Z., He, X., & Liu, F. (2016). Combustion and emission performance of a split injection diesel engine in a double swirl combustion system. *Energy, 114,* 1135–1146. https://doi.org/10.1016/j.energy.2016.08.092.
38. Dronniou, N., Lejeune, M., Balloul, I., & Higelin, P. *Combination of high EGR rates and multiple injection strategies to reduce pollutant emissions.* SAE Technical Paper 2005-01-3726. https://doi.org/10.4271/2005-01-3726.
39. Cung, K., Moiz, A., Johnson, J., Lee, S. Y., Kweon, C. B., & Montanaro, A. (2015). Spray–combustion interaction mechanism of multiple-injection under diesel engine conditions. *Proceedings of the Combustion Institute, 35,* 3061–3068. https://doi.org/10.1016/j.proci.2014.07.054.
40. Brijesh, P., & Sreedhara, S. (2016). Experimental and numerical investigations of effect of split injection strategies and dwell between injections on combustion and emissions characteristics of a diesel engine. *Clean Technologies and Environmental Policy, 18,* 2325–2334. https://doi.org/10.1007/s10098-016-1153-8.
41. Senecal, P. K., Pomraning, E., Richards, K. J., Briggs, T. E., Choi, C. Y., McDavid, R. M., & Patterson, M. A. (2003). *Multi-dimensional modeling of direct-injection diesel spray liquid length and flame lift-off length using CFD and parallel detailed chemistry*. SAE Technical Paper 2003-01-1043. https://doi.org/10.4271/2003-01-1043.
42. Han, Z., & Reitz, R. D. (1995). Turbulence modeling of internal combustion engines using RNG κ-ε models. *Combustion Science and Technology, 106,* 267–295. https://doi.org/10.1080/00102209508907782.
43. Beale, J. C., & Reitz, R. D. (1999). Modeling spray atomization with the Kelvin-Helmholtz/Rayleigh-Taylor hybrid model. *Atomization and Sprays, 9,* 632–650. https://doi.org/10.1615/AtomizSpr.v9.i6.40.
44. Schmidt, D. P., & Rutland, C. J. (2000). A new droplet collision algorithm. *Journal of Computational Physics, 164,* 62–80. https://doi.org/10.1006/jcph.2000.6568.
45. Han, Z., & Reitz, R. D. (1997). A temperature wall function formulation for variable-density turbulent flows with application to engine convective heat transfer modeling. *International Journal of Heat and Mass Transfer, 40,* 613–625. https://doi.org/10.1016/0017-9310(96)00117-2.
46. Zeldovich, Y. B., Barenblatt, G. I., Librovich, V. B., & Makhviladze, G. M. (1986). *The mathematical theory of combustion and explosions*. Consultants Bureau.
47. Hiroyasu, H., & Kadota, T. (1976). *Models for combustion and formation of nitric oxide and soot in direct injection diesel engines.* SAE Technical Paper 760129. https://doi.org/10.4271/760129.
48. Nagle, J. (1962). Oxidation of carbon between 1000–2000 °C. In *Proceedings Fifth Carbon Conference* (Vol. 1, pp. 154–164).